NASA/CR—1999–209428

Development of a Practical Methodology for Elastic-Plastic and Fully Plastic Fatigue Crack Growth

R.C. McClung, G.G. Chell, and Y.-D. Lee
Southwest Research Institute, San Antonio, Texas

D.A. Russell and G.E. Orient
Rocketdyne Division, Boeing North American, Canoga Park, California

Prepared for Marshall Space Flight Center
under Contract NAS8–37828

July 1999

Acknowledgments

The results described in this report would not have been possible without the support of many other colleagues. The authors are pleased to acknowledge the significant contributions of Chris Kuhlman (SwRI), Tim Grant (SwRI), and Kaung J. Chang (Rocketdyne), who performed some of the computations; Vic Aaron and Tom Masden, SwRI laboratory technicians who performed the Inconel 718 crack growth experiments; Steve Hudak (SwRI), who provided both management support and technical advice; and Luz Escobedo and Patty Soriano, SwRI secretaries who prepared all the reports, including this final report.

The technical staff of NASA Marshall Space Flight Center are especially thanked for maintaining a strong, cordial working relationship throughout the contract. In particular, Wayne Gregg, Gwyn Faile, Carmelo Bianca, and former NASA employee Chris Wilson provided encouragement and guidance that was essential to the success of this program.

Development of the NASGRO modules would not have been possible without the support of technical staff at NASA Johnson Space Center. The assistance of Royce Forman and Sambi Mettu (Lockheed) is gratefully acknowledged.

Numerous professional colleagues cooperated by providing data, software, or technical advice during the course of the program. The authors extend their special thanks to Jim Newman (NASA Langley Research Center), Joe Bloom (McDermott International, Inc.), and Monir Sharobeam (Stockton State College, New Jersey).

Available from:

NASA Center for AeroSpace Information
800 Elkridge Landing Road
Linthicum Heights, MD 21090–2934
(301) 621–0390

National Technical Information Service
5285 Port Royal Road
Springfield, VA 22161
(703) 487–4650

TABLE OF CONTENTS

Page

1. BACKGROUND 1
   1.1 The Demands of Space Propulsion 1
   1.2 Previous Capabilities for Fatigue Crack Growth Analysis 2
   1.3 Selection of a Governing Parameter for Elastic-Plastic Fatigue Crack Growth 3
      1.3.1 Historical Background 3
      1.3.2 Criteria for Parameter Selection 5
      1.3.3 Evaluation of Delta *J* 7
      1.3.4 Evaluation of Alternative Parameters 9
   1.4 Overview of the Program and Final Report 11

2. DEVELOPMENT AND VERIFICATION OF *J*-INTEGRAL SOLUTIONS 14
   2.1 Introduction 14
   2.2 Existing Solutions 19
   2.3 New Solutions 20
      2.3.1 Surface, Corner, and Embedded Cracks in Plates 20
         2.3.1.1 Finite Element Solutions 20
         2.3.1.2 Reference Stress Solutions 20
      2.3.2 Cracks at Stress Concentrations 23
         2.3.2.1 Finite Element Solutions 23
         2.3.2.2 Reference Stress Solutions 26
      2.3.3 Reference Stress Solutions for Through Cracks in Plates 27
   2.4 Estimation Methods for Combined Mechanical Loading 28
   2.5 Estimation Methods for Combined Primary and Secondary Loading 29
   2.6 Estimation Methods for Multiaxial Loading 31

3. DEVELOPMENT AND VERIFICATION OF PRACTICAL CRACK GROWTH ALGORITHMS 33
   3.1 Introduction 33
   3.2 Formulation of Closure-Corrected ΔJ 34
   3.3 Algorithms to Estimate Crack Opening Stresses 40
      3.3.1 Effects of Maximum Stress, Stress Ratio, and Stress State 43
      3.3.2 Effect of Specimen Geometry 47
      3.3.3 Effect of Net-Section and Gross Yielding 50
      3.3.4 Effect of Stress Concentrations 55
      3.3.5 Effect of Multiaxial Stresses 58
      3.3.6 Effects of Combined Loading 62
   3.4 Algorithms for Crack Instability 64
   3.5 Algorithms to Estimate Fatigue, Constitutive, and Fracture Properties 65
      3.5.1 Fatigue Crack Growth Properties 65
      3.5.2 Constitutive Properties 69
      3.5.3 Fracture Properties 73

TABLE OF CONTENTS (CONTINUED)

Page

3.6 Load Interaction Effects 74
3.7 Creep-Fatigue Effects 78

4. DEVELOPMENT AND VERIFICATION OF NASGRO SOFTWARE MODULES 81
4.1 Introduction 81
4.2 J and ΔJ Solutions 83
4.3 Failure Algorithms 83
4.4 Elastic-Plastic Fatigue Crack Growth 84

5. SUMMARY AND CONCLUSIONS 86
5.1 Summary of J-Integral Solutions 86
5.2 Summary of Practical Crack Growth Algorithms 87
5.3 Summary of NASGRO Modules 88

6. REFERENCES 86

APPENDIX A. EVALUATION OF ALTERNATIVE GOVERNING PARAMETERS A.1
A.1 Introduction A.1
A.1.1 Potential Limitations of ΔJ A.1
A.1.2 Possible Alternative Parameters A.1
A.2 Critical Evaluation of Alternative Parameters A.2
A.2.1 Previous Studies of Alternative Parameters A.2
A.2.2 Summary and Discussion A.4
A.3 A Re-Evaluation of ΔJ A.6
A.4 General Remarks About All EPFCG Governing Parameters A.8
A.5 Conclusions and Recommendations A.9

APPENDIX B. A SURVEY OF CURRENTLY AVAILABLE J SOLUTIONS B.1

APPENDIX C. FINITE ELEMENT J SOLUTIONS FOR SURFACE AND CORNER FLAWS C.1

APPENDIX D. A J ESTIMATION SCHEME FOR CRACKS AT NOTCHES D.1
D.1 Introduction D.1
D.2 J Estimation Schemes D.1
D.2.1 EPRI Scheme D.1
D.2.2 Proposed Estimation Scheme (Modified RSM) D.4
D.2.3 Standard RSM Scheme D.5
D.3 Validation of J Estimation Scheme D.6

TABLE OF CONTENTS (CONTINUED)

Page

D.3.1 Significance of $V(a/b, D/R)$ D.8
D.3.2 Validation of Equation (D.19) D.8
D.4 Summary D.9

APPENDIX E. AN APPROXIMATE METHOD FOR DERIVING *J* SOLUTIONS FOR TWO SIMULTANEOUSLY APPLIED MECHANICAL LOADS FROM *J* SOLUTIONS FOR THE TWO LOADS ACTING SEPARATELY E.1
E.1 Introduction E.1
E.2 EPRI *J* Estimation Scheme for Single Loads E.2
E.3 Reference Stress Approach E.3
E.4 Optimum Choice for P_o^* E.4
E.5 Extension to Combined Loading E.7
E.6 Estimating the Optimum Yield Load for Combined Loading E.8
E.7 Application to Single Edge Cracked Plates (SECP) E.9
E.8 Application to Circumferential Through-wall Defect (CTWD) E.11
E.9 Sensitivity to Choice of $P_o(\lambda)$ E.12
E.10 Summary of Procedure for Estimating J_p for Combined Loading E.13
E.11 Discussion E.14
E.12 Conclusions E.15

APPENDIX F. *J* ESTIMATION PROCEDURES FOR COMBINED PRIMARY AND SECONDARY LOADS F.1
F.1 Introduction F.2
F.2 Definition of Primary and Secondary Loads and Elastic Follow-up F.2
F.2.1 Primary and Secondary Loads F.2
F.2.2 Elastic Follow-up F.3
F.3 Effects of Secondary Loads on Fracture F.3
F.4 Review of Presently Available Methods of Estimating *J* for Combined Loading . . . F.4
F.4.1 The EPRI Scheme F.4
F.4.2 The R6 Method F.6
F.4.3 Chell's Approach F.9
F.4.4 Proposed Modification to the R6 Approach F.16
F.5 Treatment of Elastic Follow-up Due to Imposed Displacements and Rotations . . . F.18
F.6 Comparison of Methods F.19
F.7 A Recommended Procedure for Determining *J* for Combined Primary and Secondary Loads F.20
F.7.1 Stress Analysis F.21
F.7.2 Determination of J for Primary Loads using EPRI Solutions and Reference Stress Methods F.21

TABLE OF CONTENTS (CONTINUED)

Page

F.7.3 Prescribed Displacements F.23
F.7.4 Primary and Secondary Components of Stress F.23
F.7.5 Evaluate the Stress Intensity Factor Due to Secondary Loading F.24
F.7.6 Determine the Effective Crack Size, a_e' F.25
F.7.7 Calculate the First Order Plastically Corrected Stress Intensity Factor F.25
F.7.8 Derive an Equivalent Load Ratio for the Secondary Loads F.25
F.7.9 Evaluate the Primary Load Ratio F.26
F.7.10 Determine the Equivalent Load Ratio for the Combined Loading F.27
F.7.11 Calculate the SIF for the Combined Loading F.27
F.7.12 Calculate the Value of J for the Combined Loading F.27
F.8 Issues Still Outstanding and Requiring Validation F.28
F.9 Conclusions F.28

APPENDIX G. SIMPLE J ESTIMATION TECHNIQUES FOR MODE I CRACKS UNDER MULTIAXIAL LOADS G.1

APPENDIX H. FINITE ELEMENT ANALYSIS OF SPECIMEN GEOMETRY EFFECTS ON FATIGUE CRACK CLOSURE H.1
H.1 Introduction H.1
H.2 Finite Element Model H.2
H.3 Results H.4
H.4 Discussion H.10
H.5 Conclusions H.15

APPENDIX I. ALGORITHMS FOR CRACK INSTABILITY I.1
I.1 Introduction I.2
I.2 Criteria for Crack Instability I.2
I.2.1 Brittle Fracture Criterion I.2
I.2.2 Ductile Fracture Criterion I.4
I.3 Criteria for Accelerated Fatigue Crack Growth Due to Incipient Instability I.4
I.3.1 Contribution of Brittle Fracture Mechanisms to Crack Growth I.4
I.3.2 Contribution of Ductile Fracture Mechanisms to Crack Growth I.7
I.3.2.1 Memory Model I.7
I.3.2.2 Loss of Memory Model I.9
I.3.3 Practical Guidelines for Applying the Tear-Fatigue Crack Growth Law .. I.11
I.3.3.1 Guidelines for Applying the Memory Model I.11
I.3.3.2 Guidelines for Applying the Loss of Memory Model I.12
I.3.3.3 Guidelines for Determining the Stress Ratio and Its Effect on Fracture I.13

TABLE OF CONTENTS (CONTINUED)

Page

I.4 Material Property Characterization for Crack Instability and Tear-fatigue I.14
I.4.1 Characterization of J_R-Curves I.14
I.4.2 Assessing the Importance of Constraint I.15
I.4.2.1 Brittle (Cleavage) Failure I.16
I.4.2.2 Effects of Constraint on the J_R-Curve I.16
I.4.3 Estimating Upper and Lower Bounds for *J-R* Behavior I.17
I.4.4 Choice of J_{mat} I.17
I.5 Practical Considerations in Evaluating the Service Life I.18
I.5.1 Characterization of Toughness for Service Applications I.18
I.5.2 Leak-Before-Break I.19
I.5.3 Stable Crack Growth After Leak I.20

APPENDIX J. A CREEP-FATIGUE CRACK GROWTH ASSESSMENT METHODOLOGY J.1
J.1 Introduction J.1
J.2 Creep-Fatigue Crack Growth J.2
J.3 Time Dependent Fracture Mechanics and C_t J.4
J.3.1 Constitutive Creep Laws J.4
J.3.2 Transition times and C_t J.5
J.3.3 Expressions for C_t J.7
J.4 Considerations Related to Cyclic Loading J.10
J.4.1 General Aspects of Creep-Fatigue J.10
J.4.2 Material Property Requirements J.10
J.4.3 Cyclic Deformation and Crack Tip Recovery J.11
J.5 Other Aspects of Creep-Fatigue J.14
J.5.1 Combined Mechanical and Thermal Loading J.14
J.5.2 Crack Tip Plasticity J.15
J.5.3 Constraint J.16
J.5.4 Crack Closure J.16
J.5.5 Displacement Loading and Elastic Follow-up J.17
J.5.6 Crack Growth Initiation J.18
J.5.7 Effects of Loading Ramp Rate J.18
J.5.8 Effects of Temperature Changes During a Load Cycle J.18
J.6 Remaining Life Estimation under Creep-Fatigue Conditions J.18
J.7 Conclusions J.19

APPENDIX K. USER'S MANUAL FOR NASGRO ELASTIC-PLASTIC FRACTURE MECHANICS MODULES K.1
See detailed Table of Contents for Appendix K ..... K.i

TABLE OF CONTENTS (CONTINUED)

Page

APPENDIX L. EXPERIMENTAL VERIFICATION OF NASGRO ELASTIC-PLASTIC FATIGUE CRACK GROWTH MODULE L.1
L.1 Introduction L.1
L.2 Material Characterization L.1
L.3 Specimen Geometries L.2
L.4 Crack Growth Experiments L.4
L.5 NASGRO Calculations L.6
L.6 Discussion and Conclusions L.10

LIST OF TABLES

Page

Table 2.1 Summary of Existing J Solutions 19

Table 3.1 Relationship between strain hardening exponent and ratio of ultimate to yield strengths, based on Eqn. 3.39 71

Table B.1 Survey of Existing J Solutions B.2

Table C.1 Surface flaw, membrane loading - elastic solution quality; comparison with results from FLAGRO 2.0 . . . . . C.6

Table C.2 Corner flaw, membrane loading - elastic solution quality; comparison with results from FLAGRO 2.0 . . . . . C.6

Table C.3 Surface flaw, membrane loading - h_1 factors by angular position for $n = 5$ C.7

Table C.4 Surface flaw, membrane loading - h_1 factors by angular position for $n = 10$ C.7

Table C.5 Surface flaw, membrane loading - h_1 factors for $n = 15$ C.8

Table C.6 Corner flaw, membrane loading - h_1 factors for $n = 5$ C.8

Table C.7 Corner flaw, membrane loading - h_1 factors for $n = 10$ C.9

Table C.8 Corner flaw, membrane loading - h_1 factors for $n = 15$ C.9

Table D.1 Summary of finite element J solutions for cracks emanating from notches D.10

Table E.1 h_1 functions for a plane strain SECP under combined tension and bending for the case of λ=0.125 . . . . . E.16

Table E.2 h_1 functions for a through-crack in a cylinder under combined tension and bending E.17

Table F.1 Summary of J solutions used to validate the EPRI approach F.7

Table F.2 Summary of J solutions used to validate the R6 (Revision 3) approach F.11

Table F.3 Summary of J solutions used to validate the Chell approach F.16

Table F.4 Summary of J solutions used to validate the Budden approach F.18

LIST OF TABLES

Page

Table G.1 Comparison of Jansson FEM results for multiaxial J with simple estimates based on an effective stress approach for a range of λ, n, and a/b values G.8

Table H.1 Geometry correction factors used to calculate stress intensity factor H.7

Table L.1 Chemical composition of the Inconel 718 test material L.2

Table L.2 Summary of NASGRO EPFCG verification test conditions L.6

LIST OF FIGURES

Page

Figure 2.1 Schematic defining geometry parameters for semi-elliptical surface crack infinite plate 21

Figure 2.2 Schematic showing geometrical relationship between notch depth (D), notch root radius (R), crack depth (d), notch plus crack depth (a), and half plate width (b) 25

Figure 2.3 Estimated versus finite element h_1 values for combined mechanical loads (tension plus bending) 30

Figure 3.1 Schematic representation of hysteresis loop showing opening stress level and corresponding estimates of effective stress and strain ranges 37

Figure 3.2 Normalized crack opening stresses based on Newman equation 44

Figure 3.3 Effective stress range ratio based on Newman equation 44

Figure 3.4 Comparison of crack opening stresses based on Newman equation and finite element modeling for a low or zero hardening material 45

Figure 3.5 Comparison of crack opening stresses based on Newman equation, finite element modeling, and experimental measurements for a high hardening material 45

Figure 3.6 Normalized crack opening stress as a function of normalized stress intensity factor 49

Figure 3.7 Finite element simulation of a growing fatigue crack showing decreases in crack opening levels as net-section yielding is approached 52

Figure 3.8 Normalized crack opening stress as a function of normalized stress intensity factor for conditions of significant ligament plasticity 53

Figure 3.9 Schematic outline of simple model to predict crack opening stresses for cracks growing out of notches 56

Figure 3.10 Normalized crack opening stress as a function of normalized maximum stress for different biaxial stress ratios 60

LIST OF FIGURES (CONTINUED)

Page

Figure 3.11 Comparison of predicted and FE crack opening stresses for negataive biaxial stress ratios 63

Figure 3.12 Finite element simulations showing effect of stress amplitude on crack closure following a single overload cycle 75

Figure 3.13 Effect of stress amplitude on crack closure following a single overload cycle . . . 77

Figure C.1 Sample finite element mesh for new *J* solutions C.2

Figure C.2 Elements and volumes C.2

Figure C.3 Load dependence of *J* integral C.4

Figure C.4 Angular dependence of *J* integral C.4

Figure C.5 Surface flaw, membrane loading - angular variation of the *J*-integral for $a/t = 0.2$ C.10

Figure C.6 Surface flaw, membrane loading - angular variation of the *J*-integral for $a/t = 0.5$ C.10

Figure C.7 Surface flaw, membrane loading - angular variation of the *J*-integral for $a/t = 0.8$ C.11

Figure C.8 Corner flaw, membrane loading - angular variation of the *J*-integral for $a/t = 0.2$ C.11

Figure C.9 Corner flaw, membrane loading - angular variation of the *J*-integral for $a/t = 0.5$ C.12

Figure C.10 Corner flaw, membrane loading - angular variation of the *J*-integral for $a/t = 0.8$ C.12

Figure D.1 Schematic showing geometrical relationships between notch depth (D), notch root radius (R), crack depth (d), notch plus crack depth (a), and half plate width (b) D.2

LIST OF FIGURES (CONTINUED)

Page

Figure D.2 Comparison of EPRI finite element resuults (dashed line) with the optimized RSM (solid line) for a single crack at a round hole subjected to biaxial stressing: d/R=0.125, K_t=2.8, n=5 . . . . . D.11

Figure D.3 Comparison of EPRI finite element results (dashed line) with the optimized RSM (solid line) for a single crack at a round hole subjected to biaxial stressing: d/R=0.250, K_t=2.8, n=5 . . . . . D.12

Figure D.4 Comparison of EPRI finite element results (dashed line) with the optimized RSM (solid line) for a single crack at a round hole subjected to biaxial stressing: d/R=0.500, K_t=2.8, n=5 . . . . . D.13

Figure D.5 Comparison of EPRI finite element results (dashed line) with the optimized RSM (solid line) for a single crack at a round hole subjected to biaxial stressing: d/R=0.750, K_t=2.8, n=5 . . . . . D.14

Figure D.6 Comparison of EPRI finite element results (dashed line) with the optimized RSM (solid line) for a single crack at a round hole subjected to biaxial stressing: d/R=1.000, K_t=2.8, n=5 . . . . . D.15

Figure D.7 Comparison of finite element results (open circles) with the modified (dotted line) and standard (solid line) RSM's for symmetrical cracks in double edge notched plates subjected to uniaxial stressing: d/R=0.1194, K_t=4.2, n=10 . . . . D.16

Figure D.8 Comparison of finite element results (open circles) with the modified (dotted line) and standard (solid line) RSM's for symmetrical cracks in double edge notched plates subjected to uniaxial stressing: d/R=0.2067, K_t=4.2, n=10 . . . . D.17

Figure D.9 Comparison of finite element results (open circles) with the modified (dotted line) and standard (solid line) RSM's for symmetrical cracks in double edge notched plates subjected to uniaxial stressing: d/R=0.2940, K_t=4.2, n=10 . . . . D.18

Figure D.10 Comparison of finite element results (open circles) with the modified (dotted line) and standard (solid line) RSM's for symmetrical cracks in double edge notched plates subjected to uniaxial stressing: d/R=0.3813, K_t=4.2, n=10 . . . . D.19

Figure D.11 Comparison of finite element results (open circles) with the modified (dotted line) and standard (solid line) RSM's for symmetrical cracks in double edge notched plates subjected to uniaxial stressing: d/R=0.4685, K_t=4.2, n=10 . . . . D.20

Figure D.12 Comparison of finite element results (open circles) with the modified (dotted line) and standard (solid line) RSM's for symmetrical cracks in double edge notched plates subjected to uniaxial stressing: d/R=0.5558, K_t=4.2, n=10 . . . . D.21

LIST OF FIGURES (CONTINUED)

Page

Figure D.13 Comparison of finite element results (open circles) with the modified (dotted line) and standard (solid line) RSM's for symmetrical cracks in double edge notched plates subjected to uniaxial stressing: d/R=0.6431, K_t=4.2, n=10 .... D.22

Figure D.14 Comparison of finite element results (open circles) with the modified (dotted line) and standard (solid line) RSM's for symmetrical cracks in double edge notched plates subjected to uniaxial stressing: d/R=0.3063, K_t=6.3, n=10 .... D.23

Figure D.15 Comparison of finite element results (open circles) with the modified (dotted line) and standard (solid line) RSM's for symmetrical cracks in double edge notched plates subjected to uniaxial stressing: d/R=0.5248, K_t=6.3, n=10 .... D.24

Figure D.16 Comparison of finite element results (open circles) with the modified (dotted line) and standard (solid line) RSM's for symmetrical cracks in double edge notched plates subjected to uniaxial stressing: d/R=0.7540, K_t=6.3, n=10 .... D.25

Figure D.17 Comparison of finite element results (open circles) with the modified (dotted line) and standard (solid line) RSM's for symmetrical cracks in double edge notched plates subjected to uniaxial stressing: d/R=0.9779, K_t=6.3, n=10 .... D.26

Figure D.18 Comparison of finite element results (open circles) with the modified (dotted line) and standard (solid line) RSM's for symmetrical cracks in double edge notched plates subjected to uniaxial stressing: d/R=1.2018, K_t=6.3, n=10 .... D.27

Figure D.19 Comparison of finite element results (open circles) with the modified (dotted line) and standard (solid line) RSM's for symmetrical cracks in double edge notched plates subjected to uniaxial stressing: d/R=1.4256, K_t=6.3, n=10 .... D.28

Figure D.20 Comparison of finite element results (open circles) with the modified (dotted line) and standard (solid line) RSM's for symmetrical cracks in double edge notched plates subjected to uniaxial stressing: d/R=1.6495, K_t=6.3, n=10 .... D.29

Figure D.21 Comparison of finite element results (open circles) with the modified (dotted line) and standard (solid line) RSM's for symmetrical cracks in double edge notched plates subjected to uniaxial stressing: d/R=0.1550, K_t=8.4, n=10 .... D.30

Figure D.22 Comparison of finite element results (open circles) with the modified (dotted line) and standard (solid line) RSM's for symmetrical cracks in double edge notched plates subjected to uniaxial stressing: d/R=0.5759, K_t=8.4, n=10 .... D.31

Figure D.23 Comparison of finite element results (open circles) with the modified (dotted line) and standard (solid line) RSM's for symmetrical cracks in double edge notched plates subjected to uniaxial stressing: d/R=0.9967, K_t=8.4, n=10 .... D.32

LIST OF FIGURES (CONTINUED)

Page

Figure D.24 Comparison of finite element results (open circles) with the modified (dotted line) and standard (solid line) RSM's for symmetrical cracks in double edge notched plates subjected to uniaxial stressing: d/R=1.4175, K_t=8.4, n=10 . . . . D.33

Figure D.25 Comparison of finite element results (open circles) with the modified (dotted line) and standard (solid line) RSM's for symmetrical cracks in double edge notched plates subjected to uniaxial stressing: d/R=1.8383, K_t=8.4, n=10 . . . . D.34

Figure D.26 Comparison of finite element results (open circles) with the modified (dotted line) and standard (solid line) RSM's for symmetrical cracks in double edge notched plates subjected to uniaxial stressing: d/R=2.2591, K_t=8.4, n=10 . . . . D.35

Figure D.27 Comparison of finite element results (open circles) with the modified (dotted line) and standard (solid line) RSM's for symmetrical cracks in double edge notched plates subjected to uniaxial stressing: d/R=2.6800, K_t=8.4, n=10 . . . . D.36

Figure D.28 Comparison of finite element results (open circles) with the modified (dotted line) and standard (solid line) RSM's for symmetrical cracks in double edge notched plates subjected to uniaxial stressing: d/R=3.1008, K_t=8.4, n=10 . . . . D.37

Figure D.29 Comparison of finite element results (open circles) with the modified RSM using the actual value of $V(a/b, D/R)$ (dashed line) and V=1 (solid line) for symmetrical cracks in double edge notched plates subjected to uniaxial stressing: d/R=0.1194, K_t=4.2, n=10 . . . . . D.38

Figure D.30 Comparison of finite element results (open circles) with the modified RSM using the actual value of $V(a/b, D/R)$ (dashed line) and V=1 (solid line) for symmetrical cracks in double edge notched plates subjected to uniaxial stressing: d/R=0.6431, K_t=4.2, n=10 . . . . . D.39

Figure D.31 Comparison of finite element results (open circles) with the modified RSM using the actual value of $V(a/b, D/R)$ (dashed line) and V=1 (solid line) for symmetrical cracks in double edge notched plates subjected to uniaxial stressing: d/R=0.3063, K_t=6.3, n=10 . . . . . D.40

Figure D.32 Comparison of finite element results (open circles) with the modified RSM using the actual value of $V(a/b, D/R)$ (dashed line) and V=1 (solid line) for symmetrical cracks in double edge notched plates subjected to uniaxial stressing: d/R=1.6495, K_t=6.3, n=10 . . . . . D.41

LIST OF FIGURES (CONTINUED)

Page

Figure D.33 Comparison of finite element results (open circles) with the modified RSM using the actual value of $V(a/b, D/R)$ (dashed line) and V=1 (solid line) for symmetrical cracks in double edge notched plates subjected to uniaxial stressing: d/R=0.1550, K_t=8.4, n=10 . . . . . D.42

Figure D.34 Comparison of finite element results (open circles) with the modified RSM using the actual value of $V(a/b, D/R)$ (dashed line) and V=1 (solid line) for symmetrical cracks in double edge notched plates subjected to uniaxial stressing: d/R=3.1008, K_t=8.4, n=10 . . . . . D.43

Figure E.1 Schematic of variation of J with load, P, for materials with different strain hardening capacities E.18

Figure E.2 Graphical construction of the optimum combined yield load E.19

Figure E.3 Normalized yield loads for a circumferential through-wall defect as a function of λ for a/b = 0.25 . . . . . E.20

Figure F.1 Above general yield the failure load (P_f) and critical crack size (a_f) become increasingly insensitive to toughness, J_{Ic}, and hence J F.10

Figure F.2 High primary loads "shake out" the effects of secondary loads F.13

Figure F.3 Variation of P_p/P_y' for different combinations of primary P/P_y and secondary P_s/P_y' loads F.15

Figure F.4 Flow chart illustrating the steps and decision in the procedure for determining J for combined loads F.22

Figure F.5 Effects of crack tip plasticity on the stiffness $[C^{-1}(Q_1, Q_2, ...)]$ of the cracked section F.32

Figure F.6 First order plastic correction and recharacterization of embedded elliptical defect centered on C F.35

Figure G.1 Comparison of fully plastic J solutions for cracks in infinite plates under biaxial loading G.7

Figure H.1 Typical mesh for finite element analysis of crack closure: (a) entire mesh (b) near-tip fine mesh region H.3

LIST OF FIGURES (CONTINUED)

Page

Figure H.2 Three different specimen geometries modeled in this investigation H.5

Figure H.3 Normalized crack opening stresses as a function of normalized maximum stress H.6

Figure H.4 Normalized crack opening stresses as a function of the maximum stress intensity factor H.8

Figure H.5 Normalized crack opening stresses as a function of normalized stress intensity factor H.9

Figure H.6 Normalized crack opening stresses as a function of normalized stress intensity factor for conditions of significant ligament plasticity H.13

Figure I.1 Schematic showing instability criterion for ductile materials I.21

Figure I.2 Schematic representation of tear-fatigue Memory Model I.22

Figure I.3 Schematic representation of tear-fatigue loss of Memory Model I.23

Figure I.4 Definition of the constants, C, R, and T, that appear in Equations (I.29) to (I.32) that can be used to mathematically represent J_R-curves I.24

Figure I.5 Example crack growth resistance curves for Inconel 718 . . . . . I.25

Figure I.6 The offset procedure used to define J_{Ic} according to ASTM Test Method E813 . . . . . I.26

Figure I.7 Predicted tear-fatigue crack growth rates versus measured values for a mild steel I.31

Figure I.8 Example of the suppression of tearing during a tear-fatigue test when a control mode change reduced dJ_{max}/dN from 22.6 kN/m to 0 kN/m I.32

Figure J.1 Creep crack growth, da/dt, expressed as a function of stress intensity factor, K J.21

Figure J.2 Creep crack growth data as shown in Figure J.1 expressed as a function of the time dependent fracture mechanics parameter, C_t J.22

Figure J.3 Schematic showing the development of primary and secondary creep zones at the crack tip, and the transition times t_1 and t_2 . . . . . J.23

LIST OF FIGURES (CONTINUED)

Page

Figure J.4 Effects of cyclic loading: (a) Pressure cycling due to start-up and shut-down. (b) Deformation in cyclic zone at crack tip, (c) Deformation outside the plastic zone J.24

Figure J.5 Schematic showing different C_t behavior for cyclic recovery and no recovery . J.25

Figure J.6 Examples of the effect on the remaining life of a pressure vessel operating in the creep regime of assuming various recovery models and creep constitutive laws J.26

Figure J.7 Illustration showing the effect of increasing thermal loading on the transition of $C(t)$, the crack tip field characterizing TDFM parameter, to its steady state value, C^*, which is determined only by the primary loading J.27

Figure J.8 Illustration showing the effect of increasing crack tip plasticity on the transition of C_t to its steady state value, C^* J.28

Figure L.1 Baseline specimen geometry for NASGRO EPFCG verification experiments . . L.3

Figure L.2 Comparison of actual and predicted numbers of crack growth cycles L.8

Figure L.3 Correlation of measured crack growth rates with calculated values of ΔJ_{eff} L.9

Figure L.4 Comparisons of predicted a and c values for SC01 geometries under elastic-plastic cycling, demonstrating stable semi-circular shapes L.12

DEFINITION OF SYMBOLS

a	crack size; for a semi-elliptical surface crack, the depth dimension
a_{crit}	critical crack length
a_e	effective crack size ($= a + \phi r_y$)
a_f	critical defect size for failure
a_{init}	initial crack size for ductile tearing
a_e'	effective crack depth ($= a + r_y$)
a_0	initial crack size
A	coefficient in Norton's Law for secondary creep rate (material constant)
A	area under load-deflection curve
A_k	empirical constant in NASGRO expression for K_C as fraction of thickness
A_0, A_1, A_2, A_3	coefficients in Newman closure equations
b	for some geometries, length of uncracked ligament; alternatively, half-width of a cracked plate
b	in fatigue life equations, the fatigue strength exponent
B	coefficient in primary creep law (material constant)
B	specimen thickness
B_k	empirical constant in NASGRO expression for K_C as function of thickness
c	crack size; for a semi-elliptical surface crack, half the surface length
c	in fatigue life equations, the fatigue ductility exponent
c	uncracked ligament (for a double edge-cracked plate)
c_e	effective crack size ($= c + \phi r_y$)
c_i	initial crack length
c_{crit}	critical crack length
c_e^{Δ}	effective crack length for cyclic loading
C	empirical coefficient in Paris equation for FCG based on ΔJ_{eff} (closure corrected)
C	in general resistance curve form, Δa value on the asymptotic blunting line which corresponds to $J_R = R$
C_h^*, C_p^*	path independent integrals characterizing crack-tip stress field under large scale primary creep
C_k	empirical constant in NASGRO expression for K_C as function of thickness
C^0, C_{ss}^0, C_{sp}^0	compliances
C_S^*	path independent integral characterizing crack-tip stress field under large-scale secondary creep
C_t	time-dependent fracture mechanics parameter
$C(t)$	time-dependent fracture mechanics parameter
C_0	empirical coefficient in Paris equation for FCG based on ΔK (no closure correction)
C_1	empirical coefficient in Paris equation for FCG based on ΔJ (no closure correction)
C_2	empirical coefficient in Paris equation for FCG based on ΔK_{eff} (closure-corrected)

DEFINITION OF SYMBOLS (CONTINUED)

C^*	time-dependent fracture mechanics parameter for steady state creep
d	depth of crack growing from notch root
da/dN	average fatigue crack growth rate (increase in crack size per cycle)
$(da/dN)_f$	crack growth rate per cycle due to fatigue
$(da/dN)_t$	crack growth per cycle due to tearing
$(da/dN)_{time}$	crack growth rate per cycle due to time-dependent creep crack extension
da/dt	average change in crack size with time
d_e	effective value of $d(= d + \phi r_y)$
d_s	increment of arc length in definition of J-integral
D	temperature-dependent coefficient in Paris equation for FCG with hold times
D	normalized structural parameter in some EPRI J solutions
D	notch depth for double edge notched plate
E	Young's elastic modulus
E'	effective elastic modulus
F	geometry factor in stress intensity factor solution
F	in the $R6$ method for combined loading, a particular function of the applied load and the constitutive relationship
F	force
g	geometric term that makes λ dimensionless
G	elastic strain energy release rate
h_0	nondimensional factor in multiaxial J_p solution
h_0'	nondimensional factor in uniaxial J_p solution
h_1	non-dimensional factor in EPRI estimation scheme for J_p
h_1^*	plastic influence function appearing in reference stress J formulation
h_2	nondimensional factor in the multiaxial plane strain J_p solution
H	coefficient in creep crack growth expression in terms of C_t
H	factor in formulation of optimum yield load
I_m	numerical constant dependent on m which is related to crack tip stress field
J	J-integral
J_c	critical value of J for cleavage fracture
J_e or J^e	elastic component of J
J_{Ic}	a measure of fracture toughness corresponding approximately to the onset of ductile tearing
J_{min}	minimum value of J
J_{mat}	an elastic-plastic measure of fracture toughness at the initiation of crack extension
J_{max}	maximum value of J
J_p or J^p	plastic component of J
J_p^{RSM}	plastic component of J estimated using reference stress method
J_R	elastic-plastic fracture toughness (resistance to crack extension) corresponding to a particular tear length
J_0, J_1, J_2	empirical constants in power law or quadratic forms of resistance curve

DEFINITION OF SYMBOLS (CONTINUED)

$\dot{J}^*$	J^* integral rate
J^*	a path-independent integral proposed by Blackburn
$\hat{J}$	a path-independent integral proposed by Kishimato
$\dot{\hat{J}}$	$\hat{J}$ integral rate
K	stress intensity factor
K_c	thickness-dependent material fracture toughness
K_{flow}	$\sigma_{flow}\sqrt{\pi a}$
K_{Ic}	plane strain fracture toughness
K_{I_e}	fracture toughness of part-through surface crack
K_{mat}	a measure of fracture toughness at the initiation of crack extension
K_{max}	maximum value of stress intensity factor
K_{min}	minimum value of stress intensity factor
K_{open}	value of K at which crack first becomes fully open
K_r	parameter in FAD equal to $\sqrt{J_e/J}$
K_R	fracture toughness (resistance to crack extension) corresponding to a particular tear length
K_t	theoretical stress concentration factor (based on gross section stress)
K^σ	actual local stress concentration factor
K^ε	actual local strain concentration factor
K_0	$\sigma_0\sqrt{\pi a}$ (in the context of FE closure analysis)
l	temperature-dependent exponent in Paris equation for FCG with hold times
L_r	net section stress parameter in Failure Assessment Diagram (= P/P_0)
L_r^*	value of L_r based on P_0^*
m	exponent on stress in primary creep law (material constant)
m	empirical exponent in Paris equation for FCG based on ΔJ_{eff} (closure corrected)
m_0	empirical exponent in Paris equation for FCG based on ΔK (no closure correction)
m_1	empirical exponent in Paris equation for FCG based on ΔJ (no closure correction)
m_2	empirical exponent in Paris equation for FCG based on ΔK_{eff} (closure-corrected)
M	coefficient in blunting line equation (usually = 2)
M	applied moment
M_L	limit moment per unit thickness
M_0	characteristic yield moment
M_0^*	optimized characteristic yield moment
n	exponent in Norton's Law for secondary creep rate (material constant)
n	strain hardening exponent in Ramberg-Osgood equation

DEFINITION OF SYMBOLS (CONTINUED)

n'	stable cyclic value of strain hardening exponent in Ramberg-Osgood equation
N	cycle of fatigue loading
N_f	number of fatigue cycles to failure
N_r	number of allowable remaining service cycles
P	applied (primary) load
P	factor in primary creep law (material constant)
P_f	critical load for failure
P_p	applied mechanical load
P_{ps}/P_y'	equivalent primary load ratio in Chell scheme for combined loading
P_s	effective primary load arising from a secondary load
P_s/P_y'	secondary load ratio in Chell scheme for combined loading
P_y	general yield load of cracked structure in $R6$ method
P_0	characteristic yield load
P_0^*	optimum characteristic yield load
$\hat{P}$	combined primary and secondary load
q	exponent in creep crack growth expression in terms of C_t
q	material constant in NASGRO FCG equation describing crack growth near instability
Q	elastic-plastic fracture mechanics parameter characterizing constraint in terms of crack-tip stress fields
r_c	crack-tip creep zone size
$\dot{r}_c$	rate of expansion of crack-tip creep zone
$r(x)$, $r_1(x)$	factors in $R6$ method for combined primary and secondary loading characterizing the plasticity interactions between primary and secondary loads
r_y	monotonic crack-tip plastic zone size
$r(\lambda)$	ratio of yield loads
R	in general resistance curve form, intercept of tearing line with $\Delta a = 0$ axis
R	stress intensity factor ratio = K_{min}/K_{max}
R	internal radius of a cracked cylinder
R	notch root radius
s_{ij}	stress deviator
S	in the context of combined primary and secondary loading, a secondary load
S	in the context of biaxial loading, a remote stress applied in a direction normal to the plane of the crack
S	in the context of finite element analysis of crack closure, a nominal (far-field) applied stress
S_0	uniform stress applied to a NASGRO cracked geometry
S_1, S_2	outer fiber bending stress applied to NASGRO cracked geometries
$\bar{S}$	plastically relaxed secondary load
t	section thickness
t	time (in the context of creep-fatigue effects on crack growth)

DEFINITION OF SYMBOLS (CONTINUED)

t_h	hold time
t_{net}	net section thickness
t_0	characteristic value of thickness for plane strain conditions
t_1, t_2, t_3	transition times in TDFM
T	in general resistance curve form, asymptotic slope of the tearing line
T	in the context of biaxial loading, a remote stress applied in a direction transverse to the axis of stress S
T_i	surface traction
T^*, T_p^*, ΔT_p^*, ΔT_p	path-independent integrals proposed by Atluri and colleagues
$\dot{T}_p^*$	T_P^* integral rate
u_i	displacement
U	effective stress intensity factor range ratio, which characterizes crack closure
U_0	value of U for baseline FCG data
V	dimensionless structural parameter in reference stress method estimate of J_p (of order 1)
V_a	value of V at the a-tip
V_c	value of V at the c-tip
W	section width (or half-width, for certain geometries)
W_e	strain energy density
x	a rectangular coordinate
y	a rectangular coordinate
Z	a parameter characterizing the amount of elastic follow-up in a structure under creep conditions
α	material constant in Ramberg-Osgood equation
α_c	constraint factor in Newman closure equations
α'	stable cyclic value of α
β	stress state dependent factor in expression for crack-tip plastic zone size
β_R	NASGRO surface correction factor to compensate for surface constant effects
Γ	contour in definition of J-integral
δ_t	crack tip opening displacement
Δa_b, Δc_b	amount of crack tip blunting up to the point of fracture
$\Delta a_{f,n}$	total crack extension due to fatigue after n cycles
Δa_t	tear length
$\Delta a_{t,n}$	total ductile tearing after n fatigue cycles
ΔJ	range of the J-integral (actually, the ΔJ-integral)
ΔJ_e	range of J_e
ΔJ_e^{eff}	effective (closure-corrected) value of elastic ΔJ
ΔJ_{eff}	effective range of the J-integral (closure-corrected)
ΔJ_P^{eff}	effective (closure-corrected) value of plastic ΔJ
ΔJ^*	range of J^* integral
$\Delta \hat{J}$	range of $\hat{J}$ integral
ΔK	range of the stress intensity factor

DEFINITION OF SYMBOLS (CONTINUED)

ΔK_{eff}	effective range of the stress intensity factor (closure-corrected)
ΔK_{th}	threshold stress intensity factor range
ΔK_{ε}	range of the strain intensity factor
ΔP	primary load range
Δr_y	cyclic plastic zone size
ΔX	range of an elastic-plastic fatigue crack growth parameter
$\Delta\varepsilon$	total strain range
$\Delta\varepsilon_e$	elastic strain range
$\Delta\varepsilon_p$	plastic strain range
$\Delta\sigma$	stress range
$\dot{\varepsilon}$	total creep strain rate
ε_e or ε^e	elastic strain
ε_{ef}	effective strain
ε'_f	fatigue ductility coefficient in a fatigue life equation
ε_{ij}	strain tensor
ε_p or ε^p	plastic strain
$\dot{\varepsilon}_p$	primary creep strain rate
ε_{ref}	reference strain
ε^p_{ref}	reference plastic strain
$\dot{\varepsilon}_s$	secondary creep strain rate
ε_0	yield strain in Ramberg-Osgood equation = σ_0/E
ε'_0	stable cyclic value of ε_0
η	geometry factor in EPRI yield load solution for TC02
θ	angle subtended by circumferential crack of half-length in a cylindrical pipe
λ	in combined loading, dimensionless ratio of two applied loads
λ	biaxiality ratio = T/S
μ	dimensionless factor in J estimates (function of Poisson's ratio and stress state)
ν	Poisson's ratio (typically elastic value)
ν_e	elastic value of Poisson's ratio
ν_p	plastic value of Poisson's ratio
σ_{ef}	effective (von Mises) stress
σ_{flow}	flow stress
σ_{ij}	stress tensor
σ^{max}_{yy}	local stress normal to the crack plane at maximum load
σ_{open}	crack opening stress
σ_P	primary stress
σ_{ref}	reference stress
σ_S	secondary stress
σ^{tot}_S	total linear elastic secondary stress distribution

DEFINITION OF SYMBOLS (CONTINUED)

$\bar{\sigma}_S$	plastically relaxed secondary stress
$\bar{\sigma}_S^{tot}$	total elastic-plastic secondary stress distribution
$\bar{\sigma}^{tot}$	total elastic-plastic stress distribution due to all the applied loads
σ^{tot}	total linear elastic stress distribution due to all the applied loads
σ_{ult}	ultimate strength
σ_{ys}	yield strength
σ_0	yield stress in Ramberg-Osgood equation
σ_0	in the context of FE closure analysis, the yield stress in a bilinear stress-strain curve
σ'_f	fatigue strength coefficient in a fatigue life equation
σ'_0	stable cyclic value of σ_0
σ_∞, σ^∞	remote applied stress
ϕ	interpolating parameter in expression for C_e
ϕ^Δ	value of interpolating parameter in expression for C_e^Δ
ϕ^*	value of ϕ based on P_0^*
Φ	angular position around perimeter of surface crack or corner crack
Φ	in context of tear-fatigue, crack-tip opening displacement and degree of blunting

NONSTANDARD ABBREVIATIONS

ABAQUS	Commercial finite element program
ANSYS	Commercial finite element program
ASTM	American Society for Testing and Materials
CC01	NASGRO designation for quarter-elliptical Corner Crack in finite plate
CCP	Center Cracked Plate fracture mechanics geometry
CEGB	Central Electricity Generating Board
CMOD	Crack Mouth Opening Displacement
COD	Crack Opening Displacement
CT, C(T)	Compact Tension fracture mechanics geometry
CTWD	Circumferential Through-Wall Defect
DECP	Double Edge Cracked Plate
DEN	Double Edge Notch
EC01	NASGRO designation for elliptical Embedded Crack in finite plate
EDM	Electro-Discharge Machining
EPFCG	Elastic-Plastic Fatigue Crack Growth
EPFM	Elastic-Plastic Fracture Mechanics
EPRI	Electric Power Research Institute
FAD	Failure Assessment Diagram
FASTRAN	NASA computer code for crack closure analysis
FCG	Fatigue Crack Growth
FE	Finite Element
FEM	Finite Element Method
FLAGRO	A general-purpose NASA fracture mechanics computer code (now called NASGRO)
GE	General Electric
GUI	Graphical User Interface
HRR	Hutchinson-Rice-Rosengren
ISY	Intermediate Scale Yielding
LEFM	Linear Elastic Fracture Mechanics
LSY	Large Scale Yielding
MCPT	Multiple Cycle Proof Testing
NASA	National Aeronautics and Space Administration
NASCRAC	A general-purpose NASA fracture mechanics computer code
NASGRO	A general-purpose NASA fracture mechanics computer code (formerly called FLAGRO)
PZS	crack-tip Plastic Zone Size
RSM	Reference Stress Method
SECP	Single Edge Cracked Plate
SECP-B	Single Edge Cracked Plate under Bending
SECP-T	Single Edge Cracked Plate under Tension
SC01	NASGRO designation for semi-elliptical Surface Crack in finite plate
SSME	Space Shuttle Main Engine
SSY	Small-Scale Yielding
STA	Solution Treated and Aged
SURFLAW	Rocketdyne computer program for *J*-integral computation
SwRI	Southwest Research Institute
TC01	NASGRO designation for central Through Crack in finite plate
TC02	NASGRO designation for edge Through Crack in finite plate
TMF	Thermo-Mechanical Fatigue
TDFM	Time Dependent Fracture Mechanics

EXECUTIVE SUMMARY

A practical engineering methodology has been developed to analyze and predict fatigue crack growth rates under elastic-plastic and fully-plastic conditions. Under small-scale yielding conditions, the methodology reduces to the customary LEFM approach to FCG analysis based on ΔK.

The methodology employs the closure-corrected effective range of the J-integral, ΔJ_{eff}, as the governing parameter. Delta J was selected because it best satisfied the simultaneous criteria of theoretical validity, practicality, and demonstrated usefulness. Alternative parameters based on other path-area integrals were critically reviewed and found to be less satisfactory.

The first major component of the methodology is a set of J (and ΔJ) solutions for specific geometries, along with general J estimation methods for other geometries and loading conditions. Solutions of the plastic component of J generally follow either the EPRI estimation scheme or the reference stress method. Solutions of the elastic component of J are based on the linear elastic stress intensity factor with a first-order plastic correction based on the crack-tip plastic zone size.

Existing J solutions for standard fracture mechanics geometries, including many NASGRO geometries, are documented. Elastic-plastic finite element methods are employed to generate new plastic J solutions, and these and other FE results are then used to derive new optimized reference stress solutions. These solution forms are conservatively extended to construct reference stress solutions for other geometries without available FE solutions. General schemes are developed to estimate J under various types of combined loading. New reference stress methods are developed and verified for combined mechanical loading and combined primary and secondary loading. A J estimation method for two-dimensional Mode I cracks under biaxial loading is also developed and verified.

The second major component of the methodology is a set of specific practical algorithms that translate a J solution into a specific quantitative prediction of fatigue crack growth rate or life. Solutions for ΔJ follow the same general form as the EPRI and reference stress schemes for J, with single values of applied parameters replaced by their respective ranges, and employing a cyclic constitutive law. Corrections for crack closure are applied independently to elastic and plastic J terms based on energy considerations.

Crack opening stresses are calculated from closed-form equations derived by Newman. FE studies show that these equations could be extended to the EPFCG regime, to different geometries, and to combined loading by replacing the normalized maximum stress term with a normalized maximum stress intensity factor term. Simple, verified algorithms are identified for the stress concentration effects and multiaxial effects on closure.

Simple algorithms are developed to evaluate the instability of cracks subjected to monotonic and cyclic loading in materials that behave in a brittle or ductile manner, and fatigue crack growth equations are recommended for describing the acceleration in FCG rates due to incipient instability. Algorithms are developed to estimate fatigue and constitutive properties needed for elastic-plastic FCG analysis that might not be readily available. The general outlines of potential methods for load interaction effects and creep-fatigue effects are presented and discussed.

A critical core of the J solutions and practical crack growth algorithms is implemented in software form in new elastic-plastic NASGRO modules. Solutions for J and ΔJ under combined primary and secondary loading are provided for five existing NASGRO geometries: TC01, TC02, CC01, SC01, and EC01. Failure algorithms compute critical crack sizes and critical loads for these geometries. EPFCG lives are calculated from closure-corrected ΔJ_{eff} solutions and a Paris equation for crack growth rates. The new modules are independent and do not require the main NASGRO code, but emulate the current NASGRO code and employ existing NASGRO routines wherever possible. A User's Manual provides complete details of the capabilities of the new modules, along with brief documentation of the theoretical background, verification, and validity limits of the modules.

The NASGRO EPFCG module is independently verified by comparing its predictions with actual experimental crack growth data for Inconel 718 for three different geometries, deformation conditions ranging from SSY to LSY, and stress ratios ranging from $R = 0$ to $R = -1$. The NASGRO module is found to be highly successful in predicting crack growth lives and crack shapes and correlating crack growth rate data.

1. BACKGROUND

1.1 The Demands of Space Propulsion

The current reusable rocket propulsion system supporting America's space program, the Space Shuttle Main Engine (SSME), is an advanced, high performance liquid hydrogen/liquid oxygen propulsion system. The requirements of building a reliable, reusable, and lightweight high pressure rocket engine which fits in a small space has made the SSME the most sophisticated and highly engineered liquid propellant rocket engine ever built. Future rocket engine design supporting X-vehicles, Reusable Launch Vehicles (RLV), and liquid fly-back boosters, for example, will place an even greater demand upon system performance and structural capability, resulting in increased dependence upon advanced fracture mechanics methods in order to ensure structural adequacy.

The SSME and future reusable rocket engines are faced with a number of relatively unique challenges in addition to the concerns commonly encountered with traditional gas turbines and expendable rocket engines. The combination of the small volume and stringent lightweight requirements on reusable engine components dictates the development of thin structural design and relatively higher operating stresses. Furthermore, reusable hydrogen fueled propulsion system components, exposed to the potentially detrimental effects of high pressure hydrogen environments, are more at risk due to their extended environmental exposure. The components of the more conventional expendable rocket engines, due to their much more limited operational lifetime, are not nearly as susceptible to the combined damaging effects associated with repeated high stress and strain cycles and high pressure hydrogen. In addition, the high film heat transfer coefficient of hydrogen, coupled with extensive hydrogen cooling of reusable engine structures, can cause large thermal gradients in the components as well as aggravate the effect of any temperature spikes during engine start-up or cut-off. The result is that reusable space propulsion systems typically experience a much broader range of temperatures, larger plastic strain ranges, and higher strain rates than do either gas turbine or expendable rocket engines.

SSME operating experience can be used to illustrate the wide range of operating conditions. The temperatures typically range from as low as −423°F up to roughly 1500°F. However, thermal spikes can drastically exceed the upper, steady state temperature. The environment can be liquid and gaseous hydrogen or oxygen, as well as steam and any mixture thereof. The components have to endure rapid loading rates as evidenced by thermal spikes, but also relatively long hold times of approximately nine minutes each flight. The mean stress can result from pressure loads (exceeding 6000 psi), thermal effects, external mechanical loads, preload, and residual stresses from fabrication, misalignment or fit-up. The component alternating stress can stem from phenomena such as mechanical vibration, acoustic loading, and fluid flow. The load history of the SSME typically includes load cycles due to proof testing, assembly/disassembly, engine start-up, steady state operation, and shut-down. Several changes in the engine power level can occur during each engine test or flight. Furthermore, high vibratory loads consisting of random and superimposed sinusoidal components at a mean stress close to yield, act in combination with the previously mentioned low cycle fatigue loads. Also, since current and future space propulsion systems are principally pressure vessels, crack geometries of interest are predominantly surface and embedded cracks.

Experience with life-limited hardware and occasional component cracking on the SSME greatly assists in identifying the most relevant issues and concerns. Cracking problems associated with inelastic loading have been attributed to thermal shocks, local notch effects, hydrogen assisted cracking, internal hydrogen concentration, large thermal gradients, preload stresses, and localized regions of low strength materials. Required elastic-plastic and fully plastic analysis methods include the prediction of crack growth due to fatigue and time dependent effects (e.g., true corrosion fatigue, stress corrosion fatigue, creep, and creep-fatigue), instability and plastic collapse, leak before break, and leakage areas. Additional analysis complexities arise due to the existence of complex component geometries, multiaxial loading, variable states of stress, and various component boundary conditions (e.g., from purely load to purely displacement control).

1.2 Previous Capabilities for Fatigue Crack Growth Analysis

Engineering approaches to characterization of fatigue crack growth (FCG) rates naturally began with the more common and conceptually simpler case of fatigue cracks in nominally elastic bodies. Here the zone of plastic deformation at the tip of the crack is relatively small in comparison to other characteristic dimensions such as component width or crack length. Under these conditions of "small-scale yielding" (SSY), the linear elastic stress intensity factor K, which scales the elastic crack tip stress field, was found to be a suitable parameter to describe the behavior of the crack. The landmark research in this area was conducted in the early 1960s by Paris (Paris, Gomez, and Anderson, 1961; Paris, 1964), who showed conclusively that the range of the stress intensity factor, K, could be used in a power-law expression to describe crack growth rates:

$$\frac{da}{dN} = C_0(\Delta K)^{m_0} \tag{1.1}$$

Here da/dN is the average increase in the crack length per cycle of loading and C_0 and m_0 are empirical constants. With relatively few exceptions, K has remained unchallenged to this day as the parameter of choice for engineering analysis of FCG rates under SSY conditions.

Previous National Aeronautics and Space Administration (NASA) capabilities for the analysis of FCG have employed this conventional ΔK approach to the SSY regime. The primary NASA tool for fracture mechanics analysis of fatigue is NASGRO, formerly known as NASA/FLAGRO (Forman et al., 1988). NASGRO was originally developed to address the Space Shuttle Orbiter structure and payloads, and is now being used by a much broader audience for a wide range of aircraft, propulsion, and space structure applications. NASGRO currently provides (Forman et al., 1997) a wide range of stress intensity factor solutions, a robust crack growth equation, several load interaction models, an extensive materials data base, facilities to accommodate complex load spectra, and many other features. However, the currently released version of NASGRO is strictly limited to linear elastic fracture mechanics.

NASCRAC is another general-purpose fracture analysis computer code developed for NASA (NASCRAC, 1989; Harris et al., 1987). Although that program was originally envisioned to address

not only elastic but also elastic-plastic conditions to some significant degree, the final product was heavily weighted towards the analysis of traditional SSY FCG. While a large number of library K-solutions were programmed into the code and extensive capabilities were provided for the generation of new K-solutions when needed, only limited attention was given to J. J-integral solutions for only eight crack geometries were included in Version 2.0 of the main code, all copied directly from the earliest edition of the Electric Power Research Institute (EPRI) elastic-plastic fracture handbook (Kumar, German, and Shih, 1981), and only a few of these geometries were of practical value to the analysis of actual hardware. Version 2.0 of NASCRAC does contain an optional stand-alone module for calculation of J using a nontraditional 2-D finite element approach, but this module has very limited functionality. Moreover, the module is completely detached from the main NASCRAC software, and no mechanism is provided to incorporate new J solutions into the main NASCRAC code for evaluation of fracture mechanics life.

Furthermore, J solutions in the main NASCRAC code can only be used within the established framework of SSY FCG technology. The first step after retrieval of a given J solution is to convert it into the equivalent K value. Subsequent calculations use SSY crack growth laws, SSY variable amplitude loading algorithms, and SSY criteria for final fracture. This approach ignores any fundamental differences between SSY and elastic-plastic or fully-plastic fatigue crack growth. As will be shown later, these differences are considerable in many instances.

The previously available NASA tools for fracture mechanics analysis of fatigue are clearly inadequate to address the full range of applications problems in reusable space propulsion systems, where (as noted above) significant plasticity can accompany fatigue crack growth. The need to develop improved fracture mechanics methods and tools that could satisfactorily address those demanding applications problems was the motivation for the current contract.

1.3 Selection of a Governing Parameter for Elastic-Plastic Fatigue Crack Growth

The first and most fundamental challenge in developing practical engineering methods for analysis of elastic-plastic fatigue crack growth (EPFCG) is to select a governing parameter to replace or supplement the linear-elastic parameter ΔK.

1.3.1 Historical Background

The development of parameters and engineering methods to describe fatigue crack growth under elastic-plastic and fully-plastic conditions, where SSY is no longer satisfied and K is no longer an accurate description of the near-tip stress field, began somewhat later than the development of the ΔK approach but proceeded at a much slower rate. One of the first attempts to develop a FCG parameter for large scale yielding (LSY) was reported by Boettner, Laird, and McEvily (1965). They successfully correlated crack growth rates at very large strains in a variety of materials with a so-called "strain intensity factor", the product of remote plastic strain range, $\Delta\varepsilon_p$, and the square root of crack length, $\sqrt{a}$. McEvily (1969) later replaced $\Delta\varepsilon_p$ with $\Delta\varepsilon$, the total strain range. Another related but slightly different form was proposed by Solomon (1972), who calculated his "pseudostress intensity factor" as $E\delta\varepsilon\sqrt{a}$ where E is the elastic modulus. This general approach was

re-popularized in the late 1970s and early 1980s as the strain intensity factor, ΔK_ε, by El Haddad, Smith, and Topper (1979a, 1979b) and by Skelton and co-workers (Haigh and Skelton, 1978; Starkey and Skelton, 1982; Skelton, 1982).

One of the few competitors to K in early basic studies of SSY FCG was the crack tip opening displacement (CTOD), δ_t. The CTOD also attracted some early attention from McEvily, Beukelmann, and Tanaka (1974) as a characteristic parameter for FCG under LSY, and Tomkins (1975, 1980) later extended this concept. Both McEvily and Tomkins developed estimates of δ_t from the Bilby-Cottrell-Swinden (BCS) model for an idealized monotonically loaded crack with appropriate modifications to accommodate cyclic loading and large-scale deformation. They both also suggested some direct physical relationship between δ_t and the size of the crack growth increment, but others (for example, Tanaka, Hoshide, and Sakai, 1984; Brown, de los Rios, and Miller, 1988) have since used estimates of δ_t in a more general Paris-type power law crack growth expression (similar to Eqn. (1.1)).

Dowling and Begley (1976) at Westinghouse were the first to propose the range of the J-integral as a correlating parameter for elastic-plastic fatigue crack growth. The J-integral had previously been proposed by Rice (1968) as a characteristic parameter for near-tip stress-strain fields in elastic-plastic fracture. Working from the fundamental identity of J as an energy term, Dowling and Begley estimated ΔJ from load-deflection curves for deeply-cracked compact tension and center crack specimens. Advancing to the more complex semi-elliptical surface flaw in a smooth axial fatigue specimen, for which no similar approximation formula was available, Dowling (1977) developed an expression for ΔJ based on the suggestion of Shih and Hutchinson (1976) that J could be estimated by summing independent elastic and plastic components.

Delta J has been by far the most common elastic-plastic FCG parameter in use in the past twenty years. The list of different authors who have demonstrated its successful application to a wide range of materials, specimen and crack geometries, and temperatures is much too long to cite here. The specific methods of application remain varied: some researchers have calculated J with some form of the Shih and Hutchinson elastic-plastic summation technique, now firmly established in the EPRI elastic-plastic fracture handbook (Kumar, German, and Shih, 1981), while others have continued to estimate J from experimental load-deflection information. This experimental approach, of course, is not applicable to engineering design and analysis outside of the laboratory.

It is important to note, however, that ΔJ has been controversial since its first introduction. Early objections stemmed from the original definition of J, which was based on the deformation theory of plasticity and hence did not admit unloading. Later objections addressed the complications introduced by fatigue crack closure, the inability of simple J to rigorously accommodate variations in temperature, and other issues. Some of these objections have not been satisfied by strict mathematical counter-arguments. Nevertheless, the demonstrated success of ΔJ as an engineering tool (and the absence of alternative parameters with equally demonstrated success) left it intact as the current parameter of choice for many analysts. This success also seems to suggest that, in spite of theoretical objections, the parameter still captures enough of the correct physics to describe with sufficient accuracy the driving forces for fatigue crack advance under many conditions.

Nevertheless, these concerns prompted some additional searches for alternative elastic-plastic fatigue (and ductile fracture) parameters. Most notable among these are the J^* integral of Blackburn (1972), the $\hat{J}$ integral of Kishimoto, Aoki, and Sakata (1980), and the $\Delta T_p{}^*$ integral of Atluri, Nishioka, and Nakagaki (1984). It is best to label these as path-area integrals since the far-field representation includes both a path and an area contribution. A theoretical review of these parameters with particular reference to elastic-plastic fatigue crack growth is available in Kim and Orange, 1988. It can be shown that many of these quantities, including J, are derivable from a global energy balance with different restrictions invoked. Typically, the new parameters have a greater range of strict mathematical validity than the original J integral, particularly for problems involving plastic loading and unloading, temperature changes, and crack growth. However, these new parameters have not been evaluated outside of a very few research laboratories and are not yet accepted as engineering tools.

1.3.2 Criteria for Parameter Selection

The selection of a governing parameter for SSY FCG is typically a non-issue because of the wide acceptance of ΔK. For elastic-plastic FCG, however, the selection of the governing parameter is perhaps the most significant issue to be addressed and likely the most controversial one. As was discussed earlier, a number of parameters have been proposed and used. While ΔJ is the most widely used parameter in the engineering community at present, it has remained controversial from a theoretical standpoint.

The selection of a governing parameter must be guided equally by at least three considerations. The first is that the parameter must represent with sufficient accuracy the actual driving force for crack extension or the actual crack growth mechanism. That is, the parameter must be *theoretically valid.* The second is that the parameter must be easily and accurately calculated or estimated for a variety of actual materials, loads, and crack configurations: the parameter must be *practical.* The third is that the parameter must have demonstrated success in the actual consolidation of fatigue crack growth rate data and the prediction of fatigue crack growth lives under different conditions: the parameter must be *useful.*

Theoretical considerations include the validity and uniqueness of the parameter under complex load and environmental conditions including nonproportional loading and plastic unloading, thermal gradients and cycling, and material inhomogeneity. An integral parameter should ideally be sufficiently path-independent that the parameter value does not depend arbitrarily on the region over which it is evaluated. Another key theoretical issue is that the parameter should describe some physically-meaningful quantity which is somehow genuinely descriptive of the driving force for crack growth. Finally, the ideal theoretical parameter should also permit some direct physical measurement of its numerical value in order to validate computational methods. These theoretical considerations were the primary focus of the NASA-funded General Electric (GE) review (Kim and Orange, 1988) of the alternative path-area integrals.

Practical considerations are of equal importance for an engineering methodology, but have often been neglected. The chosen parameter should be easily and accurately calculated for a variety

of materials, loads, structural geometries, and crack configurations. A parameter which requires a sophisticated numerical analysis is less useful than a parameter which can be easily estimated from handbook tables or simple equations. However, the mere availability of simple estimation schemes is insufficient unless the estimation schemes used to estimate actual numerical values for the different parameters retain the theoretical distinctions between the parameters (McClung and Sehitoglu, 1991). The typical calculation schemes for three of the leading "simple" parameters (ΔJ, δ_t, and ΔK_ε) have been shown to give exactly the same functional form,

$$\Delta X = A_e a \Delta\sigma \{\Delta\varepsilon_e + A_p \Delta\varepsilon_p\} \tag{1.2}$$

where ΔX is the range of the parameter, $\Delta\sigma$ is the applied stress range, $\Delta\varepsilon_e$ and $\Delta\varepsilon_p$ are the nominal elastic and plastic strain ranges, a is the crack length, and A_e and A_p are general coefficients. An exact knowledge of the proper driving force is of little value unless that driving force can be either exactly calculated with sufficient economy or estimated with sufficient accuracy. For example, the crack opening displacement is one of the more attractive parameters from a conceptual or theoretical standpoint. Unfortunately, the COD is typically estimated from an unvalidated modification of the simple Dugdale crack model, which is technically limited to a center crack under plane stress SSY in an elastic-perfectly plastic material. Any exactness present in the concept is likely lost in the estimate. If the theoretical uniqueness of a given parameter is critical, then the estimation scheme must retain sufficient accuracy to capture this uniqueness.

A related factor in this question of practicality is the crack and component geometry. Most analytical solutions and most simple crack models correspond to simple reference crack configurations, such as the center-cracked infinite plate subject to uniform stressing. Most real cracks and real components, of course, are much more complex. An important criterion for a crack growth parameter will be how easily and accurately the effects of different crack and component geometries can be calculated. For ΔK this is simple, because many handbook solutions have been accumulated through the years and can be readily integrated into a computer code. For most elastic-plastic parameters, however, this information is totally unknown.

Yet another practical issue is the availability of a material data base. Existing data bases for fatigue crack growth are almost exclusively limited to SSY conditions, where ΔK is the correlating parameter. The chosen elastic-plastic and fully plastic FCG parameter should be able to employ this data base as much as possible to minimize the need for further baseline testing. This implies that the ideal parameter should have some clear relationship to ΔK and that its use should be entirely consistent with established approaches to SSY FCG as plasticity effects diminish.

The third set of selection criteria requires that the parameter have demonstrated success in the correlation of fatigue crack growth rate data in regimes which are relevant to the intended applications. No parameter, no matter how conceptually satisfying, should be used in engineering applications without a substantial experience base of successful use to correlate crack growth rates for different loads and geometries on a consistent basis. This success implies that confident predictions of growth rates and lives can be carried out from engineering calculations of the

parameter in conjunction with a standard data base of material properties that describe crack growth resistance in benchmark laboratory tests.

1.3.3 Evaluation of Delta J

Theoretical Considerations. The most frequent objections raised to Delta J following its introduction by Dowling and Begley (1976) argued that since the J-integral was based on the theory of deformation plasticity, which does not allow unloading or nonproportional plasticity, then it could not be applied to cyclic loading. However, Lamba (1975) had already demonstrated that a properly defined ΔJ maintained path independence in his studies of notch deformation. Wuthrich (1982; Wuthrich and Hoffelner, 1984) and Tanaka (1983) independently proved the path-independence and validity of ΔJ in application to fatigue cracking problems.

All three authors emphasized that "Delta J" must be properly formulated to maintain this validity. The original J-integral was defined by Rice (1968) for two-dimensional problems as

$$J = \int_{\Gamma} W_{\varepsilon} dy - T_i \frac{\partial u_i}{\partial x} ds \tag{1.3}$$

where x and y are rectangular coordinates normal to the crack front, ds is an increment of arc length along any contour, Γ, beginning along the bottom surface of the crack and ending along the top surface, T_i is the surface traction exerted on the material within the contour, and u_i is the displacement. The strain energy density W_ε is given by the equation

$$W_{\varepsilon} = \int \sigma_{ij} \, d\varepsilon_{ij} \tag{1.4}$$

where σ_{ij} and ϵ_{ij} are the stress and strain tensors, respectively. The correct "operational" definition of ΔJ, then, is given by

$$\Delta J = \int_{\Gamma} \Delta W_{\varepsilon} \, dy - \Delta T_i \frac{\partial(\Delta u_i)}{\partial x} ds \tag{1.5}$$

where

$$\Delta W_{\varepsilon} = \int \Delta\sigma_{ij} \, d(\Delta\varepsilon_{ij}) \tag{1.6}$$

Here the increments Δ of the stress, strain, traction, and displacement quantities designate the changes in these quantities from their respective reference values. However, the "Δ" in ΔJ and ΔW_ε do not represent changes in J and W_ε; instead, ΔJ and ΔW_ε are single-valued functions of their arguments. In other words, $\Delta J \neq J_{max} - J_{min}$. In this sense, "Delta J" is something of a misnomer, and Wuthrich (1982) has even argued that the term should not be used for this reason. It is therefore perhaps more appropriate to speak of the "ΔJ-Integral" rather than the "range of the J-Integral." For

elastic-plastic, cyclically saturated materials, the path-independence of ΔJ is satisfied since $\Delta\epsilon$ is a single-valued function of $\Delta\sigma$ during the loading portion of the cycle. The stress range field, $\Delta\sigma_{ij}$, and strain range field, $\Delta\epsilon_{ij}$, within the cyclic plastic zone at the crack tip follow the usual HRR-singular forms with ΔJ characterizing their amplitudes. Further tutorial background is provided in Saxena (1998).

By analogy to the original J-integral, then, ΔJ properly defined appears to have significant physical meaning. Delta J is related to the rate of change of potential energy with change in crack size, and (as noted above) scales the stress and strain fields in the crack tip deformation zone. Furthermore, ΔJ is a quantity that can be directly measured experimentally. For example, Dowling and Begley (1976) measured ΔJ in deeply cracked compact tension specimens according to

$$\Delta J = \frac{2A}{Bb} \tag{1.7}$$

where A is the area under the load-deflection curve, B is the specimen thickness, and b is the length of the uncracked ligament. Here, again, the analogy with the original J-integral was employed.

Delta J does have some remaining theoretical limitations, primarily related to variability in material properties in the crack tip region. Yoon and Saxena (1991), for example, have pointed out that path independence will not be strictly satisfied for materials that are not cyclically saturated. Temperature-dependent constitutive property variations for cracks growing in significant thermal fields may also violate path-independence. The practical significance of these limitations, and the possibility of pragmatic solutions to overcome the limitations, remains to be evaluated from experience.

A final set of potential theoretical limitations is the potential loss of J-dominance under certain conditions. When applied loads are severe, especially in low constraint geometries, the crack tip stress field may not be adequately characterized by the J-integral (McMeeking and Parks, 1979; Dodds et al., 1993), and so J alone may not be an adequate predictor of crack growth or fracture. Current approaches to this problem in the international fracture community typically employ an additional parameter, such as Q, to characterize the stress field more completely. In principle, the same limitations may apply to the ΔJ-integral, although the magnitude of ΔJ in a fatigue crack growth analysis will typically be less than the maximum value of J in a ductile fracture analysis, and so the problem may be less significant. It is also possible that the different crack advance mechanisms associated with fatigue crack growth have a decreased functional dependence on loss of constraint. Specimen size or geometry effects on EPFCG rates have not been noted as they have been observed for ductile fracture. However, this limitation has related implications for the practical characterization of crack instability (treated in Appendix I), where constraint has an apparent effect on fracture toughness that is actually related to changes in the crack driving force.

Practical Considerations. Further taking advantage of the direct analogy to the original J-integral, ΔJ also satisfies most of the aforementioned practical considerations. Delta J can be relatively easily and accurately calculated for different materials, loads, structural geometries, and crack configurations. As will be discussed in Chapter 2, numerous J solutions are already available.

New J solutions can be generated with finite element analysis, and powerful reference stress techniques can be used to generalize the discrete numerical solutions or even estimate J in the absence of finite element results. These estimation techniques, while simple, can be applied to practical, complex geometries, and they preserve the distinctive information about the particular geometry and material. As will be discussed in Chapter 3, all of these monotonic J solution forms can easily be employed to calculate ΔJ.

As will be shown in Chapter 3, ΔJ is directly related to ΔK in the SSY regime. This provides a basis for employing conventional (SSY) fatigue crack growth data bases in elastic-plastic FCG analyses, thereby minimizing the need for additional property generation. Furthermore, this relationship between ΔK-controlled SSY FCG and ΔJ-controlled EPFCG suggests that tools for EPFCG can easily be built into current tools for SSY FCG analysis, employing some of the same practical crack growth algorithms.

Finally, it must be emphasized that ΔJ has been successfully used by many researchers to correlate fatigue crack growth rate data and fatigue lives. While different researchers have employed slightly different forms of ΔJ, all have generally followed similar conceptual approaches. An exhaustive bibliography of this experience is neither practical nor needed, but selected citations are useful to illustrate the breadth of the experience base (Dowling and Begley, 1976; Dowling, 1976, 1977; Mowbray, 1979; Sadananda and Shahinian, 1979; El Haddad et al., 1980; Huang and Pelloux, 1980; Musava and Radon, 1980; Reger and Remy, 1982; Vardar, 1982; El Haddad and Mukherjee, 1983; Wang et al., 1983; Heitmann et al., 1984; Tanaka et al., 1984; Jolles, 1985; Obrtlik and Polak, 1985; Grin' et al., 1987; Horikawa and Cho, 1987; Hoshide and Socie, 1987; Rie and Schubert, 1987; Zheng and Liu, 1986; Hoshide et al., 1988; Bicego, 1989; Hatanaka et al., 1989; Jablonski, 1989; Yang and Lu, 1989; Earthman, 1991; Vormwald and Seeger, 1991; McDowell and Berard, 1992; Miura et al., 1994; Mu et al., 1996; Rie and Wittke, 1996; Rahman et al., 1997).

1.3.4 Evaluation of Alternative Parameters

The current contract effort was initiated by NASA-Marshall with the preliminary judgment that the range of the J-integral was the most appropriate choice for the elastic-plastic governing parameter around which a practical methodology could be developed. This judgment was based on an assessment of the available information about EPFCG, including many of the factors reviewed in the previous section.

Nevertheless, it was recognized at the outset that ΔJ was not necessarily a perfect parameter, or even the optimum parameter for all EPFCG applications. Therefore, a comprehensive literature review and critical evaluation of various governing parameters for EPFCG was conducted as part of the research program. The review was primarily focused on the alternative path-area integrals referenced earlier in the historical survey. The main criteria for evaluation were the considerations described in Section 1.3.2: theoretical rigor and validity, ease of use for practical applications, and demonstrated success in crack growth rate data consolidation and life prediction.

This review and evaluation is documented at some length in **Appendix A**. For convenience, the major conclusions are reproduced in the paragraphs that follow.

The simple alternative parameters such as ΔK_t and COD have clear practical and theoretical limitations. They share the same practical limitations of J in addressing temperature-dependent changes in material properties. In practice, these simple parameters are usually estimated directly from computations of J or K, and as such they retain the same theoretical limitations of those two fundamental parameters. Since most of the estimation techniques used to calculate the simple alternative parameters produce exactly the same functional form as ΔJ, any potentially important theoretical distinctions between the different parameters are lost entirely in the estimation schemes.

The alternative integral parameters clearly have some desirable theoretical capabilities, and their general success in correlating EPFCG data in the GE studies is encouraging. However, these advanced parameters possess some major practical limitations at the present time. First of all, their computation depends entirely upon complex elastic-plastic finite element analyses of growing cracks. This type of analysis is difficult and expensive for simplified (two-dimensional) laboratory specimen configurations, and totally unfeasible for actual (fully three-dimensional) component geometries and temperature-load histories. Second, several ambiguities remain regarding theoretical interpretation and application. Several of the parameters cannot be measured experimentally, so direct validation is not possible. The physical meaning of several parameters for the crack growth process is not yet evident and may not exist. Because of this absence of clear mechanistic justification, the parameters may give incorrect results in some applications.

The GE study found the two parameters ΔJ^* and $\Delta \hat{J}$ (and their rate forms) to be the most promising alternative parameters for a wide range of EPFCG, Thermo-Mechanical Fatigue (TMF), and creep crack growth applications. In view of the GE results, and in view of other potential limitations of other proposed integral parameters, this seems to be a reasonable conclusion. However, the practical use of these alternative parameters will likely depend on the development of simplified estimation techniques.

Extensive development work will be required before these new parameters can be used with confidence in actual applications. Therefore, although these parameters have exhibited some promise in research settings, their engineering implementation in the near term is not viable.

Considering all evaluation criteria, the original choice of ΔJ appears to be the optimum choice at the present time as the governing parameter for practical assessment of EPFCG. Delta J best addresses a broad range of both theoretical and practical issues. For example, robust estimation schemes are available to calculate ΔJ accurately and efficiently for a wide range of crack and component geometries; a ΔJ methodology enables the existing ΔK crack growth data base to be employed; and ΔJ has an established history of successful use in the characterization of crack growth.

Delta J is not a perfect parameter. Several mathematical conditions required by the original theoretical formulation of J will not be strictly satisfied for some practical EPFCG problems.

Thermal gradients and temperature-dependent material properties may degrade the path-independence of J and introduce practical difficulties in computing a single representative value.

However, researchers have shown repeatedly that ΔJ is successful in correlating EPFCG data under isothermal conditions. This success has been explained in terms of an "operational" definition of ΔJ which satisfies the essential spirit of the mathematical formulation. Several researchers have also used simple estimates of ΔJ with moderate success to correlate TMF and other elevated temperature fatigue crack growth data.

It should be noted that even a "perfect" governing parameter, one which exactly characterizes the crack-tip stresses and strains and the manner in which they facilitate crack advance, may be inadequate to completely describe crack growth rates in elevated temperature applications. Potential changes in crack growth damage mechanisms due to environmental and metallurgical effects may also be significant, and so some information about changes in material resistance to crack growth may be required. The scope of the current contract, however, is limited primarily to addressing the effects of mechanical plasticity on the "driving force" for crack growth.

In summary, NASA-Marshall appears to have made a wise choice in their preliminary selection of ΔJ as the governing parameter for EPFCG. There is an immediate need to develop practical tools for analysis of existing and planned hardware. Delta J has an extensive track record of successful use for the analysis of elastic-plastic fatigue crack growth, considerably more extensive than any competing parameter. The technology is available to address most of the detailed questions relating to actual implementation of an engineering method. Hence, it is possible to assemble a practical and reliable engineering tool in a relatively short time frame and with relatively limited resources.

1.4 Overview of the Program and Final Report

Technical efforts under the current contract may be broadly grouped into three major areas, and those three areas also provide the organizational scheme for this final report.

The first major area is the development and verification of additional J-integral solutions for crack geometries of particular significance to advanced reusable propulsion systems. A few relevant J solutions were already available, and needed only to be adapted for NASA use. Other general J solutions were derived from available finite element solutions. In other cases, new elastic-plastic finite element solutions were generated for specific geometries and then used to derive more general reference stress solutions applicable to a wider range of geometries. Finally, methods were developed to estimate J for various combined loading cases, including combined primary loading, combined primary and secondary loading, and multiaxial loading. The development and verification of new J-integral solutions is described in Chapter 2.

The second major area is the development and verification of practical crack growth algorithms. These algorithms translate a general calculation of J for some crack geometry into a specific quantitative prediction of FCG rate and FCG life. The first steps in this translation are the

appropriate formulation of a cyclic ΔJ estimate from a monotonic J solution and the correct implementation of crack closure information into an estimate of the effective cyclic J, ΔJ_{eff}. Methods were developed to estimate crack opening stresses for different applied stresses, stress ratios, stress states, and specimen and crack geometries. Other algorithms were developed to predict the conditions for crack instability (final fracture) and the potential acceleration of the FCG rate due to incipient instability. An important set of algorithms provides guidance for determining needed material properties, including the estimation of some properties from readily available information when a complete experimental characterization has not been performed. Finally, general guidance was provided for the development of practical algorithms to address creep-fatigue effects and load interaction effects in variable amplitude cycling. The development and verification of practical crack growth algorithms is described in Chapter 3.

The third major area is the development and verification of NASGRO software modules. The original contractual scope of work was dedicated to the development and verification of new methodologies. This work scope was later expanded to address the implementation of the methodologies in engineering software tools. The NASGRO work scope to date, however, has been limited to the implementation of the critical core methodologies: J solutions for primary and secondary loading for five common geometries; failure algorithms to compute critical crack size or critical load at fracture; and simple elastic-plastic fatigue crack growth calculations for the five implemented geometries. The development and verification of NASGRO software modules is documented in Chapter 4.

Many new elastic-plastic fracture mechanics methodologies have been developed and verified in the current contract effort. Some of these new developments have been documented in considerable detail in earlier monthly technical progress reports and topical reports. For convenience, the current final report is comprehensive, containing thorough descriptions of all work performed under the current contract, with appropriate integration of earlier progress reports. However, to preserve the readability of the final report, many of the detailed investigations are documented in appendices. The main body of this final report is designed to be more of an overview document that provides a general description of the work completed and organizes the detailed discussions in the appendices. For convenience, all references for the main body and the appendices are collected into a comprehensive list at the end of the report.

The contracting team of Southwest Research Institute and Rocketdyne (now part of Boeing North American) also performed two other technology contracts for NASA-Marshall on related topics during the period of performance of the current contract. These other two contracts were both focused on the elastic-plastic fracture mechanics analysis of proof testing, and both contracts employed J-integral methods to describe crack growth and instability. The two proof testing contracts have now both been completed and documented (McClung et al., 1996b; Chell et al., 1997a). The investigations conducted under the proof testing contracts provided a number of useful results to this elastic-plastic fatigue crack growth contract, and vice versa, and the interactions between the three contracts were recognized and managed by NASA-Marshall. This synergism between the three contracts greatly enhanced the productivity and efficiency of all three. While the

investigations documented in detail in this final report were supported by the current contract, key results from the other two contracts are implemented and cited as appropriate.

Due to the exceptional breadth of the developed methodology, the symbolic nomenclature employed in this final report is extensive and complex. Symbols have sometimes been assigned multiple meanings, and multiple symbols have sometimes been used to identify the same quantity, in order to maintain clarity and consistency with historical usage. While every attempt has been made to minimize any confusion arising from these conflicts (and, in fact, many "conflicts" have been maintained to minimize collateral confusion from changes in historical usage), the list of symbols provided in the preliminary paging cannot provide a definitive guide to all symbol meanings or a complete list of all symbol variants. The primary meaning of all symbols has been clearly identified in the immediate context of each usage, and this immediate context (not the comprehensive list of symbols) must be the primary means of identifying symbol definitions when conflicts arise.

2. DEVELOPMENT AND VERIFICATION OF *J*-INTEGRAL SOLUTIONS

2.1 Introduction

Given that ΔJ has been chosen as the governing parameter, the task remains to obtain an accurate J solution for a given combination of material, load, and geometry.

For small-scale yielding (SSY) FCG, the task of calculating the governing parameter is relatively straightforward. The governing parameter K is based on linear elastic fracture mechanics (LEFM) and may be calculated to very high accuracy in a number of different ways. A very large number of solutions are already available in the literature, and many different numerical analysis techniques have been established to calculate new values with a minimum of additional effort. Furthermore, the form of K can be normalized so that it is independent of load magnitude (i.e., K merely scales with applied load), although it is dependent on the spatial variation in stress resulting from the load. Since K is usually independent of material properties, its other major dependence is on geometry.

In contrast, the task of estimating an elastic-plastic parameter is generally more difficult. The J-integral, like other elastic-plastic parameters, is a nonlinear function of both applied load and material strain hardening, and may also be a nonlinear function of the customary geometry parameters. Simple linear mechanics methods are not adequate to meet this challenge.

The general engineering approach to estimating J for primary loading developed originally under EPRI sponsorship (Kumar et al., 1981) can be written as

$$J(c,P) = J_e(c_e,P) + J_p(c,P) \tag{2.1}$$

Here J_e is a first-order plastic corrected value of the linear elastic solution for J that interpolates between linear elastic and fully plastic behavior. It is related directly to the stress intensity factor through the expression

$$J_e(c_e,P) = \frac{K^2(c_e,P)}{E'} \tag{2.2}$$

The EPRI J estimation scheme defines the effective crack length, c_e, according to

$$c_e = c + \phi r_y \tag{2.3}$$

including a crack tip plastic zone size correction determined by the terms ϕ and r_y that are defined respectively as

$$\phi = \frac{1}{1+\left(\frac{P}{P_o(c)}\right)^2} \tag{2.4}$$

$$r_y = \frac{1}{\beta\pi}\left(\frac{n-1}{n+1}\right)\left(\frac{K(c,P)}{\sigma_o}\right)^2 \tag{2.5}$$

In these equations, β equals 2 for plane stress and 6 for plane strain based on arguments about the size of the crack-tip plastic zone, P is the applied load, and P_o a characteristic normalizing net section yield load. The effective elastic modulus E' is equal to E for plane stress and $E/(1-\nu^2)$ for plane strain, where E is Young's modulus and ν is Poisson's ratio. The parameters n and σ_o appear in the Ramberg-Osgood equation describing stress-strain behavior (see Eqn 2.7).

Although the analytical forms of the fully-plastic component, J_p, used in the EPRI scheme differ slightly depending on the cracked structure, for illustrative purposes the following expression is used here

$$J_p(c,P) = \alpha\epsilon_o\sigma_o\frac{c}{W}(W-c)h_1\left(\frac{c}{W},n\right)\left(\frac{P}{P_o(c)}\right)^{n+1} \tag{2.6}$$

where W is the section width. This particular estimation scheme was developed for materials whose stress-strain behavior can be described by a Ramberg-Osgood equation of the form

$$\frac{\varepsilon}{\varepsilon_0} = \frac{\sigma}{\sigma_0} + \alpha\left(\frac{\sigma}{\sigma_0}\right)^n \tag{2.7}$$

where ϵ is the total strain (elastic plus plastic) due to the stress, σ, α, and n are material constants, and ϵ_o is a "yield" strain corresponding to the "yield" stress σ_o, where $\epsilon_o=\sigma_o/E$. The first term on the right hand side of this equation represents the component of elastic strain, ϵ^e, and the second term represents the plastic strain, ϵ^p.

The nondimensional factor h_1 in Eqn 2.6 is, in general, a function of both constitutive relationship (e.g., strain hardening exponent) and geometry (e.g., crack length). The values of the function h_1 are typically obtained from detailed finite element (FE) analysis, and the EPRI handbooks contain tabulated values of h_1 for various cracked geometries, normalized crack sizes (e.g., c/W), and values of n. The different functional forms of Eqn 2.6 arise from different normalization schemes used to define h_1. The handbooks also give equations for evaluating the yield load P_o. This

parameter depends on the Ramberg-Osgood yield stress, σ_o, and structural dimensions (for example, wall thickness and radius in the case of cylindrical pressure vessels).

Finite element approaches to J calculation for a general-purpose fatigue crack growth analysis code have at least two significant limitations, however. First of all, the finite element solutions are exactly correct for only a single combination of material properties and crack/component dimensions. Estimation of J for any other combination of properties and dimensions typically requires empirical interpolation of tables containing multiple solutions, likely with some loss of accuracy. Purely interpolative approaches are even more impractical for fully three-dimensional crack configurations. For example, a surface crack in a finite sized plate is characterized by the crack aspect ratio (a/c) and two width-to-thickness ratios (a/t and c/b) in addition to the h/b value.

The second major limitation is the significant cost associated with the generation of original J solutions by the finite element method. Mesh generation alone for the finite element analysis of complex crack problems is extremely time-consuming, to say nothing of the computer costs associated with solution of a large three-dimensional elastic-plastic problem. Original finite element analysis is a reasonable approach to obtaining a limited number of new J solutions, but certainly not to obtaining all J solutions needed in the program.

An alternative option for J estimation is the reference stress method (Ainsworth, 1984) developed at the former Central Electricity Generating Board (CEGB) in the UK. The method is now incorporated into the R6 procedure for structural integrity assessment (Milne et al., 1986) and is widely used by designers and analysts. The reference stress method (RSM) requires only three basic inputs: (1) a K solution; (2) a description of the elastic-plastic constitutive response of the material (e.g., Ramberg-Osgood constants, Eqn. 2.7); and (3) an estimate of the limit load for the cracked member, assuming elastic-perfectly plastic material behavior. The J estimate can be written in the simple form

$$J = \frac{K^2}{E'}\left(\frac{E\varepsilon_{ref}}{\sigma_{ref}}\right) \tag{2.8}$$

The reference stress σ_{ref} is calculated as

$$\sigma_{ref} = \frac{P}{P_0}\sigma_0 \tag{2.9}$$

where P is the applied load and P_0 is the plastic limit load for a (cracked) rigid plastic material of yield stress σ_0. The reference strain ϵ_{ref} is then calculated from the constitutive relationship as the uniaxial strain corresponding to σ_{ref}. The RSM expression can be expanded to include a first-order plastic correction to K, and it can also be reformulated for Ramberg-Osgood materials to define an equivalent h_1 factor in the manner of Eqn.2.6.

The RSM approach is a particularly powerful means of estimating J for practical engineering problems, especially when detailed FE solutions are not available. Since K solutions are readily available or calculable for many geometries, and stress-strain relationships are also commonly

available, the generation of a J estimate is typically reduced to the task of defining an appropriate limit load solution. A required limit load solution may be obtained from existing compendia (Miller, 1988) or estimated from simple mechanics arguments.

Alternatively, an optimized limit load solution can be derived from a limited number of existing FE J solutions. This approach insures that the RSM solution is acceptably accurate while providing a means of "extending" the FE solution to a much wider range of load, geometry, and material parameters. Such an approach—the collaboration of selective FE analysis with general RSM formulations—has been employed to great advantage in the current contract, as described further below.

The general form of the optimized RSM estimate of J_p for a Ramberg-Osgood material employed in this work is (Chell et al., 1997b)

$$J_p^{RSM}(c,P)=\mu V\left(\frac{c}{W}\right)\alpha J_e(c,P)\left(\frac{P}{P_o^*(c)}\right)^{n-1} \tag{2.10}$$

where P_o^* is the optimized net section yield load evaluated using the Ramberg-Osgood yield stress, σ_o. In general, P_o^* will not equal the EPRI normalizing yield load, P_o, although it may have a form very similar to it. V is a dimensionless "structural" parameter that, in general, has a value of around 1, and

$$\mu=\frac{1-\nu_p^2}{1-\nu_e^2}\ (plane\ strain),\quad \mu=1\ (plane\ stress) \tag{2.11}$$

where ν_e is the elastic value of Poisson's ratio, and ν_p is the plastic value.

The general form of Eqn 2.10 offers several advantages over the conventional EPRI scheme. Making the assumption that V=1, then Eqn 2.10 provides a relatively simple expression for J_p that can be used for defective hardware for which EPRI handbook solutions are not available. This is possible because J_e can be readily evaluated for a wide range of geometries using existing K solutions, and the net section yield load, P_o^*, can be estimated from existing compendia of solutions (Miller, 1988), or estimated using plastic limit analysis. In addition, if the material stress-strain curve cannot be adequately represented by a Ramberg-Osgood equation, then J_p^{RSM} can still be evaluated using a generalized version of Eqn 2.10,

$$J_p^{RSM}(c,P)=\mu V J_e(c,P)\left(\frac{E\epsilon_{ref}^p}{\sigma_{ref}}\right) \tag{2.12}$$

where the reference stress, σ_{ref}, is defined as

$$\sigma_{ref} = \left(\frac{P}{P_o^*} \right) \sigma_o \tag{2.13}$$

and the reference plastic strain, ϵ^p_{ref}, is the uniaxial plastic strain corresponding to σ_{ref}. For a Ramberg-Osgood material,

$$\epsilon^p_{ref} = \alpha \frac{\sigma_o}{E} \left(\frac{\sigma_{ref}}{\sigma_o} \right)^n \tag{2.14}$$

Additional modifications to reference stress estimates are possible that employ empirical modifications to the optimum yield load or the structural parameter that introduce an additional dependency on the strain hardening exponent, n. Some modifications of this nature were explored under the current contract. When supporting data are available, the extra degrees of freedom associated with these modifications permit some increases in the accuracy of the J solutions. However, these modifications are possible only when more extensive finite element data are available, and the validity of the modification outside the bounds of the available data cannot be assured. Furthermore, the reference stress method modified in this way can no longer be extended to non-Ramberg-Osgood materials. Therefore, the contractor has chosen not to employ these modified reference stress solutions in the delivered methodology. However, future work could demonstrate the validity and usefulness of these modifications in certain situations.

Chapter 2 summarizes activities under the current contract to develop and verify new J-integral solutions. Previously existing J solutions are surveyed and summarized. New reference stress J solutions are derived from existing FE solutions for two-dimensional through cracks. New finite element J solutions are generated for a limited matrix of surface and corner cracks, these FE solutions are employed to develop improved reference stress solutions with greater generality, and the reference stress solutions are then independently verified with another set of recent FE solutions. New finite element J solutions are generated for cracks emanating from double edge notches, and the FE solutions (along with existing EPRI solutions) are used to verify a new reference stress technique for cracks growing from any stress concentrator. New reference stress J solutions for through cracks in finite plates are derived from existing FE solutions and verified. General J estimation methods for combined mechanical loading based on the reference stress technique are developed and verified. Various J estimation methods for combined primary and secondary loading are critically reviewed, and a new procedure combining the reference stress technique with a first-order plasticity correction is forwarded. A J estimation technique for two-dimensional Mode I cracks subjected to biaxial loading is presented and verified. As noted earlier, many of the details of these methods and their verification are provided as appendices to the main body of the report.

2.2 Existing Solutions

The great majority of formal J solutions currently available have been generated in work supported by the Electric Power Research Institute (EPRI). The EPRI handbooks (e.g., Kumar, German and Shih, 1981; Zahoor, 1989-1991) typically contain tables of h_1 values for discrete values of n, a/t, etc., derived from extensive finite element (FE) computations, along with appropriate formulae for K (often borrowed from existing compendia of K solutions). A limited number of additional J solutions are available in the literature, primarily analytical solutions for cracks in infinite bodies and isolated FE solutions for special geometries. These isolated FE results are typically insufficient to support a general expression for J. The major J solutions available are summarized in Table 2.1. Nearly all of these solutions are limited to uniform tensile loading (or internal pressure, for hollow cylinders), with only a few solutions for pure bending or combined bending-tension. A more detailed compilation of existing J solutions is provided in **Appendix B**.

Table 2.1 Summary of Existing J Solutions

	Existing Solutions	
	Thorough	Limited
STANDARD SPECIMENS		
Compact Tension Specimen, SS02	X	
Three-Point Bend Specimen, SS05	X	
THROUGH-THICKNESS CRACKS IN PLATES AND SHELLS		
Through Crack in an Infinite Plate	X	
Through Crack at Center of Plate, TC01	X	
Through Crack at Edge of Plate, TC02	X	
Double-Edge Cracked Plate	X	
Axial Through Crack in a Pressurized Cylinder, TC07		X
Circumferential Through Crack in a Cylinder, TC08	X	
Through Crack from Hole in a Finite Plate, TC09		X
EMBEDDED CRACKS		
Embedded Elliptical Crack, EC01		X
SURFACE CRACKS		
Semi-Elliptical Surface Crack in a Plate, SC01		X
Semi-Elliptical Axial Surface Crack in a Hollow Cylinder, SC04	X	
Internal Axial Surface Crack (Constant Depth) in a Hollow Cylinder	X	
Semi-Elliptical Circumferential Surface Crack in a Hollow Cylinder, SC05	X	
Internal Circumferential Surface Crack (Constant Depth) in a Hollow Cylinder, SC06	X	
External Circumferential Surface Crack (Constant Depth) in a Hollow Cylinder, SC06	X	

2.3 New Solutions

2.3.1 Surface, Corner, and Embedded Cracks in Plates

The finite element method and the reference stress method were employed in partnership to construct new J solutions for quarter-elliptical corner cracks (NASGRO designation CC01), semi-elliptical surface cracks (NASGRO designation SC01), and elliptical embedded cracks in finite plates (NASGRO designation EC01). These idealized crack configurations are commonly employed in many applications problems.

2.3.1.1 Finite Element Solutions

While a number of FE results have been published for the surface crack geometry, the available solutions alone are not sufficient to construct a general tabular interpolation solution for all possible degrees of freedom, including variations in a/t, a/c, c/b, strain hardening exponent (n), and angular position (Φ) (the geometry parameters associated with the surface crack are defined in Figure 2.1). No literature J solutions were available for the corner crack geometry, and embedded crack solutions were available only for infinite bodies.

In order to facilitate the development of RSM estimates, a matrix of additional finite element J solutions were generated for surface cracks and corner cracks under uniform tension using the commercial finite element program ABAQUS. The matrix included three a/t values, three a/c values, and three n values for a fixed $c/b = 4.0$. Elastic solutions were validated by comparison with the most recent benchmark K solutions in NASGRO. Fully-plastic h_1 values were obtained at eleven angular positions along the crack front. Further descriptions of the finite element analyses, along with detailed tabular and graphical results, are given in **Appendix C**.

2.3.1.2 Reference Stress Solutions

Reference stress solutions were derived from the FEM J results for SC01 and CC01 under uniform tension and the results of Yagawa et al. (1993) for SC01 under bending using the optimization scheme developed by Chell et al. (1997b). The specific forms of the plastic J solutions employed were

$$J_P^{RSM}\left(\frac{a}{t},\frac{a}{c},\frac{c}{b}\right) = J_e\left(\frac{a}{t},\frac{a}{c},\frac{c}{b}\right)\mu V\alpha\left(\frac{P}{P_o^*}\right)^{n-1} \quad \text{, for CC01 or SC01 under tension}$$

$$J_P^{RSM}\left(\frac{a}{t},\frac{a}{c},\frac{c}{b}\right) = J_e\left(\frac{a}{t},\frac{a}{c},\frac{c}{b}\right)\mu V\alpha\left(\frac{M}{M_o^*}\right)^{n-1} \quad \text{, for SC01 under bending} \qquad (2.15)$$

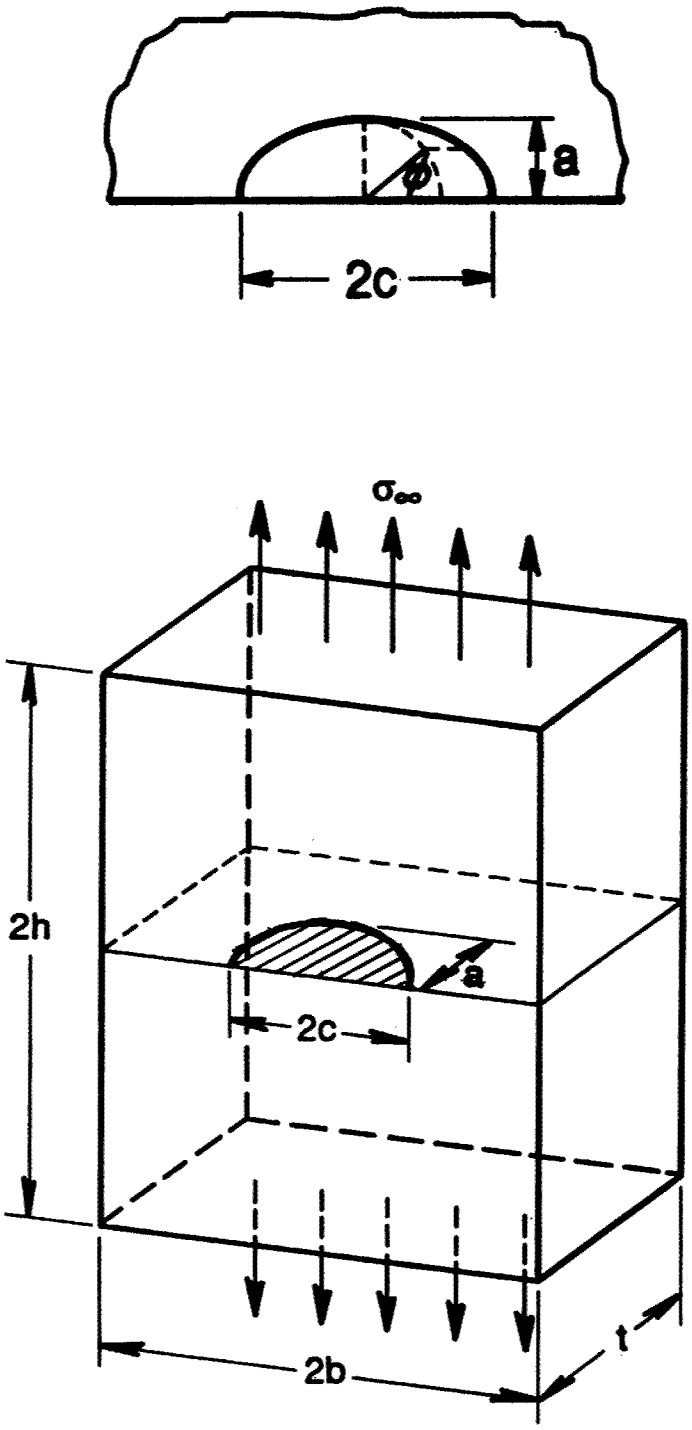

Figure 2.1 Schematic defining geometry parameters for semi-elliptical surface crack in finite plate

Here the optimized yield load, P_o^*, the optimized yield moment, M_o^*, and the structural parameter, V, are dependent on geometrical parameters only and are independent of the strain hardening exponent, n. To generalize the solution to arbitrary c/b values, the structural parameter V was taken to be a constant associated with each specific model type and the crack front location, and independent of a/t and a/c ratios. For model type SC01 under tension or bending, two values of V for the deepest ($\Phi = 90°$) crack tip and the near surface ($\Phi = 9°$) crack tip, $(V_a)_{avg}$ and $(V_c)_{avg}$, were evaluated as the arithmetic mean of optimized V values for all a/t and a/c ratios. Respectively, $(V_a)_{avg}$ and $(V_c)_{avg}$ are equal to 1.8164 and 1.2561 for SC01 under tension and 1.0412 and 0.9730 for SC01 under bending. For model type CC01 under tension, V was taken as the maximum of the two arithmetic means at the Φ=9° and Φ=81° near surface crack tip locations. In this case, $V=V_{max}=\max((V_a)_{avg},(V_c)_{avg})= 1.4329$.

The optimization scheme also found that for tension-loaded SC01 and CC01 flaw geometries, the optimized net section yield load was approximately given by the reduction in the load bearing area of the flawed section

$$P_o^* = \begin{cases} \sigma_o\left(Wt - \dfrac{\pi ac}{4}\right), & \textit{for CC01 where } W=b \\ \sigma_o\left(Wt - \dfrac{\pi ac}{2}\right), & \textit{for SC01 where } W=2b \end{cases} \tag{2.16}$$

The net section yield moments, M_o^*, for SC01 and CC01 were approximated from plastic limit analysis.

In the absence of finite element J_p solutions to use as data to optimize or verify the RSM solutions for model types EC01 under tension and CC01 under bending, the RSM approach was still used but with P_o^* estimated from plastic limit theory and with a conservatively chosen V=1.873. This constant value of V corresponds to plus two standard deviations from the mean value derived from a statistical analysis of V values for a wide range of cracked structures (Chell et al., 1997b). There is a 97% confidence that computed V values will fall below this statistical upper bound.

The new RSM solutions were verified by comparing the results against the original FE results generated in this contract for SC01 and CC01 under uniform tension and the Yagawa et al. (1993) results for SC01 under bending. In addition, independent FE results in the literature were used for further verification. Sharobeam and Landes (1995) have reported J results for SC01 under uniform tension which cover a wide range of values for crack depths ($0.16 \le a/t \le 0.82$), aspect ratios ($0.46 \le a/c \le 2.0$), and plate dimensions characterized by the width to crack length ($2.28 \le b/c \le 17.1$) and half-height to thickness ($4 \le h/t \le 16$) ratios. In all, they calculated 21 J solutions covering n values of 5, 10, and 15. Their results represent a widely varied, almost randomly selected, set of solutions.

The correlation between the Sharobeam and Landes results and the RSM estimates was found to be strong. Agreement was good even when the load bearing area was large compared with the crack area (the smallest ratio of crack area to total plate area was 0.018). Hence load redistribution due to the presence of the flaw appears to be able to occur over a wide area.

The variation in the value of V reflects both an explicit crack size dependence and also possible inaccuracies in the computed values of h_1. It is not yet possible to see how the value of V can be estimated a priori, and the limited data base of results currently available is not sufficient to warrant performing a parametric fit of V to a/t and a/c. However, the results demonstrate that it is possible to employ average (or perhaps bounding) values of V and generate relatively accurate J_p solutions, especially at the deepest point of the crack.

Further details of the development and verification of all the RSM solutions for SC01, CC01, and EC01 are given in **Appendix K**, the User's Manual for the NASGRO elastic-plastic fracture mechanics modules. Included in Appendix K are extensive tables of V and normalized optimum yield loads, along with graphical representations of all verifications, and a table showing limits of applicability (both geometric and material) of all J solutions in NASGRO.

2.3.2 Cracks at Stress Concentrations

Cracks at stress concentrations are another important class of elastic-plastic fracture mechanics problems, since the geometric discontinuity may substantially elevate the local stresses and may even introduce plastic enclaves in the uncracked body.

There are only two known sets of J solutions available for cracks emanating from stress concentrating features, and both are for defects at round holes. Sumpter (1973) presented graphical J values for symmetric defects at a hole under uniform uniaxial nominal stressing in a non-work hardening material. Results were given for ratios of defect depth to hole radius, a/R, of 0.05, 0.1, and 1. The EPRI handbooks (Kumar, German, and Shih, 1981) included J solutions in the usual EPRI parametric form for a single defect emanating from a hole subjected to biaxial nominal stressing, where the ratio of the stress components parallel and perpendicular to the plane of the defect is 0.5. Results were given for a/R ratios of 0.125, 0.25, 0.5, 0.75, and 1, and strain hardening exponents of 1, 2, 3, and 5.

2.3.2.1 Finite Element Solutions

In order to support the development and validation of a general reference solution method for cracks at stress concentrations, a set of J solutions were generated using the elastic-plastic finite element method. These FE solutions were developed under the companion contract on multiple cycle proof testing (MCPT), not the current contract, since the elastic-plastic fracture mechanics behavior of cracks at stress concentrations was a particularly significant problem for the assessment of MCPT. A more detailed description of the FE methods and results is given in the MCPT final report (McClung et al., 1996b). For convenience, a short summary is given here.

Three double edge notch geometries under plane stress tensile loading were considered in the investigation, corresponding to K_t values of 4.29, 6.43, and 8.57 where

$$K_t = \frac{stress\ at\ notch}{gross\ section\ stress} \tag{2.17}$$

Corresponding values of D/R were 2.41, 6.2, and 11.6. Here, b is half the width of the plate and R is the radius of the semi-circular notch tip. The relationships between d, a, R, D, and b, are shown schematically in Figure 2.2. The notches extended 30% across the section ($D = 0.3b = 1.5$ inch, where $b = 5$ inch) and had root radii of 0.622 inch, 0.2425 inch, and 0.129 inch.

The finite element analyses were first verified under linear elastic conditions by comparison with known solutions. Then the fully plastic component of J, J_p, was calculated for various crack depths and strain hardening exponents, n, assuming a Ramberg-Osgood stress-strain law (Eqn. 2.3) with a characteristic yield stress $\sigma_o = 60$ ksi and Young's Modulus $E = 30{,}000$ ksi. The constant $\alpha = 100$ was chosen to have a very high value in order to induce high levels of plasticity at relatively low stress levels. Values of $n = 1, 3, 5, 10$, and 15 were used in the analysis, and for each value the applied load, P, was incremented in the computations until $J_e/J < 0.0005$ (where J_e is the elastic component of J), which ensured that the fully plastic solution had been reached. Following the EPRI handbook (Kumar, German, and Shih, 1981) form for double edge cracked plates (DECP), J_p was expressed in the form

$$J_p = \left(J - J_e\right) = \alpha\sigma_o\epsilon_o c h_1\left(\frac{a}{b}, n, \frac{D}{R}\right)\left\{\frac{P}{P_o}\right\}^{n+1} \tag{2.18}$$

so that the EPRI J solutions would be recovered at relatively large d values ($d > 0.5R$) when the notch plus crack could be represented to a good approximation as a crack of effective depth, $a = D + d$ subjected to the nominal stress. In this equation, P is the applied load, P_o is a characteristic yield load per unit breadth of plate given by

$$P_o = \frac{4}{\sqrt{3}} c\sigma_o \tag{2.19}$$

$c = b - a$, and $h_1(a/b, n, D/R)$ is a function whose values were derived from the FE results. At large d values, $h_1\ (a/b,\ n,\ D/R)$ becomes independent of D/R, and the h_1 values tabulated in the EPRI handbook for the double edge cracked plate were approximately recovered. These results showed that, as in the linear elastic case, the effect of the notch is limited to crack depths, d, that are less than about half the root radius, R, of the notch.

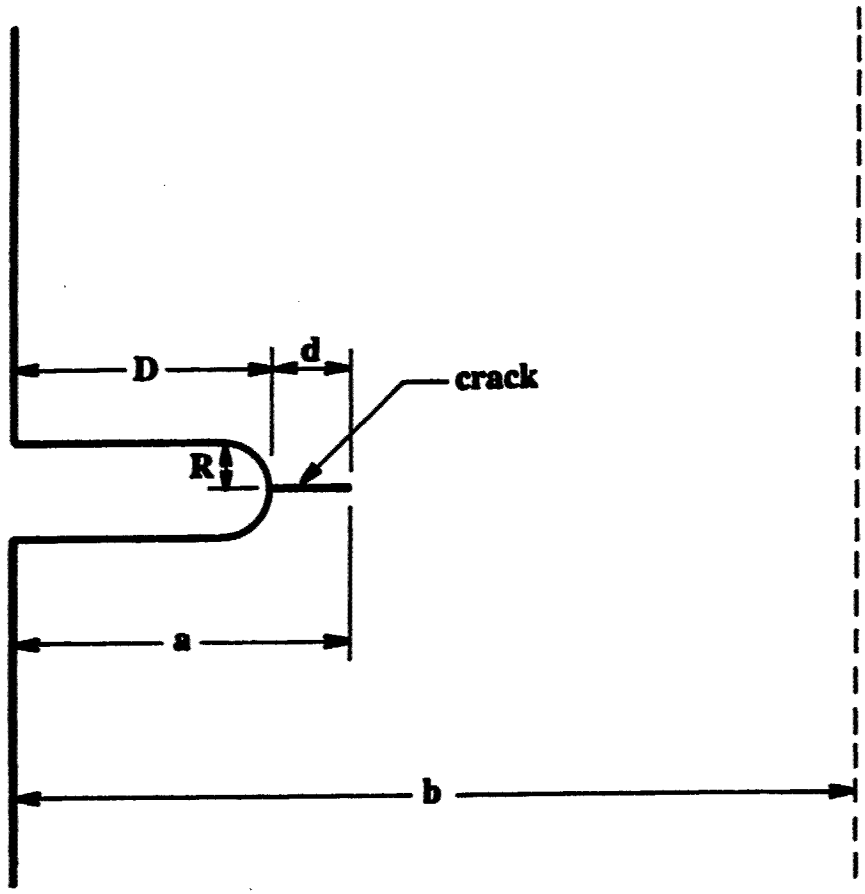

Figure 2.2. Schematic showing geometrical relationship between notch depth (D), notch root radius (R), crack depth (d), notch plus crack depth (a), and half plate width (b)

2.3.2.2 Reference Stress Solutions

A new J estimation method was developed that combines the scheme adopted by EPRI and used in the elastic-plastic handbooks, with the reference stress method (RSM).

In the new scheme, hereafter referred to as the modified RSM, first order plasticity effects are included in J via a first order plastically corrected value for the linear elastic solution, J_e. This insures that the correct linear elastic limit is recovered by the scheme.

The fully plastic contribution to J, J_p is evaluated using the RSM. For the purposes of validating the approach, the optimized RSM is employed. In this method, a yield load, P_o^*, and structural parameter, $V(a/b,D/R)$, are derived from finite element solutions for J_p. (In the present instance, the J_p solutions were available from the new FE solutions and the EPRI handbooks.) The values of P_o^* and $V(a/b,D/R)$ were chosen so as to optimize the fit of the RSM estimate of J_p to the finite element solutions for a range of n values. This approach ensured that the correct fully plastic limit is recovered by the scheme.

Note that in general, the values of P_o^* and $V(a/b,D/R)$ are not known a priori in the absence of appropriate finite element solutions for J_p, P_o^* is often approximated by P_o, and $V(a/b,D/R)$ is assumed to have the value of unity. Using the optimized approach provides an accurate representation of the fully plastic solution, enabling the accuracy of the modified RSM to be explicitly investigated in the important elastic-plastic regime which interpolates between linear elastic and fully plastic behavior.

The optimized RSM expression for J_p used here was

$$J_p = J_e(d)\ V(a/b,D/R) \left[\frac{E\epsilon_{ref}^p}{\sigma_{ref}}\right] \tag{2.20}$$

where ϵ_{ref}^p is the plastic component of the reference strain which, for Ramberg-Osgood materials, is given by

$$\epsilon_{ref}^p = \alpha \left(\frac{P}{P_o^*}\right)^n \tag{2.21}$$

and

$$\sigma_{ref} = \frac{P}{P_o^*}\ \sigma_o \tag{2.22}$$

The total J estimate was then written as

$$J = J_e(d + \phi^* r_y) + J_e(d)\ V(a/b,D/R) \left[\frac{E\epsilon^p_{ref}}{\sigma_{ref}}\right] \tag{2.23}$$

where

$$\phi^* = \frac{1}{1 + \left(\frac{P}{P_o^*}\right)^2} \tag{2.24}$$

The new method was verified through detailed comparison with both the EPRI and new FE solutions. Agreement was excellent for all the crack depths analyzed ($0.1194 \leq d/R \leq 0.6431$) and at all load levels.

In principle, this new estimation method for cracks at stress concentrators should be applicable to any notched geometry for which a K solution is available, along with a J_p solution for the cracked geometry in the absence of the notch. The geometric limitations of the new J solution for the crack at a notch would be the same as the limitations of the constituent K and J_p solutions. The reference stress formulation would permit application of the solution for Ramberg-Osgood materials with any $n > 1$, and ultimately for materials with other stress-strain relationships. However, specific validity limits for specific solutions to be developed in the future would need to be established through suitable verification analyses.

Further details of the new J estimation method for cracks at notches, along with extensive documentation of the verification studies, are given in **Appendix D**.

2.3.3 Reference Stress Solutions for Through Cracks in Plates

Finite element J solutions were available in the EPRI handbook (Kumar et al., 1981) for the through crack at the center of a finite plate (NASGRO designation TC01) under uniform tension for plane strain and plane stress, and for the through crack at the edge of a finite plate (NASGRO designation TC02) under uniform tension or bending for plane strain and plane stress. In order to increase the generality of the solutions for these geometries, optimized reference stress solutions were also derived from the finite element solutions.

The reference stress solutions for the plastic J term, J_p^{RSM}, took the following general forms:

TC01 with b=$W/2$ and TC02 under tension with b=W:

$$J_p^{RSM}\left(\frac{c}{b}\right) = J_e\left(\frac{c}{b}\right)\mu V\left(\frac{c}{b}\right)\alpha\left(\frac{P}{P_0^*}\right)^{n-1} \tag{2.25}$$

TC02 under bending with $b=W$:

$$J_p^{RSM}\left(\frac{c}{b}\right) = J_e\left(\frac{c}{b}\right)\mu V\left(\frac{c}{b}\right)\alpha\left(\frac{M}{M_o^*}\right)^{n-1} \tag{2.26}$$

Here W is the plate width, and the crack size is $2c$ for TC01 and c for TC02. The optimized yield loads, P_o^* or M_o^*, and the structural parameter, V, were derived from the EPRI finite element results for different strain hardening exponents, but are themselves dependent on geometrical parameters only and are independent of the strain hardening exponent. Discrete values of the optimized yield loads and V's are given in **Appendix K**. Appendix K also documents the verification of the reference stress solutions by direct comparison with the established EPRI finite element results.

These new RSM solutions share the same geometric limitations as the EPRI solutions from which they were derived (see Table 15 in Appendix K), but may be employed with larger strain hardening values than the $n = 20$ upper bound of the EPRI solutions. For Ramberg-Osgood materials with $n < 20$, the RSM and EPRI solutions should give nearly identical results. The primary advantage of the RSM formulation is that it permits future extension to materials that do not follow a Ramberg-Osgood stress-strain equation.

2.4 Estimation Methods for Combined Mechanical Loading

In the linear elastic regime, K due to combined mechanical loading (e.g., tension + bending) can be easily computed by summing the independent K values calculated for the loads acting separately. In the nonlinear plastic regime, however, this linear superposition does not hold for the computation of J under combined mechanical loading. No rigorous procedure to perform this combination was previously available.

An approximate method has now been developed to estimate J for two simultaneously applied mechanical loads, given that J solutions are available for the two loads acting separately. This combined J solution can be expressed in terms of the linear elastic component of J for the combined loading, and a material dependent function of an appropriate combined yield load. The latter is called the optimum yield load, and represents the load to cause net-section yielding of a defective structure of non-strain hardening material. The derivation of J for the combined loading is thus reduced to finding an expression for the optimum combined yield load. The concept of the optimum yield load is discussed further in Chell et al. (1997b).

The methodology has been validated against computed fully plastic J solutions for single edge cracked plates (Kumar et al., 1984a), and cylinders containing circumferential through-wall defects (Kumar and German, 1988), simultaneously subjected to tensile forces and pure bending moments. The agreement between the approximate solutions and the computed J values is generally good, as summarized in Figure 2.3. The accuracy of the method is dependent on the accuracy of the combined yield load chosen as an interpolation function between the two extreme loading conditions corresponding to pure tension and pure bend. The developed methodology has the added benefit of allowing solutions obtained for Ramberg-Osgood materials to be extended to materials that display arbitrary stress-strain behavior.

In principle, this new estimation method for cracks under combined mechanical loading should be applicable to any geometry for which J solutions are available for the two loads acting separately, and for which a combined yield load solution can be formulated. The geometric limitations for the new solutions would be determined by the minimum capabilities of the individual J solutions and combined yield load solution. The reference stress formulation would permit application of the solution for Ramberg-Osgood materials with any $n > 1$, and ultimately for materials with other stress-strain relationships. However, specific validity limits for specific solutions to be developed in the future would need to be established through suitable verification analyses.

More complete details of the estimation method and its validation are given in **Appendix E**. This appendix also includes further background on the optimum yield load concept.

2.5 Estimation Methods for Combined Primary and Secondary Loading

Procedures for determining J for primary (mechanical) loads are now relatively well-established, as discussed in the preceding sections. However, parallel procedures for secondary (i.e., thermal, residual, displacement imposed) loads are far less advanced. This is due, in large extent, to the variety of such loads, which makes a general characterization of them (e.g., a handbook approach) difficult, if not impossible. Furthermore, these secondary loads can have a significantly different and much more complex effect on a total J solution than do primary loads, and their effect is also dependent on the manner in which they are combined with primary loads.

Four major methods for estimating J for combined primary and secondary loads have been forwarded previously: the EPRI handbook approach (Kumar et al., 1984) which incorporates the effect of secondary loading through a first-order plasticity correction to the elastic component of J; the R6 structural integrity procedure (Milne et al., 1986) which includes a term characterizing the interaction between primary and secondary loads; the method of Chell (1986) which combines a first-order plasticity correction with the RSM approach; and a proposed modification to the R6 procedure (Budden, 1989) based on the Neuber principle. None of these methods are totally satisfactory as they stand.

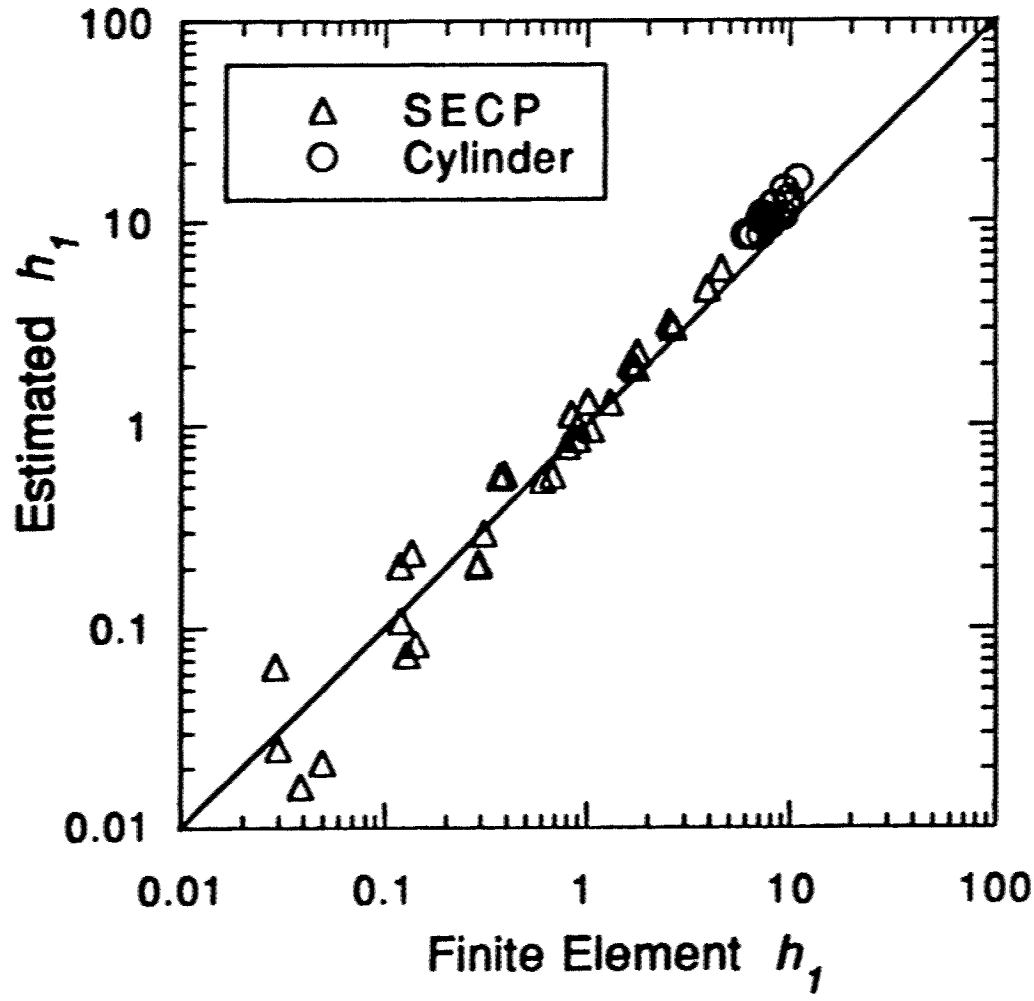

Figure 2.3. Estimated versus finite element h_1 values for combined mechanical loads (tension plus bending)

A new procedure has been developed based on improvements in the Chell approach. This procedure allows credit to be taken for situations where stress relaxation occurs due to plastic deformation in the defect free structure, although it is not generally applicable to situations where significant elastic follow-up occurs. The latter problem can be addressed by simulating the secondary loading with imposed displacements, and a method of solution for this approach has been outlined. The method has been validated against available FE solutions for combined mechanical-thermal loading. Further work is needed to validate certain aspects of the method. Of particular concern are J estimates when the secondary load produces a plastic enclave large in size compared to the crack. The recommended procedure is not applicable to cases where it is known that load history effects are important (the order of application of primary and secondary loads). The method assumes that the primary load is superimposed on an existing secondary load.

Appendix F contains a detailed discussion of the four previous methods and the new improved procedure.

2.6 Estimation Methods for Multiaxial Loading

As noted earlier, most existing J solutions are limited to simple uniaxial load configurations such as pure tension or bending. However, multiaxial stress states occur frequently in reusable aerospace propulsion systems. Solution of the complete multiaxial problem was beyond the scope of the current contract, but some simple estimation techniques have been developed and evaluated. A more complete discussion of these methods is available in **Appendix G**.

The approach is based on an approximation scheme for infinite bodies first introduced by He and Hutchinson (1981) and later amplified by Dowling (1987). For a stress, S, applied remote from the crack in a direction normal to the plane of the crack, and remotely applied transverse stresses, T, normal to the axis of stress S, the multiaxial, fully plastic J solution can be written in the general form

$$J_p = \alpha \varepsilon_0 \sigma_0 a\, h_0 \left(\frac{S}{\sigma_0} \right)^{n+1} \tag{2.27}$$

where σ_0, ε_0, and n are material constants in the Ramberg-Osgood constitutive relationship, Eqn 2.7. The effects of multiaxiality are captured in the factor h_0. For plane strain, h_0 is given by

$$h_0 = h_0^{/} \{|1 - \lambda|\}^{n-1} \tag{2.28}$$

where h'_0 is the uniaxial solution and the biaxiality ratio $\lambda = T/S$. For plane stress, the form is

$$h_0 = h_0' \left\{ \sqrt{1 - \lambda + \lambda^2} \right\}^{n-1} \tag{2.29}$$

This approach has been validated against the rigorous numerical results of He (1986) for through-thickness cracks in infinite plates under both plane stress and plane strain at biaxiality ratios ranging from -1 to +2. Quantitative agreement is generally excellent for λ values between -1 and +1, which is the range of practical importance.

The only available set of biaxial J results for cracks in finite bodies is that of Jansson (1986), who published fully plastic plane stress FE solutions for biaxially-loaded center-cracked plates at $\lambda = \pm 1$, ± 0.5, and 0. Agreement of the simple estimation scheme with the Jansson results is reasonably good but gradually deteriorates for deeper cracks ($a/t \geq 0.5$), especially with larger strain hardening exponents ($n \geq 13$). This crack depth effect is largely due to rigid boundary displacement constraints imposed by Jansson which cannot be emulated by the simple estimation scheme. Estimates were found to be conservative (higher than FE values) for $\lambda = \pm 1.0$, 0.0, and -0.5, but not $\lambda = +0.5$.

This new estimation method for J under multiaxial loads is currently limited to two-dimensional geometries with Mode I through cracks for which J solutions under uniaxial loading are available. The accuracy for large cracks in finite geometries, especially under significant levels of structural constraint, cannot be assured without further validation. The geometric and material limits of applicability of specific solutions would also be bounded by the geometric and material limits of the constituent uniaxial solution, and the method is currently limited to Ramberg-Osgood materials.

3. DEVELOPMENT AND VERIFICATION OF PRACTICAL CRACK GROWTH ALGORITHMS

3.1 Introduction

The role of the practical crack growth algorithms is to move from a general calculation of J for some component and crack geometry to a specific quantitative prediction of fatigue crack growth life under various conditions; i.e., to estimate properly the accumulation of relevant damage. These algorithms must be sufficiently simple to admit incorporation into an efficient computer code for general purpose fatigue crack growth analysis and must be sufficiently robust to address accurately a wide range of components, materials, and loading conditions.

Much less research has been conducted on fatigue crack growth under elastic-plastic conditions than under small-scale yielding (SSY) conditions, where ΔK is generally acceptable as the correlating parameter for crack growth rates. As a result, relatively few practical algorithms have been proposed for EPFCG, and much less background information is available to support the development of these algorithms. The algorithms presented in this report are based on the best available analytical and experimental data, but it must be emphasized that this data base is limited in size and scope for many problems. Existing data were employed wherever possible, and some new analytical and experimental investigations were conducted as needed to address critical needs for new information. The technical challenge is a large one, and comprehensive answers to all important questions are far beyond the scope of any single research program.

It should be noted that the algorithms presented in this report have been derived and assembled using a modular approach wherever possible. As new insights or data become available, or as engineering experience identifies significant shortcomings associated with certain approaches, individual algorithms can be replaced by revised versions.

Crack growth algorithms for SSY conditions have already been proposed, and in some cases also validated, for some of the problems addressed here. In some cases, these SSY algorithms can be applied to EPFCG conditions with equal or at least acceptable accuracy. In some cases, SSY algorithms require modifications to enable their extension into the EPFCG regime. In other cases, SSY algorithms (especially those with a predominantly empirical basis) are known to predict the wrong trends under EPFCG conditions, and must be replaced entirely.

The goal of this research program, and of this report, has been to lay out a general framework to solve the comprehensive EPFCG problem, even if all relevant issues are not yet resolved. The intended approach is relatively exhaustive, attempting to identify and mention most key issues, and to propose at least one approach to each significant technical challenge. Limitations and important unknowns are identified where possible, and needs/priorities for future research are highlighted.

The basic engineering philosophy which undergirds most of the practical crack growth algorithms for EPFCG is that accurate predictions of crack growth rates due to fatigue crack growth mechanisms will result from an accurate characterization of the effective range of the J-integral,

ΔJ_{eff}. The specific technical arguments supporting this philosophy follow in subsequent sections. In practice, this implies that accurate crack growth algorithms depend on three basic calculations or characterizations: (1) an accurate estimate of the (monotonic) J-integral for the specific loads, material, and geometry (discussed at some length in Chapter 2); (2) an accurate estimate of crack closure behavior for the specific loads, material, and geometry; and (3) an accurate means of incorporating stress and strain ranges and closure information into the cyclic EPFCG parameter, ΔJ_{eff}. The primary exceptions to this engineering approach are those applications in which alternative crack growth mechanisms come into play, such as ductile tearing near instability, or creep-fatigue mechanisms at appropriate temperatures and times.

Characterization of the primitive parameters–loads, materials, and geometries–is addressed to only a limited extent in this report. The general task of component stress analysis is clearly beyond the scope of this contract, although some recommendations for the characterization of local stress or strain fields are given where appropriate. The task of identifying the appropriate component and crack geometry for a given application is also left to the reader. In general, the correlating parameters J and K are given for idealized geometries. Some assistance is given for the task of identifying or characterizing relevant material properties. While specific data bases or test methods are not addressed, material property requirements are clearly identified, and recommendations are forwarded for estimating those necessary properties that may not be readily available from data which are more likely available.

The presentation and discussion of crack growth algorithms that follows begins with remarks about the construction of the effective cyclic range of the J-integral, ΔJ_{eff}, from a monotonic J estimation form. Included here are discussions of the rationale and proper manner for the incorporation of closure information into the parameter estimate. Detailed descriptions of different analytical methods to quantify specific crack closure behavior in different situations are then presented. Subsequent discussions address specific algorithms for crack instability and the estimation of material properties, followed by general discussions of issues associated with load interaction effects and creep-fatigue effects.

3.2 Formulation of Closure-Corrected ΔJ

As noted in Chapter 1, the correct mathematical definition of ΔJ is not $J_{max} - J_{min}$, but is instead given by replacing the stress, strain, traction, and displacement quantities in the original integral equation for J with their respective ranges. Following this argument, it is possible to derive an engineering expression for ΔJ from the monotonic J equations presented in Chapter 2 by appropriately replacing single values of the load, stress, and strain with their respective ranges.

In doing this, however, it is essential to observe the differences between monotonic and cyclic constitutive relationships. According to Masing's hypothesis, the cyclic (hysteretic) stress-strain relationship can be obtained approximately for materials that exhibit symmetric behavior in tension and compression by "doubling" the monotonic stress-strain curve (Bannantine, Comer, and Handrock 1990). The original monotonic constitutive equations may be used to describe cyclic hysteretic behavior if the original single values of stress and strain are replaced by the stress

and strain amplitudes. For a Ramberg-Osgood material, for example, the cyclic constitutive law can be written as

$$\frac{\Delta\varepsilon}{2\varepsilon_0} = \frac{\Delta\sigma}{2\sigma_0} + \alpha\left(\frac{\Delta\sigma}{2\sigma_0}\right)^n \tag{3.1}$$

Note that this constitutive relationship may change further if the material cyclically hardens or softens. In this case, the functional form of Eqn 3.1 stays the same, but the values of the Ramberg-Osgood constants are replaced by their stable cyclic counterparts α', σ_0', ε_0', and n'.

The other critical difference between the monotonic J expression and the cyclic ΔJ expression is the influence of crack closure. Dowling and Begley (1976) and Dowling (1976), in their groundbreaking investigations of ΔJ as a correlating parameter for EPFCG, recognized that the fatigue crack was closed during a portion of the loading cycle. The significant impact of this crack closure on the energy associated with crack extension was immediately obvious from the load vs. load line displacement data. Since Dowling and Begley were measuring ΔJ, according to an energy definition, from the area under the load-displacement curve (Eqn 1.7), they recognized the need to identify the crack closure level and incorporate this information into their estimate of ΔJ. Dowling (1977) did not account for crack closure in his first ΔJ estimates for small semi-elliptical surface cracks in smooth, axial specimens only because he was unable to identify a crack opening level from remote hysteresis loops or low-power optical microscopy.

Subsequent researchers have been remarkably strong in their agreement that crack closure is an important element of accurate ΔJ estimates. For example, of the thirty-three papers cited in Section 1.2.3 to illustrate the breadth of research experience with ΔJ, twenty-three papers incorporated crack closure information into their calculations of ΔJ. Most of the ten papers that omitted closure information from ΔJ did so only because their authors were unable to detect or measure closure levels for very small cracks, and chose instead to assume conservatively that the crack was open throughout the fatigue cycle. This overwhelming majority is all the more remarkable in view of the considerable controversy in the area of SSY fatigue crack growth studies regarding the existence and utility of crack closure as a characterizing feature of fatigue cracking in that regime.

Concerns have been raised previously about whether crack closure effects compromise the path-independence of ΔJ. The work of Lamba (1975), Wuthrich (1982), and Tanaka (1983) in demonstrating the path-independence of a properly-defined ΔJ was cited in Chapter 1, but those authors did not consider the closure phenomenon, and it is not clear how to include closure considerations in a rigorous proof of path-independence. However, Kubo et al. (1989) have performed an important numerical analysis of ΔJ with an elastic-plastic finite element simulation of a growing fatigue crack. They calculated ΔJ numerically and demonstrated path-independence when the crack opening point was employed as a reference point for the evaluation. Kubo et al. also showed that ΔJ based on the crack opening load appropriately characterized the range of the stress, strain, and displacement in the vicinity of the crack tip.

The cited authors did employ a variety of methods to incorporate closure into their parameter estimates. The approach adopted here is illustrated in Figure 3.1, which shows the influence of crack closure on the effective hysteresis loop energy: the effective elastic and plastic strain energies are denoted in the figure by the cross-hatched areas. This approach is conceptually consistent with the fundamental definition of J as a measure of energy. The elastic strain energy in the absence of closure would be equal to the product $\frac{1}{2}\Delta\sigma\Delta\varepsilon_e$. The effective elastic strain energy associated with the hysteresis loop is then given by $\frac{1}{2}U^2\Delta\sigma\Delta\varepsilon_e$, where U is the effective stress intensity factor range ratio that characterizes crack closure

$$U = \frac{K_{max} - K_{open}}{K_{max} - K_{min}} \tag{3.2}$$

Here K_{open} is the applied stress intensity factor at which the crack first becomes fully open during the load-increasing portion of the cycle, and K_{max} and K_{min} are the maximum and minimum stress intensity factors in the cycle, respectively. The plastic strain energy in the absence of closure is a large fraction of the product $\Delta\sigma\Delta\varepsilon_p$; for an elastic-perfectly plastic material it would be exactly equal to that simple product. The effective plastic strain energy, taking closure into account, is then approximately equal to $U\Delta\sigma\Delta\varepsilon_p$: the height of the hysteresis loop is decreased by the factor U, whereas the width of the hysteresis loop is roughly unchanged for typical crack opening stresses. Therefore, the crack closure factor U should have an impact on both the elastic and plastic terms of ΔJ, but not the same impact on both terms.

Returning now to the fundamental definition of the cyclic ΔJ as the J-integral with single values of stresses, strains, and loads replaced by their ranges, it is possible to write simple equations for ΔJ by analogy to Eqns 2.1 through 2.14 for the monotonic J.

The general engineering expression for the closure-corrected cyclic ΔJ, therefore, comprises elastic and plastic components where

$$\Delta J_{eff}(c,\Delta P) = \Delta J_e^{eff}(c_e,\Delta P) + \Delta J_p^{eff}(c,\Delta P) \tag{3.3}$$

The first-order plastic corrected value of the effective elastic ΔJ_e is related directly to the effective stress intensity factor range by the expression

$$\Delta J_e^{eff}(c_e,\Delta P) = \frac{\left[U\,\Delta K(c_e,\Delta P)\right]^2}{E'} \tag{3.4}$$

Note that this formulation predicts a U^2 influence of closure on the elastic term, consistent with the energy-based argument of Figure 3.1.

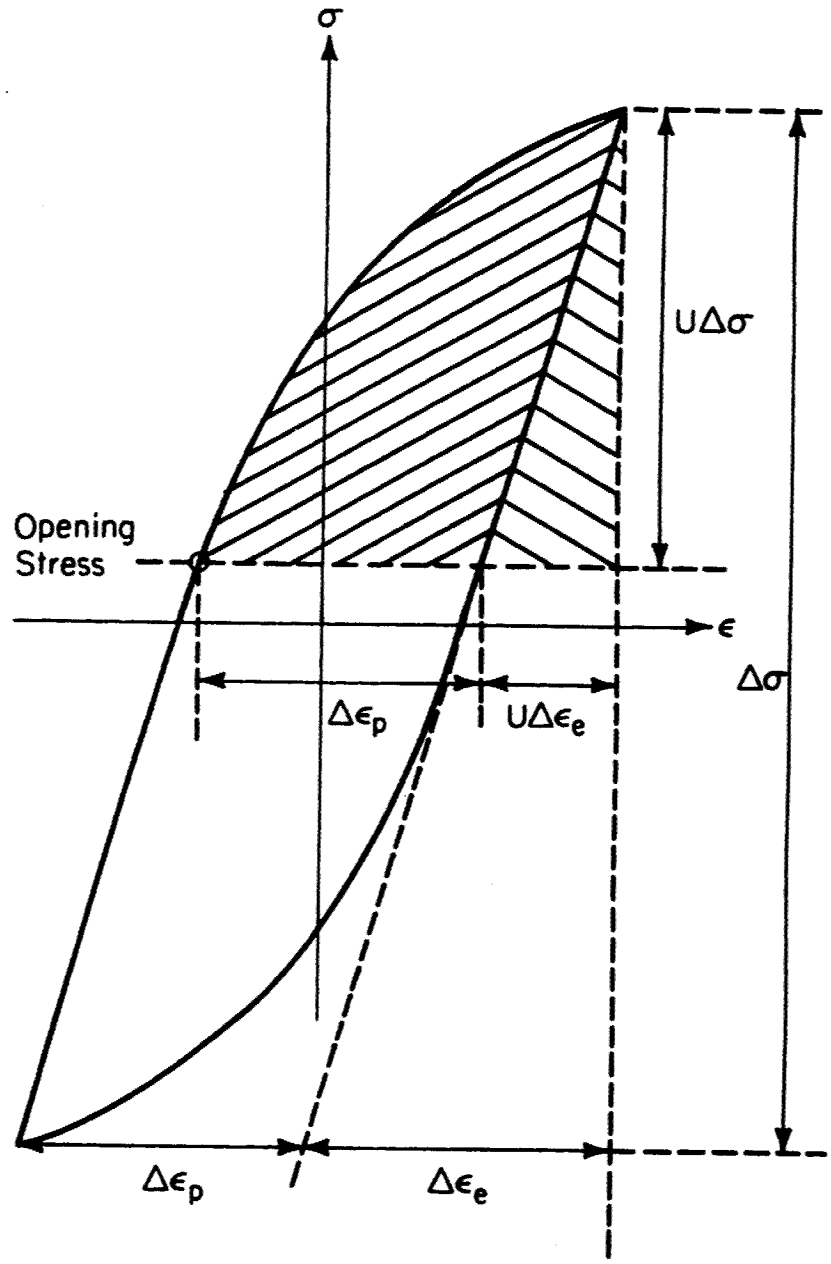

Figure 3.1. Schematic representation of hysteresis loop showing opening stress level and corresponding estimates of effective stress and strain ranges.

The effective crack length for cyclic loading, c_e^{Δ} (here the adjective "effective" indicates a plasticity-modified crack length, not the influence of crack closure), is now given by

$$c_e^{\Delta} = c + \phi^{\Delta} \Delta r_y \tag{3.5}$$

where the cyclic crack tip plastic zone size correction is determined by the terms ϕ^{Δ} and Δr_y that are defined respectively as

$$\phi^{\Delta} = \frac{1}{1 + \left(\frac{\Delta P}{2P_o(c)} \right)^2} \tag{3.6}$$

$$\Delta r_y = \frac{1}{\beta\pi} \left(\frac{n-1}{n+1} \right) \left(\frac{\Delta K(c, \Delta P)}{2\sigma_o} \right)^2 \tag{3.7}$$

Note that the effective crack length is calculated on the basis of the cyclic plastic zone size rather than the monotonic plastic zone size, and that the cyclic plastic zone size is computed on the basis of the cyclic yield stress $2\sigma_0$, consistent with the original formulation of Rice (1967). This is all consistent with the approach of Newman (1992a), who investigated the growth of small fatigue cracks under intermediate scale yielding. Newman suggested that the effective crack length was best given by

$$c_e^{\Delta} = c + \frac{\Delta r_y}{4} \tag{3.8}$$

where Δr_y is given by

$$\Delta r_y = \left(1 - \frac{K_{open}}{K_{max}} \right)^2 \frac{r_y}{4} \tag{3.9}$$

and the monotonic plastic zone size r_y is calculated using the maximum applied stress intensity factor.

Newman is correct that crack closure has a direct influence on the size of the cyclic plastic zone (McClung, 1991b), although the actual influence is slightly more complex than his simplified expression, which can underestimate Δr_y. However, for simplicity, the effect of closure to reduce the plastic zone size has been conservatively neglected in the present formulation. But this simplification is not particularly significant. Dowling (1987) has shown that the effective crack length correction term is numerically significant in a J solution only for a narrow range of the intermediate scale yielding regime. In small-scale yielding, $\Delta r_y << a$, and the correction is minimal. In large-scale yielding, $J_p >> J_e$, and so a small correction in the elastic term is not significant. In the intermediate scale yielding regime, if $\Delta K/(2\sigma_0)$ is large enough to cause a potentially significant crack length correction, then the crack opening level is probably relatively close to zero, so that the

effect of the Newman $(1-K_{open}/K_{max})^2$ term is still relatively small. For increased accuracy (reduced conservatism), however, it may be useful to investigate this correction in more detail in future work.

In general, the Newman formulation for the effective crack length, Eqn 3.8, gives an apparently smaller crack length correction than the formulation in the present methodology. However, his formulation was based on a Dugdale estimate of the plastic zone size, which gives a slightly larger value than the Irwin-type estimate employed in the present methodology.

By analogy with the monotonic fully-plastic component of J (Eqn 2.6), the fully-plastic component of ΔJ_{eff} can be written in the EPRI scheme as

$$\Delta J_p^{eff}(c,\Delta P) = 4U\alpha\epsilon_o\sigma_o\frac{c}{W}(W-c)h_1\left(\frac{c}{W},n\right)\left(\frac{\Delta P}{2P_o(c)}\right)^{n+1} \tag{3.10}$$

Note the multiplier of two on the yield load and the leading factor of four on the entire expression; both of these factors arise from the cyclic (hysteretic) doubling of the stress-strain curve (Eqn 3.1). Note, also, the closure correction by the simple multiplier U (not U^2 as in the elastic term). The correctness of this choice is perhaps more obvious in the context of an equivalent but simpler version of the EPRI fully-plastic scheme. The original normalizations of He and Hutchinson (1981) were written in the general form

$$J_p = \sigma\varepsilon_p a\, h_1 \tag{3.11}$$

where the subscripts p have been added to clarify that He and Hutchinson were treating a fully plastic material. The cyclic analog of Eqn 3.11 (replacing single values by their ranges) is the simple form

$$\Delta J_p = \Delta\sigma\Delta\varepsilon_p a\, h_1 \tag{3.12}$$

The energy considerations associated with Figure 3.1 indicated that the effective value of the plastic component should then be written

$$\Delta J_p^{eff} = U\Delta\sigma\Delta\varepsilon_p a\, h_1 \tag{3.13}$$

This equation can be expanded by expressing the cyclic plastic strain in terms of the cyclic stress for a cyclic Ramberg-Osgood material to give the general form

$$\Delta J_p^{eff} = 4U\alpha\sigma_o\varepsilon_o a\, h_1\left(\frac{\Delta\sigma_\infty}{2\sigma_0}\right)^{n+1} \tag{3.14}$$

which is generically the same form as Eqn (3.10).

In order to preserve this same functional dependence of ΔJ_p^{eff} on U in reference stress estimates for ΔJ_p^{eff}, we must write the form

$$\Delta J_p^{eff}(c,P) = U\mu V\left(\frac{c}{W}\right)\alpha\,\Delta J_e(c,P)\left(\frac{\Delta P}{2P_o^*(c)}\right)^{n-1} \tag{3.15}$$

Note here that U is not included in the ΔJ_e term, because that would introduce an inappropriate U^2 factor on ΔJ_p^{eff}. This RSM formulation can also be easily extended to materials with arbitrary stress-strain behavior, being careful to observe the cyclic hysteretic doubling of whatever constitutive relationship is employed.

3.3 Algorithms to Estimate Crack Opening Stresses

The earliest characterizations of crack opening stresses were based on direct experimental measurements, beginning with the original investigations of Elber (1970, 1971). Many test data have been reported for closure under SSY conditions, but relatively few experimental results are available under elastic-plastic conditions. Dowling and Begley (1976) and Mowbray (1979), in their early work on ΔJ, estimated closure levels from the cusp in the unloading line of the load-displacement curve. When cracks are small relative to overall specimen dimensions, which is typically the case for practical EPFCG problems, no global compliance changes are visible, and this technique fails. McClung and Sehitoglu (1988) measured closure in small edge cracks under elastic-plastic cycling with a high-magnification replica technique. Iyyer and Dowling (1986), Rie and Schubert (1987), and Hatanaka et al. (1987a, 1987b) attempted to measure closure for surface cracks in low-cycle fatigue specimens via low-magnification inspection of the crack opening displacements at the specimen surface, but this technique is disadvantaged by several difficulties (McClung and Sehitoglu, 1991).

A more satisfying approach to determining crack opening stresses in the context of practical crack growth algorithms is based on rigorous mechanics analyses of the closure phenomenon. The limited experimental data available, although insufficient to construct empirical closure models, is nonetheless important as a means of verifying the mechanics models.

The first mechanics models of closure were all generally based on a Dugdale (1960) or Bilby-Cottrell-Swinden (1963) strip-yield model that has been modified to leave material in the wake of the advancing crack tip. These include the early efforts of Dill and Saff (1976), Shiratori et al. (1977), Fuhring and Seeger (1979), and Budiansky and Hutchinson (1978); the slightly later and more extensive work of Newman (1981, 1982), and the more recent contributions of Sehitoglu (1985a, 1985b) and Ibrahim et al. (1986). The first significant research in elastic-plastic finite element (FE) modeling of growing fatigue cracks was conducted independently by Newman (1976) and Ohji et al. (1974) in the early 1970s, and in the ensuing twenty years the FE method has been

applied to study plasticity-induced crack closure in over seventy additional publications (McClung and Sehitoglu, 1989a; McClung, 1992). Limited studies of closure based on the boundary element method (Cruse and Raveendra, 1988) and superdislocation models (Kanninen and Atkinson, 1980) are also available.

It is not the purpose of this report to compare the results of all the various closure models exhaustively. Some comparisons, along with critical discussions of the various modeling issues which impact on the accuracy and validity of the results, are available elsewhere (McClung and Sehitoglu, 1989a). While the specific numerical results vary from model to model, the general trends of crack opening stresses with various parameters are nearly always similar, and those models that satisfy certain modeling criteria are usually in reasonably good quantitative agreement. Disagreements in U rarely exceed ten or twenty percent, which is usually a negligible contribution to the total uncertainty in crack growth rate.

Newman has exercised his modified-Dugdale closure model, available to the general public as the FASTRAN-II computer code (Newman, 1992b), to develop a simple closed-form equation (Newman, 1984) which gives crack opening stresses as a function of applied stress, stress ratio, and crack-tip constraint. This equation is written as

$$\sigma_{open}/\sigma_{\max} = A_0 + A_1 R + A_2 R^2 + A_3 R^3 \qquad \text{for } R \geq 0 \tag{3.16}$$

$$\sigma_{open}/\sigma_{\max} = A_0 + A_1 R \qquad \text{for } -2 < R < 0 \tag{3.17}$$

when $\sigma_{open} \geq \sigma_{min}$. The coefficients are

$$A_0 = \left(0.825 - 0.34\alpha_c + 0.05\alpha_c^2\right)\left[\cos\left(\pi\sigma_{\max}/2\sigma_{flow}\right)\right]^{1/\alpha_c} \tag{3.18}$$

$$A_1 = \left(0.415 - 0.071\alpha_c\right)\sigma_{\max}/\sigma_{flow} \tag{3.19}$$

$$A_2 = 1 - A_0 - A_1 - A_3 \tag{(3.20}$$

$$A_3 = 2A_0 + A_1 - 1 \tag{3.21}$$

Here α_c is the constraint factor (the subscript has been added here to avoid confusion with the similar symbol in the Ramberg-Osgood equation). For pure plane stress conditions, α_c is set equal to 1.0. The pure plane strain limit was originally identified by Newman as $\alpha_c = 3.0$, but smaller values of α_c (e.g., 1.73) (McClintock and Irwin, 1965) have also been chosen to represent plane strain in some applications. The flow stress σ_{flow} is originally the yield stress for the Dugdale perfectly-plastic

material, but it has been re-interpreted as the average of the uniaxial yield (σ_{ys}) and ultimate (σ_{ult}) strengths in order to account approximately for strain hardening behavior. Suggestions on alternative means of estimating σ_{flow} for strain hardening materials, or for materials that cyclically harden or soften, in the face of limited material property data are discussed in Section 3.5.2.

This equation has been chosen as the primary means of estimating crack closure behavior for the practical EPFCG crack growth algorithms, for the following reasons. First of all, only Newman (1984) and Ibrahim et al. (1986) have derived such a simple closed-form equation. All other closure analyses are available only as graphical or tabular results, and for any given model, typically only limited results are available. Development of any new set of simple equations to predict closure would not only be a time-consuming exercise, it would likely not be supported by a sufficiently broad data base. The Ibrahim et al. equation gives generally similar results to the Newman equation under some conditions, but it considers only plane stress, not plane strain or any other constraint state.

The Newman equation gives satisfactory agreement with the results of more advanced closure models, such as FE models, and it is nearly always conservative if not highly accurate. It should be noted that the original Newman model actually addresses only central cracks in infinite, elastic-perfectly plastic bodies under pure mode I loading, and the influence of constraint is addressed only approximately. However, systematic comparisons with detailed FE closure results have confirmed that the Newman model agrees relatively well under those limited conditions. More important, these comparisons have indicated how the Newman equation can be interpreted and applied to predict closure levels satisfactorily under a much wider range of load, geometry, and material conditions. Some of these comparisons are shown in conjunction with later discussions.

In short, the Newman equation has been adopted because it is robust (it addresses a wide variety of crack growth problems), it is simple (the closed-form equation permits a rapid, direct computation of crack opening stress), it is accurate (it has shown acceptable agreement with relevant experimental and advanced numerical results), and it is generally conservative under those conditions when its exact accuracy is less certain.

It should be noted that crack closure can arise from other sources besides crack wake plasticity, such as crack surface roughness and crack surface oxides (Suresh, 1991). However, roughness and oxide effects are generally more significant in the near-threshold regime and for cracks that are microstructurally-small. Crack wake plasticity and the associated residual stresses ahead of the crack tip are generally the dominant closure mechanism in the Paris regime, especially for large amplitude fatigue cycles that can crush asperities or oxide debris on the crack surface and hence reduce their contributions to closure. For these reasons, modeling of crack closure in the current methodology is limited to plasticity-induced phenomena. Fortunately, this closure mechanism is by far the most mature from the modeling perspective. However, it should be emphasized that the Newman approach adopted here may not be accurate in the SSY near-threshold regime when other closure mechanisms come into play.

3.3.1. *Effects of Maximum Stress, Stress Ratio, and Stress State*

The predictions of the Newman equation for a variety of applied stresses, stress ratios, and stress states are illustrated in Figures 3.2 and 3.3. The figures show, first of all, that normalized crack opening stresses are typically a strong function of normalized maximum stress. This result is particularly significant for EPFCG, because $\sigma_{max}/\sigma_{flow}$ values under elastic-plastic conditions are typically much larger than under small-scale yielding conditions. A failure to recognize and address this effect can lead to nonconservative crack growth rate predictions.

This important result is consistent with a wealth of other experimental, analytical, and numerical evidence for cracked configurations which are outside the near-threshold regime and the near-net-section-yielding regime (McClung, 1991c). These two alternative regimes are discussed later in the report. Agreement between the Newman equations and recent FE closure results for a low-hardening plane stress material at two stress ratios is shown in Figure 3.4. The $R = 0$ comparison is a good example of a situation in which the Newman model is conservative when its apparent accuracy may be lower.

One of the "limitations" of the original Newman model is that the Dugdale crack upon which it is based is a small-scale yielding model without strict applicability to general elastic-plastic behavior. In addition, the FASTRAN computer code experiences numerical difficulties above $\sigma_{max}/\sigma_{flow}$ values around 0.7, and the closed-form equation was derived from results between $\sigma_{max}/\sigma_{flow} = 0.2$ and 0.8. In order to solve a complete range of EPFCG problems, however, it must be possible to accommodate larger values of the normalized maximum stress.

Fortunately, the Newman equation is sufficiently smooth and well-behaved that it also gives good predictions at higher values of $\sigma_{max}/\sigma_{flow}$. Note in Figure 3.4 the good agreement between simple equation and FE results out to maximum stresses approaching the flow stress, especially for the significant fully-reversed condition. The Newman equation also gives the correct limiting result that $U = 1$ for $R \geq 0$ whenever the maximum stress approaches or exceeds the flow stress. Another confirmation of the validity of this "extrapolation" is the excellent agreement between the Newman equation and actual experimental measurements of crack closure at large maximum stresses (McClung and Sehitoglu, 1988), as shown in Figure 3.5. The experimental and model material here was a 1026 steel with significant strain hardening (the FE model directly incorporated a linear hardening constitutive law with large slope), so the comparison also confirms the validity of the $\sigma_{flow} = (\sigma_{ys} + \sigma_{ult})/2$ approach to accommodating strain hardening with the Newman model. This is one of the few conditions where the Newman model predicts higher crack opening levels than the FE model, but it is interesting to note that the Newman model agrees more closely with the experimental data.

Therefore, it appears to be reasonable to apply the Newman equation to higher maximum stresses, not because the original Newman model is strictly valid under those conditions, but because the derived equation agrees well with comparable experimental and numerical results in that expanded regime.

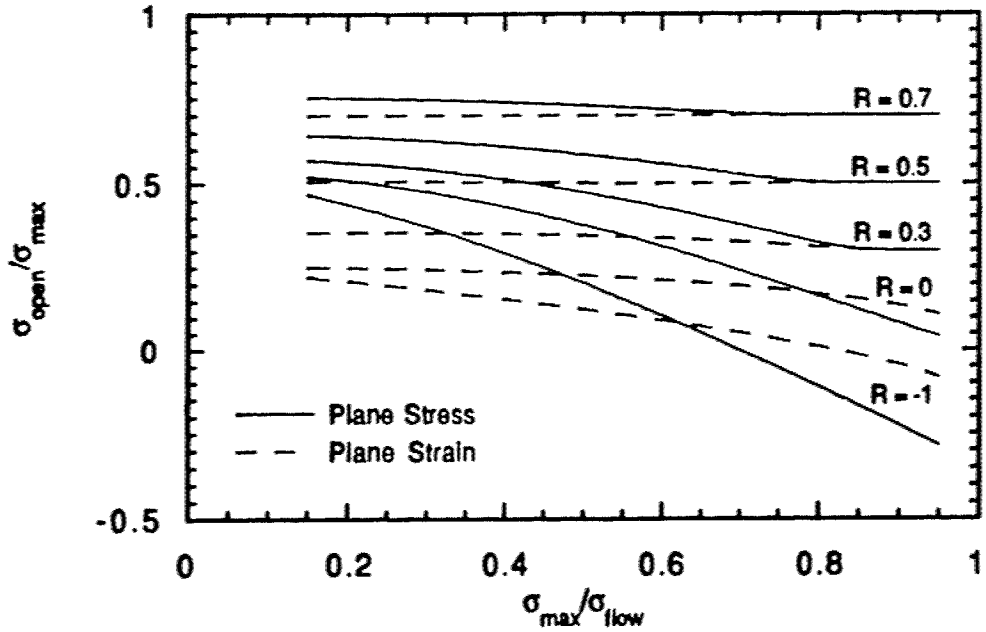

Figure 3.2. Normalized crack opening stresses based on Newman equation

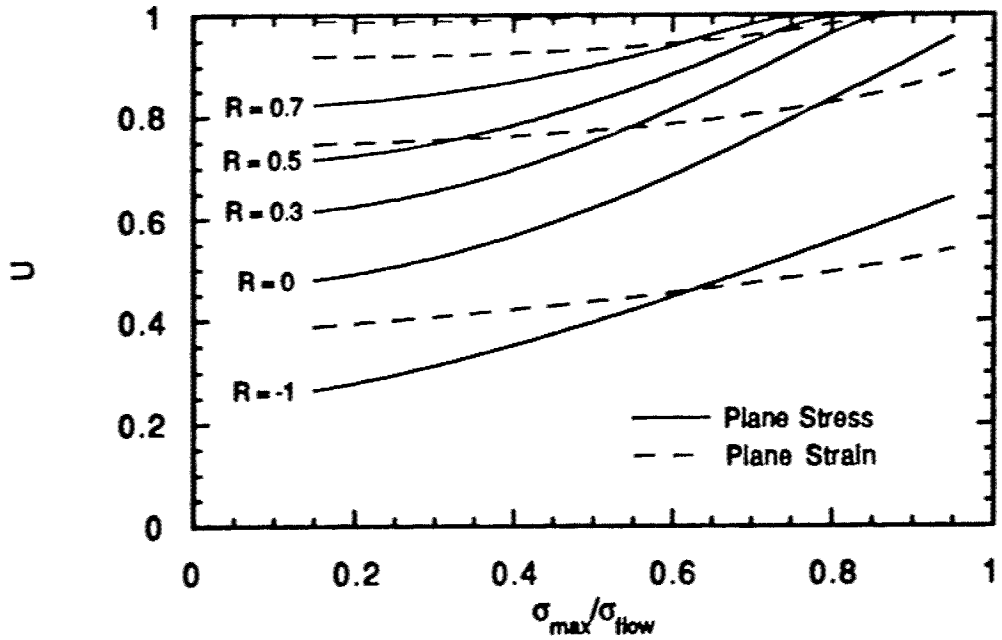

Figure 3.3. Effective stress range ratio based on Newman equation

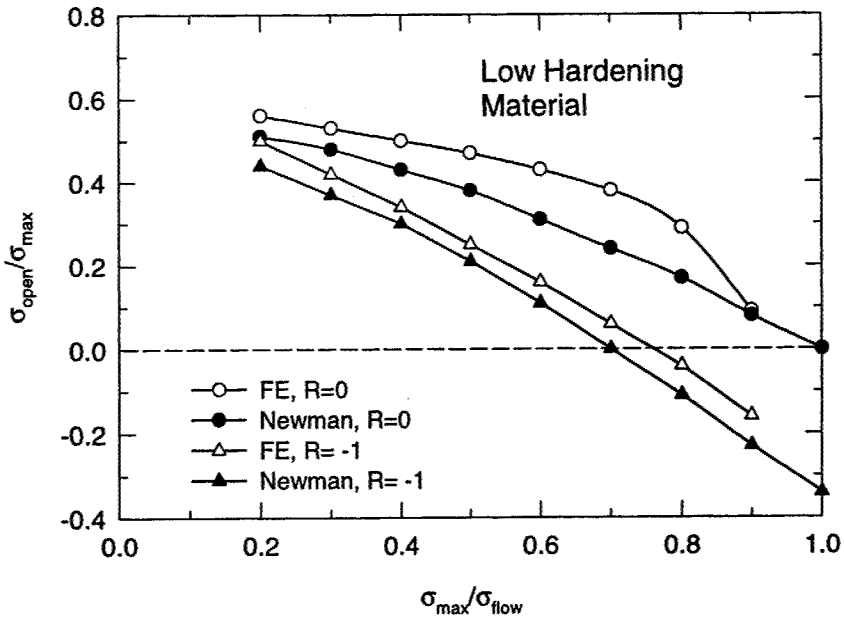

Figure 3.4. Comparison of crack opening stresses based on Newman equation and finite element modeling for a low or zero hardening material

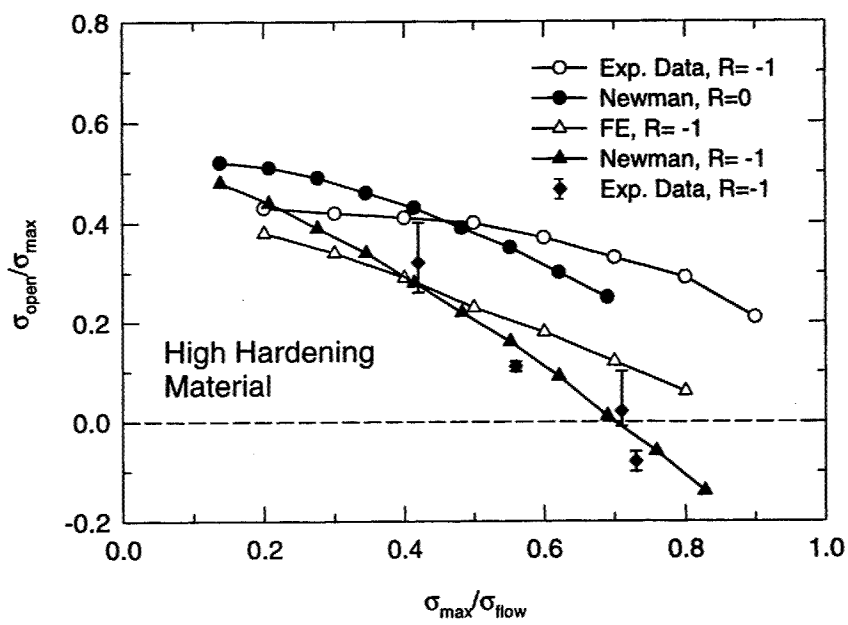

Figure 3.5. Comparison of crack opening stresses based on Newman equation, finite element modeling, and experimental measurements for a high hardening material

In a similar vein, the Newman equation was limited to $R \geq -1$ in its original derivation and publication. The equation appears to be well-behaved for slightly lower stress ratios (more negative), however, so small extrapolations are probably reasonable. Very few experimental data are available for comparison in this range, but some recent crack growth rate studies have suggested that the Newman equation predicts the correct trends at $R = -2$ (Bloom, 1994). Note that at higher positive stress ratios, the Newman model correctly indicates that crack closure occurs less and less (U approaches 1.0 more quickly).

As the Newman results indicate, crack opening stresses are typically lower in plane strain (higher constraint) than in plane stress at low and intermediate values of $\sigma_{max}/\sigma_{flow}$. At slightly higher $\sigma_{max}/\sigma_{flow}$ values, around 0.6 to 0.8, closure levels are relatively independent of stress state. As will be noted later, this regime is relatively common in EPFCG problems. At even higher applied stresses, when σ_{max} approaches σ_{flow}, crack opening stresses are actually computed to be slightly higher in plane strain than in plane stress. This somewhat surprising result has not yet been evaluated experimentally, primarily because of the great difficulty in making any experimental measurements of crack closure in true plane strain conditions, but the stress state trends of the Newman model have been independently confirmed and rationalized by finite element closure analyses (Lalor and Sehitoglu, 1988; Sun and Sehitoglu, 1992).

Quantitative estimation of crack opening stresses therefore requires an assessment of the appropriate stress state: plane stress, plane strain, or some intermediate constraint. In the context of the Newman modified Dugdale model, this choice is quantified in terms of the constraint factor α_c.

At least two basic approaches are possible to select the appropriate value of α_c. One approach is to make some sort of rigorous quantitative assessment of stress state. The traditional method for two-dimensional laboratory specimen geometries has been to compare the crack tip plastic zone size (the width ahead of the crack tip) with the specimen thickness. Full plane strain constraint is frequently assumed to exist (Clark, 1971; McGowan and Liu, 1980; Daiuto and Hillberry, 1984) whenever a criterion similar to that specified in ASTM E 399 (1998) is satisfied,

$$B \geq 2.5\left(\frac{K_{max}}{\sigma_{ys}}\right)^2 \tag{3.22}$$

where B is specimen thickness. Full plane stress conditions are typically assumed (Daiuto and Hillberry, 1984; Shahinian, 1976; Hertzberg and Paris, 1965) when the crack tip plastic zone width is on the order of one-half the specimen thickness or greater

$$B \leq \frac{2}{\pi}\left(\frac{K_{max}}{\sigma_{ys}}\right)^2 \tag{3.23}$$

When neither of these criteria is satisfied, partial constraint is assumed.

For three-dimensional configurations, it has been traditional to assume that quarter-elliptical corner cracks, semi-elliptical surface cracks, and elliptical embedded cracks are characterized by plane strain in the specimen interior, but that surface or corner cracks exhibit plane stress deformation at the specimen surface. However, this traditional approach leaves open two questions. First of all, which "plane strain" value of α_c is most appropriate: 3.0? 1.73? Or some other value? And second, how is constraint diminished under elastic-plastic conditions when plasticity becomes widespread? If constraint in two-dimensional configurations decreases when the crack-tip plastic zone size becomes large compared to the specimen thickness, how does constraint in three-dimensional configurations change when the crack-tip plastic zone size becomes large compared to the remaining ligament?

A second approach to selecting α_c is more empirical in nature: the optimum α_c is chosen on the basis of which value will best correlate the current experimental fatigue crack growth rate data. For example, α_c may be used as a fitting parameter to optimize the regression of FCG data at different stress ratios. This is the approach adopted in the current NASGRO computer code. Newman also follows this approach, although he also imposes stress state transitions as the crack grows and the plastic zone size grows larger in comparison to specimen dimensions (Newman et al., 1986; Newman, 1996).

In the absence of rigorous quantitative answers to the previous questions about the numerical characterization of stress state, and for consistency with the current NASGRO approach, it appears prudent to adopt the more empirical approach to the selection of α_c. However, in the absence of adequate experimental data (as will often be the case), it appears prudent to assign $\alpha_c = 3$ (full plane strain) to surface, corner, and embedded cracks under elastic-plastic conditions. This approach generally gives the most conservative (lowest) crack opening stresses. A constraint parameter of $\alpha_c = 3.0$ is also recommended for two-dimensional plane strain configurations, because the Newman model with $\alpha_c = 3.0$ agrees most closely with the limited experimental and numerical data for plane strain closure (McClung, Thacker, and Roy, 1991). In the absence of supporting experimental data under elastic-plastic conditions, it does not appear prudent to impose rigorous stress state transitions as the crack grows.

These stress state issues are investigated further in the experimental verification of the NASGRO EPFCG module, Appendix L.

3.3.2 Effect of Specimen Geometry

The original Newman FASTRAN model and most other mechanics analyses of crack closure have focused on the center-cracked plate under uniform tension, usually with a small ratio of crack length to specimen width so that finite width effects were minimized (or eliminated entirely, for infinite plate models). Systematic parameter studies of geometrical issues such as specimen configuration or large changes in crack length were virtually non-existent. Therefore, it has not been clear to what extent the "benchmark" center-cracked plate closure results were applicable to other specimen or structural geometries. For example, does the same functional dependence of $\sigma_{open}/\sigma_{max}$ on $\sigma_{max}/\sigma_{flow}$ hold, or does it somehow change for significantly different geometries?

In order to address these issues, a series of analytical investigations utilizing a FE closure model were conducted. The model was used to study closure at three different crack lengths for three different specimen geometries: center-cracked plate, single-edge-cracked plate under tension, and single-edge-cracked plate under pure bend. The details of these investigations are summarized in **Appendix H**.

The key result of these investigations, as shown in Figure 3.6, is that crack opening stresses $\sigma_{open}/\sigma_{max}$ are more accurately correlated by K_{max}/K_{flow} than by $\sigma_{max}/\sigma_{flow}$, where K_{max}/K_{flow} is given by*

$$\frac{K_{max}}{K_{flow}} = \frac{F\sigma_{max}\sqrt{\pi a}}{\sigma_{flow}\sqrt{\pi a}} \tag{3.24}$$

For the center-cracked infinite plate, $F = 1$, and so $K_{max}/K_{flow} = \sigma_{max}/\sigma_{flow}$. This implies that the Newman equations can be used equally well to predict crack opening stresses in other specimen geometries simply by replacing $\sigma_{max}/\sigma_{flow}$ in equations 3.16-3.21 with the calculated K_{max}/K_{flow}. The FE studies also showed that the Newman equation interpreted in this manner provided an accurate or slightly conservative lower bound to nearly all FE closure results obtained. The quality of the K_{max}/K_{flow} geometry correlation does deteriorate at larger values of K_{max}/K_{flow} (farther outside the small-scale yielding regime), but the Newman equation remains a conservative estimate.

Appendix H was published as an independent journal article in slightly modified form earlier in the contract (McClung, 1994). This publication prompted Liu and Wu (1997) to investigate further the effects of specimen geometry on crack closure using an extension of the Newman strip yield closure model that incorporated a two-dimensional weight function method. They studied the same three geometries plus one notched geometry at various stress ratios and obtained similar results. They confirmed that K_{max}/K_{flow} was a successful correlating parameter, especially in the small-scale yielding regime, slowly deteriorating outside this regime. They reported slightly stronger correlations at $R \geq 0$ and slightly weaker correlations at $R = -1$.

It appears reasonable to apply this same K_{max}/K_{flow} criterion to other specimen geometries which have not yet been explicitly studied, in the absence of other information. This unvalidated extension is supported by several factors. First of all, the criterion has an attractive rational foundation: it is entirely reasonable and perhaps even expected to characterize crack tip behavior in terms of the stress intensity factor rather than simply the nominal stress. Second, the geometries

---

* Note that in Figure 3.8 and some following figures, and in Appendix H, the term K_{flow} is denoted as $K_0 = \sigma_0\sqrt{\pi a}$. This nomenclature follows from historical usage in the finite element closure analysis, where the characteristic strength variable is σ_0, the intersection of the elastic and plastic lines in a bilinear stress-strain curve. For the low hardening materials represented in these figures, $\sigma_0 = \sigma_{flow}$, and so $K_0 = K_{flow}$. Furthermore, in some of these figures, and throughout Appendix H, the applied stress is denoted as S rather than σ, again following historical usage, to emphasize that the finite element stress is a nominal, far-field quantity, not the local stress in the vicinity of the crack tip.

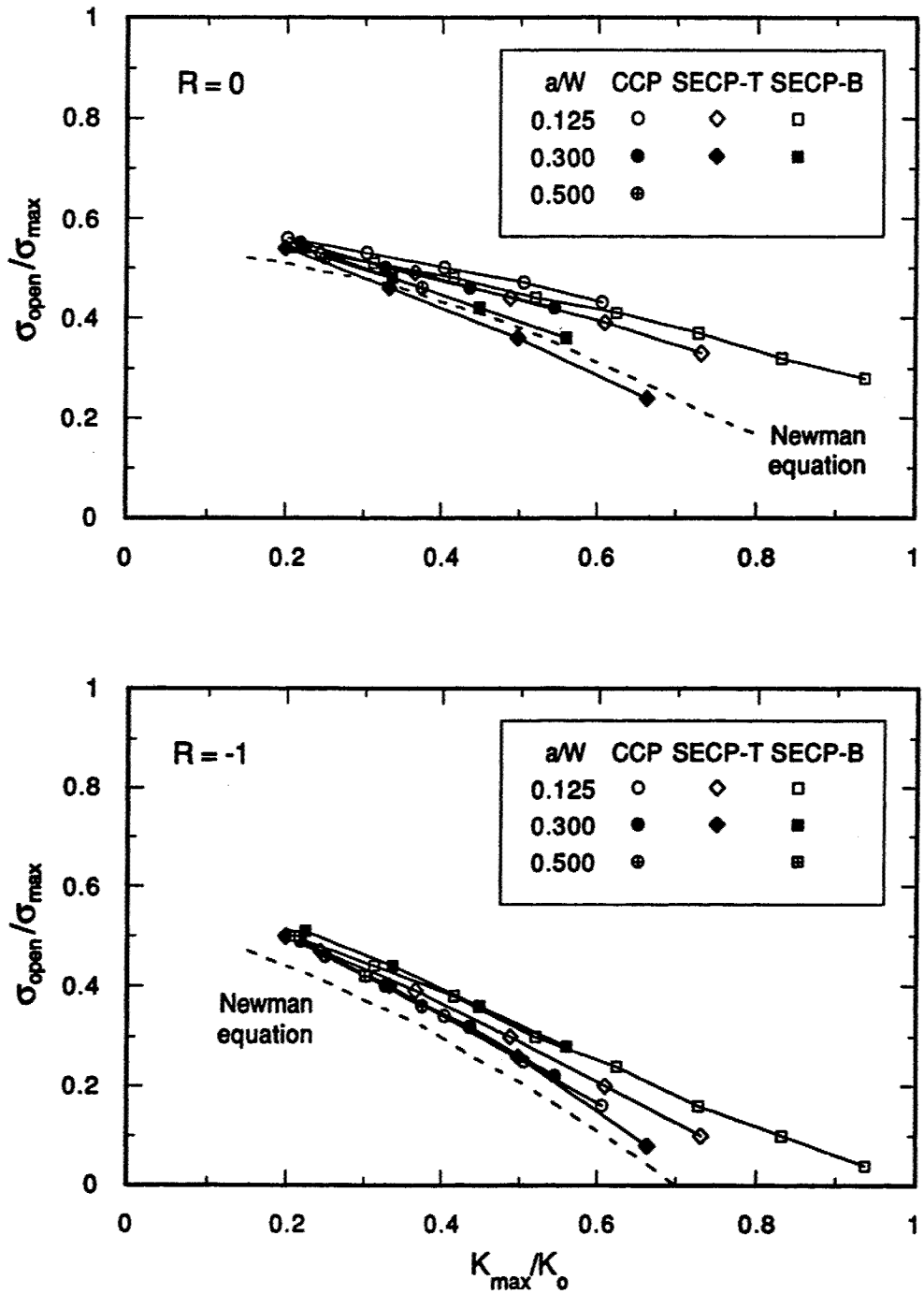

Figure 3.6. Normalized crack opening stress as a function of normalized stress intensity factor (top) $R = 0$ (bottom) $R = -1$

which have been examined directly represent an extreme range of configurations, with F values ranging from 1.0 to 2.8 and normalized crack depths ranging from $a/t = 0$ to 0.5, and including both tension and pure bend loading. Relatively few F or a/t values encountered in practical situations will exceed these values.

Of particular interest are three-dimensional geometries such as surface cracks, which are of great significance in reusable aerospace propulsion systems and other engineering applications. For these geometries, the F values at the maximum depth position can be as small as 0.64 for semi-circular cracks in uniform tension (and even smaller for larger $a/2c$ ratios), and so a K_{max}/K_{flow} criterion would suggest a slightly less pronounced effect of $\sigma_{max}/\sigma_{flow}$ on crack opening stresses. Unfortunately, since the surface flaw is a genuinely three-dimensional geometry, rigorous closure analyses are much more difficult and largely beyond the practical limits of current models or computing power. Furthermore, experimental measurements of closure for these configurations are also impractical. Therefore, this particular application of the criterion cannot be directly verified at the present time. The criterion can be indirectly verified, however, by comparing actual experimental FCG rate data with predictions based on these assumptions.

The use of an LEFM criterion such as K_{max}/K_{flow} (as opposed to some EPFM criterion based on J) to characterize closure behavior seems appropriate for several reasons. First of all, verification of the K_{max}/K_{flow} approach (and the $\sigma_{max}/\sigma_{flow}$ approach on which it is based) has been performed well outside the small-scale yielding regime; i.e., outside the normal region of K validity. Second, as deformation becomes increasingly elastic-plastic and K becomes less accurate as a descriptor of the crack tip fields, closure behavior approaches limiting conditions (e.g., no closure at $R = 0$), and this limit state is satisfactorily described by the K_{max}/K_{flow} approach (as described in the next section). Third, the K_{max}/K_{flow} approach provides an unambiguous criterion for secondary loading conditions, when J effects are considerably more complex.

One postscript on stress state effects is in order: As was observed earlier, the predicted crack closure levels for all constraint conditions (α_c ranging from 1 to 3) are all relatively similar when $\sigma_{max}/\sigma_{flow}$ (K_{max}/K_{flow}) is around 0.6 to 0.8. This is roughly the range of expected K_{max}/K_{flow} values for semi-circular surface cracks when σ_{max} approaches σ_{flow}, which may be satisfied in EPFCG problems. Therefore, stress state assessments in conjunction with closure predictions may not be required to be extremely accurate.

3.3.3 Effect of Net-Section and Gross Yielding

As discussed in the previous section, crack opening stresses in a variety of geometries appear to be correlated by the parameter K_{max}/K_{flow}. This correlation is strong in the SSY regime and generally holds into the ISY regime, although the quality of the correlation gradually deteriorates. A corollary of this relationship is that changes in the crack length do not cause changes in the crack opening stress, unless those changes in crack length also introduce significant changes in the geometry correction factor, F, contained in the expression for K. This corollary is consistent with a wealth of experimental and analytical evidence (McClung, 1991c).

However, as the crack length (or the applied stress) increases to the point that the remaining ligament is significantly plastic, this relationship between K_{max}/K_{flow} and $\sigma_{open}/\sigma_{max}$ appears to deteriorate (McClung, 1991c). Crack opening stresses drop off with additional crack growth. This change likely occurs because the elastic constraint which confines the residual plasticity in the vicinity and wake of the crack tip (the fundamental mechanism of plasticity-induced closure) is significantly diminished.

This effect is illustrated in Figure 3.7, which shows crack opening stresses from a FE simulation of a single growing fatigue crack (center crack, nominal a/W around 0.5) at $R = 0$ and an applied stress of $\sigma_{max}/\sigma_{flow} = 0.41$. Initially, σ_{open} remains constant as the crack extends. As the nominal net section stress reaches about $0.8\sigma_0$, however, σ_{open} begins to drop off. The deterioration in σ_{open} is appreciable by the time the nominal net section stress reaches σ_0, such that σ_{open} appears to be rapidly approaching zero.

The ASTM standard test method E647 for measurement of fatigue crack growth rates requires that the nominal net-section stresses in center-crack tension (ASTM designation M(T), middle-crack tension) specimens remain lower than 0.80 of yield. A related validity criterion for the compact tension specimen requires than the nominal crack-tip plastic zone size (PZS) be less than 0.25 of the remaining ligament, b. This PZS/b criterion is nearly the same as the nominal net-section stress criterion for the MT specimen. Limited FE closure investigations suggest that these two criteria may also provide rough rules-of-thumb to indicate when crack closure behavior begins to be influenced by ligament plasticity effects. However, it should be emphasized that these criteria have not been systematically validated for this particular purpose.

Finite element closure results that violate one or both of these two criteria are shown in Figure 3.8. The specimen geometries (and the specific FE models) are the same as those considered previously in studies of specimen geometry effects. In order to apply the net-section stress criterion to the SECP-bend geometry, the criterion was reinterpreted in terms of the relationship between the nominal applied stress and the nominal limit stress for an elastic-perfectly plastic material. Details are given in Appendix H. In Figure 3.8, the ratio of applied stress to limit stress ranges from 0.8 to about 1.1, and the ratio of PZS to b ranges from 0.25 to about 0.35. The trend lines from other analyses satisfying both criteria (smaller K_{max}/K_{flow}) were included on the figure for comparison purposes. In general, σ_{open} dropped off somewhat more rapidly with increasing K_{max}/K_{flow} when either criterion was violated, especially at $R = 0$. However, the crack opening stresses continued to follow expected trends for some configurations, especially at $R = -1$. Note, also, that the Newman equation is still an approximate lower bound for most of the data shown.

However, several questions remain. First, is it more appropriate to characterize net-section yield (or limit stress) and PZS sizes in terms of the yield stress (e.g., the 0.2 percent offset yield stress) or the flow stress (typically, the average of yield and ultimate)? The ASTM criteria for FCG testing cited above are formally expressed in terms of the yield stress. However, the test method recognizes that for materials exhibiting appreciable strain hardening, this approach may be unnecessarily conservative. Therefore, the ASTM test method offers an alternative set of criteria based on the flow stress. Since the flow stress has already been adopted in these practical algorithms

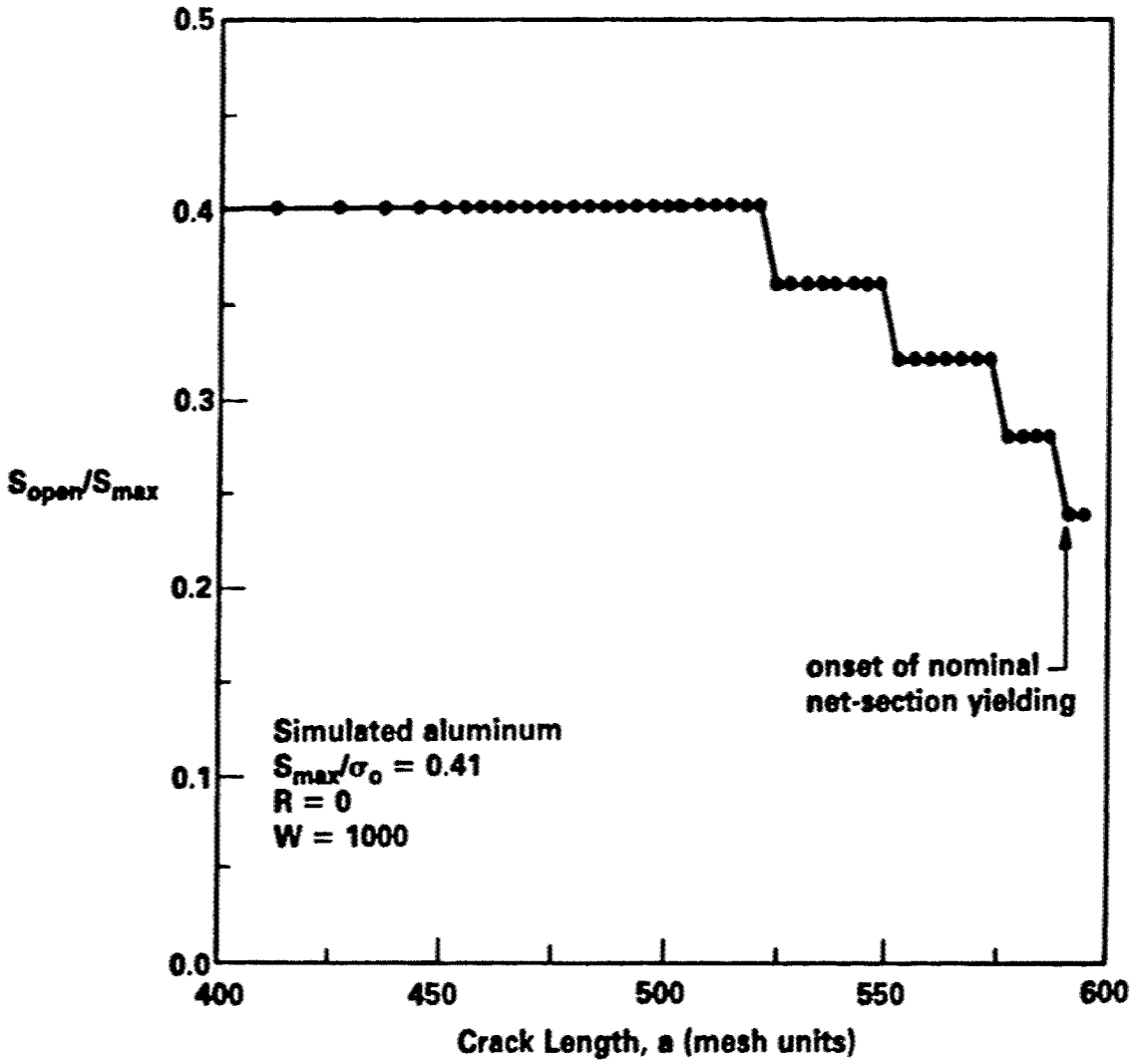

Figure 3.7. Finite element simulation of a growing fatigue crack showing decreases in crack opening levels as net-section yielding is approached.

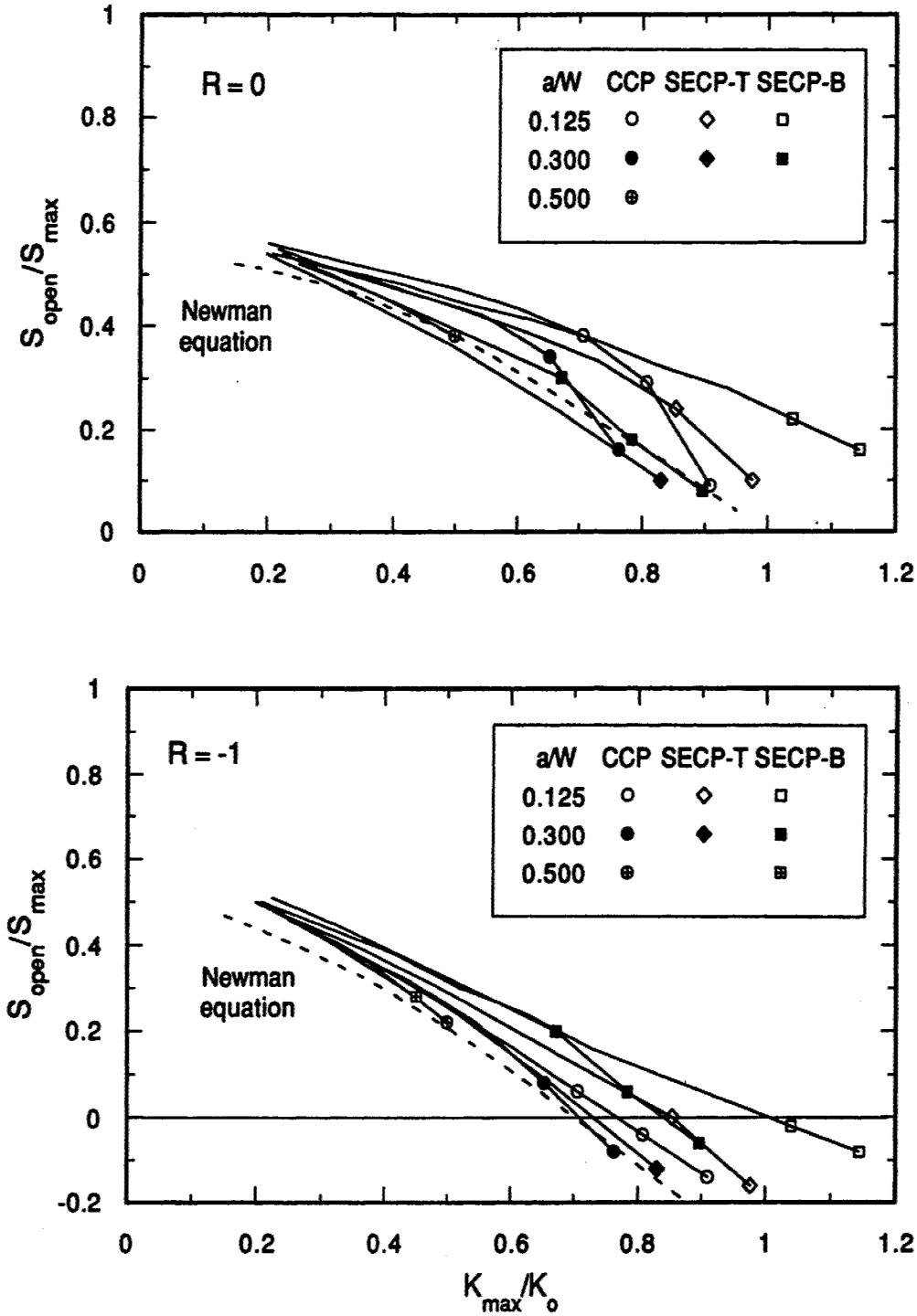

Figure 3.8. Normalized crack opening stress as a function of normalized stress intensity factor for conditions of significant ligament plasticity. (top) $R = 0$ (bottom) $R = -1$

as an acceptable (albeit approximate) means of addressing the effects of strain hardening on closure, it appears reasonable to continue the use of the flow stress in criteria for ligament plasticity effects. This choice further delays the predicted onset of net-section yielding effects.

A second question is the proper manner in which to apply the K_{max}/K_{flow} approach when σ_{max} is greater than yield. For example, when the maximum (near-surface) stresses in a bending configuration are greater than σ_{ys}, some stress redistribution will occur, and the actual maximum stresses at the outer fiber will be less than the values predicted by elasticity theory. Which stresses, elastic or actual, should be used to calculate K_{max}/K_{flow} and then $\sigma_{open}/\sigma_{max}$? Almost no direct evidence is available to support any recommendation. For consistency with the recommended treatment of combined primary and secondary stresses, it may be prudent to calculate K_{max}/K_{flow} on the basis of the actual (plastically-relaxed) stress distribution. This would generally require an additional computation of K for a non-uniform stress distribution, but this computation may be required to determine J in the recommended manner. In this calculation, the yield stress should be interpreted as σ_{ys}, not σ_{flow}. In the event that the elastic-plastic stress distribution is not available and cannot be easily calculated, the use of the elastic stress distribution (e.g., the usual linear distribution for bending) in the computation of K_{max}/K_{flow} and then $\sigma_{open}/\sigma_{max}$ should be conservative. Unfortunately, this result may be unnecessarily conservative in some applications.

A third question addresses the ambiguity of net-section yield definitions for three-dimensional geometries. Consider, for example, a deep semi-elliptical surface crack in a finite plate such that the maximum depth of the flaw is approaching the back surface. The crack-tip plastic zone size at the maximum depth of the crack may be a very large fraction of the remaining ligament at that point (perhaps even exceeding the ligament size). However, a short distance around the crack perimeter, where the remaining ligament is larger, the crack-tip plastic zone may not exceed net-section yield criteria. Closure behavior at the two positions, however, will certainly be related. Furthermore, plastic relaxation at the maximum depth position may introduce local load shedding to neighboring ligaments that further complicates the local stress state and closure response.

In view of these unanswered questions, and in view of the general success of the Newman model in bounding closure behavior even when net-section yielding (defined in terms of σ_{flow}) is approached, it may be adequate at the present time to introduce no rigorous modifications to the crack closure algorithms to accommodate net-section yield effects. It should also be noted that under elastic-plastic conditions, when stresses are severe and net-section yielding is more likely, the nominal calculated closure stresses already approach zero (as K_{max}/K_{flow} approaches 1). However, net-section yield effects could be more significant for large cracks under lower applied stresses, where nominal closure stresses are relatively high (especially in plane stress) and the decreases in closure stresses due to net-section yield effects can be more pronounced (as in Figure 3.7). Further study is required to resolve these issues.

Based on the considerations discussed in Sections 3.3.1 through 3.3.3, it is useful to summarize the limits of applicability of the Newman closure algorithm as employed here. The algorithm can be applied to any cracked geometry under uniaxial primary loading for which K solutions are available, for K_{max}/K_{flow} values less than 1, although its accuracy may deteriorate under

net section yielding. The algorithm can be applied down to arbitrarily low values of K_{max}/K_{flow}, although it may not give accurate answers in the near-threshold SSY regime, when ΔK approaches ΔK_{th}. The algorithm can be applied to stress ratios in the range $-2 < R < 1$. As discussed in Section 3.3.6, extension of the algorithm to combined primary and secondary loading appears to be valid but has not been rigorously verified. The algorithm can be applied to any material for which a flow stress can be defined.

3.3.4 Effect of Stress Concentrations

The growth of cracks near stress concentrations, such as holes or notches, is one of the classic problems in fatigue. Broek (1972) was one of the first to note that growth rates are often higher than might be expected from nominal ΔK values when the crack is still small relative to the dimensions of the concentrator. Numerous researchers have experimentally measured crack opening levels for cracks growing from holes or notches and found that gradual changes in closure with increasing crack length corresponded to changes in growth rates (Tanaka and Nakai, 1983; Ogura et al., 1985; Shin and Smith, 1985, 1988; Sehitoglu, 1985a, 1985b; Savaidis and Seeger, 1994). McClung and Sehitoglu (1992) and others have studied the problem more closely with careful literature reviews, crack growth experiments, and coordinated finite element closure analyses, and have confirmed that accurate assessment of crack opening stresses is a key step in describing the growth of these fatigue cracks.

This observation introduces the question of how best to estimate crack opening stresses for cracks near stress concentrations. McClung (1991a) has proposed and validated a simple model which may be easily extended to cover a broader range of elastic-plastic FCG problems. The accuracy of this model has subsequently been independently confirmed in research by Savaidis et al. (1995). The heart of this simple model is the same fundamental dependence of $\sigma_{open}/\sigma_{max}$ on $\sigma_{max}/\sigma_{flow}$ predicted by the Newman closure analysis and used to address other closure problems, as described above. The unique feature of the simple model is the manner in which σ_{max} is defined.

The simple model is summarized schematically in Figure 3.9. First, the local stress at maximum load, σ_{yy}^{max}, at the location of the crack tip in an equivalent <u>notched</u> but <u>uncracked</u> body is determined. Second, the ratio of this local maximum stress to the flow stress is set equal to the normalized nominal maximum stress, $\sigma_{max}/\sigma_{flow}$ in a corresponding <u>cracked</u> but <u>unnotched</u> body. Finally, based on this $\sigma_{max}/\sigma_{flow}$ value, the normalized crack opening stress $\sigma_{open}/\sigma_{max}$ is estimated from a suitable closure analysis and assigned to this particular crack-tip location in the original notched, cracked body. Note that in Figure 3.9, the symbol "S" is used to denote nominal or far-field applied stresses, and the symbol "σ" is used to denote local stresses.

The first and third steps in this simple model require additional computations to be completed, for which algorithms must be specified. The first step involves estimation of the local stress field in the equivalent notched, uncracked body. This determination can be carried out in several different ways. The most accurate (and typically most expensive) method is to perform an elastic-plastic finite element analysis. For some applications, this FE analysis may already be available. In general, it will not be available, and the extra expense is probably not warranted to

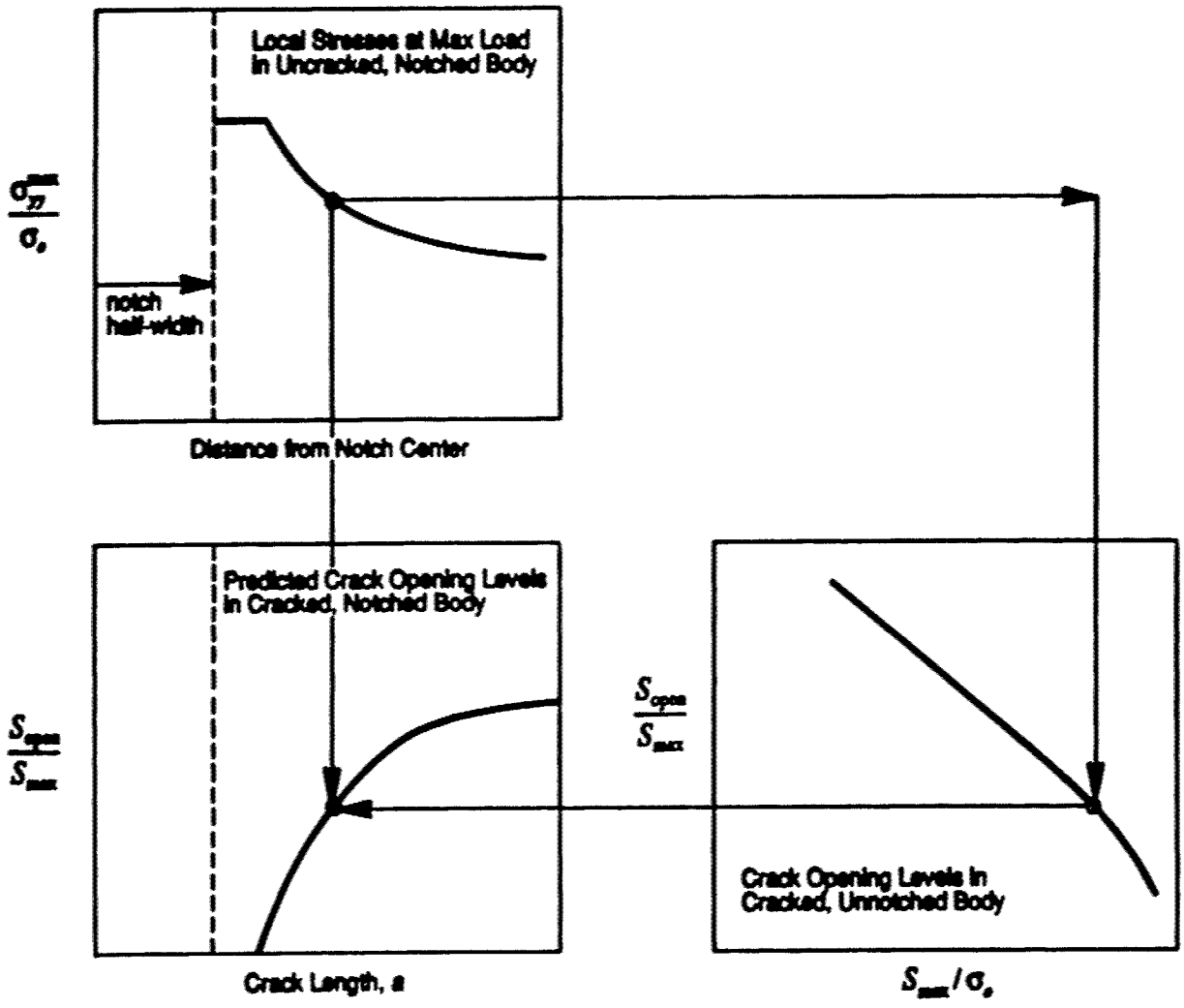

Figure 3.9. Schematic outline of simple model to predict crack opening stresses for cracks growing out of notches

solve only the closure problem. Alternative approaches involve estimating the elastic-plastic stress distribution from the elastic stress distribution. Glinka (1985a, 1985b) has published a detailed analysis scheme to determine this elastic-plastic field from the elastic field in a manner that takes into account different states of stress (plane stress vs. plane strain) and the stress redistribution brought on by notch plasticity. A simpler and more well-known approach to the same task employs the Neuber relationship,

$$K_t = \sqrt{K^{\sigma} K^{\varepsilon}} \tag{3.25}$$

where K_t is the theoretical stress concentration factor, and K^{σ} and K^{ε} are the corresponding concentration factors for local stress and strain, respectively. The Neuber form neglects stress redistribution due to yielding, and it is known to slightly overestimate stresses at the notch root in many cases, but these two effects may roughly compensate for each other in some applications. The Neuber method requires fewer computations, and its accuracy is expected to be entirely suitable for most closure assessments.

Use of either the Neuber or Glinka methods does require prior information about the theoretical elastic stress distribution near the stress concentration. Closed-form solutions are available for some common notch geometries. For example, the original solution by Inglis (1913) is available for a center hole in a plate. Amstutz and Seeger (1995) and Glinka and Newport (1987) have developed simple methods to estimate the elastic stress field ahead of the notch based on the remote stress, the stress concentration factor, and the notch root radius.

The third step is to estimate $\sigma_{open}/\sigma_{max}$ from $\sigma_{max}/\sigma_{flow}$. For consistency, this step should be carried out using the same Newman closed-form equation presented earlier. Use of this relationship raises the same question posed before about the use of a $\sigma_{max}/\sigma_{flow}$ criterion for widely differing geometries. Previously it was noted that $\sigma_{max}/\sigma_{flow}$ should be interpreted as K_{max}/K_{flow} when the geometry correction factor F in the stress intensity factor expression was significantly different from 1. Previous validation exercises for the $\sigma_{max}/\sigma_{flow}$ approach to crack closure at notches and holes considered only center cracks or short edge cracks, where F was approximately equal to 1. Applications of this approach to other configurations have not yet been validated, but this small extension seems reasonable. Note that the F value used to calculate K_{max}/K_{flow} from $\sigma_{max}/\sigma_{flow}$ should be based on an equivalent crack length in a corresponding unnotched body, to avoid double counting of the stress concentration effect. Further studies are required to evaluate use of this approach for cracks growing from notches or holes embedded in global stress gradients, such as bending configurations.

It is interesting to note that the K_{max}/K_{flow} criterion appears suitable to address the entire notch closure problem (independent of the computation of a local stress σ_{yy}^{max}), at least qualitatively. For very short cracks at notch roots, the stress intensity factor is known to be approximately given by $K_{max} = 1.12 K_t \sigma_{max} \sqrt{\pi a}$, where a is measured from the root of the notch. The stress concentration factor K_t is typically around 3.0 or greater for many notches or holes. If K_{flow} is equal to $\sigma_{flow} \sqrt{\pi a}$, then K_{max}/K_{flow} will be around 1.0 or even greater even when $\sigma_{max}/\sigma_{flow}$ is as small as 0.3. This result

correctly predicts the general trend that crack opening levels are quite low for very short cracks at notches. In the other extreme, for very long cracks at notches, the stress intensity factor is given by the usual $K_{max} = F\sigma_{max}\sqrt{\pi(a+c)}$, where F is the usual geometry correction factor for the notch-independent long crack configuration and c is the notch half-width, so that K is actually independent of the notch stress field. Since the corresponding long crack K_{flow} is $\sigma_{flow}\sqrt{\pi(a+c)}$, $K_{max}/K_{flow} = F\sigma_{max}/\sigma_{flow}$, and the notch is correctly predicted to have no influence on crack opening stresses.

The particular attractiveness of this alternative approach is that a consistent closure algorithm could be used for both notched and unnotched geometries. Since previously cited studies of closure in unnotched bodies with stress gradients (bend geometries) found that opening stresses were correlated by K_{max}/K_{flow} rather than the nominal (uncracked) stress at the crack tip location, it may be that K_{max}/K_{flow} is theoretically a better parameter for notches as well. The use of a K_{max}/K_{flow} criterion could also facilitate a more general treatment of the closure problem when notches are superimposed on nominal stress gradients, such as notches in bending.

A key unsolved problem, however, is the proper manner to carry out a smooth transition from the short crack K_{flow} to the long crack K_{flow}. For the short crack K_{flow}, the reference crack size is just a, the crack length measured from the notch root, but for the long crack K_{flow}, the reference crack size is the total length $(a + c)$. Application of the K_{max}/K_{flow} concept will require the identification of the crack size at which the long crack criterion should be adopted and some means of transitioning smoothly from the short crack to the long crack K_{flow} solution. The transition crack size, for example, could be estimated by the intersection of the short crack and long crack stress intensity factor solutions (Dowling, 1979), by the original notch plastic zone boundary, or perhaps indicated in some way by the closure solutions themselves. Once a suitable transition size is identified, some sort of interpolation scheme might be used to perform the transition with adequate smoothness. These nontrivial unresolved issues prevent a simple application of the K_{max}/K_{flow} criterion to the notch problem at the present time. Further study is required.

The approach based on local stresses and $\sigma_{max}/\sigma_{flow}$ has been shown previously to address adequately the effects of stress ratio, nominal maximum stress, strain hardening, and notch shape on crack closure behavior near stress concentrators. Further details are available elsewhere (McClung, 1991a). While the original simple closure model was employed in conjunction with FCG rate calculations based on ΔK_{eff}, there appears to be no reason why the closure information could not be used successfully to inform a ΔJ_{eff} approach to FCG rate prediction. The task of estimating J for cracks near notches is treated separately in Section 2.3.2.

3.3.5 Effect of Multiaxial Stresses

The SwRI finite element (FE) model of a growing fatigue crack was exercised to study crack closure under biaxial loading. A brief description of the general FE model is given in Appendix H. For these biaxial studies, the only specimen geometry considered was the center-cracked plate with a/W around 0.125. The ratio of plastic to elastic modulus was $H/E = 0.01$. The applied stress state was characterized by the biaxiality ratio $\lambda = \sigma_x/\sigma_y$, where σ_x and σ_y are the applied (nominal) stresses parallel and perpendicular to the crack line, respectively. Five different biaxial stress ratios were

considered: $\lambda = 0$ (ordinary uniaxial loading), +1 (equibiaxial loading), +1/2, −1/2, and −1 (which is equivalent to pure shear). All applied loading was proportional, either fully in-phase (positive lambda) or 180° out-of-phase (negative lambda). The crack is always growing perpendicular to the axis of the maximum principal stress (traditional Mode I loading). Further background information is available in (McClung, 1989a), which reports on some earlier analyses of biaxial effects conducted with an earlier version of the FE closure code.

The crack opening results are summarized in Figure 3.10 for $R = 0$ (top) and $R = -1$ (bottom). In these figures, σ_{open} and σ_{max} denote σ_y stresses (stresses perpendicular to the crack line), consistent with the usual definition for uniaxial loading. Several general trends are evident. First of all, at lower applied stresses (below $\sigma_{max}/\sigma_0 = 0.3$ or 0.4), the biaxial stress ratio has essentially no effect on crack opening stresses. This is consistent with experimental observations that under small-scale yielding conditions, different biaxial stress ratios have no significant effect on fatigue crack growth (FCG) rates (McClung and Sehitoglu, 1988). Second, there is a general trend at larger applied stresses (moving into the intermediate-scale and large-scale yielding regime) to lower crack opening levels for increasingly negative biaxial stress ratios, and to higher crack opening levels for positive biaxial stress ratios. Again, this is generally consistent with available experimental FCG rate data (Brown and Miller, 1985; Hoshide, Tanaka, and Yamada, 1981). Predictions of FCG rates based on the finite element closure results and a closure-corrected Paris Law relationship agree rather well with these available experimental *da/dN* data (McClung, 1989a). These numerical results are also generally consistent with limited experimental measurements of closure (McClung, 1989a). Note that the effect of biaxiality on crack opening behavior is more pronounced for negative lambda values than for positive lambda.

These FE results, while interesting and valuable, are not suitable in their present form for incorporation into practical algorithms for elastic-plastic FCG analysis, because they are not sufficiently general. The general approach chosen to characterize crack opening levels in the practical EPFCG methodology is the simple set of equations derived from the Newman FASTRAN model. This model has been shown previously to give an acceptably accurate lower bound to the crack opening levels given by the more sophisticated FE analyses for various uniaxial loading cases. Although the Newman equation provides a means for describing the effects of applied stress, uniaxial stress ratio (R), out-of-plane stress state, and material hardening on crack opening stresses, it does not provide an intrinsic means of incorporating the effects of biaxial stress ratio on crack closure.

Based on Rocketdyne experience, the most common biaxial stress states which are expected to be encountered in reusable aerospace propulsion systems are positive lambda values. These include cracks growing in pressurized cylinders, where the pressure-induced axial stress is traditionally one-half the value of the hoop stress ($\lambda = +1/2$), and cracks growing in equibiaxial thermal stress fields ($\lambda = +1$). For these biaxial ratios, the effect of biaxiality on crack closure is often minimal. If positive biaxial stress ratios are simply neglected, the crack opening stresses corresponding to uniaxial loading ($\lambda = 0$) are always a slightly conservative estimate, and this may be an optimum approach at the present time.

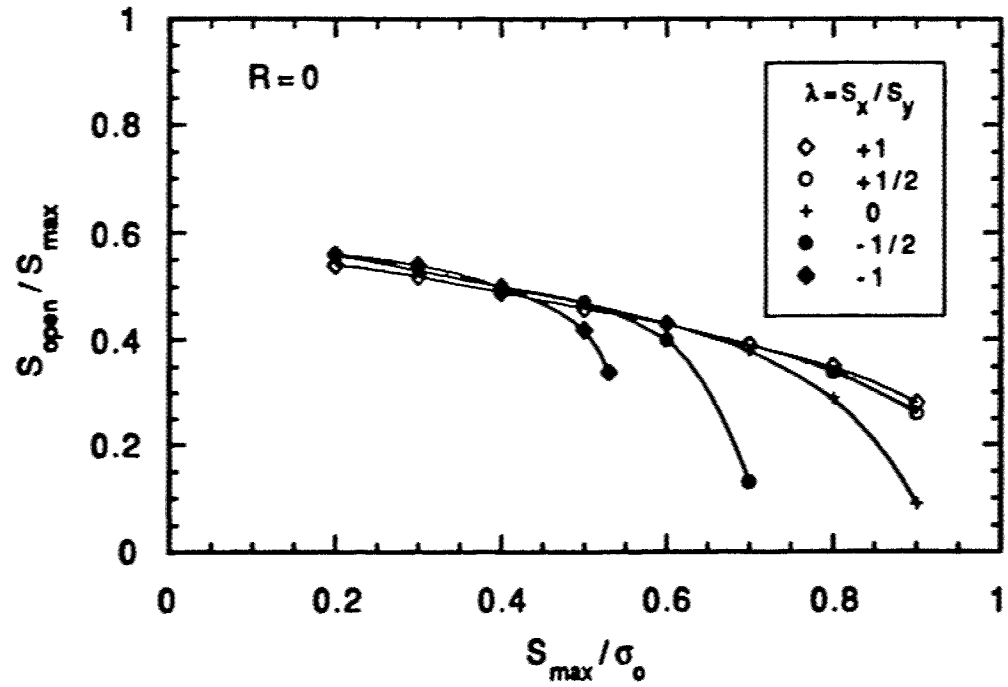

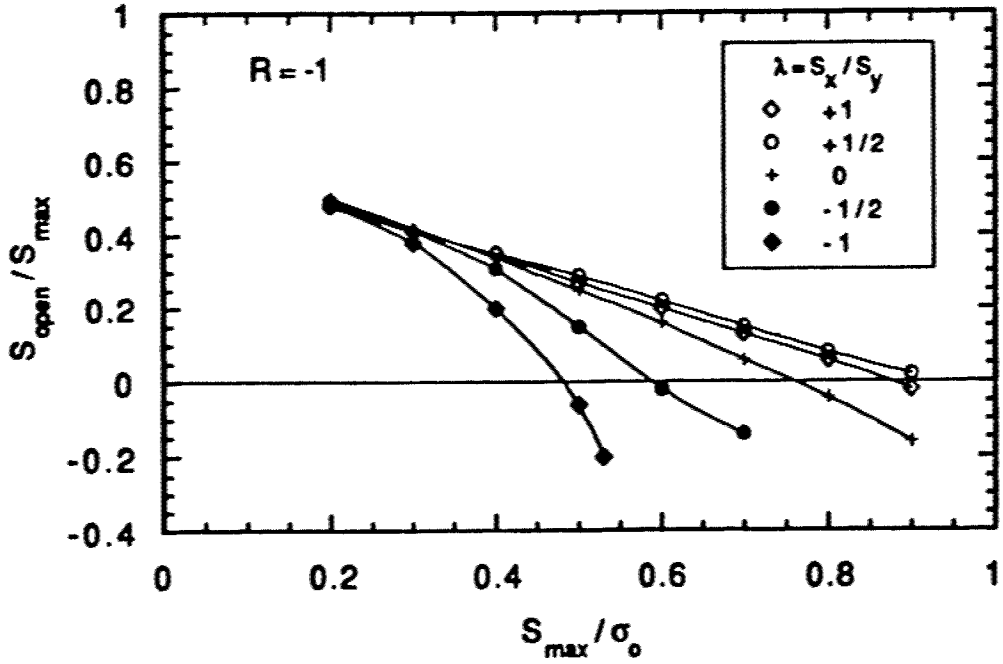

Figure 3.10. Normalized crack opening stress as a function of normalized maximum stress for different biaxial stress ratios. (top) $R = 0$ (bottom) $R = -1$

A corresponding practical approach for negative biaxial stress ratios is not immediately apparent. The difference between uniaxial and biaxial results increases with increasing maximum stress and increasingly negative lambda. Ultimately, crack opening stresses for negative biaxial stress ratios appear to drop off sharply as nominal gross yielding conditions are approached. For example, when $\lambda = -1$, the von Mises yield criterion indicates that general yielding is satisfied when $\sigma_y = -\sigma_x = 0.577\sigma_0$ and σ_0 is the uniaxial yield stress. From Figure 10, the crack opening level is seen to drop off sharply as σ_{max} approaches $0.577\sigma_0$. This suggests that the effective (von Mises) stress, σ_{eff}, may play some useful role in characterizing the applied loading. However, at lower applied stresses, the biaxial stress ratio has no effect on crack opening behavior, so the effective stress alone will not be suitable as a predictive parameter.

This discussion invites a more theoretical consideration of exactly why and how biaxiality influences crack opening behavior. At least two factors appear to be involved. The first, as noted earlier, is the effective von Mises stress. However, the von Mises stress alone is not consistent with several results. The absence of von Mises effects on closure at lower applied stresses has already been pointed out. In addition, the effective stress at $\lambda = +1$ is the same as the effective stress at $\lambda = 0$, but the closure results are not the same. And according to effective stress arguments, since $\lambda = +1/2$ corresponds to a minimum in the nominal stress vs. effective stress relationship ($\sigma_{eff} = 0.76\sigma_y$), it might be expected that $\lambda = +1/2$ would correspond to the highest crack opening levels. This is barely true for $R = -1$ and not true for $R = 0$.

The second factor which likely influences crack closure behavior is crack tip constraint, particularly as influenced directly by near-tip stresses parallel to the crack. The crack closure phenomenon itself is motivated by elastic constraint of the near-tip plastic deformation. A loss of constraint, such as that which occurs when applied stresses increase and crack tip plastic zones grow large relative to the crack and remaining ligament, generally leads to a decrease in crack closure levels. Positive stresses applied parallel to the crack cause an increase in constraint, along with a corresponding small reduction in the size of the crack tip plastic zone (McClung, 1989a), and it appears reasonable that this may cause some increase in crack closure levels.

This constraint effect caused by remotely applied stresses may also be related to the effects of different "T-stresses" on crack tip behavior. The T-stress is the non-singular stress term parallel to the crack in the near-tip field. Leevers and Radon (1982) have shown that the T-stress, which influences the near-tip constraint, varies widely from geometry to geometry. These T-stress effects may also help to explain why crack closure results differ slightly from geometry to geometry, as discussed in Appendix H. In that appendix, it was observed that specimen geometry effects nearly vanished under small-scale yielding conditions when opening data were correlated on the basis of K_{max}/K_0, but that the quality of this correlation gradually deteriorated at higher stress levels. This is similar to the loss of agreement between uniaxial and biaxial results at higher stresses, especially for positive biaxial stress ratios. Implicit T-stresses influence the near-tip field in a similar, but not identical, manner to remotely applied biaxial stresses.

These theoretical considerations may provide some guidance for the development of more rigorous algorithms to predict the effects of biaxiality on crack closure. It should be noted, however,

that negative biaxial ratios are not expected to occur frequently in SSME applications. When they do occur, it is also possible that resulting crack growth may be mixed-mode in nature, and mixed-mode growth is clearly beyond the scope of the current program.

In view of the limited information available, a simple semi-empirical algorithm has been developed to predict crack opening levels for negative biaxiality ratios from uniaxial closure data. This algorithm calculates a closure-equivalent applied stress from the applied biaxial stress. The closure-equivalent applied stress is the equivalent uniaxial applied stress which generates the same crack opening response as the biaxial applied stress. The equation developed is

$$\frac{\sigma_{closure\text{-}equivalent}}{\sigma_0} = \frac{\dfrac{\sigma_y^{biaxial}}{\sigma_0}\left(1 - \dfrac{\sigma_{cutoff}}{\sigma_0}\right) + \dfrac{\sigma_{cutoff}}{\sigma_0}\left(\dfrac{\sigma_y^{biaxial}}{\sigma_{eff}} - 1\right)}{\dfrac{\sigma_y^{biaxial}}{\sigma_{eff}} - \dfrac{\sigma_{cutoff}}{\sigma_0}} \tag{3.26}$$

where $\sigma_y^{biaxial}$ is the applied stress σ_y in the biaxial loading case, σ_{eff} is the von Mises effective stress, and σ_{cutoff} is the applied stress σ_y below which uniaxial and biaxial crack opening stresses are identical. For example, $\sigma_y^{biaxial}/\sigma_{eff}$ is 0.577 for $\lambda = -1$ and 0.756 for $\lambda = 0$. For $R = -1$, σ_{cutoff}/σ_0 is approximately 0.25, and for $R = 0$, σ_{cutoff}/σ_0 ranges from 0.45 to 0.55. It is not possible at this time to predict the value of σ_{cutoff}/σ_0 over a general range of R and λ. When in doubt, a lower value of σ_{cutoff}/σ_0 will generally always give more conservative (lower) values of $\sigma_{open}/\sigma_{max}$. The predictions of crack opening stresses for negative lambda values, based on equation 3.26 and available FE results for uniaxial stressing, are compared with available biaxial FE results in Figure 3.11.

It should also be noted that no numerical results are yet feasible for more common (and complex) geometries such as surface cracks. Furthermore, no experimental data revealing how biaxiality affects FCG rates for surface cracks or other three-dimensional geometries have been published. The generation of additional closure information or predictive algorithms for multiaxial loading is beyond the scope of the current investigation.

These multiaxial closure algorithms are currently limited to two-dimensional geometries with Mode I through cracks under uniform biaxial loading, to stress ratios in the range $-1 \le R \le 0$, and to biaxiality ratios in the range $-1 \le \lambda \le +1$. Further investigations should permit extension to a broader range of conditions.

3.3.6 Effects of Combined Loading

It appears that the effects of combined mechanical (primary) loading on crack opening levels can be addressed adequately with the standard K_{max}/K_{flow} criterion (Section 3.3.2). For example, a common form of combined mechanical loading is combined bending and tension. Each loading mode independently defines a value of K_{max}, and the total K_{max} can be obtained by superposition. The

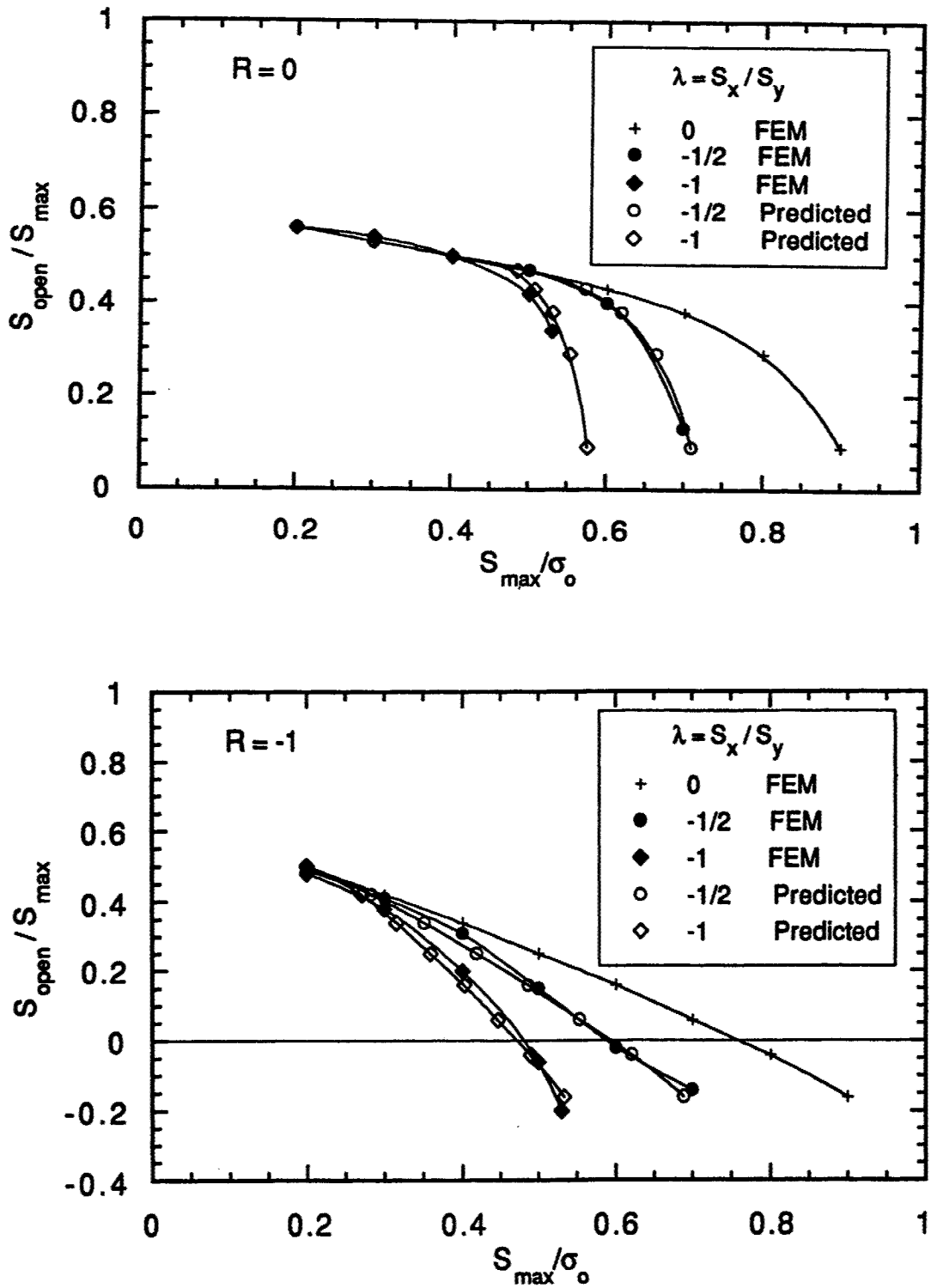

Figure 3.11. Comparison of predicted and FE crack opening stresses for negative biaxial stress ratios. (top) $R = 0$ (bottom) $R = -1$

nominal K_{flow} is chosen in the usual way, and then $\sigma_{open}/\sigma_{max}$ is calculated on the basis of K_{max}/K_{flow} from the usual Newman closure equation. This approach has been verified for edge cracks under combined bending and tension using the finite element method (see Appendix H). The extension of this method to other geometries and other forms of combined mechanical loading appears reasonable, although further validation is not possible at this time.

The effects of combined primary and secondary loading on crack closure behavior are undoubtedly complex, and no analytical or experimental information is available to guide the development of specific algorithms or to validate those algorithms. Furthermore, the development of this information is well beyond the scope of the current investigation. However, it appears reasonable to adopt the same K_{max}/K_{flow} approach proposed earlier to address different specimen geometries as well as combined mechanical loading. In this case, the total K_{max} value employed will be the linear superposition of contributions to the elastic stress intensity factor from both primary and secondary loading. This value is also required by the J-estimation scheme for combined primary and secondary loading (as discussed in Appendix F) and therefore should be readily available.

A remaining ambiguity is the proper choice of the normalizing flow strength σ_0 in the expression for K_{flow}, when the crack is growing through a thermal gradient (secondary stresses are thermal) and when the flow stress is significantly temperature-dependent. A reasonable choice for σ_0 would seem to be the value corresponding to the temperature at the current crack tip location. However, this is only a speculative suggestion and has not been confirmed. A more conservative assumption may be appropriate in view of the uncertainty.

Finally, it should be noted that other complexities often associated with combined primary and secondary loading, such as thermo-mechanical fatigue (TMF) loading and time-dependent (creep) deformation, can also influence crack closure behavior. For example, Sehitoglu and Sun (1989), using an enhanced FE closure code, have shown that time-dependent deformation in the vicinity of the crack tip can have a significant effect on crack closure stresses. They developed a simple expression to predict the dependence of crack opening stresses on material and test variables, but this expression is not sufficiently general for present purposes. Palazotto and Bednarz (1989) have presented results from other finite element studies based on a time-dependent constitutive formulation which show some influence of viscoplasticity on closure levels. Further studies of TMF and creep effects on crack closure remain well beyond the scope of the present investigation.

3.4 Algorithms for Crack Instability

The onset of crack instability defines the end of the fatigue crack growth life. Furthermore, incipient instability can cause an acceleration in the fatigue crack growth rate due to the contribution of static failure modes to crack extension during the load-up part of a fatigue cycle. The fundamental failure criteria governing these crack instability phenomena in materials that exhibit brittle or ductile behavior are now reasonably well-established. The main feature differentiating fracture in brittle and ductile materials is that the latter display an increase in toughness as a crack extends under a rising load, whereas in the former crack extension and instability are coincident.

Practical algorithms that address these crack instability issues are described in detail in **Appendix I**. In that appendix, criteria for evaluating the instability of cracks subjected to monotonic and cyclic loading under linear elastic and elastic-plastic conditions are reviewed and practical guidelines provided for implementing the criteria for brittle and ductile materials. Emphasis is placed on ductile materials because of the more complicated instability criterion governing these materials, and because they are a major constituent of advanced reusable aerospace propulsion systems. Fatigue crack growth equations are recommended for describing the acceleration in FCG rates due to incipient instability. This acceleration depends on the magnitude of the crack tip driving force at the maximum load in the cycle and the fracture resistance of the material.

In general, the instantaneous enhancement in cyclic crack propagation rate will depend on the previous cyclic load history. Rules are provided in the appendix for determining the influence of this load history. In the case of ductile materials, which can undergo simultaneous stable tearing and fatigue crack growth, the rules are formulated in terms of Memory and Loss of Memory Models. In the Memory Model, the ductile fracture process zone at the crack tip retains information about the previous cyclic loading, while in the Loss of Memory Model this information is assumed lost. The latter model predicts more conservative crack growth rates than the former. Available experimental evidence providing verification of the Memory Model is summarized in an endnote to Appendix I.

The characterization of fracture properties for use in the instability criteria is discussed in Appendix I, as well as the effects of plastic constraint on fracture toughness and J_R-curves. Practical considerations pertaining to the application of the crack instability criteria to predicting failure in service life assessments are addressed.

3.5 Algorithms to Estimate Fatigue, Constitutive, and Fracture Properties

The development and use of practical algorithms for the prediction of elastic-plastic fatigue crack growth rates requires an appropriate material data base. This data base must include information about material resistance to fatigue crack growth; some characterization of the material constitutive (stress-strain) response, with attention to both monotonic and cyclic properties; and a description of the material resistance to fracture instability by tearing or cleavage. Discussions of material properties requirements and recommended estimation techniques for FCG, constitutive, and fracture properties follow below.

3.5.1 Fatigue Crack Growth Properties

The most obvious requirement for materials data is some characterization of the resistance to fatigue crack growth: appropriate material constants for an equation which relates the applied driving force to the resulting crack growth rate da/dN. Unfortunately, data bases do not currently exist for experimental elastic-plastic fatigue crack growth behavior. Relatively few EPFCG test programs have been conducted, nearly all in a research environment, and no standardized test method (e.g., ASTM) has been developed. The FCG data bases that do exist are nearly all for small-scale yielding conditions in which ΔK has been used as the correlating parameter. The

available SSY FCG data bases are actually quite extensive and cover a broad range of structural materials.

Fortunately, it appears possible to convert these SSY FCG data bases for use with predictive algorithms for elastic-plastic FCG. The J-integral is directly related to the stress intensity factor, K, in the linear elastic or SSY regime according to the relationship

$$J = \frac{K^2}{E'} \tag{3.27}$$

where $E' = E$ for plane stress and $E/(1-\nu^2)$ for plane strain, and E is Young's elastic modulus. This relationship can easily be exploited to convert a crack growth expression which is written in terms of ΔK to an expression written in terms of ΔJ. Furthermore, it has been shown by experience that this same crack growth relationship in the SSY regime can be successfully extrapolated upwards into the elastic-plastic and fully-plastic regimes, so that a single crack growth expression adequately describes FCG data spanning as many as five orders of magnitude in da/dN (Dowling, 1976; McClung and Sehitoglu, 1991; McClung and Hudak, 1994). In other words, a ΔJ (or ΔJ_{eff}) vs. da/dN relationship which is valid in the SSY regime is also valid in the EPFCG regime.

The use of material data bases (empirical constants) which are keyed to SSY FCG relationships presents an additional question: which SSY FCG equation to use? The simplest and most common equation is the so-called Paris Law, the power law relationship written as

$$\frac{da}{dN} = C_0(\Delta K)^{m_0} \tag{3.28}$$

where C_0 and m_0 are the empirical (material) constants, typically based on a least-squares regression of experimental crack growth data. Several other crack equations have been proposed, however, and some are in common use. The NASCRAC (1989) computer code, for example, permits the use of the Forman, Walker, Collipriest, and Hop-Rau models. These alternative models were developed primarily to follow observed deviations from standard power law behavior at very low applied stress intensities (near threshold) or at very high applied stress intensities (near final instability and fracture).

The best choice for EPFCG analysis appears to be the simple Paris Law form. There is no evidence that EPFCG data exhibit traditional threshold behavior at very low applied values of ΔJ. In fact, small cracks in elastic-plastic deformation fields typically grow at rates significantly faster than near-threshold (large) cracks, at equivalent ΔK values well below the nominal threshold stress intensity factor range, ΔK_{th}; this is one-manifestation of the so-called small crack effect (McClung et al., 1996a). At the other extreme, EPFCG data generally exhibit standard power law behavior at very high applied values, perhaps deviating only when the critical value of the J-integral for the initiation of ductile tearing, J_{Ic}, is approached or exceeded. While some deviation from power law

behavior is expected at these limits, in EPFCG it appears preferable to address this phenomenon directly through consideration of ductile fracture equations rather than through some modification to the FCG equation. These issues are discussed further in Section 3.4. If the only available SSY FCG data are expressed in terms of one of the more complex crack growth equations, some further algebra may be required to obtain the equivalent C_0 and m_0 values.

If the material resistance to SSY fatigue crack growth is described by C_0 and m_0 as written in Eqn. 3.28, then the material resistance to EPFCG can be written according to

$$\frac{da}{dN} = C_1(\Delta J)^{m_1} \tag{3.29}$$

where

$$C_1 = C_0(E')^{m_0/2} \tag{3.30}$$

$$m_1 = \frac{m_0}{2} \tag{3.31}$$

As discussed in Section 3.2, the driving force for elastic-plastic fatigue crack growth is best expressed in terms of a closure-corrected ΔJ_{eff}. However, the original SSY FCG data base is most likely defined in terms of a nominal ΔK value which has not been corrected for closure. It is not valid to insert a closure-corrected driving force into a material resistance equation written in terms of a closure-independent driving force. Therefore, the original SSY FCG constants must be adjusted for closure by computing the original closure-corrected ΔK_{eff} values and determining the new SSY FCG constants which will give the same FCG rate. Since, in general, crack closure stresses would not have been measured during the generation of the baseline SSY FCG data, these closure stresses must be estimated.

A variety of experimental observations and analytical models are available to estimate closure levels, as discussed in Section 3.3. The correct closure stress will depend on the stress state (plane stress vs. plane strain), the applied maximum stress as a fraction of the flow stress, and the stress ratio. Most baseline SSY FCG testing is performed at relatively low applied stresses (perhaps on the order of 0.1 to 0.3 of the yield stress) and at stress ratios ranging from $R = 0$ to 0.1. The stress state can vary from plane stress to plane strain, depending primarily on the thickness of the test specimen (as discussed below). For these applied stresses and stress ratios, a reasonable estimate of crack closure behavior under plane strain conditions is about $U_0 = 0.75$ to 0.8, where U_0 denotes the effective stress intensity factor range ratio for baseline SSY FCG data. This estimate is conservatively consistent with the limited number of experimental measurements (Fleck and Smith, 1982) and analyses (Chermahini et al., 1989; McClung et al., 1991; Newman, 1984) available for plane strain. A reasonable estimate for plane stress is about $U_0 = 0.5$ (see Appendix H). Minor variations from these levels will not cause significant errors. If the specific load history and specimen geometry for the baseline SSY tests are both known, then the closure levels can be

estimated from available information such as the Newman closure equations (Newman, 1984) cited in Section 3.3.

Algebraic adjustments in the material constants for closure are straightforward. A closure-corrected Paris equation in the SSY regime can be written as

$$\frac{da}{dN} = C_2(\Delta K_{eff})^{m_2} \tag{3.32}$$

where

$$C_2 = \frac{C}{U_0^{m_0}} \tag{3.33}$$

$$m_2 = m_0 \tag{3.34}$$

Combining the closure and SSY vs. EPFCG corrections, then, the final form may be written as

$$\frac{da}{dN} = C\left(\Delta J_{eff}\right)^m \tag{3.35}$$

where

$$C = \frac{C_0\left(E'\right)^{m_0/2}}{U_0^{m_0}} \tag{3.36}$$

$$m = \frac{m_0}{2} \tag{3.37}$$

in terms of the original SSY FCG data base constants.

The decision to treat the original SSY data as either plane stress or plane strain has implications for the selection of both E' and U_0. In reality, of course, the deformation fields near fatigue cracks are complex and three-dimensional, and the degree of constraint gradually changes with increasing distance from the crack tip or with proximity to the specimen surface. The ideas of plane stress or plane strain are actually only limiting representations of constraint between which most of reality occurs. However, it is often convenient to choose one or the other extremes as a

simple description of stress state. The traditional criteria for two-dimensional geometries were reviewed in Section 3.3.1. Much of the available SSY FCG data is expected to satisfy full plane strain conditions, especially for high strength aerospace structural materials.

The current NASGRO database contains a large quantity of fatigue crack growth data expressed in terms of ΔK, including tabulation of all parameters associated with the NASGRO crack growth equation. Unfortunately, due to the complex nature of the NASGRO equation (*da/dN* is a function not only of ΔK but also of K_{th}, K_c, R, a crack closure factor derived from the Newman closure equations, and three other empirical exponents), it is not possible to use the NASGRO value of C directly in either Eqn. 3.35 or 3.36. In most cases, however, the NASGRO value of the crack growth exponent n can be set equal to the exponent m_0 in Eqn. 3.37 to determine m (this should be checked carefully due to possible complications from the near-threshold and near-instability terms in the NASGRO equation). However, it should be possible to use the raw data (numerical or graphical) in the NASGRO database, in conjunction with the given exponent (n) value, to calculate or estimate C_0 in Eqn. 3.36. Furthermore, the value of the Newman constraint factor α_c (denoted as α in the NASGRO manual) should provide some insight as to the stress state associated with the baseline data.

3.5.2 Constitutive Properties

A quantitative description of the material constitutive response is required both to compute the driving force ΔJ_{eff} and to estimate the crack closure parameter U. Ideally, the available material data base will include direct experimental information on both the standard tensile properties σ_{ys} (yield strength) and σ_{ult} (ultimate tensile strength) as well as some representation of the stress-strain relationship. This relationship is often expressed in the Ramberg-Osgood form,

$$\frac{\varepsilon}{\varepsilon_0} = \frac{\sigma}{\sigma_0} + \alpha\left(\frac{\sigma}{\sigma_0}\right)^n \tag{3.38}$$

where ε_0, σ_0, α, and n are the material constants, usually determined empirically through a least squares regression of stress vs. strain data from a tensile test. This is the form assumed by the EPRI handbook approach to estimating J and by most elastic-plastic finite element J solutions. The constitutive response of some materials is not well described by the Ramberg-Osgood form, however, and alternate forms such as a bilinear stress-strain relationship may be more appropriate.

Stress-strain relationships such as the Ramberg-Osgood equation can be written in terms of *engineering* stress and strain or *true* stress and strain as derived from tensile test data. True stresses and strains are corrected for changes in the instantaneous cross-sectional area and length of the tensile specimen due to deformation during the test, whereas engineering quantities are based on the original nominal dimensions of the tensile specimen at the beginning of the test (Bannantine, et al., 1990). The common yield and ultimate strengths are customarily given as engineering quantities. The engineering and true stress-strain curves are very similar except at large values of strain

approaching necking, and so values of the Ramberg-Osgood constants will generally be similar for engineering and true quantities unless the data from which they were derived include very large strains. Current usage of the Ramberg-Osgood equation in EPFM applications by various practitioners is mixed between engineering and true quantities. Pragmatically, the engineering stress and strain values will be more commonly available, and their use in this context appears acceptable. Engineering quantities were recommended in the recently completed proof testing handbook (Chell et al., 1997a). However, true values are also acceptable in the current context, and are preferred by some users of *J*-integral methods.

In some cases, however, the available data base may not include all this direct experimental information on the specific material of interest. If only some information is available, it may still be possible to estimate the remaining information using some simple engineering rules-of-thumb. For example, if the only tensile data available are the traditional yield and ultimate strengths, an approximate Ramberg-Osgood relationship can be constructed. It can be shown that the strain hardening exponent in Eqn. 3.38, n, is related to the ratio of yield and ultimate strengths by the expression (Bannantine et al., 1990)

$$\frac{\sigma_{ult}}{\sigma_{ys}} = \left\{\frac{1}{n(0.002)}\right\}^{\frac{1}{n}} \exp\left(-\frac{1}{n}\right) \tag{3.39}$$

if α is set equal to 1 and the yield strength σ_{ys} corresponds to a 0.2 percent (0.002) offset. In this particular expression, σ_{ys} and σ_{ult} are engineering quantities and n is the exponent in a true stress-true strain relationship. However, considering the approximate nature of the estimate, the mixed formulation should be acceptable. For the IN-718 considered in this program, for example, the strain hardening exponent was calculated as 15.8 from the original experimental stress-strain data. Based on Eqn. 3.39, the ratio of ultimate over yield was predicted to be 1.17. The actual average values of σ_{ys} and σ_{ult} from the same two tensile tests were 166.4 and 195.2 ksi, respectively. The ratio of these two values is 195.2/166.4 = 1.17. A compilation of σ_{ult}/σ_{ys} vs. n values based on Eqn. 3.39 is given in Table 3.1. Note that direct computation of n from σ_{ult}/σ_{ys} will require an iterative solution (inversion) of Eqn. 3.39. Once n is determined, σ_0 can be estimated from

$$\sigma_0 = \left\{\frac{0.002\,E}{(\sigma_{ys})^n}\right\}^{\frac{1}{1-n}} \tag{3.40}$$

and ε_0 is given by

$$\varepsilon_0 = \frac{\sigma_0}{E} \tag{3.41}$$

In order to use the Newman modified-Dugdale model to compute crack opening stresses (see Section 3.3.1), an estimate of the so-called flow stress, σ_{flow}, is required, where σ_{flow} is the average of yield and ultimate strengths: $\sigma_{ys} = (\sigma_{ys} + \sigma_{ult})/2$. If Ramberg-Osgood or related power-law relationships are available for the material of interest, σ_{flow} can be estimated with the aid of Eqns. 3.39 and 3.40.

Table 3.1. Relationship between strain hardening exponent and ratio of ultimate to yield strengths, based on Eqn. 3.39.

n	σ_{ult}/σ_{ys}
3	3.943
3.5	3.102
4	2.604
4.5	2.281
5	2.057
5.5	1.893
6	1.769
6.5	1.672
7	1.595
7.5	1.532
8	1.480
8.5	1.436
9	1.398
9.5	1.366
10	1.338
10.5	1.313
11	1.292

n	σ_{ult}/σ_{ys}
11.5	1.273
12	1.255
12.5	1.240
13	1.226
13.5	1.213
14	1.202
14.5	1.191
15	1.182
15.5	1.173
16	1.165
16.5	1.157
17	1.150
17.5	1.144
18	1.138
18.5	1.132
19	1.127
19.5	1.122
20	1.117

A very important note is that the constitutive response of some materials can change significantly after substantial cyclic deformation (in the elastic-plastic regime) has occurred. Depending on the initial metallurgical condition of a material, the stress-strain response may exhibit gradual cyclic strain hardening, cyclic strain softening, little or no change, or mixed behavior in which relative softening may occur at one strain range and relative hardening at another. These changes can directly affect the material properties required for both J calculation (e.g., Ramberg-Osgood constants) and closure analysis (e.g., σ_{flow}).

It is not possible to predict cyclic properties directly from monotonic properties, but it is possible to anticipate when cyclic hardening or softening may occur. In general, materials which

have particularly "soft" monotonic properties tend to harden following cycling, while materials which are initially quite "hard" tend to soften. This can sometimes be predicted on the basis of the monotonic strain hardening exponents: if $n < 5$, then cyclic hardening will often occur, while if $n > 10$, cyclic softening is more likely. Many materials tend to cyclically stabilize around $n' = 6$ or 7. Consider, for example, IN-718 in the STA-1 condition: the monotonic strain hardening exponent is about 15.8. This material cyclically softens, and the cyclic strain hardening exponent is about 6.2. Manson and Hirschberg (1964, p. 133) proposed an alternative criterion for hardening or softening based on the ratio of the monotonic ultimate strength to the monotonic yield strength. If $\sigma_{ult}/\sigma_{ys} > 1.4$, then cyclic hardening is predicted; if $\sigma_{ult}/\sigma_{ys} < 1.2$, then cyclic softening is predicted. A large change in cyclic response is not expected for ratios between 1.2 and 1.4.

Directly measured cyclic values for the yield and ultimate strengths are generally not available, although the cyclic yield strength can be computed directly from a cyclic Ramberg-Osgood relationship and the "cyclic ultimate strength" can be estimated with the aid of Eqn. 3.39. These computations will typically be required in order to estimate the cyclic flow stress σ'_{flow} needed for closure calculations. If no experimental information is available on the cyclic constitutive relationship (e.g., Ramberg-Osgood), then no direct means is available to compute or estimate any of the cyclic tensile properties. If Coffin-Manson total strain vs. fatigue life data of the general form

$$\frac{\Delta\varepsilon}{2} = \frac{\sigma_f'}{E}(2N_f)^b + \varepsilon_f'(2N_f)^c \tag{3.42}$$

are available, then the cyclic strain hardening exponent, n', can be approximately estimated from the relationship (Morrow, 1965; Bannantine et al., 1990)

$$n' = \frac{c}{b} \tag{3.43}$$

where c is the fatigue ductility exponent and b the fatigue strength exponent in a fatigue life equation of the form above. In practice, cumulative regression errors can degrade the accuracy of this relationship. Based on energy arguments, Morrow (1965) has suggested that the cyclic strain hardening exponent can also be roughly estimated from either b or c according to the relationships

$$c = \frac{-n'}{n' + 5} \tag{3.44}$$

$$b = \frac{-1}{n' + 5} \tag{3.45}$$

It is not always clear whether monotonic or cyclic property data should be used in specific applications. The application of cyclic loading to a given material does not alone imply that cyclic properties are appropriate. The cyclic loading must be intense enough (maximum stresses approaching or exceeding yield, or cyclic deformation including a significant plastic component) and long enough (a significant number of cycles) to cause a complete transition to stable cyclic properties. No simple rules-of-thumb are available to estimate when a change will or will not occur, or how long is required for the change to occur. If cyclic softening or hardening does occur, then the stable state will often be reached after about 20 to 40 percent of the total expected low cycle fatigue (LCF) life, so some initial assessments may be possible based on nominal strains and LCF properties. If it is suspected that cyclic hardening or softening may occur but it is not clear, then it may be prudent to choose the constitutive properties which will give the most conservative prediction of crack growth rates.

The issue of cyclic vs. monotonic constitutive properties suggests a related question: does a change from a monotonic to a cyclic material state also influence the material resistance to fatigue crack growth? The earlier observation that SSY FCG and EPFCG data can be consistently correlated by the same power law relationship suggests that the FCG resistance does not change appreciably. This is probably true because the FCG resistance is primarily controlled by near-tip material response. Near the crack tip, due to the intense cyclic deformation, the material experiencing separation is probably always approximately cyclically stable, even if the remote properties are nominally monotonic.

As noted earlier, tabulated Ramberg-Osgood constants are not readily available in the public domain for common metals used in space propulsion systems. Some limited information on stress-strain properties for various structural alloys is available in the *Aerospace Structural Metals Handbook* (Brown et al., 1996) and the *Structural Alloys Handbook* (Holt et al., 1996). These data are typically in the form of stress-strain curves (which could be digitized and then fitted to estimate the Ramberg-Osgood constants) or in the form of tabulated or graphical values of yield and ultimate strengths (which could be used to estimate the Ramberg-Osgood constants following the procedures outlined earlier).

3.5.3 Fracture Properties

As discussed in detail in Appendix I, material property requirements to characterize ductile fracture include (as a minimum) some measure of the critical value of J for the initiation of ductile tearing, J_{mat}, and (ideally) a complete J-resistance curve (J vs. Δa). Unfortunately, tabulated or graphical values of these properties are not generally available in the public domain in any quantity.

More commonly available in the public domain are data for the fracture toughness expressed in terms of K. For example, the NASGRO database contains values for the plane strain fracture toughness, K_{Ic}, and the fracture toughness (measured or estimated) for part-through flaws, K_{Ie}. In the absence of other information, a first estimate of the value of J_{mat} can be obtained by setting K_{mat} equal to the available, appropriate fracture toughness (K_{Ic}, K_{Ie}, or K_c), depending on the application of interest, and then calculating J_{mat} as

$$J_{mat} = \frac{(K_{mat})^2}{E'} \tag{3.46}$$

Limited additional toughness data are available in the *Aerospace Structural Metals Handbook* (Brown et al., 1996) and the *Structural Alloys Handbook* (Holt et al., 1996).

No reliable estimation techniques are currently known for constructing a complete *J*-resistance curve without performing the necessary elastic-plastic fracture mechanics tests. However, the blunting line of the *J*-resistance curve can be estimated as

$$J = (2\sigma_{ys})\Delta a \tag{3.47}$$

An approximate lower bound to the actual resistance curve would then follow the blunting line up to J_{mat}, with no increase in toughness above J_{mat} (in other words, assume that fracture occurs whenever J_{max} exceeds J_{mat}). An approximate upper bound to the actual resistance curve would follow the blunting line at all values of *J*.

3.6 Load Interaction Effects

Perhaps no other advanced topic in SSY fatigue crack growth has received more attention over the years than variable amplitude loading. A variety of specialized algorithms to predict crack growth rates under variable amplitude loading have been proposed, several of them specifically designed to address the often observed phenomenon of crack growth retardation following an overload. This retardation effect has been directly linked by experiment to crack closure behavior and the associated residual stresses and plastic zone introduced by the overload. Most of the variable amplitude crack growth models, however, such as the Wheeler (1972) and Willenborg (Willenborg, Engle, and Wood, 1971) models, are empirical in nature and require the determination of multiple empirical constants. As such, they do not accurately reflect the mechanics and physics of the crack growth mechanisms. Another model, the FASTRAN approach of Newman mentioned earlier in the discussion of crack closure, is based directly on the mechanics of crack closure. This model has been successfully applied to a variety of fatigue life prediction problems (e.g., Newman, 1981) and has also been demonstrated to predict the key trends observed in high-resolution crack-tip measurements following overloads (Dexter, Hudak, and Davidson, 1989; Davidson, Hudak, and Dexter, 1985, 1987).

In comparison, very few detailed studies of variable amplitude effects in elastic-plastic and fully-plastic fatigue crack growth have been reported. The limited data available suggest, however, that crack closure remains a key issue (McClung and Sehitoglu, 1988; Socie, 1977). Furthermore, studies of LSY FCG indicate that some of the rules-of-thumb about variable-amplitude loading effects under SSY conditions may give entirely wrong answers when applied to LSY. For example, consider Figure 3.12, which shows in schematic a simple SSY history (top) and a simple LSY history (bottom). The SSY history is well known to produce significant crack growth retardation due to

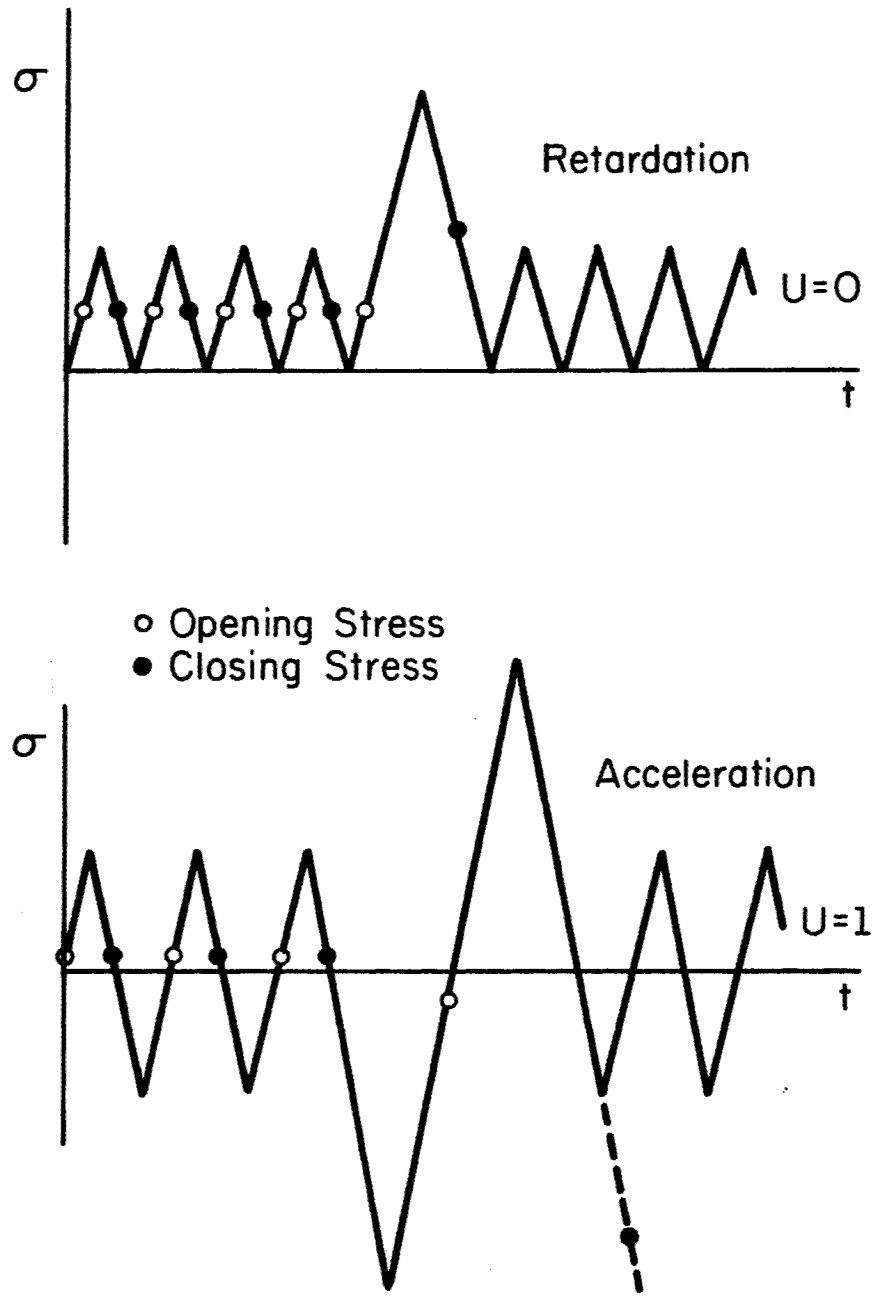

Figure 3.12 Finite element simulations showing effect of stress amplitude on crack closure following a single overload cycle

closure effects, and by the same line of conventional reasoning the LSY history would also be expected to produce retardation. But in practice, the LSY history can lead to a major acceleration in the crack growth rate and a reduction in the fatigue crack propagation life by nearly a factor of four in comparison to linear damage estimates which neglect closure altogether (McClung and Sehitoglu, 1988).

The motivation for this acceleration is again closure (or lack thereof following the overload), but it is a uniquely LSY closure effect. At large maximum stresses (in this case, greater than the yield stress) and at low stress ratios (in this case, $R = -1$), the major cycle opening stress and closing stress (normalized by the yield stress) both decrease significantly, the closing stress dropping off sharply with increasing maximum stress. The major cycle closure behavior can cause large changes in subcycle closure behavior and greatly increase subcycle damage, even if the major cycle occurs infrequently. These closure phenomena have also been directly observed experimentally (McClung and Sehitoglu, 1988). Such changes in closure behavior may cause load cycles that are nominally below the threshold for fatigue damage to cause significant crack growth.

Finite element closure studies have identified more clearly the differences—and similarities—between SSY and ISY/LSY load interaction effects (McClung, 1992). Figure 3.13 shows the results of three different FCG simulations in which changes in normalized crack opening levels following a single overload were tracked. All three simulations involved $R = 0$ cycling with a single 100% overload. The lowest amplitude simulation had a baseline maximum stress of $0.2\sigma_0$, so the overload maximum stress was $0.4\sigma_0$—still in the SSY regime. The highest amplitude simulation had a baseline maximum stress of $0.4\sigma_0$, and therefore an overload maximum stress of $0.8\sigma_0$—well into the ISY regime. At the lowest stress amplitude, the post-overload closure behavior shows a momentary decrease in closure levels, and then a sharp rise in closure levels. This is entirely consistent with the customary retardation in FCG rates following overloads in the SSY regime. Furthermore, the simulation demonstrates why this retardation is typically delayed, beginning not immediately after the overload but some number of cycles later, following a very brief acceleration in growth rates (Ling and Schijve, 1990). The closure behavior in the highest stress amplitude simulation is similar in that closure levels drop immediately following the overload, and then rise substantially. The critical differences are that the immediate drop is much more pronounced, causing a much more pronounced temporary acceleration in growth rate, and that the subsequent rise in closure level occurs at a much more gradual rate. In fact, if the overload cycle occurs repetitively, even infrequently, it is likely that the overload cycle will repeat before the subcycle closure level ever returns to its previous stable level. In this case, the load interaction effect would be entirely acceleration, never retardation.

The key to successful prediction of variable amplitude loading effects in elastic-plastic FCG, then, is to focus on the physical mechanisms which cause nonlinear damage accumulation. The primary mechanisms of interest here relate to crack closure and the associated changes in plastic strains and residual stresses. Empirical models developed for SSY conditions will be of limited value. The mechanics-based FASTRAN approach appears to hold considerable promise, although its general applicability to ISY and LSY conditions has not been fully established and may be

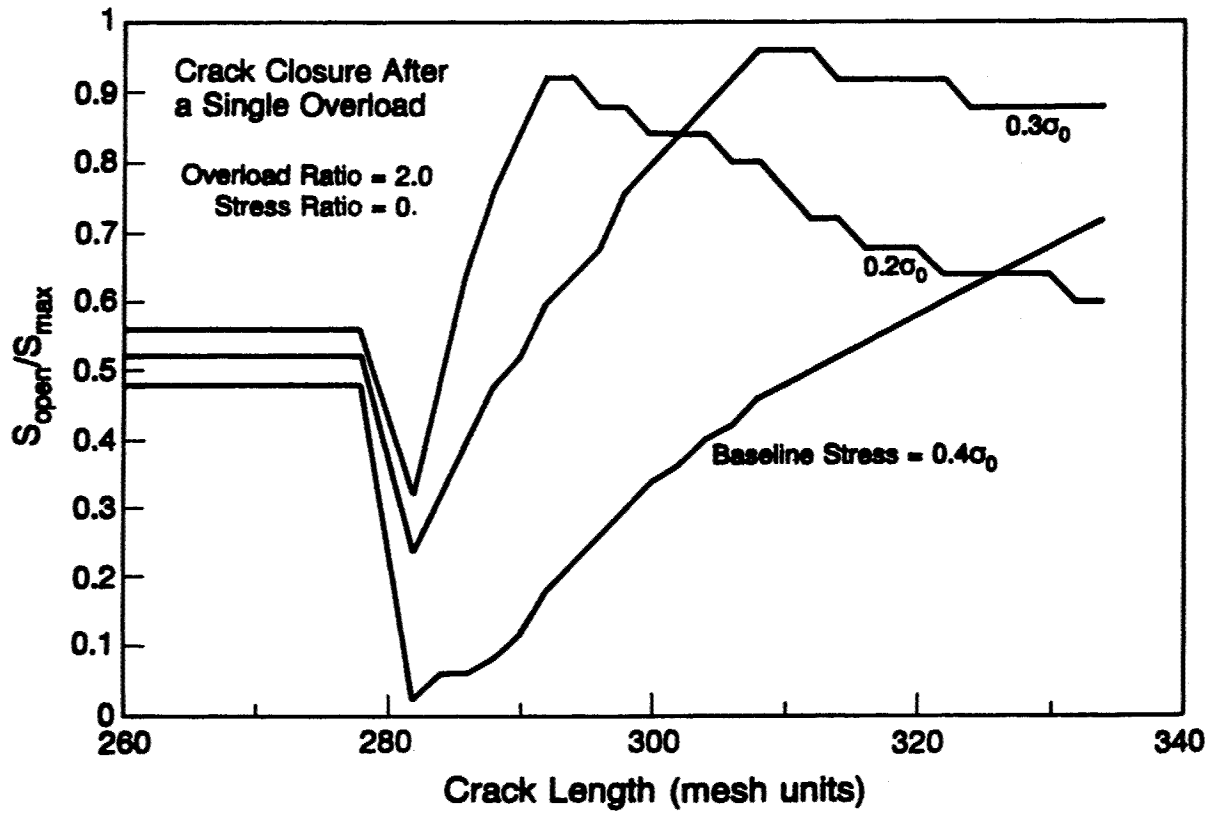

Figure 3.13 Effect of stress amplitude on crack closure following a single overload cycle

restricted. However, the FASTRAN approach is not consistent with the structure of the NASGRO elastic-plastic fracture mechanics modules.

In general, it is known that for "short" loading spectra, the crack closure behavior is controlled almost entirely by the major or dominant cycle in the spectrum (Socie, 1977). For "longer" spectra, the subcycles play an increasingly important role in setting the closure levels. A practical approach to variable amplitude crack growth analysis might begin by defining the opening and closing levels in terms of the major cycle and then developing an estimate of the subcycle crack growth distance which is required to overcome this effect. An ad hoc model of this type was used successfully to correlate crack growth rates by McClung and Sehitoglu (1988). Vormwald and Seeger (1991) and Topper et al. (1992) have also employed fade-out models to describe the gradual changes in crack closure with crack growth following large amplitude overload or underload cycles, qualitatively similar to the trends in the FE results shown above. Vormwald and Seeger (1991) further proposed an elementary algorithm to predict crack opening stresses under elastic-plastic variable amplitude loading, and their recommendations deserves more careful study in future development of load interaction rules. For loading spectra which are more random in nature and which are not dominated by any one cycle, it may be reasonable to calculate statistically some effective average crack opening level and apply it to the entire history (Newman, 1981).

Other variable loading effects may also be important. For example, a limited number of large amplitude cycles could cause significant cyclic hardening or softening that might otherwise not occur under the remaining small amplitude cycles. These changes in the constitutive properties could significantly influence the value of ΔJ and thereby significantly influence fatigue crack growth rates. This effect is related to the periodic overstrain effect described by Brose et al. (1974) for smooth specimen fatigue lives under variable amplitude loading.

Due to the complexity of the problem and the limited available data, it is not possible at this time to develop and verify a rigorous quantitative algorithm for load interaction effects in EPFCG. Until such an algorithm is developed, simple linear damage rules (i.e., assuming the absence of either beneficial or deleterious load interaction effects) should be employed. This is consistent with the approach taken by NASGRO for SSY FCG analysis, where load interaction algorithms have not been implemented until Version 3.

3.7 Creep-Fatigue Effects

As noted in Section 1.1, the operating conditions for reusable aerospace propulsion system hardware include elevated temperatures and significant hold times. Under these conditions, it is possible that creep deformation and the resulting damage at the crack tip can contribute substantially to the crack growth process. A synergistic interaction can also occur between creep and fatigue mechanisms.

Unfortunately, although the traditional fracture mechanics parameters K and J have proven to be successful parameters for characterizing time independent static and cyclic crack behavior, they are not adequate for characterizing time dependent creep deformation at a crack tip. A time

dependent fracture mechanics (TDFM) parameter that correlates *da/dt* data for different cracked geometries and loading systems may be required for the fracture control of some reusable aerospace propulsion system components. Although the formal development of practical TDFM algorithms is beyond the scope of the current contract, it is useful to develop the general outline of a suitable approach and thereby lay the foundation for future work. As will be shown, the appropriate TDFM methodology employs much of the new elastic-plastic fracture mechanics technology developed under the current contract to facilitate a *J*-based approach to fracture control.

To overcome the shortcomings of K and J, Landes and Begley (1976) proposed the use of a new parameter, C^*, to characterize creep deformation under steady loading conditions. C^* is the creep analog of the *J*-integral, and hence can be estimated with the same general procedures previously described for J. While C^* has been widely accepted as the correlating parameter for creep crack growth under large-scale creep, it is not applicable for components undergoing transient behavior, such as cyclic loading.

C^* was later generalized to include transient, as well as steady state, creep deformation by Saxena and co-workers (Saxena, 1986; Saxena and Liaw, 1986; Leung et al., 1988; Bassini et al., 1989), and the new parameter was denoted C_t. Unlike C^*, C_t is an explicit function of time as well as crack size and applied load. C_t does not characterize the crack tip fields, except under steady state conditions when it reduces to C^*, but it does have an interpretation related to the rate of change of the power input from the loading system as the crack extends (Saxena, 1986). A time dependent crack field characterizing parameter, $C(t)$, has been developed by Riedel (1987). This parameter also reduces to C^* under steady state conditions. The parameter $C(t)$ provides important information on typical transition times between the transient and steady states, and between small and large scale crack tip creep conditions.

Appendix J outlines a practical approach to the characterization of creep-fatigue crack growth under cyclic loading conditions involving a hold time at steady load. The crack growth rate per cycle is expressed as the linear sum of two contributions: that due to fatigue crack extension, and that due to creep crack growth during the hold time

$$da/dN = (da/dN)_f + (da/dN)_{time} \tag{3.48}$$

Here $(da/dN)_f$ is the fatigue crack growth rate,

$$(da/dN)_f = D(\Delta K)^l \tag{3.49}$$

and D and l are temperature dependent material constants that may also depend on the hold time. The effects of cyclic plasticity can be addressed by replacing ΔK with $(E' \Delta J)^{1/2}$. The creep crack extension, $(da/dN)_{time}$, that occurs during the hold time, t_h, is evaluated according to

$$(da/dN)_{time} = \int_0^{t_h} (da/dt)\,dt = \int_0^{t_h} H C_t^q \, dt \tag{3.50}$$

where H and q are material constants.

The parameter C_t consists of transient (short time) and steady state (long time) components, both of which depend on the constitutive law which relates creep strain rate to stress. The value of C_t is also dependent on whether creep deformation recovery due to cycling can occur at the crack tip. If the zone of creep deformation which spreads out from the tip is smaller than the cyclic crack tip plastic zone, then creep recovery will occur and all history effects from previous cyclic load changes are lost. If the creep zone is much larger than the cyclic plastic zone, then recovery is unlikely, and information regarding the previous load history is retained with creep deformation evolving with time as if no cyclic loading had occurred.

The transient component of C_t is characterized by the applied stress intensity factor, and derivatives of it. Expressions for the steady state component can be readily derived from available fully plastic J solutions, or a reference stress approach, by employing the analogy between plastic and creep deformation. Hence, C_t can be calculated from material property data and fracture mechanics parameters. The effects of thermal loading can be incorporated into C_t by adding the thermal stress intensity factor to the stress intensity factor arising from primary loading, and evaluating $C_t(t \to 0)$ using the total value. The steady state component, C^*, is unaffected by thermal loading and depends only on the applied primary load. The foregoing are applicable even when widespread crack tip plasticity is present.

Further details of the methodology are provided in Appendix J, including methods of calculating C_t, procedures for performing a remaining life assessment, and discussions of other important factors such as crack growth incubation, loading ramp rate, and temperature changes during the cycling.

Because the approach to creep-fatigue effects outlined here has not yet been developed into a formal set of algorithms, it is not possible or appropriate to characterize the limits of applicability at this time.

4. DEVELOPMENT AND VERIFICATION OF NASGRO SOFTWARE MODULES

4.1 Introduction

The original Statement of Work (SOW) in this contract called for the development of practical engineering methods for the analysis of elastic-plastic and fully plastic fatigue crack growth, but did not address the implementation of these methods in engineering software. NASA-Marshall had originally intended that the methods would be implemented in software form, but the decisions about when and how to perform that implementation were postponed until the methods themselves had begun to take shape.

As the engineering methods for EPFCG were developed and documented, and as performance of the original SOW was nearing completion, NASA-Marshall addressed the software implementation issues. Amendments to the SOW were executed in order to transfer the EPFCG technology to the practicing engineer through the development of computer software to implement the analytical tools.

NASA-Marshall directed that the EPFCG methodology should be implemented into NASGRO, an existing linear-elastic fracture mechanics program used extensively throughout the NASA centers and the aerospace community. NASGRO, which was originally titled NASA/ FLAGRO, has broad capabilities for the computation of stress intensity factors and the calculation of fracture mechanics remaining life under small-scale yielding conditions. The original NASA/ FLAGRO program, itself based on an earlier computer program known as FLAGRO4 (Forman and Hu, 1984), was first released over ten years ago (Forman et al., 1988). New versions have been released as major enhancements were completed. Version 2.0 was released in 1994 (Forman et al., 1994). Version 3.0, the first to be denoted as "NASGRO," is in Beta prerelease at this writing (Forman et al., 1997), and is expected to be officially released during late 1998.

NASGRO, like nearly all other LEFM computer codes for FCG, employs the range of the stress intensity factor as the correlating parameter for crack growth rates. As noted earlier in this report, although ΔK is inadequate as a correlating parameter under elastic-plastic conditions, the computation of an appropriate EPFCG parameter such as ΔJ_{eff} requires values of ΔK as input. Therefore, an LEFM computer code is an appropriate starting point for the development of an EPFCG computer code.

The new elastic-plastic fracture mechanics NASGRO modules were developed as independent modules that do not require compilation or execution of the main NASGRO code. NASA may choose to integrate the new modules more closely with the main NASGRO code in a future release of NASGRO, and the design of the modules will facilitate this integration. However, the modules were developed as an independent code at this time for several reasons. First, NASA and its onsite contractors properly control the source code for the main NASGRO code, and control the release of new official versions of NASGRO. Therefore, the current contractor team was not in a position to deliver a new version of the main NASGRO code. Furthermore, development and delivery of the new modules as an independent program insures that the software is now available

to NASA both as source code and as executable code for immediate use, without waiting on the development and release of a new NASGRO version.

Because the new modules were developed as an independent program, no changes were made to the main NASGRO program itself. However, for consistency and compatibility with the main NASGRO code, the new modules emulate NASGRO wherever possible. Existing NASGRO subroutines or subprograms (for example, interpolation routines) were employed wherever possible in the development of the new elastic-plastic modules. All K solutions employed in the new modules were taken directly from the current NASGRO version without modification. General NASGRO protocols for text-based input and output were followed, including batch file mode. No graphical user interface (GUI) was included in the SOW or developed.

Since the new elastic-plastic methodology reduces to a conventional SSY methodology when loads are relatively low and plastic strains are negligible, the new modules perform almost identically to the existing NASGRO program in the SSY regime. However, some minor changes to current NASGRO methods were implemented in some aspects of the program where necessary for compatibility with the new elastic-plastic methodology, so the new modules will not always give the identical answer to NASGRO in the SSY regime. For example, current NASGRO methods for closure corrections to the driving force ΔK were modified to accommodate the new K_{max}/K_{flow} criterion for crack opening values. Also, the complex NASGRO crack growth equation, which employs nonlinear crack growth curves in the near-threshold and near-instability regimes, was replaced with a simple linear Paris equation, since EPFCG does not exhibit threshold behavior, and since near-instability EPFCG behavior is better described with methods that explicitly treat the interactions between monotonic and cyclic crack growth mechanisms.

The new elastic-plastic fracture mechanics NASGRO modules were specifically tailored for the NASGRO environment. Therefore, the capabilities of the current NASGRO main program had some influence on, and in some cases limited, the capabilities of the new elastic-plastic modules. For example, the current EC01 K solutions in the main NASGRO program are limited to uniform tension applied to a centrally-located symmetric flaw. Therefore, the current EC01 solutions in the new elastic-plastic modules share the same limitations, and nonuniform secondary stress distributions are conservatively recharacterized as calculated average uniform stresses.

It must be emphasized that the elastic-plastic NASGRO modules developed to date and described in this report represent only a subset of the EPFCG methodology developed and verified under the current contract. As evidenced by this final report, that EPFCG methodology includes a very broad range of capabilities and addresses a very broad range of problems. The intent of the NASGRO module development conducted in the current contract was to implement a critical core of this methodology and provide a solid foundation for further software development in the future. Therefore, the new NASGRO modules are limited to a small number of common geometries and to a basic set of crack growth capabilities. Many of the more advanced features of the methodology, such as the treatment of notched geometries, multiaxial loading, combined mechanical loading, creep-fatigue interactions, etc., have not yet been implemented. In other cases, simpler versions of methodologies have been implemented. For example, treatment of combined primary-secondary

loading follows the EPRI handbook procedure rather than the more complex procedures recommended in Appendix F. These and other features could be implemented in future versions of the NASGRO elastic-plastic modules.

Complete details of the capabilities of the new NASGRO modules is provided in Appendix K, which serves as a User's Manual for the new modules. This User's Manual was designed to function as a stand-alone document. Therefore, Appendix K contains some brief additional documentation of the theoretical background to the methods implemented in the modules, along with documentation of the module verification and validity limits. The appendix also includes detailed instructions on how to run the program, including line-by-line documentation of interactive screen input.

Portions of this final report serve as a more comprehensive "theoretical manual" for the user. The experimental verification of the EPFCG submodule is independently documented in Appendix L.

For convenience, a brief description of the capabilities of the elastic-plastic NASGRO modules follows below.

4.2 *J* and ΔJ Solutions

Solutions for the *J*-integral and the closure-corrected range of the *J*-integral are provided for five existing NASGRO geometries: central through crack, TC01; edge through crack, TC02; quarter-elliptical corner crack, CC01; semi-elliptical surface crack, SC01; and elliptical embedded crack, EC01. All five geometries have solutions for uniform tensile loading, and TC02, SC01, and CC01 also have solutions for bending. Combined tension and bending loading is not supported.

All five geometries have reference stress solution modules, and TC01 and TC02 also have solution modules based on the EPRI handbook. The reference stress solutions for TC01, TC02, SC01 (tension), and CC01 (tension) are based on optimized limit loads derived from available finite element *J* solutions. The reference stress solutions for SC01 (bend), CC01 (bend), and EC01 are conservatively based on limit loads estimated from plastic limit theory and bounding values of a structural parameter that appears in the optimized reference stress solutions.

All five geometries support combined primary and secondary loading based on the EPRI handbook method, which incorporates the effect of secondary loading through a first-order plasticity correction to the elastic component of *J* and ΔJ. Secondary stress gradients are conservatively recharacterized to generate uniform and linear stress fields admissible to the NASGRO *K* solutions.

4.3 Failure Algorithms

The failure algorithms compute critical crack sizes and critical loads for the five NASGRO geometries subjected to combined primary and secondary loading. The critical load computation is based on the primary load, with secondary loads being held constant. For brittle materials containing

cracks with two degrees of freedom, assessments are carried out at both the a-tip and the c-tip, but for materials that behave in a ductile manner, the assessments are made restrictively at the a-tip. Cracks with more than one degree of freedom (i.e., CC01, SC01, EC01) are reduced to one degree of freedom in growth by restricting crack size changes either to maintain constant aspect ratio, or to maintain the size in the c-direction fixed while permitting growth in the a-direction.

Instability analysis for materials that behave in a ductile manner is based upon crack resistance curves that describe increasing toughness with crack extension. Failure is assumed to occur when the applied J and the gradient of applied J with increasing crack length, dJ/da, simultaneously exceed the material toughness and the gradient in toughness with respect to tear length. J-resistance curves are described with simple quadratic or power law equations.

4.4 Elastic-Plastic Fatigue Crack Growth

Elastic-plastic fatigue crack growth lives for cyclic changes in combined primary and secondary loads are calculated from closure-corrected ΔJ solutions and a Paris equation for crack growth rates. Closure corrections are based on the equations derived by Newman from his modified-Dugdale closure model, interpreted in terms of K_{max}/K_{flow} values. Chosen values of the constraint factor in the Newman equations, α_c, can be applied independently to each location for two-degree-of-freedom cracks (CC01, SC01, EC01), although the use of a common value at both locations is recommended based on verification studies conducted to date. The NASGRO surface correction factor β_R is applied to the ΔJ solution at points where the crack front intersects a free surface (the c-tip for SC01 and the a-tip and c-tip for CC01). Material property constants for the Paris equation written in terms of ΔJ are derived from the corresponding constants in a SSY Paris equation written in terms of ΔK, (without closure corrections) and an independent estimate of closure in the SSY data.

The EPFCG module permits variable amplitude stress histories and employs simple linear damage rules, so no load interaction effects are incorporated. Existing NASGRO protocols are followed to define fatigue load spectrums or schedules.

Starting from a user-specified initial crack size, the module computes crack sizes, maximum J values, ΔJ values, and values of the effective stress range ratio, U. These quantities are calculated and output at both locations for a two-degree-of-freedom crack, at specified numbers of cycles to a predefined limiting number of cycles or until failure. Determination of crack instability (failure) in the EPFCG module is currently based on simple exceedance of a specified critical J value.

The NASGRO EPFCG module was independently verified by comparing its predictions with actual experimental crack growth data from critical tests performed on specimens of Inconel 718. Experiments included three different specimen geometries (TC01, SC01, and CC01). Some tests were conducted under SSY conditions, while others were conducted under intermediate or large-scale yielding conditions. Stress ratios were $R = 0$, $R = 0.1$, or $R = -1$. The SSY tests were used to determine baseline crack growth properties, and then these properties were used to make independent predictions for the remaining tests. The NASGRO module was found to be highly successful in predicting crack growth lives and correlating crack growth rate data. All lifetime predictions were

conservative and within a factor of two of the actual observed life. The NASGRO module also generally predicted the correct crack shape development for two-degree-of-freedom surface cracks.

5. SUMMARY AND CONCLUSIONS

A practical engineering methodology has been developed to analyze and predict fatigue crack growth rates under elastic-plastic and fully-plastic conditions. The methodology employs the closure-corrected effective range of the J-integral, ΔJ_{eff}, as the governing parameter. Under small-scale yielding conditions, the elastic-plastic methodology reduces to the customary linear elastic fracture mechanics approach to FCG analysis based on ΔK, although still closure-corrected.

The range of the J-integral was selected as the governing parameter because it best satisfied the simultaneous criteria of theoretical validity, practicality, and demonstrated usefulness. Alternative parameter choices based on other path-area integrals were critically reviewed and found to be less satisfactory based on the same criteria. Although ΔJ does possess some limitations, it appears to be the best available parameter at the present time.

The methodology comprises two major components. The first major component is a set of specific solutions for the J-integral for specific geometries, along with a general methodology for calculating J under a wide range of different conditions, including combined loading. The second major component is a set of specific practical algorithms that translate a J solution into a specific quantitative prediction of fatigue crack growth rate or life, including general equation forms for ΔJ_{eff}, and algorithms for determining crack opening levels, crack instability conditions, and material properties. A core subset of the J solutions and the practical algorithms has been implemented into special elastic-plastic NASGRO modules. All components of the entire methodology, including the NASGRO modules, have been verified through analysis and experiment, and limits of applicability have been identified.

The details of the J solution methods, the practical crack growth algorithms, and the NASGRO modules, along with documentation of the verification exercises and identification of the limits of applicability, are provided in three preceding chapters and in twelve accompanying appendices. A brief summary of the individual elements of the methodology follows.

5.1 Summary of J-Integral Solutions

Solutions of the plastic component of the J-integral generally follow either the EPRI estimation scheme, which is based directly on normalized finite element results, or the optimized reference stress method, which employs an estimation scheme based on the stress intensity factor solution, the constitutive equation, and an optimized limit load solution. The solutions are generally applicable to materials described by a Ramberg-Osgood constitutive relationship, although the reference stress form permits extension to materials that obey an arbitrary stress-strain law. Solutions of the elastic component of the J-integral are generally based on the linear elastic stress intensity factor with a first-order plastic correction based on the crack-tip plastic zone size.

Existing J solutions for standardized fracture mechanics geometries, including many NASGRO geometries, were documented and tabulated. Most of these solutions are found in EPRI handbooks, with a few additional solutions scattered in the literature.

Elastic-plastic finite element methods were employed to generate new plastic J solutions for semi-elliptical surface cracks and quarter-elliptical corner cracks in finite plates under uniform tension. These FE results were then used to derive new optimized reference stress solutions for the same configurations. The solutions were further verified against independent literature FE results. Optimized reference stress solutions for surface cracks under bending were derived from other literature FE results. These solution forms were then conservatively extended to construct reference stress solutions for corner cracks under bending and elliptical embedded cracks under tension, for which no finite element results were available.

Elastic-plastic finite element methods were used to generate new J solutions for a specific set of cracked double edge notch geometries. These FE results were then employed to develop and verify a new optimized reference stress solution method for the general problem of a crack at a stress concentrator. The method was further verified against available FE results in the EPRI handbook.

Optimized reference stress solutions were derived for through cracks in plates under tension or bending from FE results in the EPRI handbook.

General reference stress methods were developed for estimating J under combined mechanical loading (combined tension and bending, for example). The methodology is based on the identification of an optimum combined yield load. Verification of the methodology was accomplished through comparison with limited available solutions in the EPRI handbook for two different geometries.

Four previously proposed methods for estimating J for combined primary and secondary loading were critically reviewed, and a new procedure was developed based on improvements in one of the four previous methods. The method has been verified through comparison with available FE solutions for combined mechanical and thermal loading.

A general J estimation method for two-dimensional Mode I cracks under biaxial loading was developed and verified by comparison with available literature solutions.

5.2 Summary of Practical Crack Growth Algorithms

Solutions for ΔJ follow the same general form as the EPRI and reference stress schemes for J, with single values of applied load, stress, or stress intensity factor replaced by their respective ranges, and employing a cyclic Ramberg-Osgood constitutive form. Corrections for crack closure are applied independently to elastic and plastic J terms based on energy arguments.

Crack opening stresses as a function of normalized maximum stress, stress ratio, and stress state are calculated from a simple set of closed-form equations derived by Newman from his modified-Dugdale closure model of a center-cracked plate. These equations were shown to compare favorably with more sophisticated finite element models and with experimental measurements in the elastic-plastic regime. Finite element closure studies showed that the Newman equations could be extended to address a wider variety of geometries as well as combined loading by replacing the

normalized maximum stress term with a normalized maximum stress intensity factor term. The effects of net-section yielding on closure behavior were identified. A simple, verified algorithm was identified that predicted crack closure levels for cracks growing out of stress concentrations. A simple modification to the Newman equations was developed to describe the effects of multiaxial applied stresses on the closure of Mode I cracks.

Simple algorithms were developed to evaluate the instability of cracks subjected to monotonic and cyclic loading in materials that behave in a brittle or ductile manner. Resistance curve methods were employed for ductile materials under elastic-plastic conditions. Fatigue crack growth equations were recommended for describing the acceleration in FCG rates due to incipient instability. Rules were developed to determine the influence of previous load history on simultaneous tearing and fatigue crack growth mechanisms.

Algorithms were developed to estimate fatigue, constitutive, and fracture properties needed for elastic-plastic FCG analysis that might not be readily available. These algorithms included equations to estimate elastic-plastic FCG equation constants from available ΔK-based small-scale yielding FCG equations, equations to estimate Ramberg-Osgood constitutive properties from conventional tensile properties, and equations to estimate cyclic constitutive properties from low cycle fatigue data.

Important issues associated with the treatment of load interaction effects were discussed, and general guidelines for analytical treatments were suggested, but a specific algorithm was not proposed due to the complexity of the problem.

The general outline of a methodology for creep-fatigue effects on crack growth was presented and discussed. The methodology is based on a linear summation of the crack growth contributions due to creep and fatigue. The time-dependent parameter C_t is employed to characterize the creep crack growth rates.

5.3 Summary of NASGRO Modules

A critical core of the J solutions and practical crack algorithms was implemented in software form in new elastic-plastic NASGRO modules. The new modules are independent and do not require compilation or execution of the main NASGRO code, but emulate the current NASGRO code and employ existing NASGRO routines (such as K solutions) wherever possible. Complete details of the capabilities of the new modules are provided in a User's Manual, which also includes brief documentation of the theoretical background, verification, and validity limits of the modules.

Solutions for J and ΔJ are provided for five existing NASGRO geometries: TC01, TC02, CC01, SC01, and EC01. All five geometries have solutions for uniform tensile loading, and TC02, SC01, and CC01 also have solutions for bending. Combined tension and bending loading is not supported. All five geometries have reference stress solution modules, and TC01 and TC02 also have solution modules based on the EPRI handbook. All five geometries support combined primary

and secondary loading based on the EPRI handbook method, which incorporates the effect of secondary loading through a first-order plasticity correction to the elastic component of J and ΔJ.

The failure algorithms compute critical crack sizes and critical loads for the five NASGRO geometries subjected to combined primary and secondary loading. The critical load computation is based on the primary load, with secondary loads being fixed during iteration. Cracks with more than one degree of freedom are reduced to one degree of freedom in growth by maintaining constant aspect ratio, or by maintaining one crack dimension fixed. Instability analysis for materials that behave in a ductile manner is based upon crack resistance curves that describe increasing toughness with crack extension.

EPFCG lives are calculated from closure-corrected ΔJ solutions and a Paris equation for crack growth rates. Closure corrections are based on the equations derived by Newman from his modified-Dugdale closure model, interpreted in terms of K_{max}/K_{flow} values. The NASGRO surface correction factor β_R is applied to the ΔJ solution at points where the crack front intersects a free surface. Material property constants for the Paris equation written in terms of closure-corrected ΔJ are derived from the corresponding constants in a SSY Paris equation written in terms of closure-independent ΔK. The EPFCG module permits variable amplitude stress histories and employs simple linear damage rules (no load interaction effects). Starting from a user-specified initial crack size, the module computes crack sizes, maximum J values, ΔJ values, and U values at specified numbers of cycles to a predefined limiting number of cycles or until failure.

The NASGRO EPFCG module was independently verified by comparing its predictions with actual experimental crack growth data for Inconel 718. Experiments included three different specimen geometries (TC01, SC01, and CC01), a wide range of deformation conditions (SSY, ISY, and LSY), and stress ratios ranging from $R = 0$ to $R = -1$. The SSY tests were used to determine baseline crack growth properties, and then these properties were used to make independent predictions for the remaining tests. The NASGRO module was found to be highly successful in predicting crack growth lives and correlating crack growth rate data. All lifetime predictions were conservative and within a factor of two of the actual observed life. The NASGRO module also generally predicted the correct crack shape development for two-degree-of-freedom surface cracks.

6. REFERENCES

Adefris, N., A. Saxena, and D. L. McDowell, 1996, "Creep-Fatigue Crack Behavior in 1Cr-1Mo-0.25V Steel II: Crack Growth Behavior and Models," *Fatigue and Fracture of Engineering Materials and Structures*, Vol. 19, pp. 401-411.

Ainsworth, R. A., 1992a, "Practical Aspects of the Calculation and Application of C^*," *Materials at High Temperatures*, Vol. 10, pp. 119-126.

Ainsworth, R. A., 1992b, "Singular Fields at Defects in Creeping Structures Subjected to Mechanical Loading Combined with Thermal Stresses," Conference on 'Behavior of Defects at High Temperatures,' Sheffield, U.K.

Ainsworth, R. A., M. B. Ruggles, and Y. Takagashi, 1992, "Flaw Assessment Procedure for High Temperature Reactor Components," *Journal of Pressure Vessel Technology*, Vol. 114, pp. 166-170.

Ainsworth, R. A., G. G. Chell, M. C. Coleman, I. W. Goodall, D. J. Gooch, J. R. Haigh, S. T. Kimmins, and G. J. Neate, 1987, "CEGB Assessment Procedure for Defects in Plant Operating in the Creep Range", *Fatigue and Fracture of Engineering Materials and Structures*, Vol. 10, pp. 115-127.

Ainsworth, R. A., 1984, "The Assessment of Defects in Structures of Strain Hardening Material," *Engineering Fracture Mechanics*, Vol. 19, pp. 633-642.

Ainsworth, R. A., 1982, "The Initiation of Creep Crack Growth," *International Journal of Solids and Structures*, Vol. 18, pp. 873-881.

Ainsworth, R. A., B. K. Neale, and R. H. Price, 1978, "Fracture Behaviour in the Presence of Thermal Strains", Proc. Conf. on Tolerance of Flaws in Pressurized Components, I. Mech. E., London, Paper C96/78, pp. 197-204.

Amstutz, H., and T. Seeger, 1995, "Accurate and Approximate Elastic Stress Distribution in the Vicinity of Notches in Plates Under Tension," unpublished manuscript, referenced in Savaidis, Dankert, and Seeger, 1995.

Anderson, T. L., 1995, **Fracture Mechanics: Fundamentals and Applications**, CRC Press.

ASTM E 399, 1998, "Standard Test Method for Plane-Strain Fracture Toughness of Metallic Materials," *Annual Book of ASTM Standards*, Vol. 03.01.

ASTM E 647, 1998, "Standard Test Method for Measurement of Fatigue Crack Growth Rates," *Annual Book of ASTM Standards*, Vol. 03.01.

ASTM E 1457, 1998, "Standard Test Method for Measurement of Creep Crack Growth Rates in Metals", *Annual Book of ASTM Standards*, Vol. 03.01.

ASTM E 1737, 1998, "Standard Test Method for *J*-Integral Characterization of Fracture Toughness," *Annual Book of ASTM Standards*, Vol. 03.01.

Atluri, S. N., T. Nishioka, and M. Nakagaki, 1984, "Incremental Path-Independent Integrals in Inelastic and Dynamic Fracture," *Engineering Fracture Mechanics*, Vol. 20, pp. 209-244.

Bannantine, J. A., J. J. Comer, and J. L. Handrock, 1990, **Fundamentals of Metal Fatigue Analysis**, Prentice Hall, Englewood Cliffs, New Jersey.

Bass, B. R., R. H. Bryan, J. W. Bryson, and J. G. Merkle, 1982, Applications of Energy Release Rate Techniques to Part-Through Cracks in Experimental Pressure Vessels," *ASME Journal of Pressure Vessel Technology*, Vol. 104, pp. 308-316.

Bassini, J. L., D.E. Hawk, and A. Saxena, 1989, "Evaluation of the C_t Parameter for Characterizing Creep Crack Growth Rate in the Transient Regime," *Nonlinear Fracture Mechanics ASTM STP 995*, American Society for Testing and Materials, pp. 7-26.

Bhandari, S., S. Charif D'Ouazzane, and C. Faidy, 1984, "Establishment of Governing Parameters for Fatigue Crack Growth Analysis in Areas of High Nominal Strain", ASME publication 84-PVP-20.

Bicego, V., 1989, "Low Cycle Fatigue Life Predictions in Terms of an EPFM Small Crack Model," *Engineering Fracture Mechanics*, Vol. 32, pp. 339-349.

Bilby, B. A., A. H. Cottrell, and K. H. Swinden, 1963, "Plastic Yielding from Sharp Notches," *Proceedings of the Royal Society, Series A*, Vol. 272, pp. 304-314.

Blackburn, W. S., 1972, "Path Independent Integrals to Predict Onset of Crack Instability in an Elastic-Plastic Material," *International Journal of Fracture Mechanics*, Vol. 8, pp. 343-346.

Bloom, J. M., 1994, "An Approach to Account for Negative R-Ratio Effects in Fatigue Crack Growth Calculations for Pressure Vessels Based on Crack Closure Concepts," *ASME Journal of Pressure Vessel Technology*, Vol. 116, pp. 30-35.

Boettner, R. C., C. Laird, and A. J. McEvily, Jr., 1965, "Crack Nucleation and Growth in High Strain-Low Cycle Fatigue," *Trans. Met. Soc. AIME*, Vol. 233, pp. 279-387.

Bradford, R., 1988, "A Structural Approach to the Calculation of *J*," *Engineering Fracture Mechanics*, Vol. 29, pp. 683-696.

Bradford, R., 1987, "Elastic-plastic J-analysis of a Thermally and Mechanically Loaded Cracked Cylinder by the Reference Stress Approach", CEGB Report OED/STM/87/10050/N, Bedminster Down, Bristol, England.

Brocks, W., and H.-D. Noack, 1988, "J-Integral and Stresses at an Inner Surface Flaw in a Pressure Vessel," *International Journal of Pressure Vessels and Piping*, Vol. 31, pp. 187-203.

Broek, D., 1972, "The Propagation of Fatigue Cracks Emanating From Holes," Report NLR TR-72134C, National Aerospace Laboratory, Amsterdam, The Netherlands.

Brose, W. R., N. E. Dowling, and J. Morrow, 1974, "Effect of Periodic Large Strain Cycles on the Fatigue Behavior of Steels," SAE Paper 740221.

Brown, W. F., Jr., H. Mindlin, and C. Y. Ho, 1996, **Aerospace Structural Metals Handbook**, 5 volumes, CINDAS/USAF CRDA Handbooks Operation, Purdue University.

Brown, M. W., E. R. de los Rios, and K. J. Miller, 1988, "A Critical Comparison of Proposed Parameters for High Strain Fatigue Crack Growth," *Basic Questions in Fatigue: Volume I, ASTM STP 924*, American Society for Testing and Materials, pp. 233-259.

Brown, M. W., and K. J. Miller, 1985, "Mode I Fatigue Crack Growth Under Biaxial Stress at Room and Elevated Temperature," *Multiaxial Fatigue, ASTM STP 853*, American Society for Testing and Materials, pp. 135-152.

Brown, W. F., and J. E. Srawley, 1966, *Plane Strain Crack Toughness Testing of High Strength Metallic Materials, ASTM STP 410*, American Society for Testing and Materials.

Brust, F. W., M. Nakagaki, and P. Gilles, 1990, "Comparison of Elastic-Plastic Fracture Mechanics Techniques," *Fracture Mechanics: Twenty-First Symposium, ASTM STP 1074*, pp. 448-469.

Brust, F. W., M. Nakagaki, and C. Springfield, 1989, "Integral Parameters for Thermal Fracture," *Engineering Fracture Mechanics*, Vol. 33, pp. 561-579.

Brust, F. W., J. J. McGowan, and S. N. Atluri, 1986, "A Combined Numerical/Experimental Study of Ductile Crack Growth After a Large Unloading, Using T^*, J, and CTOA Criteria," *Engineering Fracture Mechanics*, Vol. 23, pp. 537-550.

Bryan, R. H., B. R. Bass, J. W. Bryson, and J. G. Merkle, 1984, "Experimental Investigation of Tearing Behavior of a Flaw in a Thick Pressure Vessel," 1984 Light Water Reactor Structural Integrity, Proc. 3rd Int. Seminar on Assuring Structural Integrity of Steel Reactor Pressure Boundary Components, Elsevier, pp. 175-209.

Budden, P. J., 1989, "Fracture Assessment of Combined Thermal and Mechanical Loads Using Uncracked Body Stress Analysis," CEGB Report RD/B/6158/R89, Berkeley Nuclear Laboratories, Berkeley, England.

Budianski, B., and J. W. Hutchinson, 1978, "Analysis of Closure in Fatigue Crack Growth," *ASME Journal of Applied Mechanics*, Vol. 45, pp. 267-276.

Bueckner, H. F., 1958, "The propagation of cracks and the energy of elastic deformation", *Journal of Applied Mechanics Trans. ASME*, Vol. 80E, pp. 1225-30.

Casper, S., 1986, "J-integral and Plastic Zone Analysis of the Combined Thermal Mechanical Loading of a Centre-Crack Plate", CEGB, *[Referenced as note in draft in the validation section of Milne, et al. (1986)].*

Chan, K. S., J. Lankford, and D. L. Davidson, 1986, "A Comparison of Crack-Tip Field Parameters for Large and Small Cracks," *ASME Journal of Engineering Materials and Technology*, Vol. 108, pp. 206-213.

Chell, G. G., R. C. McClung, C. J. Kuhlman, D. A. Russell, K. Garr, and B. Donnelly, 1997a, "Guidelines for Proof Test Analysis," Final Report to NASA Marshall Space Flight Center, Contract NAS8-39380, to be published as a NASA Contractor Report.

Chell, G. G., C. J. Kuhlman, H. R. Millwater, and D. S. Riha, 1997b, "Application of Reference Stress and Probabilistic Methodologies to Assessing Creep Crack Growth," *Elevated Temperature Effects on Fatigue and Fracture, ASTM STP 1297,* American Society for Testing and Materials, pp. 54-73.

Chell, G. G., S. J. Hudak, V. P. Swaminathan, C.-P. Leung, and A. Saxena, 1993, "A High Temperature Fitness for Service Assessment Methodology for Petrochemical Processing Vessels," *Service Experience and Life Management: Nuclear, Fossil, and Petrochemical Plants*, ASME PVP-Vol. 261, pp. 213-234.

Chell, G. G., 1990, "Application of the CEGB Failure Assessment Procedure, R6, to Surface Flaws", *Fracture Mechanics: 21st Symposium, ASTM STP 1074*, American Society for Testing and Materials, pp. 525-544.

Chell, G. G., 1986, "A *J* Estimation Procedure for Combined Mechanical, Thermal, and Residual Stresses," *International Journal of Pressure Vessels and Piping*, Vol. 23, pp. 187-213.

Chell, G. G., 1984, "Fatigue Crack Growth Laws for Brittle and Ductile Materials Including the Effects of Static Modes and Elastic-Plastic Deformation," *Fatigue of Engineering Materials and Structures*, Vol. 7, pp. 237-250.

Chell, G. G., 1979, "A Procedure for Incorporating Thermal and Residual Stresses into the Concept of a Failure Assessment Diagram", *Elastic-Plastic Fracture, ASTM STP 668*, American Society for Testing and Materials, pp. 581-605.

Chermahini, R. G., K. N. Shivakumar, J. C. Newman, Jr., and A. F. Blom, 1989, "Three-Dimensional Aspects of Plasticity-Induced Fatigue Crack Closure," *Engineering Fracture Mechanics*, Vol. 34, pp. 393-401.

Clark, W. G., Jr., 1971, "Effect of Temperature and Section Size on Fatigue Crack Growth in Pressure Vessel Steel," *Journal of Materials*, Vol. 6, pp. 134-149.

Cruse, T. A., and S. T. Raveendra, 1988, "Advanced Modeling for Fatigue Growth of Small Surface Cracks," Final Report, AFOSR Contract No. F49620-86-C-0048.

Daiuto, R. A., and B. M. Hillberry, 1984, "Effect of Thickness on Fatigue Crack Propagation in 7475-T731 Aluminum Alloy Sheet," NASA CR-172367.

Davidson, D. L., S. J. Hudak, Jr., and R. J. Dexter, 1987, "Fatigue Crack Growth with Single Overload: Measurement and Modeling," *Load and Thermal History Effects on Mechanical Properties*, TMS, pp. 63-79.

Davidson, D. L., S. J. Hudak, Jr., and R. J. Dexter, 1985, "Measurement and Analysis of Critical Crack-Tip Processes During Fatigue Crack Growth," NASA CR-172597.

de Lorenzi, H. G., 1982, "On the Energy Release Rate and the J Integral for 3-D Crack Configurations," *International Journal of Fracture*, Vol. 19, pp. 183-194.

Dexter, R. J., S. J. Hudak, Jr., and D. L. Davidson, 1989, "Modelling and Measurement of Crack Closure and Crack Growth Following Overloads and Underloads," *Engineering Fracture Mechanics*, Vol. 33, pp. 855-870.

Dill, H. D., and C. R. Saff, 1976, "Spectrum Crack Growth Prediction Method Based on Crack Surface Displacement and Contact Analysis," *Fatigue Crack Growth Under Spectrum Loads, ASTM STP 595*, American Society for Testing and Materials, pp. 306-319.

Dodds, R. H., Jr., C. F. Shih, and T. L. Anderson, 1993, "Continuum and Micromechanics Treatment of Constraint in Fracture," *International Journal of Fracture*, Vol. 64, pp. 101-133.

Dowling, N. E., 1987, "J-Integral Estimates for Cracks in Infinite Bodies," *Engineering Fracture Mechanics*, Vol. 26, pp. 333-348.

Dowling, N. E., 1979, "Notched Member Fatigue Life Predictions Combining Crack Initiation and Propagation," *Fatigue of Engineering Materials and Structures*, Vol. 2, pp. 129-138.

Dowling, N. E., 1977, "Crack Growth During Low-Cycle Fatigue of Smooth Axial Specimens," *Cyclic Stress-Strain and Plastic Deformation Aspects of Fatigue Crack Growth, ASTM STP 637*, American Society for Testing and Materials, pp. 97-121.

Dowling, N. E., 1976, "Geometry Effects and the J-Integral Approach to Elastic-Plastic Fatigue Crack Growth," *Cracks and Fracture, ASTM STP 601*, American Society for Testing and Materials, pp. 19-32.

Dowling, N. E., and J. A. Begley, 1976, "Fatigue Crack Growth During Gross Plasticity and the J-Integral," *Mechanics of Crack Growth, ASTM STP 590*, American Society for Testing and Materials, pp. 82-103.

Dugdale, D. S., 1960, "Yielding of Steel Sheets Containing Slits," *Journal of the Mechanics and Physics of Solids*, Vol. 8, pp. 100-104.

Earthman, J. C., 1991, "Characterization of Small Crack Growth in 12% CrMoV Steel under High Temperature, Low Cycle Fatigue Conditions," *Materials Science and Engineering*, Vol. A132, pp. 89-95.

El Haddad, M. H., and B. Mukherjee, 1983, "Elastic-Plastic Fracture Mechanics Analysis of Fatigue Crack Growth," *Elastic-Plastic Fracture: Second Symposium, Volume II–Fracture Resistance Curves and Engineering Applications, ASTM STP 803*, American Society for Testing and Materials, pp. II-689–II-707.

El Haddad, M. H., N. E. Dowling, T. H. Topper, and K. N. Smith, 1980, "*J* Integral Applications for Short Fatigue Cracks at Notches," *International Journal of Fracture*, Vol. 16, pp. 15-30.

El Haddad, M. H., K. N. Smith, and T. H. Topper, 1979a, "A Strain Based Intensity Factor Solution for Short Fatigue Cracks Initiating from Notches," *Fracture Mechanics, ASTM STP 677*, American Society for Testing and Materials, pp. 274-289.

El Haddad, M. H., K. N. Smith, and T. H. Topper, 1979b, "Fatigue Crack Propagation of Short Cracks," *ASME Journal of Engineering Materials and Technology*, Vol. 101, pp. 42-46.

Elber, W., 1971, "The Significance of Fatigue Crack Closure," *Damage Tolerance in Aircraft Structures, ASTM STP 486*, American Society for Testing and Materials, pp. 230-242.

Elber, W., 1970, "Fatigue Crack Closure Under Cyclic Tension," *Engineering Fracture Mechanics*, Vol. 2, pp. 37-45.

Fleck, N. A., 1986, "Finite Element Analysis of Plasticity-Induced Crack Closure Under Plane Strain Conditions," *Engineering Fracture Mechanics*, Vol. 25, pp. 441-449.

Fleck, N. A., and R. A. Smith, 1982, "Crack Closure—Is It Just a Surface Phenomenon?", *International Journal of Fatigue*, Vol. 4, pp. 157-160.

Forman, R. G., et al., 1997, "Fatigue Crack Growth Computer Program NASGRO Version 3.00," JSC-22267B (DRAFT), NASA Lyndon B. Johnson Space Center.

Forman, R. G., et al., 1994, "Fatigue Crack Growth Computer Program NASA/FLAGRO Version 2.0," JSC-22267A, NASA Lyndon B. Johnson Space Center.

Forman, R. G., V. Shivakumar, J. C. Newman, Jr., S. M. Piotrowski, and L. C. Williams, 1988, "Development of the NASA/FLAGRO Computer Program," *Fracture Mechanics: Eighteenth Symposium, ASTM STP 945*, American Society for Testing and Materials, Philadelphia, pp. 781-803.

Forman, R. G., and T. Hu, 1984, "Application of Fracture Mechanics on the Space Shuttle," *Damage Tolerance of Metallic Structures, ASTM STP 842*, American Society for Testing and Materials, Philadelphia, pp. 108-133.

Fuhring, H., and T. Seeger, 1979, "Dugdale Crack Closure Analysis of Fatigue Cracks Under Constant Amplitude Loading," *Engineering Fracture Mechanics*, Vol. 11, pp. 99-122.

Gao, X., J. Faleskog, C. F. Shih, and R. H. Dodds, Jr., 1998, "Ductile Tearing in Part-Through Cracks: Experiments and Cell-Model Predictions," *Engineering Fracture Mechanics*, Vol. 59, pp. 761-777.

Ghonem, H., T. Nicholas, and A. Pineau, 1993, "Elevated Temperature Fatigue Crack Growth in Alloy 718 Part I: Effects of Mechanical Variables, and Part II: Effects of Environmental and Material Variables," *Engineering Fracture Mechanics*, Vol. 16, pp. 565-576 and pp. 577-590.

Glinka, G., and A. Newport, 1987, "Universal Features of Elastic Notch-Tip Stress Fields," *International Journal of Fatigue*, Vol. 9, pp. 143-150.

Glinka, G., 1985a, "Energy Density Approach to Calculation of Inelastic Strain-Stress Near Notches and Cracks," *Engineering Fracture Mechanics*, Vol. 22, pp. 485-508.

Glinka, G., 1985b, "Calculation of Inelastic Notch-Tip Strain-Stress Histories Under Cyclic Loading," *Engineering Fracture Mechanics*, Vol. 22, pp. 839-854.

Grin', E. A., D. M. Shur, and A. G. Mazepa, 1987, "Study of the Kinetics of Growth of a Low-Cycle Fatigue Crack with the Use of the *J*-Integral (Translation)," *Problemy Prochnosti* (USSR), Vol. 19, pp. 1325-1329.

Haigh, J. R., and R. P. Skelton, 1978, "A Strain Intensity Approach to High Temperature Fatigue Crack Growth and Failure," *Materials Science and Engineering*, Vol. 36, pp. 133-137.

Harris, D. O., C. J. Bianca, E. D. Eason, L. D. Salter, and J. M. Thomas, 1987, "NASCRAC: A Computer Code for Fracture Mechanics Analysis of Crack Growth," Proc. AIAA/ASME/ASCE/AHS 28th Structures, Structural Dynamics, and Materials Conference, Part 1, pp. 662-667.

Hatanaka, K., T. Fujimitsu, and S. Shiraishi, 1989, "An Analysis of Surface Crack Growth in Circumferentially Grooved Components under Low-Cycle Fatigue," *JSME International Journal*, Series I, Vol. 32, pp. 245-255.

Hatanaka, K., T. Fujimitsu, and H. Ichiymama, 1987a, "Effects of Mean Stress and Strain on Crack Growth and Crack Closure in Low Cycle Fatigue," *Trans. JSME*, Series A, Vol. 53, pp. 748-754 (in Japanese).

Hatanaka, K., T. Fujimitsu, and S. Shiraishi, 1987b, "Effect of Mean Stress on Closure and Growth of Short Cracks in Low Cycle Fatigue," *Trans. JSME*, Series A, Vol. 53, pp. 740-747 (in Japanese).

He, M., 1986, "Through-the-Thickness Crack in Biaxial Stress Field," Institute of Scientific and Technical Information of China, Technical Report C 000039, Beijing (available NTIS). See also Proc. ICF Int. Symp. Fracture Mechanics (Beijing), Science Press, Beijing, China, 1983, pp. 42-49.

He, M. Y., and J. W. Hutchinson, 1983a, "Bounds for Fully Plastic Crack Problems for Infinite Bodies," *Elastic-Plastic Fracture, Volume I: Inelastic Crack Analysis, ASTM STP 803*, American Society for Testing and Materials, pp. I-277 - I-290.

He, M. Y., and John W. Hutchinson, 1983b, "Penny-Shaped Crack in a Round Bar of Power-Law Hardening Material," *Elastic-Plastic Fracture: Second Symposium, Volume I - Inelastic Crack Analysis, ASTM STP 803*, American Society for Testing and Materials, pp. I-291 - I-305.

He, M. Y., and J. W. Hutchinson, 1981, "The Penny-Shaped Crack and the Plane Strain Crack in an Infinite Body of Power-Law Material," *ASME Journal of Applied Mechanics*, Vol. 48, pp. 830-840.

Heald, P. T., T. C. Lindley, and C. E. Richards, 1972, "The Influence of Stress Intensity and Microstructure of Fatigue Crack Growth Propagation in 1% Carbon Steel," *Materials Science and Engineering*, Vol. 10, pp. 235-240.

Heaton, M. D., 1976, "On the Calculation of Stress Intensity Factors Due to Thermal and Residual Stress Fields", CEGB Research Report NW/SSD/RR/158/78, CEGB Northwestern Region Scientific Services Department.

Heitmann, H. H., H. Vehoff, and P Neumann, 1984, "Life Prediction for Random Load Fatigue Based on the Growth Behavior of Microcracks," *Advances in Fracture Research, Fracture '84*, Proc. ICF6, Vol. 5, pp. 3599-3606.

Hellen, T. K., and W. S. Blackburn, 1987, "Post-Yield Fracture Mechanics Analysis of the Combined Thermal and Mechanical Loading of a Centre-Cracked Plate," *International Journal of Fracture*, Vol. 32, pp. 185-199.

Hellen, T. K., and W. S. Blackburn, 1985, "Post-yield Fracture Mechanics Analysis of the Combined Thermal and Mechanical Loading of a Centre Cracked Panel", CEGB Report TPRD/B/0613/R85, Berkeley Nuclear Laboratories, Gloucestershire, England.

Hertzberg, R. W., and P. C. Paris, 1965, "Application of Electron Fractography and Fracture Mechanics to Fatigue Crack Propagation," Proc. First Int. Conf. Fracture, Sendai, Japan, Vol. 1, pp. 459-478.

Hodulak, L., and H. Stöckl, 1985, "Bestimmung von J-Risswiderstandskurven an Platten mit Oberflächenrissen," Report W11/85, Fraunhofer-Institut der Werkstoffmechanik, Freiburg, Germany.

Holt, J. M., H. Mindlin, and C. Y. Ho, 1996, **Structural Alloys Handbook**, 3 volumes, CINDAS/ Purdue University.

Horikawa, K., and S.-M. Cho, 1987, "Initial Fatigue Crack Growth Behavior in a Notched Component (Report II)," *Transactions of Japan Welding Research Institute*, Vol. 16, pp. 167-175.

Hoshide, T., M. Miyahara, and T. Inoue, 1988, "Elastic-Plastic Behavior of Short Fatigue Crack in Smooth Specimen," *Basic Questions in Fatigue: Volume I, ASTM STP 924*, American Society for Testing and Materials, pp. 312-322.

Hoshide, T., and D. F. Socie, 1987, "Mechanics of Mixed Mode Small Fatigue Crack Growth," *Engineering Fracture Mechanics*, Vol. 26, pp. 841-850.

Hoshide, T., K. Tanaka, and A. Yamada, 1981, "Stress-Ratio Effect of Fatigue Crack Propagation in a Biaxial Stress Field," *Fatigue of Engineering Materials and Structures*, Vol. 4, pp. 355-366.

Huang, J. S., and R. M. Pelloux, 1980, "Low Cycle Fatigue Crack Propagation in Hastelloy-X at 25 and 760 °C," *Metallurgical Transactions A*, Vol. 11A, pp. 899-904.

Ibrahim, F. K., J. C. Thompson, and T. H. Topper, 1986, "A Study of the Effect of Mechanical Variables on Fatigue Crack Closure and Propagation," *International Journal of Fatigue*, Vol. 8, pp. 135-142.

Inglis, C. E., 1913, "Stresses in a Plate due to the Presence of Cracks and Sharp Corners," *Trans. of the Royal Institute of Naval Architects, London*, Vol. 55, pp. 219-230.

Irving, P. E., and L. N. McCartney, 1977, "Prediction of Fatigue Crack Growth Rates: Theory, Mechanisms and Experimental Results," *Metal Science*, Vol. 11, pp. 351-361.

Isida, M., 1971, "Effect of Width and Length on Stress Intensity Factors of Internally Cracked Plates Under Various Boundary Conditions," *International Journal of Fracture*, Vol. 7, pp. 301-316.

Iyyer, N. S., and N. E. Dowling, 1986, "Opening and Closing of Cracks at High Cyclic Strains," *Small Fatigue Cracks*, TMS, pp. 213-223.

Jablonski, D. A., 1989, "An Experimental Study of the Validity of a Delta *J* Criterion for Fatigue Crack Growth," *Nonlinear Fracture Mechanics: Volume I–Time Dependent Fracture, ASTM STP 995*, American Society for Testing and Materials, pp. 361-387.

Jansson, S., 1986, "Fully Plastic Plane Stress Solutions for Biaxially Loaded Center-Cracked Plates," *ASME Journal of Applied Mechanics*, Vol. 53, pp. 555-560.

Joch, J., and R.A. Ainsworth, 1992a, "The Effect of Geometry on the Development of Creep Singular Fields for Defects Under Step-Load Controlled Loading," *Fatigue and Fracture of Engineering Materials and Structures*, Vol. 15, pp. 229-240.

Joch, J., and R.A. Ainsworth, 1992b, "The Development of Creep Singular Fields for Defects in Thermally Loaded Structures," *Fatigue and Fracture of Engineering Materials and Structures*, Vol. 15, pp. 685-693.

Jolles, M., 1985, "Effects of Load Gradient on Applicability of a Fatigue Crack Growth Rate–Cyclic *J* Relation," *Fracture Mechanics: Sixteenth Symposium, ASTM STP 868*, American Society for Testing and Materials, pp. 381-391.

Jordan, E. H., and G. J. Meyers, 1989, "Fracture Mechanics Applied to Elevated Temperature Crack Growth," *ASME Journal of Engineering Materials and Technology*, Vol. 111, pp. 306-313.

Jordan, E. H., and G. J. Meyers, 1986, "Fracture Mechanics Applied to Nonisothermal Fatigue Crack Growth," *Engineering Fracture Mechanics*, Vol. 23, pp. 345-358.

Joyce, J. A., and V. Culafic, 1988, "Characterization of Interaction Effects Between Ductile Tearing and Intense Fatigue Cycling," *International Journal of Fracture*, Vol. 36, pp. 89-100.

Kaiser, S., 1983, "On the Relation Between Stable Crack Growth and Fatigue," *Fatigue of Engineering Materials and Structures*, Vol. 6, pp. 33-50.

Kanninen, M. F., and C. Atkinson, 1980, "Application of an Inclined-Strip-Yield Crack Tip Plasticity Model to Predict Constant Amplitude Fatigue Crack Growth," *International Journal of Fracture*, Vol. 16, pp. 53-69.

Kim, K. S., and R. H. Van Stone, 1997, "Crack Growth Under Thermo-Mechanical and Temperature Gradient Loads," *Engineering Fracture Mechanics*, Vol. 58, pp. 133-147.

Kim, K. S., and R. H. Van Stone, 1995a, "Time-Dependent Crack Growth Characterization Using Rate Integrals," *International Journal of Fracture*, Vol. 70, pp. 167-181.

Kim, K. S., and R. H. Van Stone, 1995b, "Hold Time Crack Growth Analyses at Elevated Temperatures," *Engineering Fracture Mechanics*, Vol. 52, pp. 433-444.

Kim, K. S., and R. H. Van Stone, 1995c, "Characterization of Elevated Temperature Crack Growth in Hastelloy-X Using Integral Parameters," *ASME Journal of Engineering Materials and Technology*, Vol. 117, pp. 299-304.

Kim, K. S., and R. H. Van Stone, 1992, "Elevated Temperature Crack Growth," NASA CR 189191, prepared for NASA Lewis Research Center.

Kim, K. S., and T. W. Orange, 1988, "A Review of Path-Independent Integrals in Elastic-Plastic Fracture Mechanics," *Fracture Mechanics: Eighteenth Symposium, ASTM STP 945*, American Society for Testing and Materials, pp. 713-729.

Kim, K. S., R. H. Van Stone, S. N. Malik, and J. H. Laflen, 1988a, "Elevated Temperature Crack Growth," *Lewis Structures Technology - 1988*, NASA CP-3003, Vol. 3, pp. 3-187 - 3-198.

Kim, K. S., R. H. Van Stone, S. N. Malik, and J. H. Laflen, 1988b, "Elevated Temperature Crack Growth," NASA CR 182247, prepared for NASA Lewis Research Center.

Kirk, M. T., and R. H. Dodds, Jr., 1992, "Approximate Techniques of J Estimation Applicable to Part-Through Surface Cracks," *Engineering Fracture Mechanics*, Vol. 43, pp. 123-136.

Kishimoto, K., S. Aoki, and M. Sakata, 1980, "On the Path Independent Integral-$\hat{J}$," *Engineering Fracture Mechanics*, Vol. 13, pp. 841-850.

Kubo, S., T. Yafuso, M. Nohara, T. Ishimaru, and K. Ohji, 1989, "Investigation on Path-Integral Expression of the *J*-Integral Range Using Numerical Simulations of Fatigue Crack Growth," *JSME International Journal*, Series I, Vol. 32, pp. 237-244.

Kumar, V., and M. D. German, 1988, "Elastic-Plastic Fracture Analysis of Through Wall and Surface Flaws in Cylinders," Report NP-5596, Electric Power Research Institute.

Kumar, V., M. D. German, W. W. Wilkening, W. R. Andrews, H. G. deLorenzi, and D. F. Mowbray, 1984a, "Advances in Elastic-Plastic Fracture Analysis," Report NP-3607, Electric Power Research Institute.

Kumar, V., B. I. Schumacher, and M. D. German, 1984b, "Development of a Procedure for Incorporating Secondary Stresses in the Engineering Approach", Report NP-3607, Section 7, Electric Power Research Institute.

Kumar, V., W. W. Wilkening, W. R. Andrews, M. D. German, H. G. deLorenzi, and D. F. Mowbray, 1982, "Estimation Techniques for the Prediction of Elastic-Plastic Fracture of Structural Components of Nuclear Systems," 5th and 6th Semiannual Report to EPRI, Contract RP1237-1, February 1, 1981- January 31, 1982.

Kumar, V., M. D. German, and C. F. Shih, 1981, "An Engineering Approach for Elastic-Plastic Fracture Analysis," Report NP-1931, Electric Power Research Institute.

Laird, C., and G. C. Smith, 1962, "Crack Propagation in High Stress Fatigue," *Philosophical Magazine*, Vol. 7, pp. 847-857.

Lalor, P., and H. Sehitoglu, 1988, "Fatigue Crack Closure Outside Small Scale Yielding Regime," *Mechanics of Fatigue Crack Closure, ASTM STP 982*, American Society for Testing and Materials, pp. 342-360.

Lamba, H. S., 1975, "The *J*-Integral Applied to Cyclic Loading," *Engineering Fracture Mechanics*, Vol. 7, pp. 693-703.

Landes, J. D., and J.A. Begley, 1976, "A Fracture Mechanics Approach to Creep Crack Growth," *Mechanics of Crack Growth, ASTM STP 590*, American Society for Testing and Materials, pp. 128-148.

Larsson, S. G., and A. J. Carlsson, 1973, "Influence of Non-Singular Stress Terms and Specimen Geometry on Small-Scale Yielding at Crack Tips in Elastic-Plastic Materials," *Journal of the Mechanics and Physics of Solids*, Vol. 21, pp. 263-277.

Leevers, P. S., and J. C. Radon, 1982, "Inherent Stress Biaxiality in Various Fracture Specimen Geometries," *International Journal of Fracture*, Vol. 19, pp. 311-325.

Leung, C.-P., D. L. McDowell, and A. Saxena, 1990, "Estimation of the C_t Parameter: Experimental Implications," *ASTM Journal of Testing and Evaluation*, Vol. 18, pp. 25-37.

Leung, C.-P., and D. L. McDowell, 1990, "Inclusion of Primary Creep in the Estimation of the C_t Parameter," August, *International Journal of Fracture*, Vol. 46, pp. 81-104.

Leung, C. P., D.L. McDowell, and A. Saxena, 1988, "Influence of Primary Creep in the Estimation of C_t Parameter," *International Journal of Fracture*, Vol. 36, pp. 275-289.

Liaw, P. K., A. Saxena and J. Schaeffer, 1989, "Estimating Remaining Life of Elevated Temperature Steam Pipes — Part II: Fracture Mechanics Analyses," *Engineering Fracture Mechanics*, Vol. 32, pp. 709-722.

Ling, M. R., and J. Schijve, 1990, "Fractographic Analysis of Crack Growth and Shear Lip Development Under Simple Variable-Amplitude Loading," *Fatigue and Fracture of Engineering Materials and Structures*, Vol. 13, pp. 443-456.

Liu, J. Z., and X. R. Wu, 1997, "Study on Fatigue Crack Closure Behavior for Various Cracked Geometries," *Engineering Fracture Mechanics*, Vol. 57, pp. 475-491.

Manson, S. S., and M. H. Hirschberg, 1964, **Fatigue: An Interdisciplinary Approach**, Syracuse University Press, Syracuse, New York.

Marchand, N. J., R. M. Pelloux, and B. Ilschner, 1988, "A Fracture Mechanics Criterion For Thermal-Mechanical Fatigue Crack Growth of Gas Turbine Materials," *Engineering Fracture Mechanics*, Vol. 31, pp. 535-551.

Marchand, N. J., R. M. Pelloux, and B. Ilschner, 1987, "Non-Isothermal Fatigue Crack Growth in Hastelloy-X," *Fatigue and Fracture of Engineering Materials and Structures*," Vol. 10, pp. 59-74.

Marschall, C. W., and G. M. Wilkowski, 1989, "Effect of Cyclic Loads on Ductile Fracture Resistance," *Advances in Fracture and Fatigue for the 1990's, Vol. 1: Load History Effects of Fracture Resistance*, PVP-Vol. 166, ASME, pp. 1-13.

McClintock, F., and G. Irwin, 1965, "Plasticity Aspects of Fracture Mechanics," *Fracture Toughness Testing and Its Applications, ASTM STP 381*, American Society for Testing and Materials, pp. 85-109.

McClung, R. C., K. S. Chan, S. J. Hudak, Jr., and D. L. Davidson, 1996a, "Behavior of Small Fatigue Cracks," *ASM Handbook, Volume 19: Fatigue and Fracture*, ASM International, pp. 153-158.

McClung, R. C., G. G. Chell, H. R. Millwater, D. A. Russell, and G. E. Orient, 1996b, "A Comparison of Single-Cycle Versus Multiple Cycle Proof Testing Strategies: Final Report," Final Report to NASA Marshall Space Flight Center, Contract NAS8-37451, to be published as a NASA Contractor Report.

McClung, R. C., 1994, "Finite Element Analysis of Specimen Geometry Effects on Fatigue Crack Closure," *Fatigue and Fracture of Engineering Materials and Structures*, Vol. 17, pp. 861-872.

McClung, R. C., and S. J. Hudak, Jr., 1994, "Surface Crack Growth in Inconel 718 During Large Unload-Reload Cycles," *Fracture Mechanics: Twenty-Fourth Volume, ASTM STP 1207*, American Society for Testing and Materials, pp. 706-721.

McClung, R. C., S. J. Hudak, Jr., M. L. Bartlett, and J. H. FitzGerald, 1993, "Growth of Surface Cracks During Large Elastic-Plastic Loading Cycles," *Fracture Mechanics: Twenty-Third Symposium, ASTM STP 1189*, American Society for Testing and Materials, pp. 265-283.

McClung, R. C., 1992, "Finite Element Modeling of Fatigue Crack Growth," *Theoretical Concepts and Numerical Analysis of Fatigue*, Engineering Materials Advisory Services, pp. 153-172.

McClung, R. C., and H. Sehitoglu, 1992, "Closure and Growth of Fatigue Cracks at Notches," *ASME Journal of Engineering Materials and Technology*, Vol. 114, pp. 1-7.

McClung, R. C., 1991a, "A Simple Model for Fatigue Crack Growth Near Stress Concentrations," *ASME Journal of Pressure Vessel Technology*, Vol. 113, pp. 542-548.

McClung, R. C., 1991b, "Crack Closure and Plastic Zone Sizes in Fatigue," *Fatigue and Fracture of Engineering Materials and Structures*, Vol. 14, pp. 455-468.

McClung, R. C., 1991c, "The Influence of Applied Stress, Crack Length, and Stress Intensity Factor on Crack Closure," *Metallurgical Transactions A*, Vol. 22A, pp. 1559-1571.

McClung, R. C., and H. Sehitoglu, 1991, "Characterization of Fatigue Crack Growth in Intermediate and Large Scale Yielding," *ASME Journal of Engineering Materials and Technology*, Vol. 113, pp. 15-22.

McClung, R. C., B. H. Thacker, and S. Roy, 1991, "Finite Element Visualization of Fatigue Crack Closure in Plane Stress and Plane Strain," *International Journal of Fracture*, Vol. 50, pp. 27-49.

McClung, R. C., 1989a, "Closure and Growth of Mode I Cracks in Biaxial Fatigue," *Fatigue and Fracture of Engineering Materials and Structures,* Vol. 12, pp. 447-460.

McClung, R. C., 1989b, "A Simple Model for Fatigue Crack Growth Near Stress Concentrations," *Innovative Approaches to Irradiation Damage and Fracture Analysis,* PVP - Vol. 170, ASME Pressure Vessels and Piping Conference, Honolulu, Hawaii, pp. 31-39.

McClung, R. C., and H. Sehitoglu, 1989a, "On the Finite Element Analysis of Fatigue Crack Closure — 1. Basic Modeling Issues," *Engineering Fracture Mechanics*, Vol. 33, pp. 237-252.

McClung, R. C., and H. Sehitoglu, 1989b, "On the Finite Element Analysis of Fatigue Crack Closure — 2. Numerical Results," *Engineering Fracture Mechanics*, Vol. 33, pp. 253-272.

McClung, R. C., and H. Sehitoglu, 1988, "Closure Behavior of Small Cracks Under High Strain Fatigue Histories," *Mechanics of Fatigue Crack Closure, ASTM STP 982*, American Society for Testing and Materials, Philadelphia, pp. 279-299.

McDowell, D. L., and J.-Y. Berard, 1992, "A ΔJ-Based Approach to Biaxial Fatigue," *Fatigue and Fracture of Engineering Materials and Structures*, Vol. 15, pp. 719-741.

McEvily, A. J., D. Beukelmann, and K. Tanaka, 1974, "On Large-Scale Plasticity Effects in Fatigue Crack Propagation," Proc. Symp. Mechanical Behavior of Materials, Kyoto, Japan, Society of Materials Science, Japan, Vol. 1, pp. 269-281.

McEvily, A. J., 1969, "Fatigue Crack Growth and the Strain Intensity Factor," Proc. Air Force Conf. on Fatigue and Fracture of Aircraft Structures and Materials, Miami Beach, AFFDL-TR-70-144, pp. 451-458.

McGowan, J. J., and H. W. Liu, 1980, "The Role of Three-Dimensional Effects in Constant Amplitude Fatigue Crack Growth Testing," *ASME Journal of Engineering Materials and Technology*, Vol. 102, pp. 341-346.

McMeeking, R. M., and D. M. Parks, 1979, "On Criteria for *J*-Dominance of Crack-Tip Fields In Large-Scale Yielding," *Elastic-Plastic Fracture, ASTM STP 668*, American Society for Testing and Materials, pp. 175-194.

Meyers, G. J., 1982, "Fracture Mechanics Criteria for Turbine Engine Hot Section Components," Final Report, NASA CR-167896.

Miller, M. P., D. L. McDowell, R. T. T. Oehmke, and S. D. Antolovich, 1993, "A Life Prediction Model for Thermomechanical Fatigue Based on Microcrack Propagation," *Thermomechanical Fatigue Behavior of Materials, ASTM STP 1186*, American Society for Testing and Materials, pp. 35-49.

Miller, A. G., 1988, "Review of Limit Loads of Structures Containing Defects," *International Journal of Pressure Vessels & Piping*, Vol. 32, pp. 197-327.

Miller, A, G., 1986, "J Estimation for Surface Defects", Report TPRD/B/0811/R86, Central Electricity Generating Board, Berkeley Nuclear Laboratories, Gloucestershire, U.K.

Milne, I., R. A. Ainsworth, A. R. Dowling, and A. T. Stewart, 1986, "Assessment of the Integrity of Structures Containing Defects," CEGB Report R/H/R6-Revision 3, Central Electricity Generating Board, Sudbury House, London.

Miura, N., T. Fujioka, K. Kashima, S. Kanno, M. Hayashi, M. Ishiwata, and N. Gotoh, 1994, "Low Cycle Fatigue and Ductile Fracture for Japanese Carbon Steel Piping Under Dynamic Loading," *Nuclear Engineering and Design*, Vol. 153, pp. 57-69.

Moran, B., and C. F. Shih, 1987, "Crack Tip and Associated Domain Integrals from Momentum and Energy Balance," *Engineering Fracture Mechanics*, Vol. 27, pp. 614-642.

Morrow, J., 1965, "Cyclic Plastic Strain Energy and Fatigue of Metals," *Internal Friction, Damping, and Cyclic Plasticity, ASTM STP 378*, American Society for Testing and Materials, pp. 45-87.

Mowbray, D. F., 1979, "Use of a Compact-Type Strip Specimen for Fatigue Crack Growth Rate Testing in the High-Rate Regime," *Elastic-Plastic Fracture, ASTM STP 668*, American Society for Testing and Materials, pp. 736-752.

Mu, Z., H. Vehoff, M. Brede, and P. Neumann, 1996, "Behavior of Short Cracks in Alloy 800HT Under Biaxial Fatigue," *Materials Science and Technology*, Vol. 12, pp. 416-420.

Murakami, Y., 1987, 1989, 1992, **Stress Intensity Factors Handbook**, 3 volumes, Pergamon Press.

Musava, J. K., and J. C. Radon, 1980, "An Elastic-Plastic Crack Growth Analysis Using the *J*-Integral Concept," *Fracture and Fatigue: Elasto-Plasticity, Thin Sheet, and Micromechanisms Problems*, Proc. 3rd Colloquium on Fracture, Pergamon, pp. 129-141.

Muscati, A., 1985, "Elastic-plastic Fracture Analysis of a Thick Walled Cylinder Subjected to Combined Thermal and Mechanical Loading", CEGB Report SWR/SSD/0626/N85, Bedminster Down, Bristol, England.

NASCRAC User's Manual and *NASCRAC Theory Manual*, 1989, Version 2.0, Failure Analysis Associates.

Neuber, H., 1961, "Theory of Stress Concentration for Shear Strained Prismatical Bodies with Arbitrary Non-linear Stress-strain Law", *ASME Journal of Applied Mechanics*, Vol. 28, pp. 544-550.

Newman, J. C., Jr., J. D. Bland, and R. F. Berry, Jr., 1998, "Fracture Toughness and Critical Crack Sizes for the Space Shuttle Solid Rocket Motor D6AC Steel Case," *Fracture Mechanics: 26th Volume, ASTM STP 1256*, American Society for Testing and Materials, pp. 799-821.

Newman, J. C., Jr., 1996, "Application of a Closure Model to Predict Crack Growth in Three Engine Disc Materials," *International Journal of Fracture*, Vol. 80, pp. 193-218.

Newman, J. C., Jr., 1992a, "Fracture Mechanics Parameters for Small Fatigue Cracks," *Small-Crack Test Methods, ASTM STP 1149*, American Society for Testing and Materials, pp. 6-33.

Newman, J. C., Jr., 1992b, "FASTRAN-II A Fatigue Crack Growth Structural Analysis Program," NASA TM 104159.

Newman, J. C., Jr., D. S. Dawicke, and C. A. Bigelow, 1992, "Finite-Element Analyses and Fracture Simulation in Thin-Sheet Aluminum Alloy," NASA TM 107662, also published in Proceedings, International Workshop on Structural Integrity of Aging Airplanes, Atlanta, Georgia, 1992.

Newman, J. C., Jr., M. H. Swain, and E. P. Phillips, 1986, "An Assessment of the Small-Crack Effect for 2024-T3 Aluminum Alloy," *Small Fatigue Cracks*, The Metallurgical Society, pp. 427-452.

Newman, J. C., Jr., 1984, "A Crack Opening Stress Equation for Fatigue Crack Growth," *International Journal of Fracture*, Vol. 24, pp. R131-R135.

Newman, J. C., Jr., 1982, "A Nonlinear Fracture Mechanics Approach to the Growth of Small Cracks," *Behavior of Short Cracks in Airframe Components*, AGARD Conf. Proc. No. 328, pp. 6.1-6.26.

Newman, J. C., Jr., 1981, "A Crack-Closure Model for Predicting Fatigue Crack Growth Under Aircraft Spectrum Loading," *Methods and Models for Predicting Fatigue Crack Growth Under Random Loading, ASTM STP 748*, American Society for Testing and Materials, pp. 53-84.

Newman, J. C., Jr., and I. S. Raju, 1981, "An Empirical Stress-Intensity Factor Equation for the Surface Crack," *Engineering Fracture Mechanics*, Vol. 15, pp. 185-192.

Newman, J. C., Jr., 1976, "A Finite-Element Analysis of Fatigue Crack Closure," *Mechanics of Crack Growth, ASTM STP 590*, American Society for Testing and Materials, pp. 281-301.

Nikishkov, G. P., and S. N. Atluri, 1988, "Three-Dimensional Elastic-Plastic J-Integral Calculations for Semielliptical Surface Cracks in a Tensile Plate," *Engineering Fracture Mechanics*, Vol. 29, pp. 81-87.

Nix, K. J., G. G. Chell, N. Knee, and T. C. Lindley, 1989, "An Investigation of the Interaction Between Ductile Tearing and Fatigue in a Low Alloy Steel," *Advances in Fracture and Fatigue for the 1990's, Vol. 1: Load History Effects of Fracture Resistance*, PVP-Vol. 166, ASME, pp. 33-39.

Nix, K. J., T. C. Lindley, N. Knee, and G. G. Chell, 1988, "An Investigation of Fatigue Crack Growth in a Ductile Material at High Growth Rates," *Fatigue of Engineering Materials and Structures*, Vol. 11, pp. 205-220.

Obrtlik, K., and J. Polak, 1985, "Fatigue Growth of Surface Cracks in the Elastic-Plastic Region," *Fatigue and Fracture of Engineering Materials and Structures*, Vol. 8, pp. 23-31.

Ogura, K., Y. Miyoshi, and I. Nishikawa, 1985, "Fatigue Crack Growth and Closure of Small Cracks at the Notch Root," *Current Research on Fatigue Cracks, MRS 1*, Society of Materials Science, Japan, pp. 57-78.

Ohji, K., K. Ogura, and Y. Ohkubo, 1974, "On the Closure of Fatigue Cracks Under Cyclic Tensile Loading," *International Journal of Fracture*, Vol. 10, pp. 123-124.

Okazaki, M., I. Hattori, F. Shiraiwa, and T. Koizumi, 1983, "Effect of Strain Wave Shape on Low-Cycle Fatigue Crack Propagation of SUS 304 Stainless Steel at Elevated Temperatures," *Metallurgical Transactions A*, Vol. 14A, pp. 1649-1659.

Okazaki, M., and T. Koizumi, 1983, "Crack Propagation of Steels during Low Cycle Thermal-Mechanical and Isothermal Fatigue at Elevated Temperatures," *Metallurgical Transactions A*, Vol. 14A, pp. 1641-1648.

Orange, T. W., 1990, "Methods and Models for R-Curve Instability Calculations," *Fracture Mechanics: Twenty-First Symposium, ASTM STP 1074*, American Society for Testing and Materials, pp. 545-559.

Palazotto, A., and E. Bednarz, 1989, "A Finite-Element Investigation of Viscoplastic-Induced Closure of Short Cracks at High Temperatures," *Fracture Mechanics: Perspectives and Directions (Twentieth Symposium), ASTM STP 1020*, American Society for Testing and Materials, pp. 530-547.

Paris, P. C., 1964, "The Fracture Mechanics Approach to Fatigue," *Fatigue - An Interdisciplinary Approach*, Proc. 10th Sagamore Army Materials Research Conf., Syracuse Univ. Press, pp. 107-132.

Paris, P. C., M. P. Gomez, and W. E. Anderson, 1961, "A Rational Analytic Theory of Fatigue," *The Trend in Engineering*, University of Washington, January, pp. 9-14.

Parks, D. M., and Y.-Y. Wang, 1988, "Elastic-Plastic Analysis of Part-Through Surface Cracks," *Analytical, Numerical, and Experimental Aspects of Three Dimensional Fracture Processes*, AMD - Vol. 91, ASME, pp. 19-32.

Pelloux, R. M., and N. Marchand, 1986, "Thermal-Mechanical Fatigue Behavior of Nickel-Base Superalloys," NASA CR 175048, Prepared for NASA Lewis Research Center.

Rahman, S., G. Wilkowski, and R. Mohan, 1997, "Low-Cycle Fatigue Crack Growth Considerations in Pipe Fracture Analysis," *Nuclear Engineering and Design*, Vol. 168, pp. 105-118.

Reger, M., and L. Remy, 1982, "Influence of Environment on Microcrack Propagation in High Temperature Low Cycle Fatigue," *Fracture and the Role of Microstructure*, Proc. 4th European Conference on Fracture, EMAS, Vol. 2, pp. 531-538.

Rice, J. R., 1972, "Some Remarks on Elastic Crack Tip Stress Fields", *International Journal of Solids and Structures*, Vol. 8, pp. 751-758.

Rice, J. R., 1968, "A Path Independent Integral and the Approximate Analysis of Strain Concentration by Notches and Cracks," *ASME Journal of Applied Mechanics*, Vol. 35, pp. 379-386.

Rice, J. R., 1967, "Mechanics of Crack Tip Deformation and Extension by Fatigue," *Fatigue Crack Propagation, ASTM STP 415*, American Society for Testing and Materials, pp. 247-309.

Rie, K.-T., and H. Wittke, 1996, "New Approach for Estimation of ΔJ and for Measurement of Crack Growth at Elevated Temperature," *Fatigue and Fracture of Engineering Materials and Structures*, Vol. 19, pp. 975-983.

Rie, K. T., and R. Schubert, 1987, "Note on the Crack Closure Phenomenon in Low-Cycle Fatigue," Proc. Second International Conference on Low Cycle Fatigue and Elastic-Plastic Behavior of Materials, Munich, pp. 575-580.

Riedel, H., 1987, **Fracture at High Temperatures**, Springer-Verlag.

Romanoski, G. R., Jr., and R. M. Pelloux, 1990, "The Fatigue Behavior of Small Cracks in an Aircraft Turbine Disk Alloy," *Elevated Temperature Crack Growth*, MD - Vol. 18, ASME, pp. 7-23.

Rooke, D. P., and D. J. Cartwright, 1976, **Compendium of Stress Intensity Factors**, Her Majesty's Stationery Office, London.

Ruggieri, C., T. L. Panontin, and R. H. Dodds, Jr., 1996, "Numerical Modeling of Ductile Crack Growth in 3-D Using Computational Cell Elements," *International Journal of Fracture*, Vol. 82, pp. 67-95.

Sadananda, K., and P. Shahinian, 1979, "A Fracture Mechanics Approach to High Temperature Fatigue Crack Growth in Udimet 700," *Engineering Fracture Mechanics*, Vol. 11, pp. 73-86.

Savaidis, G., M. Dankert, and T. Seeger, 1995, "An Analytical Procedure for Predicting Opening Loads of Cracks at Notches," *Fatigue and Fracture of Engineering Materials and Structures*, Vol. 18, pp. 425-442.

Savaidis, G., and T. Seeger, 1994, "An Experimental Study on the Opening and Closure Behavior of Fatigue Surface, Corner, and Through-Thickness Cracks at Notches," *Fatigue and Fracture of Engineering Materials and Structures*, Vol. 17, pp. 1343-1356.

Saxena, A., 1998, **Nonlinear Fracture Mechanics for Engineers**, CRC Press.

Saxena, A., 1991, "Creep Crack Growth in High Temperature Ductile Materials," *Engineering Fracture Mechanics*, Vol. 40, pp. 721-736.

Saxena, A., 1986, "Creep Crack Growth Under Non-Steady-State Conditions," *Fracture Mechanics: Seventeenth Volume, ASTM STP 905*, American Society for Testing and Materials, pp. 185-201.

Saxena, A., and P. K. Liaw, 1986, "Remaining Life Estimation of Boiler Pressure Parts - Crack Growth Studies," EPRI-CS-4688, Electric Power Research Institute, Palo Alto, CA.

Sehitoglu, H., and W. Sun, 1991, "Modeling of Plane Strain Fatigue Crack Closure," *ASME Journal of Engineering Materials and Technology*, Vol. 113, pp. 31-40.

Sehitoglu, H., and W. Sun, 1989, "The Significance of Crack Closure Under High Temperature Fatigue Crack Growth with Hold Periods," *Engineering Fracture Mechanics*, Vol. 33, pp. 371-388.

Sehitoglu, H., 1985a, "Crack Opening and Closure in Fatigue," *Engineering Fracture Mechanics*, Vol. 21, pp. 329-339.

Sehitoglu, H., 1985b, "Characterization of Crack Closure," *Fracture Mechanics: Sixteenth Symposium, ASTM STP 868*, pp. 361-380.

Shahinian, P., 1976, "Influence of Section Thickness on Fatigue Crack Growth in Type 304 Stainless Steel," *Nuclear Technology*, Vol. 30, pp. 390-397.

Sharobeam, M. H., and J. D. Landes, 1995, "A Single Specimen Approach for *J*-Integral Evaluation for Semi-Elliptical Surface Cracks," *Fracture Mechanics: 25th Volume, ASTM STP 1220*, American Society for Testing and Materials, pp. 397-414.

Shih, C. F., and J. W. Hutchinson, 1976, "Fully Plastic Solutions and Large Scale Yielding Estimates for Plane Stress Crack Problems," *ASME Journal of Engineering Materials and Technology*, Vol. 98, pp. 289-295.

Shih, C. F., 1983, "Tables of Hutchinson-Rice-Rosengren Singular Field Quantities," Materials Research Laboratory Report MRL E-147, Brown University.

Shin, C. S., and R. A. Smith, 1988, "Fatigue Crack Growth at Stress Concentrations–The Role of Notch Plasticity and Crack Closure," *Engineering Fracture Mechanics*, Vol. 29, pp. 301-315.

Shin, C. S., and R. A. Smith, 1985, "Fatigue Crack Growth from Sharp Notches," *International Journal of Fatigue*, Vol. 7, pp. 87-93.

Shiratori, M., T. Miyoshi, H. Miyamoto, and T. Mori, 1977, "A Computer Simulation of Fatigue Crack Propagation Based on the Crack Closure Concept," *Adv. in Research on the Strength and Fracture of Materials (Fracture 1977)*, ICF4, Waterloo, Canada, Vol. 2B, pp. 1091-1098.

Sih, G.C., 1973, **Handbook of Stress Intensity Factors**, Institute of Fracture and Solid Mechanics, Lehigh University, Bethlehem, PA.

Skelton, R. P., 1982, "Growth of Short Cracks During High Strain Fatigue and Thermal Cycling," *Low-Cycle Fatigue and Life Prediction, ASTM STP 770*, American Society for Testing and Materials, pp. 337-381.

Socie, D. F., 1977, "Prediction of Fatigue Crack Growth in Notched Members Under Variable Amplitude Loading Histories," *Engineering Fracture Mechanics*, Vol. 9, pp. 849-865.

Solomon, H. D., 1972, "Low Cycle Fatigue Crack Propagation in 1018 Steel," *Journal of Materials*, Vol. 7, pp. 299-306.

Starkey, M. S., and R. P. Skelton, 1982, "A Comparison of the Strain Intensity and Cyclic J Approaches to Crack Growth," *Fatigue of Engineering Materials and Structures*, Vol. 5, pp. 329-341.

Sumpter, J. D. G., 1973, "Elastic-Plastic Analysis and Design Using the Finite Element Method", Ph.D. Thesis, Department of Mechanical Engineering, Imperial College of Science and Technology, London.

Sun, W., and H. Sehitoglu, 1992, "Residual Stress Fields During Fatigue Crack Growth," *Fatigue and Fracture of Engineering Materials and Structures*, Vol. 15, pp. 115-128.

Suresh, S., 1991, **Fatigue of Materials**, Cambridge University Press.

Tada, H., P. Paris, and G.R. Irwin, 1985, **The Stress Analysis of Cracks Handbook**, 2nd Edition, Del Research Corporation.

Tanaka, K., T. Hoshide, and N. Sakai, 1984, "Mechanics of Fatigue Crack Propagation by Crack-Tip Plastic Blunting," *Engineering Fracture Mechanics*, Vol. 19, pp. 805-825.

Tanaka, K., 1983, "The Cyclic *J*-Integral as a Criterion for Fatigue Crack Growth," *International Journal of Fracture*, Vol. 22, pp. 91-104.

Tanaka, K., and Y. Nakai, 1983, "Propagation and Non-propagation of Short Fatigue Cracks at a Sharp Notch," *Fatigue of Engineering Materials and Structures*, Vol. 6, pp. 315-327.

Tomkins, B., 1980, "Micromechanisms of Fatigue Crack Growth at High Stress," *Metal Science*, Vol. 14, pp. 408-417.

Tomkins, B., 1975, "The Development of Fatigue Crack Propagation Models for Engineering Applications at Elevated Temperatures," *ASME Journal of Engineering Materials and Technology*, Vol. 97, pp. 289-297.

Topper, T. H., D. L. DuQuesnay, and M. A. Pompetzki, 1992, "Crack Closure, Damage, and Short Crack Growth Under Variable Amplitude Loading," *Theoretical Concepts and Numerical Analysis of Fatigue*, Engineering Materials Advisory Services, pp. 201-235.

Trantina, G. G., H. G. deLorenzi, and W. W. Wilkening, 1983, "Three-Dimensional Elastic-Plastic Finite Element Analysis of Small Surface Cracks," *Engineering Fracture Mechanics*, Vol. 18, pp. 925-938.

Vardar, O., 1982, "Fatigue Crack Propagation Beyond General Yield," *ASME Journal of Engineering Materials and Technology*, Vol. 104, pp. 192-199.

Vormwald, M., and T. Seeger, 1991, "The Consequences of Short Crack Closure On Fatigue Crack Growth Under Variable Amplitude Loading," *Fatigue and Fracture of Engineering Materials and Structures*, Vol. 14, pp. 205-225.

Wang, S.-Z., Z. Yang, and M.-K. Kang, 1983, "Fatigue Crack Growth Rate Under Full Yielding Condition for 15CDV6 Steel," *Engineering Fracture Mechanics*, Vol. 18, pp. 895-902.

Wang, X., S. B. Lambert, and G. Glinka, 1998, "Approximate Weight Functions for Embedded Elliptical Cracks," *Engineering Fracture Mechanics*, Vol. 59, pp. 381-392.

Wang, Yongyi, 1988, "Analysis of Fracture Initiation in Surface-Cracked Plates," M. S. Thesis, Massachusetts Institute of Technology.

Wang, Yongyi, 1991, "A Two-Parameter Characterization of Elastic-Plastic Crack Tip Fields and Applications to Cleavage Fracture," Ph.D. Thesis, Massachusetts Institute of Technology.

Weertman, J., 1969, "Theory of Rate of Growth of Fatigue Cracks Under Combined Static and Cyclic Stresses," *International Journal of Fracture Mechanics*, Vol. 5, pp. 13-15.

Wheeler, O. E., 1972, "Spectrum Loading and Crack Growth," *Journal of Basic Engineering, Trans. ASME*, Vol. 94, pp. 181-186.

Wilkening, W. W., H. G. deLorenzi, and M. Barishpolsky, 1984, "Elastic-Plastic Analyses of Surface Flaws in a Reactor Vessel," *ASME Journal of Pressure Vessel Technology*, Vol. 106, pp. 247-254.

Wilkowski, G. M., et al., 1992, "Short Cracks in Piping and Piping Welds," Semiannual Report (April-September 1991), NUREG/CR-4599, Vol. 2, No. 1.

Willenborg, J., R. M. Engle, and H. A. Wood, 1971, "A Crack Growth Retardation Model Using an Effective Stress Concept," Air Force Flight Dynamics Laboratory Technical Memorandum 71-1-FBR.

Wilson, W. K., and I. W. Yu, 1979, "The Use of the J Integral in Thermal Stress Crack Problems", *International Journal of Fracture*, Vol. 15, pp. 377-87.

Wuthrich, C., and W. Hoffelner, 1984, "Fatigue Crack Growth at High Strain Amplitudes," *Mechanical Behavior of Materials - IV*, Proc. 4th International Conference, Pergamon Press, Vol. 2, pp. 911-917.

Wuthrich, C., 1982, "The Extension of the *J*-Integral Concept to Fatigue Cracks," *International Journal of Fracture*, Vol. 20, pp. R35-R37.

Xia, L., C. F. Shih, and J. W. Hutchinson, 1995, "A Computational Approach to Ductile Crack Growth Under Large Scale Yielding Conditions," *Journal of the Mechanics and Physics of Solids*, Vol. 43, pp. 389-413.

Yagawa, G., Y. Kitajima, and H. Ueda, 1993, "Three Dimensional Fully Plastic Solutions for Semi-Elliptical Surface Cracks," *International Journal of Pressure Vessels and Piping*, Vol. 53, pp. 457-510.

Yagawa, G., H. Ueda, and Y. Takahashi, 1985, "Surface Crack Behavior in Ductile Materials," Proc. 8th SMIRT Conference, Paper G6/2, pp. 249-252.

Yang, S., and Y. Lu, 1989, "Surface Crack Growth in a Plate Under the Remote High Strain-Controlled Cyclic Loading," *Fatigue and Fracture of Engineering Materials and Structures*, Vol. 12, pp. 399-407.

Yoon, K. B., and A. Saxena, 1991, "An Interpretation of ΔJ for Cyclically Unsaturated Materials," *International Journal of Fracture*, Vol. 49, pp. R3-R9.

Yoon, K. B., 1990, "Characterization of Creep Fatigue Crack Growth Behavior Using the C_t Parameter," Ph.D. Thesis, Georgia Institute of Technology, Atlanta, Georgia.

Zahoor, A., 1991, *Ductile Fracture Handbook*, NP-6301-D, Vol. 3, Electric Power Research Institute.

Zahoor, A., 1990, *Ductile Fracture Handbook*, NP-6301-D, Vol. 2, Electric Power Research Institute.

Zahoor, A., 1989, *Ductile Fracture Handbook*, NP-6301-D, Vol. 1, Electric Power Research Institute.

Zahoor, A., 1989, "*J*-Integral Analysis of Three-Point Bend Specimen," and "*J*-Integral Analysis of the Compact Tension Specimen," *Journal of Engineering Materials and Technology, Trans. ASME*, Vol. 111, pp. 132-137, 138-144.

Zheng, M., and H. W. Liu, 1986, "Fatigue Crack Growth Under General-Yielding Cyclic Loading," *ASME Journal of Engineering Materials and Technology*, Vol. 108, pp. 201-205.

APPENDIX A

EVALUATION OF ALTERNATIVE GOVERNING PARAMETERS

A.1 Introduction

A.1.1 Potential Limitations of ΔJ

Several potential limitations of J and ΔJ have been identified during the past two decades, and these issues may be grouped into three broad categories. The first set of concerns, which were raised relatively soon after ΔJ was first proposed as a governing parameter for EPFCG, addressed the fundamental suitability of ΔJ to characterize crack growth under cyclic loading. How could a parameter which was originally based on nonlinear elasticity theory and the deformation theory of plasticity be valid when elastic-plastic unloading occurred? How could path-independence be maintained during not only unloading but also crack closure? Some of these fundamental issues are addressed elsewhere in the final report, citing satisfactory responses from the literature.

A second set of concerns involves the particular theoretical and practical suitability of J and ΔJ to characterize crack-tip fields when temperatures are changing temporally and/or spatially in the cracked component. Since elastic-plastic conditions are often associated with severe thermal conditions, this is potentially a significant concern. Researchers have suggested that ΔJ can lose its path-independence in the presence of thermal gradients or material inhomogeneities, such as changes in constitutive properties with changing temperatures. A related practical problem confronting simple estimation schemes for ΔJ is how to choose appropriate material properties when these thermal effects are significant.

Finally, a third set of concerns currently receiving significant attention in the (monotonic) fracture community is the potential loss of J-dominance under certain conditions. When applied loads are severe, especially in low constraint geometries, the crack tip stress field may not be adequately characterized by the J-integral, and so J alone may not be a successful predictor of crack growth or fracture. Ongoing studies are currently emphasizing the use of an additional parameter (for example, Q) to characterize more completely the crack-tip stress field. The potential implications of these issues for EPFCG have not been addressed to date.

A.1.2 Possible Alternative Parameters

Delta J is not the only candidate parameter for an EPFCG methodology. As noted in the background, several other "simple" parameters were developed in the early days of EPFCG research. These include the strain intensity factor and the crack tip opening displacement. More recently, a number of sophisticated path-area integrals have been proposed to address concerns about ΔJ. Most notable among these are the J^* integral of Blackburn (1972), the $\hat{J}$integral of Kishimoto, Aoki, and Sakata (1980), and the $\Delta T_p{}^*$ integral of Atluri, Nishioka, and Nakagaki (1984). A theoretical review of these parameters with particular reference to elastic-plastic fatigue crack growth is given by Kim and Orange (1988). It can be shown that many of these quantities are derivable from a global energy balance with different restrictions invoked. Typically, the new parameters have a greater range of strict mathematical validity than the original J integral, particularly for problems involving plastic loading and unloading, temperature changes, and crack growth.

A.2 Critical Evaluation of Alternative Parameters

A.2.1 Previous Studies of Alternative Parameters

The current contract did not permit original investigations of alternative parameters in detail. However, a number of studies in the literature have evaluated different parameters from different perspectives, and it is useful to critically review these different studies.

General Electric. The only comprehensive study of the various integral parameters was conducted by GE Aircraft Engines under NASA-Lewis sponsorship (Kim and Orange, 1988; Kim *et al.*, 1988a, 1988b; Kim and Van Stone, 1992, 1995a, 1995b, 1995c, 1997). This study included a theoretical assessment of the parameters, along with numerical and experimental evaluation of the parameters under a variety of load and temperature histories.

The theoretical survey (Kim and Orange, 1988) investigated eight different integral parameters. The survey concluded that there existed as yet no integral parameter with a well-established physical background and all the desirable features required for engine applications. The four parameters ΔJ^*, $\Delta \dot{J}$, $\Delta T_p{}^*$, and ΔT_p were found to maintain theoretical path-independence for more general elastic-plastic problems, including nonproportional loading, unloading, temperature gradients, and material inhomogeneities. This was not true of the simple ΔJ and its closely related derivative parameters.

On the other hand, the GE/NASA study found that the physical meaning of the four advanced integral parameters was either vague or totally unknown. The physical meaning of ΔJ is well-established for those applications where theoretical validity has also been established. Neither J^* nor $\dot{J}$ can be measured experimentally, since neither can be expressed as the rate of a potential or as a line integral along the boundary of the structure (both include an area integral). $\Delta T_p{}^*$ can be measured experimentally only for proportional loading. ΔT_p, along with ΔJ and its derivative parameters, can be measured experimentally, although ΔT_p is related to the near crack-tip stress field only for proportional loading.

The GE/NASA study also investigated the ability of the four advanced integral parameters to correlate experimental crack growth rate data under several different types of load and temperature histories. In all cases, the parameters were computed from elastic-plastic finite element (FE) analyses of the cracked components, including FE simulation of crack growth and crack closure. Original experiments were performed at GE with buttonhead single edge notch specimens of Alloy 718. Total strain ranges varied from 0.50% to 1.70%. Some analyses were also conducted for experiments conducted previously by Jordan and Meyers (1989; 1986) with Hastelloy X.

All four advanced integral parameters did a good job of correlating Alloy 718 isothermal tests at 538C for three different strain ranges. The performance of ΔJ, which retains general theoretical validity under these conditions, was not investigated. The advanced parameters also did a reasonably good job of correlating Alloy 718 TMF crack growth data with the 538C isothermal data. Thermal gradient tests in which the crack tip region was at higher temperatures (649C) were reported to be

consistent with 649C isothermal tests, although those isothermal tests were not analyzed with the alternative parameters. The thermal gradient tests were not consistently correlated with the TMF or 538C isothermal tests, perhaps indicating some independent time-dependent or environmental effects at the higher temperature.

The success of the advanced parameters in correlating the Meyers Hastelloy X data was somewhat mixed. Three of the four advanced parameters did a good job with the isothermal tests at each of five different temperatures, but ΔT_p did not perform well at some higher temperatures and was eliminated from further evaluation. Trend lines from different temperatures were significantly different. Correlation of TMF data was not as strong. A few out-of-phase tests at lower temperature ranges were correlated well, but agreement between different TMF tests at higher maximum temperatures was poor.

It is worthy of special note that Jordan and Meyers also evaluated different correlating parameters for their data. They used much simpler estimation techniques (no numerical analysis) and therefore were limited to evaluating simpler parameters: ΔK, ΔK_ε, ΔJ, and COD. Their resulting correlations were generally of similar quality to the GE advanced parameter correlations for the isothermal tests (worse at lower temperatures, sometimes slightly better at higher temperatures) and generally much better than the GE correlations for the TMF tests. The Jordan-Meyers analyses are discussed in more detail below.

GE also conducted a limited number of studies on strain histories with hold times, investigating both the advanced integrals J^*, $\hat{J}$, T_p^* and their rate integral counterparts $\dot{J}^*$, $\dot{\hat{J}}$, and $\dot{T}_p^*$. The rate forms of the parameters were required to correlate Alloy 718 growth rate data with hold times, although $\dot{T}_p^*$ did not perform satisfactorily. Correlation of data from tests with combined cycling and hold times required an empirical superposition technique. Further consideration of these tests and analyses is beyond the scope of the current report, however.

Jordan and Meyers. As noted above, Jordan and Meyers conducted isothermal (1989) and TMF (1986) tests on tubular specimens of Hastelloy-X as part of an earlier NASA-Lewis contract effort at Pratt & Whitney (Meyers, 1982). Several different simple parameters, including ΔK, ΔK_ε, ΔJ, and COD, were evaluated. Each parameter was estimated from simple analytical expressions, and crack closure was not considered. Jordan and Meyers generally concluded that all of the elastic-plastic parameters performed somewhat similarly. Under isothermal conditions, they did a relatively poor job at low temperatures and a relatively good job at elevated temperatures. The COD estimate, which was derived from a ΔJ calculation, did the best job of correlating isothermal data from different temperatures. The elastic ΔK was always unsatisfactory. The three parameters ΔK, ΔK_ε, and ΔJ were all reasonably successful in correlating data from three different types of TMF cycles within a factor of two. Note that total strain ranges were 0.15% to 0.40%, lower than the GE tests, so the plasticity was less severe.

Estimation of ΔJ presented special challenges due to cyclic hardening as well as temperature-dependent changes in modulus and strain hardening exponent during TMF cycling. These challenges are among the theoretical limitations of ΔJ cited in the GE study. Jordan and

Meyers developed simple estimation techniques to address each challenge. The cyclic hardening problem was handled by reformulating ΔJ in terms of plastic work measured at the ends of the gage length, and then measuring this quantity periodically during the test. A constant average value of elastic modulus for a variable temperature cycle was chosen that gave the same strain energy at peak load as the actual temperature-dependent modulus. An effective value of the strain hardening exponent was computed from the measured stress range and strain range values in the TMF tests.

Marchand and Pelloux. Marchand and Pelloux (Marchand, Pelloux, and Ilschner, 1987, 1988; Pelloux and Marchand, 1986), in conjunction with another NASA-Lewis contract, examined fracture mechanics approaches to isothermal and TMF crack growth data in several different gas turbine materials using an SEN specimen. Total strain ranges were 0.25% and 0.50%. Again, they focused their evaluations on simple parameters that could be easily estimated: ΔK and ΔK_t, ΔJ computed using some of the same techniques as Jordan and Meyers, and a modified ΔK which corrected for the effects of specimen compliance changes at longer crack lengths. They concluded that ΔK and ΔK_t provided poor correlations of the data and that ΔJ provided a better but still inadequate description. The modified ΔK parameter gave reasonably strong correlations. The best performer was identified as an alternative version of the modified ΔK parameter which accommodated crack closure considerations based on measured crack opening stresses. The influence of closure on the other parameters was not explored.

Others. Other researchers have argued for the use of advanced alternative parameters on theoretical grounds but have not provided experimental validation. Brust (Brust, Nakagaki, and Gilles, 1990; Brust, McGowan, and Atluri, 1986; Brust, Nakagaki, and Springfield, 1989), for example, is an advocate of T^* and the related family of crack-tip integrals for use in a wide range of history-dependent and temperature-dependent fracture problems. However, no original experimental evidence has been presented to support these claims for elastic-plastic fatigue crack growth, other than an isolated unload-reload ductile crack growth test. Brust points out that "there is still much work needed before an integral parameter, whether T^* or any other, can be used with confidence for arbitrarily cracked structures" (Brust, Nakagaki, and Gilles, 1990).

A.2.2 Summary and Discussion

The simple alternative parameters such as ΔK_t and COD have clear practical and theoretical limitations. They share the same practical limitations of J in addressing temperature-dependent changes in material properties. In practice, these simple parameters are usually estimated directly from computations of J or K, and as such they retain the same theoretical limitations of those two fundamental parameters. Parameters which cannot be estimated from J or K generally cannot rigorously accommodate geometry effects, since only J and K have well-developed libraries of geometry correction factors (and techniques to compute the same). Furthermore, as noted earlier, most of the estimation techniques used to calculate the simple alternative parameters produce exactly the same functional form as ΔJ. Therefore, any potentially important theoretical distinctions between the different parameters may be lost entirely in the estimation schemes.

The alternative integral parameters clearly have some desirable theoretical capabilities, and their general success in correlating EPFCG data in the GE studies is encouraging. However, these advanced parameters possess some major practical limitations at the present time.

First of all, their computation depends entirely upon complex elastic-plastic finite element analyses of growing cracks. This type of analysis is difficult and expensive for simplified (two-dimensional) laboratory specimen configurations, and totally unfeasible for actual (fully three-dimensional) component geometries and temperature-load histories. Several modeling issues remain unresolved for even the simplified research problem. For example, GE pointed out that the finite element mesh size, the loading step size, and the node release scheme for crack growth all need further investigation (Kim and Van Stone, 1992). The effects of crack closure on these advanced parameters have not been fully addressed in the numerical modeling. The computation of rate integrals for histories with hold times requires information about the time for the crack to advance incrementally in the FE model, but this information is not available *a priori*. Calculation of T^* can be arbitrarily dependent on the choice of the characteristic distance, ε, locating the integration path around the crack tip, and no theoretical guidance is yet available to select an appropriately consistent value of ε for laboratory and application configurations.

Second, several ambiguities remain regarding theoretical interpretation and application. Several of the parameters cannot be measured experimentally, so direct validation is not possible. The physical meaning of several parameters for the crack growth process is not yet evident and may not exist. Because of this absence of clear mechanistic justification, the parameters may give incorrect results in some applications. For example, Brust, McGowan, and Atluri (1986) have advocated T^* for elastic-plastic unload-reload applications because it was uniquely successful in predicting observed ductile crack advance below the previous maximum load on the second cycle of an experiment with A508 steel. However, this type of crack advance behavior is not typical for unload-reload histories in the ductile fracture regime (Marschall and Wilkowski, 1989). Therefore, it is possible that in other applications, T^* would predict crack advance where it is not observed experimentally.

The GE study found the two parameters ΔJ^* and $\Delta \hat{J}$ (and their rate forms) to be the most promising alternative parameters for a wide range of EPFCG, TMF, and creep crack growth applications. In view of the GE results, and in view of other potential limitations of other proposed integral parameters, this seems to be a reasonable conclusion.

However, the practical use of these alternative parameters will likely depend on the development of simplified estimation techniques. As noted earlier, a dependence on extremely complex finite element analyses will not be acceptable for engineering methodologies in the foreseeable future. Instead, simplified estimation schemes must be developed. These estimation schemes should permit the relatively rapid, approximate computation of ΔJ^* or $\Delta \hat{J}$ for realistic geometries and time-temperature-load histories. The estimation schemes could employ simplified analytical methodologies such as K solutions, J solutions, temperature-dependent constitutive laws, etc. Some tabular approaches which incorporate representative finite element results (cf. the EPRI handbook methodology for J) may be appropriate. In particular, the most promising approaches may

be those which begin with some existing J estimation scheme but which capture the uniqueness of the alternative integral formulation, at least in part. At the present time, it is not clear if simplified estimation schemes of this type, or of any type, can be developed.

The practical limitations of the advanced parameters suggest that their engineering implementation is not feasible in the near future. Therefore, it seems appropriate to revisit the original ΔJ parameter, re-assessing its potential theoretical limitations and evaluating the practical significance of those limitations.

A.3 A Re-Evaluation of ΔJ

At the outset of this re-evaluation, it should be reiterated that ΔJ is not a perfect parameter. Several mathematical conditions required by the original theoretical formulation of J will not be strictly satisfied for some practical EPFCG problems. Thermal gradients and temperature-dependent material properties may degrade the path-independence of J and introduce practical difficulties in computing a single representative value. This re-evaluation should not be construed as an attempt to "sweep under the rug" these potential complications.

However, researchers have shown repeatedly that ΔJ is successful in correlating EPFCG data under isothermal conditions, despite arguments about mathematical rigor to the contrary. This success has been explained in terms of an "operational" definition of ΔJ which satisfies the essential spirit of the mathematical formulation, if not its letter. And it is from this perspective that we evaluate whether ΔJ may still have adequate engineering utility to address more complex EPFCG histories involving significant thermal effects.

First of all, it is useful to remember that several researchers have used simple estimates of ΔJ with moderate success to correlate TMF and other elevated temperature fatigue crack growth data. The work of Jordan and Meyers and also of Marchand has already been cited. Romanoski and Pelloux (1990) found that a closure-corrected ΔJ_{eff} gave excellent consolidation of elastic and elastic-plastic small crack data in IN100 at 649C. Okazaki and colleagues (Okazaki and Koizumi, 1983; Okazaki *et al.*, 1983) have published several papers in which ΔJ was used successfully to correlate TMF and isothermal fatigue crack growth data in different steels. Their work included several examples in which a rate form of ΔJ was used to characterize time-dependent effects such as strain rate.

Furthermore, the monotonic parameter J is currently being employed in other industries to solve problems which are primarily driven by thermal stresses arising from transient thermal gradients. For example, J is currently the parameter most often used to address the pressurized thermal shock (PTS) problem facing nuclear pressure vessels. This fact does not prove that J is a perfect parameter for the job, but it does suggest that other researchers have concluded that, for the time being, J is the best available choice.

It is not clear to what extent a loss of theoretical path-independence will cause practical difficulties for ΔJ in an engineering context. Chan, Lankford, and Davidson (1986) have shown

from high-resolution experimental measurements that at the microscale, path-independence is not strictly satisfied even under simple isothermal elastic-plastic cycling. This violation, however, has not invalidated the use of ΔJ for crack growth rate correlation under these conditions. Path independence is not necessarily a strong selection criterion for cyclic loading. Characterization of cyclic changes in the parameter are more important. Miller *et al.* (1993) have argued for the interpretation of ΔJ as a local parameter which reflects the crack tip opening behavior, in which case they claim that path independence is irrelevant. The use of ΔJ in this manner, however, requires an estimation scheme which genuinely reflects local behavior and which can be carried out consistently in a wide range of applications. The "operational definition" of ΔJ employed previously in isothermal problems may be sufficient to solve non-isothermal problems as well.

The theoretical limitations of ΔJ should become most significant when cyclic plasticity is relatively large. When cyclic plasticity is more limited (e.g., contained plasticity at a stress concentrator, or along the outer fibers of a member experiencing a large thermal gradient), or when the plasticity arises entirely from secondary loading (e.g., thermal loading), the total ΔJ solution may be more closely linked to the corresponding elastic ΔK solution. Minor computational errors arising from path dependence or other theoretical transgressions will be of relatively less consequence. The GE experiments emphasized extensive plasticity: uniform global strain ranges as high as 1.70%. While this may have been an appropriate choice to test the suitability of various parameters under diagnostically extreme conditions, it does not necessarily reflect the types of nonlinear deformation likely to be encountered commonly in SSME and other aerospace propulsion applications.

The moderate success of Jordan-Meyers and Marchand in using simple parameters more closely linked to ΔK appears to be consistent with this argument about limited plasticity, although some of their successes may have been fortuitous. It is slightly bewildering why (in a few situations) the correlations employing estimates of ΔJ, which were based on ΔK solutions, gave slightly less satisfying correlations than the elastic ΔK itself. This disagreement suggests that some errors may have been introduced by the particular estimation scheme used to compute the plastic ΔJ component.

It appears that it would be useful to conduct further studies of simple ΔJ estimation schemes (i.e., schemes which do not require FE analysis) for non-isothermal conditions, including both thermal gradients and thermal cycling. Some of the "simpler" alternative integral parameters reviewed and quickly dismissed by the GE study represent attempts to address thermal stress issues without necessarily addressing the fundamental theoretical limitations of the J formulation. These parameters may provide some insight for a more robust J estimation scheme.

Special attention should be given to appropriate means of accommodating temperature-dependent material property changes as well as thermal stresses. The simple algorithms derived by Jordan and Meyers to address temperature-dependent changes in modulus and strain hardening exponent provide a starting point, but improved methods may be possible. Bounding techniques which ensure conservatism may be adequate for many engineering purposes.

Although these estimation schemes should not be dependent on FE analysis, it is recommended that limited FE studies be conducted in conjunction with development of the

estimation schemes to validate and optimize the simple approaches. These FE studies would also permit further evaluation of the extent and significance of path dependence.

The potential role of crack closure in these thermal problems should be investigated further. Both Marchand and Romanoski found that simple closure corrections significantly improved the quality of their correlations with simple ΔK and ΔJ estimates. The GE finite element studies found that closure was significant for all of the advanced integral parameters: contributions to the path-area integral were negligible when the crack was closed. Unfortunately, little is known about potentially unique closure phenomena motivated by thermal effects, but simple approaches based on well-characterized stress-dependent (isothermal) effects may be adequate.

These improved simple estimation schemes for ΔJ under non-isothermal conditions could be evaluated by applying them to the available crack growth data from GE, Jordan-Meyers, Marchand, etc. At some point, it may also be useful to conduct additional original experimental investigations, particularly as it becomes possible to identify a series of critical diagnostic tests. It should be recognized, however, that these will not be inexpensive experiments.

Experimental evaluation of the improved ΔJ estimation schemes should permit a clearer understanding of the limitations of ΔJ from both theoretical and pragmatic perspectives. In turn, this exercise should more sharply focus the potential need for advanced alternative parameters, and perhaps evaluate the ability of the alternative parameters to provide improved correlations.

A.4 General Remarks About All EPFCG Governing Parameters

Before closing, it is useful to discuss briefly two important issues pertaining to all of the proposed governing parameters for EPFCG, especially under non-isothermal conditions.

The first issue is that these parameters characterize only the mechanical "driving force" for crack growth: some measure of the strength of the stress and strain fields in the vicinity of the crack tip, as influenced by externally applied loads (mechanical, thermal, etc.) and the constitutive response of the material. This is not so much a "limitation" of the parameter as it is simply a recognition that the kinetics of crack growth includes both "driving force" and "material resistance" factors. Driving force parameters (such as ΔK, ΔJ, ΔJ^*, etc.) do not (and were never intended to) address potential changes in the material resistance to crack growth under various test or application conditions. For example, a significant change in the crack-tip temperature may induce a change in the crack growth mechanism from intergranular to transgranular. Environmental effects on crack growth which are dependent on time and/or temperature may become important. Other issues such as hydrogen effects may also play some role.

Some of these effects have been noted in studies of elevated temperature EPFCG. For example, Marchand, Pelloux and Ilschner (1987) constructed two different correlations of his isothermal and TMF data for Hastelloy X, one incorporating intergranular crack advance modes and one incorporating data which involved transgranular cracking. He suggested that the mode of fracture depended primarily on the temperature at which σ_{max} occurred. Ghonem, Nicholas, and

Pineau (1993) have reviewed the variety of crack growth damage mechanisms which can be operative in Inconel 718 at elevated temperatures. They concluded that these damage mechanisms ranged from fully cycle-dependent to fully environment-dependent, depending solely on the slip character in the crack-tip region.

The challenge of correlating crack growth data from complex EPFCG conditions such as TMF, therefore, is much more than simply identifying the proper mechanical parameter to characterize the crack-tip deformation. Some correlation of crack growth damage mechanisms must also be performed. From a pragmatic standpoint, the quest for these correlations will likely include questions about the practical relationship between TMF and isothermal cycling (perhaps at the maximum or minimum temperature of the TMF cycle), and the corresponding relationship between isothermal cycling at different temperatures. Even the most theoretically correct alternative integral parameters will be insufficient to address these questions alone.

The second issue is the extent to which a single crack-tip parameter genuinely and uniquely reflects the important near-tip stress and strain fields. As noted in the Introduction, under some conditions (especially low constraint) the crack-tip stress field itself is not adequately characterized by the J-integral alone. This loss of J-dominance has been linked to apparent changes in fracture behavior during monotonic loading when attempts are made to characterize fracture solely in terms of J. This limitation would be shared by all of the alternative integral parameters as well, so in this regard the newer approaches offer no benefit. However, it is not clear if these constraint effects will also be important for EPFCG applications. The constraint effects were identified in fracture problems when different geometries exhibited substantially different failure behavior. In EPFCG studies, however, data from contrasting geometries and contrasting load regimes have been shown to agree closely (Dowling, 1976), and so it is possible that the loss of J-dominance is not practically significant for fatigue crack growth. In general, crack-tip deformation will be much less severe in most EPFCG applications than in the types of ductile tearing problems exhibiting large constraint effects, and this is a possible explanation. Further work is needed to clarify whether constraint effects exist or are significant for EPFCG.

A.5 Conclusions and Recommendations

Two of the advanced integral parameters, ΔJ^* and $\Delta \hat{J}$, along with their rate forms, appear to be promising alternatives to ΔJ in applications which involve extensive plasticity and large temperature changes. Other alternative parameters, including both simple and advanced formulations, have been shown to be less promising.

However, currently available methods for computing these advanced parameters involve complex finite element analysis which is impractical for engineering applications. Additional work is required to develop simpler estimatior. schemes, if this is even possible. Furthermore, numerous other theoretical and practical issues about the calculation and application of these parameters remain outstanding. Extensive development work ($$$ and time) will be required before these parameters can be used with confidence in actual applications. Therefore, although these parameters have exhibited some promise in research settings, their practical use in the near term is not viable.

Considering all evaluation criteria, the original choice of ΔJ appears to be the optimum choice at the present time as the governing parameter for practical assessment of EPFCG. Delta J best addresses a broad range of both theoretical and practical issues. For example, robust estimation schemes are available to calculate ΔJ accurately and efficiently for a wide range of crack and component geometries; a ΔJ methodology enables the existing ΔK crack growth data base to be employed; and ΔJ has an established history of successful use in the characterization of crack growth.

Therefore, in the short term, further development of ΔJ to address potential limitations appears to be preferable. These development activities should include more careful studies of practical schemes to address various temperature dependencies in the calculation and application of ΔJ. Application of these new estimation schemes will help identify uses of ΔJ which maintain adequate conservatism for engineering life assessment, and may also facilitate a more thorough assessment of the practical limitations of ΔJ. The previous uses of ΔJ to characterize elevated temperature crack growth data in which theoretical validity was not strictly satisfied suggests that some of these validity questions may be of less practical significance in engineering applications.

Finally, it should be noted that even a "perfect" governing parameter, one which exactly characterizes the crack-tip stresses and strains and the manner in which they facilitate crack advance, may be inadequate to completely describe crack growth rates in elevated temperature applications. Potential changes in crack growth damage mechanisms due to environmental and metallurgical effects may also be significant, and so some information about changes in material resistance to crack growth may be required. The scope of the current contract, however, is limited primarily to addressing the effects of mechanical plasticity on the "driving force" for crack growth.

APPENDIX B

A SURVEY OF CURRENTLY AVAILABLE *J* SOLUTIONS

This appendix summarizes the J solutions that are currently available in tabulated or closed form (not including new J solutions generated in the current contract effort). Included in the survey of available solutions are many common geometries in NASGRO (with NASGRO designation cited), geometries identified by NASA as being of particular interest, and additional geometries of particular relevance to pressurized systems. The results of the survey are summarized in Table B.1. Note that many geometries of interest have no available solutions for the plastic component of J.

Many of these solutions are taken or adapted from the various handbooks that have been published by EPRI over the past seventeen years. In these handbooks, tabulated solutions are typically given for discrete values of normalized crack and component dimensions and the strain hardening exponent.

In general, a complete J solution requires both an elastic J solution, which is typically derived directly from a K solution (either tabulated or closed-form), and a plastic J solution, which is based either on tabulated FEM results or a closed-form analytical estimate. The plastic J solution is typically based on a power law constitutive relationship, and so the total J solution reflects a material obeying a Ramberg-Osgood constitutive relationship between total stress and total strain.

Since most J estimation techniques, including the EPRI handbook and CEGB reference stress approaches, require a linear elastic K solution to construct a total J solution, sources for appropriate K solutions have also been noted for convenience. However, the detailed cataloguing of K solutions is outside the scope of the current contract. Many other K solutions can be found in equation, tabular, or graphical form in standard handbooks, textbooks, or manuals such as Rooke and Cartwright (1976), Murakami (1987), Anderson (1995), and the NASGRO computer code and user's manual.

The specific solutions for either K or J are not given in this appendix, but instead references are given that identify where the equations or tables can be found. For convenience, some additional references are given for isolated J solutions published in individual reports or journal articles. Often these solutions are given as total J values (either tabular or graphical) based on limited FEM calculations.

This compilation is inevitably incomplete. A systematic literature search was performed early in the contract effort to identify existing J solutions, and some new solutions were published and identified later in the contract effort; but some later publications may have been missed. Furthermore, some J solutions are available only in reports that have not been formally published, widely circulated, or indexed, and hence may have escaped detection during the literature search.

The symbols used in this particular appendix are, in many cases, the symbols employed in the cited references. Those original references should be consulted for specific symbol meanings; no attempt is made here to define or harmonize all of the cited symbols.

Table B.1. Survey of Existing *J* Solutions

	Existing Solutions	
	Thorough	Limited
STANDARD SPECIMENS		
Compact Tension Specimen, SS02	X	
Disc-Shaped Compact Tension Specimen, SS03		
Arc-Shaped Tension Specimen, SS04		
Three-Point Bend Specimen, SS05	X	
THROUGH-THICKNESS CRACKS IN PLATES AND SHELLS		
Through Crack in an Infinite Plate	X	
Through Crack at Center of Plate, TC01	X	
Through Crack at Edge of Plate, TC02	X	
Double-Edge Cracked Plate	X	
Through Crack From Hole in a Lug, TC04		
Through Crack in a Hollow Sphere, TC06		
Axial Through Crack in a Pressurized Cylinder, TC07		X
Circumferential Through Crack in a Cylinder, TC08	X	
Through Crack from Hole in a Finite Plate, TC09		X
Radial Through Crack (Internal) in a Hollow Disk		
Radial Through Crack (External) in a Hollow Disk		
EMBEDDED CRACKS		
Embedded Elliptical Crack, EC01		X
CORNER CRACKS		
Quarter-Elliptical Corner Crack in a Plate, CC01		
Quarter-Elliptical Corner Crack from Hole in a Plate, CC02		
Quarter-Elliptical Corner Crack from Hole in a Lug, CC03		
SURFACE CRACKS		
Semi-Elliptical Surface Crack in a Plate, SC01 and SC02		X
Semi-Elliptical Axial Surface Crack in a Hollow Cylinder, SC04	X	
Internal Axial Surface Crack (Constant Depth) in a Hollow Cylinder	X	
Semi-Elliptical Circumferential Surface Crack in a Hollow Cylinder, SC05	X	
Internal Circumferential Surface Crack (Constant Depth) in a Hollow Cylinder, SC06	X	
External Circumferential Surface Crack (Constant Depth) in a Hollow Cylinder, SC06	X	
Semi-Elliptical Surface Crack in a Solid Circular Bar, SC07		
Circumferential Surface Crack (Constant Depth) in a Solid Cylinder		

STANDARD SPECIMENS

Compact Tension Specimen, SS02

K solution available in NASGRO, Anderson (1995)

Plastic *J* solutions available in tabulated form for
$a/W = 0.25, 0.375, 0.5, 0.625, 0.75, 1.0$
$n = 1, 2, 3, 5, 7, 10, 13, 16, 20$
plane stress or plane strain
Source: Kumar et al. (1981) EPRI Handbook, Section 3.1

Disc-Shaped Compact Type Specimen, SS03

K solution available in NASGRO, Anderson (1995)

No plastic *J* solution currently available

Arc-Shaped Tension Specimen, SS04

K solution available in NASGRO, Anderson (1995)

No plastic *J* solution currently available

Three-Point Bend Specimen, SS05

K solution available in NASGRO, Anderson (1995)

Plastic *J* solutions available in tabulated form for
$a/W = 0.125, 0.25, 0.375, 0.5, 0.625, 0.75, .875$
$n = 1, 2, 3, 5, 7, 10, 13, 16, 20$
plane stress or plane strain
$2L/b = 4$
Source: Kumar et al. (1981) EPRI Handbook, Section 3.4

THROUGH-THICKNESS CRACKS IN PLATES AND SHELLS

Through Crack in an Infinite Plate

K solution is trivial

Plastic J solution for uniform tension based on closed form expression (good for all n values)
plane stress and plane strain
Source: Shih and Hutchinson (1976), He and Hutchinson (1981)

Through Crack at Center of Plate, TC01

K solution available in NASGRO, Anderson (1995)

Plastic J solutions available in tabulated form for uniform tension
a/W = 0.125, 0.25, 0.375, 0.5, 0.625, 0.75, .875
n = 1, 2, 3, 5, 7, 10, 13, 16, 20
plane stress and plane strain
Source: Kumar et al. (1981) EPRI Handbook, Section 3.3

Note: this plastic J solution can be extended continuously back to a/W = 0. by polynomial interpolation between larger crack sizes and the infinite plate solution (2.1).

Plastic J solutions available in tabulated form for biaxially loaded center-cracked plates
a/W = 0.125 to 0.625 in 0.125 steps
n = 1, 2, 3, 5, 7, 10, 13, 16, 20
plane stress only
load ratios S_x/S_y = ±0.5 and ±1.0
Source: Jansson (1986)

Limited FEM J solutions for combined thermal and mechanical loading in Kumar et al. (1984a) EPRI Report, Section 7, and also in Hellen and Blackburn (1987)

Through Crack at Edge of Plate, TC02

K solution available in NASGRO, Anderson (1995)

Plastic J solutions available in tabulated form for uniform tension
a/W = 0.125, 0.25, 0.375, 0.5, 0.625, 0.75, .875
n = 1, 2, 3, 5, 7, 10, 13, 16, 20
plane stress and plane strain
Source: Kumar et al. (1981) EPRI Handbook, Section 3.3

Plastic J solutions available in tabulated form for pure bending

details not currently available
Source: Kumar et al. (1982) EPRI Report

Plastic J solutions available in tabulated form for combined tension and bending
$a/W = 0.125, 0.25, 0.375, 0.5, 0.625, 0.75, .875$
$n = 1, 2, 3, 5, 7, 10$
plane strain only
5 discrete values of tension-to-bending ratio
Source: Kumar et al. (1984a) EPRI Report, Section 2

Limited FEM J solutions for combined thermal and mechanical loading in Kumar et al. (1984a) EPRI Report, Section 7

Double-Edge Cracked Plate

K solutions available in Anderson (1995)

Plastic J solutions available in tabulated form for uniform tension
$a/W = 0.125, 0.25, 0.375, 0.5, 0.625, 0.75, .875$
$n = 1, 2, 3, 5, 7, 10, 13, 16, 20$
plane stress or plane strain
Source: Kumar et al. (1981) EPRI Handbook, Section 3.6

Through Crack From Hole in a Lug, TC04

K solution available in NASGRO

No plastic J solutions currently available

Through Crack in a Hollow Sphere, TC06

K solution available in NASGRO

No plastic J solutions currently available

Axial Through Crack in a Pressurized Cylinder, TC07

K solution available in Zahoor (1990) EPRI Handbook, Section 6.1, for $0 < c/(Rt)^{0.5} < 5$
also see NASGRO

Zahoor (1990), Section 6.2, also gives an approximate total J solution based on a Dugdale model

No FEM plastic J solutions currently available

Circumferential Through Crack in a Cylinder, TC08

K solutions available in Zahoor (1989) EPRI Handbook, Section 1, for axial tension, bending, internal pressure
also see NASGRO

Plastic J solutions available in tabulated form for
axial tension, bending, combined tension + bending
$R/t = 5, 10, 20$
$n = 1, 2, 3, 5, 7, 10$
θ/π ranges from 0 to 0.5 in small steps
Source: Zahoor (1989) EPRI Handbook, Section 2, including solutions from earlier Kumar et al. handbooks
Some improved solutions are available in Wilkowski et al. (1992) for bending, small θ/π

Through Crack From Hole in a Finite Plate, TC09

No closed form K solutions available, but several tabular solutions have been published
see Murakami (1987), Chapter 5
NASGRO has a series solution for tension and bending plus biaxial tension

Limited plastic J solutions available for narrow range of a/R values in a biaxial stress field
see Zahoor (1991) EPRI Handbook, Section 11.2

Radial Through Crack (Inside) in a Hollow Disk

Apparently no closed form K solution available
Graphical K solution available in Murakami (1987), Section 6.5, for rotating disk

No plastic J solutions currently available

Radial Through Crack (Outside) in a Hollow Disk

Apparently no closed form K solution available

No plastic J solutions currently available

EMBEDDED CRACKS

Embedded Elliptical Crack

No closed form *K* solutions available for the general 4 DOF problem
some graphical and tabular solutions available in Murakami (1987), Chapter 9
one closed form solution available in NASGRO for
embedded elliptical crack centered in a finite thickness plate (EC01)
Closed form *K* solutions available for buried elliptical crack in infinite body
under uniform tension or bending; see Murakami (1987), Chapter 9
Weight function solutions available for buried elliptical crack in infinite body
under general bivariant stress field; see Wang et al. (1998)

No FEM plastic *J* solutions currently available for general 4 DOF problem
closed-form plastic *J* solution (based on FEM results) available for penny-shaped crack in infinite body
Source: He and Hutchinson (1981)
limited FEM results also available for penny-shaped crack in finite diameter round bar
Source: He and Hutchinson (1983b)

CORNER CRACKS

Quarter-Elliptical Corner Crack in a Plate, CC01

K solution available in NASGRO for uniform tension, bending

No FEM plastic *J* solutions currently available

Quarter-Elliptical Corner Crack from Hole in a Plate, CC02

K solution available in NASGRO

No FEM plastic *J* solutions currently available

Quarter-Elliptical Corner Crack from Hole in a Lug, CC03

K solution available in NASGRO

No FEM plastic *J* solutions currently available

SURFACE CRACKS

Semi-Elliptical Surface Crack in a Plate, SC01, SC02

Closed-form (Newman and Raju, 1981) *K* solutions available in NASGRO for uniform tension and bending; NASGRO also contains general weight function solutions for arbitrary stress distribution

limited number of plastic *J* FEM solutions available from Yagawa et al. (1993)
limited number of total *J* FEM solutions available from Kirk and Dodds (1992), Wang (1988, 1991), Parks and Wang (1988), Dodds et al. (1993), Sharobeam and Landes (1995)
very limited total *J* solutions also published by Nikishkov and Atluri (1988), Trantina et al. (1983), and Hodulak and Stöckl (1985)

Comment: Although several different sets of FEM *J* solutions have been published for surface cracks in plates, no single author has published a sufficient number of reliable results to faciliate a general tabular interpolation solution, as in the EPRI handbooks. Furthermore, the results of different authors sometimes disagree.

Semi-Elliptical Axial Surface Crack in a Hollow Cylinder, SC04

Closed-form *K* solutions available in Zahoor (1991) EPRI Handbook, Section 8.1, for internal pressure, various stress distributions
Weight function *K* solution in NASGRO
Some additional tabulated *K* solutions available in Murakami (1987), Section 9.36

Plastic *J* solutions available in tabulated form for internal pressure only
a/t = 0.1 to 0.8 in 0.025 or 0.05 steps
$a/2c$ = 1/3, 1/4, 1/6, 1/10, 1/20, and 1/40
n = 1, 2, 3, 5, 7
R/t = 10 only
Source: Zahoor (1991) EPRI Handbook, Section 8.2

also see very limited FEM total *J* solutions by Wilkening et al. (1984) and Brocks and Noack (1988)

Bass et al. (1982) and Bryan et al. (1984) have published very limited FEM total *J* solutions for external axial semi-elliptical surface flaw in cylinder

Internal Axial Surface Crack (Constant Depth) in a Hollow Cylinder

K solutions available for internal pressure and arbitrary stress distribution
Source: Zahoor (1991) EPRI Handbook, Section 7.1

Plastic *J* solutions available in tabulated form for internal pressure only

R/t = 5, 10, 20
a/t = 0.0 to 0.8 in 0.05 steps
n = 1, 2, 3, 5, 7, 10, 20
Source: Zahoor (1991) EPRI Handbook, Section 7.2

also see solutions for external axial crack in pressurized cylinder, Kumar et al. (1982) EPRI Report

Limited FEM J solutions for combined thermal and mechanical loading in Kumar et al. (1984a) EPRI Report, Section 7

Semi-Elliptical Circumferential Surface Crack in a Hollow Cylinder, SC05

Closed-form K solutions available in Zahoor (1990) EPRI Handbook, Section 3.1, for axial tension, bending moment, arbitrary stress distribution (internal crack; limitations on crack size/shape)
NASGRO K solution for uniform tension, bending

FEM plastic J solutions available in tabulated form for axial load (internal crack)
a/t = 0.1 to 0.8 in 0.025 or 0.05 steps
n = 1, 2, 5, 10
θ/π = 0.05 to 1.00 in 0.05 steps
R/t = 10 only
Source: Zahoor (1990) EPRI Handbook, Section 3.2

FEM plastic J solutions also available for constant depth circumferential surface cracks
independent uniform axial load or bending moment
same a/t, n, θ/π, and R/t values as semi-elliptical surface crack solutions above
Source: Zahoor (1990) EPRI Handbook, Section 2.2 (K solutions in Section 2.1)

Very limited number of FEM plastic J solutions published by Yagawa et al. (1985) for a nearly semi-elliptical shape

Internal Circumferential Surface Crack (Constant Depth) in a Hollow Cylinder, SC06

K solutions available in Zahoor (1990) EPRI Handbook, Section 4.1, for axial load and arbitrary stress distribution
weight function K solutions also available in NASGRO for arbitrary stress distribution

plastic J solutions available in tabulated form for axial load
a/t = 0.0 to 0.8 in 0.05 steps
n = 1, 2, 3, 5, 7, 10, 20
R/t = 5, 10, 20
Source: Zahoor (1990) EPRI Handbook, Section 4.2

Limited FEM J solutions for combined thermal and mechanical loading in Kumar et al. (1984a) EPRI Report, Section 7, and in Muscati (1985)

External Circumferential Surface Crack (Constant Depth) in a Hollow Cylinder, SC06

K solutions available in Rooke and Cartwright (1976), Section 3.2.1, for uniform axial tension
weight function K solutions also available in NASGRO for arbitrary stress distribution

Plastic J solutions available in Kumar et al. (1982) EPRI Report

Semi-Elliptical Surface Crack in a Solid Circular Bar, SC07

K solutions available in NASGRO for uniform tension and bending

No plastic J solutions currently available

Circumferential Surface Crack (Constant Depth) in a Solid Cylinder

K solutions available in Rooke and Cartwright (1976), Section 3.2.1, for uniform axial tension (limiting case of solution for hollow cylinder)

no plastic solutions currently available

APPENDIX C

FINITE ELEMENT J SOLUTIONS FOR SURFACE AND CORNER FLAWS

New *J*-integral solutions based on original elastic-plastic finite element analysis were developed at Rocketdyne for semi-elliptical surface flaws and quarter-elliptical corner flaws. Some of the results were generated in conjunction with parallel Rocketdyne internal research activities.

A parametric quarter-elliptical flaw model was employed. The model was originally developed to interface with 3D models of components, and it can also be used to generate fully plastic *J*-integral solutions for 3D surface or corner flaws. The basic solid entities and their meshing and load application macros were set up in ANSYS 5.0, resulting in a typical mesh as shown in Figure C.1. Flaw modeling employed solid modeling techniques including area concatenation and extensive programmability capabilities. The model was broken up into sub-volumes so that each volume could be map-meshed with eight-noded bricks. The vicinity of the crack tip was deleted facilitating convergence of the plastic solution for materials with high hardening exponents. A mesh and volume division is shown for a particular geometry and mesh refinement in Figure C.2. A flag is used to generate boundary conditions for surface or corner cracks, and the far field load can be perpendicular to or parallel with the crack plane. The opening and the parallel stresses may have different polynomial forms, varying only through the plate thickness.

Reviews of the literature indicate that the fully plastic results published by different researchers do not agree uniformly. Furthermore, even the elastic values may not agree with the Newman-Raju tables in some cases. Therefore, criteria for various aspects of solution quality such as attainment of fully plastic behavior, infinite boundaries, and convergence with respect to element refinement must be established and clearly stated when documenting the results. An adaptive scheme based on optimization was applied to make sure that all the criteria were satisfied with the least amount of function evaluations. A *J*-integral evaluation script incorporating meshing, solution, *J*-integral extraction and quality checking as well as the algorithm to satisfy conditions of convergence with respect to element size, attainment of fully plastic deformation and appropriate model extent was developed.

J-integral solutions were generated with ABAQUS, using its *J*-integral evaluation capabilities and the recently implemented Ramberg-Osgood material model. Utility programs were written to extract *J*-integral values at each load step and integration path. Values associated with integration paths were screened against a path independence criterion. The quality of the mesh (closely tied to material nonlinearity and load level) was characterized by the number of 'good' paths and the maximum difference between the averaged *J* value and the *J*-integral on any of the retained paths. All these steps were implemented in a C shell script called SURFLAW that generates a table of *J*-integral values corresponding to input material properties, load conditions and mesh refinement parameters.

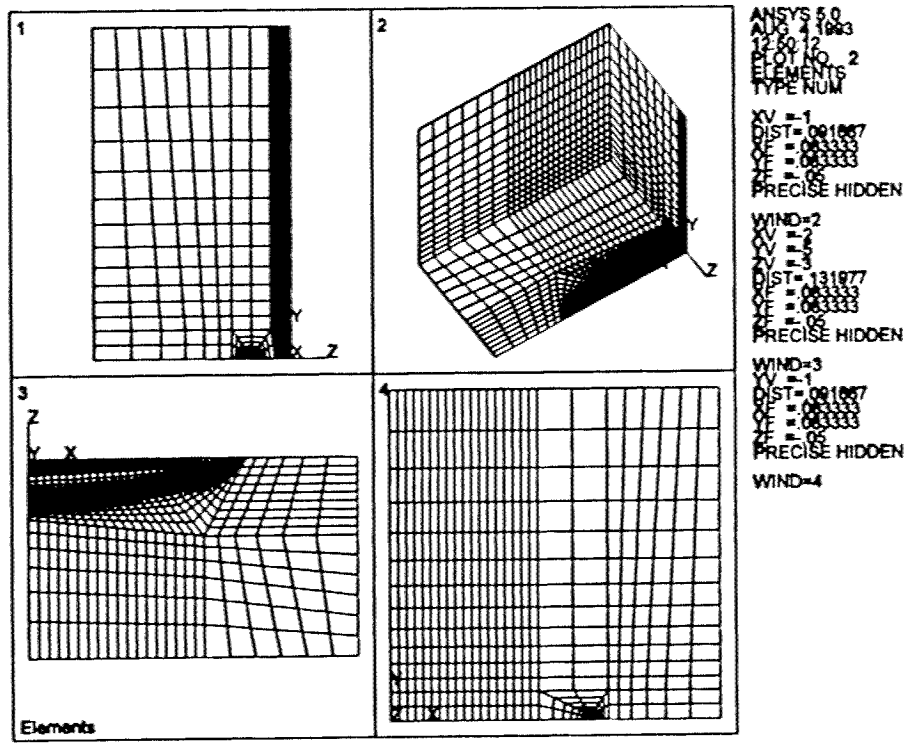

Figure C.1. Sample finite element mesh for new *J* solutions

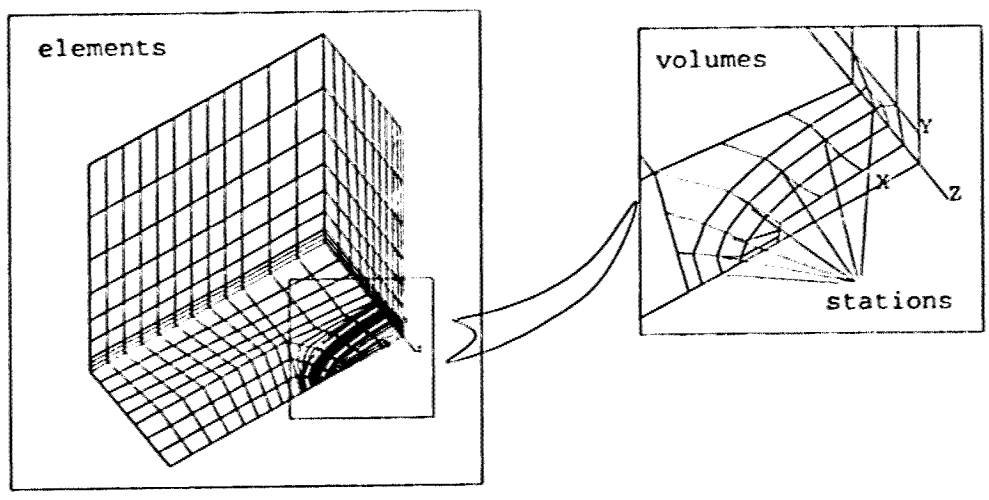

Figure C.2. Elements and volumes

Comparisons of results from SURFLAW with literature J solutions were favorable, as indicated in Figures C.3 and C.4. The Dodds solution (Dodds et al., 1993) shown corresponded to medium hardening and flaw geometry conditions ($2c/a = 6$, $a/t = 0.25$, $2b/t = 4$, $E = 500$, $\nu = 0.3$, $n = 10$, $\sigma_0 = 1$, $\alpha = 1$). Model refinement was characterized by the number of stations along the crack front, the number of elements at a station, referred to as the number of sectors, and the radial element size. The stations were uniformly distributed along the elliptical angle, Φ. First, a mesh refinement study was performed. Comparisons with Dodds' results showed that at the deep point of the crack front and at the free surface the results matched even with relatively coarse mesh designs. The angular dependence, however, differed as shown in Figure C.4. The refinement study demonstrated that the current parametric model converged to the angular dependence given in Figure C.4. The number of elements surrounding the crack front was found to be the most important factor to convergence at the deep end and at the free surface, probably related to the resolution of the angular dependence in the near-tip field.

The fully plastic solution generation procedure was eventually automated. The version of ABAQUS used in this effort had only an elastic-plastic material model, and therefore the fully plastic solution had to be extracted using an EPRI-type scheme. Since the additivity of elastic and plastic J-integral contribution is already an approximation, the logic was to apply large enough load level so that the elastic contribution is negligible and then separate the plastic contribution from the calculated total J-integral. The initial guess for this load level was calculated using a simple reference stress method (McClung et al., 1996b) to estimate the plastic contribution and then solving for the load that results in negligible elastic J. Subsequently, the model was solved using elastic and elastic-plastic materials. The load level that satisfied the criterion for small elastic J to total J ratio was then calculated by a few iterations adjusting the estimated load value. While the 'fully plastic' load level is found, the proper $(n+1)$ power dependence is monitored to assure that the deformation mode does not shift in the gross yielding regime. Once the fully plastic h_1 factors were extracted, the governing script stepped to a higher mesh refinement level until consecutive h_1 values converged at the free surface and at the depth direction. Refinement typically increased the number of degrees of freedom by 1.5× - 2×, largely concentrated in the vicinity of the crack front.

Tables of the fully plastic h_1 factor were generated for surface flaws and corner flaws under membrane loading. Here h_1 was defined as

$$h_1 = \frac{J_p}{\alpha \sigma_0 \varepsilon_0 t \left(\frac{\sigma_\infty}{\sigma_0} \right)^{n+1}} \qquad \textbf{(C.1)}$$

where σ_0, ε_0, α, and n are the usual Ramberg-Osgood constants. Three different a/t values (0.2, 0.5, 0.8) and three different a/c values (0.2, 0.6, 1.0) were considered (a total of nine different combinations). These are the same crack shapes and sizes considered in the Yagawa finite element results (Yagawa et al., 1993) for surface cracks. Three different values of the strain hardening exponent were considered: $n = 5$, 10, and 15. Yagawa and most authors have considered only n less than or equal to 10. The geometry ratios $h/c = 4$ and $c/b = 0.25$ were held constant in all analyses.

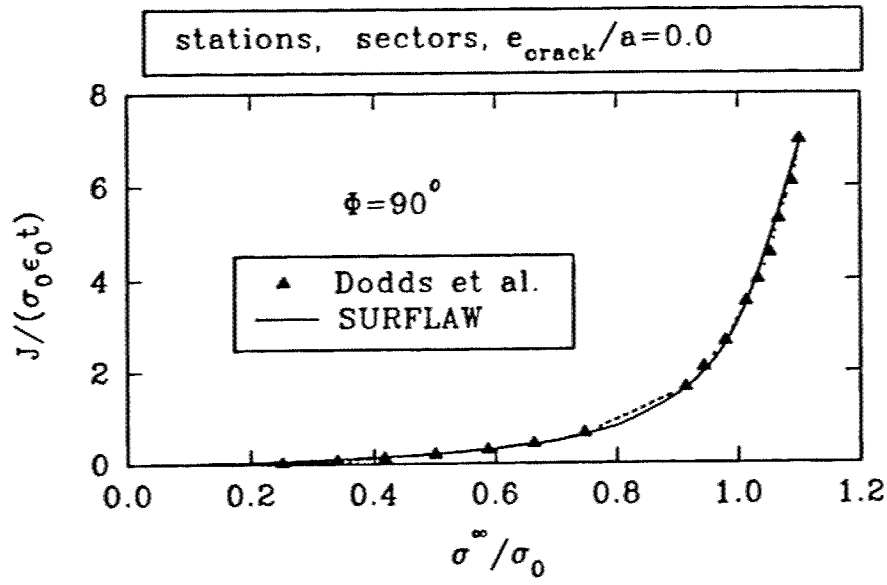

Figure C.3. Load dependence of *J* integral

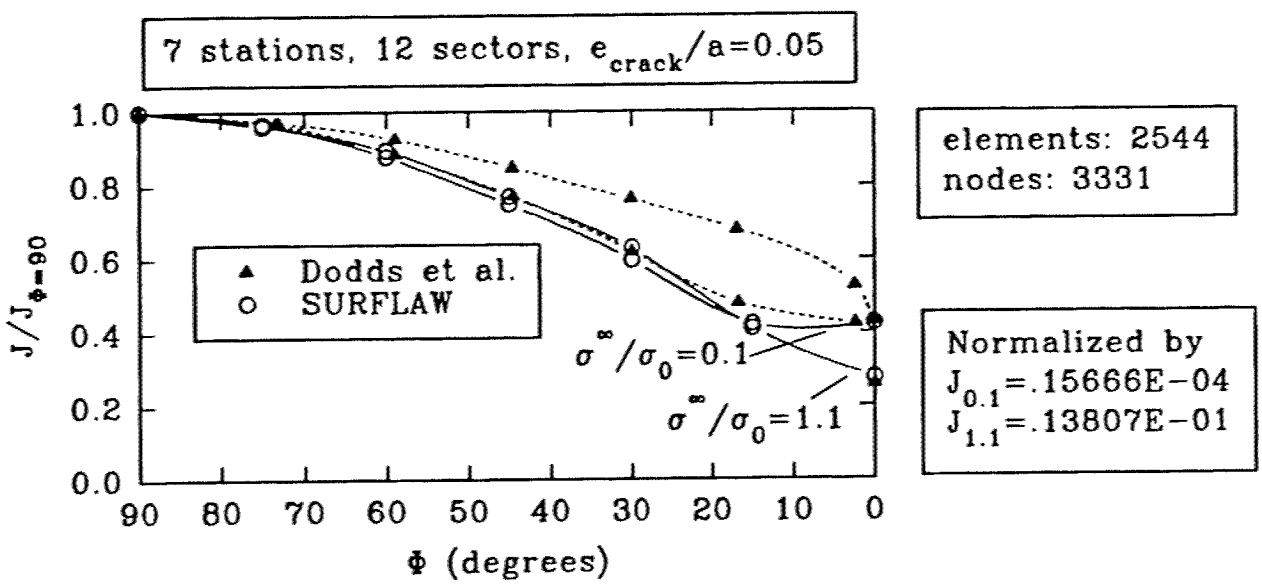

Figure C.4. Angular dependence of *J* integral

Tables C.1 and C.2 show comparisons of elastic solutions with the most recent benchmark K solutions, developed at NASA-Johnson and incorporated in version 2.0 of NASGRO. The elastic solutions were obtained with standard 8-noded elements in ABAQUS. At the free surfaces, the stress intensity factors have been calculated using a plane stress assumption, while plane strain was used at all other stations. The third and fourth columns of these tables show the percentage difference between the new ABAQUS results and the FLAGRO solutions at the plate surface ($\Phi = 0$) and at the deepest point in the thickness direction ($\Phi = 90$). The fifth, sixth, and seventh columns of these tables give information related to the mesh refinement and size of the FE models: the number of sectors perpendicular to the crack front, the ratio of the element size to the minimum of a and b, and the total number of degrees of freedom (NDOF). Agreement is relatively strong for the surface crack but not as good for the corner flaw.

Fully-plastic h_1 values were calculated with the hybrid version of the ABAQUS 8-noded element, which is expected to perform better under conditions of incompressibility than the standard displacement-formulated elements. Tables C.3 - C.8 furnish the numerical values of the h_1 factors, while Figures C.5 - C.10 illustrate the same information graphically. The columns of the tables represent values at stations at equidistant elliptical angle (Φ). In the current study, 11 stations were specified. It is apparent that for high values of the strain hardening exponent, the calculated J values oscillate slightly with angular position. This problem is worse for elongated flaws. Also, in some surface crack computations, the symmetry condition requiring that the J-integral plot along the crack front have zero slope at $\Phi = 90$ is not apparent, judging from the plots.

Table C.1. Surface flaw, membrane loading - elastic solution quality; comparison with results from FLAGRO 2.0

a/t	*a/c*	% e(0)	% e(90)	nsec	cerat	NDOF
.20	.20	9.24	-1.46	9	.012	15240
.20	.60	-.27	-.52	9	.017	10503
.20	1.00	.79	-1.64	9	.017	8469
.50	.20	6.17	-4.76	9	.012	13518
.50	.60	-2.61	-2.97	9	.017	9801
.50	1.00	-1.76	-2.36	9	.017	8235
.80	.20	4.90	-4.09	9	.012	12396
.80	.60	-4.05	-2.33	9	.017	8400
.80	1.00	-3.52	-3.06	9	.017	7524

Table C.2. Corner flaw, membrane loading - elastic solution quality; comparison with results from FLAGRO 2.0

a/t	*a/c*	% e(0)	% e(90)	nsec	cerat	NDOF
.20	.20	8.80	2.29	9	.012	15240
.20	.60	-1.43	.48	9	.017	10503
.20	1.00	-2.09	-2.24	9	.017	8469
.50	.20	3.45	-3.74	9	.012	13518
.50	.60	-6.40	-4.32	9	.017	9801
.50	1.00	-5.82	-6.42	9	.017	8235
.80	.20	-2.40	-9.32	9	.012	12396
.80	.60	-10.78	-9.13	9	.017	8400
.80	1.00	-10.82	-10.95	9	.017	7524

Table C.3. Surface flaw, membrane loading - h_1 factors by angular position for $n = 5$

a/t	*a/c*	0°	9°	18°	27°	36°	45°	54°	63°	72°	81°	90°
.20	.20	.164	.252	.407	.544	.676	.789	.897	.988	1.062	1.103	1.117
.20	.60	.286	.352	.441	.480	.533	.570	.605	.631	.652	.666	.672
.20	1.00	.321	.383	.446	.440	.452	.446	.447	.442	.439	.435	.435
.50	.20	1.325	2.139	3.357	4.384	5.480	6.371	7.136	7.764	8.222	8.428	8.516
.50	.60	1.502	1.916	2.412	2.548	2.764	2.860	2.917	2.938	2.968	2.973	2.976
.50	1.00	1.377	1.658	1.931	1.867	1.894	1.839	1.800	1.730	1.677	1.637	1.630
.80	.20	7.224	11.273	15.743	18.150	21.870	21.460	20.632	20.051	18.960	18.993	19.369
.80	.60	4.983	6.449	7.582	7.389	8.421	7.750	7.034	6.695	6.266	6.114	6.178
.80	1.00	3.910	4.728	5.251	4.849	5.142	4.775	4.080	3.734	3.397	3.285	3.270

Table C.4. Surface flaw, membrane loading - h_1 factors by angular position for $n = 10$

a/t	*a/c*	0°	9°	18°	27°	36°	45°	54°	63°	72°	81°	90°
.20	.20	.198	.320	.523	.703	.863	.996	1.133	1.250	1.345	1.398	1.416
.20	.60	.324	.416	.544	.604	.671	.715	.759	.792	.820	.839	.847
.20	1.00	.358	.450	.550	.553	.571	.565	.569	.566	.562	.557	.556
.50	.20	2.539	4.512	6.957	8.841	10.665	11.979	13.048	13.953	14.546	14.712	14.811
.50	.60	2.319	3.205	4.264	4.561	4.967	5.128	5.189	5.209	5.231	5.200	5.186
.50	1.00	2.007	2.599	3.210	3.179	3.272	3.218	3.168	3.040	2.921	2.827	2.804
.80	.20	17.731	29.512	39.550	43.774	49.600	46.576	44.854	43.844	43.706	45.805	47.496
.80	.60	9.688	13.685	16.725	15.850	19.174	17.318	15.896	14.776	14.068	14.323	14.780
.80	1.00	7.242	9.472	11.077	10.311	11.898	11.108	9.239	8.398	7.536	7.533	7.625

Table C.5. Surface flaw, membrane loading - h_I factors for $n = 15$

a/t	*a/c*	0°	9°	18°	27°	36°	45°	54°	63°	72°	81°	90°
.20	.20	.223	.370	.608	.821	1.001	1.148	1.310	1.447	1.560	1.623	1.644
.20	.60	.356	.465	.622	.698	.774	.823	.875	.915	.948	.971	.981
.20	1.00	.389	.503	.628	.638	.659	.653	.657	.657	.653	.646	.646
.50	.20	4.085	7.615	11.602	14.488	17.057	18.798	20.228	21.434	22.129	22.212	22.309
.50	.60	3.336	4.808	6.564	7.048	7.697	7.939	8.000	8.021	8.019	7.922	7.881
.50	1.00	2.774	3.738	4.750	4.759	4.932	4.891	4.816	4.613	4.407	4.243	4.198
.80	.20	37.609	63.511	82.404	91.460	99.198	92.725	90.097	88.292	89.548	95.447	98.941
.80	.60	17.660	25.890	32.760	30.172	37.828	34.002	31.546	28.972	28.224	29.095	30.806
.80	1.00	12.667	17.231	20.882	19.281	23.029	21.124	18.005	16.467	14.557	15.003	15.533

Table C.6. Corner flaw, membrane loading - h_I factors for $n = 5$

a/t	*a/c*	0°	9°	18°	27°	36°	45°	54°	63°	72°	81°	90°
.20	.20	.178	.269	.439	.576	.740	.871	1.065	1.198	1.420	1.375	1.047
.20	.60	.332	.436	.566	.612	.687	.729	.789	.795	.857	.724	.559
.20	1.00	.357	.456	.559	.558	.587	.581	.588	.561	.562	.460	.355
.50	.20	1.624	2.620	4.074	5.173	6.600	7.543	8.700	9.330	10.971	11.047	8.743
.50	.60	1.758	2.351	3.041	3.217	3.554	3.679	3.883	3.909	4.249	3.635	2.840
.50	1.00	1.586	2.032	2.491	2.474	2.593	2.549	2.540	2.397	2.389	1.957	1.534
.80	.20	10.547	16.218	22.113	25.204	30.867	30.298	30.327	31.659	32.942	37.593	37.708
.80	.60	6.745	9.171	11.182	11.176	13.035	11.897	11.417	11.116	11.877	12.845	11.941
.80	1.00	5.043	6.621	7.934	7.725	8.562	7.809	6.905	6.564	6.762	6.896	6.177

Table C.7. Corner flaw, membrane loading - h_1 factors for $n = 10$

a/t	*a/c*	0°	9°	18°	27°	36°	45°	54°	63°	72°	81°	90°
.20	.20	.225	.363	.591	.782	.994	1.173	1.440	1.640	1.938	1.838	1.285
.20	.60	.390	.552	.759	.836	.943	1.004	1.079	1.080	1.145	.913	.647
.20	1.00	.408	.565	.736	.755	.804	.800	.806	.759	.739	.568	.404
.50	.20	3.421	6.230	9.277	11.430	13.949	15.408	17.070	18.200	20.918	21.153	15.917
.50	.60	2.748	4.069	5.584	6.019	6.699	6.899	7.167	7.270	7.795	6.399	4.617
.50	1.00	2.295	3.208	4.224	4.343	4.665	4.639	4.577	4.268	4.129	3.189	2.347
.80	.20	29.959	50.183	64.606	71.852	79.801	76.369	79.548	86.276	94.533	109.398	102.915
.80	.60	13.894	21.145	27.580	27.336	33.214	29.540	29.170	27.742	30.372	33.628	28.082
.80	1.00	9.675	14.118	18.383	18.463	21.770	19.340	16.955	15.830	16.086	17.090	14.298

Table C.8. Corner flaw, membrane loading - h_1 factors for $n = 15$

a/t	*a/c*	0°	9°	18°	27°	36°	45°	54°	63°	72°	81°	90°
.20	.20	.263	.439	.715	.950	1.200	1.418	1.742	1.997	2.356	2.218	1.492
.20	.60	.441	.648	.916	1.018	1.153	1.230	1.315	1.315	1.383	1.077	.730
.20	1.00	.456	.657	.880	.915	.978	.977	.980	.918	.883	.659	.453
.50	.20	5.592	10.808	15.786	19.132	22.680	24.619	26.762	28.468	32.381	32.896	24.472
.50	.60	3.945	6.137	8.632	9.383	10.470	10.743	11.064	11.305	12.015	9.751	6.751
.50	1.00	3.154	4.611	6.272	6.555	7.120	7.119	6.979	6.500	6.201	4.673	3.339
.80	.20	74.186	130.370	161.082	179.972	189.422	181.685	191.746	207.090	224.200	260.682	240.016
.80	.60	28.924	46.897	63.166	61.199	76.402	67.139	66.817	62.233	69.675	78.743	60.777
.80	1.00	18.993	29.158	39.744	40.303	48.572	42.573	37.144	34.238	34.758	37.577	30.002

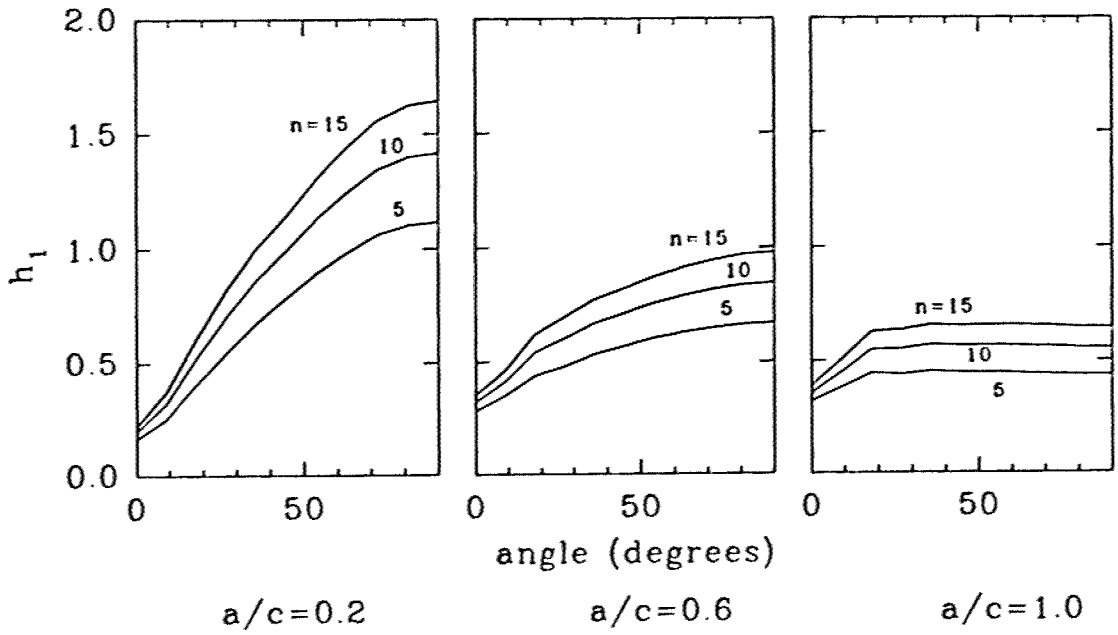

Figure C.5. Surface flaw, membrane loading - angular variation of the *J*-integral for $a/t = 0.2$

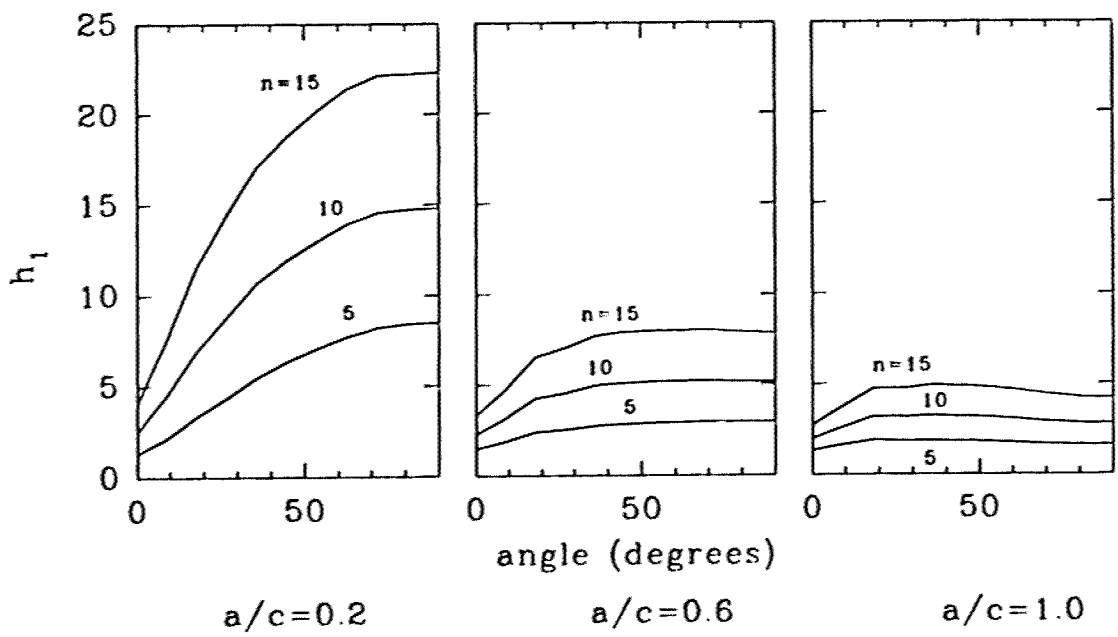

Figure C.6. Surface flaw, membrane loading - angular variation of the *J*-integral for $a/t = 0.5$

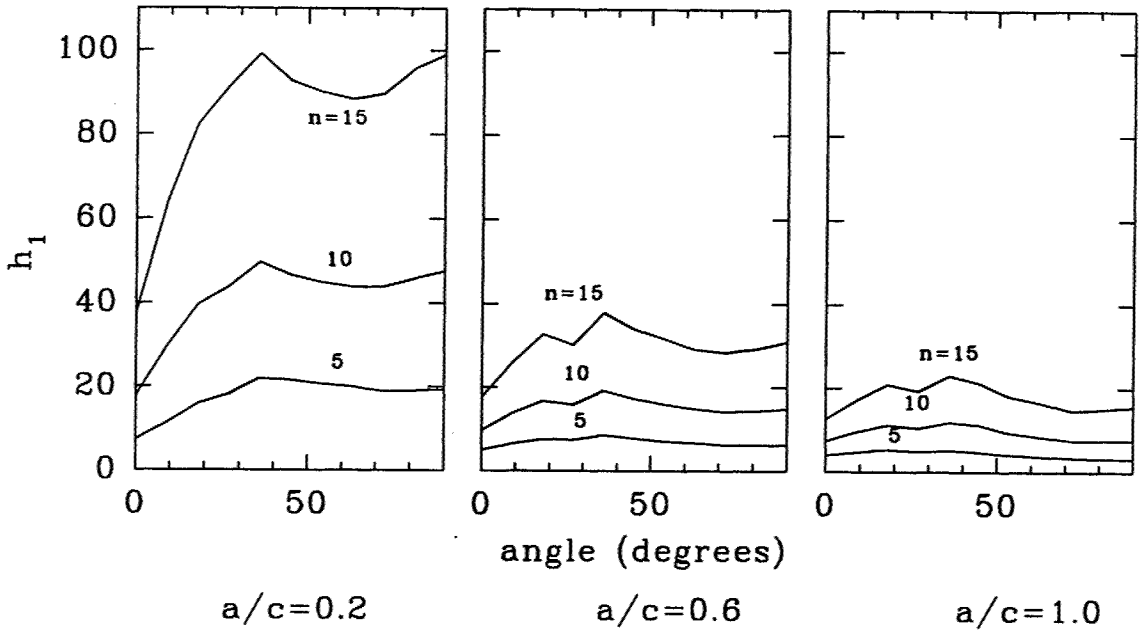

Figure C.7. Surface flaw, membrane loading - angular variation of the *J*-integral for $a/t = 0.8$

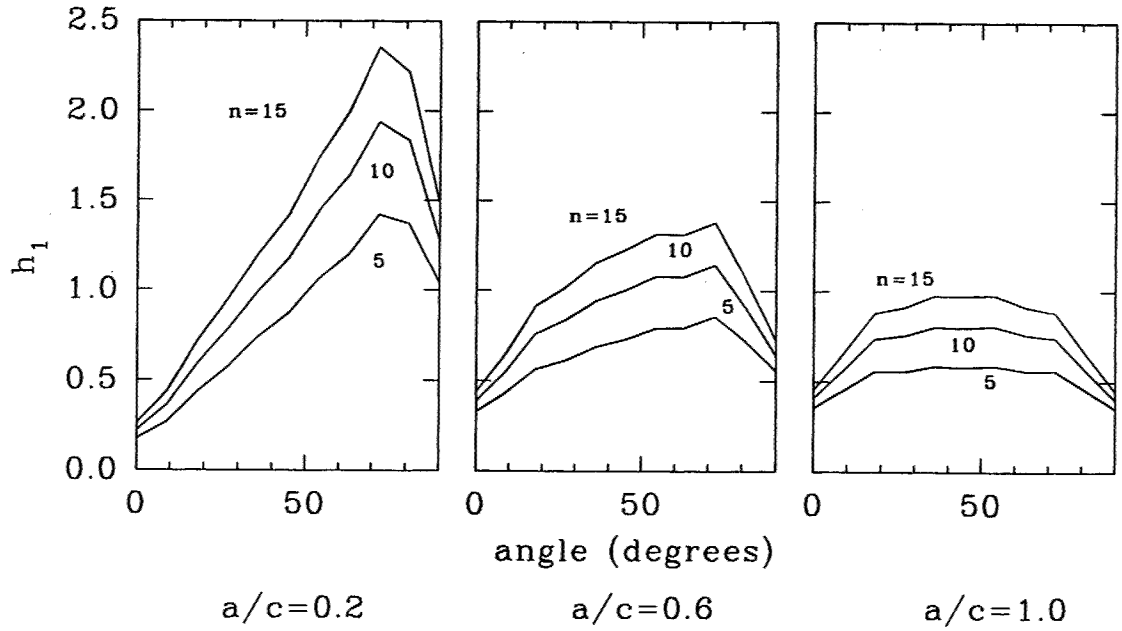

Figure C.8. Corner flaw, membrane loading - angular variation of the *J*-integral for $a/t = 0.2$

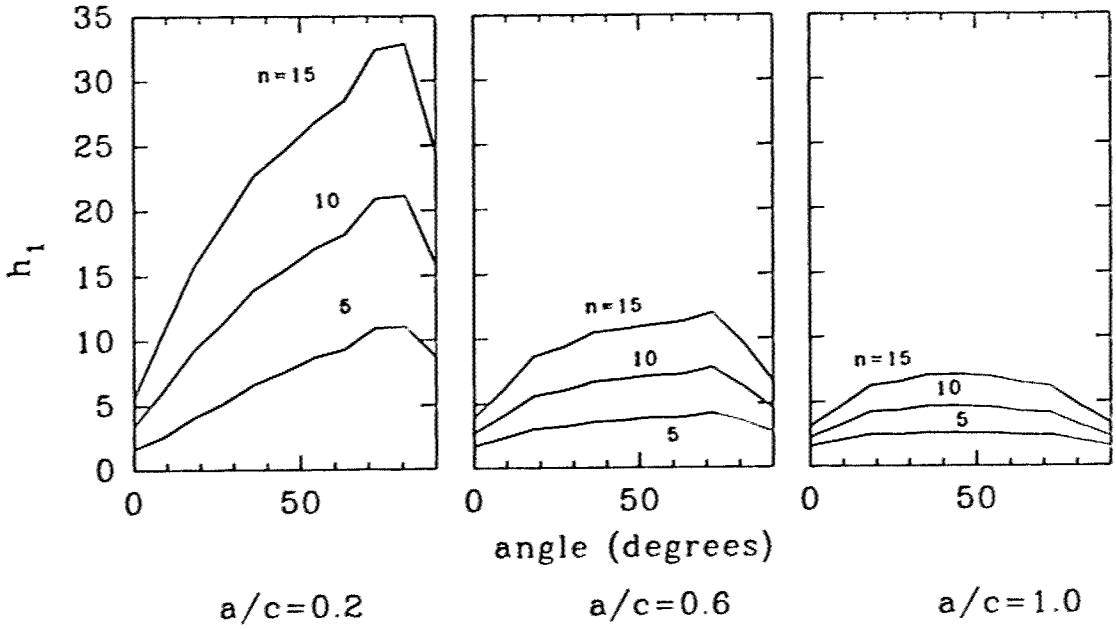

Figure C.9. Corner flaw, membrane loading - angular variation of the *J*-integral for $a/t = 0.5$

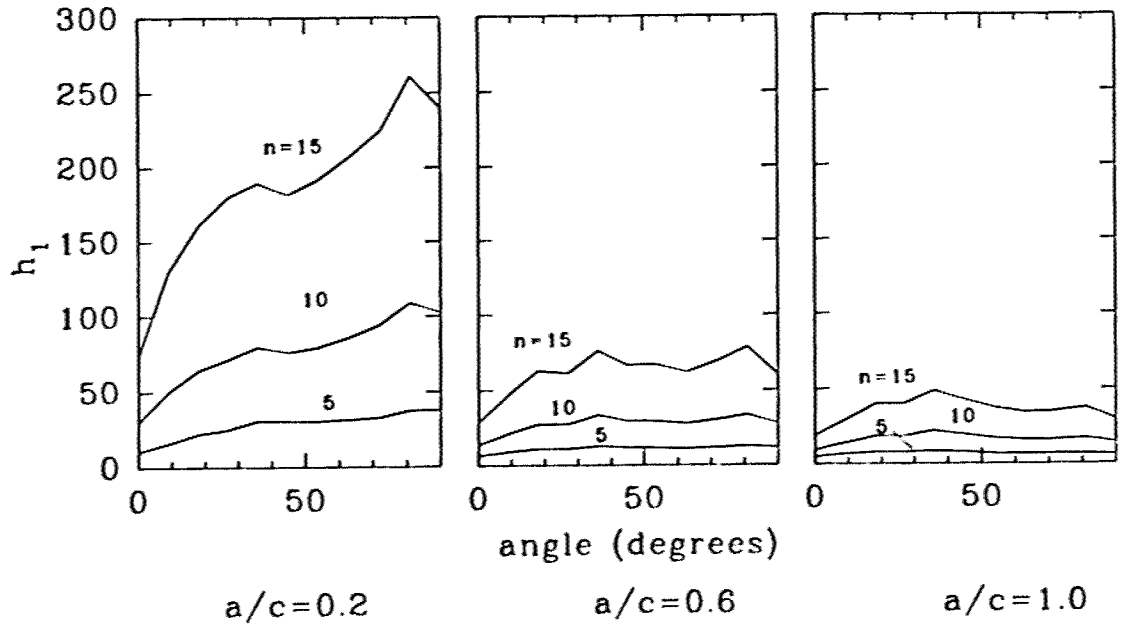

Figure C.10. Corner flaw, membrane loading - angular variation of the *J*-integral for $a/t = 0.8$

APPENDIX D

A J ESTIMATION SCHEME FOR CRACKS AT NOTCHES

D.1 Introduction

In this Appendix, a J estimation scheme is proposed and validated against original finite element J results and existing results presented in the EPRI elastic-plastic fracture handbook (Zahoor, 1991). The new FE results are elastic-plastic J solutions for symmetrical cracks emanating from parallel sided double edge notches (DEN) in plates subjected to tensile forces and undergoing plane stress deformation. The EPRI solutions were derived for a single crack emanating from a round hole in an infinite body subjected to uniform biaxial stressing, the stress normal to the crack plane being equal to twice the value of the stress acting parallel to the crack plane. Both sets of solutions were obtained for material stress-strain behavior governed by the Ramberg-Osgood law

$$\frac{\epsilon}{\epsilon_o} = \frac{\sigma}{\sigma_o} + \alpha \left(\frac{\sigma}{\sigma_o} \right)^n \qquad \textbf{(D.1)}$$

where ϵ_o, α, n, and σ_o are material constants, and $\epsilon_o=\sigma_o/E$, E is Young's modulus, and ϵ is the strain corresponding to the uniaxial stress, σ.

The cracked DEN J solutions were computed for various a/b and n values and for D/R=2.41, 6.2, and 11.6 which correspond to stress concentration factors, K_t, of 4.2, 6.3, and 8.4, where

$$K_t = \frac{stress\ at\ notch}{gross\ section\ stress} \qquad \textbf{(D.2)}$$

Here, $a=D+d$, where D is the depth of the notch, d is the depth of the crack measured from the root of the notch, b is half the width of the plate, and R is the radius of the semi-circular notch tip. The EPRI solutions are for a crack at a embedded round hole with $D/R=1$ and K_t=2.8. Hence, these two sets of results provide a comprehensive range of solutions which cover most stress concentration features of practical interest. The relationships between d, a, R, D, and b, are shown schematically in Figure D.1.

D.2 J Estimation Schemes

D.2.1 EPRI Scheme

In the EPRI handbook, the plane stress solution for J is expressed in the form

$$J = J_e + J_p \qquad \textbf{(D.3)}$$

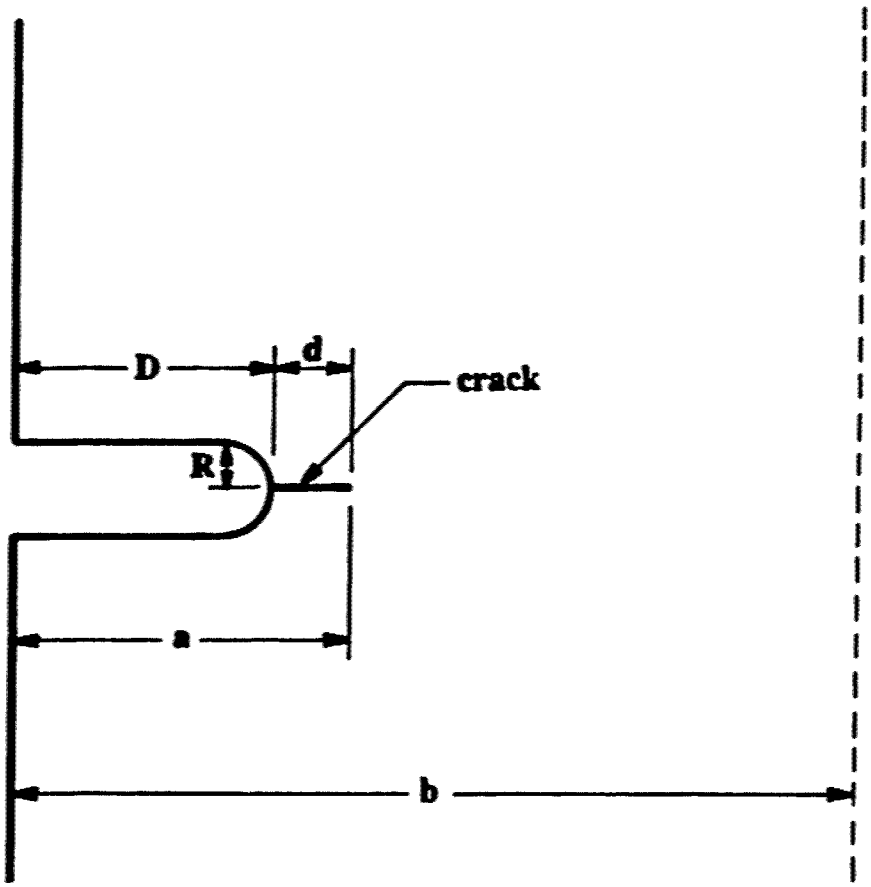

Figure D.1 Schematic showing geometrical relationships between notch depth (*D*), notch root radius (*R*), crack depth (*d*), notch plus crack depth (*a*) and half plate width (*b*).

where J_e is a first order plastically corrected value of the linear elastic solution for J and is given by

$$J_e(d_e) = J_e(d + \phi r_y) \tag{D.4}$$

where

$$J_e = \frac{K^2}{E} \tag{D.5}$$

and K is the stress intensity factor. The effective depth, $d_e = d + \phi r_y$, includes a plastic zone correction determined by the terms ϕ and r_y which are defined as

$$\phi = \frac{1}{1 + \left(\frac{P}{P_o}\right)^2} \tag{D.6}$$

$$r_y = \frac{1}{\beta\pi}\left[\frac{n-1}{n+1}\right]\left(\frac{K}{\sigma_o}\right)^2 \tag{D.7}$$

Here β equals 2 for plane stress, and 6 for plane strain.

The plastic component of J, J_p, is expressed as

$$J_p = \alpha\ \epsilon_o\ \sigma_o\ d\ h_1(d/R, n, \lambda)\left(\frac{P}{P_o}\right)^{n+1} \tag{D.8}$$

where the values of the function h_1 are tabulated in the EPRI handbook for various values of d/R and n, and for a biaxial stress factor, λ=0.5. P is the applied load, and P_o a characteristic yield load.

The cracked DEN results were expressed in a similar form to the EPRI handbook solution for double edge cracked plates. For example, the plastic component of J_p was written as

$$J_p = \alpha \ \epsilon_o \ \sigma_o \ c \ h_1(a/b,n,D/R) \left(\frac{P}{P_o} \right)^{n+1} \tag{D.9}$$

where $c=b-a$. The characteristic yield load, P_o was defined for the double edge cracked plate in plane stress as

$$P_o = \frac{4}{\sqrt{3}} \ c \ \sigma_o \tag{D.10}$$

D.2.2 Proposed Estimation Scheme (Modified RSM)

The proposed J estimation scheme combines the scheme adopted by EPRI and used in the elastic-plastic handbooks, with the reference stress method. In the proposed scheme, hereafter referred to as the modified RSM, first order plasticity effects are included in J via a first order plastically corrected value for the linear elastic solution, J_e, given by equations (D.4) and (D.5). This ensures that the correct linear elastic limit is recovered by the scheme.

The fully plastic contribution to J, J_p is evaluated using the RSM. For the purposes of validating the approach, the optimized RSM is employed. In this method, a yield load, P_o^*, and structural parameter, $V(a/b,D/R)$, are derived from finite element solutions for J_p. (In the present instance, the J_p solutions are available from the new FE results and the EPRI handbooks.) The values of P_o^* and $V(a/b,D/R)$ are chosen so as to optimize the fit of the RSM estimate of J_p to the finite element solutions for a range of n values. This approach ensures that the correct fully plastic limit is recovered by the scheme.

Note that in general, the values of P_o^* and $V(a/b,D/R)$ are not known a priori in the absence of appropriate finite element solutions for J_p, P_o^* is often approximated by P_o, and $V(a/b,D/R)$ is assumed to have the value of unity. Using the optimized approach provides an accurate representation of the fully plastic solution, enabling the accuracy of the modified RSM to be investigated explicitly in the important elastic-plastic regime which interpolates between linear elastic and fully plastic behavior.

The optimized RSM expression for J_p is

$$J_p = J_e(d) \ V(a/b,D/R) \left[\frac{E\epsilon^p_{ref}}{\sigma_{ref}} \right] \tag{D.11}$$

where ϵ^p_{ref} is the plastic component of the reference strain which, for Ramberg-Osgood materials, is given by

$$\epsilon^p_{ref} = \alpha \left(\frac{P}{P_o^*} \right)^n \tag{D.12}$$

and

$$\sigma_{ref} = \frac{P}{P_o^*} \sigma_o \tag{D.13}$$

In summary, in the proposed modified RSM J estimation scheme for cracks at notches, J is written as

$$J = J_e(d + \phi^* r_y) + J_e(d) \; V(a/b,D/R) \left[\frac{E\epsilon^p_{ref}}{\sigma_{ref}} \right] \tag{D.14}$$

where

$$\phi^* = \frac{1}{1 + \left(\frac{P}{P_o^*} \right)^2} \tag{D.15}$$

D.2.3 Standard RSM Scheme

For comparison purposes, it is useful to review the standard RSM scheme. The standard optimized RSM expression is

$$J = J_e(d) \left\{ 1 + \frac{\frac{1}{2} L_r^{*2}}{\left[\frac{E\epsilon_{ref}}{\sigma_{ref}} \right]} \right\} + J_e(d) \; V(a/b,D/R) \; \frac{E\epsilon^p_{ref}}{\sigma_{ref}} \tag{D.16}$$

where ϵ_{ref} is the reference strain derived from Equation (D.1) by replacing σ by σ_{ref}, and $L_r^* = P/P_o^*$. In this equation, the first term on the right hand side provides a first order plastic correction similar

to that appearing in Equation (D.15). However, note that whereas the modified RSM approach explicitly includes local notch tip plasticity effects through the dependence of J_e on $\phi^* r_y$, these effects are not directly accounted for in the standard RSM approach, where small scale plasticity is assumed to depend on the net section stress parameter, L_r^*.

D.3 Validation of *J* Estimation Scheme

It is convenient to transfer the *J* results obtained from the finite element computations and the optimized modified RSM to the Failure Assessment Diagram (FAD) to facilitate a comparison of the two sets of solutions, and to identify trends in behavior as the value of K_r changes. The FAD provides a simple diagrammatic representation of *J* solutions which makes apparent the effect of increasing crack tip plasticity as the applied load is increased. The FAD can be generated by evaluating the parameters L_r and K_r as a function of the load *P* using the equations

$$L_r = \frac{P}{P_o(a/b)} \quad , \quad K_r = \sqrt{\frac{J_e(d,P)}{J(d,P)}} \tag{D.17}$$

The value of L_r measures the nearness of the flawed structure to net section yielding (by definition, L_r=1 corresponds to net section yielding), and the value of K_r determines the effects of crack tip plasticity with respect to linear elastic behavior. (By definition, K_r=1 corresponds to J=J_e, and linear elastic fracture mechanics may be applied, whereas a value of K_r«1 indicates that fully plastic behavior is appropriate and $J \approx J_p$.)

FAD's have been constructed using Equation (D.17) for the *J* solutions given in the EPRI handbooks and the new cracked DEN solutions. (Note that L_r in this equation is evaluated using the EPRI expressions for the characteristic yield loads.) In all cases, Ramberg-Osgood constants given by α=1 and σ_o=60 ksi were used. A summary of the *J* solutions analyzed in terms of the FAD is shown in Table D.1. FAD's have also been constructed for the notch geometries listed in Table 1 using *J* values derived according to the modified RSM and the standard RSM. In all, a total of 10 EPRI *J* solutions and 88 new cracked DEN *J* solutions were analyzed in this way. A representative set of the results are displayed in Figures D.2 through D.6 for the EPRI geometry and n=5, and Figures D.7 through D.28 for the cracked DEN geometry and n=10.

Although the source values for *J* are not given in the EPRI handbook, the EPRI solutions validate the modified RSM approach to estimating *J* since the EPRI handbook gives the solutions already resolved into J_e and J_p components, as defined in equations (D.3) through (D.8). These equations are equivalent to equation (D.14) since in equation (D.14) the plastic component, J_p, is the optimized RSM solution derived directly from equation (D.8). Figures D.2 through D.6 enable the accuracy of the standard optimized RSM (equation (D.16), indicated by solid lines in the figures) to be compared with the EPRI finite element solutions (dashed lines), bearing in mind that the standard RSM does not explicitly incorporate the effect of the notch on crack tip plasticity in the small scale yielding regime. The RSM estimate of *J* will be conservative compared to the finite element results when the RSM failure curve falls inside the finite element failure curve, but will

underestimate the finite element J value when the reverse situation occurs. For a given applied load (L_r value) the ratio of J solutions is given by

$$\frac{J\ (RSM)}{J\ (finite\ \ element)} = \left[\frac{K_r(finite\ \ element)}{K_r(RSM)} \right]^2 \qquad \textbf{(D.18)}$$

From Figures D.2 through D.6 it can be seen that the standard optimized RSM method provides a good approximation to the EPRI finite element values of J, even for the smallest crack (d/R=0.125) where the stress concentration of the hole will have the most effect on crack tip plasticity.

In Figures D.7 through D.13 the finite element FAD's derived from the new cracked DEN J solutions for K_t=4.2 (open circles) are compared with the FAD's constructed using the modified RSM (dotted lines) and the standard RSM (solid lines). These figures illustrate some important points:

- The FAD's constructed using the modified RSM are in excellent agreement with the finite element solutions for all the crack depths analyzed ($0.1194 \le d/R \le 0.6431$) and at all load levels (L_r values).

- The effects of the concentration of stress and strain at the notch root on crack tip plasticity are clearly apparent for shallow cracks (d/R<0.2940). This is indicated by the shape of the FAD's at low values of the applied load (low L_r values). In this regime, the values of K_r derived from the finite element and modified RSM are significantly less than 1, whereas the standard RSM (which does not incorporate the effect of the notch on small scale crack tip yielding) is still predicting values which are close to 1.

- The standard RSM estimation scheme for J could significantly underestimate J for shallow cracks at notches for low to moderate load levels. Hence, the standard RSM estimation for J will be non-conservative in these cases.

- At high loads where plastic deformation has extended across the net section (L_r>1), local effects at the notch root become insignificant for all the cracks analyzed. In this regime, the FAD's calculated from the finite element J values, and using the modified and standard RSM's, are all in good agreement.

- The FAD's derived from the three methods are in good agreement at all load levels for relatively deep cracks ($d/R \ge 0.2940$). This indicates that local notch stress concentration effects on crack tip plasticity are small for these types of cracks. In these cases, the J solutions for the notch plus crack are very similar to the J solutions for a crack of depth $a=D+d$ subjected to the nominal load. This kind of behavior is well known in linear elastic fracture mechanics and could have been anticipated to occur also in the elastic-plastic fracture regime.

The FAD's for the cracked geometries where K_t=6.3 are shown in Figures D.14 through D.20. Similar conclusions can be drawn from these results as for those for K_t=4.2, with, in particular, local notch concentration effects being most important for shallow cracks where $d/R \leq 0.3063$. Similar conclusions can also be drawn from the results presented in Figures D.21 through D.28 for the cracked geometries where K_t=8.4.

D.3.1 Significance of V(a/b,D/R)

Whereas, in the absence of appropriate fully plastic J solutions, the value of the yield load, P_o^*, can be estimated from plastic limit load theory, it is not possible to determine the value of $V(a/b,D/R)$ without these solutions. The value of P_o^* is not dependent on local notch stress concentrations, and is a function of the remaining uncracked section (net section) and the nominal applied load. In contrast, the value of $V(a/b,D/R)$ for shallow cracks ($d/R<0.3$) will be sensitive to notch concentration effects. For example, in the case of double edge notched plates V typically had a value of around 1.4 for the very shallow cracks, which decreased to around 1.2 for the deepest cracks. These values are consistent with an average values for V of about 1 which has been derived from the analysis a wide range of cracked structural geometries. Furthermore, the value of V only influences the value of J in the fully plastic regime.

Hence, it is proposed that a value of 1 be assumed for V, and the following expression be used to evaluate J in cases where finite element elastic-plastic results are not available

$$J = J_e\left(d + \phi^* r_y\right) + J_e(d)\left[\frac{E\epsilon_{ref}^p}{\sigma_{ref}}\right] \qquad \textbf{(D.19)}$$

D.3.2 Validation of Equation (D.19)

Validation in support of equation (D.19) is shown in Figures D.29 through D.34 which show FAD's constructed using equations (D.14) (dashed lines) and (D.19) (solid lines), and FAD's derived from the cracked DEN finite element J analyses for n=10 (open circles). The figures cover FAD's for shallow and deep cracks emanating from notches with K_t values of 4.2, 6.3 and 8.4. The modified RSM approximations to J represented by equations (D.14) and (D.19) were evaluated using optimized yield loads, P_o^*.

The agreement between FAD's derived using the modified RSM based on assuming V=1 and the finite element FAD's is good, indicating that the accuracy of the modified RSM approach to estimating J will be sufficient for engineering applications. As previously stated, the assumption that V=1 will only significantly influence the accuracy of FAD's derived using the modified RSM approach in the fully plastic regime (L_r>1). This conclusion is supported by comparing the results in Figures D.29 through D.34 for the two modified RSM approaches based on using an explicit value for V and assuming V=1.

D.4 Summary

The elastic-plastic value of J for cracks at notches can be estimated by combining the EPRI and RSM estimation schemes. The EPRI scheme provides a means of evaluating J in the linear elastic and small scale crack tip yielding regimes which incorporates local notch stress concentration effects. The RSM approach provides a way of estimating the effects of widespread plasticity (net section yielding) on J. Combining these schemes provides the following equation for J which may be applied at all levels of crack tip plasticity, from the linear elastic limit through to the fully plastic limit, and for all crack depths

$$J = J_e\left(d + \phi^* \, r_y\right) + J_e(d) \left[\frac{E\epsilon^p_{ref}}{\sigma_{ref}}\right] \qquad \textbf{(D.20)}$$

where $\sigma_{ref} = P/P_o^*$, P_o^* is an estimated yield load for the cracked structure, based on the remaining uncracked section, and ϕ^* and r_y are evaluated according to equations (D.15) and (D.7), respectively.

Table D.1. Summary of finite element *J* solutions for cracks emanating from notches.

a/b	*d/R*	*R/D*	K_t
EPRI plane stress solutions for single crack emanating from round hole subject to biaxial stressing: n = 1, 3, 5.			
0.000	0.125	1.00	2.8
0.000	0.250	1.00	2.8
0.000	0.500	1.00	2.8
0.000	0.750	1.00	2.8
0.000	1.000	1.00	2.8
Plane stress solutions for cracks emanating from double edge notched plates, D/b=0.3: n = 1, 3, 5, 10, 15.			
0.315	0.119	2.41	4.2
0.326	0.206	2.41	4.2
0.337	0.294	2.41	4.2
0.347	0.381	2.41	4.2
0.358	0.469	2.41	4.2
0.369	0.556	2.41	4.2
0.380	0.643	2.41	4.2
0.315	0.306	6.19	6.3
0.326	0.525	6.19	6.3
0.337	0.754	6.19	6.3
0.347	0.978	6.19	6.3
0.358	1.202	6.19	6.3
0.369	1.426	6.19	6.3
0.380	1.650	6.19	6.3
0.304	0.155	11.63	8.4
0.315	0.576	11.63	8.4
0.326	0.997	11.63	8.4
0.337	1.418	11.63	8.4
0.347	1.838	11.63	8.4
0.358	2.259	11.63	8.4
0.369	2.680	11.63	8.4
0.380	3.101	11.63	8.4

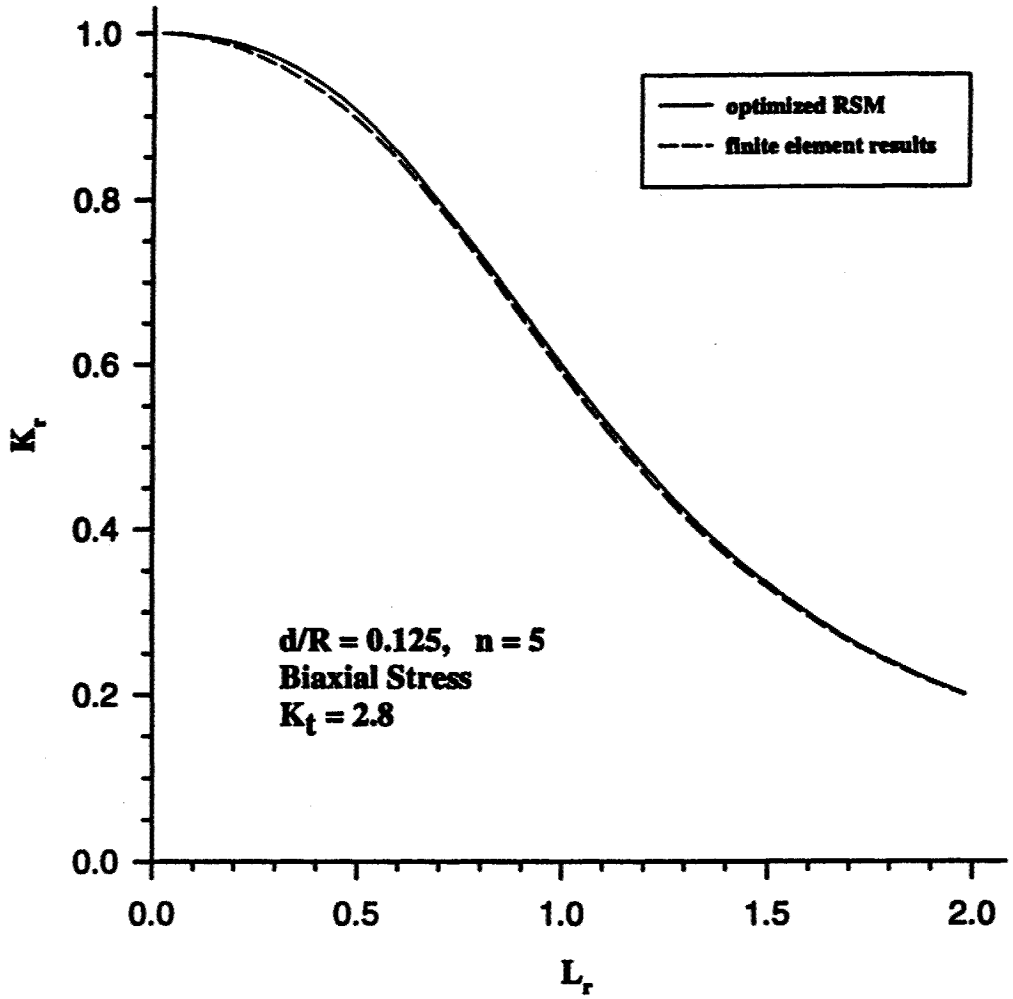

Figure D.2 Comparison of EPRI finite element results (dashed line) with the optimized RSM (solid line) for a single crack at a round hole subjected to biaxial stressing: d/R=0.125, K_t=2.8, n=5.

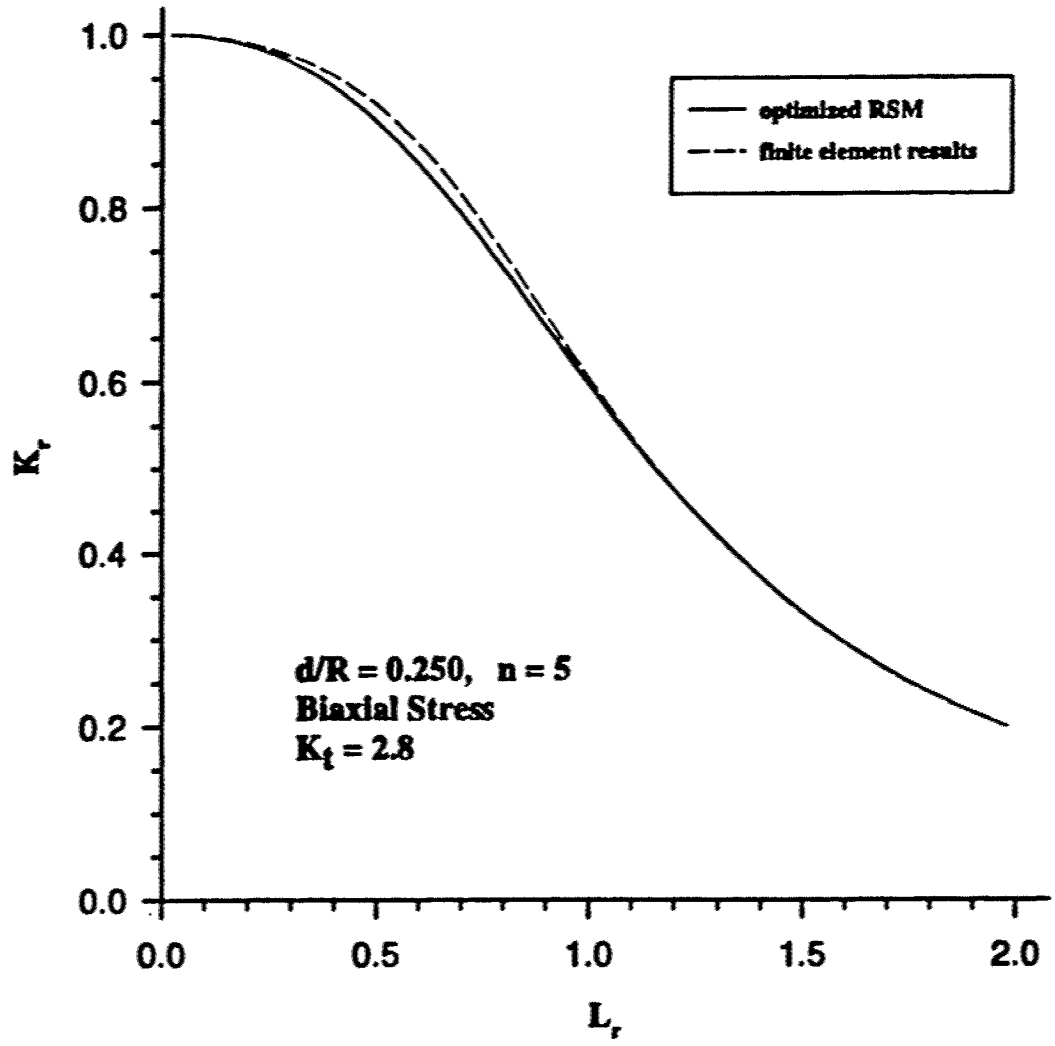

Figure D.3 Comparison of EPRI finite element results (dashed line) with the optimized RSM (solid line) for a single crack at a round hole subjected to biaxial stressing: d/R=0.250, K_t=2.8, n=5.

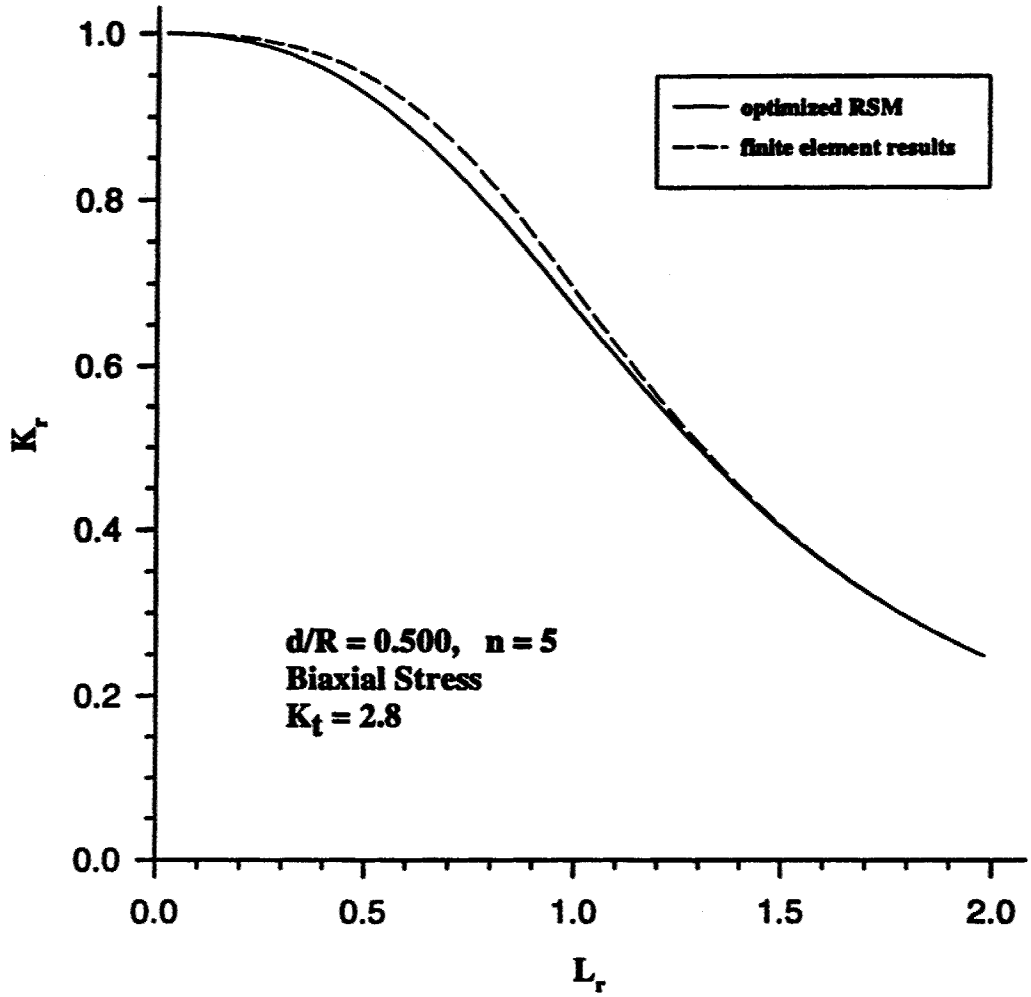

Figure D.4 Comparison of EPRI finite element results (dashed line) with the optimized RSM (solid line) for a single crack at a round hole subjected to biaxial stressing: d/R=0.500, K_t=2.8, n=5.

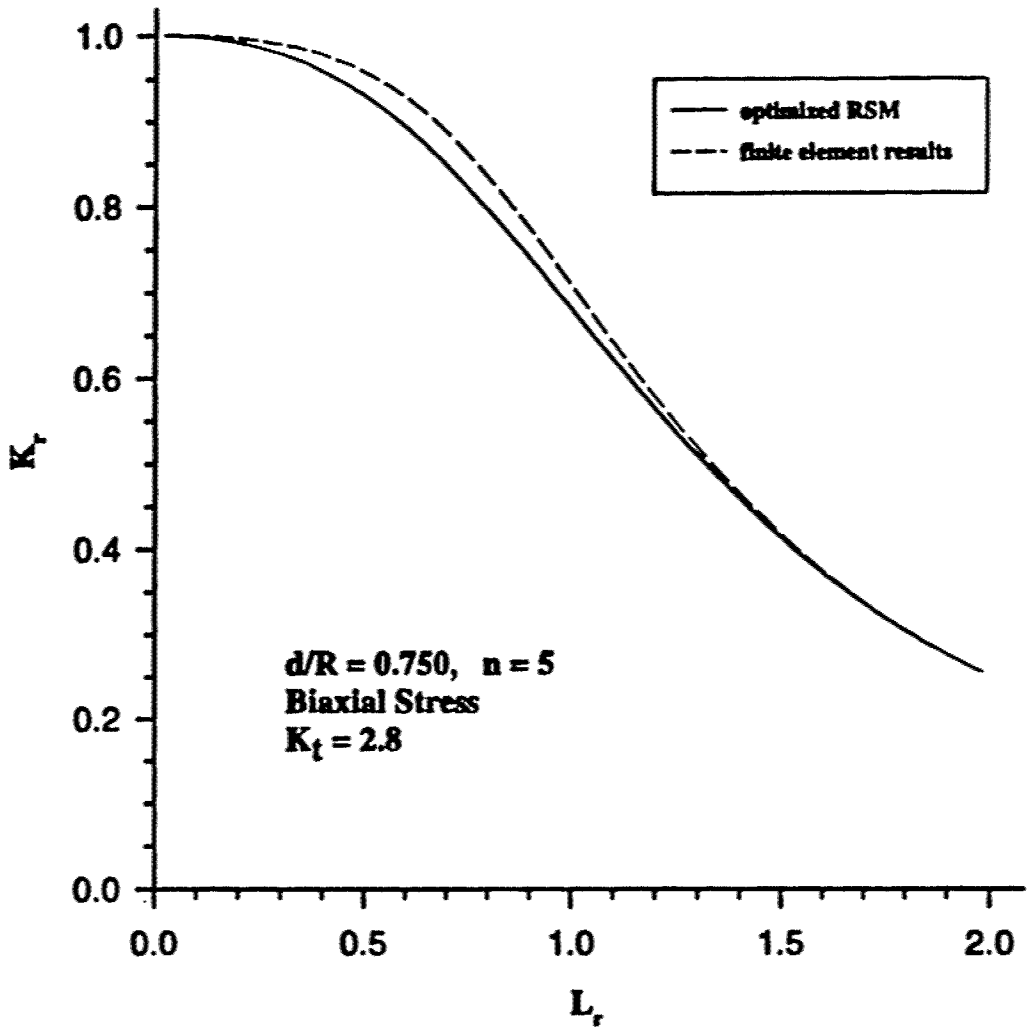

Figure D.5 Comparison of EPRI finite element results (dashed line) with the optimized RSM (solid line) for a single crack at a round hole subjected to biaxial stressing: d/R=0.750, K_t=2.8, n=5.

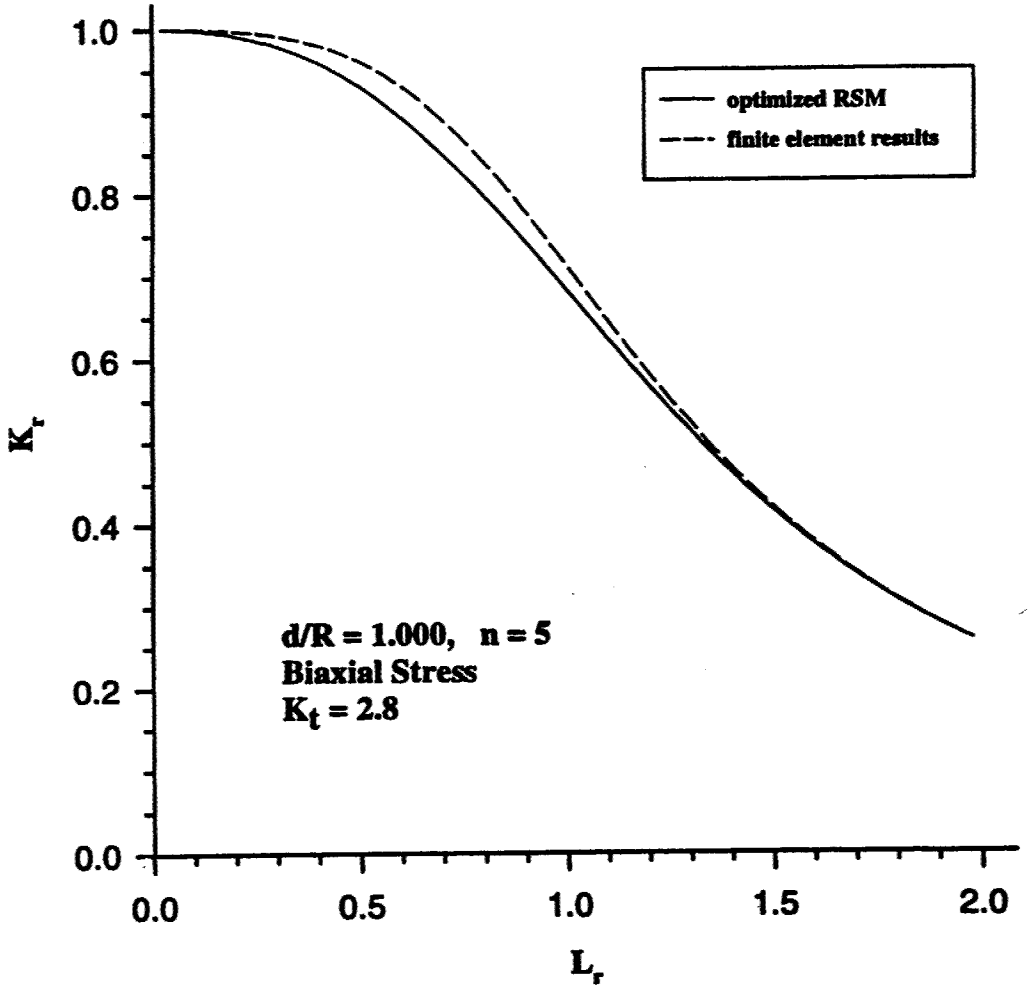

Figure D.6 Comparison of EPRI finite element results (dashed line) with the optimized RSM (solid line) for a single crack at a round hole subjected to biaxial stressing: d/R=1.000, K_t=2.8, n=5.

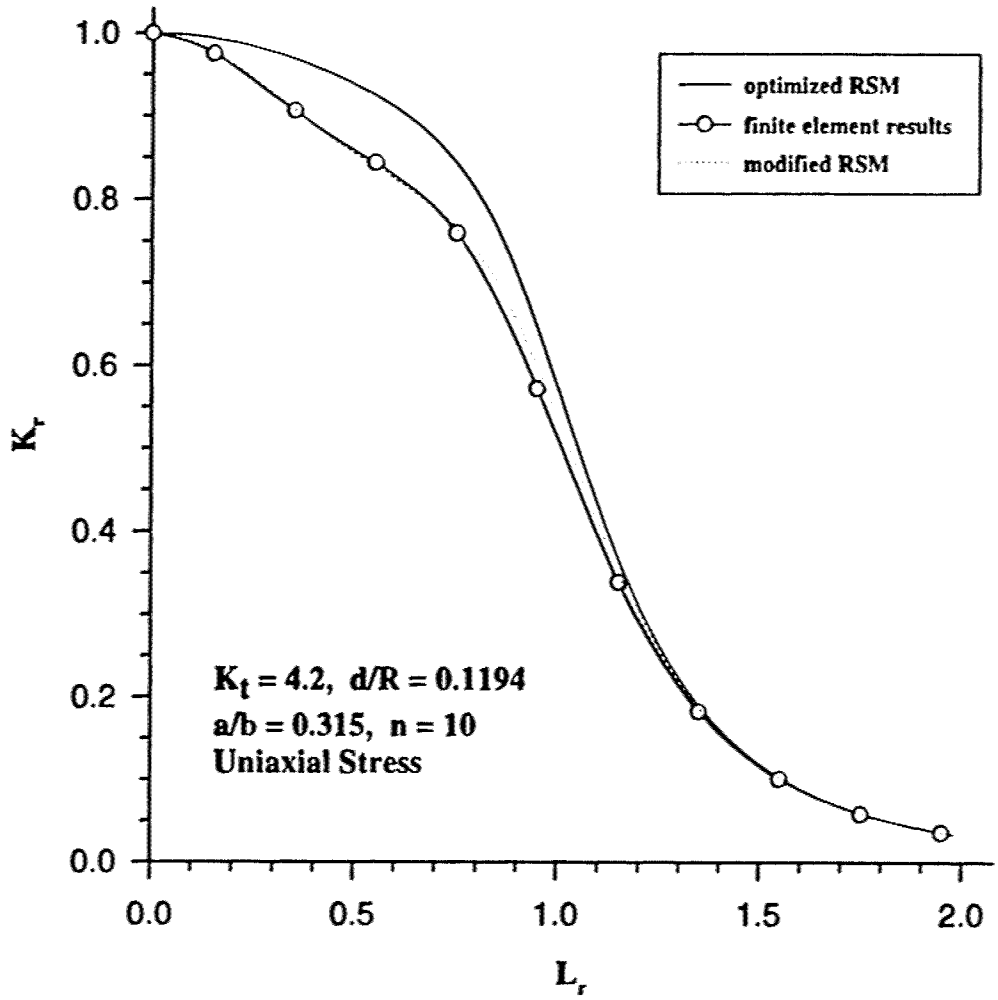

Figure D.7 Comparison of finite element results (open circles) with the modified (dotted line) and standard (solid line) RSM's for symmetrical cracks in double edge notched plates subjected to uniaxial stressing: d/R=0.1194, K_t=4.2, n=10.

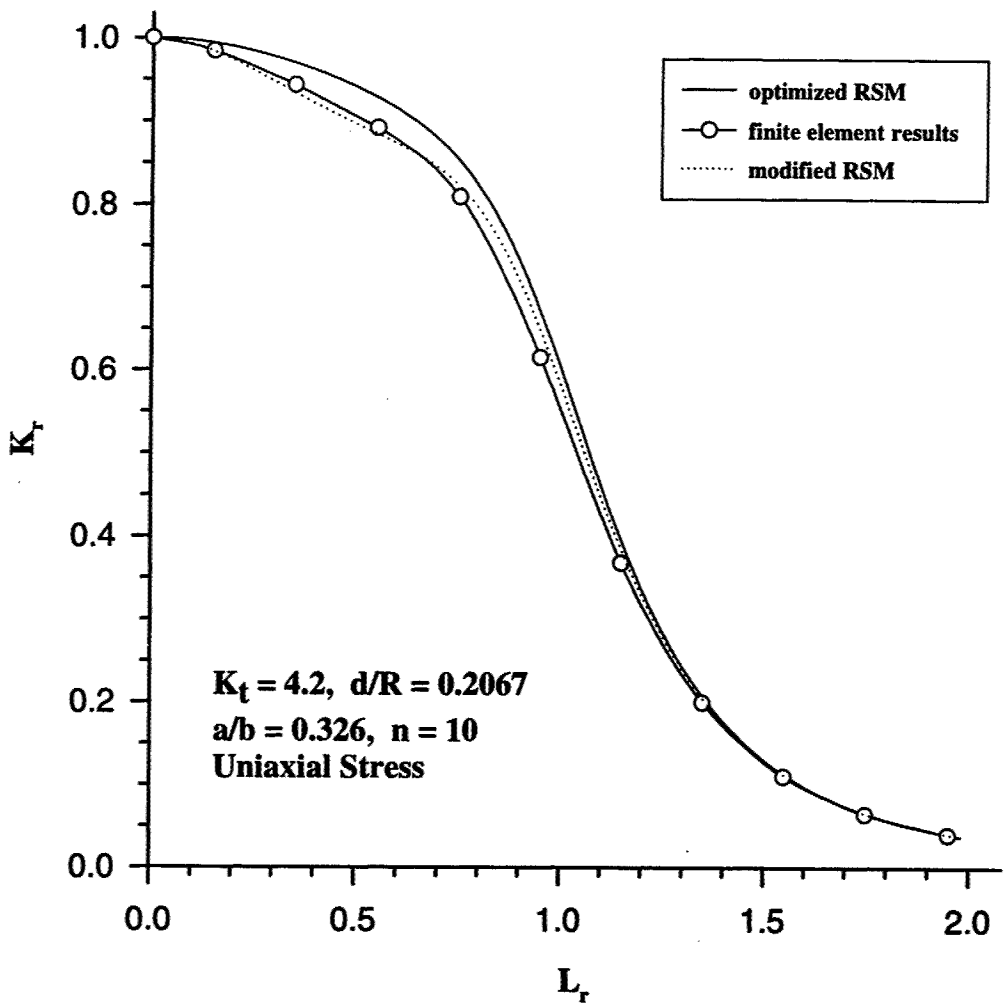

Figure D.8 Comparison of finite element results (open circles) with the modified (dotted line) and standard (solid line) RSM's for symmetrical cracks in double edge notched plates subjected to uniaxial stressing: d/R=0.2067, K_t=4.2, n=10.

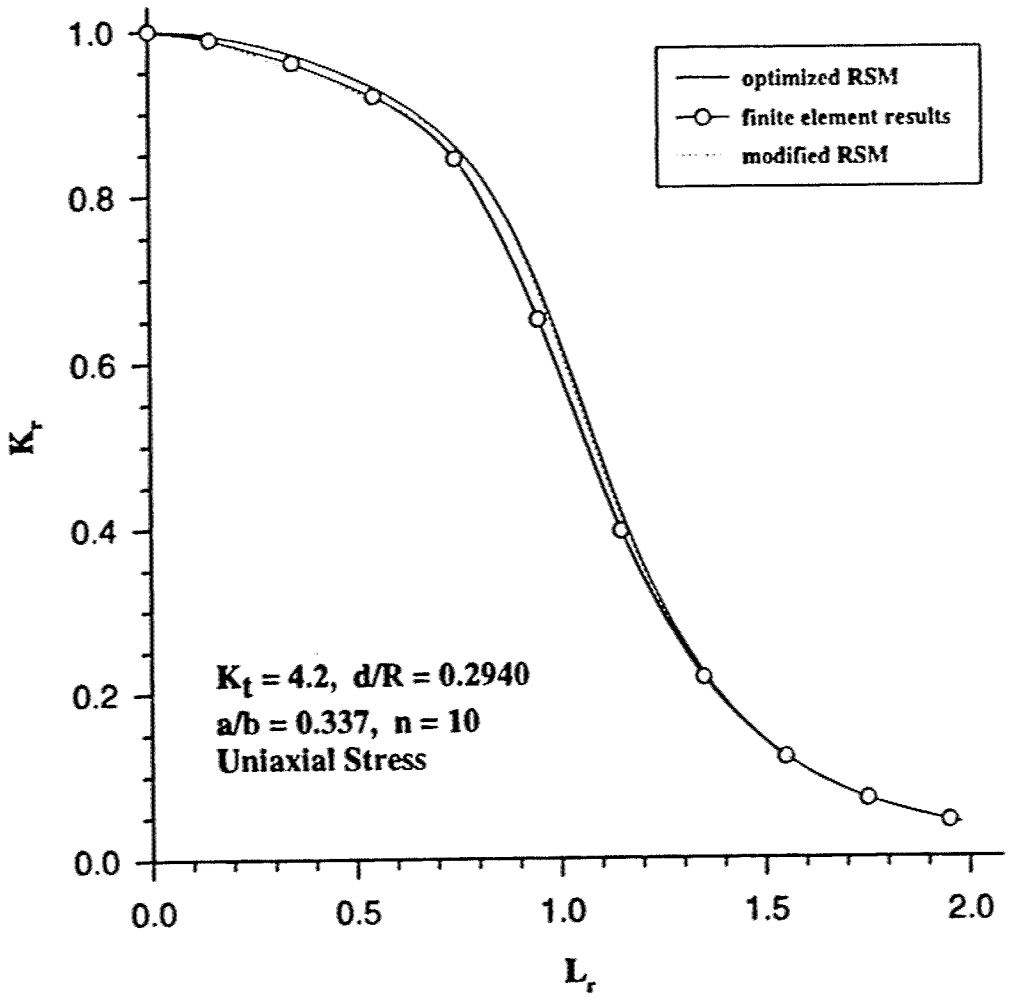

Figure D.9 Comparison of finite element results (open circles) with the modified (dotted line) and standard (solid line) RSM's for symmetrical cracks in double edge notched plates subjected to uniaxial stressing: d/R=0.2940, K_t=4.2, n=10.

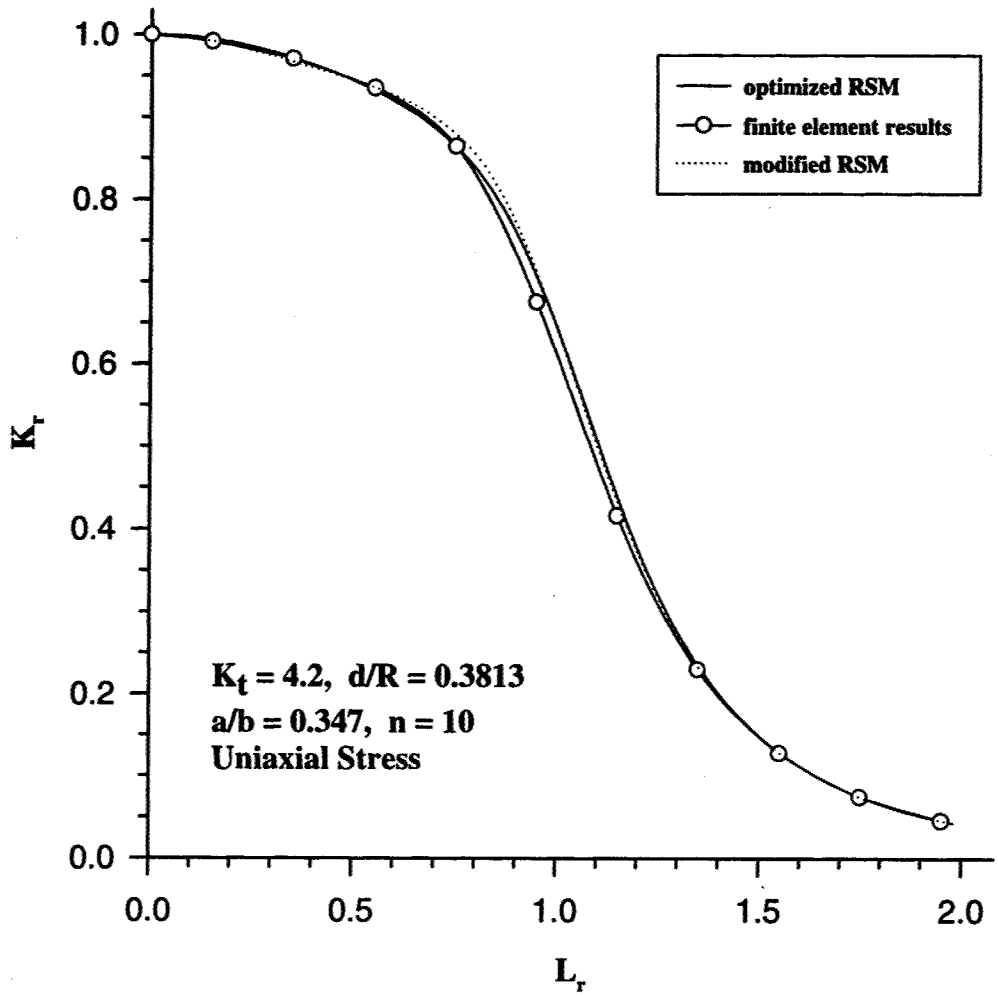

Figure D.10 Comparison of finite element results (open circles) with the modified (dotted line) and standard (solid line) RSM's for symmetrical cracks in double edge notched plates subjected to uniaxial stressing: d/R=0.3813, K_t=4.2, n=10.

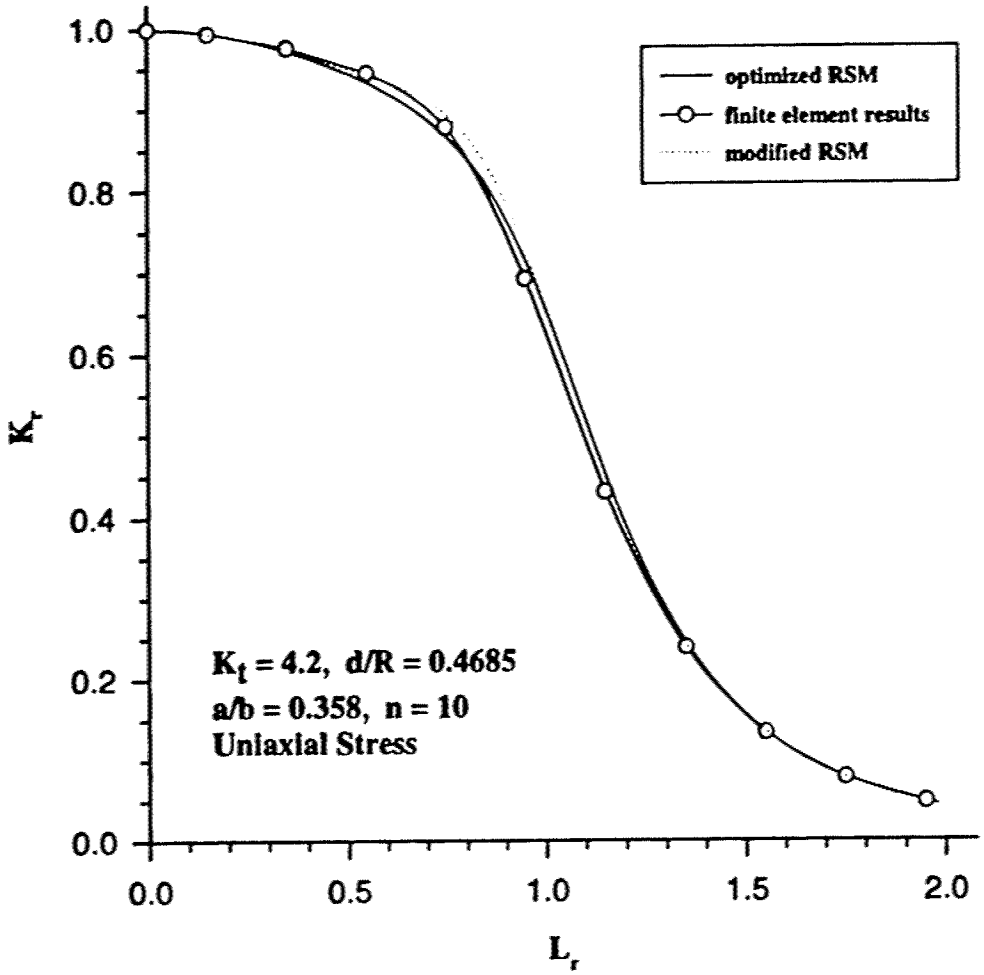

Figure D.11 Comparison of finite element results (open circles) with the modified (dotted line) and standard (solid line) RSM's for symmetrical cracks in double edge notched plates subjected to uniaxial stressing: d/R=0.4685, K_t=4.2, n=10.

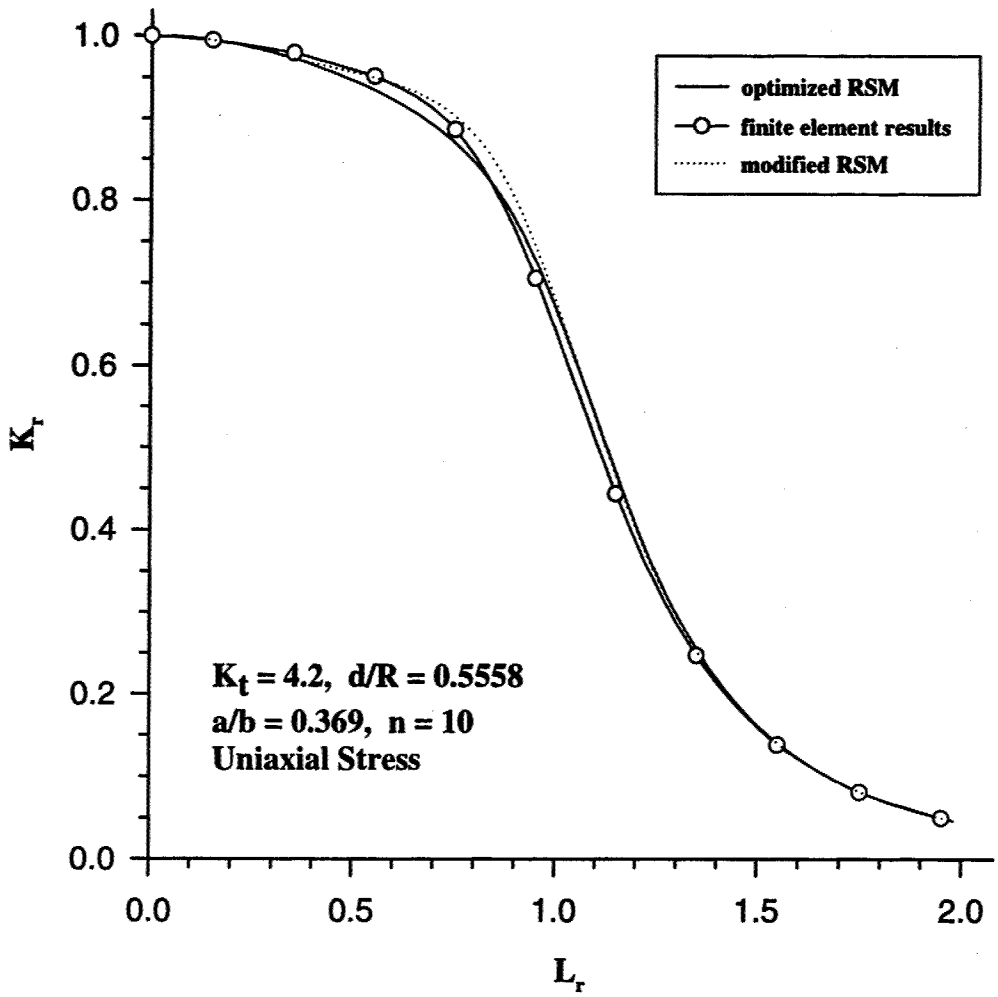

Figure D.12 Comparison of finite element results (open circles) with the modified (dotted line) and standard (solid line) RSM's for symmetrical cracks in double edge notched plates subjected to uniaxial stressing: d/R=0.5558, K_t=4.2, n=10.

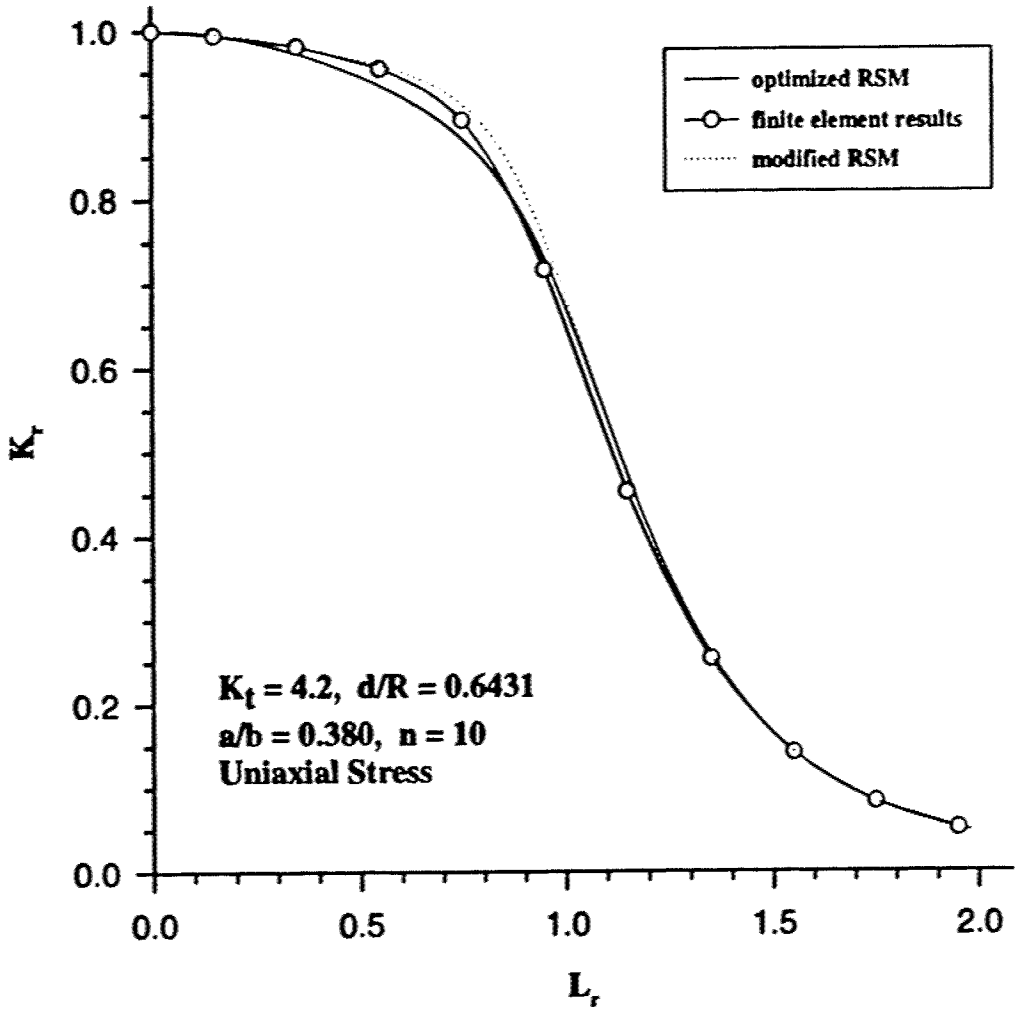

Figure D.13 Comparison of finite element results (open circles) with the modified (dotted line) and standard (solid line) RSM's for symmetrical cracks in double edge notched plates subjected to uniaxial stressing: d/R=0.6431, K_t=4.2, n=10.

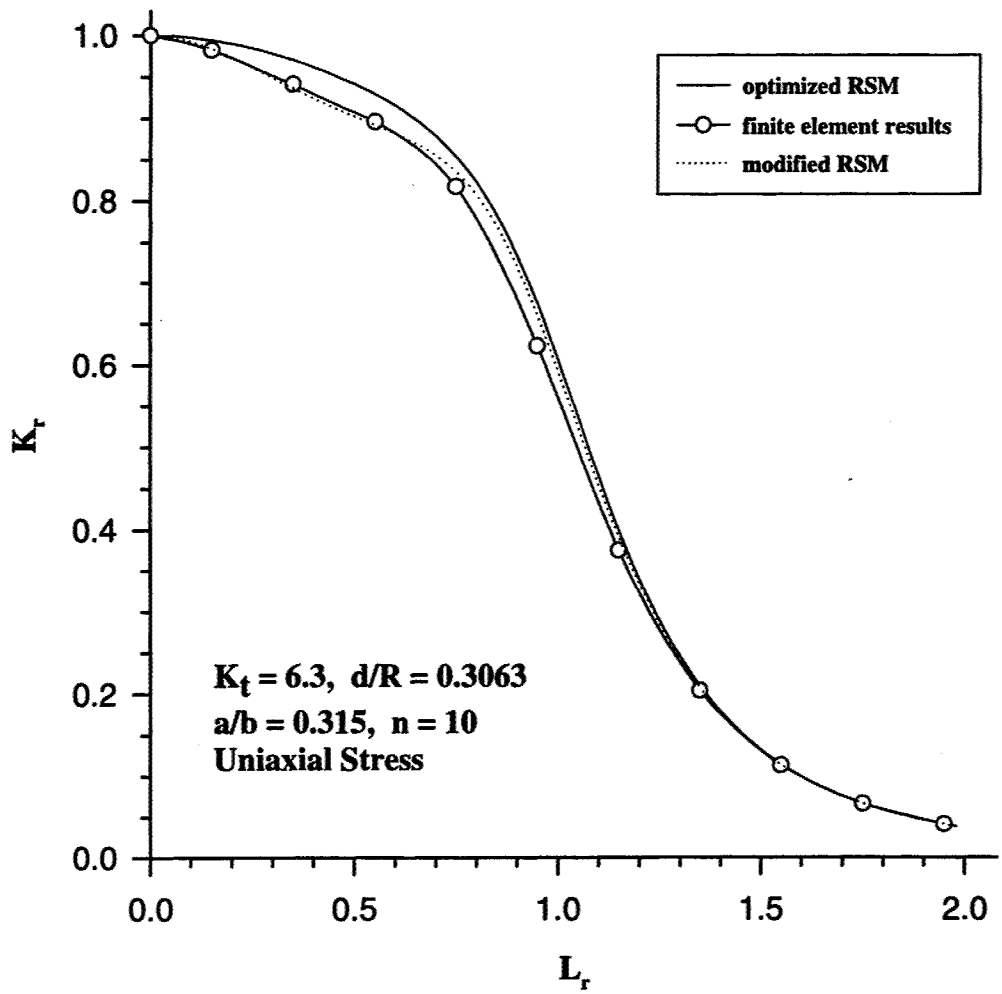

Figure D.14 Comparison of finite element results (open circles) with the modified (dotted line) and standard (solid line) RSM's for symmetrical cracks in double edge notched plates subjected to uniaxial stressing: d/R=0.3063, K_t=6.3, n=10.

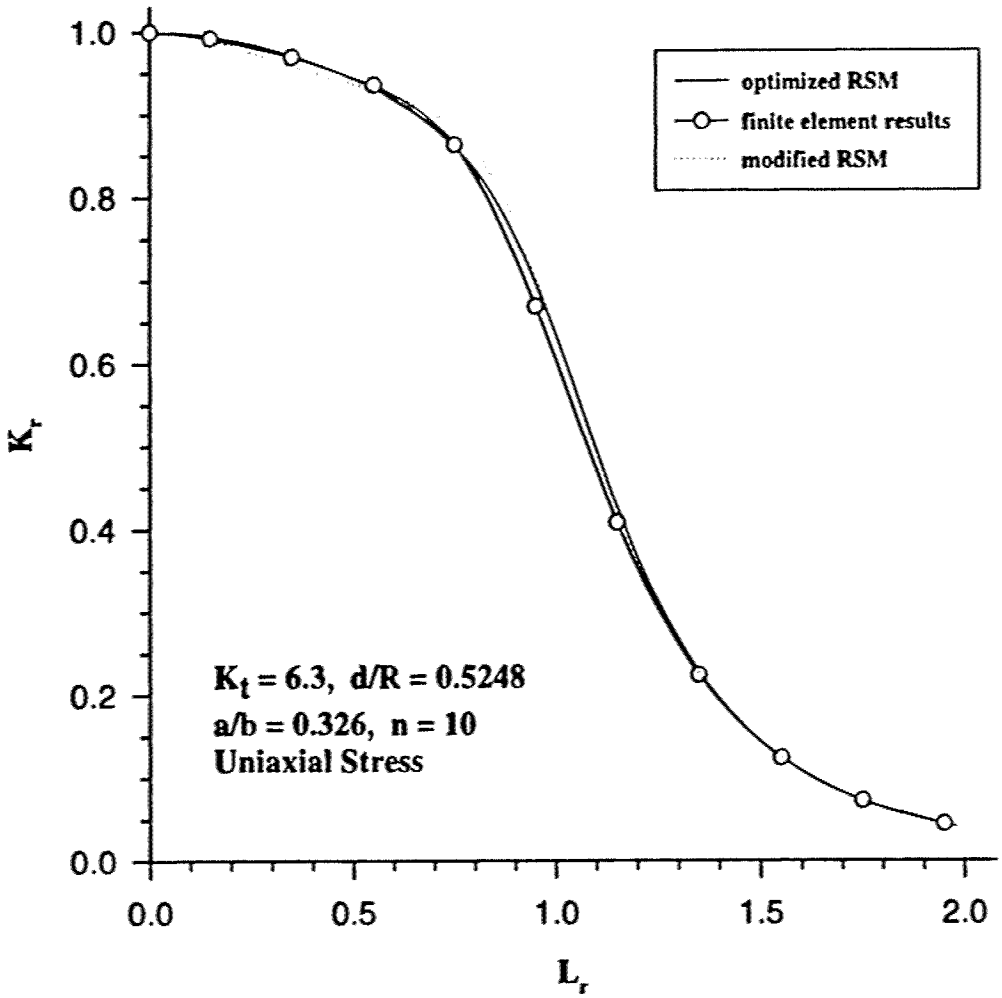

Figure D.15 Comparison of finite element results (open circles) with the modified (dotted line) and standard (solid line) RSM's for symmetrical cracks in double edge notched plates subjected to uniaxial stressing: d/R=0.5248, K_t=6.3, n=10.

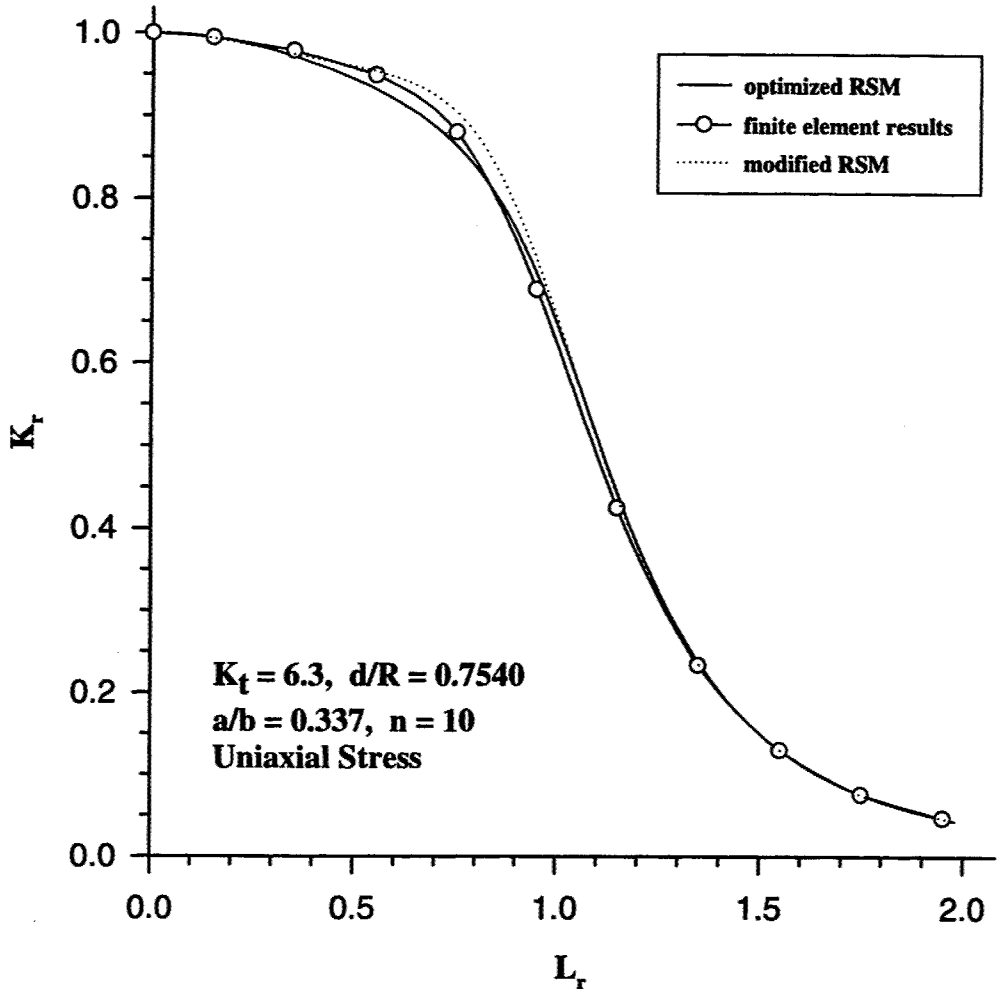

Figure D.16 Comparison of finite element results (open circles) with the modified (dotted line) and standard (solid line) RSM's for symmetrical cracks in double edge notched plates subjected to uniaxial stressing: d/R=0.7540, K_t=6.3, n=10.

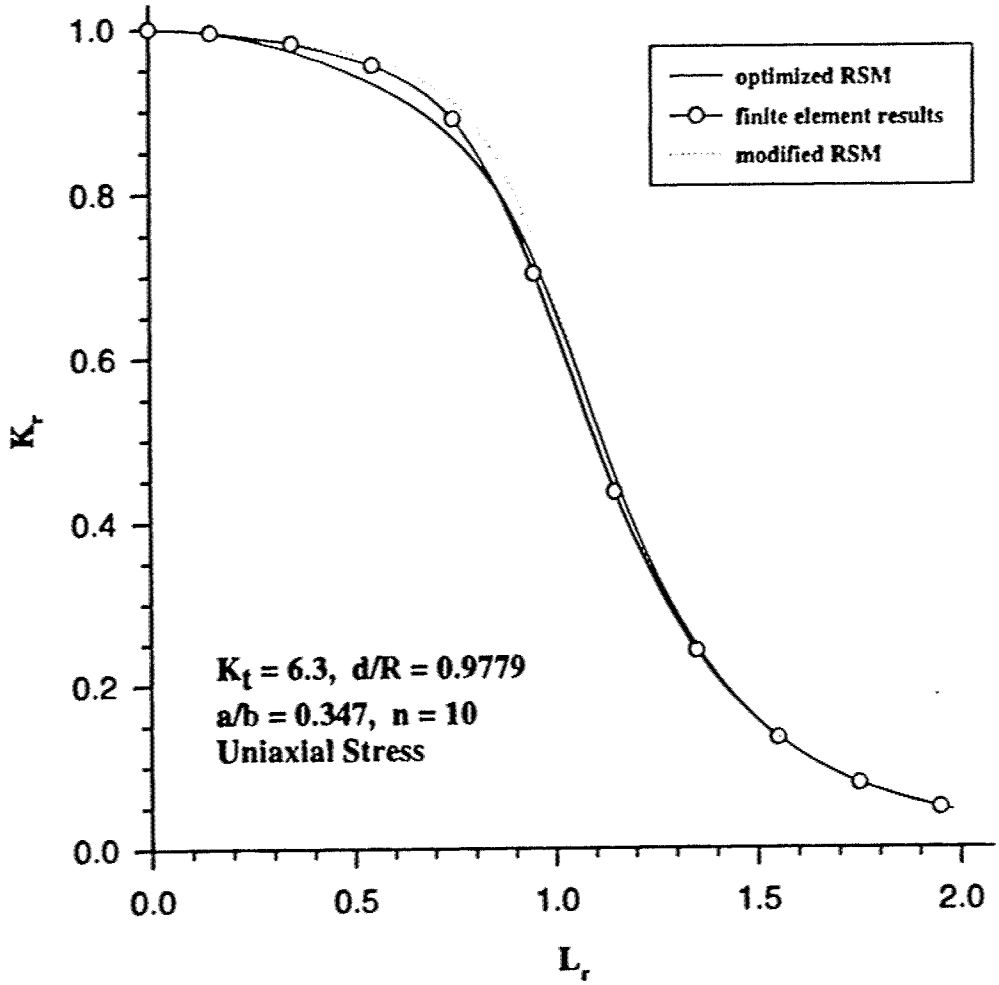

Figure D.17 Comparison of finite element results (open circles) with the modified (dotted line) and standard (solid line) RSM's for symmetrical cracks in double edge notched plates subjected to uniaxial stressing: d/R=0.9779, K_t=6.3, n=10.

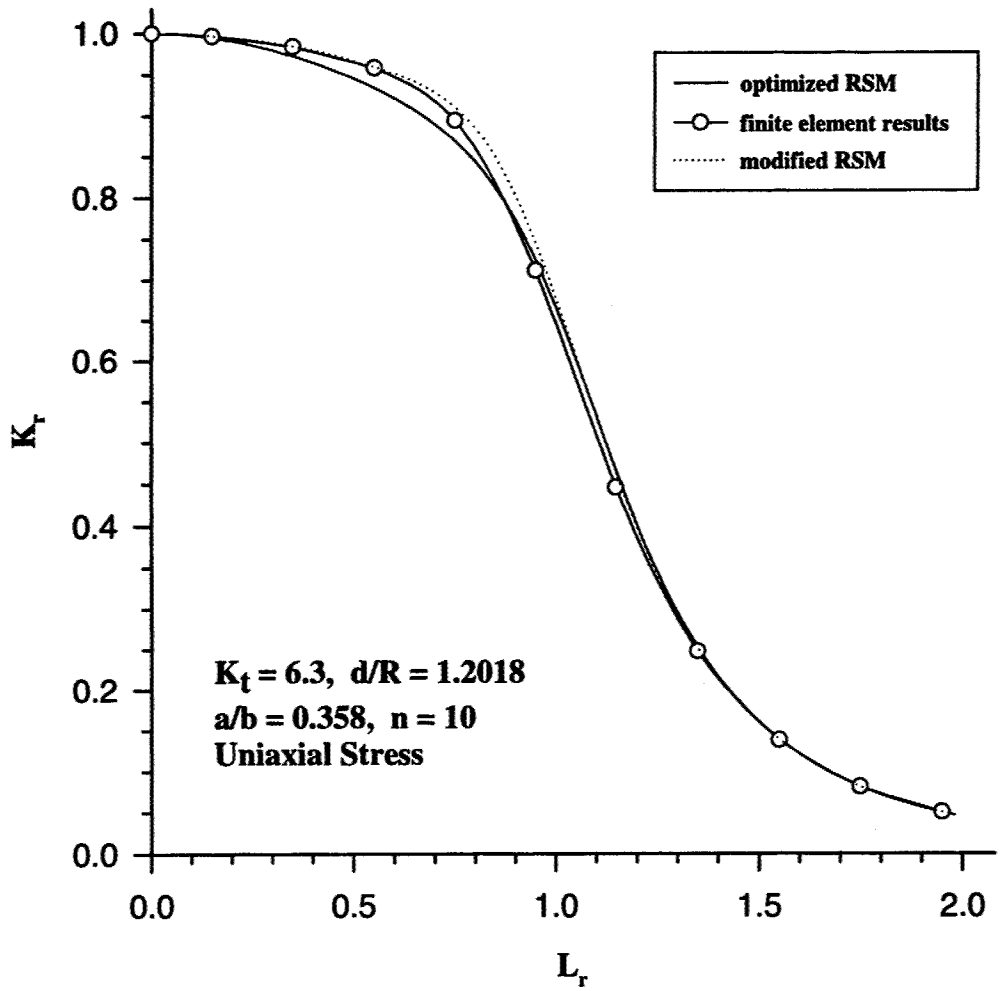

Figure D.18 Comparison of finite element results (open circles) with the modified (dotted line) and standard (solid line) RSM's for symmetrical cracks in double edge notched plates subjected to uniaxial stressing: d/R=1.2018, K_t=6.3, n=10.

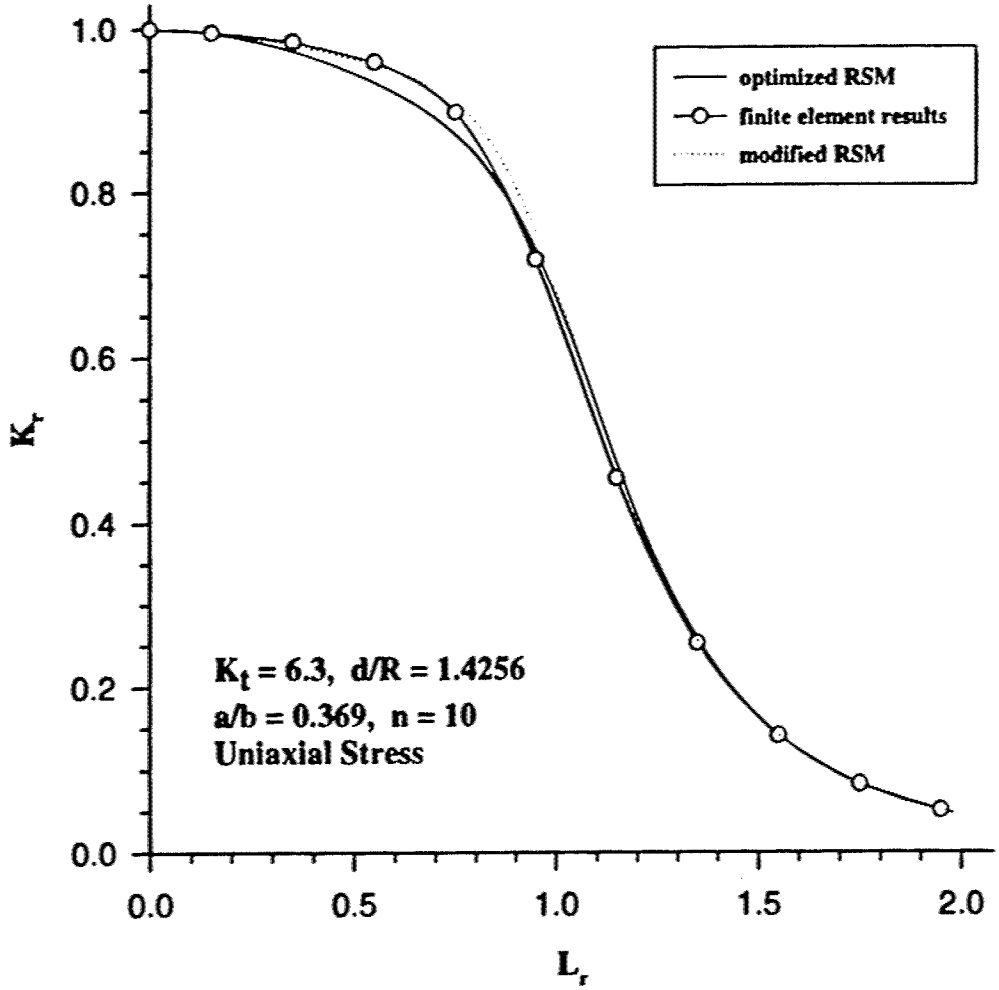

Figure D.19 Comparison of finite element results (open circles) with the modified (dotted line) and standard (solid line) RSM's for symmetrical cracks in double edge notched plates subjected to uniaxial stressing: d/R=1.4256, K_t=6.3, n=10.

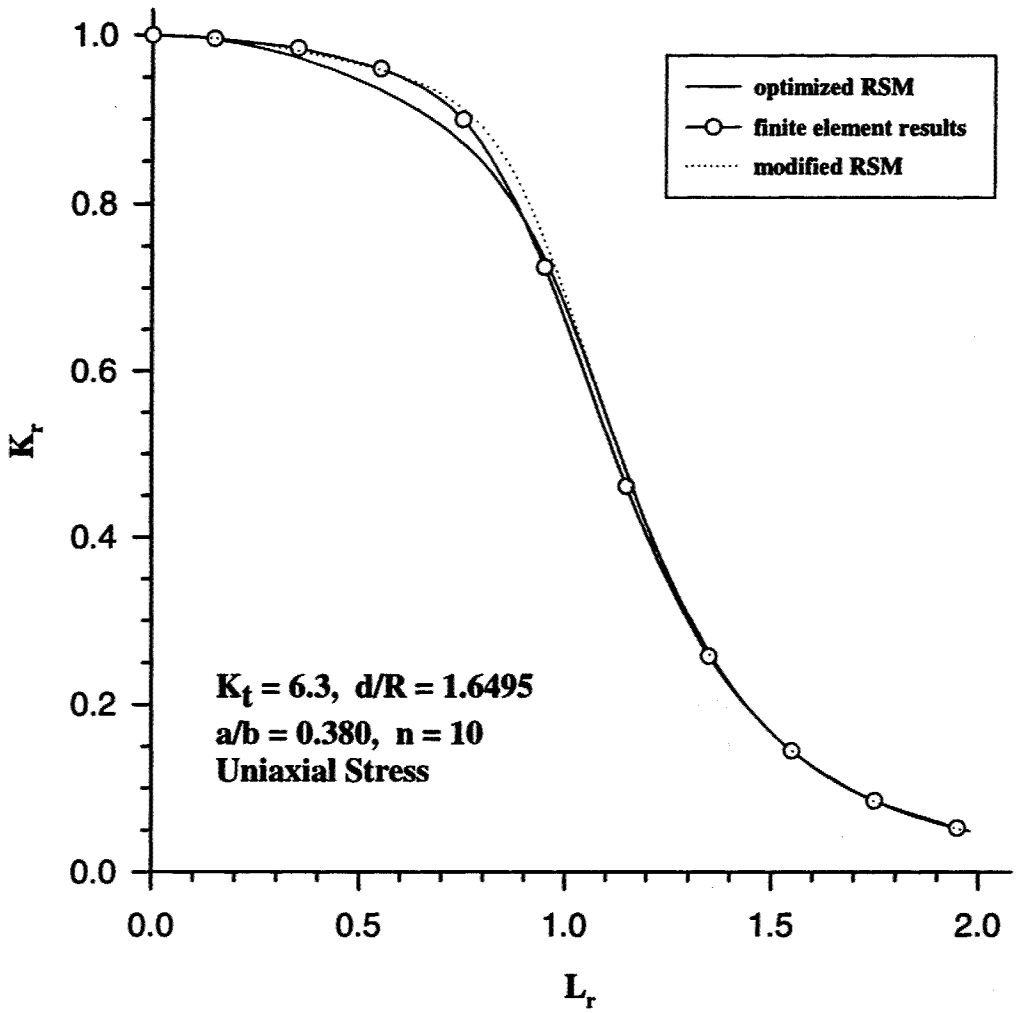

Figure D.20 Comparison of finite element results (open circles) with the modified (dotted line) and standard (solid line) RSM's for symmetrical cracks in double edge notched plates subjected to uniaxial stressing: d/R=1.6495, K_t=6.3, n=10.

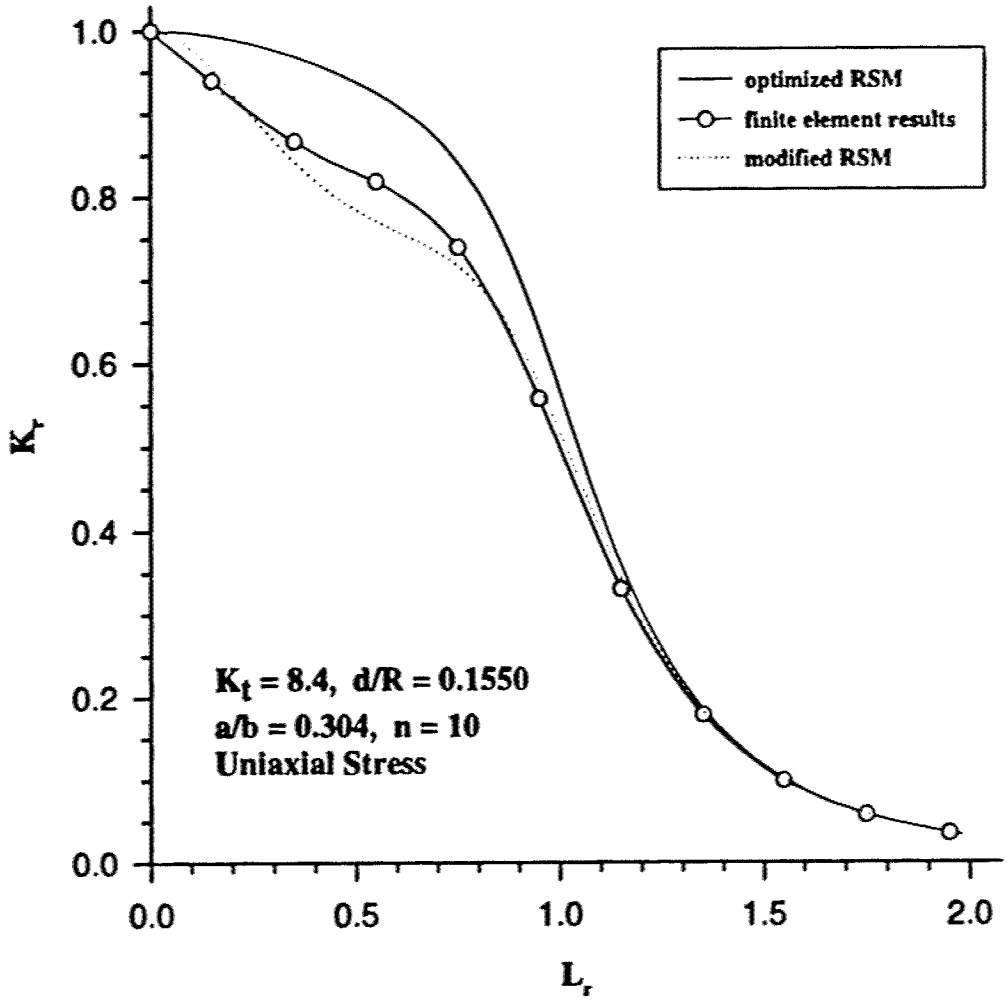

Figure D.21 Comparison of finite element results (open circles) with the modified (dotted line) and standard (solid line) RSM's for symmetrical cracks in double edge notched plates subjected to uniaxial stressing: d/R=0.1550, K_t=8.4, n=10.

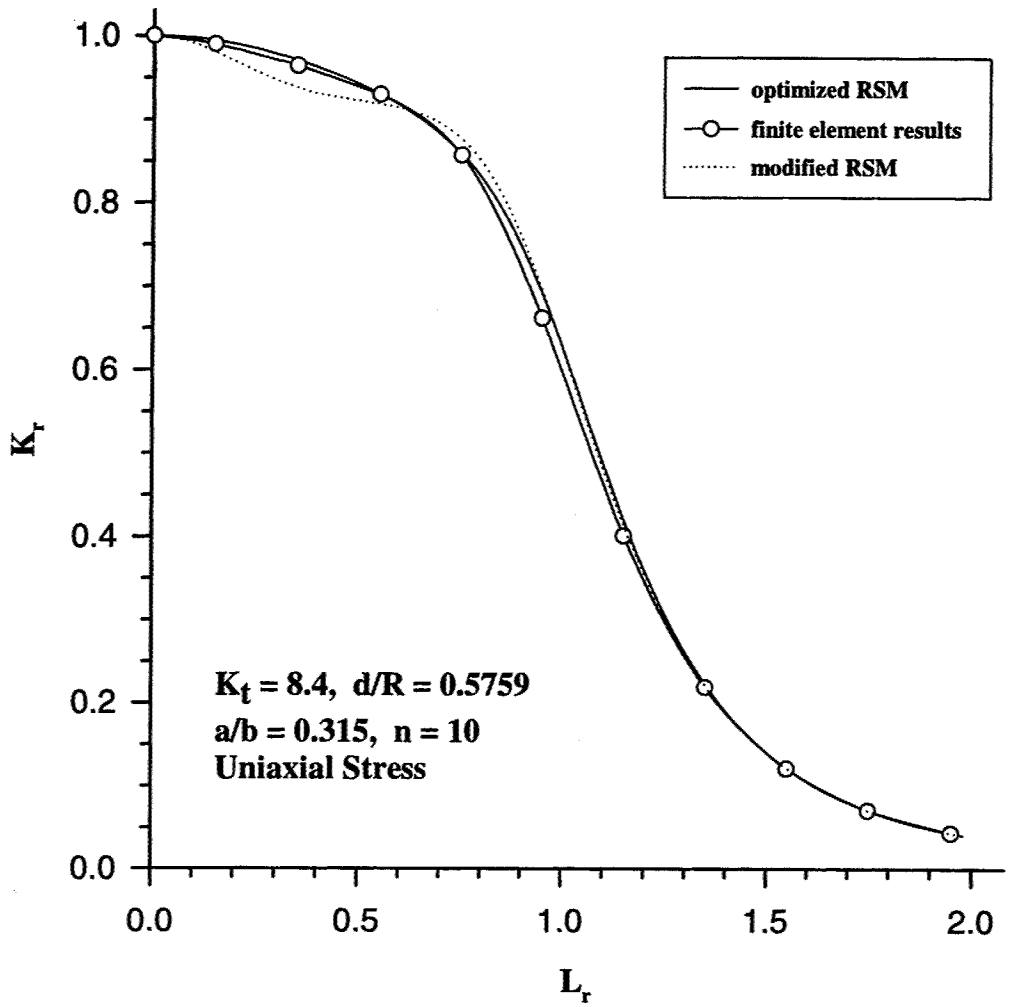

Figure D.22 Comparison of finite element results (open circles) with the modified (dotted line) and standard (solid line) RSM's for symmetrical cracks in double edge notched plates subjected to uniaxial stressing: d/R=0.5759, K_t=8.4, n=10.

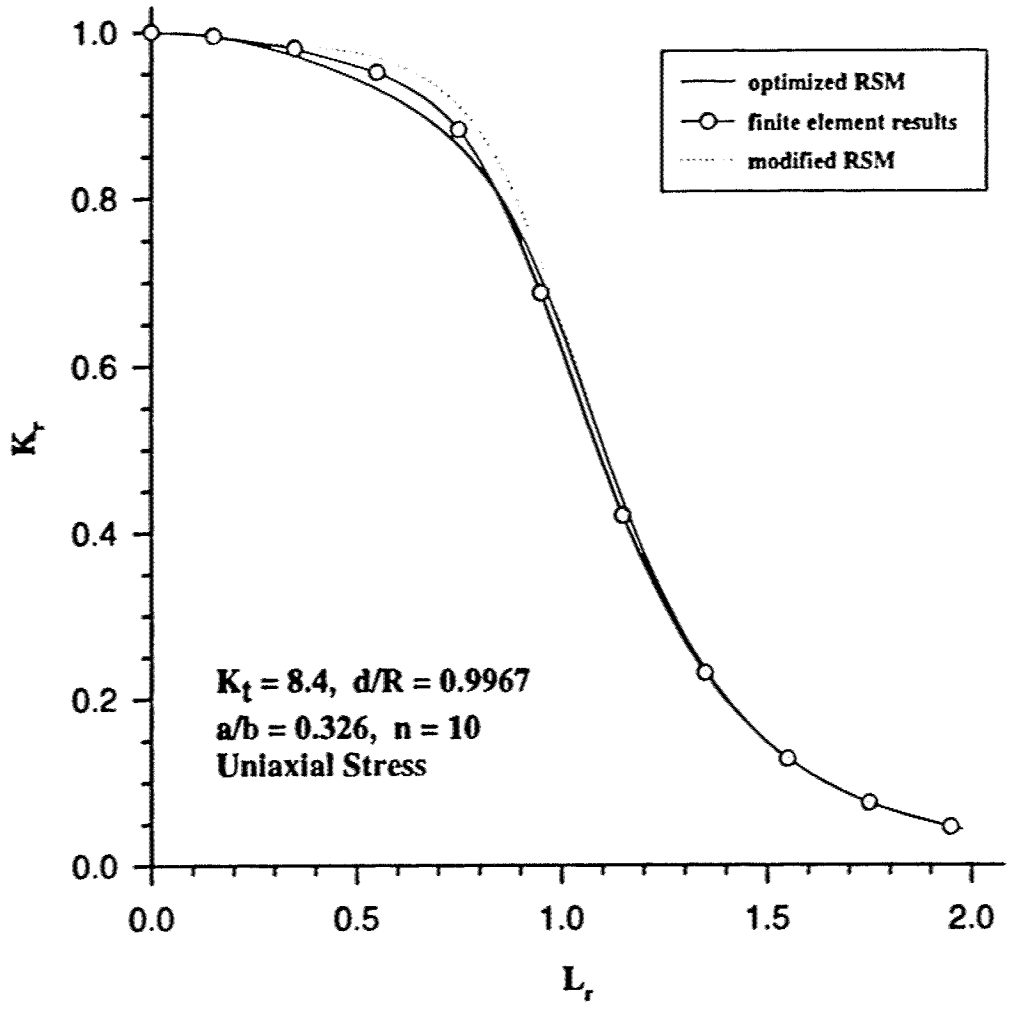

Figure D.23 Comparison of finite element results (open circles) with the modified (dotted line) and standard (solid line) RSM's for symmetrical cracks in double edge notched plates subjected to uniaxial stressing: d/R=0.9967, K_t=8.4, n=10.

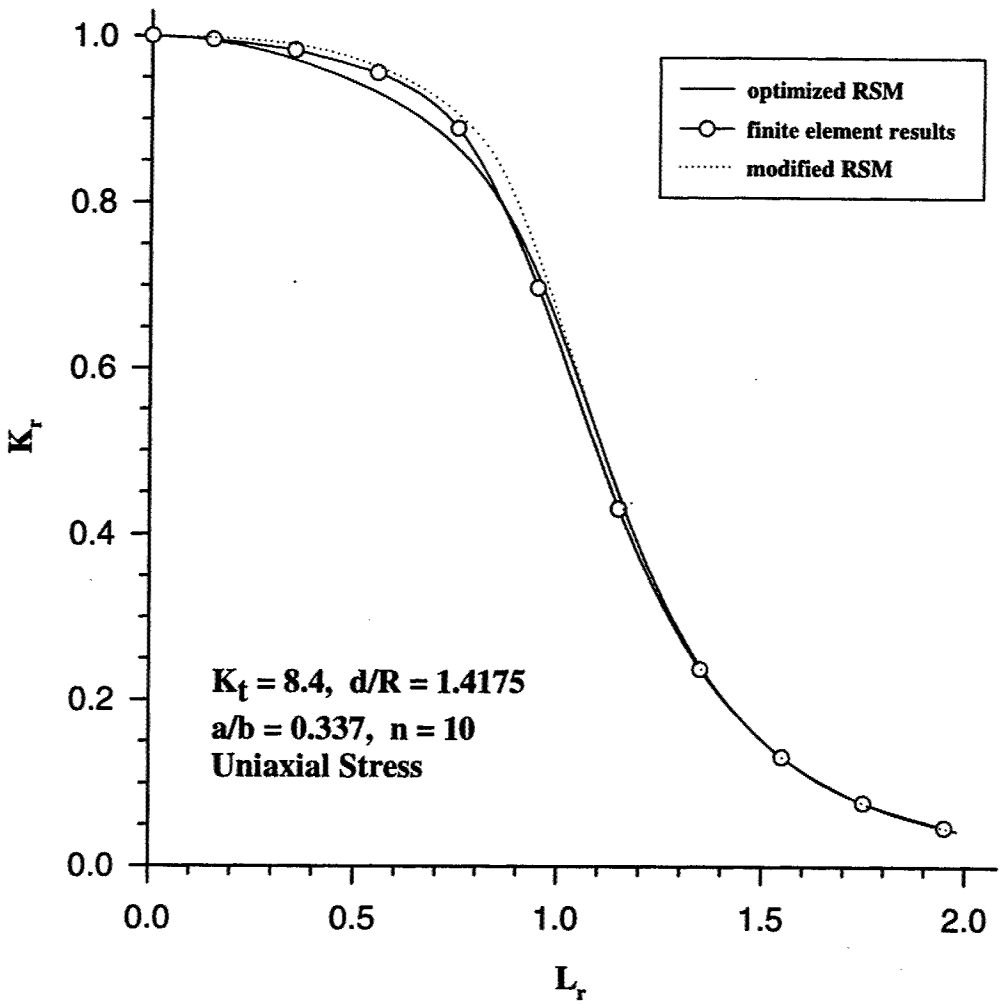

Figure D.24 Comparison of finite element results (open circles) with the modified (dotted line) and standard (solid line) RSM's for symmetrical cracks in double edge notched plates subjected to uniaxial stressing: d/R=1.4175, K_t=8.4, n=10.

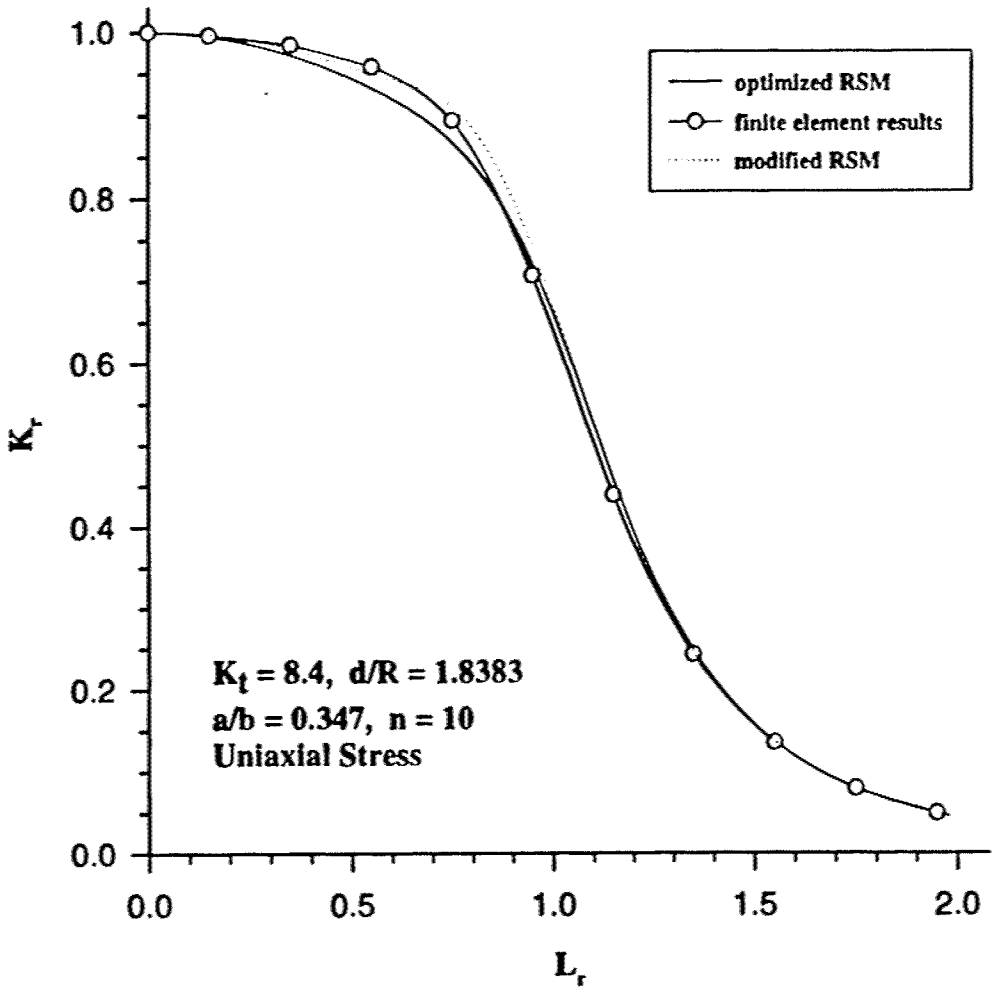

Figure D.25 Comparison of finite element results (open circles) with the modified (dotted line) and standard (solid line) RSM's for symmetrical cracks in double edge notched plates subjected to uniaxial stressing: d/R=1.8383, K_t=8.4, n=10.

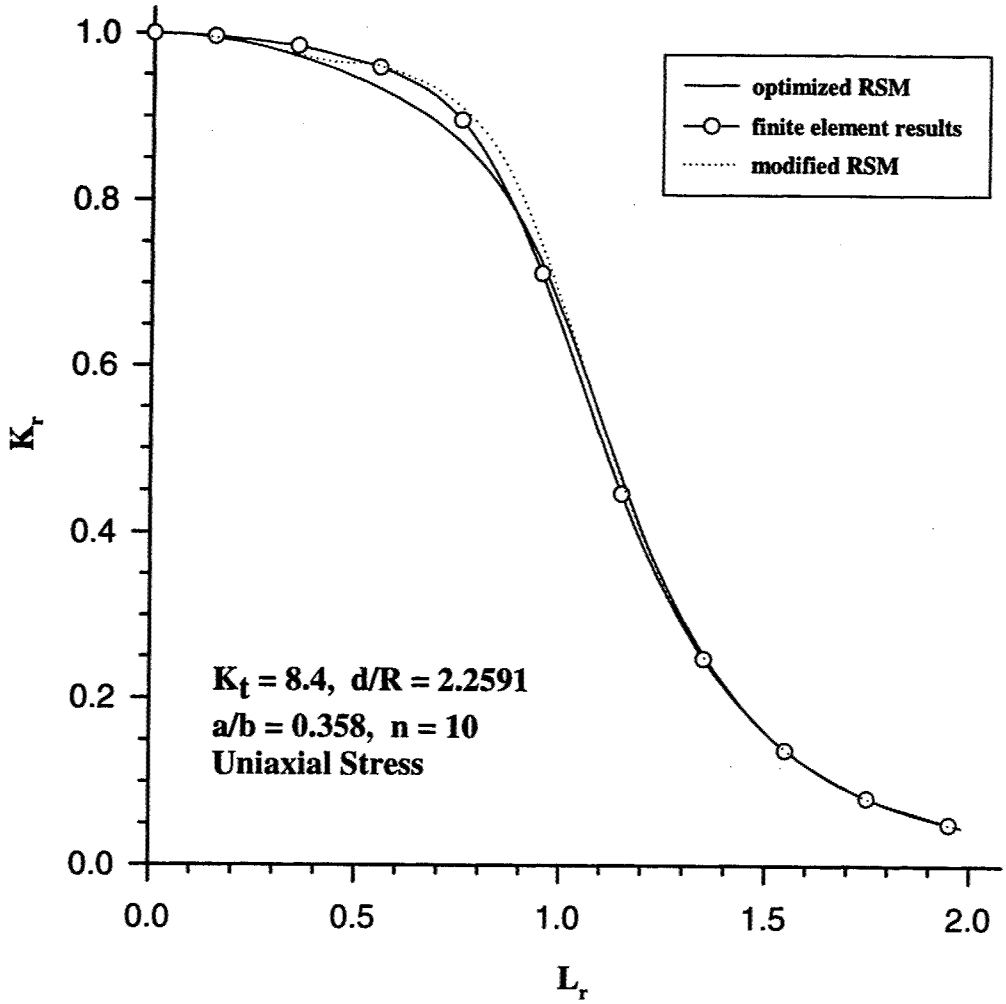

Figure D.26 Comparison of finite element results (open circles) with the modified (dotted line) and standard (solid line) RSM's for symmetrical cracks in double edge notched plates subjected to uniaxial stressing: d/R=2.2591, K_t=8.4, n=10.

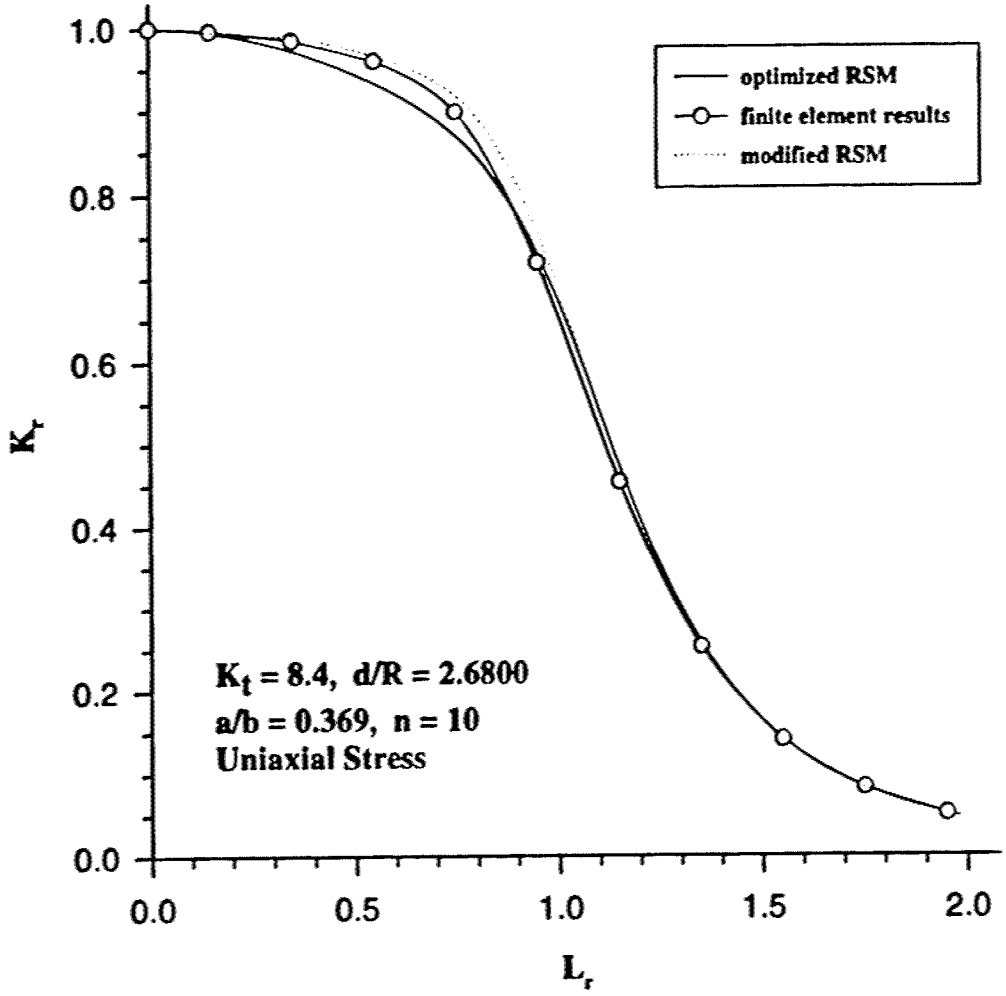

Figure D.27 Comparison of finite element results (open circles) with the modified (dotted line) and standard (solid line) RSM's for symmetrical cracks in double edge notched plates subjected to uniaxial stressing: d/R=2.6800, K_t=8.4, n=10.

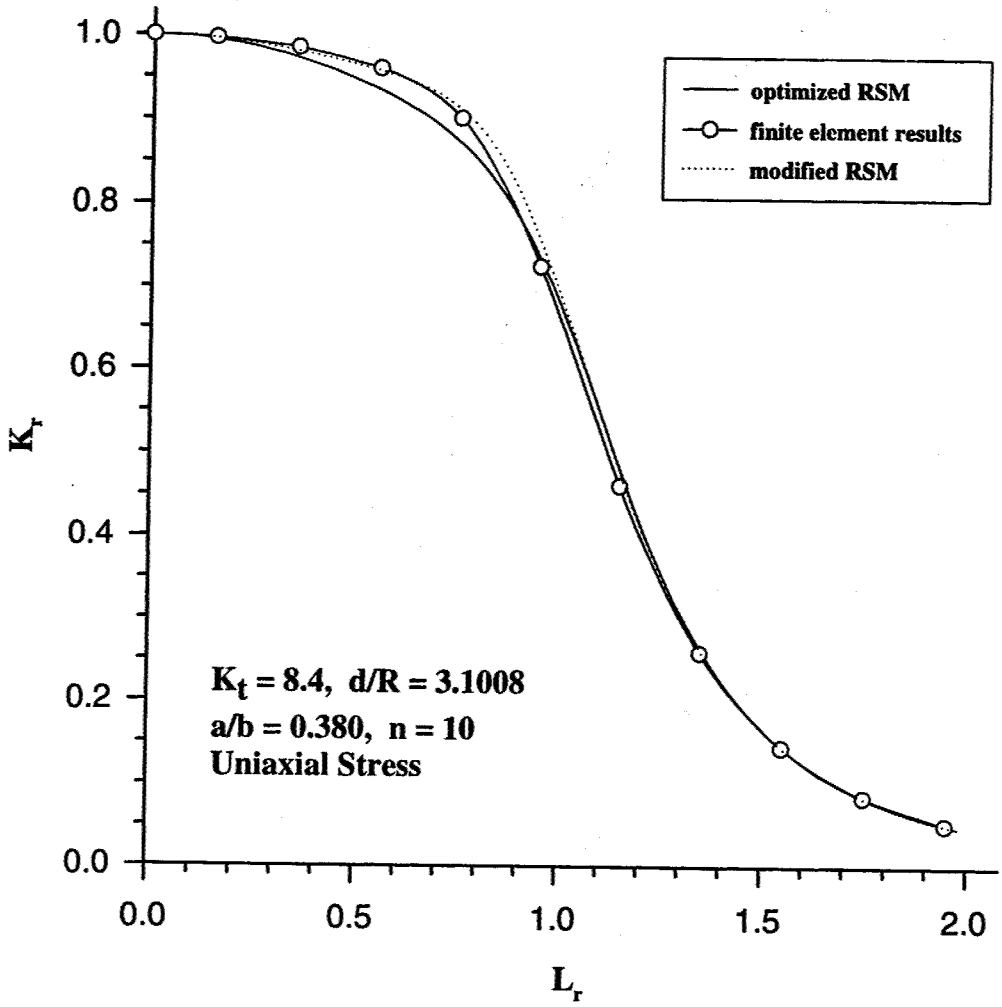

Figure D.28 Comparison of finite element results (open circles) with the modified (dotted line) and standard (solid line) RSM's for symmetrical cracks in double edge notched plates subjected to uniaxial stressing: d/R=3.1008, K_t=8.4, n=10.

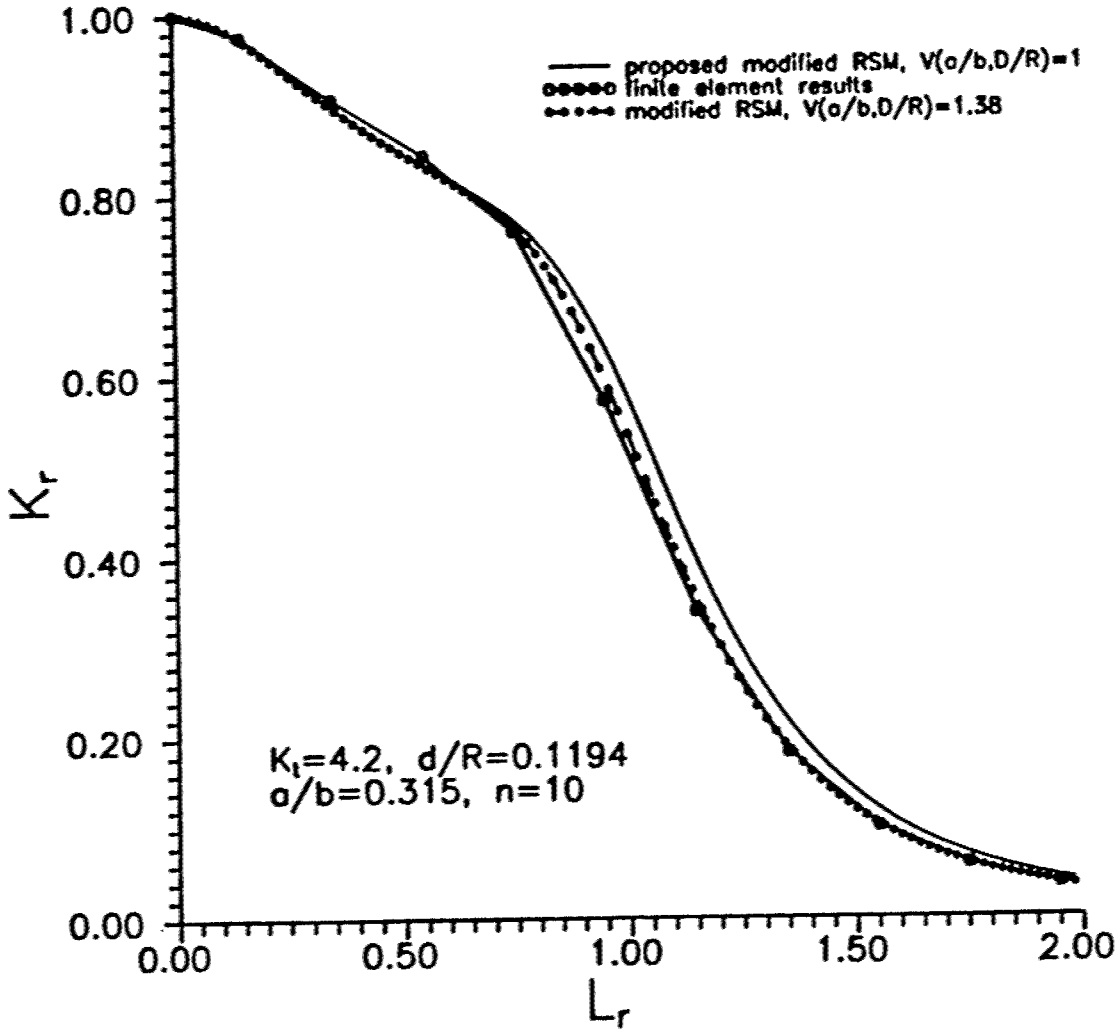

Figure D.29 Comparison of finite element results (open circles) with the modified RSM using the actual value of $V(a/b,D/R)$ (dashed line) and V=1 (solid line) for symmetrical cracks in double edge notched plates subjected to uniaxial stressing: d/R=0.1194, K_t=4.2, n=10.

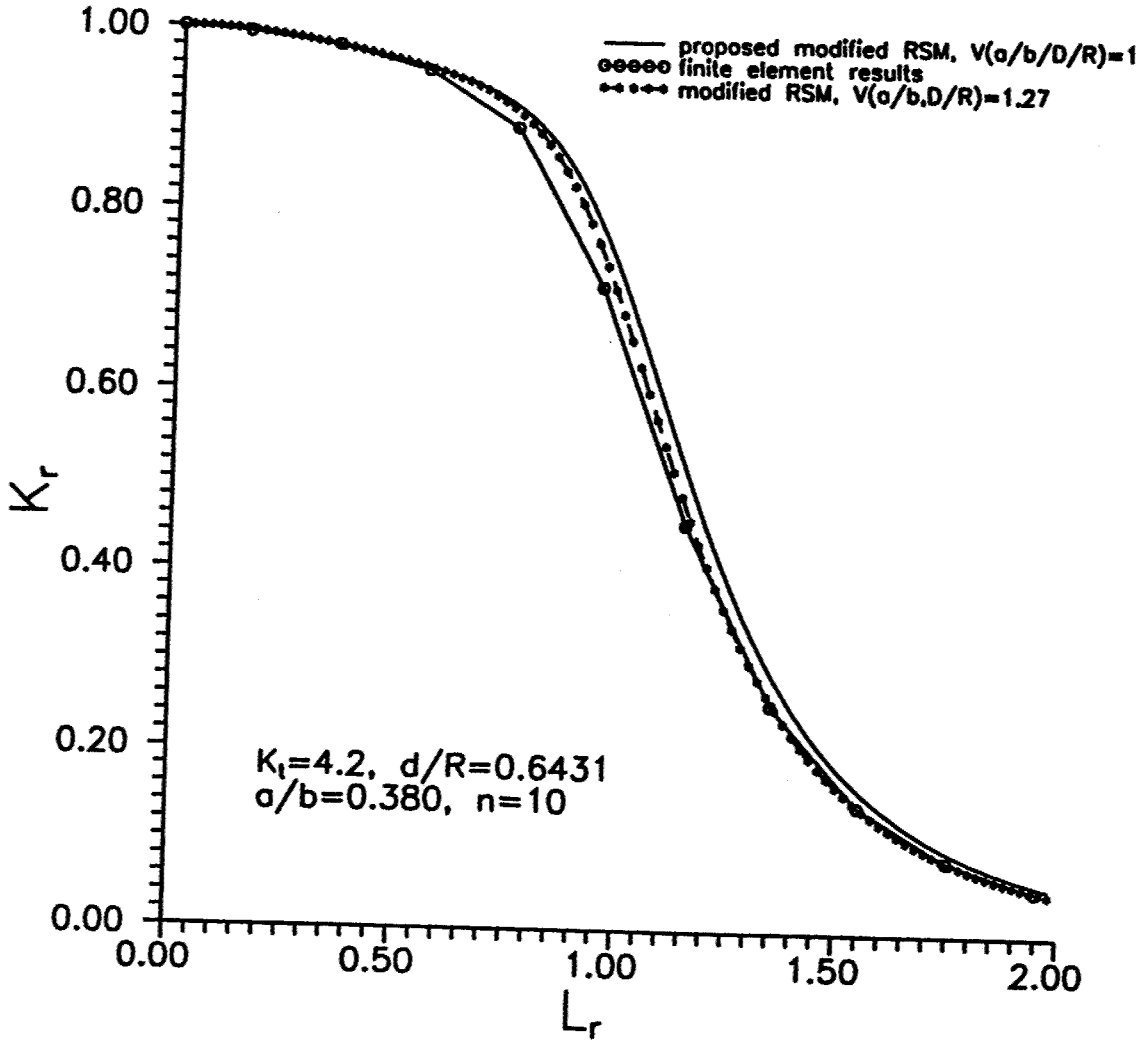

Figure D.30 Comparison of finite element results (open circles) with the modified RSM using the actual value of *V(a/b,D/R)* (dashed line) and *V*=1 (solid line) for symmetrical cracks in double edge notched plates subjected to uniaxial stressing: *d/R*=0.6431, K_t=4.2, *n*=10.

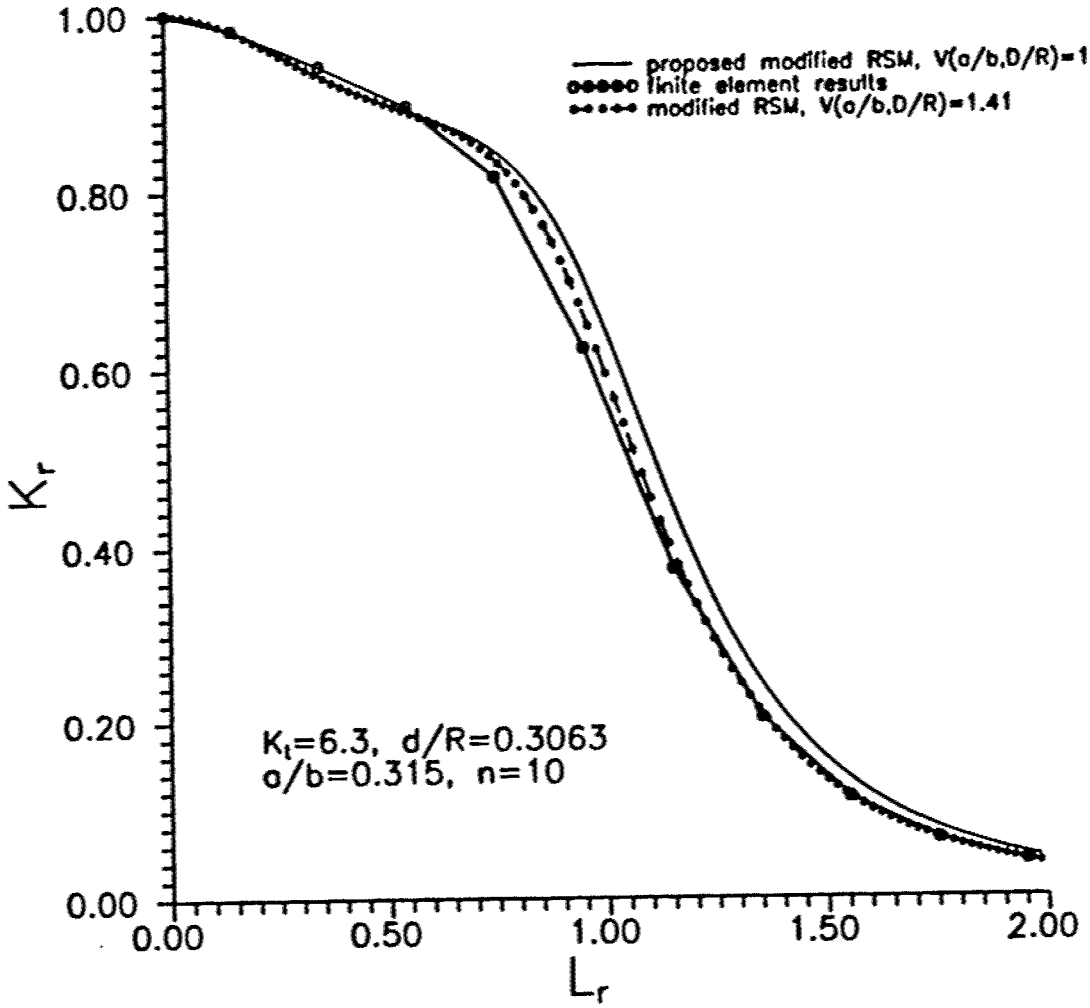

Figure D.31 Comparison of finite element results (open circles) with the modified RSM using the actual value of $V(a/b,D/R)$ (dashed line) and V=1 (solid line) for symmetrical cracks in double edge notched plates subjected to uniaxial stressing: d/R=0.3063, K_t=6.3, n=10.

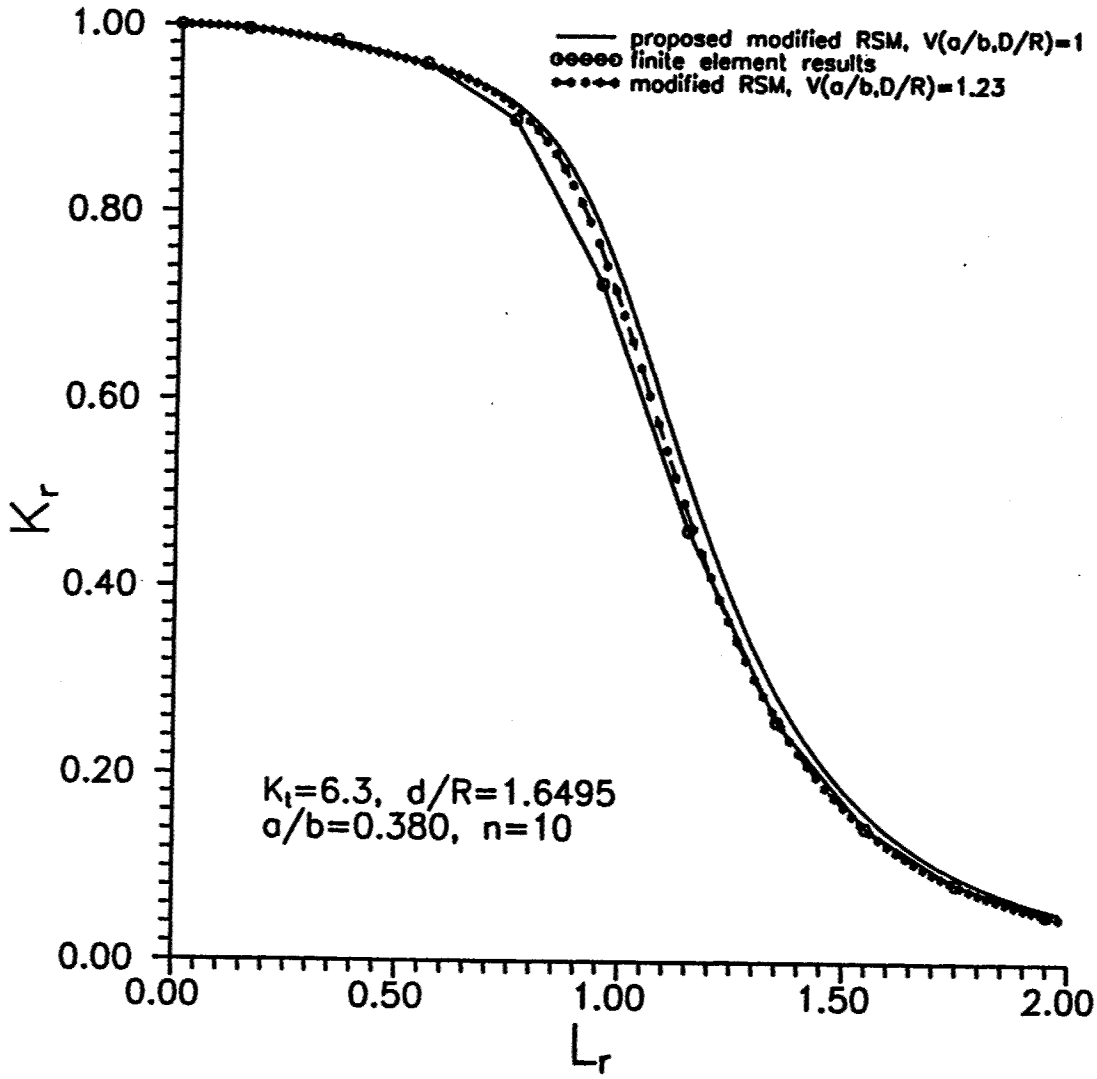

Figure D.32 Comparison of finite element results (open circles) with the modified RSM using the actual value of *V(a/b,D/R)* (dashed line) and *V*=1 (solid line) for symmetrical cracks in double edge notched plates subjected to uniaxial stressing: *d/R*=1.6495, K_t=6.3, *n*=10.

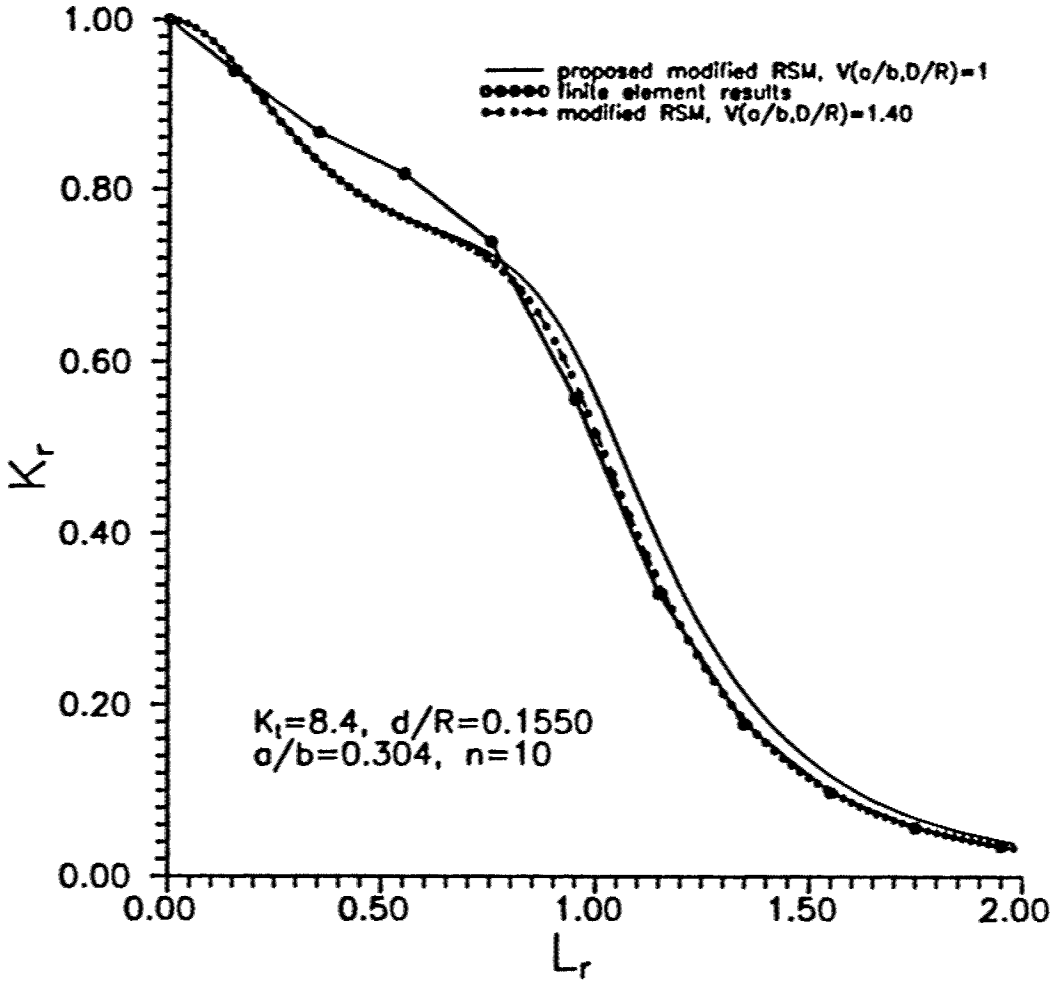

Figure D.33 Comparison of finite element results (open circles) with the modified RSM using the actual value of $V(a/b,D/R)$ (dashed line) and V=1 (solid line) for symmetrical cracks in double edge notched plates subjected to uniaxial stressing: d/R=0.1550, K_t=8.4, n=10.

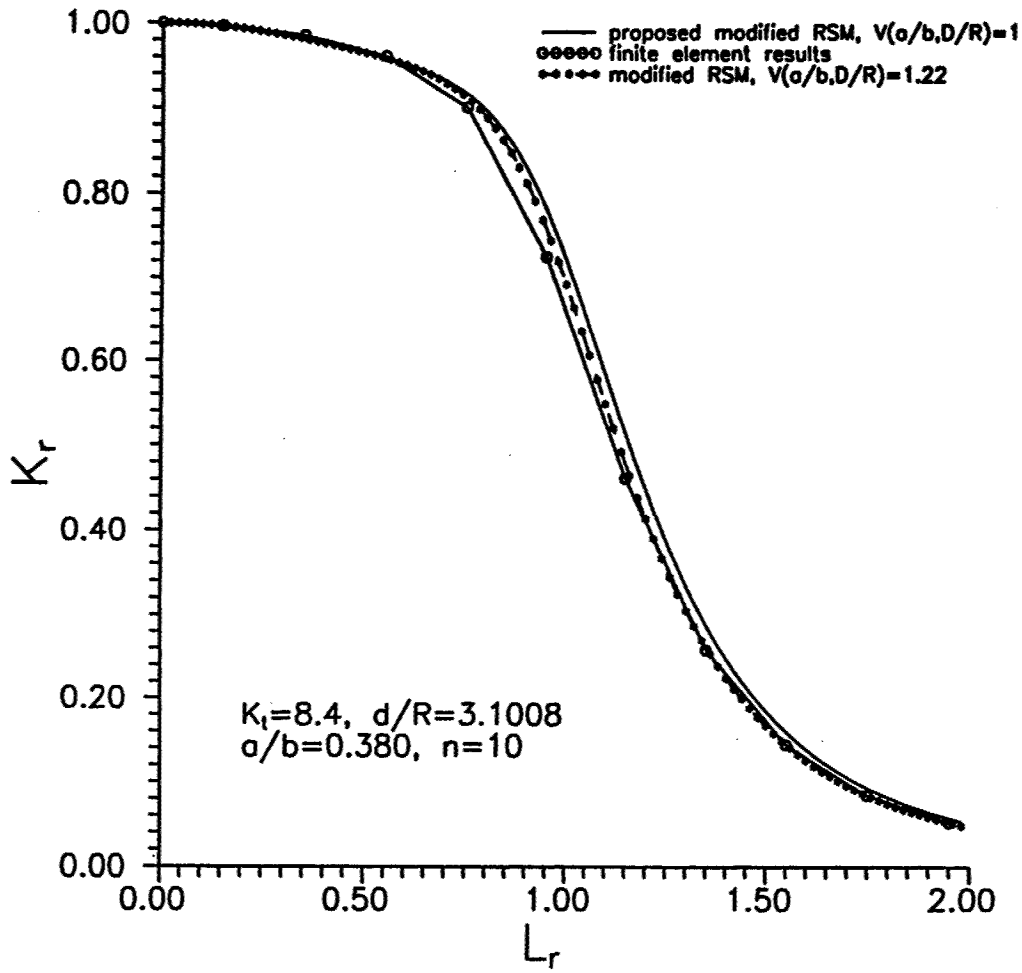

Figure D.34 Comparison of finite element results (open circles) with the modified RSM using the actual value of *V(a/b,D/R)* (dashed line) and *V*=1 (solid line) for symmetrical cracks in double edge notched plates subjected to uniaxial stressing: *d/R*=3.1008, K_t=8.4, *n*=10.

APPENDIX E

AN APPROXIMATE METHOD FOR DERIVING J SOLUTIONS FOR TWO SIMULTANEOUSLY APPLIED MECHANICAL LOADS FROM J SOLUTIONS FOR THE TWO LOADS ACTING SEPARATELY

Summary

It is shown that the J solution for two mechanical loads applied simultaneously can be expressed in terms of the linear elastic component of J for the combined loading, and a material dependent function of an appropriate combined yield load. The latter is called here the optimum yield load, and represents the true yield load of a defective structure of non-strain hardening material. The derivation of J for the combined loading is thus reduced to finding an expression for the optimum combined yield load. An approximate method for deriving this load is described using reference stress concepts and published fully plastic J solutions for single mechanical loads. The methodology is validated against computed fully plastic J solutions for single edge cracked plates, and cylinders containing circumferential through-wall defects, simultaneously subjected to tensile forces and pure bending moments. The agreement between the approximate solutions and the computed J values is good. The accuracy of the method is dependent on the accuracy of the combined yield load chosen as an interpolation function between the two extreme loading conditions corresponding to pure tension and pure bend.

The methodology can be used to generate tables of values for the optimum yield loads, and then J solutions for materials with arbitrary stress-strain behavior. This extension of the EPRI J solutions for specific strain hardening exponents to the general case, is one of the major benefits that can be derived from applying the reference stress method. It offers the opportunity for re-analyzing the extensive J solutions contained in the EPRI handbooks in order to generalize the single load solutions to arbitrary stress-strain behavior, and hence utilize these, where appropriate, to generate solutions for combined loading cases. These developments will help facilitate the inclusion of J solutions in computer programs, such as NASGRO, which may be extended to incorporate elastic-plastic fracture mechanics.

E.1 Introduction

The Electric Power Research Institute (EPRI) has sponsored the calculation of elastic-plastic J solutions for a variety of structural and laboratory specimen geometries (Kumar, German, and Shih, 1981; Kumar et al., 1984a; Kumar and German, 1988). Nearly all the solutions pertain to the application of single mechanical loads, or mechanical loads combined with thermal loading. Only a limited number of solutions have been derived for combined tensile forces and bending moments.

The purpose of this Appendix is to describe the development of an approximate method for deriving J solutions for two simultaneously applied loads from existing solutions for single loads. It is assumed that no J solutions are available for the combined loading case. If these solutions are available they can be used, together with interpolation and/or extrapolation procedures, to derive the desired solutions.

The approach adopted is based on the reference stress method proposed by Ainsworth (1984) for characterizing the plastic deformation at a crack tip. These concepts are used to identify an optimum yield load from which a reference stress may be derived. In general, the optimum yield load does not correspond to any of the yield loads used in the J estimation scheme described in the EPRI

handbooks, nor to the yield loads normally derived from plastic limit load theory. As will be seen, to solve the combined mechanical loading problem requires knowing the optimum yield load for the combined loading. An approximate method for constructing this is given in the Appendix, based on estimating plastic limit loads for the combined loading.

The developed methodology for combined loads is used to generate approximate J solutions for tensile forces and bending moments applied to single edge cracked plates (SECP) and cylinders containing circumferential through-wall defects (CTWD). These are validated against J solutions contained in the EPRI handbooks for the same loads and geometries (Kumar et al., 1984; Kumar and German, 1988).

E.2 EPRI *J* Estimation Scheme for Single Loads

In the EPRI estimation scheme the J-integral is written as the superposition of elastic (J_e) and plastic (J_p) components

$$J = J_e + J_p \tag{E.1}$$

J solutions reported in references (Kumar, German, and Shih, 1981; Kumar et al., 1984a; Kumar and German, 1988) were derived from elastic-plastic finite element analyses for materials obeying the Ramberg-Osgood stress-plastic strain constitutive law

$$\epsilon^p/\epsilon_o = \alpha[\sigma/\sigma_o]^n \tag{E.2}$$

where ϵ^p is plastic strain, σ is the applied stress, and ϵ_o, σ_o, α and n are material constants.

The elastic component of J is related to the applied stress intensity factor (K) through the equation

$$J_e = K^2(a_e)/E' \tag{E.3}$$

where $E'=E$, Young's modulus, for plane stress, and $E'=E/(1-\nu^2)$, for plane strain, where ν is Poisson's ratio. The effective crack depth a_e is evaluated from first order plasticity theory and is given for a Ramberg-Osgood power law by

$$a_e = a + \frac{\phi}{\pi\beta}\frac{(n-1)}{(n+1)}\left(\frac{K}{\sigma_o}\right)^2 \tag{E.4}$$

where

$$\phi = \frac{1}{1 + \frac{1}{2}\left(\frac{P}{P_o}\right)^2} \tag{E.5}$$

and a is the crack depth and P_o a characterizing yield load chosen as a convenient normalizing load parameter. β is equal to 2 for plane stress, and 6 for plane strain conditions.

Expressions for J_p for single mechanical loads can be obtained from the EPRI handbooks (Kumar, German, and Shih, 1981; Kumar et al., 1984a; Kumar and German, 1988) as

$$J_P = \alpha\sigma_o\epsilon_o c\left[\frac{a}{b}\right]h_1\left(\frac{a}{b},n,D\right)\left[\frac{P}{P_o}\right]^{n+1} \tag{E.6}$$

where b is the section size and $c=b-a$ is the uncracked ligament.

The function h_1 depends on a/b, n and, in general, a normalized structural parameter, D (for example, for cylindrical geometries $D = R/t$, where R is the mean radius and t the wall thickness). Values of h_1 are tabulated in the EPRI handbooks for various structural and laboratory geometries. It is convenient to omit some or all of the functional dependencies of h_1 in the ensuing discussions, and to include explicitly only those dependencies which are relevant to the subject at hand.

E.3 Reference Stress Approach

The basic assumption of the reference stress method is that, for a particular structural geometry, defect, and loading condition, there exists a reference point in J-load space through which all the J solutions pass, irrespective of the constitutive equation describing the material stress-strain response. The principle is shown schematically in Figure E.1, where P represents the applied load. The value of P corresponding to the reference point is hereafter called the optimum yield load, P_o^*. This load is equal to the true yield load of a defective structure: the J-load curve for a non-hardening (elastic-perfectly plastic) material also passes through the reference point.

The idea of a reference stress originates from the study of creep deformation. In the creep context, the reference point corresponds to the spatial point in the structure where the steady state value of the stress is invariant to changes in the constitutive law relating strain rate to uniaxial stress. The value of the stress at this point is frequently used as a one parameter characterization of creep deformation in the structure, and is called the reference stress. These concepts can be transferred to plasticity by invoking the analogy between creep and plastic deformation. This analogy states that, for similar constitutive equations between creep deformation (the law relating creep rate and stress) and plastic deformation (the law relating plastic strain and stress), the results for a plastic stress analysis can be obtained from creep analysis by replacing creep strain rate and displacement rate by plastic strain and displacement. It is clear from this that a reference stress exists that characterizes plastic deformation. This stress corresponds to the value of stress at the spatial point in the structure

where the stress is invariant with respect to changes in the constitutive law relating plastic strain and uniaxial stress. To the authors' knowledge, the validity of transferring these concepts to plastic fracture mechanics, where changes in the applied value of J replace changes in a spatial coordinate, has not been formally established.

When applied to estimating J solutions, the aim of the reference stress approach is to optimize the choice of yield load so that the dependence of h_1 on n is eliminated or reduced to an insignificant level. Thus, in terms of the optimum yield load, J_p can be written as

$$J_p = \alpha\sigma_o\epsilon_o c\left[\frac{a}{b}\right] h_1^*\left(\frac{a}{b},D\right)\left[\frac{P}{P_o^*}\right]^{n+1} \qquad \textbf{(E.7)}$$

where, by comparison with equation (E.6), h_1^* is given by

$$h_1^*\left(\frac{a}{b},D\right) = h_1\left(\frac{a}{b},n,D\right)\left(\frac{P_o^*}{P_o}\right)^{n+1} \qquad \textbf{(E.8)}$$

Although n appears as an argument in the terms on the right hand side of equation (E.8), it is assumed in the reference stress approach that the product of these terms is independent of n. It can be seen from equation (E.7) that all values of J_p for a given defective structure and applied load are equal when $P=P_o^*$, irrespective of the value of n. This value of J_p is the value at the reference point in J-load space (see Figure E.1).

The optimum yield load allows an optimum reference stress to be defined. This stress provides a single parameter characterization (for given plastic constraint) of the plastic deformation in the uncracked ligament (Ainsworth, 1984). The optimum reference stress, σ_{ref}, is related to the optimum yield load by the equation

$$\sigma_{ref} = (P/P_o^*)\sigma_o \qquad \textbf{(E.9)}$$

where σ_o is the yield stress.

E.4 Optimum Choice for P_o^*

Equation (E.6) has to reduce to the LEFM expression for J when n=1 but with the elastic value of Poisson's ratio, ν, replaced by the plastic value, ν_p. Writing

$$K = (\pi a)^{1/2}(P/A)F\left(\frac{a}{b}\right) \qquad \textbf{(E.10)}$$

where A is a geometric constant of the dimensions of area, and F is an influence function which depends on geometry, then

$$\mu J_e = \mu \frac{(\pi a)}{E'} \left(\frac{PF}{A} \right)^2 \tag{E.11}$$

where $\mu = \left(1 - \nu_p^2\right) / \left(1 - \nu^2\right)$. Comparing equation (E.11) to equation (E.6) with n=1 and α=1 yields the following expression for $h_1(1)$

$$h_1(1) = HP_o^{\,2} \tag{E.12}$$

where use has been made of the relationship $E\epsilon_o = \sigma_o$ and

$$H = \left(\frac{E}{E'} \right) \left(\frac{\pi}{c/b} \right) \left(\frac{F}{A\sigma_o} \right)^2 \mu \tag{E.13}$$

Rewriting equation (E.8) as

$$\frac{h_1^*}{P_o^{*n+1}} = \frac{h_1(n)}{P_o^{\,n+1}} \tag{E.14}$$

then from equation (E.12) it can be seen that both the left hand and right hand sides of equation (E.14) are <u>independent of the choice of yield load</u> when n=1. This is an important observation which influences the method chosen to determine P_o^*, but one that should be expected in the linear elastic limit.

In order to find the optimum choice for P_o^*, and to allow for uncertainties in the calculated value of $h_1(n)$, equation (E.14) is rewritten as:

$$\frac{HP_o^{*2}(1)}{P_o^{*n+1}(n)} = \frac{h_1(n)}{P_o^{n+1}} \tag{E.15}$$

where the $P_o^*(n)$ are unknown yield loads whose values are to be determined. Re-arranging this equation yields the following expression for $P_o^*(n)$

$$P_o^*(n) = P_o\left[\frac{HP_o^{*2}(1)}{h_1(n)}\right]^{1/(n+1)} \tag{E.16}$$

This equation contains two unknowns when $n>1$, namely, $P_o^*(1)$ and $P_o^*(n)$, and reduces to equation (E.12) when $n=1$.

Inaccuracies in the computed values of $h_1(n)$ may arise from a number of causes, for example, the quality of the finite element mesh, and, in the case of the EPRI handbook solutions, the goodness of fit to the J results obtained using equations (E.1), (E.3), and (E.6). These computational inaccuracies are manifested as uncertainties in the value of the optimum yield load, and, instead of the J curves passing through a single point in J-load space as in Figure E.1, the intersections of the curves for different strain hardening capacities will be spread over a finite area of this space. Thus, even though $P_o^*(1)$ in equation (E.16) is known precisely, inaccuracies in the value of $h_1(n)$ will produce an apparent n dependence of the optimum yield load, which is shown explicitly in equation (E.16). Hence, a procedure is required for estimating the most likely, or optimum, value of P_o^* taking into account these uncertainties.

The optimization procedure followed here consists of using $P_o^*(1)$ as a variational parameter, chosen to minimize the dependence of the yield loads $P_o^*(n)$ on n for $n>1$. In other words, a value for $P_o^*(1)$ is sought such that $P_o^*(n)=P_o^*$, a constant independent of n, when $n>1$. A possible numerical procedure for implementing this optimization scheme is described in Section 7.

Once these values of $P_o^*(1)$ and P_o^* have been determined, then, using equations (E.7), (E.11), to (E.14), J_p can be written for $n>1$ as

$$J_p = \mu J_e\left[\frac{P_o^*(1)}{P_o^*}\right]^2 \alpha\left[\frac{P}{P_o^*}\right]^{n-1} \tag{E.17}$$

This equation is surprising because it shows that the plastic component of J is related to the elastic component. Furthermore, using the Ramberg-Osgood law as specified in equation (E.2), and the definition of the reference stress, σ_{ref}, given in equation (E.9), then equation (E.17) can be re-written as

$$J_p = \mu J_e\left[\frac{P_o^*(1)}{P_o^*}\right]^2 \left[\frac{E\epsilon_{ref}^p}{\sigma_{ref}}\right] \tag{E.18}$$

where ϵ_{ref}^p is the reference plastic strain corresponding to the value of σ_{ref} on the uniaxial stress-strain curve. Note that J_p is now expressed in a form which is applicable to materials with arbitrary stress-

strain behavior. This important aspect of the reference stress approach enables a generalized, material dependent expression for J_p to be derived once the optimum yield load has been determined.

E.5 Extension to Combined Loading

J estimation schemes can be extended to the simultaneous application of two independent load types (e.g. tensile force and bending moment), signified as P_1 and P_2, by characterizing the load combination as P_1 and λ, where

$$\lambda = \frac{P_2}{gP_1} \tag{E.19}$$

and g is a geometric term that makes λ dimensionless. (For example, $g=b$ for a SECP, and $g=R$ for a CTWD, if P_1 is a tensile force and P_2 a bending moment). $\lambda=0$ corresponds to the application of load type P_1 only, and $\lambda=\infty$ to load type P_2 only.

Let $P_{o,1}$ and $P_{o,2}$ be the values of P_1 and P_2 at general yield when the loads are applied separately. Clearly, the values of P_1 and P_2 at general yield, when both loads are applied simultaneously, will depend on the value of λ. The combined yield load will be taken as the value of P_1 at yield, and be denoted by $P_o(\lambda)$. Hence

$$P_o(\lambda=0) = P_{o,1},\ P_o(\lambda=\infty) = \frac{P_{o,2}}{\lambda g} \tag{E.20}$$

For combined loading the EPRI expression for J_p becomes (Kumar et al., 1984a; Kumar and German, 1988)

$$J_P = \alpha\sigma_o\epsilon_o c\left[\frac{a}{b}\right]h_1\left(\frac{a}{b},n,D,\lambda\right)\left[\frac{P}{P_o(\lambda)}\right]^{n+1} \tag{E.21}$$

and, equation (E.17) becomes

$$J_p(P_1,\lambda) = \mu J_e(P_1,\lambda)\left[\frac{P_o^*(1,\lambda)}{P_o^*(\lambda)}\right]^2 \alpha\left[\frac{P_1}{P_o^*(\lambda)}\right]^{n-1} \tag{E.22}$$

The suitability of using the reference stress approach for estimating J_p for combined loading is now apparent: the dependence of J_p on a function $h_1(n,\lambda)$, about which it is assumed that nothing is known a priori (except for given solutions corresponding to the extreme values of $\lambda=0$ and $\lambda=\infty$), has been removed. The problem has been reduced to the relatively simpler (but still non-trivial) one of

estimating the optimum reference loads $P_o^*(1,\lambda)$ and $P_o^*(\lambda)$ (addressed in the next section), and evaluating the linear elastic solution for J_e.

There are now a number of compendia which give K solutions for a wide variety of structures and loads (Sih, 1973; Tada, Paris, and Irwin, 1985; Murakami, 1989) and since linear elastic solutions are linearly additive, obtaining J_e for combined loading is a relatively straightforward matter. For example, if subscript 1 and 2 indicate applied loads P_1 and P_2, then J_e for the combined loading is given by

$$J_e = (K_1 + K_2)^2 / E' \tag{E.23}$$

E.6 Estimating the Optimum Yield Load for Combined Loading

An estimate of a yield load for combined loading, denoted as $P_o(\lambda)$, can be obtained from plastic limit load theory. [For example, see the limit load compendium compiled by Miller (1988) or the EPRI handbooks (Kumar et al., 1984a; Kumar and German, 1988).] This yield load can be used as guidance in the choice of the optimum combined yield load by forcing it to recover the optimum yield load solutions for the two loads applied separately, that is, when $\lambda = 0$ and $\lambda = \infty$. This is done by defining the ratios:

$$r(\lambda = 0) = \frac{P_o^*(\lambda = 0)}{P_o(\lambda = 0)} = \frac{P_{o,1}^*}{P_{o,1}} \tag{E.24}$$

and

$$r(\lambda = \infty) = \frac{P_o^*(\lambda = \infty)}{P_o(\lambda = \infty)} = \frac{P_{o,2}^*}{P_{o,2}} \tag{E.25}$$

where $P_{o,1}^*$ and $P_{o,2}^*$ are the optimum yield loads when P_1 and P_2 act separately. These ratios can be used to force the chosen yield load, $P_o(\lambda)$, to approximate the optimum yield load, $P_o^*(\lambda)$, for arbitrary λ by writing

$$P_o^*(\lambda) = r(\lambda = 0) P_o\left(\frac{r(\lambda = 0)\lambda}{r(\lambda = \infty)}\right) \tag{E.26}$$

which reduces to the correct optimum yield loads when λ=0 and λ=∞, and provides an interpolation formula for $P_o^*(\lambda)$ between these two extremes. A graphical interpretation of this equation is shown in Figure E.2, which illustrates how the solution for $P_o(\lambda)$ is transformed into an approximate form for $P_o^*(\lambda)$.

A similar procedure can also be followed for estimating the optimum yield load $P_o^*(1,\lambda)$ based on the ratios $r(1,\lambda=0)$ and $r(1,\lambda=\infty)$ defined in a similar fashion to $r(\lambda=0)$ and $r(\lambda=\infty)$ in equations (E.24) and (E.25), and using the same yield load, $P_o(\lambda)$.

E.7 Application to Single Edge Cracked Plates (SECP)

The fracture mechanics solutions for SECP's are frequently used in structural integrity assessments. The EPRI handbooks contain plane strain J_p solutions for tensile (P_1) and bending (P_2) loads (Kumar, German, and Shih, 1981), and a limited number of solutions for combined loading for $\lambda=1/8$, and a range of negative λ values, where $\lambda=P_2/bP_1$ (Kumar et al., 1984a). The results for a negative moment are not analyzed here, due to the problems associated with crack closure, and the lack of J solutions for the case when $\lambda=-\infty$. However, the $\lambda=1/8$ solutions [see Table 2-1 in reference (Kumar et al., 1984)] provide data against which the methodology detailed in the previous sections can be judged.

Unfortunately, the yield loads used in the definition of $P_o(\lambda)$ for $\lambda=0$ and $\lambda=\infty$ in the EPRI handbooks do not reduce to the yield loads P_o^t and P_o^b used in the expressions for J_p, where superscripts t and b refer to tension and bend respectively. It is convenient to renormalize the tension and bend solutions so this is the case by replacing the EPRI functions h_1^t and h_1^b by modified values where

$$h_1(\lambda) = \frac{h_1^x}{(a/b)^m}\left[\frac{P_o(\lambda)}{P_o^x}\right]^{n+1} \qquad \textbf{(E.27)}$$

and x stands for t or b: $m=0$ and $\lambda=0$ for tension, and $m=1$ and $\lambda=\infty$ for bend. The (a/b) term is required because the expression for J_p given in the handbook for bending does not include (a/b).

Values for h_1^x are tabulated in Tables 3-7 and 3-5 of reference (Kumar, German, and Shih, 1981) for tension and three-point bending respectively, and expressions for P_o^x are given by equations (3.57) and (3.39) in the same reference. The three-point bending solutions are used in this Appendix as an approximation to the pure bending solutions.

The modified $h_1(\lambda)$ solutions defined in equation (E.27) for $\lambda=0$ and $\lambda=\infty$ were used in the optimization procedure described in Section E.4 to obtain $P_o^*(0)$ and $P_o^*(\infty)$. In this procedure, the value of $P_o^*(1)$ was varied and the values of $P_o^*(n)$ determined from equation (E.16) until the parameter, ρ, was a minimum, where

$$\rho = \sum_{n>1} (P_o^*(n) - P_o^*)^2 \qquad \textbf{(E.28)}$$

and

$$P_o^* = \frac{1}{N}\sum_{n>1} P_o^*(n) \tag{E.29}$$

N is the number of n values (where $n>1$) for which EPRI J solutions are available.

The plane strain EPRI yield load for combined loading was used as an interpolation formula for evaluating $P_o^*(\lambda)$ from equation (E.26). The EPRI solution is given by equation (2.22) of reference (Kumar et al., 1984a) as

$$P_o(\lambda) = 2\sigma_o \frac{b}{\sqrt{3}}\left[\left(\left(\left|2\lambda + \frac{a}{b}\right|\right)^2 + \left(\frac{c}{b}\right)^2\right)^{1/2} - \left|2\lambda + \frac{a}{b}\right|\right] \tag{E.30}$$

The optimized yield loads were used to determine $h_1(n,\lambda)$ from the equation

$$h_1(n,\lambda) = h_1^*(1,\lambda)\left[\frac{P_o(\lambda)}{P_o^*(\lambda)}\right]^{n-1} \tag{E.31}$$

where

$$h_1^*(1,\lambda) = H(\lambda)P_o^{*2}(1,\lambda) \tag{E.32}$$

and

$$H(\lambda) = \frac{E}{E'}\frac{\pi}{\left(\frac{c}{b}\right)}\left(\frac{F^t}{Bb} + \frac{6\lambda F^b}{Bb}\right)^2 \mu \tag{E.33}$$

Here B is the breadth of the plate. This was taken as unity in the computations, the applied loads being defined per unit breadth. The results are shown in Table E.1 together with the EPRI computed values. There is reasonable agreement between the two sets of values given the fact that the form of the optimum combined yield load has been approximated.

The conjecture that the differences between the two sets of results is due to the approximate nature of the constructed optimum combined yield load is illustrated by the following analysis. From equation (E.31)

$$\frac{h_1(n,\lambda)}{h_1(2,\lambda)} = \left[\frac{P_o(\lambda)}{P_o^*(\lambda)}\right]^{n-2} \tag{E.34}$$

and

$$\frac{P_o(\lambda)}{P_o^*(\lambda)} = \left[\frac{h_1(n+m,\lambda)}{h_1(n,\lambda)}\right]^{\frac{1}{m}} \tag{E.35}$$

These equations can be used to assess the accuracy of the approximate solutions given in Table E.1 as the following example shows. From Table E.1 the a/b=0.75 results for the EPRI solutions show that the ratio on the right hand side of equation (E.35) is about 0.7. For example, it equals 0.695 when n=3, m=4, and 0.702 when n=5, m=5. The estimated value of this ratio is 0.629, which is about 11% below the EPRI values. From equation (E.34) this indicates that the corresponding value for $h_1(10,\lambda)$ will be approximately 0.4 = $(1/1.11^8)$ times the EPRI value. As can be seen from Table E.1, this is the case.

E.8 Application to Circumferential Through-wall Defect (CTWD)

The EPRI handbooks contain J_p solutions for CTWD's subjected to a tensile force (P_1), pure bending moment (P_2), and a combination of these two load types (Kumar and German, 1988). The combined solutions for $h_1(n,R/t=10,\lambda)$, which are analyzed herein, are for λ values of 0.5, 1 and 2 [see Table 2-9 in reference (Kumar and German, 1988)], where $\lambda=P_2/RP_1$. These results provide data against which the approximate procedure for estimating J_p can be validated.

Values of h_1^t and h_1^b are tabulated in Tables 2-3 and 2-7, respectively, of (Kumar and German, 1988), and expressions for $P_{o,1}$ and $P_{o,2}$ are given by equations (2-25) and (2-50) in the same reference as

$$P_{o,1} = P_o(\lambda=0) = 2\pi\sigma_o Rt\left[1-\frac{\theta}{\pi}-\frac{2}{\pi}\sin^{-1}\left(\frac{1}{2}\sin\theta\right)\right] \tag{E.36}$$

and

$$P_{o,2} = \lambda RP_o(\lambda=\infty) = 4\sigma_o R^2 t\left[\cos(\theta/2)-\frac{1}{2}\sin\theta\right] \tag{E.37}$$

where $a/b=\theta/\pi$, a is half the total crack length, θ is the angle subtended by an arc of length a, $b=\pi R$, and t is the wall thickness. The EPRI handbook expression for $P_o(\lambda)$ is equation (2-75) in (Kumar and German, 1988)

$$P_o(\lambda) = \frac{P_{o,1}}{2}\left[\left(\left[\frac{\lambda P_{o,1}R}{P_{o,2}}\right]^2 + 4\right)^{1/2} - \frac{\lambda P_{o,1}R}{P_{o,2}}\right] \tag{E.38}$$

The optimized yield loads were determined using equation (E.38) and following a procedure similar to that described in Section E.7, where instead of equation (E.33), $H(\lambda)$ is defined as:

$$H(\lambda) = \frac{E}{E'}\frac{\pi}{\left(\frac{c}{b}\right)}\left(\frac{F^t}{2\pi Rt} + \frac{\lambda F^b}{\pi Rt}\right)^2 \mu \tag{E.39}$$

The results are shown in Table E.2 together with the EPRI solutions. As for the SECP case, there is reasonably good agreement between the two sets of results.

E.9 Sensitivity to Choice of $P_o(\lambda)$

An alternative combined yield load to that defined by equation (E.38) can be obtained by equating the force and moment corresponding to the induced stress distribution at yield to the externally applied force and moment. This results in the pair of simultaneous equations (Miller, 1988)

$$\lambda R P_o(\lambda) = 4\sigma_o R^2 t\left[\cos\alpha_1 - \frac{1}{2}\sin\theta\right] \tag{E.40}$$

and

$$\alpha_1 = \frac{\theta}{2} + \frac{P_o(\lambda)}{4\sigma_o Rt} \tag{E.41}$$

which can be combined to give the following equation for $P_o(\lambda)$

$$\frac{\lambda P_o(\lambda)}{4\sigma_o Rt} - \cos\left(\frac{\theta}{2} + \frac{P_o(\lambda)}{4\sigma_o Rt}\right) + \frac{1}{2}\sin\theta = 0 \tag{E.42}$$

This alternative yield load was used to derive a new set of $h_l(n,\lambda)$ values, displayed in Table E.2. The new solutions track the behavior of $h_l(n,\lambda)$ as n increases better than the results obtained using the EPRI yield load.

A comparison of the various combined yield loads for a/b=0.25 is shown in Figure E.3. It can be seen that the alternative yield load falls below the EPRI yield load as λ increases, and that the derived optimum yield solutions fall above the corresponding yield loads. Comparison of the combined yield loads in Figure E.3, and the corresponding results for a/b=0.25 in Table E.2, illustrates the sensitivity of $h_1(n,\lambda)$ to the choice of yield load used for interpolation purposes.

E.10 Summary of Procedure for Estimating J_p for Combined Loading

The following steps describe the procedure for determining the functions $h_1(n,\lambda)$ which define J_p through equation (E.21). It is assumed that values for $h_1(n,\lambda=0)$ and $h_1(n,\lambda=\infty)$ are available for a sufficient number of n values to enable the optimum yield loads for the two independently applied mechanical loads to be determined, and that expressions for the corresponding yield loads $P_{o,1}$ and $P_{o,2}$ are also known. These yield loads have to be compatible with the combined yield load chosen for use in equation (E.26) as an interpolation function between λ=0 and $\lambda=\infty$. This compatibility is assured if $P_o(\lambda=0)=P_{o,1}$ and $P_o(\lambda=\infty)=P_{o,2}/\lambda g$, where the parameter g is assigned to an appropriate structural dimension.

(i) Determine the optimum yield loads $P_o^*(\lambda=0)$, $P_o^*(\lambda=\infty)$, $P_o^*(1,\lambda=0)$, and $P_o^*(1,\lambda=\infty)$ from the known solutions for $h_1(n,\lambda=0)$, $h_1(n,\lambda=\infty)$, $P_o(\lambda=0)$, and $P_o(\lambda=\infty)$, using the optimization scheme described in Section 4 based on equation (E.16). A simple numerical procedure for performing this optimization is described in Section E.7 [equations (E.28) and (E.29)].

(ii) Evaluate $\lambda=P_2/gP_1$ for the required load combination, and determine the value of the function $H(\lambda)$ from the stress intensity factor solutions for the two mechanical loads using equations such as (E.33), and (E.39).

(iii) From plastic limit load considerations define a combined yield load, $P_o(\lambda)$, for arbitrary λ, such as those given in equations (E.30), (E.38), and (E.42). Approximate methods of constructing combined yield loads are discussed in reference (Miller, 1988). Equation (E.30) may be derived by applying one of these methods, which is based on a yield surface for combined tension and bending. Another technique is to use the lower bound limit load theorem which enables a yield load to be obtained by balancing the applied forces by an internal yield magnitude stress distribution consisting of tensile and compressive components. This method was used to derive equation (E.42).

(iv) Use $P_o(\lambda)$, together with $r(\lambda=0)$, $r(1,\lambda=0)$, $r(\lambda=\infty)$ and $r(1,\lambda=\infty)$, calculated from equations (E.24) and (E.25), to determine approximate values for $P_o^*(\lambda)$ and $P_o^*(1,\lambda)$ from equation (E.26). (See the equivalent graphical construction shown in Figure E.2.)

(v) Evaluate the function $h_1^*(1,\lambda)$ from equation (E.32) and hence calculate the value of $h_1(n,\lambda)$ for the desired n value from equation (E.31).

(vi) Alternatively, J_p may be calculated directly from equation (E.22), or, if J_p is desired for a non-Ramberg-Osgood material, using equation (E.9) to obtain σ_{ref}, and the uniaxial stress-

strain curve to obtain ϵ_{ref}, and hence, using the combined load equivalent of equation (E.18) and equation (E.23).

If computed J_p solutions are available for P_1 and P_2 and only a single material stress-strain curve (say, a Ramberg-Osgood law and a particular n value, or arbitrary stress-strain behavior), then values of $P_o^*(\lambda=0)$ and $P_o^*(\lambda=\infty)$ required from step (i) can still be estimated as those values which give the best agreement between equation (E.7) and the computed solutions for J, assuming that the ratios $\dfrac{P_o^*(1,0)}{P_o^*(0)}$ and $\dfrac{P_o^*(1,\infty)}{P_o^*(\infty)}$ are equal to unity.

If no computed J solutions are available for the loads P_1 and P_2, then equation (E.22) can be used to estimate J_p for the combined loading, but using best estimate values for $P_o^*(\lambda=0)$ and $P_o^*(\lambda=\infty)$ obtained from plastic limit load considerations and again assuming that the ratios $\dfrac{P_o^*(1,0)}{P_o^*(0)}$ and $\dfrac{P_o^*(1,\infty)}{P_o^*(\infty)}$ are equal to unity.

E.11 Discussion

The methodology presented for determining an expression for J_p under combined loading is approximate. The approximate nature of the method, which utilizes reference stress concepts, is in the need to determine the optimum combined yield load for arbitrary λ values from solutions which are assumed known only for the two extreme cases where $\lambda = 0$ and $\lambda = \infty$. The starting assumption for the analysis is that J solutions for the two loads applied separately are known for a range of different strain hardening materials. If this is not the case, then alternative methods can be employed, as described in Section E.10. In general, these will not be as accurate, as they are based on less precise information.

The J solutions contained in the EPRI handbooks are expressed in terms of the functions h_1 [see equations (E.6) and (E.21)], whose values are tabulated for various structural geometries, specific crack depths (a/b ratios), strain hardening exponents, and applied load types (Kumar, German, and Shih, 1981; Kumar et al., 1984a; Kumar and German, 1988). The tabular values can be used in elastic-plastic fracture mechanics assessments to determine J values based on equations (E.1), (E.6), and (E.21), together with interpolation techniques to extend the range of the available solutions.

However, a more efficient use of the methodology would be to generate tabular data for the optimum yield loads and to utilize these, together with the developed reference stress approach, in order to generate J solutions for materials with arbitrary stress-strain behavior [see equation (E.18)]. This extension of the EPRI J solutions for specific strain hardening exponents, n, to the general case, is one of the major benefits that can be derived from applying the reference stress method. Indeed,

the method offers the opportunity for re-analyzing the extensive J solutions contained in the EPRI handbooks in order to generalize the single load solutions to arbitrary stress-strain behavior, and hence, utilize these, where appropriate, to generate solutions for combined loading cases.

Methods of utilizing tabular data for calculating fracture mechanics parameters are already established in linear elastic applications: for example, in the computer program NASGRO. The methodology proposed herein of deriving J solutions for combined loading from the J solutions for the two mechanical loads applied separately, can be used to generate tabular data for use in extending linear elastic based computer codes to include elastic-plastic fracture mechanics.

Another benefit of the reference stress method is that it allows new J solutions to be estimated based on only linear elastic solutions and yield loads derived from plastic limit considerations. These solutions are immediately applicable to materials which display an arbitrary stress-strain response. The procedures for doing this are briefly described in Section E.10, and are based on equation (E.18).

E.12 Conclusions

An approximate method for evaluating J for combined mechanical loads has been developed based on reference stress principles. The accuracy of the method is determined by the accuracy with which an optimum combined yield load can be estimated. A procedure for obtaining this optimum yield load is described based on the optimum yield loads for the two mechanical loads acting separately, and plastic limit load considerations. The method has been validated against elastic-plastic finite element results for J obtained for single edge cracked plates, and circumferential through-wall defects in cylinders, subjected to simultaneously applied tensile forces and pure bending moments. The developed methodology has the added benefit of allowing solutions for J obtained for Ramberg-Osgood materials to be extended to materials which display arbitrary stress-strain behavior.

Table E.1. h_1 functions for a plane strain SECP under combined tension and bending for the case of λ=0.125: Comparison of finite element and approximate results, the latter shown in parentheses

	n value				
a/b	2	3	5	7	10
0.125	4.544	3.881	2.632	1.734	0.905
	(5.905)	(4.727)	(3.029)	(1.941)	(0.995)
0.25	2.536	1.773	0.843	0.392	0.119
	(3.201)	(2.269)	(1.140)	(0.573)	(0.204)
0.375	1.657	1.016	0.373	0.136	0.029
	(2.015)	(1.311)	(0.555)	(0.235)	(0.065)
0.5	1.305	0.804	0.310	0.120	0.030
	(1.298)	(0.791)	(0.293)	(0.109)	(0.025)
0.625	1.056	0.678	0.290	0.129	0.039
	(0.952)	(0.571)	(0.205)	(0.074)	(0.016)
0.75	0.901	0.609	0.293	0.142	0.050
	(0.855)	(0.537)	(0.212)	(0.084)	(0.021)

Table E.2. h_1 functions for a through-crack in a cylinder under combined tension and bending. Comparison of finite element and approximate results. The latter are shown in single parentheses when the EPRI yield load was used, and double parentheses when the alternative yield load was used as an interpolation formula.

		***n* value**		
λ	***a/b***	**2**	**5**	**10**
0.5	0.125	7.222	8.631	9.421
		(8.027)	(7.893)	(7.676)
		((8.574))	((10.367))	((14.228))
	0.25	6.506	6.063	6.123
		(7.682)	(5.679)	(3.432)
		((8.496))	((8.544))	((8.625))
1.0	0.125	7.925	9.604	10.958
		(9.013)	(8.543)	(7.814)
		((9.771))	((11.801))	((16.165))
	0.25	7.363	7.333	8.242
		(8.847)	(6.455)	(3.817)
		((10.036))	((10.708))	((11.930))
2.0	0.125	7.970	9.335	9.985
		(8.826)	(8.078)	(6.970)
		((9.479))	((10.646))	((12.919))
	0.25	7.438	7.156	7.519
		(8.899)	(6.410)	(3.710)
		((9.981))	((10.107))	((10.319))

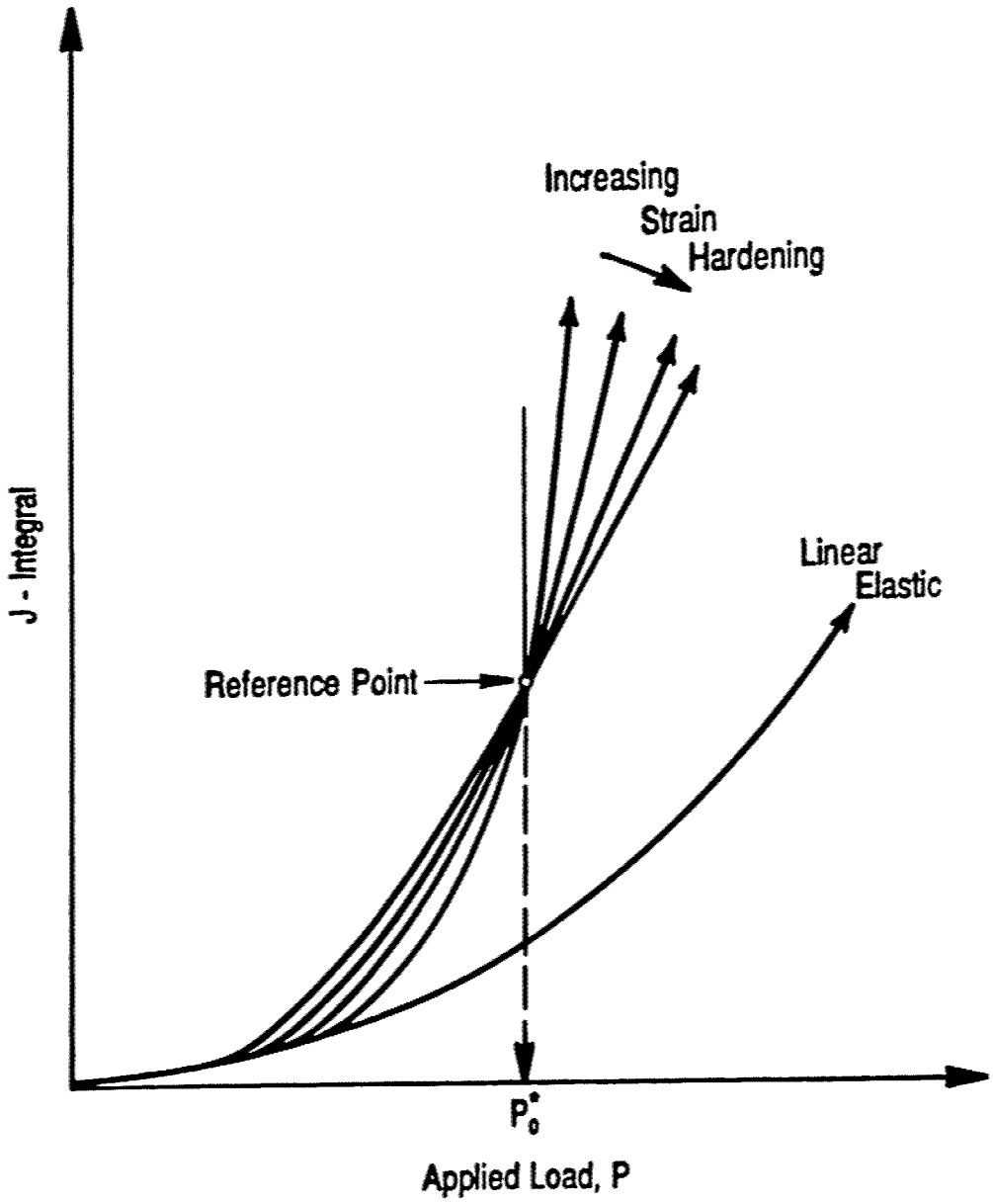

Figure E.1. Schematic of variation of J with load, P, for materials with different strain hardening capacities. At the reference point, all J values are equal, and this occurs when the load reaches the optimum yield load, P_o^*.

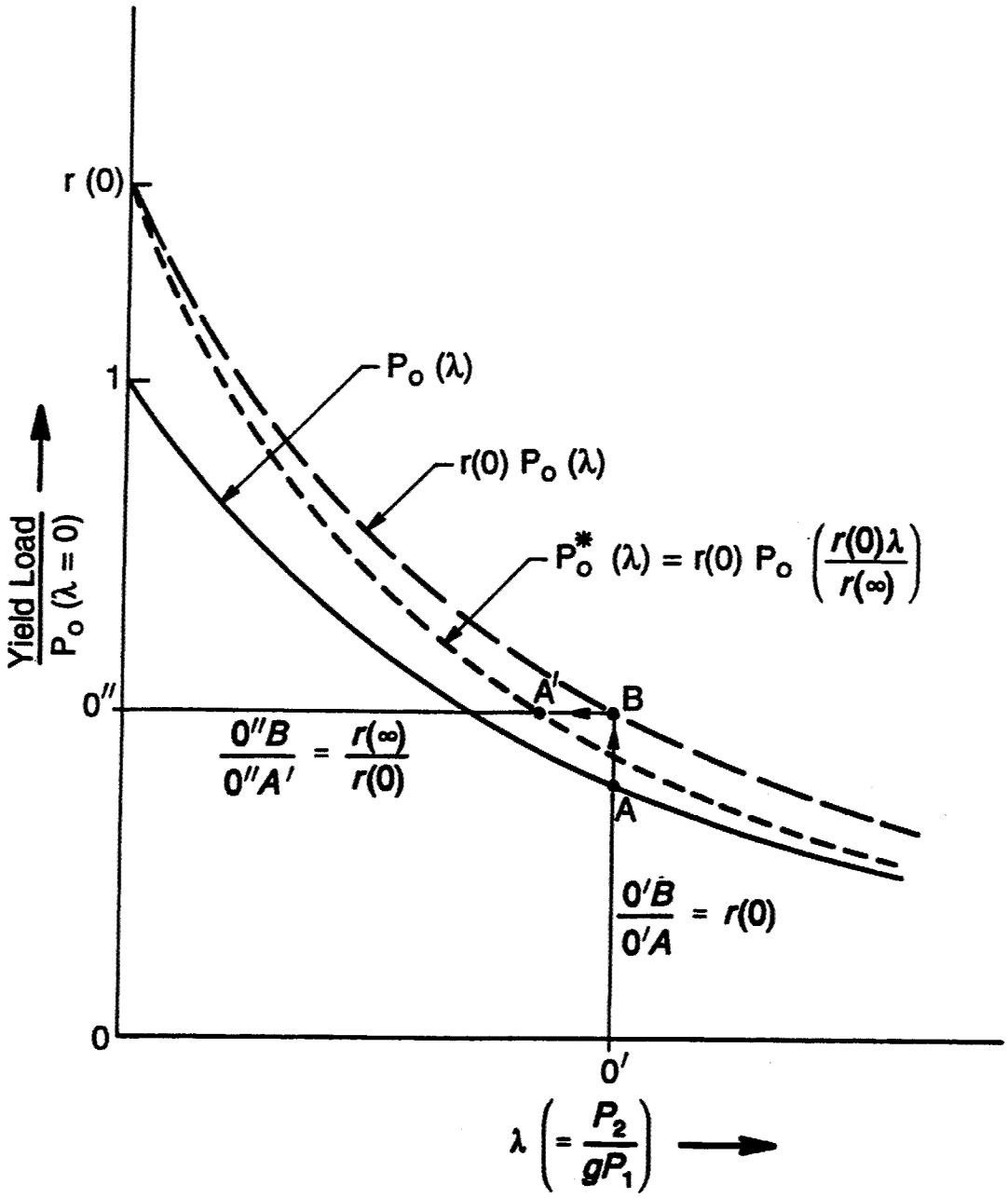

Figure E.2. Graphical construction of the optimum combined yield load.

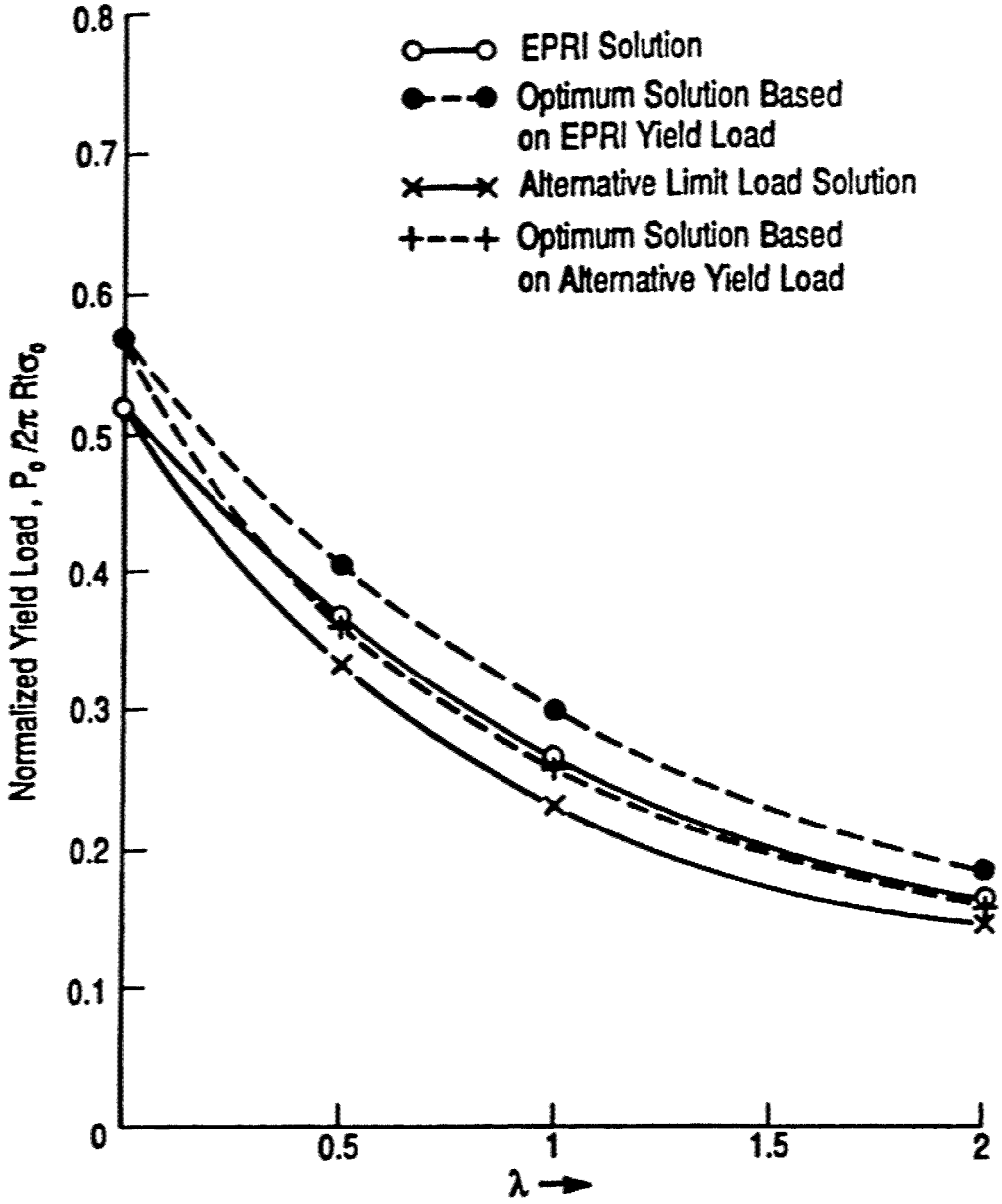

Figure E.3. Normalized yield loads for a circumferential through-wall defect as a function of λ for $a/b = 0.25$.

APPENDIX F

J ESTIMATION PROCEDURES FOR COMBINED PRIMARY AND SECONDARY LOADS

Summary

Four existing methods of estimating J for combined primary and secondary loads are reviewed. The methods are: a J estimation scheme based on the Electric Power Research Institute (EPRI) elastic-plastic handbook approach which incorporates the effects of secondary loading through a first order plasticity correction to the elastic component of J; the R6 structural integrity procedure which includes a term characterizing the interaction between primary and secondary loads; the method of Chell which combines a first order plasticity correction with the reference stress approach; and a proposed modification to the R6 procedure. None of the methods are totally satisfactory as they stand. However, a new procedure for estimating J for combined loading based on improvements in the Chell approach is developed. Parts of the procedure have not been fully validated and are based on best engineering judgement drawn from the limited information available at the present time. The procedure allows credit to be taken for situations where stress relaxation occurs due to plastic deformation in the defect free structure, but it is not generally applicable to situations where significant elastic follow-up occurs. The latter can be addressed by simulating the secondary loading by imposed displacements. This problem is not treated in detail, but a method of solution is outlined.

F.1 Introduction

Procedures for determining J for primary (mechanical) loads are now well established, either using the results of elastic-plastic finite element calculations, expressed in convenient parametric form [the EPRI J estimation scheme (Kumar, German, and Shih, 1981)], or approximate analytical methods such as those based on the reference stress approach of Ainsworth (1984). J-integral formulations have also been developed for two-dimensional geometries subjected to combined primary and secondary loads (Ainsworth, Neale, and Price, 1978; Wilson and Wu, 1979), and also for axisymmetric and other three-dimensional structures (de Lorenzi, 1982). However, the situation with regard to existing J solutions for secondary (i.e., thermal, residual, displacement imposed) loads is far less advanced than for the primary loading cases, due, to a large extent, to the variety of such loads, which makes a general characterization of them difficult, if not impossible.

The many complex forms of secondary loads obviate the possibility of developing a compendium of J solutions for these as has been done for primary loads in the elastic-plastic handbooks sponsored by EPRI (Kumar, German, and Shih, 1981). There is, thus, a need to develop and validate alternative approaches which make use of existing elastic-plastic J based methodologies, but which have the flexibility to cope with the wide variety of secondary loads encountered in practical situations. This appendix reviews some of the more promising of these methods and indicates their status as regards validation and generality. A J estimation procedure for treating primary and secondary loads is proposed based on the results of this review.

F.2 Definition of Primary and Secondary Loads and Elastic Follow-up

F.2.1 Primary and Secondary Loads

Primary loads determine the plastic collapse conditions of the structure. Secondary loads are divided into two types: self-equilibrated and non-equilibrated. Self-equilibrated loads induce stresses which integrate to produce zero net force and moments on the structure and do not affect the plastic collapse conditions. Examples are: thermal stresses in simple free standing structures (such as plates and cylinders) which are invariant along the axis of the structure; some forms of welding residual stresses generated by differential changes in the coefficient of expansion; and residual stresses resulting from plastic deformation. Non-equilibrated secondary loads induce stresses which integrate to produce a net force or moment on the structure, but do not influence the plastic collapse conditions, although they may have a significant effect on elastic-plastic fracture behavior prior to plastic collapse. In these cases the magnitude of the secondary loads is frequently related to the stiffness of the structure. An example of non-self-equilibrated loading is displacement imposed loading.

Secondary loads can give rise to technical difficulties only rarely encountered in primary loading situations. For example, severe thermal loading frequently results in localized regions of the structure where the stresses exceed yield, producing plastic enclaves and stress redistribution. In the case of displacement loading there may be a strong interaction between the effective loading

on the crack and the size of the defect due to changes in structural stiffness arising from the presence of the defect (Chell, 1979). These effects should properly be taken into account in determining *J*.

F.2.2 Elastic Follow-up

The term elastic follow-up is used to signify the ability of the structure to increase local strains by plastic yielding or creep deformation while under constant load or displacement. A structure which is thermally loaded would display no follow-up if local strains were not increased by stress relaxation due to plastic deformation. This particular situation, called strain invariance, occurs when the reduction in elastic strains due to stress relaxation is exactly balanced by the inelastic strains causing the relaxation. Although strain invariance during stress relaxation is only rarely realized, even if the stress distribution is self-equilibrated, it is often a very good approximation where inelastic strains are small compared to the elastic strains, such as occurs, for example, when the plastic zone is small and surrounded by a massive elastic matrix.

The effects of secondary stresses on fracture behavior can be enhanced by elastic follow-up in the structure. The most common form of follow-up arises from displacement loading which produces a non-equilibrated stress distribution. However, significant follow-up can also occur in cases where the structure experiences only self-equilibrated stress distributions (e.g., see Section F.4.4).

F.3 Effects of Secondary Loads on Fracture

Methods for obtaining J that include secondary loading should take into account the effects of these loads on fracture behavior in the linear elastic and fully plastic regimes. Secondary loads that induce self-equilibrated stresses will produce different effects to those where the stress distribution corresponds to a resultant non-zero force or moment. Stresses arising from displacement imposed boundary conditions come under the latter category. In these cases the secondary stresses act as if they were induced by primary loads (the sum of the reaction forces at the positions where the displacements are imposed) that decrease as the crack size increases.

It is known from the work of Bueckner (1958) and Heaton (1976) that the stress intensity factor, K_I, due to a secondary load can be determined using the stress distribution in the defect free structure. This kind of calculation can be performed using either strain energy concepts, or an equivalent method which employs a weight function. The weight function is a geometric parameter whose form depends on the geometry of the structure, the crack size and shape, and any restraints that limit deformation of the structure (Rice, 1972). The surfaces of the structure over which displacements are imposed would constitute a restraint: zero prescribed displacements are imposed on these surfaces in the calculation of the weight function. The weight function is not dependent on the form of the stresses or on the origin of their source, e.g., whether they arise due to mechanical, thermal or other causes. If the weight function is known, then the stress intensity factor is obtained by integrating the stress distribution multiplied by the weight function over the area occupied by the crack.

The fact that the stress intensity factors due to primary and secondary loads may be determined using the same weight function implies that the effects of secondary loads in the linear elastic regime is determined solely by their distribution in the structure. Any restraints which arise from surfaces of the structure where displacements (zero or non-zero) are prescribed have similar effects on K_I values determined for mechanically induced stresses as they do on K_I values corresponding to thermal, residual or displacement induced stresses. Thus, in the linear elastic fracture regime, secondary and primary loads that give rise to the same value of stress intensity factor due to similar local stress distributions will contribute equally to the possibility of fracture.

This is not the case in the fully plastic regime where the cracked section has undergone general yielding. One of the theorems used to determine lower bound plastic limit loads states that a structure will not collapse by a yielding mechanism if the applied forces can be balanced by a redistribution of the induced stress so that this nowhere exceeds the yield stress. This implies that self-equilibrated thermal and residual stresses cannot affect the plastic collapse load of the structure. These stresses do not contribute to fracture under fully plastic conditions because, by definition, they correspond to zero net force or moment acting on the structure: in principle they can be redistributed to produce a zero stress everywhere.

Although imposed displacements induce non-self-equilibrated stresses, these stresses alone do not contribute to the plastic limit load since large deformations are required before the plastic collapse mechanisms can operate. These will counter the effects of the imposed displacements, reducing the reaction forces to zero. However, it is important to note that the restraints arising from surfaces on which displacements are prescribed can affect the plastic collapse value of an independently applied primary load by inhibiting the ability of the structure to freely deform, and causing a change in the plastic collapse mechanism.

It is not clear how secondary loads will affect fracture in the transition region between the two extreme failure conditions of linear elasticity and full plasticity. In this regime an elastic-plastic analysis of secondary loads may produce results which can be either more or less onerous than the results of a failure analysis based solely on linear elastic fracture mechanics. It is in the elastic-plastic fracture regime that the results of the various methods of treating secondary loads are liable to differ most, since J estimation schemes are usually designed to include the correct linear elastic and fully plastic fracture behavior.

F.4 Review of Presently Available Methods of Estimating *J* for Combined Loading

F.4.1 The EPRI Scheme

Under EPRI sponsorship, Kumar, Schumacher, and German, have suggested a method for extending the EPRI *J* estimation scheme to thermal and residual stresses. The method was developed taking account of the different effects that secondary loads have on fracture behavior in the elastic and plastic regimes. It was proposed that these effects could be adequately simulated by including secondary loads together with primary loads in the first order plastically corrected linear elastic contribution to *J*. Thus,

$$J(a,P,S) = J^{e}(a_e,P,S) + J^{p}(a,P) \tag{F.1}$$

where a is the crack depth, a_e is an effective crack depth defined below, P and S signify mechanical (primary) and thermal (secondary) loads, and superscripts e and p signify elastic and plastic, respectively.

The expression for J^e is

$$J^{e} = \frac{\left[K(a_e,P) + K(a_e,S)\right]^2}{E'} \tag{F.2}$$

where $E' = E$, Young's modulus, for plane stress, and $E' = E/(1-\nu^2)$ for plane strain.

The effective crack depth a_e is calculated from

$$a_e = a + \phi r_y \tag{F.3a}$$

where

$$\phi = \frac{1}{\left[1 + \left(\frac{P}{P_0}\right)^2\right]} \tag{F.3b}$$

Here P is the applied load, and P_o a corresponding reference load: expressions for this are provided in the EPRI handbooks.

$$r_y = \frac{1}{\beta\pi}\left(\frac{n-1}{n+1}\right)\left[\frac{K(P,S)}{\sigma_o}\right]^2 \tag{F.3c}$$

$\beta = 2$ for plane stress, and 6 for plane strain and axisymmetric cases, and n is the exponent in the Ramberg-Osgood stress-strain equation

$$\left(\frac{\varepsilon}{\varepsilon_o}\right) = \left(\frac{\sigma}{\sigma_o}\right) + \alpha\left(\frac{\sigma}{\sigma_o}\right)^n \tag{F.4}$$

where ε is the strain due to the stress σ, $\varepsilon_o = \sigma_o/E$, and σ_o is a characterizing yield stress. α and n are material constants.

J^p is usually written for a Ramberg-Osgood stress-strain relationship of the form of Equation (F.4) as

$$J^p = \alpha\sigma_o\varepsilon_o a\left(\frac{c}{b}\right)h_1\left(\frac{a}{b},n\right)\left(\frac{P}{P_o}\right)^{n+1} \tag{F.5}$$

The function $h_1(a/b,n)$ is dependent on the type of applied loading (e.g., tension or bending), the geometry of the structure and the crack, the ratio of crack size, a, to section size b, and the strain hardening exponent, n. The remaining ligament, $c = b - a$. P_o is a reference load which, in many instances, is equivalent to the general yield load for the defective section. Expressions for P_o, and tabulated values for $h_1(a/b,n)$, are given in the EPRI handbooks which detail the J solutions (Kumar et al., 1981; Kumar et al., 1984b; Zahoor, 1989). The specific form of Equation (F.5) and the chosen dimensional normalizations may vary from geometry to geometry.

In the fully plastic regime, where $J^p >> J^e$, equation (F.1) predicts the desired physical result that secondary loads do not affect fracture behavior at or near plastic collapse.

Kumar et al. (1984b) present validation for this approach by comparing J values calculated from finite element methods with those produced by the estimation procedure for four different geometries subjected to combined mechanical and thermal loading. The results of this comparison are summarized in Table F.1 where R is the internal radius of the cylinder. The agreement between the results of the procedure and the numerical calculations is good. This agreement should be qualified by the observation that the thermal loads were not severe enough to produce significant elastic-plastic crack tip loading conditions.

The EPRI scheme does not provide advice for situations where the combined mechanical and secondary stresses exceed yield in the defect free structure, producing a plastic enclave in the region of the defect.

F.4.2 The R6 Method

The R6 procedures (Milne et al., 1986), developed by the power generation industry in the United Kingdom, enable the integrity of structures containing defects to be ascertained. The latest version (R6 [Revision 3]) employs a J estimation scheme based on the reference stress approach of Ainsworth (1984). For the purposes of this report it is not necessary to discuss the procedures in detail but to describe, in terms of J, the way that combined primary and secondary loads are treated within Option 2 of the procedures. This option is based on a material specific method of estimating J.

In the Option 2 approach J is written for mechanical loads as

$$J(a,P) = J^e(a,P)F\left(\frac{P}{P_y}\right) \tag{F.6}$$

where F is a function of the stress-strain ($\sigma - \varepsilon$) relationship and P_y is the general yield load of the cracked structure. Note that P_y in general does not equal P_o, which appears in the EPRI scheme, although the two are often the same, or closely related.

The function F is defined as

$$F\left(\frac{P}{P_y}\right) = \frac{E\varepsilon_{ref}}{\sigma_{ref}} + \frac{0.5\sigma_{ref}\left(\frac{P}{P_y}\right)^2}{\left(E\varepsilon_{ref}\right)}, \quad for \quad \frac{P}{P_y} < \frac{P_1}{P_y} \tag{F.7}$$

$$F\left(\frac{P}{P_y}\right) = \infty, \quad for \quad \frac{P}{P_y} \geq \frac{P_1}{P_y}$$

Table F.1. Summary of J solutions used to validate the EPRI approach

Geometry description	a/b	Peak thermal stress/yield	Accuracy*	Source reference
Single edge cracked plate	0.25	0.37	Good	Kumar et al. (1984a)
Single edge cracked plate	0.25	0.74	Good	Kumar et al. (1984a)
Center cracked plate	0.25	1.04	Good	Kumar et al. (1984a)
Axially cracked cylinder (R/b=10)	0.25	0.53	Good	Kumar et al. (1984a)
Axially cracked cylinder (R/b=10)	0.25	1.06	Good	Kumar et al. (1984a)
Circumferentially cracked cylinder (R/b=10)	0.25	2.75	Fair	Kumar et al. (1984a)

- The accuracy is judged against the computed results for the secondary load, and the combined secondary and primary loads.

  Good = Within 10% of computed J solutions
  Fair = Generally within 10-20% of computed J solutions

where

$$\sigma_{ref} = \left(\frac{P}{P_y}\right)\sigma_{ys} \tag{F.8}$$

$$\frac{P_1}{P_y} = \frac{(\sigma_{ys} + \sigma_{ult})}{2\sigma_{ys}} \tag{F.9}$$

and σ_{ref} is a reference stress and ε_{ref} is the corresponding reference strain obtained from the uniaxial stress-strain relationship. P_l is the plastic collapse load, σ_{ys} and σ_{ult} are the yield stress and ultimate strength. For non-hardening materials, where σ_{ys} equals σ_{ult}, the collapse load, P_1, equals the general yield load, P_y. Equation (F.9) takes credit for the strain hardening capability of the material by assuming that plastic collapse will take place with a flow stress equal to half the sum of the yield and ultimate stresses. Verification for the use of F is provided in the validation section of the R6 procedures (Milne et al., 1986) and by Ainsworth (1984).

If secondary loading is also present then the expression for J is modified to read

$$J(a,P,S) = \frac{J^e(a,P,S)F\left(\frac{P}{P_y}\right)}{\left[1 - r(x)F^{1/2}\left(\frac{P}{P_y}\right)\right]^2} \tag{F.10}$$

where

$$r(x) = r_1(x) \quad for \quad 0.8 \le \frac{P}{P_y}$$

$$r(x) = 4r_1(x)\left(1 - \frac{P}{P_y}\right) \quad for \quad 0.8 < \frac{P}{P_y} \le 1.05 \tag{F.11}$$

$$r(x) = 0 \quad for \quad 1.05 < \frac{P}{P_y}$$

and

$$r_1(x) = 0.1x^{0.714} - 0.007x^2 + 0.00003x^5, x < 5.2$$

$$r_1(x) = 0.25, x > 5.2 \tag{F.12}$$

where $x = K_I(S)P/K_1(P)_y$.

The parameter r characterizes the plasticity interaction between primary and secondary loads. Equations (F.10) and (F.11) predict that the effect of the secondary load on plasticity decreases as the primary load approaches the general yield load of the defected section: r becomes zero for loads exceeding 1.05 times the yield load. The complex form of r (its dependence on r_1 and x) was empirically chosen to pessimistically bound analytical and computed J behavior, and it has no simple physical interpretation.

Note that, unlike the EPRI scheme, secondary loads continue to affect the plastic component of J after general yielding through the dependence of J^e in Equation (F.10) on $K_I(S)$. However, this dependence has little influence on the predicted fracture behavior in the fully plastic regime because this behavior is not sensitive to the value of J, but is predominantly determined by the plastic collapse load, as schematically shown in Figure F.1. In this figure, the critical load, P_f, and critical defect size, a_f, are shown corresponding to $J=J_{Ic}$, where the toughness, J_{Ic}, is high enough to result in failure above general yield. It can be seen that, in this plastic failure regime, doubling the toughness to $2J_{Ic}$ can make little difference to the values of the critical load and crack size, which are bounded by the values of P_1 and a_1, the values corresponding to plastic collapse.

The R6 procedures do not explicitly account for plastic relaxation of the combined primary and secondary stresses in the structure, should the peak stress value exceed yield magnitude. The R6 procedure recommends that J^e be evaluated always from a linear elastic stress analysis, and no credit is taken for possible stress relaxation.

Verification for the R6 treatment of secondary loads is contained in the validation section of the procedure (Milne et al., 1986), where it is discussed in terms of the failure assessment diagram concept. The failure assessment diagram provides an alternative way of performing a J analysis, and produces results which are equivalent to a J analysis. The validation exercise demonstrates that the R6 procedures will predict conservative (safe) estimates for J in most circumstances (see Table F.2 for a summary of the J solutions used in the validation). This is consistent with the philosophy behind the R6 procedures, which is to perform a failure avoidance analysis, rather than to predict failure per se.

The one instance in the validation exercise where the R6 procedures proved to be non-conservative is identified in Table F.2. In this case the defect was very small relative to the tensile plastic enclave generated from the secondary loading in the defect free structure. The stress and strain distributions in this zone were deliberately chosen to be approximately uniform, and not to display the steep gradients which are typical of most thermal loading situations. This resulted in the J behavior being similar under the maximum applied thermal loading to that for a defect subjected to a uniform primary stress of yield point magnitude.

Currently the R6 procedures are being modified in order to remedy situations where the procedures are known to be unconservative. These modifications are discussed in more detail in Section F.4.4.

F.4.3 Chell's Approach

The R6 procedure does not exclude the use of alternative procedures for determining J in the presence of secondary loads, and recognizes that these may remove some of the pessimisms inherent in the R6 treatment of severe secondary loading. In particular, the approach adopted by Chell (1986) is mentioned as one that attempts to take credit for plastic stress relaxation.

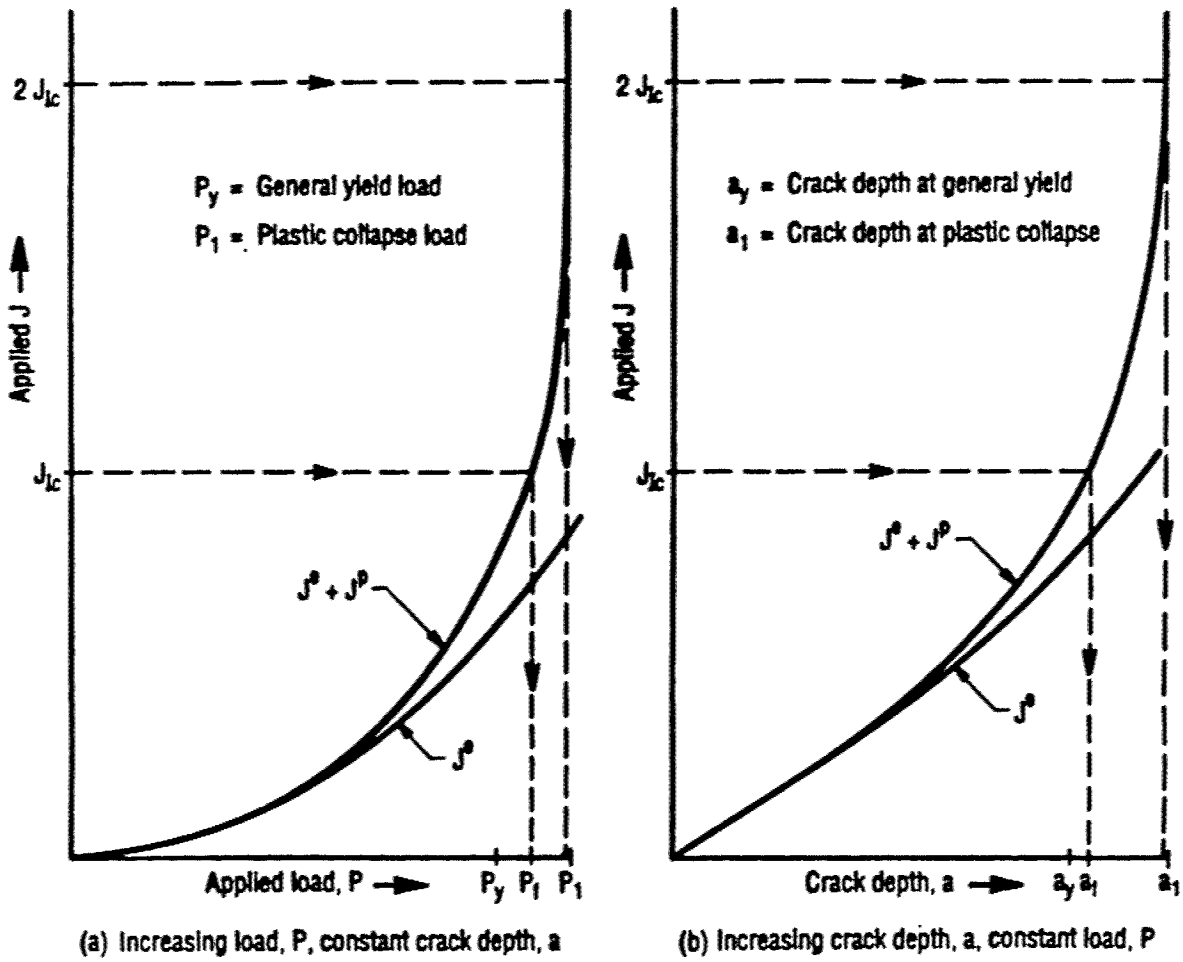

Figure F.1. Above general yield the failure load (P_f) and critical crack size (a_f) become increasingly insensitive to toughness, J_{Ic}, and hence J.

Table F.2. Summary of *J* solutions used to validate the R6 (Revision 3) approach

Geometry description	a/b	Peak thermal stress/yield	Accuracy*	Source reference
Center cracked plate	0.2	1.11	Conservative	Hellen and Blackburn (1985)
Center cracked plate	0.2	1.11 **	Conservative	Hellen and Blackburn (1985)
Center cracked plate ***	0.05	1.0	Unconservative	Casper (1986)
Center cracked plate	0.05	1.0 **	Conservative	Casper (1986)
Circumferentially cracked cylinder (R/b=0.53)	0.07	4.5	Conservative	Muscati (1985)
Circumferentially cracked cylinder (R/b=0.53)	0.225	3.97	Conservative	Muscati (1985)

* The accuracy is judged against the computed results for the secondary load, and the combined secondary and primary loads.

Conservative = Safe when applied with R6 (Revision 3) procedures
Unconservative = Unsafe when applied with R6 (Revision 3) procedures

** In this case the thermal load was superimposed on an existing mechanical load in order to study load history effects.

*** These results were for the case where the secondary stress was at tensile yield point magnitude in the central half of the plate, and at compressive yield either side of this. The defect was embedded in a plastic zone 10 times its own size.

The approach of Chell (1986) is based on the R6 *J* estimation scheme but extends a previous treatment of secondary loads (Chell, 1979) to include the effects of strain hardening and stress relaxation. The crack tip plasticity interaction between primary and secondary loads is characterized by first order plasticity theory which is re-expressed in the form of a reference load for the combined loading. This modified load is constructed so that it reduces to the plastic collapse load of the structure as the value of the mechanical load approaches this collapse load. The evaluation of the term J^e is also based on the elastic-plastic stress profile in the component. These two features mean that the value of $J(a,P,S)$ evaluated in this scheme reduces to the value of $J(a,P)$ as the primary load increases towards the value required to cause general yield of the defect free component. In other words, the influence of secondary loads on fracture behavior is diminished towards zero as plasticity becomes widespread and "shakes out" the secondary stresses as illustrated in Figure F.2. This figure shows the stress intensity factor for a defect subject to a primary, and a combined primary and secondary load. For illustrative purposes, the defect has been chosen small enough to be within the uniform tensile stress part of the secondary stress distribution, which is of magnitude equal to half

the yield stress. As the uniform primary stress is increased, the stress intensity factor for the combined loading increases linearly until the value of the primary stress exceeds half yield. For a non-hardening material, the stress intensity factor becomes constant and independent of the applied primary stress beyond this point, because plastic deformation prevents any further elevation in the tensile stress region of the combined stress distribution. The effects of the secondary stress are completely wiped out when the yield stress reaches yield magnitude, and the stress intensities for the combined and primary loads become equal.

The first stage in Chell's method is the evaluation of $J^e(a_e', S)$, the elastic component of J due to secondary loads only. This is done in a similar way to that used in the EPRI scheme, except that the effective crack depth, a_e' replaces a_e, where

$$a_e' = a + r_y \tag{F.13}$$

[If the peak secondary stress exceeds yield then the elastic-plastic stress profile should be used when evaluating J^e, compare Figure F.2. A simple approximate method for estimating this profile from the results of a linear elastic stress analysis is detailed in (Chell, 1986).] This first order plastic estimation of J^e is evaluated and used to determine an equivalent primary loading, P_s, characterized by the ratio P_s/P_y', which would produce similar crack tip plasticity results to the secondary loading. This is done using Equation (F.6), the R6 Option 2 approximation to J for primary loading, and writing

$$J^e(a_e', S) = J(a, S) = J^e(a, S) F\left(\frac{P_s}{P_y'}\right) \tag{F.14}$$

where F is the function defined by Equation (F.7). The value of the unknown ratio P_s/P_y' may be determined from Equation (F.14). The term, $F(P_s/P_y)$ accounts for crack tip plasticity due to the secondary loads, as characterized by the ratio $J^e(a_e', S)/J^e(a, S)$.

If a primary load is superposed on the secondary load then the expression for J for the combined loading is defined as

$$J(a, P, S) = J^e(a, P, S) F\left(\frac{P_{ps}}{P_y'}\right) \tag{F.15}$$

where the ratio P_{ps}/P_y' characterizes a primary load which would produce the same crack tip plasticity effects as the combined primary and secondary loads. The load ratio is given by the equation

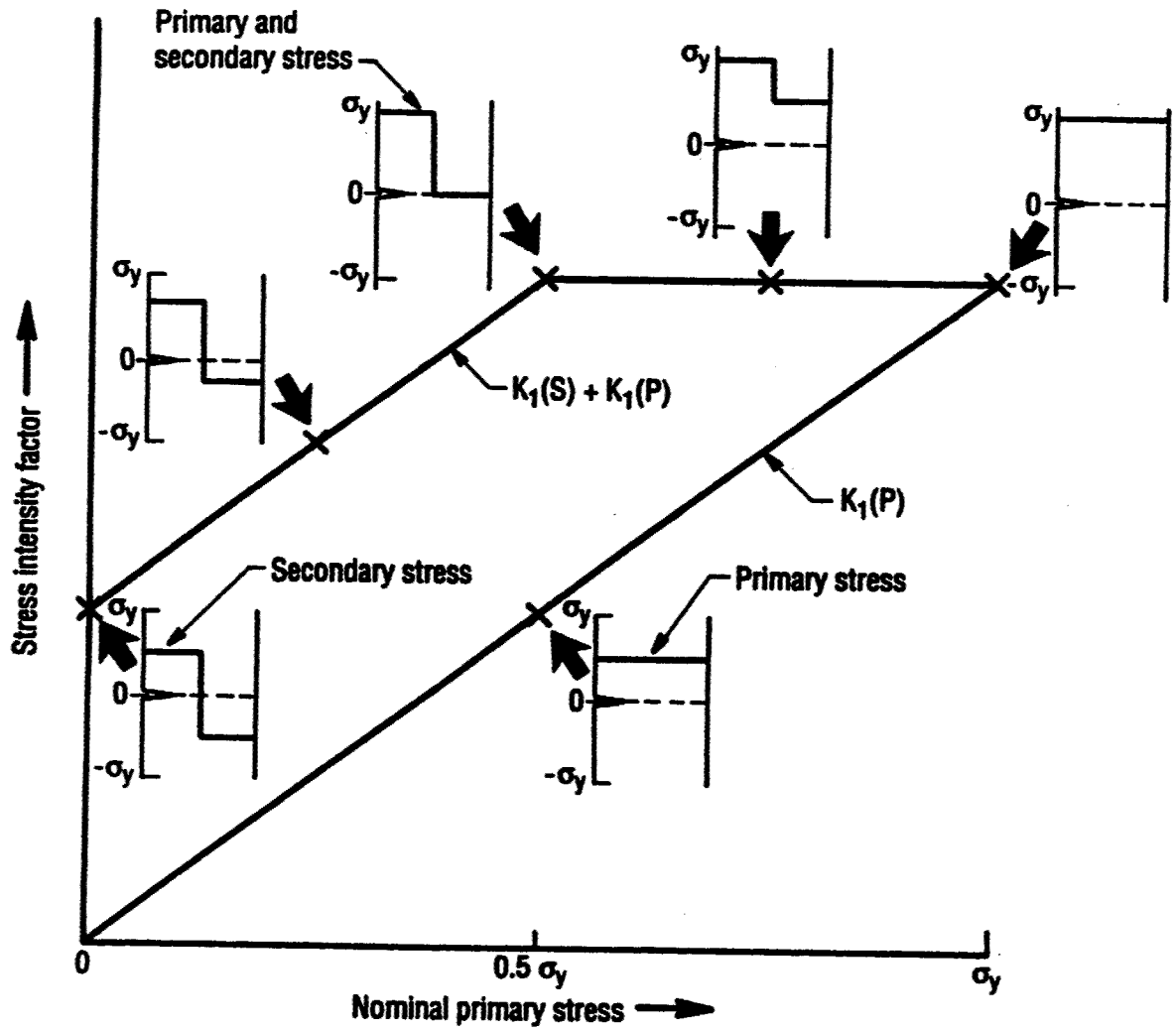

Figure F.2. High primary loads "shake out" the effects of secondary loads.

$$\frac{P_{ps}}{P_y'} = \frac{P}{P_y} + \frac{P_s}{P_y'} - \frac{\left(\frac{P}{P_y}\right)\left(\frac{P_s}{P_y'}\right)}{\left(\frac{P^*}{P_y}\right)}, \quad if \quad \frac{P}{P_y} \le \frac{P^*}{P_y} \tag{F.16}$$

$$\frac{P_{ps}}{P_y'} = \frac{P}{P_y} \qquad \frac{P}{P_y} < \frac{P^*}{P_y}$$

where $P^*/P_y = \min(P_1/P_y, 1.25)$.

This equation is empirically derived and allows secondary loads to fully contribute, through the first order plasticity term P_s/P_y', to crack tip plasticity in the small scale yielding regime, but reduces their influence as either plastic collapse is approached, or, if the material has a large capacity to strain harden, when the primary load exceeds 1.25 of the general yield load. Figure F.3 shows how the equivalent primary load ratio, P_{ps}/P_y', varies as the primary load increases, for different levels of crack tip plasticity due to a secondary load S. The effects of the secondary load are quantified by the ratio P_s/P_y', which in turn is related through Equation (F.14) to the first order crack tip plasticity correction signified by a_e'. In situations where $P/P_y > 1.25$, and stress relaxation has "shaken-out" the secondary stresses (compare Figure F.2), then Equations (F.15) and (F.16) predict $J(a,P,S)=J(a,P)$, as required on physical grounds.

Chell (1986) has validated his approach using published elastic-plastic J results for combined primary and secondary loads, including all the results reported in the EPRI handbooks. The results of this exercise are summarized in Table F.3. In general, the agreement between the estimated J and the computed J values is good, especially if the Option 2 material dependent function $F(P/P_y)$ is replaced by a function that reproduces the computed J values for the primary load. However, there was one instance where his approach underestimated the computed J values. This was the case of a small fully circumferential defect (less than 7% through the wall) in a thick cylinder subjected to very severe thermal loading, such that the peak stress determined from linear elastic theory exceeded 4 times the yield stress. Chell attributed this discrepancy to the fact that the defect was embedded in a massive plastic enclave generated by the severe thermal loading. The plastic zone in the defect free cylinder due to the thermal loading alone extended over a third of the way through the wall. Care should be exercised when applying the Chell method to these kinds of situations.

Note that the under-prediction of J using the Chell approach could be due, in part, to elastic follow-up, as his method does not make allowance for the increase in plastic strain due to stress relaxation: only the redistributed stresses are used in the calculation of $J^r(a,S)$ and $J(a,P,S)$ in Equations (F.14) and (F.15) respectively.

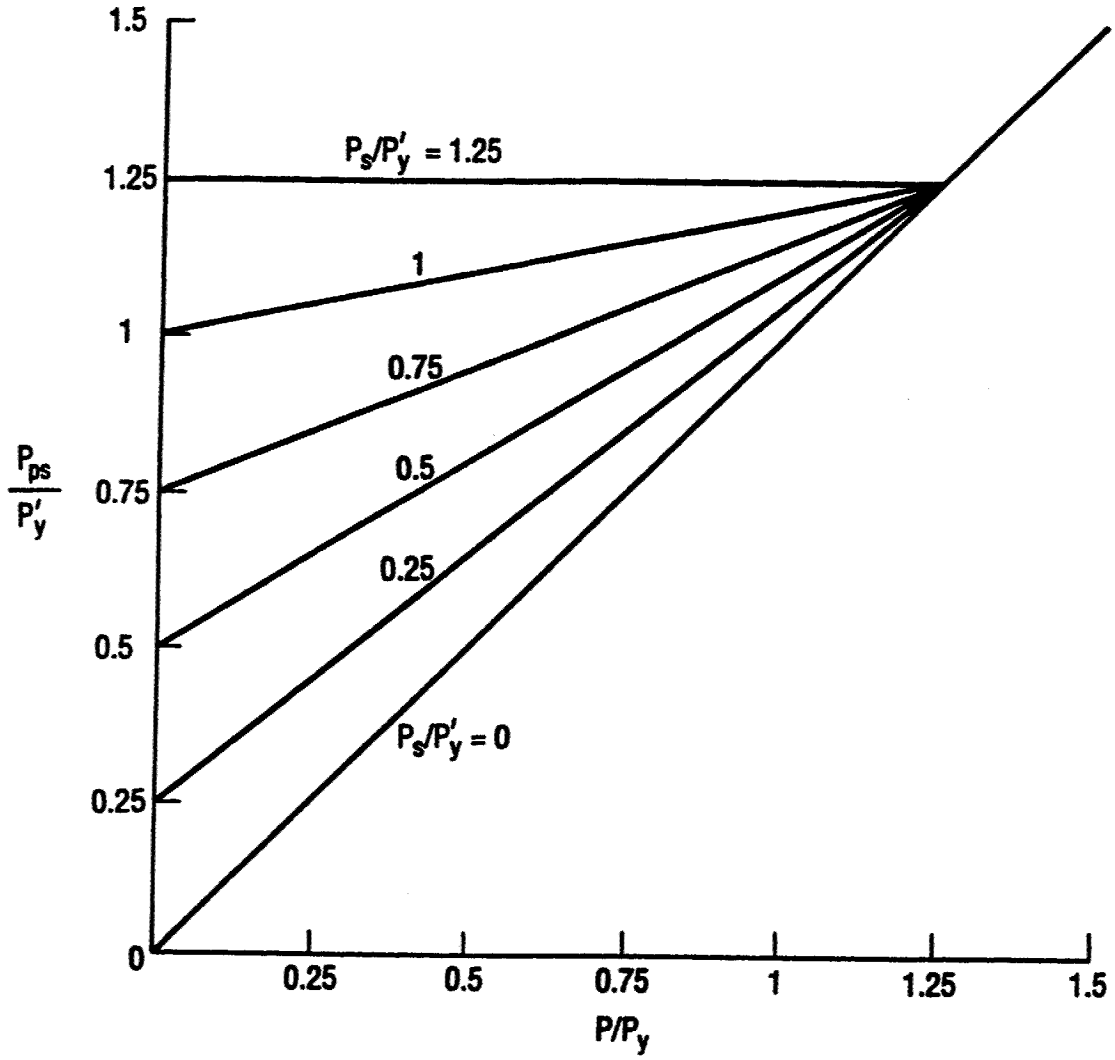

Figure F.3. Variation of P_{ps}/P_y' for different combinations of primary P/P_y and secondary P_s/P_y' loads.

Table F.3. Summary of *J* solutions used to validate the Chell approach

Geometry description	*a/b*	Peak thermal stress/yield	Accuracy*	Source reference
Single edge cracked plate	0.25	0.37	Good	Kumar et al. (1984a)
Single edge cracked plate	0.25	0.74	Good	Kumar et al. (1984a)
Center cracked plate	0.25	1.04	Good	Kumar et al. (1984a)
Axially cracked cylinder (*R/b*=10)	0.25	0.53	Good	Kumar et al. (1984a)
Axially cracked cylinder (*R/b*=10)	0.25	1.06	Good	Kumar et al. (1984a)
Circumferentially cracked cylinder (*R/b*=10)	0.25	2.75	Fair	Kumar et al. (1984a)
Center cracked plate	0.2	0.59	Good	Hellen and Blackburn (1985)
Center cracked plate	0.2	1.11	Fair	Hellen and Blackburn (1985)
Center cracked plate	0.2	1.11**	Good	Hellen and Blackburn (1985)
Circumferentially cracked cylinder (*R/b*=0.53)	0.07	1.25	Fair	Muscati (1985)
Circumferentially cracked cylinder (*R/b*=0.53)	0.07	4.5	Poor	Muscati (1985)

* The accuracy is judged against the computed results for the secondary load, and the combined secondary and primary loads.

Good = Within 10% of computed *J* solutions
Fair = Generally within 10-20% of computed *J* solutions
Poor = Generally differ by more than 20% from computed *J* solutions

** In this case the thermal load was superimposed on an existing mechanical load in order to study load history effects.

F.4.4 Proposed Modification to the R6 Approach

Evidence has been accumulating that the R6 treatment of secondary loads is not conservative in some cases. Areas of particular concern are where the secondary loads generate appreciable elastic follow-up in the structure, and where small defects are located in sensibly uniform stress fields produced by the secondary loading (see Section F.4.2). To try and overcome these difficulties, a modification to the R6 treatment has been proposed by Budden (1989) based on an approach

suggested by Bhandari, Charif D'Ouazzane and Faidy (1984). They proposed using a modified Neuber principle (Neuber, 1961) to utilize the results of an elastic-plastic stress analysis of the defect free structure in order to construct an effective stress intensity factor.

In simplified outline, the approach is as follows. The stress intensity factor K for crack depth a is determined from linear elastic theory using two stress profiles: the first profile corresponds to the actual secondary load stress distribution in the defect free body, and results in a K value of $K_{(1)}(a)$; the second profile is obtained from the computed elastic-plastic strains assuming linear elastic theory to derive a pseudo-stress profile normal to the crack plane, and has a value of $K_{(2)}(a)$. An effective crack depth, a_e', is calculated using $K_{(1)}(a)$. The effective stress intensity factor for the secondary loading, $K_{(3)}(a)$ is then evaluated from the square root of the product:

$$K_{(3)}(a) = \left[K_{(1)}(a_e')K_{(2)}(a_e')\right]^{1/2} \qquad \textbf{(F.17)}$$

The R6 procedure for estimating J, as described in Section F.3.2, is then followed with $K_{(3)}(a)$ replacing $K(S)$ in the relevant equations.

Budden (1989) provides validation for the method based on the results of elastic-plastic finite element computations for J and the computed elastic-plastic stress and strain fields in the defect free structure. He demonstrated that the method is conservative for all the cases he analyzed. Table F.4 provides a summary of this validation work. Unfortunately, the cases analyzed did not include the small defect in a center cracked panel that produced non-conservative results when analyzed according to R6 (Revision 3) (see Table F.2). However, they did include the cases where cracked cylinders were subjected to a linear axial temperature gradient which was symmetrical about the center of the cylinders. The computed J results for these cylinders indicated that significant elastic follow-up was generated by plastic deformation under the thermal loading alone, and this resulted in the elastic-plastic J values exceeding the linear elastic values.

The reason for this follow-up has been identified by Bradford (1987). He showed that for thin cylinders the axial temperature variation is equivalent to an imposed radially symmetric rotation at the symmetry plane which produces a radially symmetric bending moment. When the cylinder is cracked, this rotation is imposed on the remaining uncracked ligament only, which results in a reduction in the bending moment.

Table F.4. Summary of *J* solutions used to validate the Budden approach

Geometry description	*a/b*	Peak thermal stress/yield	Accuracy*	Source reference
Center cracked plate	0.2	1.11	Conservative	(Hellen and Blackburn, 1985)
Center cracked plate	0.2	1.11**	Conservative	(Hellen and Blackburn, 1985)
Circumferentially cracked cylinder (*R/b*=10)	0.37	4.22***	Conservative	Reported in (Budden, 1989)
Circumferentially cracked cylinder (*R/b*=100)	0.37	5.94***	Conservative	Reported in (Budden, 1989)

* The accuracy is judged against the computed results for the secondary load, and the combined secondary and primary loads.

Conservative = Safe when applied with R6 (Revision 3) procedures.

** In this case the thermal load was superimposed on an existing mechanical load in order to study load history effects

*** The thermal load was applied in the form of a linear variation of temperature along the cylinder axis. The temperature variation was symmetrical about the plane of the defect. This form of loading results in elastic follow-up.

F.5 Treatment of Elastic Follow-up Due to Imposed Displacements and Rotations

As illustrated in Section F.4.4, under the right conditions thermal loading can manifest itself in the form of an equivalent imposed rotation. Similarly, secondary stresses may also arise due to imposed displacements, either implicitly (as was the case for the rotation of the thin cylinder discussed in Section F.4.4) or explicitly. It is possible to treat these cases provided that the boundary conditions consistent with the prescribed nature of the loading can be defined. However, if more than one load type is involved, as is the case for a mechanical load independently applied to a structure subjected to imposed displacements, then proportional loading has to be assumed. Usually this assumption does not present a serious impediment to the use of the available methods.

The approach to solving the imposed displacement problem in the elastic-plastic fracture mechanics regime has been described by Chell (1979). He used the R6 procedures to formulate an expression for *J*. A similar method was adopted by Bradford (1987), in his treatment of a thin cylinder subjected to an imposed rotation. Briefly, in these approaches the displacement loading is

simulated by a set of equivalent primary loads whose magnitude changes as the crack size changes. The equivalent primary loads are given by the reactive forces at the positions where the displacements are imposed. The magnitude of the equivalent primary loads are determined by the requirement to maintain constant displacement values at these positions.

Hence, given a known form for J, and the compliance, C°, of the defect free structure, then for imposed displacements Δ which reproduce the secondary stresses in the defect free structure, an effective primary (reactive) load P_s can be obtained from the equation (see Endnote F.1)

$$\Delta = P_s(a)C_{ss}^{o} + P_p C_{sp}^{o} + \frac{d}{dP_s}\int_A J\left(a', P_s(a), P_p\right)dA \qquad \textbf{(F.18)}$$

where C_{ss}^{o} and C_{sp}^{o} are the compliances relating the applied forces P_s and P_p respectively to the corresponding displacements at the point of application of P_s, A is the area occupied by the defect, and P_p an independently applied mechanical load. The term containing the integral represents the displacement contribution arising from the presence of the defect. The load $P_s(a)$ remains constant during the integration over the area A and the dummy variable, a'. Once P_s, which is a function of the crack size a, is determined, the value of J for the secondary load is given by $J(a,P_s(a),P_p)$. In the evaluation of $J(a,P_s,P_p)$, P_s is treated as if it were a primary load and the secondary stresses are assumed to scale according to the ratio $P_s(a)/P_s(a=0)$. Equation (F.18) pertains to a single secondary load, but in principle the concepts can be applied to more complicated combinations of primary and secondary loads, although the equivalent formulation to Equation (F.18) becomes correspondingly more complicated (see Endnote F.1).

F.6 Comparison of Methods

Four approximate methods have been described for estimating J for combined primary and secondary loads: an EPRI scheme, the R6 method, an approach due to Chell, and a modified R6 procedure. Each of the methods has certain advantages and disadvantages.

The EPRI estimation scheme is the simplest method to apply as it incorporates the effects of secondary loads in J through an effective crack length term appearing in the elastic component J^e. This can be derived from a linear elastic stress analysis. However, this approach could lead to unacceptable over-estimations of J if appreciable plastic relaxation of the peak secondary stresses occurs. On the other hand, it may not adequately represent the severity of the secondary loading if this generates significant elastic follow-up in the structure. The method has limited validation based on mechanical loads superposed on moderate thermal loads.

The R6 Option 2 method for estimating J is more complicated to apply than the EPRI scheme and currently suffers from the same disadvantages. The validation section of the R6 procedures demonstrates that the approach will predict conservative values for J for combined primary and secondary loads, except where elastic follow-up is significant, or where the secondary loads produce high uniform stresses in the region of the defect. The physical basis of the R6 treatment of

secondary loads is not clear, and this can lead to anomalous situations. For example, the treatment becomes ill defined when only a secondary load is applied to a structure as the term, r, which incorporates the effects of crack tip plasticity on J, is not defined in the absence of a primary load [compare Equation (F.12)].

The approach described by Chell is based on similar principles to the R6 Option 2 method, but includes the effects of secondary loads on crack tip plasticity in a more physically meaningful way. It also takes credit for the relaxation of severe secondary stresses by plastic deformation. However, the approach does not take account of elastic follow-up effects, and has been shown to under-predict the value of J for small defects embedded in extensive plastic enclaves resulting from extreme thermal loading.

The modified R6 method uses the Neuber principle to construct an effective, plastically corrected, stress intensity factor for the secondary loading which is then used in the R6 procedure instead of the corresponding stress intensity factor. The method appears to have little, if any, physical justification, as the way that the Neuber principle is employed is far removed from the application for which it was originally proposed. It must, therefore, be considered to be an empirically based methodology. However, it allows the R6 method to take credit for plastic relaxation in the secondary stresses, and it supposedly incorporates some of the effects due to elastic follow-up. Its major disadvantage is that it adds an extra layer of complexity onto a scheme, the physical basis of which appears to be obscure.

F.7 A Recommended Procedure for Determining J for Combined Primary and Secondary Loads

None of the four approaches discussed in the previous section is suitable without modification for assessing J under combined primary and secondary loads. A new approach is required which retains the best of the technical advances that have been made, and builds on these to try and overcome the deficiencies which have been identified. The new approach should be as simple as possible to use, while at the same time pragmatically addressing important aspects of the problem, such as the effects of stress redistribution due to plastic deformation.

Consideration of the data listed in Tables F.1 through F.4 shows that the approach of Chell is the most widely validated of the four approaches. It also has a number of advantages over the other three methods. The approach allows elastic-plastic stress re-distribution to be treated, while avoiding the complexities of the method being adopted for the R6 (Rev 3) procedures (Budden, 1989). The EPRI scheme(Kumar, Schumacher, and German, 1984b) presently does not address the problem of stress relaxation and consequently would be overly pessimistic for cases of severe secondary loading which resulted in extensive plastic deformation. Furthermore, fatigue crack growth is sensitive to the fatigue stress ratio (the load at the minimum part of the cycle divided by the load at the maximum part), and the value of this quantity will depend on the assumptions made in the stress analysis. A linear elastic analysis will produce a different ratio to the result of an elastic-plastic stress analysis, which is more appropriate under cyclic elastic-plastic conditions.

A fundamental assumption made in Chell's approach, which will also be assumed in the recommended procedure described below, is that the value of J for the combined primary and secondary loads is independent of the order in which the loads are applied. This is equivalent to assuming that non-linear elastic deformation will produce results which are in good agreement with those derived using incremental plasticity theory. In the procedure outlined below, the effects of secondary loads are first addressed, and then an expression for J is determined after the primary load is superimposed on the secondary load.

The earlier approach of Chell has been modified in the new procedure to avoid the problem of under-predicting J in situations where the defect is embedded in a plastic enclave. In these cases, the first order plastic correction to the stress intensity factor for the secondary loads, which Chell calculates using the elastic-plastic stress profile, is replaced by the maximum of the stress intensity factor determined from the linear elastic stress profile for the actual defect size, and the value determined following a procedure that uses an effective crack size (see Section F.4.3).

An option has been added to the recommended procedure to enable the user to take advantage of available J solutions for the primary load alone. Chell (1986) found better agreement between his method and computed finite element J solutions for the combined loading cases when the known primary load J solutions were used in preference to the reference stress approximation.

A flow chart detailing the steps to be followed in evaluating J for combined primary and secondary loads is given in Figure F.4. This figure references parts of this section which contain more details concerning the steps in the procedure. In order to reduce the technical complexity, and to highlight the main principles involved, the procedure is written only for defects with one degree of freedom (i.e., defects that are far longer than they are deep). The extension of the procedure to defects with more degrees of freedom (such as surface breaking semi-elliptical cracks) is relatively straightforward and is described in Endnote F.2.

The following sections relate directly to the procedural steps contained in the flow chart in Figure F.4, and should be read in conjunction with that chart.

F.7.1 Stress Analysis

The loads on the structure should be classified as primary or secondary. A definition of primary and secondary loads is provided in Section F.2. If there are any doubts concerning the load classification, then it is prudent to assume that the load is primary in nature. Initially, a linear elastic stress analysis should be performed to obtain the stress distributions in the region of the structure being analyzed.

F.7.2 Determination of J for Primary Loads using EPRI Solutions and Reference Stress Methods

An estimation of J based on the EPRI scheme may be obtained for primary loads by using equations (F.1), (F.2), and (F.5), with the secondary load, signified by S, set to zero. The values for

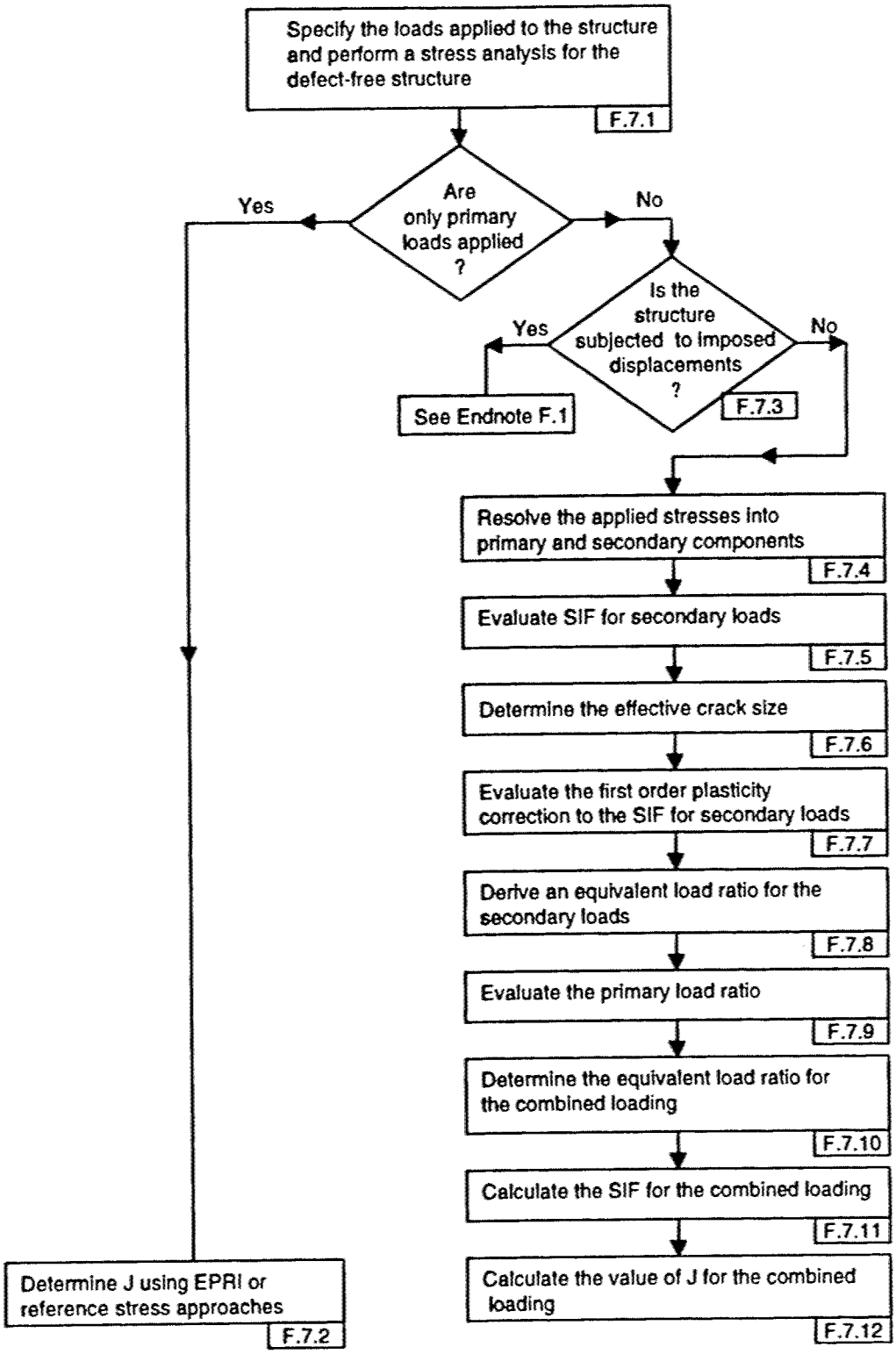

Figure F.4. Flow chart illustrating the steps and decision in the procedure for determining *J* for combined loads. The section references indicate where more information can be obtained in the main text.

the functions $h_J(a/b,n)$ may be obtained from the elastic-plastic handbooks (Kumar, German, and Shih, 1981; Kumar, Schumacher, and German, 1984b; Zahoor, 1989). The elastic component of J, J^e, can be also evaluated from Equation (F.5) by setting n=1 and α=1.

Equations (F.6) through (F.9) define J using the reference stress approach of R6. J^e can be evaluated using Equation (F.2), and expressions for $K(a,P)$ can be obtained from either the compendium of solutions (Sih, 1973; Tada, Paris, and Irwin, 1985; Murakami, 1987), or using computer codes such as NASCRAC and NASGRO. A compendium of general yield and plastic collapse loads, P_y and P_l respectively, are given by Miller (1988) for a range of defective structural geometries.

F.7.3 Prescribed Displacements

Secondary loads which manifest themselves in the form of imposed displacements require special treatment. A detailed discussion of imposed displacements is not given here, although a brief description on how these conditions can be addressed is provided in Endnote F.1.

It is only possible to give general guidance on the circumstances under which thermal and residual loads may be simulated by prescribed displacements or rotations. In practice, there are many specific factors which can influence the way secondary loads affect fracture behavior. These are related to the form of the loading, the resulting stress distribution in the structure, and the potential for elastic follow-up due to the geometric nature of the structure.

The most obvious indication that secondary loads may be acting like displacement imposed loading is when the stress distribution across the section of interest is non-self equilibrated. Steady state temperature distributions that vary through the structure, as well as across the section wall, are likely to produce long range effects that may manifest themselves in the form of elastic follow-up. In contrast, stresses that result from situations involving thermal shock, such as quenching or sudden start-up, are likely to produce self-equilibrated stresses whose effects are localized. Similarly, the process of welding two components may induce long range stresses due to the restraining influence of the structure on the components resulting from shrinkage during cooling of the weld. On the other hand, localized welding residual stresses, which are self-equilibrated, may arise due to inelastic deformation produced in the welding process, or from differences in the expansion coefficients between weld and base materials.

At this time, the complex factors affecting the behavior of secondary loads mean that an engineering judgement has to be made as to how they are to be treated for each particular case, taking into account the specific aspects related to each case. If there is justifiable doubt concerning the classification of a secondary load, then it is prudent to treat this load as primary.

F.7.4 Primary and Secondary Components of Stress

In a linear elastic fracture mechanics analysis it is not necessary to resolve the applied stress distributions into primary and secondary load components. However, this is required in elastic

plastic fracture mechanics because the secondary loads behave differently to primary loads as crack tip plasticity develops and becomes widespread. The resolution of the stresses is straightforward if independent stress analyses are performed for the different load cases, but this is not always done, particularly if the load history experienced by the component involves complicated start-up and shut-down procedures. In these latter cases, the primary loads can be identified by integrating the stresses across the section to obtain the net tensile force and moment acting on it. These loads can be represented by a linear stress distribution, chosen to balance the force and moment. The difference between this linear profile and the profile for the combined loading represents the self-equilibrated secondary stress distribution. This method of identifying the primary and secondary stress distributions is approximate, and pessimistically combines the primary and non-self equilibrated secondary load components into a single effective primary load.

The secondary loads (due to thermal and residual loads) result in the secondary stress distribution, σ_s. Under linear elastic conditions, the total secondary stress distribution, σ_s^{tot}, is equal to σ_s plus $\sigma_s(P)$. The total stress distribution due to all the applied loads, σ^{tot}, is equal to σ_s^{tot} plus σ_p.

If the combined peak values of σ_s^{tot} or σ^{tot} exceeds yield magnitude, then plastic straining and stress relaxation will occur. A pessimistic estimate for J will result from ignoring these effects, and basing the analysis on the linear elastic stress results. However, it may be considered desirable to take credit for the benefits of stress relaxation. Also, as previously mentioned, plasticity can significantly change the value of the load ratio used in fatigue crack growth analyses.

If σ_s^{tot} exceeds yield then the elastic-plastic stress distribution, $\bar{\sigma}_s^{tot}$, corresponding to σ_s plus $\sigma_s(P)$ should be calculated for the current primary load level P. The plastically relaxed stress field, $\bar{\sigma}^{tot}$, corresponding to the total linear elastic stress distribution, σ^{tot}, should also be determined.

Since the proposed procedure uses only the values of stress that result from the elastic-plastic stress analysis, then simple methods of stress analysis may justifiably be employed. Chell (1986) suggests one method, which is briefly described in Endnote F.3. However, this, and other similar methods, are mainly applicable to uniaxial, and, to a first approximation, biaxial stressing. They cannot be applied directly to situations involving multiaxial stressing, where a hydrostatic stress can result in a significant elevation above yield of one of the principal stress components. In these cases, alternative methods of stress analysis should be sought.

F.7.5 Evaluate the Stress Intensity Factor Due to Secondary Loading

$K(a,S)$ due to the total secondary loads should be determined for the linear elastic stress distribution, σ_s^{tot}, and, if plastic deformation occurs, $K(a,\bar{S})$ should also be calculated for the elastic-plastic stress distribution, $\bar{\sigma}_s^{tot}$. The stress distributions will in general be non-uniform and the SIF's will require computer codes, such as NASCRAC and FLAGRO, for their evaluation.

F.7.6 Determine the Effective Crack Size, a_e'

The effective crack size, a_e', should be evaluated using Equations (F.13) and (F.3c), with the value of β appropriate to the degree of plastic constraint at the crack tip. On occasion, and for severe secondary loads, the value of the crack tip plastic zone calculated from first order plastic theory may exceed the remaining uncracked ligament. This situation is physically unacceptable and results from a breakdown in the first order plasticity assumption that crack tip plasticity is small compared with typical dimensions associated with the defective section of the structure. To avoid this, it is recommended that the size of a_e' be set to a constant value of $(b+a)/2$ when $a_e' > (b+a)/2$, where b is section size.

F.7.7 Calculate the First Order Plastically Corrected Stress Intensity Factor

$K(a_e',S)$ due to the total secondary loads should be determined for the linear elastic stress distribution, σ_s^{tot}, and, alternatively, $K(a_e',\bar{S})$ should be calculated for the elastic-plastic stress distribution, $\bar{\sigma}_s^{tot}$ if plastic relaxation occurs. In general, these calculations will require computer codes, such as NASCRAC and FLAGRO.

Making allowance for crack tip plasticity generally increases the crack tip driving force J with respect a linear elastic estimate of J, but this is not always the case. Therefore, if the applied loads result in only linear elastic behavior in the defect-free structure, and $K(a_e',S) < K(a,S)$, then $K(a_e',S)$ should be given the value of $K(a,S)$. This situation can occur when the value of σ_s^{tot} rapidly falls and produces a SIF which decreases with increasing crack length. Similarly, if account is taken of plastic relaxation and $K(a_e',\bar{S}) < K(a,S)$, then $K(a_e',\bar{S})$ should be set to the value of $K(a,S)$. This situation can also occur due to a decreasing stress field, or because stress relaxation has significantly reduced the stress acting over the defect. The procedure of using the maximum of $K(a_e',\bar{S})$ and $K(a,S)$ is a modification to the methodology described in Section 4.3, and avoids the under-prediction of J values when the defect size is small and embedded in a larger plastic zone.

F.7.8 Derive an Equivalent Load Ratio for the Secondary Loads

The effects of crack tip plasticity due to secondary loads on J can be characterized by an effective load ratio, P_s/P_y'. This quantity can be interpreted as the ratio of an equivalent primary load to the value of this load at ligament yielding, the value of the equivalent load being chosen so that it produces the same crack tip plasticity conditions that result from the secondary loading. It is not necessary to be specific about the absolute value or nature of the equivalent primary load in order to derive the equivalent load ratio. The ratio can be determined using Equation (F.14) and a knowledge of the values of $K(a,S)$ and $K(a_e',S)$, or the values of $K(a,\bar{S})$ and $K(a_e',\bar{S})$, whichever are appropriate.

Using the linear elastic relationship between J and K [compare Equation (F.5)], then Equation (F.14) can be re-written as

$$F(P_s/P_y') = \left[\frac{K(a_e',S)}{K(a,S)}\right]^2$$

or

$$F(P_s/P_y') = \left[\frac{K(a_e',\bar{S})}{K(a,\bar{S})}\right]^2 \qquad \textbf{(F.19)}$$

where the function $F(P_s/P_y')$ is given by Equation (F.7). The value of the ratio P_s/P_y' is chosen so that $F(P_s/P_y')$ reproduces the value on the right hand side of Equation (F.19).

The form of the function F is dependent only on the material uniaxial stress-strain behavior, and the load ratio P/P_y, and not on the absolute value of the primary load P or on the type of loading (e.g., internal pressure or bending moment). Thus, the application of the reference stress approach to determine the equivalent primary load ratio is not dependent on the absolute form of the primary load which will be superimposed on the secondary loads.

However, if a J solution is available from the EPRI handbooks, or some other source, for the specific primary load P, then this solution may be used in preference to the reference stress approach. If this route is taken, then the equivalent secondary load, P_s, may be obtained from either the equation

$$\frac{J(a,P_s)}{J^e(a,P_s)} = \left[\frac{K(a_e',S)}{K(a,S)}\right]^2$$

or

$$\frac{J(a,P_s)}{J^e(a,P_s)} = \left[\frac{K(a_e',\bar{S})}{K(a,\bar{S})}\right]^2 \qquad \textbf{(F.20)}$$

where $J(a,P)$ is the known J solution. The equivalent secondary load ratio, P_s/P_y', is then given by P_s/P_y, where P_y is the ligament yield load for the specific primary load P.

F.7.9 Evaluate the Primary Load Ratio

The primary load ratio P/P_y is required whether the reference stress approach, or a computed J solution, was used in Section F.7.8 to determine P_s/P_y'. This ratio can be determined using a general yield load obtained from the review of Miller (1988), or from the finite element results used in the computation of J for the primary load.

F.7.10 Determine the Equivalent Load Ratio for the Combined Loading

The equivalent load ratio for the combined primary and secondary loads, P_{ps}/P_y', is calculated from Equation (F.16) using the load ratios P/P_y and P_s/P_y'.

F.7.11 Calculate the SIF for the Combined Loading

$K(a,P,S)$ due to the total primary and secondary loads should be determined for the linear elastic stress distribution, σ^{tot}, or, if plastic deformation occurs, $K(a,\bar{P},\bar{S})$ should be calculated for the elastic-plastic stress distribution, $\bar{\sigma}^{tot}$. The stress distributions will, in general, be non-uniform and the SIF's will require computer codes, such as NASCRAC and FLAGRO, for their evaluation. Although $K(a,P,S)$ may be evaluated by linearly adding the components of K corresponding to the individual components of the primary and secondary loads, the same is not true of $K(a,\bar{P},\bar{S})$ because this is estimated from the elastic-plastic stress distribution corresponding to the total of all the applied loads. Thus, $K(a,P,S)$ will vary linearly with changes in the magnitude of the loads P and S, but $K(a,\bar{P},\bar{S})$ will not.

F.7.12 Calculate the Value of J for the Combined Loading

In the reference stress approach the value of $J(a,P,S)$ [or $J(a,\bar{P},\bar{S})$] for the combined primary and secondary loads can be determined from Equation (F.15) using the estimated value for the equivalent load ratio, P_{ps}/P_y', and the elastic component of $J^e(a,P,S)$ [or $J^e(a,\bar{P},\bar{S})$], where

$$J^e(a,P,S) = \frac{[K(a,P,S)]^2}{E'}$$

and **(F.21)**

$$J^e(a,\bar{P},\bar{S}) = \frac{[K(a,\bar{P},\bar{S})]^2}{E'}$$

If a computed primary load J solution, $J(a,P_s)$, had been used in the derivation of P_s/P_y', then J for the combined loading is evaluated from either the expression

$$J(a,P,S) = J^e(a,P,S) = \left[\frac{J(a,P_{ps})}{J^e(a,P_{ps})}\right]$$

or **(F.22)**

$$J(a,P,S) = J^e(a,\bar{P},\bar{S}) = \left[\frac{J(a,P_{ps})}{J^e(a,P_{ps})}\right]$$

where P_{ps} can be obtained from Equation (F.16) by replacing P_s/P_y' by the equivalent secondary load ratio P_s/P_y calculated in Section F.7.8, and using the known or computed ligament yield load P_y corresponding to the load P.

F.8 Issues Still Outstanding and Requiring Validation

One notable area where there is presently no validation is in the treatment of semi-elliptical surface defects subjected to combined loading. This is a serious omission since surface defects are of great practical importance. The approximate analysis of semi-elliptical cracks is complicated by the variation of the crack driving force along the crack front, which produces corresponding changes to the size of the crack tip plastic zone. This variation is allowed for in the recommended procedure by re-characterizing the shape and size of the defect using a first order plasticity based correction (see Endnote F.2). The correction is needed to assess the effects of the secondary loading on crack tip plasticity. However, the effects of a primary load on the plastic contribution to J also have to be determined, and this requires use of general yield loads which characterize the plastic deformation along the crack front. The issue as to whether these yield loads should take local values, or whether global values are more appropriate, is still not fully resolved (see Endnote F.2).

F.9 Conclusions

Four methods of estimating J for combined primary and secondary loads have been reviewed. These methods are: the EPRI J estimation scheme, the R6 Option 2 J estimation procedure, an approach due to Chell, and a modified R6 method based on Neuber's principle. Based on this review the conclusions are:

1) None of the above approaches provide a generally applicable method for estimating J for combined primary and secondary loads. (See conclusions 2 through 5).

2) The EPRI estimation scheme based on an elastic evaluation of J using an effective crack length is the simplest method to use. However, this approach does not allow for plastic relaxation of the secondary stresses, and, hence, may prove to be unacceptably pessimistic in some cases. An elastic-plastic stress analysis of the defect free structure is required when peak stresses exceed yield in order to reproduce the correct load ratio for use in fatigue crack growth.

3) The R6 method based on Option 2 is more complicated than the EPRI scheme, does not appear to have a well defined physical basis, and although it produces conservative estimates for J in most cases, there are instances when it under-estimates J.

4) The approach of Chell is based on first order plasticity theory and takes credit for stress relaxation due to plastic deformation. It is more complicated to apply then the EPRI scheme and may under-estimate J if the secondary load produces an extensive plastic enclave.

5) The modified R6 method based on the Neuber principle was proposed in order to allow for elastic follow-up in the structure due to secondary loads, and the effects of stress relaxation due to plastic deformation. In cases where the method has been applied, it has been demonstrated to give a conservative result. However, it is not clear how follow-up is explicitly incorporated into the methodology. Although the modified R6 approach strengthens some of the weak areas which were apparent in the original R6 procedures, the approach is complicated to apply and, because of its empirical basis, the accuracy of the method is difficult to judge.

6) A new procedure is proposed for determining J for primary and secondary loads based on modifications and additions to the approach of Chell. The method is capable of treating the effects of crack tip plasticity due to high local stresses resulting from primary loading and allows credit to be taken for plastic relaxation of the applied stresses.

7) Parts of the new procedure have not been validated. These include the treatment of defects with more than one degree of freedom, such as a semi-elliptical surface crack.

8) The effects of secondary loads on J may be enhanced if these are accompanied by elastic follow-up in the structure. None of the four methods described here rigorously address this problem. A method for treating elastic follow-up that can be simulated by imposed displacements over a defined gauge length is described. This method complements the proposed procedure.

ENDNOTE F.1

Outline of Treatment for Displacement Imposed Loading

Linear Elastic Analysis

The displacement, Δ, at the point of application of a force F in a body is given by Castigliano's theorem

$$\Delta = \frac{dU}{dF} \tag{F.23}$$

where U is the strain energy of the body. If a moment, M, is applied then the corresponding rotation, θ, is

$$\theta = \frac{dU}{dM} \tag{F.24}$$

It is convenient to generalize these equations, and to write them in the form of a generalized force Q (e.g., F or M) and the resulting generalized displacement, δ(Δ or θ)

$$\delta = \frac{dU}{dQ} \tag{F.25}$$

If a defect is present in the body, then the displacement can be resolved into uncracked and cracked components, where the displacement due to the defect, δ^d, can be written

$$\delta^d = \frac{dU^d}{dQ} \tag{F.26}$$

where U^d is the strain energy associated with the defect, given by

$$U^d = \int_A \frac{K_I^2(A')}{E'} \tag{F.27}$$

where A is the area of the defect. The compliance due to the crack is obtained from

$$C^d = \frac{d\delta^d}{dQ} \tag{F.28}$$

If many forces are being applied to the body, then the displacement δ_i^d in the direction of the i'th force, Q_i, is given by

$$\delta_i^d = \sum_j C_{ij}^d Q_j \tag{F.29}$$

where

$$C_{ij}^d = \frac{d\delta_i^d}{dQ_j} = \frac{d^2 U^d(Q_1, Q_2, \ldots)}{dQ_i dQ_j} \tag{F.30}$$

Similar expressions to Equations (F.26) through (F.30) apply for the defect free structure. Signifying these terms by the superscript o, then if there are a total of k independently applied loads, a set of k equations which are linear in the loads Q_i can be written for the total displacements of the form

$$\delta_i = \sum_j \left[C_{ij}^o + C_{ij}^d\right] Q_j \tag{F.31}$$

If m of the displacements δ_i are fixed at prescribed values, then the m equations for these fixed displacements represented by Equation (F.31) can be used to derive the variation of the corresponding m reactive loads with crack size.

The SIF is given by the sum of the SIF's corresponding to each of the loads Q_i. Similarly, for a given defect size, the load ratio P/P_y (see Section F.7.9 of the main text) should be evaluated for the multiple loads Q_i. The load ratio, P/P_y, which characterizes the nearness of the structure to general yield, will not generally be a simple function of the multiple loads, Q_i. The value of J can then be determined following a similar procedure to that described in Section F.7.3 of the main text. In general, the instantaneous loads Q_i determined from linear elastic theory will be higher (and hence, more pessimistic) than the equivalent loads derived by taking crack tip plasticity into account. This is because, as illustrated in Figure F.5, plasticity reduces the crack stiffness (increases the compliance).

Elastic-Plastic

Similar principles to those described for linear elastic behavior can be applied to determining the effects of crack tip plasticity on J under displacement imposed loading. However, the situation is complicated by the fact that crack tip plasticity results in the crack compliances, C_{ij}^d, being explicit functions of the loads Q_i (see Figure F.5). This is because J can no longer be written in terms of the square of the linear sum of individual SIF's.

In the elastic-plastic case, the compliance due to the defect can still be written as Equation (F.27) but with the strain energy defined in terms of J

$$U^d = \int_A J(A', Q_1, Q_2, \ldots) dA' \tag{F.32}$$

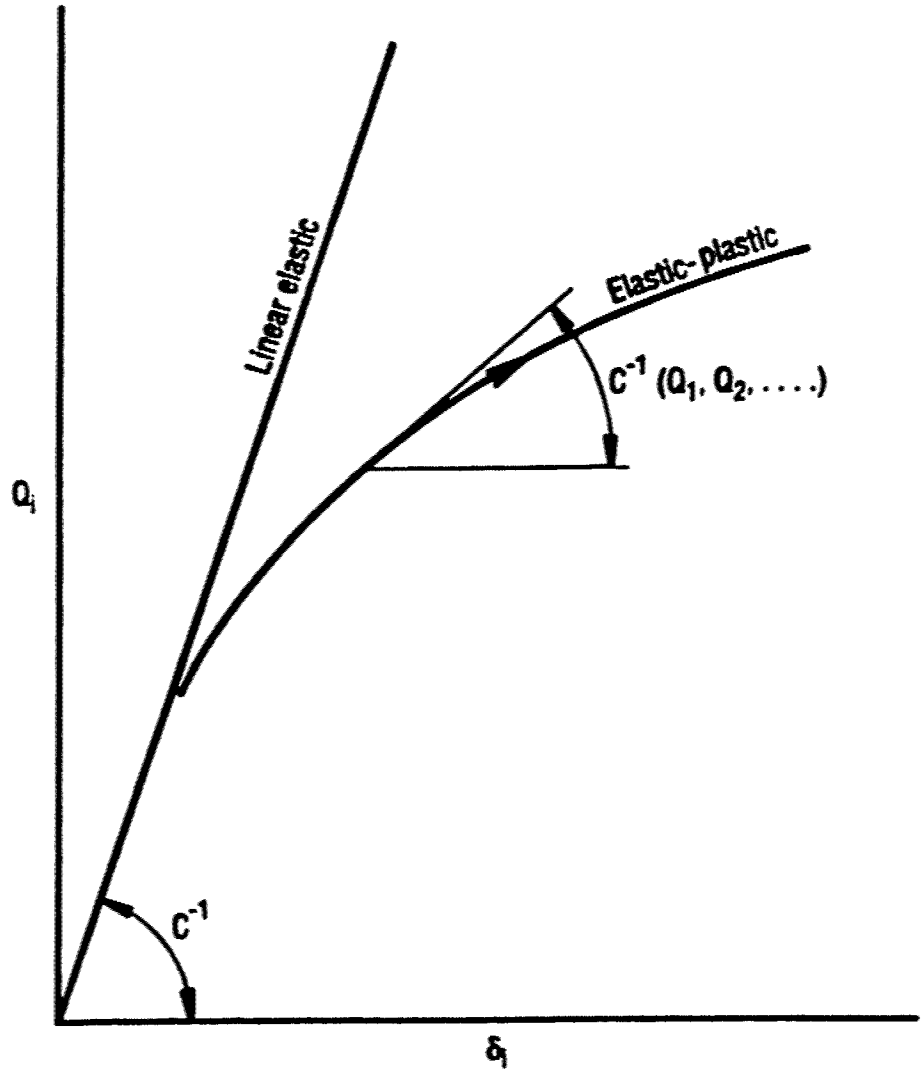

Figure F.5. Effects of crack tip plasticity on the stiffness $[C^{-1}(Q_1, Q_2, ...)]$ of the cracked section.

By comparison with Equations (F.30) and (F.31) the elastic-plastic displacements are given by

$$\delta_i = \sum_j \int_0^{Q_j} \left[C_{ij}^{o} + C_{ij}^{d}\left(Q_1, Q_2, \ldots\right) \right] dQ_j \qquad \textbf{(F.33)}$$

where the integral over dQ_j is performed assuming proportional loading (i.e., $dQ_j = Q_j\, d\lambda$, where λ is a scalar varying from 0 to 1 during the integration).

If m of the displacements δ_i are fixed at prescribed values, then the m equations for these fixed displacements represented by Equation (F.33) can be used to derive the variation of the corresponding m reactive loads with crack size. Note that, unlike the elastic counterpart, Equation (F.33) is non-linear in the loads Q_i.

Equation (F.18) of the main text is recovered from Equation (F.33) for the case of a single displacement imposed load corresponding to a reactive force P_s, and a primary applied load, P_p.

ENDNOTE F.2

Defects with more than One Degree of Freedom

The evaluation of J under combined loading for defects with more than one degree of freedom follows similar procedures to those employed for the one degree of freedom cracks. The differences arise because of the necessity of calculating J for a number of crack tip positions. This requires rules for defining the first order plastic correction for the defect when the crack tip driving force and the plastic zone size vary along the crack front. Rules are also required for applying the reference stress approach to these situations and, in particular, what is the correct reference stress and primary load ratio to use for these kinds of defect.

First Order Plastic Correction to the SIF

It is necessary to assume that the plastic zone size at a point on the defect under small scale yielding conditions is related to the value of the SIF at that point. This assumption immediately leads to a plastic zone size, $2r_y(q)$, at a point q on the defect, where $r_y(q)$ is given by Equation (F.3) with K_I interpreted as the SIF, $K_I(q)$, at q. The effective crack length, $a_e'(q)$, measured on a radial line from the center of the defect through the point q is then

$$a_e'(q) = a(q) + r_y(q) \tag{F.34}$$

Application of Equation (F.34) will, in general, lead to a re-characterized defect shape which is not readily amenable to a fracture mechanics analysis based on the available compendia of SIF solutions. It is, therefore, necessary to simplify the procedure and to restrict the determination of the effective lengths to selected points on the defect which characterize its shape. For example, for elliptically shaped defects, these positions will be the tips of the minor and major axes.

To show how this scheme should be applied, consider an embedded elliptical defect of semi-minor axis length, a, and semi-major length, c (Figure F.6). This defect is characterized by 4 SIF values, corresponding to the points on the defect signified by 1 through 4 in Figure F.6. Applying Equation (F.34) results in an effective minor axis length of $2a+r_y(1)+r_y(3)$, and an effective major axis length of $2c+r_y(2)+r_y(4)$. The center of the re-characterized defect is shifted $(r_y(1)-r_y(3))/2$ along the x-axis, and $(r_y(2)-r_y(4))/2$ along the y-axis, and has a new semi-minor axis length $a_e'=a+(r_y(1)+r_y(3))/2$, and major axis length $c_e'=c+(r_y(2)+r_y(4))/2$.

The SIF's at the selected 4 points on the re-characterized defect can then be used in Sections F.7.7 and F.7.9 to obtain the first order plastic corrections and to derive an equivalent load ratio for each of the points. Thus, in this particular example, 4 values of P_s/P_y' would be derived and used to obtain values of J for each of the 4 locations on the crack front.

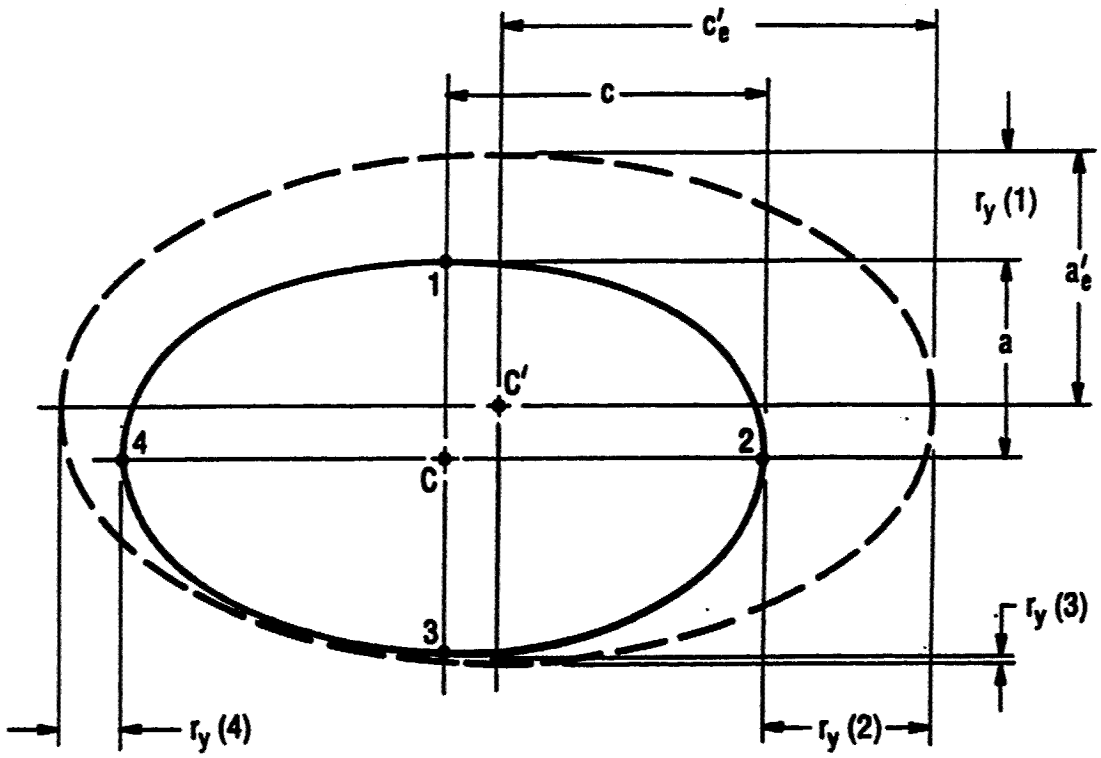

Figure F.6. First order plastic correction and recharacterization of embedded elliptical defect centered on C. The effective axes length, a_e' and c_e', are based on the center of the recharacterized defect at C′.

Primary Load Ratio

A general yield load which characterizes J at the selected crack tip locations under fully plastic conditions is required in order to determine the primary load ratio for use in Section F.7.9. It is still uncertain whether a global yield load which characterizes the plastic deformation of the defect as a whole is applicable, or whether local yield loads should be applied to determine the plastic behavior of specific points on the crack front (Miller, 1986; Chell, 1990). Local conditions can clearly affect the local value of J prior to fully plastic behavior, as is indicated by the position specific values of the first order plastic correction to the SIF. However, limited evidence suggests that the fully plastic behavior of a defect can be quantified using a global yield load which is independent of the local deformation occurring at different points on the crack front (Miller, 1986; Chell, 1990).

ENDNOTE F.3

An Approximate Method of Determining Elastic-Plastic Stress Distributions

A method is described for estimating the elastic-plastic stress distribution in a defect free structure from the results of a linear elastic analysis (Chell, 1986). The method is limited to cases where the stressing is predominantly uniaxial or biaxial, and where the shear stress components are negligible. Furthermore, it is assumed that the maximum component of stress is normal to the plane of the crack, and only the plastic relaxation of this component is considered.

Following the procedure described in Section F.7.4, the applied stress is resolved into primary, σ_p, and secondary, σ_s, components. Relaxation of σ_s is first determined using Neuber's principle (although alternative methods can be employed), and then a bounding theorem is used to obtain the relaxed stress distribution, $\bar{\sigma}^{tot}$, due to the combined relaxed secondary stress, $\bar{\sigma}_s$, and σ_p.

If $\varepsilon = \varepsilon(\sigma)$ defines the uniaxial stress-strain relationship, then a first order approximation to the plastically relaxed stress $\bar{\sigma}_s$ at all points in the crack plane can be obtained from solving the Neuber equation at each point

$$\bar{\sigma}_s \varepsilon(\bar{\sigma}_s) = (\sigma_s)^2/E \qquad \textbf{(F.35)}$$

In practice the stress increment $\sigma_s - \bar{\sigma}_s$ is redistributed over the section in order to maintain a correct force balance between the externally applied loads (these are zero in the case of self-equilibrated secondary loading) and the forces corresponding to the induced stresses. To maintain this balance, the force, δF, consistent with integration of the stress increment, $\sigma_s - \bar{\sigma}_s$, over the section, is evaluated and used to define a uniform stress increment, $\delta\sigma_s = \delta F/(\text{area of section})$. This increment is then added to σ_s at each point in the section and the Neuber equation is re-applied and the process repeated until δF becomes negligibly small. When this occurs, the relaxed stress distribution, $\bar{\sigma}_s$, exactly balances the applied forces.

A first order approximation to the combined plastically relaxed stress distribution is obtained using the bounding theorem and at each point in the section choosing a value of σ_r which minimizes the right hand side of the equation

$$\varepsilon_{\min} = \varepsilon(\sigma_p + \sigma_r) + (\bar{\sigma}_s + \sigma_r)\left[\frac{\varepsilon(\bar{\sigma}_s) - \varepsilon(\sigma_r)}{2\sigma_r}\right] \qquad \textbf{(F.36)}$$

The relaxed stress, $\bar{\sigma}^{tot}$, can be obtained as the stress corresponding to the strain $\varepsilon_{\min}$ which results from the minimization process. The force, δF, corresponding to the resulting stress difference, $\sigma_p + \bar{\sigma}_s - \bar{\sigma}^{tot}$, is calculated as for the secondary loading case, to determine a uniform stress increment, $\delta\sigma_p$, which is then added to σ_p and the whole process repeated until δF becomes neglibly small. The desired stress distribution is given by $\bar{\sigma}^{tot}$ which balances the applied forces.

The procedure described above for determining the plastically relaxed stress distributions is an elaboration on the method described in reference (Chell, 1986), which is based on the assumption that the stress in the plastic zone is constant and determined by the relaxation of the stresses at the surface of the structure. In this approximation, the stress increments, $\delta\sigma_s$ and $\delta\sigma_p$, are redistributed only onto the part of the section which remains elastic.

APPENDIX G

SIMPLE *J* ESTIMATION TECHNIQUES FOR MODE I CRACKS UNDER MULTIAXIAL LOADS

Rocketdyne experience has shown that multiaxial states of stress frequently occur in reusable aerospace propulsion system applications, and therefore some attention to the estimation of J under multiaxial conditions is needed. However, solution of the complete multiaxial J problem was clearly beyond the scope of the current contract effort. The approach taken in the current contract was to investigate and develop simple estimation techniques for multiaxial effects on two-dimensional through cracks subjected to Mode I loading, and to characterize the accuracy and limits of applicability of those techniques. This appendix summarizes the results of these investigations.

In the two-dimensional configuration under consideration here, a stress, S, is applied remote from the crack in a direction normal to the plane of the crack. Remotely applied transverse stresses, T, may also be applied normal to the axis of stress S (and therefore parallel to the crack plane). No remote shear stresses are applied. The biaxiality is characterized by the ratio $\lambda = T/S$. For uniaxial loading, $T = 0$, and the applied stress S is just the usual σ. The stress nomenclature is given here as S and T rather than specific values of the stress tensor σ_{ij} to emphasize that the formulation is general and not limited to any specific coordinate system or orientation (e.g., axisymmetric systems are also admissible).

At the outset, it should be noted that multiaxial corrections to J apply to the plastic component only. The engineering approach to J assumes that total J can be computed as the sum of elastic and plastic components,

$$J = J_e + J_p \tag{G.1}$$

The elastic component, J_e, is calculated directly from the linear elastic stress intensity factor, K, which is not influenced by multiaxial stresses of the type considered here. The effective crack length (crack tip plastic zone size) correction term that is often included in the elastic term does have some dependence on multiaxiality. But since this term is small and the change in the term due to multiaxiality even smaller, these contributions have been neglected at the present time.

He and Hutchinson (1983a) accommodated multiaxial states of stress in their numerical solutions for the J-integral in infinite bodies in terms of the von Mises effective stress and strain. Their normalization procedure for the fully plastic J was given by the form

$$\frac{J_p}{\sigma_{ef}\varepsilon_{ef}a} = h_1\left(n, \frac{S}{T}\right) \tag{G.2}$$

Here the effective stress σ_{ef} is defined in the usual way as

$$\sigma_{ef} = \left(\frac{3}{2}s_{ij}s_{ij}\right)^{1/2} \tag{G.3}$$

where s_{ij} is the stress deviator. The effective strain ε_{ef} is defined conveniently as

$$\varepsilon_{ef} = \left(\frac{2}{3} \varepsilon_{ij} \varepsilon_{ij} \right)^{1/2} \tag{G.4}$$

This coincides with the tensile strain in uniaxial tension. The effective stress and strain satisfy the same fully-plastic power-law constitutive relationship as do the uniaxial stress and strain,

$$\frac{\varepsilon}{\varepsilon_0} = \alpha \left(\frac{\sigma}{\sigma_0} \right)^n \tag{G.5}$$

The nondimensional parameter h_1 was subsequently expressed as the product of factors in n and S/T; for example, in plane strain

$$h_1 = \frac{3\pi\sqrt{n}}{4} \left(\frac{S}{\sigma_{ef}} \right)^2 \tag{G.6}$$

He and Hutchinson showed graphically how this simple analytical form based on a perturbation solution compared satisfactorily with more rigorous numerical results for both plane strain and axisymmetric cracks. Dowling (1987) has presented a similar set of comparisons for the He and Hutchinson data, showing somewhat more clearly that agreement between simple formula and numerical results was typically within ±10 percent. The only significant exception was for larger positive values of T/S ($0.67 < T/S < 1$) under axisymmetric loading (i.e., approaching triaxial tension), where the simple formulas began to significantly underpredict h_1. Dowling went on to postulate a similar approximate construction for the plane stress case, although validating numerical solutions were not available for comparison.

The basic multiaxial approximation scheme first introduced by He and Hutchinson and later amplified by Dowling may be further extended and simplified to give the following result. Begin first with a uniaxial, fully plastic J solution in the general form

$$J_p = \alpha \varepsilon_0 \sigma_0 a \, h_0' \left(\frac{S}{\sigma_0} \right)^{n+1} \tag{G.7}$$

where σ_0, ε_0, and n are material constants in the constitutive relationship, Eqn. (G.5). A corresponding multiaxial J solution for any T/S ratio can be constructing by replacing the uniaxial

h'_0 with a new multiaxial value, which is denoted as h_0. For plane strain, the relationship between h'_0 and h_0 is

$$h_0 = h_0' \{|1 - \lambda|\}^{n-1} \tag{G.8}$$

where h'_0 is the uniaxial solution and $\lambda = T/S$. For plane stress, the form is

$$h_0 = h_0' \left\{\sqrt{1-\lambda+\lambda^2}\right\}^{n-1} \tag{G.9}$$

Note that the other factors in Eqn. G.7 are not influenced by stress state. The new normalization scheme is related to the previous He and Hutchinson normalization according to $h_0 = h_1(\sigma_e/S)^2$.

He (1986) subsequently published more complete sets of numerical results for through-thickness cracks in infinite plates under both plane stress and plane strain for a variety of biaxiality ratios. For plane strain, He expressed his results in terms of a slightly different normalization scheme

$$h_2 = \frac{J_p}{\alpha\, \sigma_0\, \varepsilon_0\, a \left(\dfrac{\sqrt{3}S}{2\sigma_0}\right)^{n+1}} \tag{G.10}$$

Based on the plane strain expression for h'_0 given previously by He and Hutchinson (see Eqn. G.6), Eqn. G.8 can be appropriately modified to predict h_2 by replacing h_0 and h'_0 with h_2 and h'_2, respectively, and by setting $h'_2 = \pi\sqrt{n}$. He does not give a comparable expression for h'_0 in plane stress. Dowling (1987) suggested that a suitable plane stress estimate for use in Eqn G.9 was $h'_0 = \pi\sqrt{n}$, based on the assumption that plane stress and plane strain results are identical when appropriate corrections for the effective stress and effective strain are taken into account. Shih and Hutchinson (1976) had earlier proposed the general form

$$h_0' = 3.85\sqrt{n}\,(1 - 1/n) + \pi/n \tag{G.11}$$

for plane stress uniaxial tension, which gives similar but not identical results to the Dowling suggestion. In this study, the Shih and Hutchinson form was adopted as the uniaxial solution.

The He numerical results for plane stress and plane strain (He, 1986) are compared with the predictions of Eqns. G.8 and G.9 (based on uniaxial values and effective stress arguments) in Figure G.1. The agreement appears to be reasonably strong for all values of n and T/S. The original numerical solutions are based on energy principles which give upper and lower bound results, and their accuracy slowly decays at higher n values. The estimation techniques appear to be entirely acceptable for the infinite plate (i.e., small crack) configuration.

The only available set of biaxial J results for cracks in two-dimensional finite bodies is that of Jansson (1986), who published fully plastic plane stress solutions for biaxially-loaded center-cracked plates based on finite element (FE) calculations. He considered nine values of n ranging from $n = 1$ to 20, five values of the normalized crack width ranging from $a/b = 0.125$ to 0.625, and five values of the biaxial stress ratio λ ranging from $\lambda = +1$ to -1. Jansson presented his results in terms of a significantly different normalization scheme, and some algebra is required to express his results in the framework of Eqn G.2.

Comparisons of the Jansson FE results (in the framework of Eqn G.2) with the predictions of Eqn G.9 are given in Table G.1. Note that the h_0' solutions cited earlier (e.g., Eqn G.11) do not include the effects of finite geometry. In order to apply the multiaxial estimation scheme to finite geometries, the appropriate h_0' factors must first be determined for uniaxial loading based on elastic-plastic FE analysis or estimation procedures. Since Jansson modeled the special case where all remote boundaries were constrained to remain straight, more general uniaxial solutions (i.e., EPRI handbook) for h'_0 are not applicable. In this study, the uniaxial h'_0 was based on the Jansson results for $\lambda = 0$. This differs from the Dowling (1987) approach, where he utilized linear elastic geometry correction factors to estimate h'_0 for semi-infinite bodies.

The agreement is reasonably strong for smaller values of a/b and gradually deteriorates for larger a/b, especially at larger n. The disagreement at large a/b may be due to the influence of the rigid boundary conditions chosen by Jansson. Note that the Jansson analysis represents not only straight boundaries but also a square plate geometry. Jansson himself compared J_p results for $a/b = 0.5$ for the standard specimen with 3:1 height-to-width ratio (e.g., the EPRI handbook results) to a square plate with straight horizontal boundaries to a square plate with all boundaries held straight. His results showed that when the vertical boundaries were held straight, J_p dropped drastically, since deformation in the highly stressed region adjacent to the crack tip was restrained. This effect was also shown to be relatively small for low n and large for high n.

This boundary influence would be magnified even more for negative λ since leaving the boundary unconstrained would tend to further increase boundary curvature. Therefore, it is not surprising that large overprediction of J_p occurs for the combination of large a/b, large n, and negative λ. On the other hand, the imposed boundary influence is probably reduced for positive λ since the positive stress parallel to the crack tip is attempting to straighten the adjacent boundary itself, replacing the influence of the imposed boundary condition. In this case, using the uniaixial results to define h'_0 may overstate the beneficial effect of the boundary in reducing J_p and could result in underprediction for the biaxial case with positive λ.

From the perspective of practical algorithms for fatigue crack growth life prediction, the results are nevertheless encouraging. The predictions are always nearly exact or conservative except in the vicinity of $\lambda = +0.5$ (compare the He plane stress results and corresponding predictions at larger n in Figures G.1). The predictions are most accurate for smaller crack sizes, where the majority of the crack growth life will be expended. Many of the results are accurate within a factor of 1.5 or better. Since this inaccuracy applies only to the plastic term, which is only one contributor

to total J, errors in crack growth rate predictions (based on total ΔJ) caused by errors in h_0 should be considerably less than a factor of two in most cases.

It is somewhat discouraging that the accuracy decays so quickly at the largest n values (e.g., 20) for some λ values, since low hardening materials are commonplace in reusable aerospace propulsion systems. However, it should be remembered that any inaccuracies in the J-calculation scheme (including small errors in estimating the applied stress in service or in estimating the constitutive relationship) are greatly magnified for such large n. Even an "exact" h_0 solution does not guarantee an accurate J estimate. Although improved h_0 estimates for large n are clearly needed, this accuracy may be less significant in some applications in view of other contributors to uncertainty under these conditions.

It is instructive to review quickly the general trends of h_0 with different stress states, based on both the He and the Jansson results. In comparison with the uniaxial values, h_0 (and therefore J_p) increases dramatically with increasingly negative transverse stresses under both plane stress and plane strain. Even at small n, the difference between $\lambda = 0$ and $\lambda = -1$ values is often on the order of 10× or even 100×. It should be remembered, however, that at $\lambda = -1$ (which corresponds to pure shear), even an uncracked elastic-plastic body goes fully plastic at $S/\sigma_0 = 0.577$. Since design rules will typically keep nominal applied stresses at or below this level, the contributions of the J_p term (which is proportional to $(S/\sigma_0)^{n+1}$) will sometimes be relatively small. Furthermore, Rocketdyne experience has suggested that negative λ values are relatively rare in reusable aerospace propulsion system applications.

For positive λ values, the differences between plane stress and plane strain become very large. In plane stress, h_0 values pass through a minimum around $\lambda = +0.5$ before increasing again with increasing λ. Values of h_0 at $\lambda = +1$ are identical to those at $\lambda = 0$, according to the simple estimation scheme. The results of He and of Jansson suggest that this is nearly true for small cracks and less true for larger cracks, where h_0 is somewhat smaller at $\lambda = +1$. In plane strain, however, the simple estimation scheme suggests that the value of h_0 drops to zero at exactly $\lambda = +1$, and the He results confirm this discontinuity in the trend curves. The dramatic difference between plane stress and plane strain results at $\lambda = +1$ suggests that proper assessment of the actual out-of-plane stress state in applications is paramount for accurate J characterization. A plane stress assumption will always be conservative relative to a plane strain assumption in this region.

In summary, the simple effective stress approach to estimating the effects of multiaxial stresses on J for through-crack configurations appears to be acceptably accurate for small cracks and for some larger cracks at low and intermediate values of n. For deep cracks at large n, the estimates can be significantly in error, especially for negative λ. Errors are nearly always conservative (i.e., h_1 is predicted too large) except around $\lambda = +0.5$ in plane stress.

All of these results are for two-dimensional through cracks. The more significant geometry for reusable aerospace propulsion systems is the part-through surface crack with a semi-elliptical perimeter. Only one J result is known to be available for this type of geometry. Dodds et al. (1993) presented a comparison of J values for remote uniaxial tension vs. remote equibiaxial tension for a

semi-elliptical surface crack with the geometric parameters $a/t = 0.25$, $2c/a = 6$ in a Ramberg-Osgood material with $n = 10$. At the deepest point of the crack ($\Phi = 90°$), the total J values were identical in the SSY regime, but at $\sigma^*/\sigma_0 = 1.1$, the biaxial J value was approximately half the uniaxial J value. This difference was even more pronounced for smaller Φ values. It is not immediately obvious how to derive this result from the simple 2-D rules described above, particularly given the ambiguity about how to define the stress state in the three-dimensional configuration. In the absence of additional supporting data, it is not yet possible to develop and verify a general multiaxial J estimation scheme for three-dimensional cracks in finite bodies.

The multiaxial J estimation scheme presented here was based on methods originally developed for cracks in infinite bodies. Therefore, the multiaxial modifications to the plastic J solutions were focused on the nondimensional h factors. Extension of this approach to finite bodies requires that the effects of the finite geometry be included satisfactorily in an available h value for uniaxial loading. Such an extension was found to be moderately, but not entirely, successful in comparison to the Jansson results.

This approach, which follows the spirit of the EPRI formulations, stands in mild contrast to the reference stress J estimation schemes currently employed for other geometries and other uniaxial combined loading situations. In these schemes, the effects of finite geometries are introduced through modifications to the optimum yield load. It may be possible, therefore, to reformulate the multiaxial approach in terms of modifications to the optimum yield load, which might reflect not only changes in net section area but perhaps also changes in yielding behavior due to multiaxiality. Some preliminary work has been carried out to explore this possibility, but resolution of these questions is beyond the scope of the current contract.

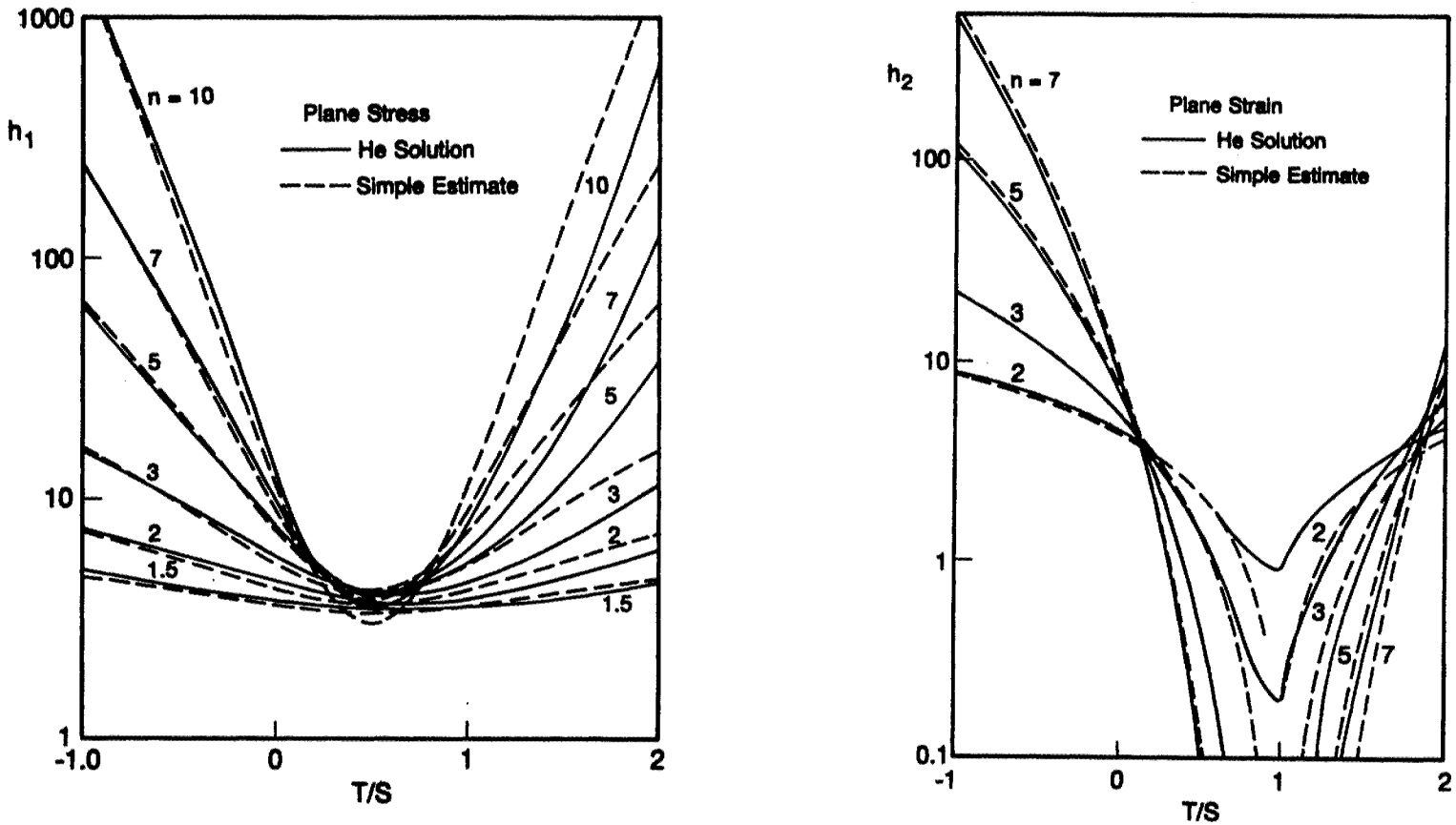

Figure G.1. Comparison of fully plastic *J* solutions for cracks in infinite plates under biaxial loading

Table G.1. Comparison of Jansson FEM results for multiaxial J with simple estimates based on an effective stress approach for a range of λ, n, and a/b values. Tabulated are the ratios of h_1 (predicted) / h_1 (Jansson FEM).

$\lambda = +1$	$n = 3$	5	7	10	13	16	20
$a/b = 0.125$	1.30	1.46	1.59	1.76	1.92	2.09	2.34
0.250	1.29	1.45	1.59	1.81	2.05	2.33	2.75
0.375	1.28	1.43	1.54	1.70	1.84	1.93	2.06
0.500	1.24	1.34	1.38	1.37	1.34	1.29	1.24
0.625	1.18	1.20	1.17	1.11	1.07	1.04	1.02

$\lambda = +0.5$	$n = 3$	5	7	10	13	16	20
$a/b = 0.125$	1.06	1.03	0.98	0.88	0.78	0.68	0.56
0.250	1.02	0.94	0.83	0.67	0.53	0.41	0.29
0.375	0.98	0.84	0.69	0.50	0.35	0.24	0.14
0.500	0.92	0.74	0.57	0.37	0.24	0.15	0.08
0.625	0.85	0.65	0.48	0.30	0.19	0.12	0.07

$\lambda = -0.5$	$n = 3$	5	7	10	13	16	20
$a/b = 0.125$	1.05	1.08	1.10	1.14	1.18	1.21	1.25
0.250	1.08	1.18	1.29	1.50	1.75	2.01	2.42
0.375	1.15	1.40	1.72	2.37	3.27	4.50	6.77
0.500	1.26	1.74	2.47	4.29	7.65	13.73	30.62
0.625	1.40	2.21	3.65	8.15	19.05	45.29	150.29

$\lambda = -1$	$n = 3$	5	7	10	13	16	20
$a/b = 0.125$	1.10	1.16	1.20	1.26	1.32	1.38	1.48
0.250	1.16	1.32	1.52	1.91	2.43	3.07	4.21
0.375	1.28	1.71	2.36	3.91	6.51	10.81	21.05
0.500	1.49	2.49	4.34	10.38	25.38	62.10	209.74
0.625	1.83	3.96	9.26	35.95	148.32	634.20	4601.86

APPENDIX H

FINITE ELEMENT ANALYSIS OF SPECIMEN GEOMETRY EFFECTS ON FATIGUE CRACK CLOSURE

H.1 Introduction

The fatigue crack closure phenomenon is an intrinsic aspect of the mechanics of growing fatigue cracks, and, in many applications, closure provides a powerful first-order correction to the crack driving force which facilitates more accurate computation of crack growth rates. Although closure can be motivated by several different physical mechanisms, including roughness or oxides on the fracture surface, extensive experimental and computational studies have shown that crack wake plasticity is often the dominant contribution to closure, particularly at higher values of the stress intensity factor.

A reasonable approach to the numerical characterization of closure, then, is to conduct an appropriate elastic-plastic continuum mechanics analysis of a body under cyclic loading with a growing crack. Numerous researchers have applied the finite element method (FEM) to the closure problem [some historical perspective is provided in (McClung and Sehitoglu, 1989a; McClung, 1992)]. Several others have explored simpler analytical approaches, such as modified versions of the Dugdale strip-yield model (see again the review in McClung and Sehitoglu, 1989a). These mechanics studies have generally agreed that the crack opening stress, typically normalized by the maximum stress in the fatigue cycle according to S_{open}/S_{max}, is a function of the stress ratio ($R = S_{min}/S_{max}$), the stress state (plane stress vs. plane strain), and the normalized maximum stress S_{max}/σ_0 (where σ_0 is the yield stress or flow stress of the material). (Note that in this appendix, the symbol S is used to denote far-field applied stress, as is customary in FEM closure studies.) These studies have also shown that crack opening stresses do not, in general, change significantly with further crack growth (McClung, 1991c), which suggests that crack opening behavior is not a function of the applied stress intensity factor alone (which, of course, changes with increasing crack length even if the applied cyclic loads remain constant). These computational results are consistent with numerous experimental measurements of crack opening stresses outside the near-threshold regime and outside the near-net-section-yielding regime (McClung, 1991c).

These numerical studies have typically been limited in scope to relatively few geometric configurations. The Dugdale model corresponds to a crack in an infinite plate under uniform tension, and most FEM studies have focused on the similar center-cracked plate (CCP) under uniform tension, usually with a small ratio of crack length to specimen width (a/W) so that finite width effects are minimized. Most other FEM analyses have addressed cracks near notches, plates with very short edge cracks, or an occasional compact tension (CT) specimen. Systematic parameter studies (methodical investigation of crack length and applied stress effects) are rare. Almost no researcher has applied the same numerical model to several contrasting geometries. The primary exceptions here are Sehitoglu and colleagues (McClung and Sehitoglu, 1989b; Sehitoglu and Sun, 1991), who investigated several applied load levels for both CCP and CT geometries, and Fleck (1986), who directly compared opening behavior for CCP and single-edge-cracked-plate bend (SECP-B) geometries at a single crack length and single applied K_{max} values. Similar experimental studies comparing different geometries are also very rare outside the near-threshold regime.

Several important questions remain unanswered, therefore. To what extent are the benchmark CCP or infinite plate closure results applicable to other specimen or structural

geometries? Does the same functional dependence of S_{open}/S_{max} on S_{max}/σ_0 hold, or does it somehow change? Are further changes introduced by very large changes in crack length for the same basic geometry? And how should closure be characterized for bend specimens or other configurations where the crack grows through a large, long-range stress gradient? Does an S_{max}/σ_0 criterion apply, and if so, how? Do crack opening stresses follow changes in the nominal (uncracked) maximum stress at the current crack tip location?

This appendix summarizes investigations which are designed to answer some of these questions. A finite element model is used to study closure at three different crack length to width ratios for three different specimen geometries: CCP, SECP-B, and single-edge-cracked-plate tension (SECP-T). The results are critically compared, and a single characteristic parameter is proposed to describe crack length, applied stress, and specimen geometry effects on closure.

H.2 Finite Element Model

The basic FEM model employed here has been described in detail in previous publications (McClung and Sehitoglu, 1989a; McClung, Thacker, and Roy, 1991). The meshes were composed of four-noded linear strain elements. At each occurrence of minimum load in the cycle, the boundary conditions at the crack tip node were changed to allow the crack to "grow" by one element length through a "nugget" of very small, uniformly sized elements along the crack line. A typical mesh is shown in Figure H.1.

Previous studies (McClung and Sehitoglu, 1989a) have found that several criteria must be satisfied to insure that the crack opening results are free of modeling artifacts. One suggested criterion was that crack tip elements must be sufficiently small relative to the crack tip plastic zone size, which implies a limitation on the smallest permissible value of the maximum applied stress intensity factor in the cycle. Since different specimen geometries were not considered in that earlier work, however, it is also possible that the crack tip element size criterion should actually reflect the smallest permissible value of the maximum applied stress in some way. A second criterion was that crack growth should extend farther than the outer boundary of the crack tip plastic zone emanating from the initial crack tip position, since crack lengths at the beginning of each analysis were set to relatively large initial sizes for efficiency. When these two criteria were met, crack opening stresses were generally stable and did not change with further crack growth, even at high stresses. The primary exception to this stability was that crack opening stresses sometimes dropped off with further crack growth if nominal net-section yielding was imminent. This behavior is addressed further in the discussion section.

All analyses discussed in this appendix were plane stress. The constitutive model followed linear kinematic hardening with $H/E = 0.01$, where E is the elastic modulus and H is $d\bar{\sigma}/d\bar{\varepsilon}_p$, the slope of the plastic line. The flow stress, σ_0, is the intersection of the elastic and plastic lines. Remote stresses were applied in many small steps (typical step size was two percent of the maximum stress). Stresses and displacements along the crack line behind the crack tip were closely monitored on each load step, and boundary conditions on the crack surfaces were appropriately changed as the crack opened or closed.

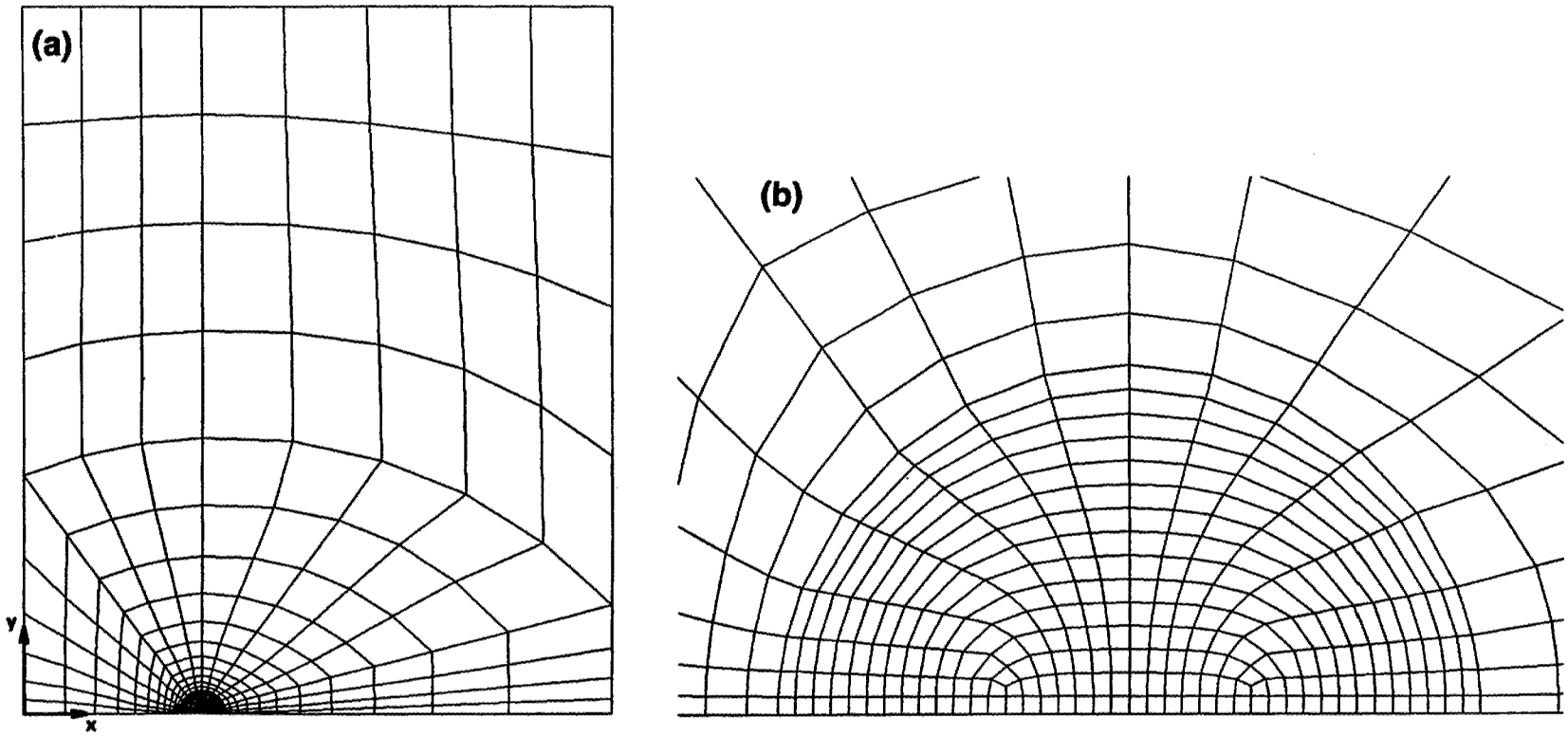

Figure H.1. Typical mesh for finite element analysis of crack closure: (a) entire mesh (b) near-tip fine mesh region

The three different specimen geometries were created using the same meshes by applying different boundary conditions. The original configuration, which simulated the CCP geometry, modeled one quadrant of the cracked plate. By replacing the central plane of symmetry normal to the crack line with a free boundary, the mesh became the upper half of a single-edge cracked plate. If the original (CCP) uniform tension loading was retained, the resulting specimen was SECP-T. The application of a pure moment to create a SECP-B configuration was simulated with a linear traction gradient across the top edge of the mesh, varying between $+S$ and $-S$. These configurations are summarized in Figure H.2.

These different boundary conditions were applied to three different meshes, each with a different range of crack length to width ratios. The "nugget" of very finely spaced nodes was roughly centered around $a/W = 0.125$, 0.3, or 0.5 in each mesh. The fine mesh spacing (i.e., the size of the smallest elements) was held constant in a given mesh, but was varied from mesh to mesh in order to keep the $\Delta a/a$ ratio in the center of the nugget roughly constant (McClung and Sehitoglu, 1989a).

H.3 Results

Calculated crack opening stresses at $R = 0$ and $R = -1$ for all specimen geometries and crack lengths are given as a function of the normalized maximum applied stress in Figure H.3. Here S_{max} was defined for the SECP-B geometry as the outer fiber stress, $S = 6M/W^2 t$, where M is the applied moment and t is the thickness. The absence of SECP-T results at $a/W = 0.5$ is due to modeling limitations, and is explained below in the discussion.

Note, first, that different specimen geometries exhibit different crack opening behaviors. For example, the SECP-T opening levels are significantly lower than the CCP opening levels, although both sets of results generally follow a smooth trend of decreasing S_{open}/S_{max} with increasing S_{max}/σ_0. Also note that large changes in crack length sometimes lead to changes in crack opening levels, especially when cracks become long relative to the specimen width (compare $a/W = 0.125$ with $a/W = 0.5$). However, a large change in crack length does not automatically lead to a large change in crack opening behavior, as illustrated by the $a/W = 0.125$ and 0.300 data for CCP and SECP-B.

Note, second, that the bend specimen results follow a similar trend with S_{max}/σ_0, where S_{max} is defined in terms of the nominal outer fiber stress rather than the local stress. If the crack opening behavior in this geometry followed the nominal stress at the crack tip location in the uncracked geometry, which decreases with increasing crack length, then we would expect the crack opening levels to increase as the crack grows. But the opposite behavior is observed: the crack opening levels gradually decrease with increasing crack length.

These results are not very appealing for engineering applications, because they suggest that a different functional relationship between S_{open}/S_{max} and S_{max}/σ_0 might be required for every new geometry, including large changes in crack length. This dilemma prompted the search for a new correlating parameter to replace S_{max}/σ_0, some parameter that describes the fundamental differences between different geometric configurations. The natural selection for such a description is the stress

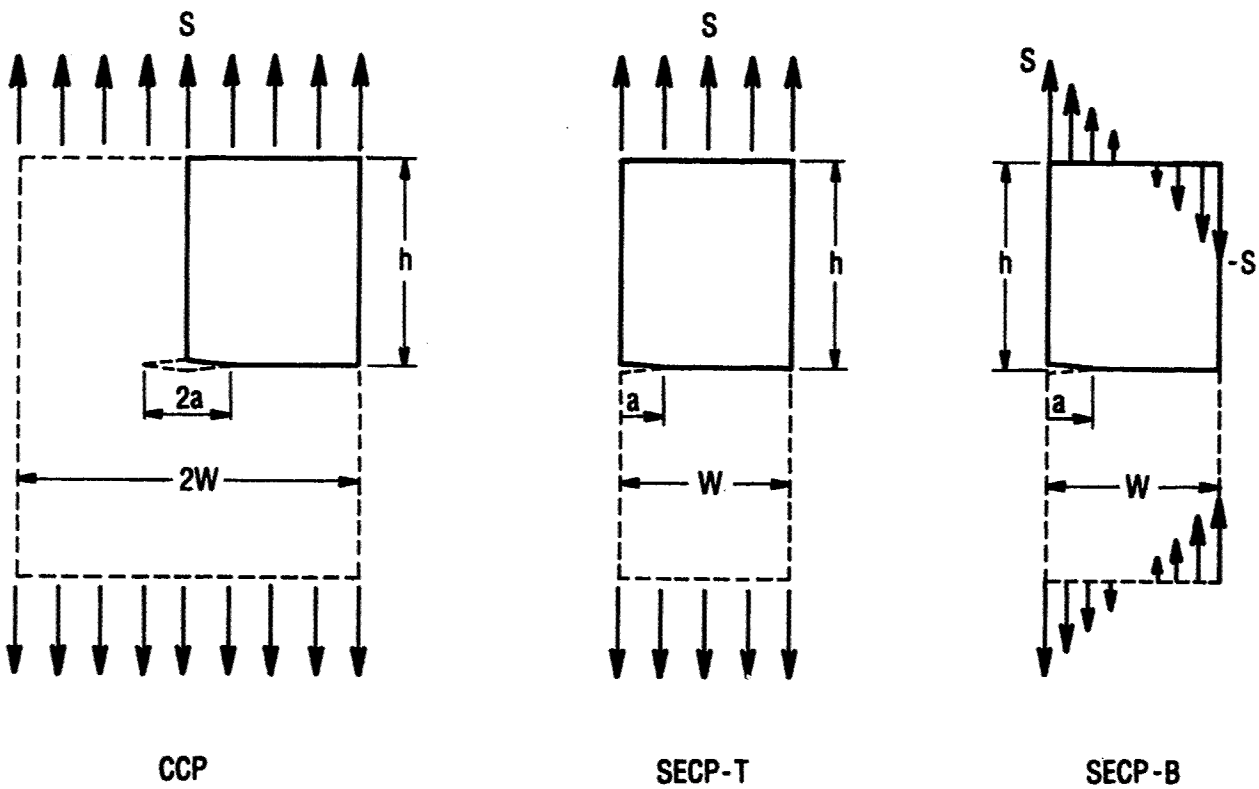

Figure H.2. Three different specimen geometries modeled in this investigation

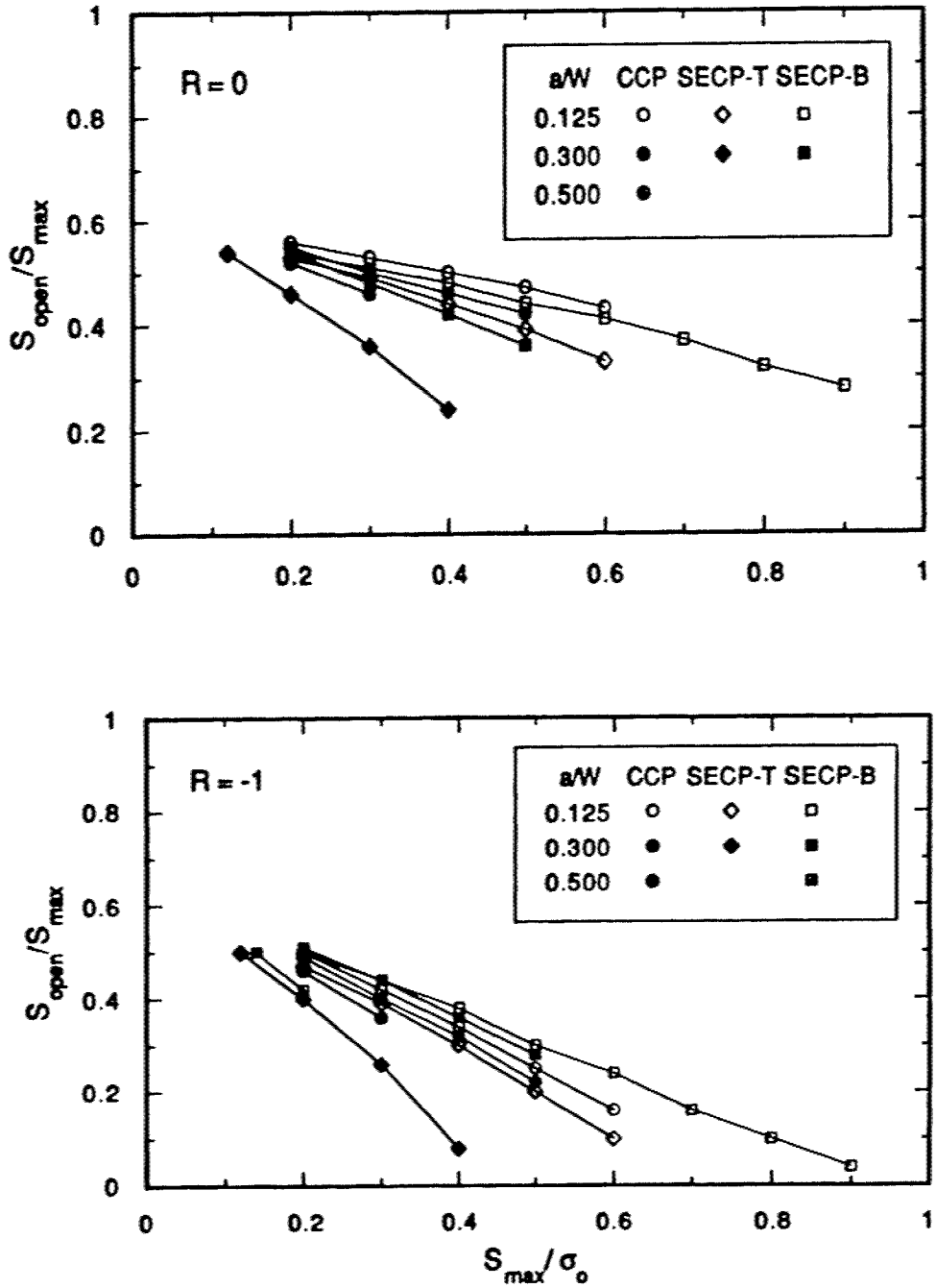

Figure H.3. Normalized crack opening stresses as a function of normalized maximum stress
(Top) $R = 0$ (Bottom) $R = -1$

intensity factor, K. As noted in the introduction, however, K alone does not lead to a satisfactory characterization of crack closure. This failure is illustrated further in Figure H.4, based on the current FEM results. Since K_{max} is a dimensional parameter, we have assigned the values $\sigma_0 = 1$ and $W = 1$ in order to provide a consistent numerical basis on which to evaluate K. Since this is an arbitrary assignment for the purposes of comparison, the absolute units or numerical values of K do not have meaning. Appropriate expressions for K were based on previously published benchmark stress intensity factor solutions (Isida, 1971; Brown and Srawley, 1966). Note that the half-height (from the crack line to the top edge of the mesh) h of the simulated specimens was 1.2 times the specimen width W. A summary of assumed values for the geometry correction factor F, where $K_{max} = F\, S_{max} \sqrt{\pi a}$, is given in Table H.1.

Table H.1. Geometry correction factors used to calculate stress intensity factor

a/W	CCP	SECP-T	SECP-B
0.125	1.01	1.22	1.04
0.3	1.07	1.66	1.12
0.5	1.25	2.83	1.50

Although K contains some valuable information about the crack tip stress and deformation fields, it seems likely that any new correlating parameter for crack closure must still retain some description of the relationship between the maximum applied stress and the yield or flow stress (the original S_{max}/σ_0). With this motivation, a hybrid parameter was formulated which combined aspects of both S_{max}/σ_0 and K. This parameter was expressed as K_{max}/K_0, where

$$\frac{K_{max}}{K_0} = \frac{F S_{max} \sqrt{\pi a}}{\sigma_0 \sqrt{\pi a}} \qquad \textbf{(H.1)}$$

Here K_{max} is calculated in the usual way, including the geometry correction factor F, while F is intentionally omitted from the normalizing quantity K_0. Note that K_{max}/K_0 is equal to $F\, S_{max}/\sigma_0$. This formulation is also suggested by the results in Figure H.3, where the calculated S_{open}/S_{max} results were approximately layered by values of F. Specimen and crack geometries exhibiting larger geometry factors tended to give lower opening stresses.

The crack opening results for both stress ratios are replotted in Figure H.5 in terms of the new correlating parameter K_{max}/K_0. Much closer agreement is observed between the various geometries. This is especially true at small values of K_{max}/K_0, where results for all three crack lengths and all

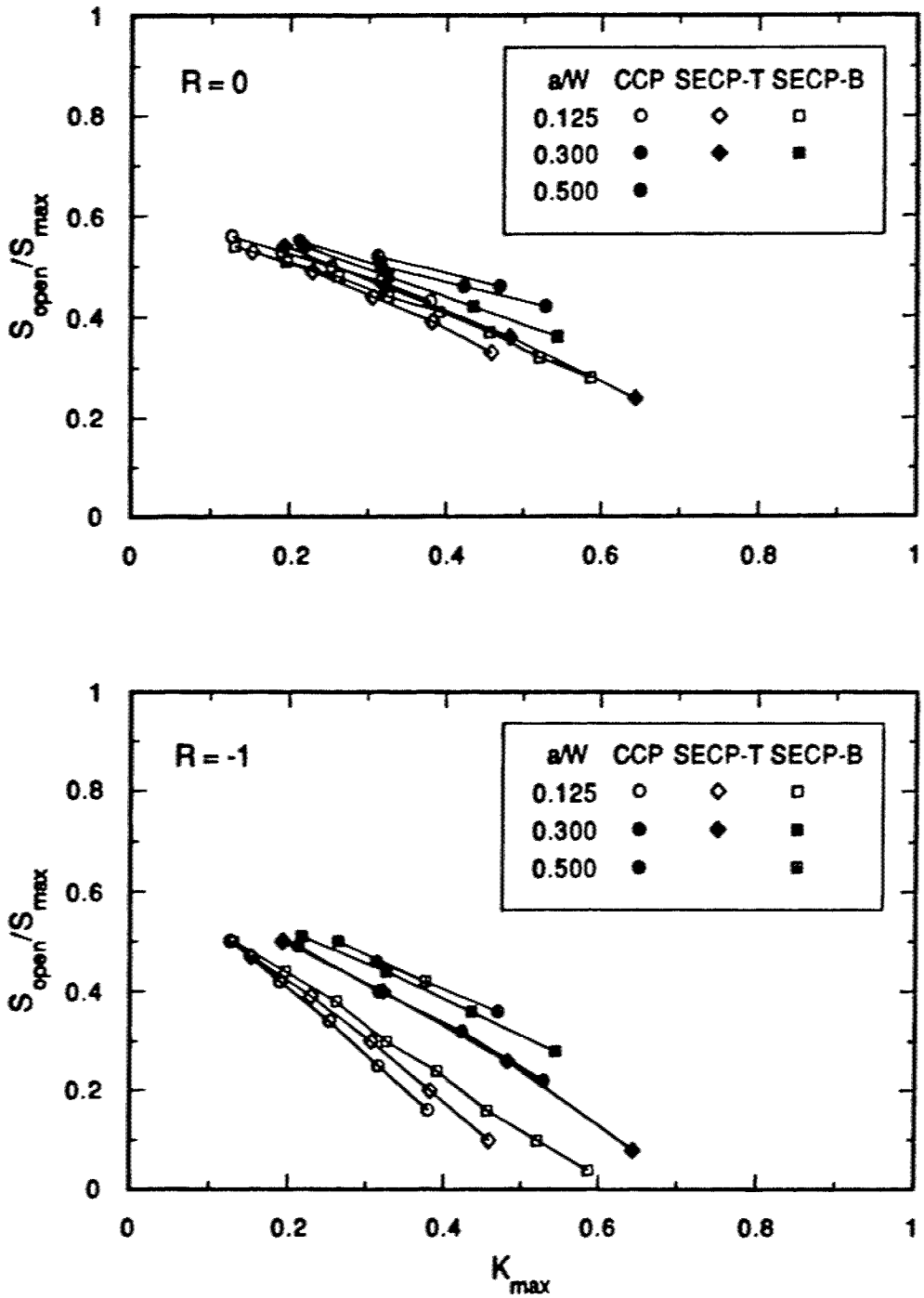

Figure H.4. Normalized crack opening stresses as a function of the maximum stress intensity factor (Top) $R = 0$ (Bottom) $R = -1$

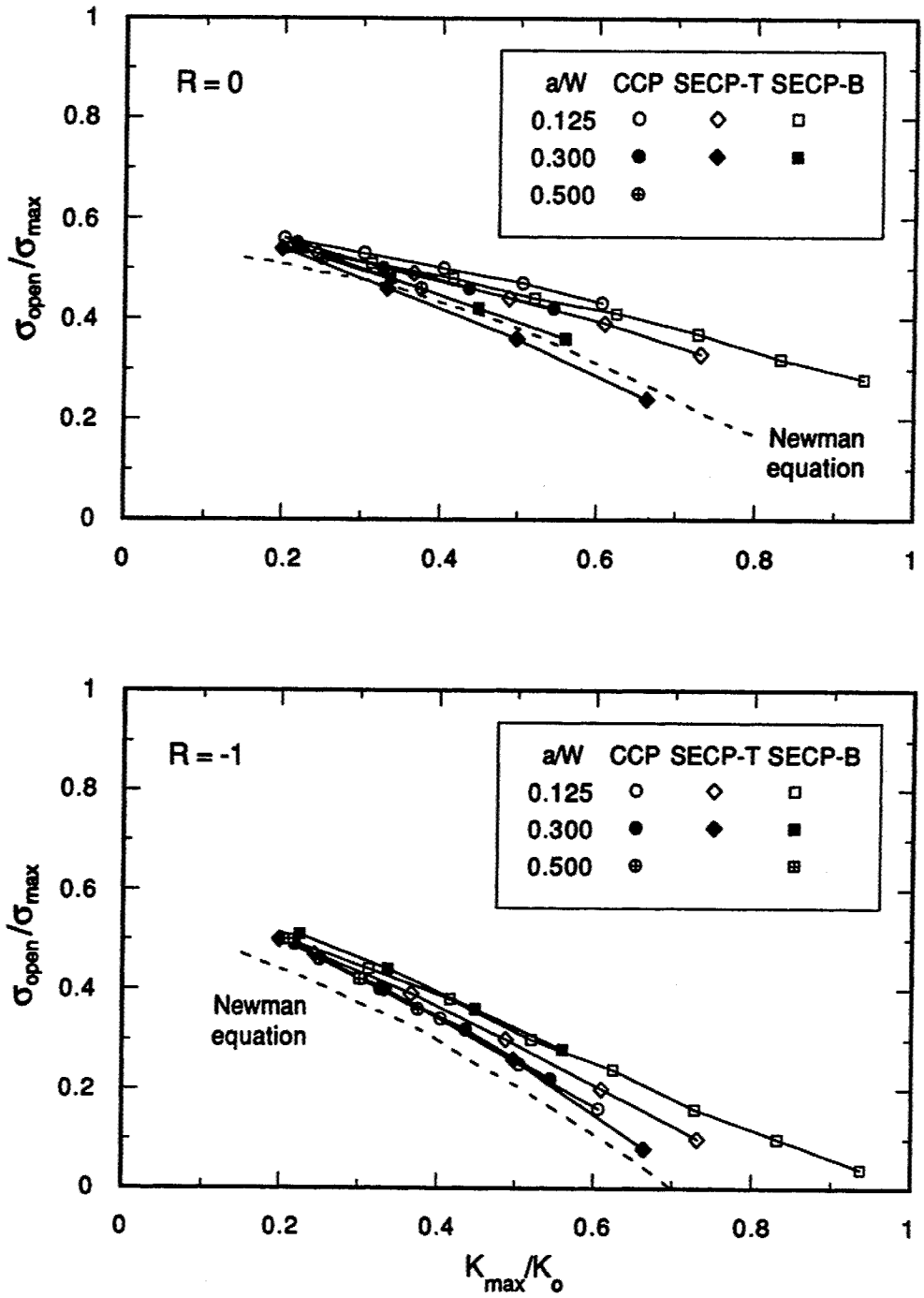

Figure H.5. Normalized crack opening stresses as a function of normalized stress intensity factor (top) $R = 0$ (bottom) $R = -1$

three specimen geometries converge very closely together. At larger K_{max}/K_0 values, the data slowly begin to spread.

Also shown for comparison in Figure H.5 are results from the modified Dugdale closure model of Newman (1981), which is implemented in the computer code FASTRAN. The specific results shown in Figure H.5 are taken from a simple closed-form equation (Newman, 1984) that describes the FASTRAN computations for a center-cracked plate in which the crack was sufficiently small that $a/W \rightarrow 0$. These results were originally expressed in terms of S_{max}/σ_0, but since the appropriate geometric correction factor is $F = 1$, we may employ the equality $K_{max}/K_0 = S_{max}/\sigma_0$. Also note that the Newman model assumes elastic-perfectly plastic material response, which is similar but not identical to the low hardening constitutive model incorporated in the FEM analysis. Although the Newman opening stresses are somewhat lower than the comparable FEM CCP ($a/W = 0.125$) results, they do serve as a convenient (but not necessarily rigorous) lower bound to nearly all of the FEM results when evaluated on a K_{max}/K_0 basis.

H.4 Discussion

The agreement among crack opening stresses as a function of K_{max}/K_0 is encouraging. The strong convergence at small K_{max}/K_0 values suggests that K_{max}/K_0 may be the theoretically proper correlating parameter under true small-scale yielding (SSY) conditions. These results are also consistent with the plane stress results of Fleck (1986) for CCP and SECP-B geometries. Fleck found identical crack opening stresses when he applied the same value of $K_{max} = 0.157\ \sigma_{ys}\ \sqrt{W}$ to both geometries (also keeping $a/W = 0.5$ constant). This corresponds to $K_{max}/K_0 = 0.125$ in the present nomenclature, well down in the SSY regime.

It perhaps should not be surprising that the quality of K_{max}/K_0 as a correlating parameter gradually deteriorates as K_{max}/K_0 increases. At progressively higher stresses and longer crack lengths, small-scale yielding gradually gives way to intermediate-scale yielding, and the linear elastic stress intensity factor K becomes less effective in characterizing the crack tip stress and deformation fields. When $K_{max}/K_0 = 0.5$, for example, the nominal crack tip plastic zone width r_p is about 0.25 of the crack length, so the SSY condition $r_p << a$ is no longer satisfied. Nevertheless, the K_{max}/K_0 correlation of crack opening behavior may still be acceptable for many engineering applications.

At higher K_{max}/K_0 values, there is a general trend to slightly lower crack opening stresses with increasing crack length and, to some degree, with increasing F values among different geometries. These trends prompted additional searches for improved correlating parameters which would be even more accurate at large K_{max}/K_0. One parameter considered was K'_{max}/K_0, where K' incorporated an effective crack length, a', defined as the sum of the physical crack length and the radius of the crack tip plastic zone. A new value of F' was also computed based on a'/W. This is a common first-order correction to K in the intermediate-scale yielding regime. This parameter gave slightly improved correlation of crack opening stresses at $R = 0$ but no improvement (perhaps even a deterioration) at $R = -1$. The alternative parameter $F\ K_{max}/K_0$ (or $F^2\ S_{max}/\sigma_0$) also improved the $R = 0$ correlation slightly but damaged the $R = -1$ correlation. The parameter $(K_{max}/K_0)^2$ performed poorly at both stress ratios. It is certainly possible that some other alternative parameter may ultimately prove to

be the optimum choice, but based upon current information, K_{max}/K_0 appears to be a reasonable selection.

On the other hand, it is not necessarily true that crack opening stresses for different geometries should correlate exactly at all applied stresses. For example, differences in the non-singular stresses parallel to the crack [the so-called *T*-stresses (Larsson and Carlsson, 1973), which are second-order terms in the crack tip stress field and do not appear in the customary *K* expressions] between different geometries could cause changes in opening behavior. FEM studies of crack closure in different biaxial stress fields (McClung, 1989a), which are indirectly related to different *T*-stresses, found that applying an equibiaxial stress parallel to the crack influenced the crack opening stress, especially at higher S_{max}/σ_0 values. On the other hand, different biaxial stresses did *not* influence S_{open}/S_{max} at lower S_{max}/σ_0 values. The *T*-stresses for CCP, SECP-T, and SECP-B are all significantly different, and *T* even changes appreciably with increasing crack length in the SECP geometries (Leevers and Radon, 1982). The influence of these *T*-stresses may help to explain some of the differences in crack opening stresses outside the small-scale yielding regime. On a different note, differences in COD (even at the same *K*) between CCP, SECP-T, and SECP-B geometries may also influence closure behavior as the fracture surfaces move relative to each other. Furthermore, it is also possible that the quality of the FEM simulation itself gradually deteriorates at these larger K_{max}/K_0 values, in view of the relative coarseness of the model (lower order linear strain elements and small strain element formulations).

A loss of *K* dominance with increasing stress and crack length ultimately leads to large scale plasticity effects, as the crack tip plastic zone size becomes large relative to the remaining ligament and the nominal net section stress approaches the yield stress. The ASTM criterion (ASTM E 647, 1998) for valid *K*-based fatigue crack growth (FCG) rate data that the nominal crack tip plastic zone size (PZS) be less than 0.25 of the remaining ligament (*b*) appears to correspond roughly to the point at which crack opening levels begin to drop off significantly with additional crack growth (McClung, 1991c). A related ASTM criterion for valid CCP FCG tests that the nominal net section stresses remain lower than 0.80 of yield also appears to coincide with a decay in crack opening stresses. This latter criterion can be interpreted as the applied stress remaining less than 0.80 of the simple limit load stress for a perfectly plastic material. This alternative interpretation provided a means of expressing the net section yield criterion for the SECP-B geometry: the applied bending moment remains less than 0.80 of the simple limit moment for a perfectly plastic material, where the limit moment per unit thickness was taken as (Miller, 1988)

$$M_L = 1.072 \frac{\sigma_0 W^2}{4} (1 - a/W)^2 \qquad \textbf{(H.2)}$$

These two ligament plasticity criteria (plastic zone size and net section stress) were applied to all of the FEM closure analyses, and FEM crack opening results were not included on Figures H.3-H.5 if either criterion was violated. This filter excluded all of the SECP-T results at $a/W = 0.5$, except when the applied stress was so low that satisfaction of the mesh refinement criteria was suspect.

However, it should be emphasized that these criteria for "normal" crack opening behavior are only rough rules-of-thumb at this point, and have not been systematically validated for this particular purpose. Figure H.6 shows a limited number of additional FEM closure results for cases in which one or both ASTM criteria were violated: $S_{applied}/S_{limit}$ ranging from 0.8 to around 1.1, and/or PZS/b ranging from 0.25 to 0.35. The trend lines from Figure H.5 (data satisfying both criteria) were included on Figure H.6 for comparison purposes. In general, the crack opening stresses dropped off more rapidly with increasing K_{max}/K_0 when either criterion was violated, especially at $R = 0$. However, the crack opening stresses continued to follow expected trends for some configurations, especially at $R = -1$, and the Newman equation is still an approximate lower bound for most of the data shown. Reliable closure results were not available at still higher applied stresses due to various difficulties with the numerical performance of the FEM code. Related difficulties also raised questions about the reliability of the closure results at large crack lengths ($a/W = 0.5$) for the SECP geometries, so most of those results have been completely omitted from this appendix.

Perhaps one of the most useful implications of the K_{max}/K_0 closure correlation is that more confident predictions can be made of crack opening stresses in other geometries, especially geometries which are not amenable to the current state-of-the-art in FEM closure modeling. Of particular interest are three-dimensional geometries such as surface cracks, which are of great significance in engineering applications. While it will probably not be possible to obtain direct experimental or analytical validation of closure predictions in these geometries in the near future, the proposed correlation seems robust enough from an engineering standpoint that it can be used with some confidence.

One example of such an application is a combined loading configuration, such as the superposition of uniform tension and bending loads. Since elastic stresses and elastic stress intensity factors superimpose linearly, it is possible to calculate a total effective K_{max} (a total effective S_{max} and F) and then predict closure behavior. In order to confirm this approach, an additional FEM closure simulation was conducted for a SECP geometry, $R = 0$, $a/W = 0.3$, with combined bending (outer fiber $S_{max} = \pm 0.15\sigma_0$) and tension (uniform $S_{max} = 0.15\sigma_0$). The individual geometry correction factors were $F = 1.66$ for tension and 1.12 for pure bending. By superposition, the total K_{max} was calculated as

$$K_{max}^{total} = F^{total} S_{max}^{total} \sqrt{\pi a} \qquad \textbf{(H.3)}$$

where the total $S_{max} = 0.3$ and the total $F = 1.39$. The combined K_{max}/K_0 value was 0.42. The computed FEM S_{open}/S_{max} value was 0.43, which falls within the scatterband of S_{open}/S_{max} results for single load configurations at $K_{max}/K_0 = 0.42$, bounded closely by the individual SECP-B and SECP-T results for $a/W = 0.3$.

It was not previously clear how to apply an S_{max}/σ_0 closure criterion to the compact tension specimen (McClung, 1991c), where a nominal stress is not clearly defined. And it is still not clear, although the present results do suggest an appropriate role for the stress intensity factor (which, of

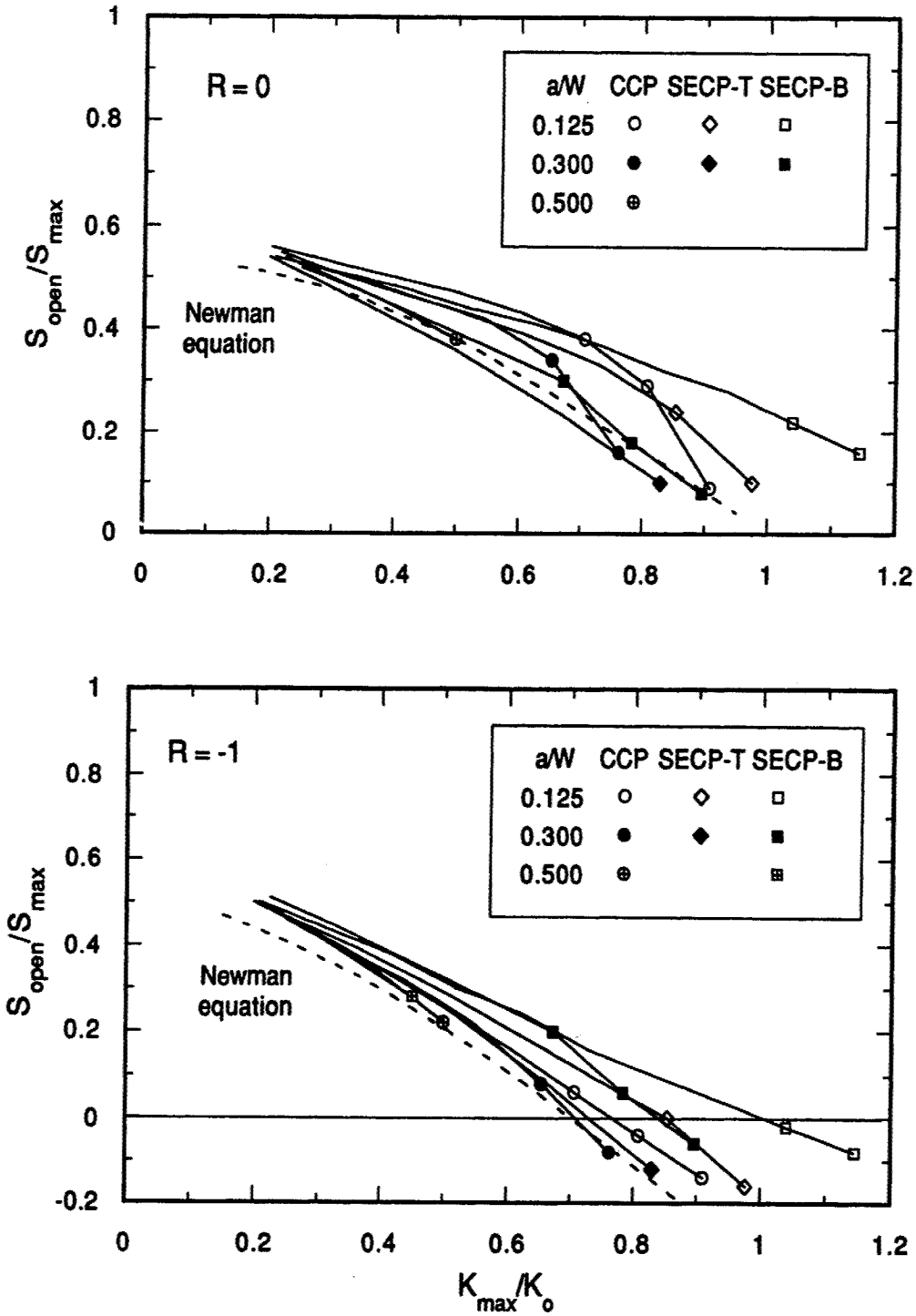

Figure H.6. Normalized crack opening stresses as a function of normalized stress intensity factor for conditions of significant ligament plasticity. (top) $R = 0$, (bottom) $R = -1$.

course, increases with crack length in the CT specimen). Some normalization of the applied load to a limit load or yield load is still needed. Sehitoglu and Sun (1991) presented their CT closure results in terms of the normalized load P_{max}/P_0, where P_0 was the limit load corresponding to the given crack length. They considered only a single narrow range of crack lengths, so it is not possible to evaluate the utility of their approach as a general correlating parameter. Comparison of their CT results with earlier CCP results from the same FEM model (McClung and Sehitoglu, 1989b) suggests that P_{max}/P_0 and S_{max}/σ_0 are not interchangeable parameters.

Newman (1992b) has suggested that CT opening levels can be related to CCP opening levels by using the CCP results and defining an equivalent maximum stress S'_{max} for the CT specimen as

$$S'_{max} = \frac{P}{Wt}\frac{F_{CT}}{F_{CCP}} \tag{H.4}$$

where the stress intensity factor for the CT specimen is expressed in the slightly modified form

$$K_{CT} = \frac{P}{Wt} F_{CT}\sqrt{\pi a} \tag{H.5}$$

Note that defining the equivalent maximum stress according to Equation H.3 in terms of the two geometry correction factors F_{CT} and F_{CCP} leads to essentially the same K_{max}/K_0 relationship proposed in this appendix. The additional assumption included in the Newman formulation is that the equivalent CT stress P/Wt normalized by the flow stress σ_0 is an appropriate characaterization of the applied stress.

The K_{max}/K_0 relationship, which was demonstrated in this appendix for plane stress, is also anticipated to correlate crack closure data for plane strain conditions. However, plane stress and plane strain data will exhibit different K_{max}/K_0 dependencies. In plane strain, the predicted dependence of S_{open}/S_{max} on S_{max}/σ_0 is often relatively weak (Newman, 1981), so the additional influence of the F factor will not be strong and may often be negligible. The unusual finite element results of Fleck (1986) in plane strain—he found only discontinuous and therefore unstable opening behavior—may have been dominated by other numerical effects. More recent finite element investigations into plane strain closure have found stable, continuous closure behavior similar to that observed under plane stress (McClung, Thacker, and Roy, 1991).

It is also anticipated that the K_{max}/K_0 correlation will hold true for materials with different strain hardening behavior, although the closure results themselves will change with different H/E (McClung, 1992). The current analyses focused on low hardening materials under plane stress because these conditions were known to motivate particularly strong variations in S_{open}/S_{max} with S_{max}/σ_0 for CCP configurations (McClung, 1992), and because they facilitated more direct comparisons with the Newman FASTRAN results.

As noted earlier, the Newman modified-Dugdale model equation provides a slightly conservative lower bound to nearly all of the FEM results considered here, if appropriate limits on plasticity in the remaining ligament are enforced. In order to function in this way, the Newman parameter S_{max}/σ_0 must be interpreted as K_{max}/K_0. For the small center crack on which the FASTRAN closed-form equation (Newman, 1984) was originally based, these two parameters are essentially identical. This is an especially useful result, because the closed-form equation addresses a wide range of stress ratios, S_{max}/σ_0 (K_{max}/K_0) values, and out-of-plane constraint (from plane strain to plane stress). This explicit equation is much more convenient for engineering applications than the FEM model, which is strictly a research tool at this time.

H.5 Conclusions

1. Different specimen geometries (in particular, CCP, SECP-T, and SECP-B configurations) exhibit different fatigue crack closure behaviors. The normalized maximum stress S_{max}/σ_0, which successfully describes closure results over small ranges of crack lengths in individual geometries, does not correlate the effect of different geometries on the normalized crack opening stress, S_{open}/S_{max}.

2. The outer fiber stress, and not the nominal stress in the vicinity of the crack tip, appears to be the appropriate characterizing stress for crack closure in SECP-bend geometries.

3. The normalized stress intensity parameter K_{max}/K_0, where $K_0 = \sigma_0\sqrt{\pi a}$ and σ_0 is the flow stress, successfully correlates crack opening stresses for the three different specimen geometries at three different ranges of crack length to width ratios. The quality of the correlation is very high at small K_{max}/K_0, and gradually deteriorates as K_{max}/K_0 increases beyond the SSY regime.

4. The K_{max}/K_0 approach to characterizing crack closure provides an engineering method to predict crack opening stresses in many other geometries and load configurations, including combined loading.

5. The Newman modified-Dugdale closure model equations, interpreted in terms of K_{max}/K_0, provide a slightly conservative lower bound to nearly all of the finite element closure results presented in this appendix, if appropriate limits on plasticity in the remaining ligament are enforced.

APPENDIX I

ALGORITHMS FOR CRACK INSTABILITY

SUMMARY

Criteria for evaluating the instability of cracks subjected to monotonic and cyclic loading under linear elastic and elastic-plastic conditions are reviewed and practical guidelines provided for implementing the criteria for brittle and ductile materials. It is shown that incipient instability results in an acceleration in the fatigue crack growth rate due to the contribution of static failure modes to crack extension during the load-up part of a fatigue cycle. Fatigue crack growth laws are recommended for describing this acceleration which depends on the magnitude of the crack tip driving force at the maximum load in the cycle and the fracture resistance of the material. In general, the instantaneous enhancement in cyclic crack propagation rate will depend on the previous cyclic load history. Rules are provided for determining the influence of this load history. In the case of ductile materials, which can undergo simultaneous stable tearing and fatigue crack growth, the rules are formulated in terms of Memory and Loss of Memory Models. In the Memory Model, the ductile fracture process zone at the crack tip retains information about the previous cyclic loading, while in the Loss of Memory Model this information is assumed lost. The latter model predicts more conservative crack growth rates than the former. The characterization of fracture properties for use in the instability criteria are discussed as well as the effects of plastic constraint on fracture toughness and J_R-curves. Practical considerations pertaining to the application of the crack instability criteria to predicting failure in service life assessments are addressed.

I.1 Introduction

Fracture mechanics based failure criteria governing crack instability in materials that exhibit brittle or ductile behavior are well defined. The main feature differentiating fracture in brittle and ductile materials is that the latter display an increase in toughness as a crack extends under a rising load, whereas in the former crack extension and instability are coincident.

In this appendix, algorithms are described which define crack instability criteria under monotonic loading conditions. These criteria are assumed applicable under cyclic loading conditions and are incorporated into fatigue crack growth algorithms in order to simulate the observed acceleration in fatigue crack growth rates due to the contribution from monotonic modes of fracture as crack instability is approached. Emphasis is placed on ductile materials because of the more complicated instability criterion governing these materials, and because they are a major constituent of the Space Shuttle Main Engine (SSME) and other advanced propulsion systems. Where possible, recommendations are proposed for modifying the algorithms for the influence of monotonic and cyclic crack-tip plasticity, and load history effects (e.g., the effect of a proof test overload on subsequent fracture behavior). Recommendations are also given regarding the material properties that are needed to implement the algorithms.

I.2 Criteria for Crack Instability

I.2.1 Brittle Fracture Criterion

In terms of linear elastic fracture mechanics (LEFM), the onset of brittle fracture occurs when

$$K\ (a,P) = K_{mat}\ (= K_{Ic}\ \textit{under plane strain conditions}) \qquad \textbf{(I.1)}$$

where $K(a,P)$ is the applied stress intensity factor which is a function on the crack depth, a, and the applied load P. K_{mat} is a measure of fracture toughness equal to the plane strain value, K_{Ic}, when flat fracture occurs, or K_c, under mixed flat and slant (plane stress) fracture conditions. K_{Ic} is determined according to the ASTM test method E399 (1998). K_c is a thickness-dependent material toughness which can be derived from K_{Ic} for some materials using the relationship proposed in the user manual for the NASA/FLAGRO (Forman et al., 1994) computer program

$$K_c = K_{Ic}\left\{1 + B_k \exp - \left[A_k \frac{t}{t_o}\right]^2\right\} \qquad \textbf{(I.2)}$$

where

$$t_o = 2.5\left(\frac{K_{Ic}}{\sigma_{ys}}\right)^2 \qquad \textbf{(I.3)}$$

and A_k and B_k are empirical constants, t the wall thickness, and σ_y the yield stress. NASGRO also gives an equation to estimate the toughness of part-through surface cracks from K_{Ic} according to

$$K_{Ie} = K_{Ic}\left(1 + C_k\, K_{Ic} / \sigma_{ys}\right) \qquad \textbf{(I.4)}$$

where C_k is an empirical constant with units of length$^{-1/2}$.

It is emphasized that Equations (I.2) and (I.4) are empirically derived and should only be used with great caution outside of their region of empirical validity.

In elastic-plastic fracture mechanics (EPFM), the LEFM fracture criterion is replaced by an equivalent criterion based on the J-Integral. In terms of the EPFM parameter, J, the onset of brittle failure occurs when

$$J\,(a,P) = J_{mat} = \frac{K_{mat}^2}{E'} \;\left(= \frac{K_{Ic}^2}{E'} \;\; \textit{under plane strain conditions}\right) \qquad \textbf{(I.5)}$$

where J_{mat} is the toughness expressed in terms of J, and $E'=E$, Young's modulus in plane stress, $E'=E/(1-\nu^2)$ in plane strain, and ν is Poisson's ratio.

In the limit of small scale crack-tip yielding, J is given by the equation

$$J = \frac{K^2}{E'} \qquad \textbf{(I.6)}$$

and Equation (I.5) reduces to the LEFM fracture criterion, Equation (I.1). Although J_{mat} is related to K_{mat}, the empirical Equations (I.2) and (I.4) are not generally applicable to failures in the EPFM regime because crack-tip plasticity will change the relationship between toughness and dimensional parameters, such as the thickness, t.

I.2.2 Ductile Fracture Criterion

The ductile failure criterion is more complicated than the brittle one as there is no single unique toughness value: the toughness depends on the instantaneous amount of ductile tearing, Δa_t. In this case, the onset of instability occurs under LEFM conditions when

$$K\left(a_o + \Delta a_t, P\right) = K_R(\Delta a_t) \ , \ \frac{dK}{da} = \frac{dK_R}{d\left(\Delta a_t\right)} \tag{I.7}$$

and under EPFM conditions when

$$J\left(a_o + \Delta a_t, P\right) = J_R(\Delta a_t) \ , \ \frac{dJ}{da} = \frac{dJ_R}{d\left(\Delta a_t\right)} \tag{I.8}$$

where a_o is the initial crack depth and $K_R(\Delta a_t)$ and $J_R(\Delta a_t)$ characterize the toughness at the tear length Δa_t. In ductile materials, K_{mat} and J_{mat} characterize the toughness at the initiation of crack extension.

The instability criteria expressed by Equations (I.7) and (I.8) correspond to conditions where the crack-tip driving force, K or J, becomes tangential to the K_R or J_R-curve (Figure I.1).

More detailed discussions concerning material toughness characterization in terms of J_R-curves are provided in Section I.4.2.

I.3 Criteria for Accelerated Fatigue Crack Growth Due to Incipient Instability

The brittle and ductile failure criteria also define instability under cyclic loading conditions. In these cases, it is known that an acceleration in the sub-critical crack growth rate occurs as the applied value of J at the maximum load in the cycle, J_{max}, approaches J_{mat} in brittle materials, and when $J_{max}>J_{mat}$ in ductile materials. To allow for this, several fatigue crack growth laws have been proposed for brittle materials (Weertman, 1969; Irving and McCartney, 1977; Heald, Lindley and Richards, 1972; Chell, 1984; Forman et al., 1994) and ductile materials (Kaiser, 1983; Chell, 1984; Nix et al., 1988; Nix et al., 1989) which result in an enhancement in the normal fatigue crack growth rate as the conditions for instability of a monotonically loaded crack are approached.

I.3.1 Contribution of Brittle Fracture Mechanisms to Crack Growth

In its simplest form, the fatigue component of the sub-critical crack extension rate, $(da/dN)_f$, is usually expressed as the Paris Equation

$$\left(\frac{da}{dN}\right)_f = C_0(\Delta K)^{m_0} \tag{I.9}$$

where C_0 and m_0 are material constants and ΔK is the cyclic range of the stress intensity factor, K_{max}-K_{min}, where subscripts *max* and *min* signify quantities evaluated at the maximum and minimum loads of a cycle, respectively. This equation is oftentimes modified to explicitly include the effects of R ratio (K_{min}/K_{max}) and near threshold behavior (e.g., see NASGRO 2.0 equation in Forman et al., 1994). For simplicity, these additional dependencies are omitted in the discussions that follow unless it is necessary to explicitly include them. (As previously noted in Section 3.5.1, EPFCG data do not exhibit traditional threshold behavior.) It is straightforward to extend the developments to be described to the more general form of the fatigue crack growth laws.

Theoretical and experimental works suggest that Equation (I.9) can be generalized to include the contribution of monotonic modes of fracture to the growth rate by writing (e.g., Heald, Lindley and Richards, 1972; Chell, 1984).

$$\frac{da}{dN} = \frac{\left(\frac{da}{dN}\right)_f}{1 - \left(\frac{K_{max}}{K_{Ic}}\right)^2} \tag{I.10}$$

The NASGRO 2.0 equation has a different form to this and can be expressed as

$$\frac{da}{dN} = \frac{\left(\frac{da}{dN}\right)_f}{\left(1 - \frac{K_{max}}{K_c}\right)^q} \tag{I.11}$$

where q is a material constant.

Both Equations (I.10) and (I.11) incorporate crack instability through the terms in their denominators, which predict infinite crack growth rates when the brittle fracture criterion is satisfied. The different forms for Equations (I.10) and (I.11) can be partly explained by the fact that Equation (I.10) is applicable to flat (plane strain) fracture, while Equation (I.11) addresses instability of through-wall flaws in thin section materials where slant (plane stress) fracture predominates.

The form of Equation (I.11), which contains a unique toughness term, K_c, is only applicable to materials which undergo brittle fracture, or materials that fail by a ductile mechanism with no significant increase in toughness with stable crack growth. Although slant fracture is a ductile mechanism, some materials used in the aerospace industry, such as some aluminum alloys, fail with little or no increase in fracture toughness after crack initiation has commenced, and for these materials Equation (I.11) provides a description of their crack growth rate behavior when K_{max} approaches K_c.

Equation (I.9) can be extended to include the effects of cyclic plasticity and crack closure by writing

$$\left(\frac{da}{dN}\right)_f = C\left(\Delta J_{eff}\right)^{m_0/2} \tag{I.12}$$

where ΔJ_{eff} reduces to $(\Delta K_{eff})^2/E'$ in the limit of small scale cyclic plasticity, ΔK_{eff} is that part of the range of ΔK where the crack is open, and $C = \left[C_0(E')^{m_0/2}\right] / \left[U_0^{m_0}\right]$, where U_0 is the effective stress intensity factor range ratio in the data from which C_0 and m_0 were derived. Following similar arguments, the effect of monotonic modes can be accounted for in the elastic-plastic regime by modifying Equations (I.10) and (I.11) to read

$$\frac{da}{dN} = \frac{\left(\frac{da}{dN}\right)_f}{1 - \left(\frac{J_{max}}{J_{Ic}}\right)} \tag{I.13}$$

and

$$\frac{da}{dN} = \frac{\left(\frac{da}{dN}\right)_f}{\left(1 - \left[\frac{J_{max}}{J_c}\right]^{1/2}\right)^q} \tag{I.14}$$

Load history effects, such as arise from overloading, will predominantly influence the fatigue component of growth, $(da/dN)_f$, through mechanisms associated with crack growth retardation and acceleration. Although materials that fail by a crack-tip stress controlled cleavage mechanism could have their toughness values increased by overloads applied at higher temperatures through

mechanisms such as warm pre-stressing, these effects will be conservatively allowed for in an assessment if toughness values measured in the absence of the overloads are used. Furthermore, sub-critical fatigue crack extension after the overload will propagate the crack tip through the process zone formed during the overload and into virgin material, eventually eliminating the effects of the overload.

I.3.2 Contribution of Ductile Fracture Mechanisms to Crack Growth

I.3.2.1 Memory Model

A simple model for including the effects of monotonic ductile fracture modes on fatigue crack growth rates has been proposed by Kaiser (1983) and Chell (1984). In this model, there is no mechanistic interaction between fracture and fatigue mechanisms, but a synergistic interaction occurs due to the increase in crack-tip driving forces from physical crack extensions resulting from each mechanism. In the model, the instantaneous crack extension per cycle, *da/dN*, is assumed equal to the linear addition of the crack growth rates from each of the mechanisms

$$\frac{da}{dN} = \left(\frac{da}{dN}\right)_f + \left(\frac{da}{dN}\right)_t \qquad \textbf{(I.15)}$$

where $(da/dN)_t$ is the contribution from tearing given by

$$\left(\frac{da}{dN}\right)_t = 0, \; if \; J_{max} \le J_{mat} \qquad \textbf{(I.16)}$$

$$\left(\frac{da}{dN}\right)_t = \frac{dJ_{max}}{dN} \Big/ \frac{dJ_R}{d(\Delta a_t)}, \quad if \;\; J_{max} > J_{mat}, \; \frac{dJ_{max}}{dN} > 0 \qquad \textbf{(I.17)}$$

$$\left(\frac{da}{dN}\right)_t = 0, \quad if \;\; \frac{dJ_{max}}{dN} \le 0 \qquad \textbf{(I.18)}$$

Using Equation (I.17) and replacing dJ_{max}/dN by $(dJ_{max}/da)(da/dN)$, then Equation (I.15) can be re-arranged into the form (Chell, 1984)

$$\frac{da}{dN} = \frac{\left(\frac{da}{dN}\right)_f}{1 - \frac{dJ_{max}}{da} / \frac{dJ_R}{d(\Delta a_t)}} \tag{I.19}$$

which predicts an infinite growth rate when the ductile instability criterion, Equation (I.8), is satisfied.

During stable crack growth the applied J must be balanced by the material's resistance to crack extension, J_R, and hence after n cycles

$$J_{max,n}\left(a_o + \Delta a_{f,n} + \Delta a_{t,n}\right) = J_R\left(\Delta a_{t,n}\right) \tag{I.20}$$

where $\Delta a_{t,n}$ is the total ductile tearing after n cycles given by

$$\Delta a_{t,n} = \sum_{i=1}^{n} \delta\Delta a_{t,i} = \sum_{i=1}^{n} \left(\Delta a_{t,i} - \Delta a_{t,i-1}\right) \tag{I.21}$$

where $\delta\Delta a_{t,i}$ is the change in tear length per cycle. The total crack extension due to fatigue after n cycles, $\Delta a_{f,n}$ is given by

$$\Delta a_{f,n} = \sum_{i=1}^{n} \left(\frac{da}{dN}\right)_{f,i} \tag{I.22}$$

where $(da/dN)_{f,i}$ is the growth rate on the i'th cycle. The crack depth after n cycles, a_n is given by $a_o + \Delta a_{f,n} + \Delta a_{t,n}$.

If at the end of n cycles the Memory Model becomes inappropriate due to a "Loss of Memory" event, then the "memory" of how the total tear length, $\Delta a_{t,n}$, was accumulated is permanently lost.

The evaluation of $\Delta a_{f,n} + \Delta a_{t,n}$ using Equations (I.20) and (I.21) is a computationally easier task than integrating Equation (I.19) over n cycles.

In the proposed tear-fatigue model:

(a) fatigue crack extension and ductile tearing are assumed to occur on the load-up part of the cycle and to be independent mechanisms that do not interact except through the mechanical interaction from physical crack extensions associated with each mechanism

(b) consistent with (a), $(da/dN)_{f,n}$ for the *n'th* cycle, is evaluated for the crack length, $a_o+\Delta a_{f,n-1}+\Delta a_{t,n-1}$

(c) provided $(dJ_{max}/dN)_n$ is positive (i.e., $dJ_{max}/da > 0$), $\Delta a_{t,n}$ is evaluated from Equation (I.20) as if $J_{max,n}$ had been applied at the beginning of the *n'th* cycle to a crack of initial depth $a_o+\Delta a_{f,n}$, and no tearing had occurred during previous cycling

(d) if $(dJ_{max}/dN)_n$ is zero or negative (i.e., J_{max} remains constant or decreases between the $(n-1)$*'th* and *n'th* cycles, and $dJ_{max}/da \leq 0$), then no tearing will occur on the *n'th* cycle even though $J_{max}>J_{mat}$. (This situation could occur if, for example, the applied loading is displacement controlled, or if the crack is subjected to thermal stressing which results in steep stress gradients.)

A simple model of fatigue crack extension that supports the assumption in item (a) is discussed in Endnote I.1. Items (c) and (d) imply that the crack-tip ductile process zone retains information about previous tearing events and tearing will not commence until $J_{max,n}$ exceeds $J_{max,n-1}$ on the load-up part of the *n'th* cycle. Hence, the proposed model is herein called the Memory Model for tear-fatigue (see Figure I.2). In contrast, if a memory of previous cyclic events was not retained within the ductile process zone, then ductile tearing would be expected to begin as soon as J_{max} exceeded J_{mat} on every load-up part of a cycle (see Figure I.3). This is herein called the Loss of Memory Model and is described in Section I.3.2.2.

Limited experimental data supports the assumption underpinning items (c) and (d) and the application of the Memory Model. This evidence is discussed in Endnote I.2.

The derivation of Equation (I.20) presupposes that the Memory Model is appropriate for the *n* service cycles. Situations where this is not the case are discussed in the next section.

I.3.2.2 Loss of Memory Model

In situations where the Memory Model is not applicable, then a conservative approach to tear-fatigue crack growth should be adopted based on the Loss of Memory Model (see Figure I.3). This situation can arise, for example, when:

(i) $J_{max,n+1} < J_{max,n}$ and $J_{max,n+1}>J_{mat}$. An example of this possibility is where a proof test or other overload event occurs part way through service.

(ii) There is a significant change in the toughness of the material at the crack tip as it propagates by tear-fatigue due to a change in through-wall metal temperature, or the time evolution of temperature, during cycling. These temperature changes could result, for example, from start-up and shut-down. However, such changes should not be an immediate cause for reverting to the Loss of Memory Model as there may be mitigating circumstances associated with thermal transient events in ductile materials which can be used to justify the continued application of the Memory Model under these conditions. (See the discussion in Item (iv) of Section I.3.3.1.)

The recommended procedure for evaluating tear-fatigue in the Loss of Memory Model is to use Equation (I.15) but with $(da/dN)_t$ defined as:

$$\left(\frac{da}{dN}\right)_{t,n} = 0, \quad if\ J_{max,n} \leq J_{mat} \tag{I.23}$$

$$\left(\frac{da}{dN}\right)_{t,n} = \delta\Delta a^{*}_{t,n}\ , \quad if\ J_{max,n} > J_{mat} \tag{I.24}$$

where $\delta\Delta a_{t,n}^{*}$ for the *n'th* cycle is obtained by solving the equation

$$J_{max,n}\left(a_o + \Delta a_{f,n} + \Delta a^{*}_{t,n-1} + \delta\Delta a^{*}_{t,n}\right) = J_R\left(\delta\Delta a^{*}_{t,n}\right) \tag{I.25}$$

and J_R is the toughness pertaining to the current service environment. The total accumulated tear after n-1 Loss of Memory cycles is given by

$$\Delta a^{*}_{t,n-1} = \sum_{i=1}^{n-1} \delta\Delta a^{*}_{t,i} \tag{I.26}$$

The superscript * signifies that ductile tearing has occurred during service under Loss of Memory conditions.

The derivation of Equation (I.25) presupposes that the Loss of Memory Model is appropriate for all the n service cycles.

I.3.3 Practical Guidelines for Applying the Tear-Fatigue Crack Growth Law

I.3.3.1 Guidelines for Applying the Memory Model

The following rules should be followed when applying Equations (I.20) and (I.21) to evaluate tear-fatigue using the Memory Model:

(i) At the start of the *n'th* load cycle the condition $J_{max,n} \geq J_{max,n-1}$ should be satisfied for the Memory Model to be applicable (irrespective of whether the cyclic loading is of constant or variable amplitude), where subscript n signifies the *n'th* cycle. This condition is equivalent to $(dJ_{max}/dN)_n \geq 0$.

This rule takes into account the basic physical assumption underpinning the Memory Model that the ductile fracture process zone should be unchanged or increase if the effects of previous load history are to influence the current toughness of material.

(ii) If $J_{max} > J_{mat}$ is satisfied on the first service load-up then Equations (I.20) and (I.21) should be applied after the first load-up. Crack extension for the first load-up should be evaluated as follows:

(a) Determine the amount of ductile tearing due to load-up, $\Delta a_{t,0}$, using Equation (I.20) with $\Delta a_{f,n}$ set to zero.
(b) Then proceed with the first cycle tear-fatigue calculations by determining $(da/dN)_{f,1}$ using the crack depth $a_o+\Delta a_{t,0}$.

This rule is intended to make sure that any ductile tearing that occurs during the first load-up is accounted for when determining crack extension due to subsequent load cycling.

(iii) If $J_{max,m} \leq J_{max,n}$, where $m \geq n+1$ then $(da/dN)_{t,m}$ should be set to zero (equivalently $\Delta a_{t,m}=\Delta a_{t,n}$). If, after a further Δn cycles, $J_{max,n+\Delta n} \geq J_{max,n}$, and provided the fatigue growth in the Δn cycles, $\delta a_{f,\Delta n} \leq 0.1 J_{max,n}/\sigma_{ys}$, then the following procedure should be followed:

(a) Determine the ductile tear, $\Delta a_{t,n+\Delta n+1}$, at the end of the $n+\Delta n+1$ load-up using Equation (I.20) with fatigue extension $\Delta a_{f,n+\Delta n}$.
(b) Then proceed to calculate the crack growth for the $n+\Delta n+2$ cycle using an instantaneous crack depth $a_{n+\Delta n+1}= a_o+\Delta a_{f,n+\Delta n}+\Delta a_{t,n+\Delta n+1}$.

If, however, $\delta a_{f,\Delta n} > 0.1 J_{max,n}/\sigma_{ys}$, then memory of the preceding load history should be assumed lost, and the Loss of Memory Model should be applied to the $n+\Delta n+1$ cycle.

This rule recognizes that very small extensions of the crack by fatigue alone which move the tip forward by only a small fraction of the ductile fracture process zone will not significantly change the process zone, and hence will not seriously degrade the information (memory) stored there. The condition $\delta a_{f,\Delta n} \leq 0.1 J_{max,n}/\sigma_{ys}$ for retaining the Memory Model has not been validated but is based on engineering judgement that memory is still retained provided crack extension is less than 10% of the ductile fracture process zone length, characterized by the crack-tip opening displacement, J_{max}/σ_{ys}.

(iv) The Memory Model can only be applied if there are no significant changes in the fracture toughness of the material due to service exposure between cycles. The Loss of Memory Model should be used when this is not the case.

This rule recognizes that material properties may significantly change during service due, for example, to thermal transients arising from start-up and shut-down which result in instantaneous through-wall temperature gradients that evolve over time. Under these conditions, the temperature in the fracture process zone changes from cycle to cycle as the crack tip extends at the maximum load of each cycle. In these circumstances, a conservative approach would be to assume that the temperature changes wipe out information in the ductile process zone related to the material's previous loading history. However, the tensile and fracture properties of ductile materials do not usually undergo drastic changes as the temperature changes and engineering judgement would suggest that it should still be possible to justify the use of the Memory Model in many cases where thermal cycling occurs. In such situations, the tensile and fracture properties used in the evaluation of the cyclic growth rate should be chosen to correspond to a time independent crack tip temperature based on the thermal cycling history and chosen to result in a conservative crack extension over the distance traveled by the tip during the growth analysis.

I.3.3.2 Guidelines for Applying the Loss of Memory Model

If cyclic loading conditions that satisfy the Memory Model are interrupted by cyclic conditions that invalidate the application of this model, then the Memory Model should be replaced by the Loss of Memory Model in further calculations of tear-fatigue. In this event, the crack depth at the end of the last cycle (say a_n if this occurs after the *n'th* cycle) for which the Memory Model was valid should be used as the initial crack depth at the start of the Loss of Memory Model. The fact that a_n consists of both fatigue and tear components is no longer relevant for the purposes of applying the Loss of Memory Model. The application of the Loss of Memory Model will always produce conservative crack growth rates compared to the predictions of the Memory Model.

The Memory Model may again become valid after a further number of cycles (say m) where the Loss of Memory Model was applied. If this occurs, then the crack depth, a_{n+m} should be used

as the initial crack depth in the Memory Model and the fact that this consists of components that arise from fatigue and tearing is not relevant.

I.3.3.3 Guidelines for Determining the Stress Ratio and its Effect on Fracture

The stress ratio, R, is normally defined as P_{min}/P_{max}, where P_{min} and P_{max} are the minimum and maximum loads in the cycle, respectively. The parameter, R, is frequently used to characterize crack closure effects since when R=0 linear-elastic fracture theory would predict the crack faces are touching at the minimum load, P_{min}. In practice, crack-tip plasticity and compressive residual stresses left behind in the wake of a propagating crack complicate this simple picture.

The definition of R in terms of a ratio of loads is limited to cases where the fatigue loading arises solely from a single mechanical load, P. It is not applicable to the many practical problems where thermal cycling is the major contributor to fatigue loading. In these cases, it is more appropriate to base the definition of R on fracture mechanics principles. A suitable definition for R based on these principles that has been used successfully in the past to characterize closure effects is

$$R = \frac{K_{\min}}{K_{\max}} \tag{I.27}$$

which reduces to P_{min}/P_{max} for the case of a single cyclic mechanical load.

The possible influences of crack closure at different stress ratios on the conditions for tearing and final instability are not well understood. Traditional instability theories assume that the crack begins to open at zero load and hence that the simple $P_{\max}$ value (relative to $P_{\min} = 0$) should be employed in calculating $J_{\max}$ for comparison with J_{mat} or J_{R}. However, the possibility that the crack opens and closes at some nonzero value of load (either positive or negative) raises the possibility that some other load value besides $P_{\max}$ is needed to characterize $J_{\max}$ properly. Newman has shown in the K domain that crack closure at positive loads during fatigue precracking or service cycling can elevate the apparent fracture toughness of a material (Newman et al., 1992, 1995). His analysis indicates that the $K_{\max}$ value at which fracture occurs is elevated by a quantity approximately equal to the (positive) K_{open} value.

However, due to an absence of information documenting this effect under fully elastic-plastic conditions, no compensation for crack closure in tear-fatigue algorithms or other instability calculations is recommended at this time. Note that under severe elastic-plastic cycling, crack opening levels are often very close to zero load, which would reduce the significance of the effect. Ignoring the effects of positive crack closure loads on fracture would be conservative. The primary conditions of potential concern (i.e., nonconservatism) would be the possibility that negative closure loads could lead to instability at lower values of $P_{\max}$. However, limited tear-fatigue studies under the MCPT contract (McClung et al., 1996) found no significant changes in tearing behavior at maximum load during severe elastic-plastic cycling at negative stress ratios.

I.4 Material Property Characterization for Crack Instability and Tear-fatigue

I.4.1 Characterization of J_R-Curves

Application of the ductile instability criteria and the tear-fatigue model is dependent on the availability of suitable material properties data. In particular, a J-resistance curve must be available for the material of interest. Unfortunately, the standard J_R-curve information contained in most material property data bases may not be the most appropriate for many reusable aerospace propulsion system applications (see Section I.4.2). However, this data still serves as the appropriate starting point for the recommended analysis procedure.

Crack growth resistance data should be based on an accepted standard test method, such as ASTM Test Method E 1737, "Standard Test Method for J-Integral Characterization of Fracture Toughness" (ASTM E 1737, 1998). This test method specifies the use of either a pin-loaded compact tension (C(T)) specimen, a single-edge crack bend (SE(B)) specimen, or a pin-loaded disk-shaped compact (DC(T)) specimen. The dimensions of the specimens used have to meet minimum requirements to ensure highly constrained plane strain deformation and J characterization of the crack-tip fields.

There are no established recommendations for fitting an equation to the J_R-curve based on first principle arguments. However, Orange (1990) has proposed several convenient empirical equations which have been demonstrated to provide satisfactory fits to experimental data. These models include an exponential form,

$$J_J = (R+T\Delta a)\left[1-\exp\left(-\frac{\Delta a}{C}\right)\right] \tag{I.29}$$

a hyperbolic form,

$$J_T = \frac{(R+T\Delta a)\Delta a}{C+\Delta a} \tag{I.30}$$

an arctangent form,

$$J_R = (R+T\Delta a)\frac{2}{\pi}\tan^{-1}\left(\frac{\pi\Delta a}{2C}\right) \tag{I.31}$$

a hyperbolic tangent form,

$$J_R = (R+T\Delta a)\ \tanh\left(\frac{\Delta a}{C}\right) \tag{I.32}$$

and a power law form,

$$J_R = J_1\ \Delta a^{J_2} \tag{I.33}$$

In all of these equations, Δa is the increment of crack advance. In the first four equations, T represents the asymptotic slope of the tearing line, R the intercept of the tearing line with the $\Delta a = 0$ axis, and C the Δa value on the asymptotic blunting line which corresponds to $J_R = R$. These parameters are illustrated schematically in Figure I.4. The specific values of all these constants are dependent not only on the material resistance data but also on the model chosen. Determination of the specific model constants involves a simple non-linear least squares regression of available experimental data. In the power law equation, J_1 and J_2 are empirical constants determined from a best fit to the whole of the resistance data, including the blunting line. A similar empirical approach employs a quadratic equation form, as is developed further in **Appendix K**.

In general, the equation chosen for subsequent application should be the form which gives the regression of highest statistical quality for a given set of data, according to traditional measures of regression error. All the parametric equations include crack-tip blunting prior to physical crack extension. This allows a complete model of tear-fatigue to be formulated which does not distinguish between blunting and physical crack growth (see Section 2 in Endnote I.1). It is particularly important that the chosen *J-R* equation describes the resistance data accurately near the "knee" of the resistance curve where crack-tip blunting transitions into physical crack extension. The majority of tear-fatigue life will generally be spent in this region of the J_R-curve. The ASTM Test Method E 1737 recognizes the general utility of a power law regression as an aid to some analyses as it is most easily mathematically inverted, which simplifies ductile tearing computations.

I.4.2 Assessing the Importance of Constraint

The dependence of measured brittle and ductile toughness values on geometry and loading mode is well documented (for example, Anderson, 1995) and is commonly attributed to the effects of crack-tip plastic constraint. This constraint is generally lower for thinner sections, higher stresses, and surface cracks under tension and pressure loading, all of which are characteristic of many reusable aerospace propulsion system applications. Conversely, constraint is higher in thick section components subjected to relatively low stresses and/or through-wall bending.

Current thinking in the international fracture community is that the change in the measured fracture resistance with specimen geometry is due to the breakdown of J as a single parameter characterization of the elastic-plastic crack-tip fields (Dodds et al., 1993). This theoretical

characterization provides the vital link between the crack-tip driving force expressed in terms of a calculable engineering parameter, J, and the physical mechanism which governs crack extension. It has been found that under certain conditions, generally associated with low crack-tip constraint, the crack-tip fields are no longer characterized by the Hutchinson-Rice-Rosengren stress fields upon which traditional J theory is based. Current attention on this so-called loss of J-dominance is focused on using J in conjunction with a stress-based parameter, Q, as a two-parameter characterization of crack-tip stress fields which includes the effects of loss of constraint.

To date, the practical applications of constraint theories have been primarily focused on elastic-plastic fracture behavior dominated by brittle fracture (cleavage). The potential applications of constraint theories to ductile tearing have only recently been explored in any detail (Xia et al., 1995; Ruggieri, et al., 1996; Gao et al., 1998). Therefore, the analytical construction of a J_R-curve for some new specimen or component geometry from a benchmark J_R-curve (e.g., measured using a C(T) specimen) is still in its early stages of development. It is possible that further advances on this topic will emerge in the next few years. The problems are much too sophisticated to admit substantial investigation under the current contract.

I.4.2.1 Brittle (Cleavage) Failure

Variations in constraint can have a dramatic impact on the measured value of J_c for cleavage (for example, see Anderson, 1995). The effect, in terms of changes in toughness values at a given temperature, can be much greater than the effect of constraint on measured tearing resistance. Fortunately, the value of J_c obtained from a C(T) or SE(B) test conducted according to standard ASTM protocols is generally a lower bound to the toughness in other configurations. Hence, problems only arise in practice if the conservatism introduced by the use of a lower bound J_c is sufficiently excessive to unreasonably penalize the integrity assessment of the hardware. However, this conservatism in the assessment may still be a relatively small contribution to the calculated fatigue life in some EPFCG problems.

Substantial progress in the use of two-parameter J-Q methods to characterize the effects of constraint on measured toughness* appears to be imminent in the international fracture community. However, this progress is still at the "academic" stage, and it is anticipated that a procedure for explicitly including the effects of plastic constraint in structural integrity assessments is still a number of years away from being realized.

I.4.2.2 Effects of Constraint on the J_R-Curve

The effect of constraint on ductile fracture behavior is illustrated in Figure I.5 with Inconel 718 data from various specimen geometries (McClung et al., 1993). Shown in the figure are J-R data from C(T) experiments which meet the validity requirements of ASTM Test Method E 1737 (ASTM E 1737, 1998), surface-crack tension experiments on 0.5-in. (12.7 mm) thick specimens, and

---

Actually, as discussed previously, constraint influences the effective crack driving force, not the material's crack growth resistance.

surface-crack tension experiments on 0.2-in. (5.1 mm) thick specimens. In each case, the data have been fitted to a power law having the general form of Equation (I.33). These results clearly show that J_R-curve for the low constraint surface crack exceeds that measured on the high constraint C(T) specimens. Also shown for comparison is the extrapolation of the blunting line corresponding to $J=2\sigma_{ys}\Delta a\ (M=2)$. This line provides an upper-bound resistance curve as it is assumed that blunting does not correspond to physical crack extension defined as coalescence of the crack tip with voids in material adjacent to it.

I.4.3 Estimating Upper and Lower Bounds for J-R Behavior

Observe in Figure I.5 that the wide range of possible *J-R* behaviors is probably bounded by two extremes. At one extreme, the highly constrained benchmark C(T) specimen J_R-curve represents a lower bound resistance to ductile tearing according to the standard ASTM test method validity requirements.

At the other extreme, the extrapolated blunting curve will serve as an engineering upper bound to crack growth resistance behavior (see Endnote I.1). In this context, it is significant that the J_R-curve for the thinner surface-crack geometry in IN-718 (Figure I.5) appears to follow the blunting curve out to greater values of Δa than does the data for the compact tension specimen. The level of constraint in these surface crack tests was extremely low, because cracks were quite deep (a/t ranging from 0.6 to 0.9), stresses were extremely high (maximum nominal stresses ranging from 155 ksi to 180 ksi, in comparison to a yield stress of 165 ksi), and the configuration was pure tension.

A lower bound approach in cases where J_R-curve data is not available is to assume that the resistance to tearing is zero, and to define the J_R-curve as equal to J_{Ic} for all tear lengths, Δa_t. This approach can be modified for part-penetrating cracks in very thin components where crack extension due to blunting may be important, by defining J_{mat}=0, and equating J_R to $2\sigma_{ys}\Delta a$ for $\Delta a<J_{Ic}/2\sigma_{ys}$, and $J_R=J_{Ic}$ otherwise. The value of J_{Ic} can be equated to the results of a fracture toughness test performed according to ASTM E 1737 standards, or to K_{Ic}^2/E', where K_{Ic} is the plane strain fracture toughness value obtained following ASTM E399 test procedures. However, care should be taken in following the latter approach as K_{Ic} is derived using a 5% offset procedure which could result in a toughness value that is appropriate to a level of ductile tearing equivalent to 2% of the depth of the crack in the test piece. Although this amount of tearing in a large test piece may be insignificant, its absolute value could be highly significant in the context of part-through cracks in thin sections.

I.4.4 Choice of J_{mat}

Application of the tear-fatigue model requires identification of the J value, J_{mat}, at which ductile tearing first initiates. The initiation of ductile tearing has been characterized by the critical value J_{Ic} measured according to ASTM Test Method E 1737 (1998) and designated in the test procedures as "a measure of fracture toughness." These quoted words reflect the fact that J_{Ic} does not in general characterize the onset of ductile tearing, which is experimentally almost impossible to identify. Instead, J_{Ic} is defined by an offset procedure similar to that used to define the

(0.2 percent offset) yield stress (see Figure I.6). An offset line of the general form $J = M\ \sigma_{ys}\Delta a$, where M is usually equal to 2 is drawn intersecting the abscissa at Δa = 0.2 mm (0.008 in.). The intersection of this offset line with the power law fit to the J-R data is defined as J_{Ic} (assuming that other validity criteria are satisfied). When $J_{max} < J_{Ic}$, it is commonly assumed that the crack only extends due to crack-tip blunting. Hence, provided $(dJ_{max}/dN)/2\sigma_{ys} << (da/dN)_f$ when $J_{max}<J_{mat}$, the contribution of tearing to (da/dN) can be ignored and J_{mat} can be equated to J_{Ic}.

The potential difficulty associated with this functional definition is that the total amount of crack growth Δa which occurs when $J_{max}= J_{Ic}$ may be relatively large compared with typical dimensions of reusable aerospace propulsion system components. For IN-718 for example , J_{Ic} for the C(T) data is defined by this procedure as 849 lb./in (see Figure I.5). The total crack growth Δa at $J_{max}=J_{Ic}$ is slightly greater than 0.01 inches (0.25 mm). Some wall thicknesses on critical SSME components are on the order of 0.01 in., so the critical amount of crack growth at instability (if instability occurs) of a part-through crack is almost certain to be substantially smaller than Δa at an applied J equal to J_{Ic}. If J_{Ic} was calculated by this procedure for one of the surface crack J_R-curves, then J_{Ic} and the corresponding Δa would be much higher and even more clearly inappropriate for most tear-fatigue analysis of SSME hardware. In these situations, it is recommended that J_{mat} is taken as zero, and a J_R-curve, designated as J_R', which includes the blunting line, is defined for use in tear-fatigue analyses instead of J_R, where

$$J_R'(\Delta a_t) = 2\sigma_{ys}\Delta a_t\,,\ J_{max} \le J_{Ic} \tag{I.34}$$

$$J_R'(\Delta a_t) = J_R(\Delta a_t),\ J_{max} > J_{Ic} \tag{I.35}$$

The justification for adopting this approach is presented in Endnote I.1.

I.5 Practical Considerations in Evaluating the Service Life

I.5.1 Characterization of Toughness for Service Applications

In many engineering evaluations, the fatigue service life will be insensitive to the value of the critical crack size at which instability is predicted. This is because the majority of the fatigue life of cracked components are spent in propagating small flaws whose size is significantly less than the critical crack size. However, there are circumstances where the life may be sensitive to the value of the critical crack size. For example, in cases when the service life consists of only a few severe fatigue cycles (which is the case for the SSME), and when fracture mechanics analyses of proof tested components are used to derive maximum flaw sizes that could be present at the start of service. In the latter case, the size of the calculated hypothetical flaw could be comparable to the critical size.

The recommended procedure to assess the importance of constraint for service applications is first to perform the FCG calculation (predicting life, or perhaps final crack length) with the tear-fatigue model based on the C(T) specimen J_R-curve. This should provide a conservative lower bound to the life, at least as far as the instability calculation is concerned. If this answer is satisfactory for the specific application at hand, then no further computation is required.

If this answer is not satisfactory, or if the analyst wishes to estimate how much conservatism may be inherent in this approach, then a second bounding calculation is recommended. In this computation, the J_R-curve is taken as the extrapolation of the blunting curve, $2\sigma_{ys}\Delta a$ and the value of J_{mat} is assumed to be the same as J_{Ic} measured for the C(T) J_R-curve. This procedure will provide an upper bound to the tearing resistance and therefore an upper bound to the life (in terms of tearing instability).

A comparison of the results for the lower bound (C(T)) and upper bound (blunting line) J_R-curves should provide an indication of how significant the uncertainty about constraint effects is for that specific life prediction problem. If the two life answers are relatively close, then further detailed analysis of the constraint effects is of little benefit. This is expected to be the case for many applications.

I.5.2 Leak-Before-Break

It is anticipated that in some reusable aerospace propulsion system applications, FCG of a part-through crack will proceed in a stable manner up to and beyond the point at which the crack fully penetrates the section thickness. This is the so-called "leak-before-break" phenomenon which is a desirable characteristic of many pressurized systems. However, in some reusable aerospace propulsion system applications, the leak associated with through-wall penetration will precipitate the release of volatile gases, potentially causing catastrophic failure of the entire propulsion system. In these applications, "failure" must therefore be redefined in terms of through-wall penetration, not the onset of ductile instability. Leak-before-break is most likely to occur where the toughness of the material is high and the crack-tip driving force is low, situations which will again be satisfied in many reusable aerospace propulsion system applications.

It practice, the modeling of surface flaw propagation in ductile materials to cause a leak is limited because of the lack of fracture mechanics solutions for very deep cracks. For example, Newman and Raju (1981) reported that the accuracy of their empirical K equations for semi-elliptical surface cracks (based on 3-D elastic FEM analyses) had not been established for $a/t > 0.8$, although they justified the use of these solutions for deeper cracks based on the concept of an equivalent through-crack. Hence, under leak-before-break conditions, the criterion governing when a surface flaw penetrates through the thickness of a structure may have to be based on the validity limits for the fracture mechanics solutions if these are violated before the failure criterion is satisfied.

I.5.3 Stable Crack Growth After Leak

In applications where full penetration of a previously part-through crack may be tolerable, it is possible to take advantage of the extra fatigue life associated with the time taken to propagate the through-wall crack to cause instability. For example, when a surface crack of surface length 2c first breaks through the thickness, the stability of a through-crack of length 2c should be assessed against ductile instability. If this through-crack is not stable, then the life calculation is terminated. If this through-crack is stable, then the FCG life calculation should continue by modeling the transition of the flaw from a surface crack to a through-crack and beyond, until the appropriate instability criterion for the through-crack is satisfied. Algorithms are already available for small scale yielding conditions (e.g., in NASCRAC) to guide the development of crack shape and the calculation of crack growth rates during the transition period. At this time, no further information is available on how these transition algorithms might require modification to accommodate the effects of larger scale-crack tip plasticity.

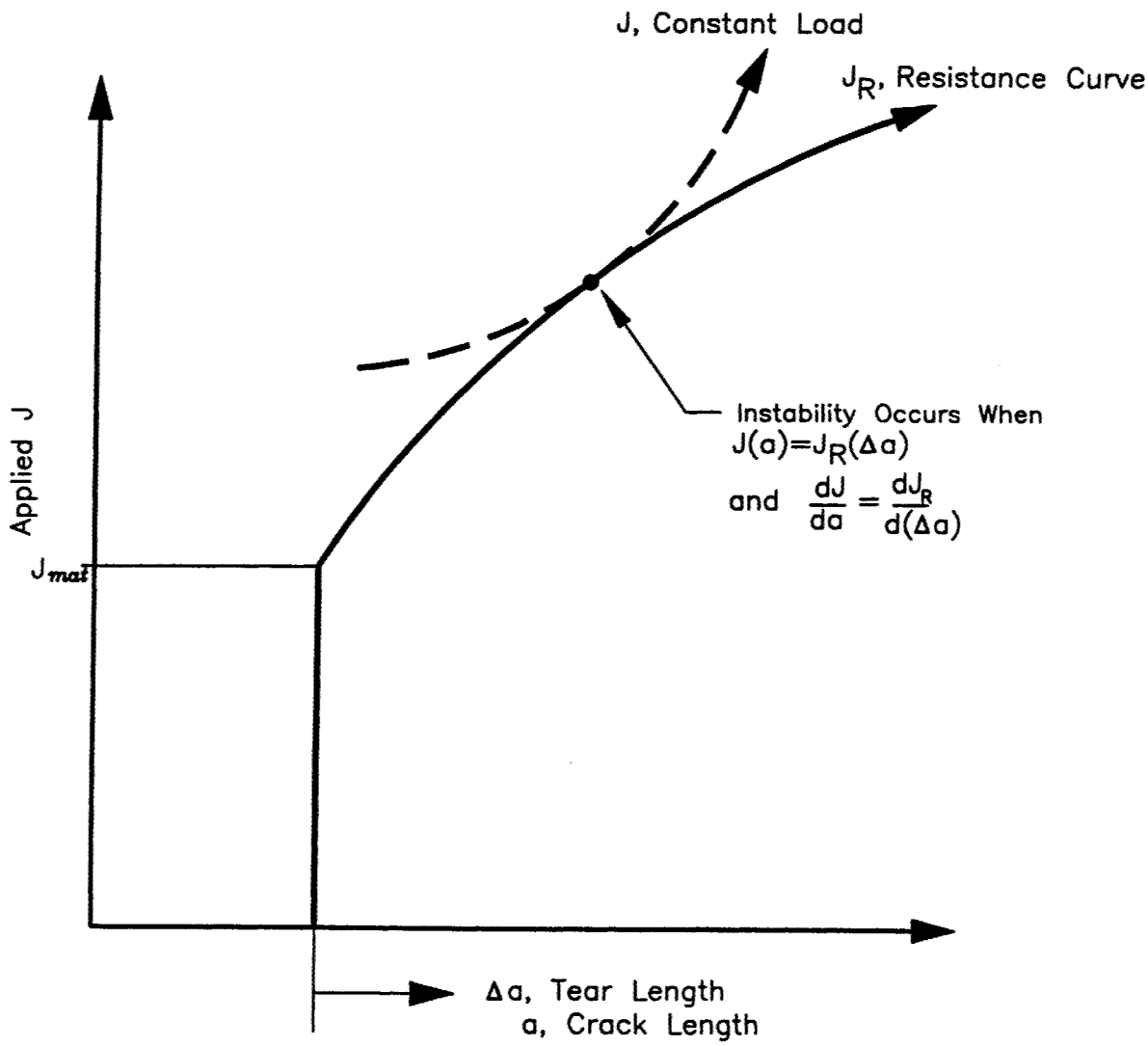

Figure I.1. Schematic showing instability criterion for ductile materials

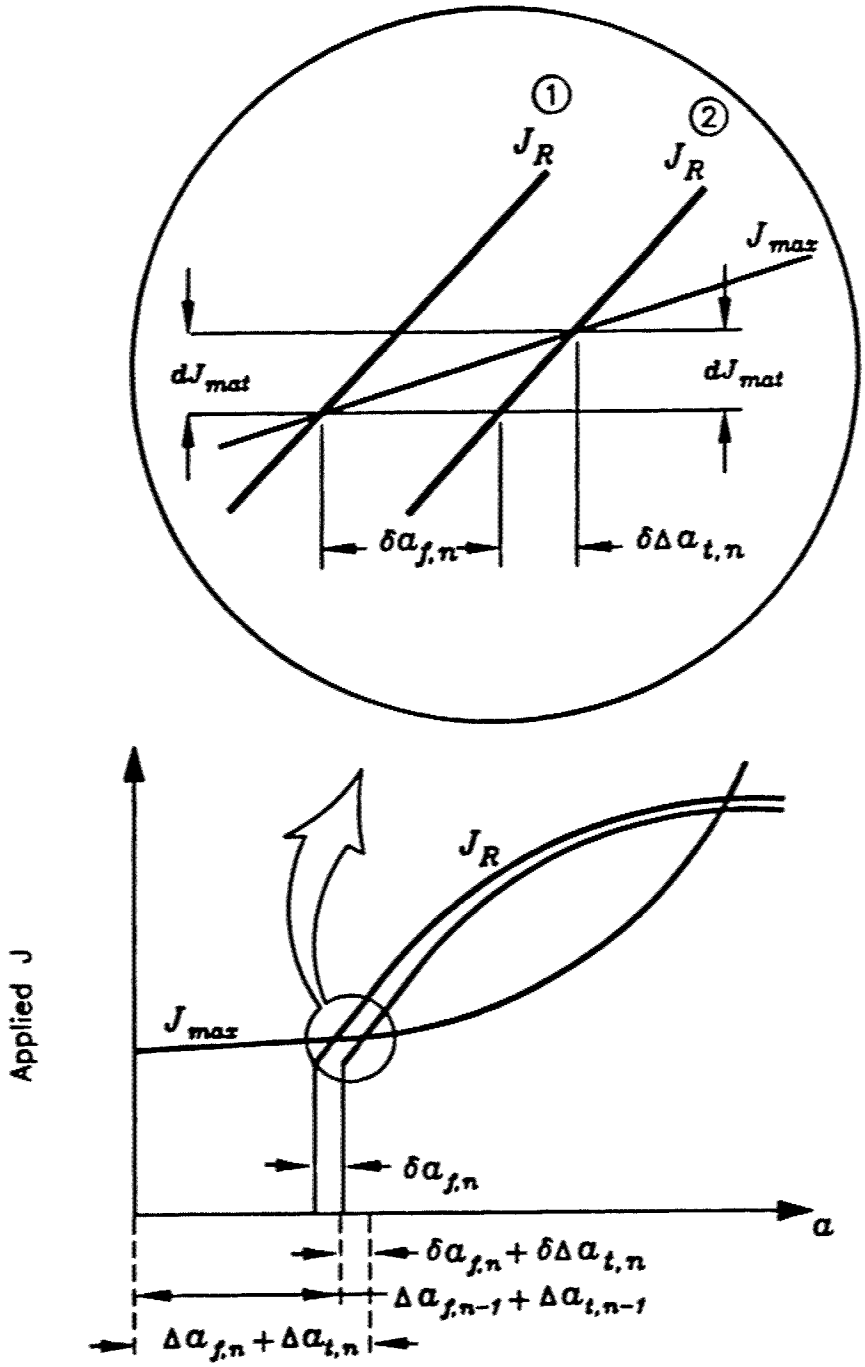

Figure I.2. Schematic representation of tear-fatigue Memory Model. The insert shows the changes in each quantity per cycle.

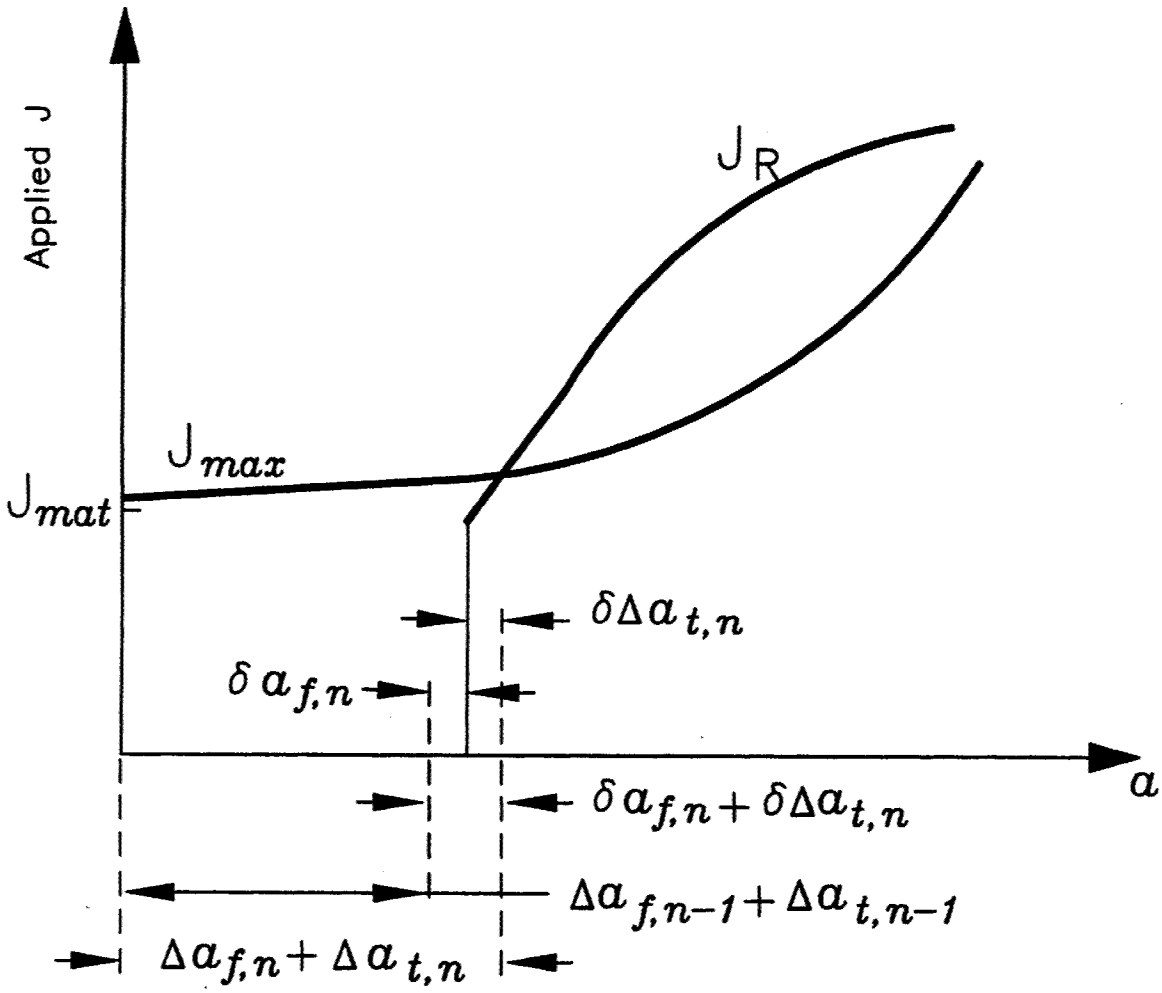

Figure I.3. Schematic representation of tear-fatigue loss of Memory Model

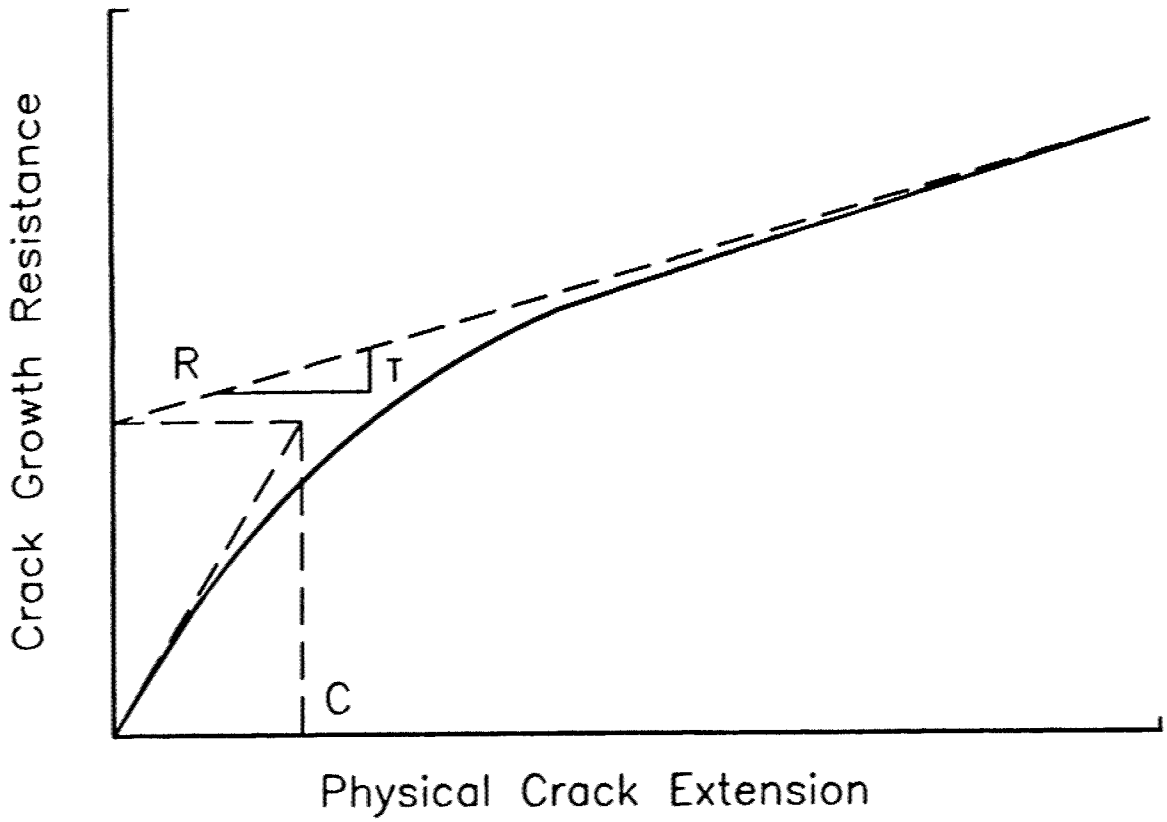

Figure I.4. Definition of the constants, C, R, and T that appear in Equations (I.29) to (I.32) that can be used to mathematically represent J_R-curves.

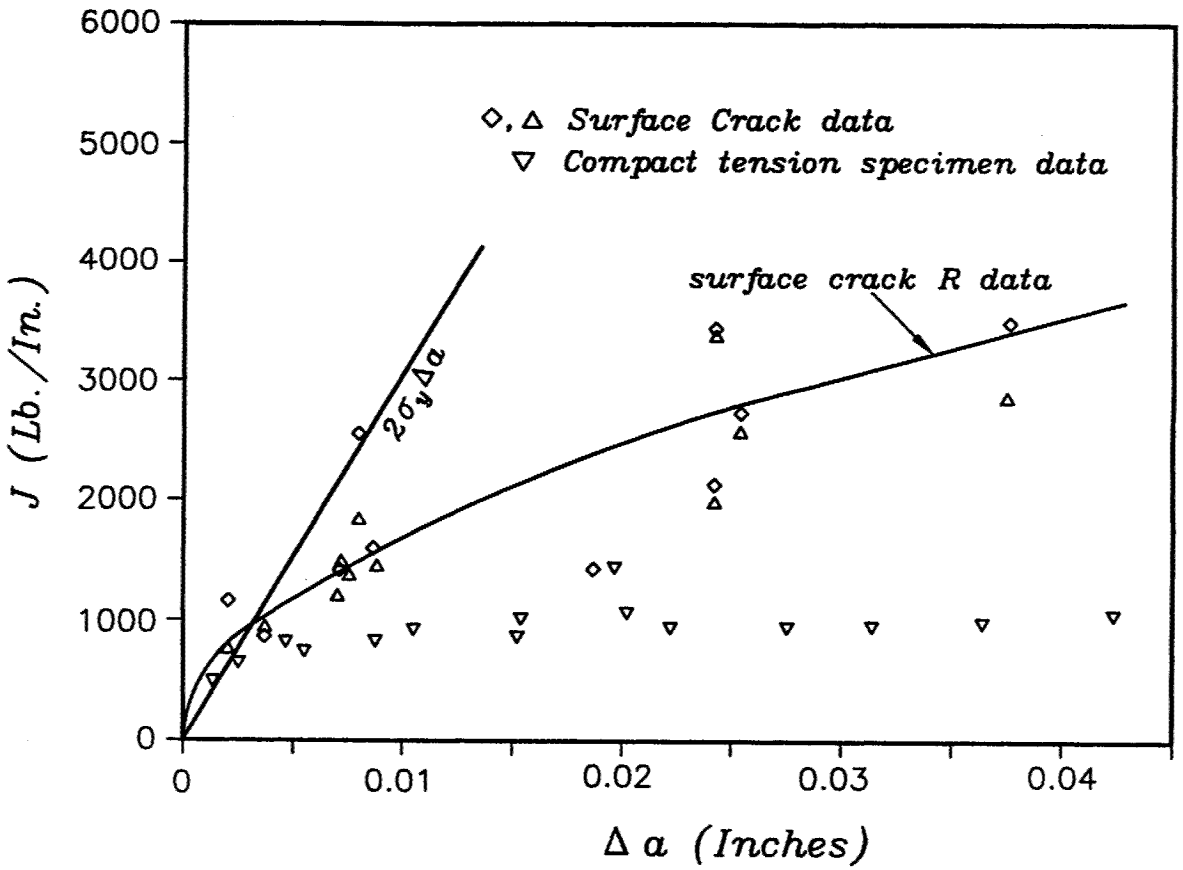

Figure I.5. Example crack growth resistance curves for Inconel 718.

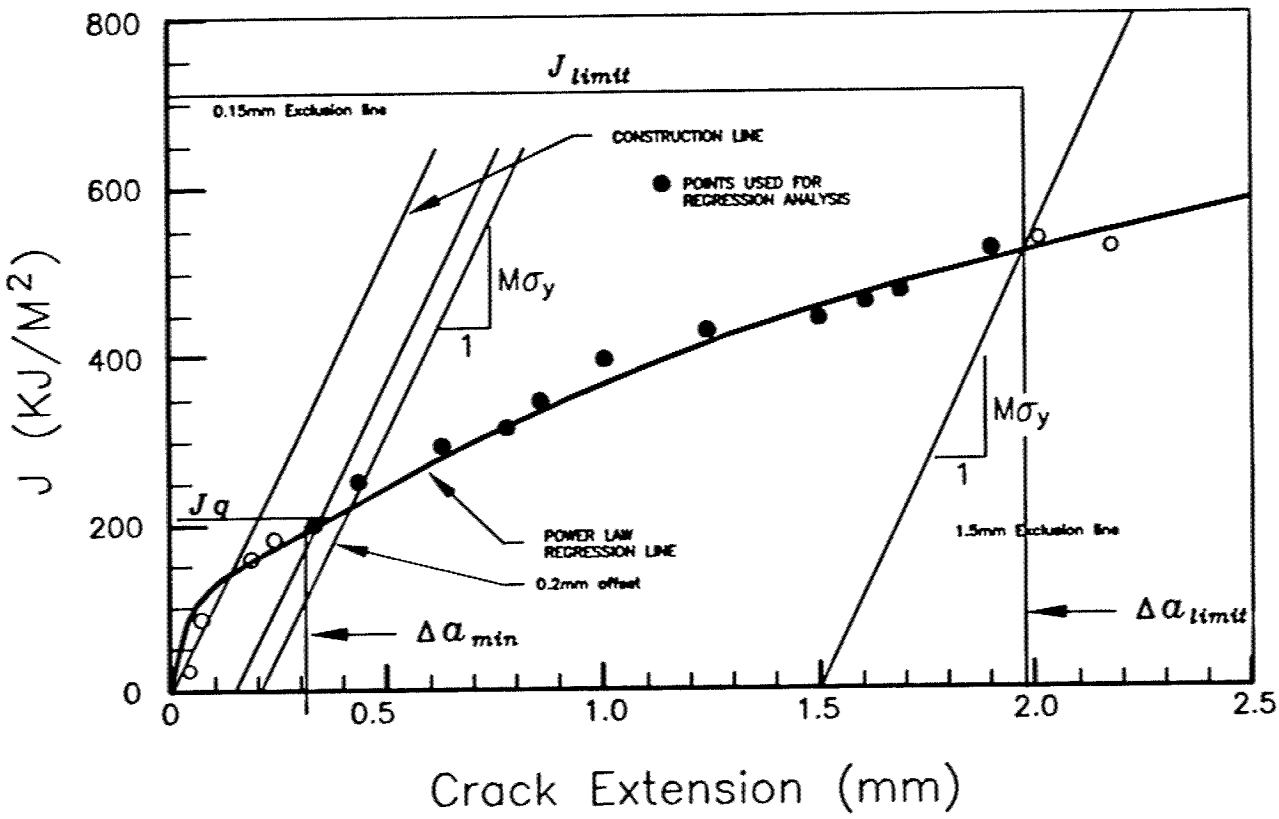

Figure I.6. The offset procedure used to define J_{Ic} according to ASTM Test Method E 1737.

ENDNOTE I.1

The Mechanics and Mechanisms of Tear-Fatigue

A Simple Mechanistic Model for Tear-Fatigue

Laird and Smith (1962) have proposed a simple model of fatigue crack growth. In this model, the first load-up part of the cycle causes crack-tip blunting, which creates new surface area at the crack tip due to the intense strain generated at the free surface. The load-down sharpens and closes the crack tip by an amount $\Delta\Phi$ where Φ is the crack-tip opening displacement. Reloading causes the crack tip to blunt and extend by an amount $\Delta\Phi/2$. Under small-scale yielding conditions, $\Delta\Phi=\Delta K^2/ME'\sigma_{ys}$, where the dimensionless constant M usually has a value of 2 under plane strain conditions. This model predicts that the value of n in Equation (I.9) should be 2. Fatigue occurs due to surface stretching and the production of **new surface area at the crack tip** due to cyclic load changes.

If $J_{max}>J_{mat}$ on the first load-up then the crack will extend by tearing. Tearing occurs through the ductile mechanism of **void growth in material in front of the crack tip**, and the link-up of these voids with the tip.

These simple models show why the ductile and fatigue crack propagation mechanisms may not interact in any significant way except through an increase in crack-driving force due to the physical increase in crack depth which each one produces.

Combined Blunting and Fatigue Crack Extension

The tear-fatigue model can be extended to include the effects of crack-tip blunting prior to ductile tearing and fatigue crack extension using the simple model described in immediately above. The interaction between blunting and fatigue can be important for cracks in very thin-walled components, as encountered in reusable aerospace propulsion systems.

Under monotonic loading conditions the degree of blunting, Φ, is determined from the equation

$$J\left(a_o+\frac{\Phi}{2}\right) = J_b\left(\frac{\Phi}{2}\right) \qquad \textbf{(I.36)}$$

where J_b is related to Φ through the equation

$$J_b = M\sigma_{ys}\frac{\Phi}{2} \qquad \textbf{(I.37)}$$

where a_o is the initial crack depth. Equation (I.36) is a mathematical statement that the crack is stable when the applied J is balanced by the materials resistance to cracking, characterized by its ability to blunt. A similar equation to Equation (I.36) must be satisfied during fatigue crack propagation if the crack is to remain stable. Hence

$$J_{max}\left(a_o+\Delta a_f+\frac{\Phi}{2}\right) = J_b\left(\frac{\Phi}{2}\right) \tag{I.38}$$

where Φ is a function of the total crack depth, $a_o+\Delta a_f$, and Δa_f is the crack extension due to fatigue mechanisms.

Let δa_f be the fatigue crack extension per cycle, and $\delta\Phi$ the corresponding increase in blunting resulting from the extension, then

$$J_{max}\left(a_o+\Delta a_f+\delta a_f+\frac{\Phi}{2}+\frac{\delta\Phi}{2}\right) = J_b\left(\frac{\Phi+\delta\Phi}{2}\right) \tag{I.39}$$

Subtracting Equation (I.38) from Equation (I.39) and expanding the appropriate functions to first order yields

$$\left(\delta a_f+\frac{\delta\Phi}{2}\right)\frac{\delta J_{max}}{\delta a} = \frac{\delta\Phi}{2}\,\frac{\delta J_b}{\delta(\Phi/2)} \tag{I.40}$$

Let $\delta a_{tot}=\delta a_f+\delta\Phi/2$ be the total crack extension (fatigue plus blunting) per cycle. then Equation (I.40) can be re-expressed in the form

$$\delta a_{tot} = \frac{\delta a_f}{1 - \frac{\delta J_{max}}{\delta a}\Big/\frac{\delta J_b}{\delta(\Phi/2)}} \tag{I.41}$$

This equation shows that blunting will cause an acceleration in the fatigue crack propagation rate. In general, the denominator in Equation (I.41) is usually very nearly equal to 1 because $\delta J_b/\delta(\Phi/2) >> \delta J_{max}/\delta a$ under normal fatigue conditions.

Note the similarity of Equation (I.41) to Equation (I.19) in the main text. These two equations would be the same if the blunting line was included as part of the J_R-curve with $\delta J_b/\delta(\Phi/2)=\delta J_R/\delta(\Delta a_t)$ on the blunting line, and J_{mat} set to zero.

Equation (I.41) predicts that $\delta a_{tot}=\delta a_f$ when $\delta J_{max}/\delta a=0$, which physically means that J_{max}, and hence J_b and Φ, remains constant during fatigue growth and blunting does not contribute to the crack extension per cycle.

ENDNOTE I.2

Evidence for Use of the Memory Model for Evaluating J_R Behavior Under Constant Amplitude Loading

The limited experimental evidence to date where the test conditions satisfied the requirements of Section I.3.3.1 show a good correlation between the measured crack growth rates and the predictions of Equations (I.15) and (I.17). This evidence encompasses the results of Kaiser (1983), Nix et al., (1988), and Nix et al., (1989) on steels. Figure I.7, taken from Nix, et al. (1988) shows typical results when the predicted growth rates are plotted against the measured rates.

Recent tear-fatigue behavior observed in fracture tests on IN-718 (a common material in reusable aerospace propulsion systems) as part of companion proof test contracts performed at SwRI for NASA-Marshall has also been analyzed and found to be in agreement with the predictions of the tear-fatigue model (McClung et al., 1996b; Chell et al., 1997a).

The prediction of the Memory Model that tearing will cease during tear-fatigue if $dJ_{max}/dN \leq 0$, even though $J_{max} > J_{mat}$, has been substantiated in test results reported by Nix et al., (1988), Joyce and Culafic (1988) and Chell et al. (1997a). Nix et al., reported a dramatic reduction in measured growth rates when a change in test conditions was made from a constant plastic load line displacement increment per cycle (where the measured dJ_{max}/dN increased each cycle), to a constant energy input per cycle (where dJ_{max}/dN was nominally zero) (see Figure I.8). Before the mode change, the measured and tear-fatigue predicted growth rates were 103 μm/cycle and 107 μm/cycle, respectively. After the mode change, the measured and predicted rates were 16 μm/cycle and 11. 5 μm/cycle, respectively, and consistent with propagation occurring by fatigue only. This result is even more remarkable when it is realized that the measured value of J_{max} after the mode change was about 1500 kN/m, and ductile tearing was suppressed even though the measured value of J_{mat} was only 141 kN/m.

Joyce and Culafic (1988) investigated load history effects in a HSLA steel. In their tests, they periodically imposed large tear steps at high load levels on specimens after they had undergone about 1 mm crack extension due to continuous cycling at lower load levels. They showed that the tearing steps had little measurable effect on the fatigue crack growth rate. In other words, tearing was suppressed after the load (J_{max}) was reduced.

Similar qualitative behavior was observed by Chell et al. (1997a) in two tests on IN-718 which involved subjecting cracked specimens to a simulated proof test overload up to incipient instability, unloading, followed by simulated service load cycling to failure. Although J_{max} at the maximum load in the service cycle exceeded J_{mat}, there was clear evidence from recorded load-line displacements that tearing did not occur under simulated service conditions until significant crack extension due to fatigue cycling had occurred.

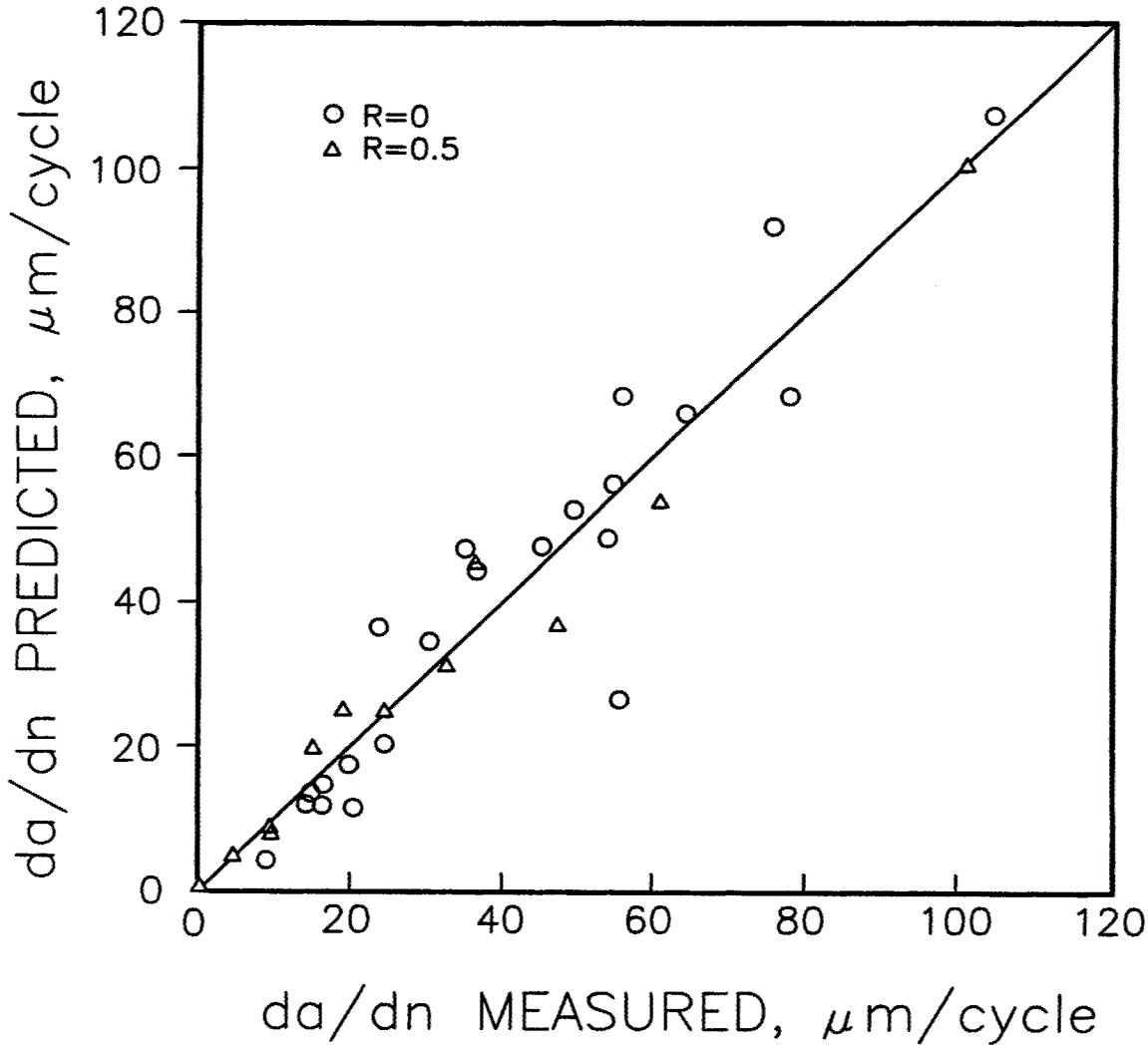

Figure I.7. Predicted tear-fatigue crack growth rates versus measured values for a mild steel. (After Nix et al., 1988).

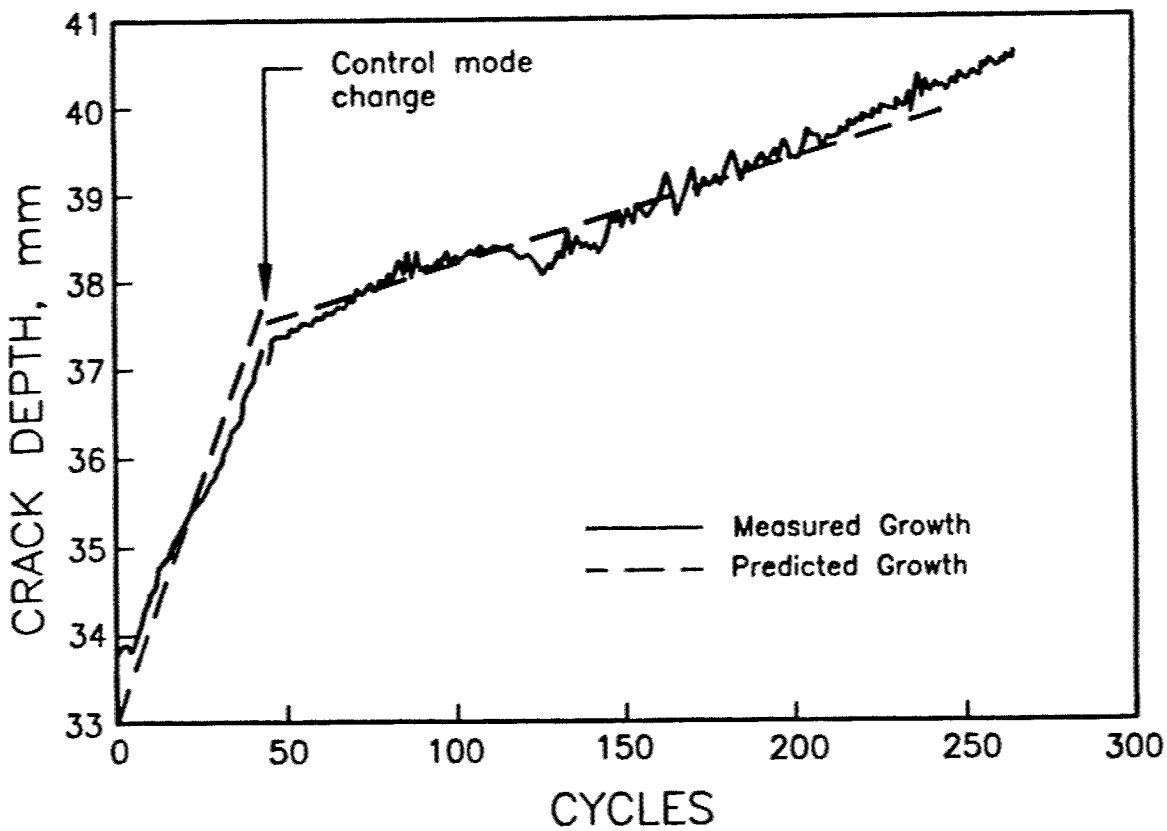

Figure I.8. Example of the suppression of tearing during a tear-fatigue test when a control mode change reduced dJ_{max}/dN from 22.6 kN/m to 0 kN/m. (After Nix et al., 1988)

APPENDIX J

A CREEP-FATIGUE CRACK GROWTH ASSESSMENT METHODOLOGY

SUMMARY

A methodology is described for evaluating creep-fatigue crack growth under cyclic loading conditions involving a hold time at steady load. The crack growth rate per cycle is expressed as the linear sum of 2 contributions: that due to fatigue crack extension, and that due to creep crack growth during the hold time. The fatigue crack growth per cycle is characterized by a Paris Law equation, where the growth constants are dependent on the hold time, and cyclic crack tip plasticity is taken into account by using the cyclic change in the *J*-Integral. The creep crack growth rate per cycle is related to an integral over the hold time of the creep crack velocity, which is characterized by the time dependent fracture mechanics parameter, C_t.

The parameter C_t consists of transient (short time) and steady state (long time) components. It is shown that these can be calculated from appropriate creep deformation data, and time independent fracture mechanics parameters. The value of C_t is influenced by the ability of the crack tip material to cyclically recover, the presence of secondary loading (thermal and displacement), crack tip plasticity and constraint. Other factors which relate to creep-fatigue are discussed, such as crack growth incubation, loading ramp rate, and temperature changes during the cycling.

A brief description is given of a procedure for evaluating the remaining life of a cracked structure under creep-fatigue conditions.

J.1 Introduction

The concepts of linear elastic (LEFM) and elastic-plastic fracture mechanics (EPFM) are now widely used by many industries to analyze defective structures. LEFM applies to situations where crack tip plasticity is small, and the stress intensity factor, *K*, characterizes the stress and strain fields at the tip, as well as the energy available to overcome the work to fracture when the crack extends. EPFM is applicable when large crack tip plastic zones develop, and the *J*-Integral replaces *K* as the appropriate characterizing parameter.

Unfortunately, although *K* and *J* have proven to be successful parameters in describing time independent fracture behavior, and this success has also carried over into the field of continuous cycling fatigue crack growth (Dowling and Begley; 1976, Dowling, 1976), they are not appropriate for characterizing time dependent creep deformation at a crack tip. This point is illustrated in Figure J.1, which shows that *K* fails to correlate creep crack growth rates, *da/dt*, in Cr-Mo-V steels obtained from compact tension (CT) specimens of different sizes containing various crack depths (Saxena, 1991).

A time dependent fracture mechanics (TDFM) parameter which correlates *da/dt* data for different cracked geometries and loading systems is essential if laboratory measured data are to be transferable to the assessment of structural components, such as the Space Shuttle Main Engine (SSME).

To overcome the shortcomings of K and J, Landes and Begley (1976) proposed the use of a parameter, C^*, to characterize creep deformation under steady loading conditions. C^* does not depend explicitly on time; it is a steady state parameter. It was later generalized to include transient, as well as steady state, creep deformation by Saxena and co-workers, and called C_t (for example, see references: Saxena, 1986; Saxena and Liaw, 1986; Leung, McDowell, and Saxena, 1988, 1990; Leung and McDowell, 1990; Bassini, Hawk, and Saxena, 1989). A much improved correlation is obtained when the *da/dt* data shown in Figure J.1 is plotted against C_t, see Figure J.2, verifying that C_t is a creep characterizing parameter which can be used for evaluating creep crack growth in structures. Unlike C^*, C_t is an explicit function of time as well as crack size and applied load.

C_t does not characterize the crack tip fields, except under steady state conditions when it reduces to C^*, but it does have an interpretation related to the rate of change of the power input from the loading system as the crack extends (Saxena, 1986). A time dependent crack field characterizing parameter, $C(t)$, has been developed by Riedel (1987). This parameter also reduces to C^* under steady state conditions. The parameter $C(t)$ provides important information on typical transition times between the transient and steady states, and between small and large scale crack tip creep conditions.

This appendix describes the linear elastic, elastic-plastic and time dependent fracture mechanics parameters needed to implement a creep-fatigue crack growth assessment methodology. It concentrates predominantly on reviewing TDFM parameters (as these are usually less familiar than time independent fracture parameters), and how they can be calculated from readily accessible or measurable engineering quantities. Section J.2 describes the creep-fatigue crack growth law used to characterize crack propagation under cyclic loading conditions where there is a steady load hold period. A brief outline of the development of the TDFM parameter, C_t, is given in Section J.3, together with methods of calculating it. Section J.4 addresses more general aspects of creep-fatigue, including material property requirements, and the effects of cycling on creep deformation at a crack tip. Section J.5 discusses other topics related to operating conditions, such as the effects of thermal and displacement loading, crack tip plasticity, loading rate and temperature cycling. Crack closure, constraint and crack growth incubation are also mentioned. The procedures to be followed in performing a remaining life assessment are briefly described in Section J.6. The conclusions drawn from this study are detailed in Section J.7.

J.2 Creep-Fatigue Crack Growth

At high operating temperatures and under steady loading conditions creep deformation and the resulting damage at the tip of crack-like defects can cause crack propagation. If the loading is cyclically applied, and the cycle includes a steady load hold period, then crack extension can occur during the cycle due to both creep and fatigue mechanisms. In this situation, a synergistic interaction can occur between the two mechanisms resulting in a crack propagation rate which exceeds the value determined by simply adding the steady state creep and continuous cycling fatigue components of crack growth (Ainsworth, Ruggles, and Takagashi, 1992). An enhancement in the fatigue component of the growth rate cannot be ruled out due to creep damage occurring in the hold time, even when no creep crack extension occurs during the hold time.

The data shown in Figure J.2 strongly indicates that the creep crack propagation rate, *da/dt*, can be correlated with C_t through an equation of the form

$$da/dt = HC_t^q \tag{J.1}$$

where H and q are material constants. Thus, C_t offers a powerful TDFM parameter for assessing creep crack growth provided that it can be expressed in a form which is relatively easily evaluated for structures.

Since C_t allows for transient effects, it has also been used to characterize creep crack extension during the hold period in a load cycle. The total crack growth rate per cycle, *da/dN*, under these creep-fatigue conditions is usually written as the simple sum of 2 components (Ainsworth, Ruggles, and Takagashi, 1992; Yoon, 1990)

$$da/dN = (da/dN)_f + (da/dN)_{time} \tag{J.2}$$

where $(da/dN)_f$ is the fatigue growth rate

$$(da/dN)_f = D(\Delta K)^l \tag{J.3}$$

D and l are temperature dependent material constants, and $(da/dN)_{time}$ is the creep crack extension that occurs during the hold time, t_h, and is evaluated by integrating Equation (J.1)

$$(da/dN)_{time} = \int_0^{t_h} (da/dt)\,dt = \int_0^{t_h} HC_t^q\,dt \tag{J.4}$$

Creep crack extension does not always immediately occur after the application of a load. An incubation period is frequently observed during which creep crack damage accumulates at the tip until a critical value is attained (Ainsworth et al., 1987). However, even if this incubation period is not exceeded in the hold time, creep may still affect the rate at which the crack extends by weakening the grain boundaries in the region of the crack tip, possibly causing crack advance during the cyclic part of the loading to be accelerated, or resulting in a change from transgranular fracture (typical of continuous cycling conditions) to intergranular fracture (typical of creep crack extension). Thus, the Paris equation constants, D and l, may themselves depend on the hold time at steady load.

The Paris equation may be extended into the low cycle fatigue regime by replacing ΔK by $(E' \Delta J)^{1/2}$ in Equation (J.3), where ΔJ is the cyclic change in the J-Integral (Ainsworth, Ruggles, and Takagashi, 1992; Yoon, 1990). Thus, a similar equation to Equation (J.1) can, in principle, be applied to describing creep-fatigue crack growth under these conditions. However, in cases where crack tip plasticity is important, these effects should also be included in the calculation of C_t (Liaw, Saxena, and Schaeffer, 1989; Joch and Ainsworth, 1992a) (see also Section J.5.2 of this appendix).

J.3 Time Dependent Fracture Mechanics and C_t

J.3.1 Constitutive Creep Laws

At elevated temperatures, the relationship between stress (σ) and strain (ϵ) depends on time (t) through a constitutive equation of the general form

$$\epsilon = f(\sigma, t) \tag{J.5}$$

Under constant stress conditions, creep deformation is usually characterized by three stages: a primary stage at early times where the strain rate decreases with time; a secondary stage where the strain rate is nominally constant and independent of time; and a tertiary stage where the creep rate increases rapidly, leading to creep rupture. These three stages can occur at a loaded crack tip as a creep zone develops and spreads across the uncracked ligament. The first two stages of deformation play an important part in this phenomenon, and are usually described by the following constitutive equation

$$\dot{\epsilon} = \dot{\epsilon}_p + \dot{\epsilon}_s \tag{J.6}$$

where $\dot{\epsilon}$ is the total creep strain rate and the subscripts p and s signify primary and secondary, respectively. The following primary creep law is frequently used for strain hardening

$$\dot{\epsilon}_p = B\, \epsilon^{-p}\, \sigma^{m(1+p)} \tag{J.7}$$

and the following for time hardening

$$\dot{\epsilon}_p = \frac{[B(1+p)]^{\frac{1}{1+p}}}{1+p}\, \sigma^m\, t^{\frac{-p}{1+p}} \tag{J.8}$$

In the strain hardening approximation used in the evaluation of creep deformation under varying stress conditions the instantaneous creep strain rate is related to the total instantaneous creep strain, while in the time hardening approximation the strain rate is related to the current time.

The secondary creep rate is given by Norton's Law,

$$\dot{\epsilon}_s = A\sigma^n \tag{J.9}$$

A, n, B, p, and *m* are material constants and ϵ is the total accumulated creep strain.

J.3.2 Transition Times and C_t

Riedel (1987) has shown that for cracked linear elastic materials under creep conditions, crack tip fields are characterized by different parameters at different times and for different creep constitutive laws. There is initially a transient phase, where the crack tip stresses relax as creep strains replace elastic strains, and simultaneously a creep zone spreads out from the tip. Eventually, after the creep zone has extended across the uncracked region of the cracked section and the primary component of the strain rate has been exhausted, steady state conditions are attained, and the crack tip stresses remain constant and no longer vary with time. The development of this large scale creep (LSC) situation from small scale creep (SSC) conditions can be described using transition times which characterize the boundaries between each stage of the process (Riedel, 1987).

For a material undergoing primary and secondary creep, the key times are:

t_1: the time taken for primary creep to develop from SSC to become LSC

t_2: the time taken for SSC due to secondary creep deformation in a zone embedded in a relatively larger primary creep zone, to develop into LSC involving predominantly secondary creep.

These transition phases are shown schematically in Figure J.3, where it is indicated how they may be combined to describe the actual creep zone development from small scale primary through to large scale secondary.

For a material which only undergoes secondary creep, the important transition time is:

t_3: the time taken for SSC due to secondary deformation to develop into large scale secondary creep.

Riedel (1987) gives the following expressions for the transition times

$$t_1 = \frac{1}{(m+1)} \left[\frac{J_e}{C_h^*} \right]^{1+p} \tag{J.10}$$

$$t_2 = \left[\frac{C_h^*}{(1+p)C_s^*} \right]^{\frac{(p+1)}{p}} \tag{J.11}$$

and

$$t_3 = \frac{J_e}{(n+1)C_s^*} \tag{J.12}$$

where $J_e = (1 - \nu^2)K^2/E$, K is the stress intensity factor, E Young's modulus, ν Poisson's ratio, and C_h^* and C_s^* are integrals which are path independent (compare the J-integral) and characterize the crack-tip stress fields under large-scale primary and secondary creep, respectively.

These times can be used in an interpolation procedure which describes the time evolution of a creep characterizing parameter, $C_t(t)$, from small-to-large scale creep (Chell et al., 1993). The result is an approximate expression for $C_t(t)$ which is applicable to combined primary and secondary creep, and for all times

$$C_t(t) = C^* + C_t(t \to 0) \tag{J.13}$$

where

$$C^* = C_p^* + C_s^* \tag{J.14a}$$

and

$$C_p^* = \frac{C_h^*}{(1+p)t^{\left(\frac{1}{1+p}\right)}} \tag{J.14b}$$

and, $C_t(t \rightarrow 0)$ describes the variation of C_t under the transient conditions which pertain in the SSC regime.

Equation (J.13) also holds for materials that only undergo secondary creep, but in this case, C_p^* is zero.

J.3.3 Expressions for C_t

The behavior of C_t at short times is dominated by the second term in Equation (J.13). Following Saxena (1986), this can be written in the form

$$C_t(t \rightarrow 0) = \left\{ \frac{J_e}{b} \beta \dot{r}_c \left(\frac{F'}{F} \right) \right\} \qquad \textbf{(J.15)}$$

where b is the uncracked section size of the component, $\dot{r}_c$ is the rate of expansion for the crack-tip creep zone at an angle of $\theta = 90°$, $\beta = 1/3$, and F and F' are derived from the stress intensity factor, K, as

$$F = K/\sigma b^{1/2}, \qquad F' = \frac{dF}{d(a/b)} \qquad \textbf{(J.16)}$$

where σ is the nominal stress.

Before Equation (J.13) can be used in a practical situation, C_s^*, C_p^* and $\dot{r}_c$ have to be defined in terms of quantities which can be evaluated for the structure. Riedel (1987) has given expressions for the creep zone size, $\dot{r}_c$, under small-scale primary and secondary creep. These can be easily differentiated with respect to time to obtain the equivalent expressions for $\dot{r}_c$ for primary creep

$$\dot{r}_c = \frac{K^2}{2\pi} \left[\frac{I_m E}{2\pi(1-\nu^2)} \right]^{\frac{2}{m-1}} \left[(1+m)(1+p)B\right]^{\frac{2}{(1+p)(m-1)}} \frac{1}{(1+p)} \left(\frac{2}{m-1} \right) t^{\left[\frac{2}{(1+p)(m-1)} - 1\right]} \tilde{r}_c \qquad \textbf{(J.17)}$$

where $\tilde{r}_c = 0.38$ for $\theta = 90°$, I_m is a numerical constant dependent on the value of m which is related to the crack tip stress field and has been tabulated by Shih (1983). For secondary creep

$$\dot{r}_c = \frac{K^2}{\pi(n-1)} \left[\frac{I_n E A(n+1)}{2\pi(1-\nu^2)} \right]^{\frac{2}{n-1}} t^{\left(\frac{2}{n-1}-1\right)} \tilde{r}_c \tag{J.18}$$

Equation (J.17) should be used for combined primary and secondary creep, and Equation (J.18) for secondary creep alone.

Note that $C_t(t\to 0)$ depends on F', essentially the derivative of K with respect to a. This means that $C_t(t\to 0)$ can become negative if F' is negative, a situation which can occur in steeply falling stress gradients. It is not clear what the physical significance of this is in terms of crack tip creep deformation. In plasticity, the equivalent to $C_t(t\to 0)$ is the first order plastic correction to J_e, and in this instance, if F' is negative, it implies that plasticity decreases J with respect to J_e, rather than increases it, as is usual. This interpretation does not carry over to the creep case, and it is suggested that $C_t(t\to 0)$ be set to zero if F' becomes negative.

The LSC components of C_t can be derived from the available fully plastic solutions, J_p, for the J-Integral by invoking the creep/plastic analogy. This states that steady state creep solutions can be obtained from the solutions for a fully plastic material by replacing strains and displacements in the equivalent fully plastic solution by strain rates and displacement rates. Thus, for example, the EPRI solutions for J_p contained in the elastic-plastic handbooks (Kumar, German, and Shih, 1981) can be written in the form

$$J_p = \alpha\, \sigma_o\, \epsilon_o\, c \left[\frac{a}{b}\right] h_1\left(\frac{a}{b}, n\right) \left(\frac{P}{P_o}\right)^{n+1} \tag{J.19}$$

for a Ramberg-Osgood law of the form

$$\left(\frac{\epsilon^p}{\epsilon_o}\right) = \alpha \left(\frac{\sigma}{\sigma_o}\right)^n \tag{J.20}$$

where $c = b - a$ is the uncracked ligament, ϵ^p the plastic strain, and ϵ_o, σ_o, α, and n are material constants. The function h_1 depends on a/b and n. Values of h_1 are tabulated in the EPRI handbooks (for example, see Kumar, German, and Shih, 1981) for various structural and laboratory geometries. P is the applied load and P_o a characterizing yield load which depends on a/b and σ_o.

By writing the Norton law coefficient as $A = \alpha\dot{\epsilon}_o/\sigma_o^n$, the J_p solutions can be converted immediately, using the analogy between plasticity and creep, into an expression for C_s^*

$$C_s^* = A\sigma_o^{n+1}\, c\left[\frac{a}{b}\right] h_1\left(\frac{a}{b}, n\right)\left(\frac{P}{P_o}\right)^{n+1} \tag{J.21}$$

Also, by writing the primary creep law, Equation (J.8), in the form of the product

$$\dot{\epsilon} = B(t)\sigma^m \tag{J.22}$$

where

$$B(t) = \frac{B}{[(1+p)t]^{p/1+p}} \tag{J.23}$$

then an equation similar to Equation (J.21) for C_s^* is also applicable to C_p^* if the constants A and n are replaced by $B(t)$ [defined in Equation (J.23)], and m, respectively.

The reference stress solutions for J_p can also be used to derive expressions for C_s^* and C_p^* following similar procedures to those employed to convert the EPRI solutions (Ainsworth et al., 1987; Chell et al., 1993). The results are

$$C_p^* = B\,\epsilon_{ref}^{-p}\,\sigma_{ref}^{m(1+p)-1}\,K^2 \qquad \text{(strain hardening)} \tag{J.24a}$$

$$C_p^* = \frac{[B(1+p)]^{\frac{1}{1+p}}}{1+p}\, t^{-\frac{p}{1+p}}\,\sigma_{ref}^{m-1}\,K^2 \qquad \text{(time hardening)} \tag{J.24b}$$

$$C_s^* = A\sigma_{ref}^{n-1}\,K^2 \tag{J.25}$$

In Equation (J.24a), ϵ_{ref} is the total accumulated strain due to both primary and secondary creep.

The reference stress, σ_{ref} is defined by the equation

$$\sigma_{ref} = \frac{P}{P_o}\sigma_o \tag{J.26}$$

and $\dot{\epsilon}_{ref}$ is the corresponding reference strain rate at the total accumulated strain ϵ_{ref} or time t obtained using uniaxial creep data.

Thus, all the terms appearing in Equation (J.13) for C_t are derivable from engineering data which should be available or calculable for the defective structure.

J.4 Considerations Related to Cyclic Loading

J.4.1 General Aspects of Creep-Fatigue

The operating histories of high temperature components cover a wide variety of circumstances, which can span the whole creep-fatigue spectrum from creep under steady load conditions without load cycling, to continuous cycling without a hold period. If a defective structure is subjected to steady load conditions over its operating lifetime, then $(da/dN)_f$ is zero, and the time integration of equation $(da/dN)_{time}$ is from zero up to the design life. At very high temperatures, or for very long hold times, crack extension by creep can still be the dominant mechanism for crack growth. In these situations $(da/dN)_{time} >> (da/dN)_f$, so that the latter can be neglected in determining crack propagation behavior. Similarly, at low temperatures, or for short hold times, where fatigue mechanisms dominate, $(da/dN)_f >> (da/dN)_{time}$, and creep effects may be neglected. Thus, consideration of the operating temperatures and cyclic load histories can often lead to simplifications in a creep-fatigue crack growth evaluation.

The crack growth law, Equation (J.1), is integrated numerically to determine the amount of crack extension that results from a specified cyclic load history. The evaluation of crack propagation during a steady load period in the cycle involves integrating $(da/dN)_{time}$ over the hold time, remembering that C_t depends on both time and crack size [see Equation (J.4)]. If the hold time is short, or if the temperature is relatively low, so that little crack extension is expected during the hold, then the integration may be made over time only, keeping the crack size constant at its initial value.

J.4.2 Material Property Requirements

To evaluate crack propagation by creep-fatigue mechanisms requires knowledge of creep deformation behavior as well as the constants which appear in the laws which relate $(da/dN)_f$ to ΔK, and $(da/dN)_{time}$ to the time dependent fracture mechanics parameter, C_t. Creep deformation mechanisms are thermally activated processes which are usually very sensitive to temperature changes, especially at very high temperatures. Hence, the material constants appearing in the creep constitutive laws specified by Equations (J.7) through (J.9) should be obtained from data derived from standard uniaxial tensile creep tests at the appropriate operating temperature. Similarly,

although they are usually less sensitive to small temperature changes, the crack growth law constants should also be obtained at the relevant operating temperatures.

In measuring the fatigue component of growth, consideration should be given to the dependence of the Paris law constants on hold time. Ideally, fatigue crack growth data should be obtained from tests that simulate the actual operating conditions of the component, which could involve both fatigue and creep crack extension during a typical load cycle. In these cases, extreme care should be taken in testing and measurement to separate crack extension during the cyclic part of the cycle, from the extension that occurs explicitly due to creep during the hold part of the cycle.

It is generally accepted that creep crack growth data obtained from laboratory tests under steady load conditions can be used in the evaluation of C_t and $(da/dN)_{time}$ under service conditions, even when the fatigue component of the total growth rate, $(da/dN)_f$, is also significant. An ASTM standard procedure for creep crack growth testing is now available and provides information regarding testing technique and data analysis (ASTM E 1457, 1998). The value of C_t can be inferred from the creep contribution to the load pin displacement rate. The ASTM test standard is designed so that only crack growth behavior under conditions of widespread creep occurs. In other words, the tests should be over in a time scale >> t_1 or t_3, so that the contribution of $C_t(t \rightarrow 0)$ to C_t is negligible.

Currently, there appears to be no standard covering the testing of materials under creep-fatigue conditions. It is not recommended that the creep growth rate be derived by subtracting the continuous cycling fatigue rate from the total measured cyclic crack growth rate. This could lead to erroneous and non-transferable data if the fatigue component of the growth is accelerated by the presence of crack tip creep damage that accumulates during the hold time.

J.4.3 Cyclic Deformation and Crack Tip Recovery

Other factors, related to the cyclic history dependence of creep deformation in the region of the crack tip, can strongly influence the computed value of C_t used in the determination of $(da/dN)_{time}$. These factors are related to the ability of the material to recover its creep deformation behavior as a result of cyclic changes in the crack tip stress field due to the cyclic changes in the applied load (Chell et al., 1993).

During load cycling, which may involve creep deformation, the crack tip region will undergo cyclic yielding. Upon reloading after the unloading and hold parts of a cycle, the crack tip stress field may return to a state similar to that which it had prior to the start of the cycle, and before any creep relaxation resulting from the hold period had occurred. Under these circumstances, the deformation history related to previous cycling events is lost. In contrast, in regions removed from the crack tip, where elastic cycling occurs, the stress field will return to a state similar to that which pertained prior to the cycling. These effects are illustrated in Figure J.4.

Figure J.4(a) shows an idealized pressure-time history with start-ups occurring during OA and DE, and a shut-down BC. The stress-strain history corresponding to the pressure history is shown in Figure J.4(b) for a material point within the cyclic plastic zone at the tip of the defect, and

Figure J.4(c) for a point outside and undergoing elastic cycling. Creep relaxation for the stress fields occurs during the steady running periods, AB and EF. The effect of the cyclic plasticity at the crack tip after the cycle OABCDE is to return a material point in the plastic zone to a stress-strain state similar to that which it had at time A, i.e., cyclic recovery occurs.

However, outside of the plastic zone elastic cycling occurs, and the effect of the cycle OABCDE is to return the deformation state of a material point to what it was just prior to the shut-down. In this case, cyclic recovery would not be expected and creep relaxation during the steady running period EF would continue from the relaxation period AB as if no cycling had occurred.

The significance of cyclic recovery in the crack-tip plastic zone will clearly depend on the size of the cyclic plastic zone (which is related to the cyclic stress intensity range corresponding to the pressure change), and the length of the steady running period (which determines the size of the creep zone relative to the cyclic plastic zone), both of which depend on material constitutive behavior.

Cyclic effects may be included in a creep crack growth methodology based on C_t by considering the following three possibilities:

1) The length of the steady running period is so long that large-scale creep deformation has occurred and the immediate crack-tip region has a negligible influence on C_t and $C_s^* + C_p^* > C_t(t \to 0)$.

2) The influence of the crack-tip region is comparable to the size of the creep zone so that $C_s^* + C_p^* \approx C_t(t \to 0)$.

3) The steady running period is short enough so that the elastic crack-tip fields still dominate creep deformation and $C_s^* + C_p^* < C_t(t \to 0)$.

Possibility (1) implies that no significant cyclic recovery occurs due to start-up/shut-down and the defective structure behaves as if it was subjected to a steady load. In this case, a static analysis is required and the expression for C_t given by Equation (J.13) is appropriate, with time t being set equal to the sum of the hold times to date. In this case the transient component, $C_t(t \to 0)$ becomes less important the longer the operating time.

Possibility (2) implies that cyclic recovery will occur near to the crack tip but not some distance away from it. This situation can be called partial recovery and may be simulated by modifying C_t so that the transient component (corresponding to $t \to 0$) is calculated assuming recovery, but the steady-state component (corresponding to $t >> 0$) does not. In this case, Equation (J.13) becomes (Chell et al., 1993)

$$C_t = C_s^*(t) + C_p^*(t) + \beta \frac{\dot{r}_c(t-t_i)}{b} \frac{F'}{F} \frac{(1-\nu^2)}{E} K^2 \qquad \textbf{(J.27)}$$

where t is the current time and t_i the time of the last cycle.

Finally, possibility (3) implies that full cyclic recovery occurs in the whole of the creep zone. In this case, all previous loading history effects are lost after cycling and the expression for C_t becomes (Chell et al., 1993)

$$C_t = C_s^*(t-t_i) + C_p^*(t-t_i) + \beta \frac{\dot{r}_c(t-t_i)}{b} \frac{F'}{F} \frac{(1-\nu^2)}{E} K^2 \qquad \textbf{(J.28)}$$

It is pessimistic to assume that full crack tip cyclic creep recovery occurs, as this maximizes the value of C_t and hence $(da/dN)_{time}$. This point is illustrated in Figure J.5 which schematically shows how C_t varies with time during cyclic loading, based on the assumptions that full recovery occurs (dotted line) and no recovery takes place, the latter being equivalent to steady state loading.

Full recovery is to be expected in situations where the creep zone size is small compared to the crack tip cyclic plastic zone, and no recovery when this situation is reversed. This conclusion has been born out by recent creep-fatigue finite element studies (Adefris, Saxena, and McDowell, 1996).

The creep zone size, r_c, which increases with time, is given by Riedel (1987) for primary and secondary creep as:

$$r_c = \frac{K^2}{2\pi} \left[\frac{I_m E}{2\pi(1-\nu^2)} \right]^{\frac{2}{(m-1)}} [(1+m)(1+p)Bt]^{\frac{2}{(1+p)(m-1)}} \tilde{r}_c \qquad \textbf{(J.29)}$$

and, for secondary creep,

$$r_c = \frac{K^2}{2\pi} \left[\frac{I_n EA(n+1)t}{2\pi(1-\nu^2)} \right]^{\frac{2}{(n-1)}} \tilde{r}_c \qquad \textbf{(J.30)}$$

The cyclic plastic zone size, Δr_y, can be estimated using the equation

$$\Delta r_y = \frac{1}{4\pi\beta'}\left(\frac{\Delta K}{\sigma_{ys}}\right)^2 \tag{J.31}$$

where ΔK is the stress intensity factor range, σ_{ys} the yield stress, and $\beta' = 2$ for plane stress, and 6 for plane strain deformation. Thus, if $r_c \leq \Delta r_y$ during the hold period, then full recovery should be assumed. It would be prudent to continue to assume full recovery even when $r_c > \Delta r_y$, or at least to assume partial recovery. Only if $r_c >> \Delta r_y$ should the assumption of no recovery be assumed in the absence of supporting experimental evidence.

The type of differences that can occur between predicted remaining lives based on the assumption of full, partial and no recover, are illustrated in Figure J.6, based on an example fitness-for-service assessment of a petrochemical processing vessel obtained using the computer code COBRA developed at Southwest Research Institute (Chell et al., 1993). These results are calculated assuming 1- and 3-year intervals between start-up and shut-down. Note that the partial and full recovery results are the same for the material that undergoes only secondary creep, this is because for these materials the steady state, or long time, component of C_t (C_s^*) does not depend explicitly on time [compare Norton's Law, Equation (J.9)], and hence recovery effects only influence the transient ($C_t(t-0)$) component of C_t.

If the hold periods occur at different temperatures during the life of the component, then it is prudent to assume full recovery.

J.5 Other Aspects of Creep-Fatigue

J.5.1 Combined Mechanical and Thermal Loading

Frequently thermal stressing due to start-up and shut-down is one of the major cyclic loading conditions that components experience. For example, components of the SSME undergo severe temperature changes over very short time scales, and although the walls can be very thin, high thermal stresses are still induced because of the rapid rate of change of temperature.

Since high thermal stresses will be relaxed over time by the substitution of creep strains for thermal strains, these stresses will not influence the long term steady state creep behavior of cracks. On the other hand, at short times into a hold period, they will load a defect and produce a corresponding stress intensity factor which will add on to the value produced by mechanical loading. This suggests the following procedure should be followed for incorporating thermal stresses into the calculation of C_t: add the thermal component of K to the mechanical component and use this value in the expression for the transient component of C_t [Equations (J.15) through (J.18)], but only

include the mechanical component in the value of K which determines the steady state value [Equations (J.24) or (J.25)][1].

These aspects have been investigated by Joch and Ainsworth (1992b) using the finite element stress analysis method. Their calculated results support the expected behavior trends, and show that it is pessimistic (i.e., produces an over-estimate of C_t), to follow the procedure suggested in the previous paragraph. (Figure J.7 shows their results plotted in terms of Riedel's (1987) crack tip characterizing parameter, $C(t)$. Very similar behavior is to be expected when $C(t)$ is replaced by C_t). In particular, the results of Joch and Ainsworth show that although $C_t(t \to 0)$ will be increased by the presence of thermal stresses, C^* will not change, and will depend only on the primary loading. Adding the initial value of the thermal K to the primary component will increase the calculated transition time, t_1 or t_3, with respect to computed finite element values, as it does not take account of the relaxation in the nominal thermal stresses due to creep, and the corresponding reduction in the thermal K with time.

J.5.2 Crack Tip Plasticity

The presence of widespread crack tip plasticity increases the crack driving force with respect to a linear elastic calculation based on K, and significantly changes the crack tip stress field compared to the linear elastic field. An initial first approximation to incorporating the effects of plasticity suggests itself: replace K in the appropriate creep equations by its elastic-plastic equivalent, $(E'J)^{1/2}$. However, after more detailed deliberations it is clear that this approach is not correct.

The reason is that under fully plastic conditions, where the cracked section has undergone general yielding, the resulting stress field will be very similar to the steady state creep stress field. (This can be seen immediately from the analogy between creep and plastic deformation.) Hence, the transition time between the initial and steady state creep solution should reduce to zero as plasticity spreads across the cracked section of a component. This behavior will not be reflected by Equation (J.15) if J_e in that equation is simply replaced by J_p. Furthermore, the reference stress solution for C^*, through its dependence on the reference stress and strain rates, already incorporates the effects of a crack tip stress field whose distribution is similar to a fully plastic field, only the magnitude of the distribution differs from the fully plastic field. However, when the applied loads are sufficient to result in general yielding, then the reference stress appearing in Equations (J.24) and (J.25) will equal the general yield value, as required. Hence it is to be expected that under fully plastic conditions, the solution for C_t will reduce to the solution for C^*.

---

[1] This approach is remarkably simple compared with the problems faced in developing elastic-plastic J estimation schemes for combined primary and secondary loads (see Appendix F). One of the reasons is that secondary stresses, although reduced by the spread of plasticity, are not totally eliminated by it. Only stresses exceeding the yield point are relaxed, and then only to the yield point level. In contrast, there is no restriction on the creep strains that can accumulate with time, and, under strain control, these will continue to replace elastic strains and relax the stress as long as a self-equilibrated stress of non-zero magnitude exists.

These conclusions have been investigated and substantiated by the results of limited finite element calculations (Joch and Ainsworth, 1992a). They have been discussed in the context of practical applications of C^* by Ainsworth (1992a). These two works suggest that crack tip plasticity can be incorporated into C_t by modifying the equation which approximates the transition from $C_t(t\to 0)$ to C^*

At this time it is premature to recommend a general formulation for C_t which includes crack tip plasticity. Clearly, if in the fully plastic regime, C_t can be replaced by C^* at all times, then C_t will be overestimated under these conditions by adding Equation (J.15) to Equation (J.24) or Equation (J.25) (see Figure J.8). Hence, in the absence of a more developed elastic-plastic procedure for creep situations, these equations should continue to be used to assess creep crack growth for all levels of plasticity, as they will overestimate the amount of crack extension compared to the actual elastic-plastic results.

J.5.3 Constraint

Unlike fully plastic behavior where large strains are generated after general yielding, large scale creep deformation can occur at reference strain levels which are moderate by comparison. Even so, the effects on calculated creep crack growth rates of assuming either plane strain or plane stress constraint can be dramatic. This is because the steady state component of C_t depends on the reference stress raised to the power $n-1$ [see Equation (J.25)], where the creep exponent n is typically about 10. The reference stress in turn is dependent on the assumed constraint conditions through its dependence on the general yield load, P_o [see Equation (J.26)].

Different creep deformation mechanisms can be driven by different equivalent stresses, so that their characterization by von Mises or Tresca equivalent stresses, or some other combination of principal stresses, may be less clear cut than is the case for plasticity. If it is not clear which constraint to assume for a particular application, it is prudent to use a plane stress reference stress based on the Tresca yield criterion. This will generally produce a higher reference stress than von Mises and plane strain solutions.

J.5.4 Crack Closure

Crack closure during cyclic crack growth can significantly change the cyclic crack tip driving force, and thus influence the crack propagation rate. In the absence of creep deformation at the crack tip, crack wake plasticity and the associated residual stress in the vicinity of the crack tip is often the dominant contribution to closure (McClung, 1991c). If significant creep deformation occurs in the load cycle, then this may influence the closure behavior. However, the crack closure phenomenon is not so well understood under creep-fatigue conditions as it is for continuous cycling.

Sehitoglu and Sun (1989) have used an elastic-plastic finite element (FE) model of a growing fatigue crack similar to that employed in Appendix H to study the effects of creep deformation on crack closure. The FE model employed a constitutive model with time-independent plastic

deformation obeying a Ramberg-Osgood type of power law, and a time-dependent creep deformation similar to Norton's law.

Sehitoglu and Sun found that creep deformation modified the crack-tip stress-strain fields and crack tip displacements, and as a result caused crack opening stresses to be lower: creep strains increased the effective stress range ratio, U, over which the crack was open. The effect was most pronounced for the higher creep rates studied. A simple semi-empirical expression was developed to predict the change in U due to creep for different applied stresses, hold times, and material properties. However, the investigations of Sehitoglu and Sun (and their resulting semi-empirical equation) were limited to $R = 0$ loading with tensile hold periods at maximum load. It is not possible at the present time to generalize these results to a wider range of load histories.

In the absence of more comprehensive analysis or any correlating experimental measurements of closure during creep-fatigue, it is not currently possible to recommend an engineering algorithm to characterize closure. When creep deformation is limited, it appears reasonable to employ the usual time-independent (plasticity-generated) estimates of crack opening stresses. When creep deformation is significant, it may be prudent to assume that no closure occurs ($U = 1$), so that the full cyclic change in the crack tip driving force is used to characterize the fatigue component of the cyclic crack growth law.

J.5.5 Displacement Loading and Elastic Follow-up

The effects of imposed displacement loading and the resulting elastic follow-up on the calculation of C_t have been discussed by Ainsworth (1992b). He concluded that the transient component of C_t at very short times, $C_t(t \to 0)$, is independent of the remote boundary conditions. Essentially, the creep zone size is too small in this regime to significantly perturb the time independent linear elastic solution. At later times, creep deformation results in stress relaxation which lowers the reference stress. In this regime, Ainsworth found that it is conservative to estimate C_t from the steady state component of C_t, C^*, provided

$$\frac{\sigma_{ref}}{\sigma^o_{ref}} \leq \frac{\left[Z - Z^{\frac{1}{(1+n)}}\right]}{[Z-1]} \qquad \textbf{(J.32)}$$

where σ^o_{ref} is the initial value of the reference stress, and σ_{ref} its instantaneous relaxed value. The parameter Z characterizes the amount of elastic follow-up in the structure: $Z = 1$ corresponds to creep deformation under constant strain conditions (such as may result from thermal loading), and $Z = \infty$ to constant load conditions. (In fact, $Z = \epsilon_c/\Delta\epsilon$, where $\Delta\epsilon$ is the elastic strain corresponding to the incremental reduction in the initial stress after time t, and ϵ_c is the accumulated creep strain after time t.) In many service situations it may be difficult to characterize the elastic follow-up in

the structure (i.e., define a value for Z) without performing a detailed and expensive time dependent stress analysis. In these cases, it is prudent to assume that no stress relaxation occurs ($Z = \infty$).

J.5.6 Crack Growth Initiation

Cracks undergo an incubation period during which creep damage accumulates at the crack tip until a critical value required for propagation is attained. Ainsworth and coworkers describe a methodology for estimating the incubation time (Chell et al., 1993; Ainsworth, 1982). An overestimate of the amount of creep crack extension will be obtained if the incubation time is assumed to be zero.

J.5.7 Effects of Loading Ramp Rate

Significant creep deformation can occur during slow loading ramps at elevated temperatures. In these cases, it is prudent to add the time of the ramping to the hold time at constant load for the purposes of calculating $(da/dN)_{time}$.

J.5.8 Effects of Temperature Changes During a Load Cycle

The effects of changes in temperature during load cycling on creep-fatigue behavior are very complex. Although synergistic effects can occur between fatigue and creep mechanisms under these conditions, it is usually considered safe, for assessment purposes, to use material property values derived for the maximum temperature experienced during the cycle.

J.6 Remaining Life Estimation under Creep-Fatigue Conditions

The remaining life is obtained by integrating the crack growth rate, da/dN, per cycle between an initial defect size, a_o, and a final size, a_f. The latter can be estimated by applying fracture mechanics, and is usually equated to the value of the maximum tolerable defect size that can just survive the worst case loading scenario to which the structure will be subjected during its design life. The number of allowable service cycles, N_r, is obtained from the equation:

$$N_r = \int_{a_o}^{a_f} \frac{1}{\left(\frac{da}{dN}\right)} da \qquad \textbf{(J.33)}$$

where, in Equation (J.2) for da/dN,

$$\left(\frac{da}{dN}\right)_f = A(t_h)(\Delta K)^{m(t_h)} \qquad \textbf{(J.34)}$$

and

$$\left(\frac{da}{dN}\right)_t = \int_0^{t_h} H\left[C_t\left(a,t^*+t\right)\right]^q dt \qquad \textbf{(J.35)}$$

In Equation (J.35), the value of t^* depends on whether cyclic recovery occurs in the crack tip region. If it does, then $t^* = 0$. If no recovery takes place then t^* should be set equal to the operating time up to the start of the current load cycle.

Equations (J.33) through (J.35) can be readily generalized to the case where the cyclic loading conditions vary during the operating history.

J.7 Conclusions

Cyclic crack extension under creep-fatigue conditions can be determined by linearly adding the growth rates per cycle due to fatigue and creep. The fatigue growth rate can be estimated using the Paris equation, but the constants appearing in that law will, in general, depend on the hold time in the cycle. The effects of cyclic plasticity can be accounted for by replacing ΔK in the Paris equation by $(E'\Delta J)^{1/2}$.

The creep crack growth rate per cycle is calculated by integrating a creep crack growth law, characterized by the time dependent fracture mechanics parameter, C_t, over the hold time. It has been shown that laboratory measured C_t values correlate creep crack growth rates from different test specimens, and hence, this parameter facilitates the transfer of these data to structural components.

The parameter, C_t, consists of transient and steady state components, both of which depend on the constitutive law which relates creep strain rate to stress. The value of C_t is also dependent on whether creep deformation recovery due to cycling can occur at the crack tip. If the zone of creep deformation which spreads out from the tip is smaller than the cyclic crack tip plastic zone, then creep recovery will occur and all history effects from previous cyclic load changes are lost. If the creep zone is much larger than the cyclic plastic zone, then recovery is unlikely, and information regarding the previous load history is retained with creep deformation evolving with time as if no cyclic loading had occurred.

The transient component of C_t is characterized by the applied stress intensity factor, and derivatives of it. Expressions for the steady state component can be readily derived from available fully plastic J solutions, or a reference stress approach, by employing the analogy between plastic and creep deformation. Hence, C_t can be calculated from material property data and fracture mechanics parameters. The effects of thermal loading can be incorporated into C_t by adding the thermal stress intensity factor to the stress intensity factor arising from primary loading, and evaluating $C_t(t\rightarrow 0)$ using the total value. The steady state component, C^*, is unaffected by thermal

loading and depends only on the applied primary load. The foregoing are applicable even when widespread crack tip plasticity is present.

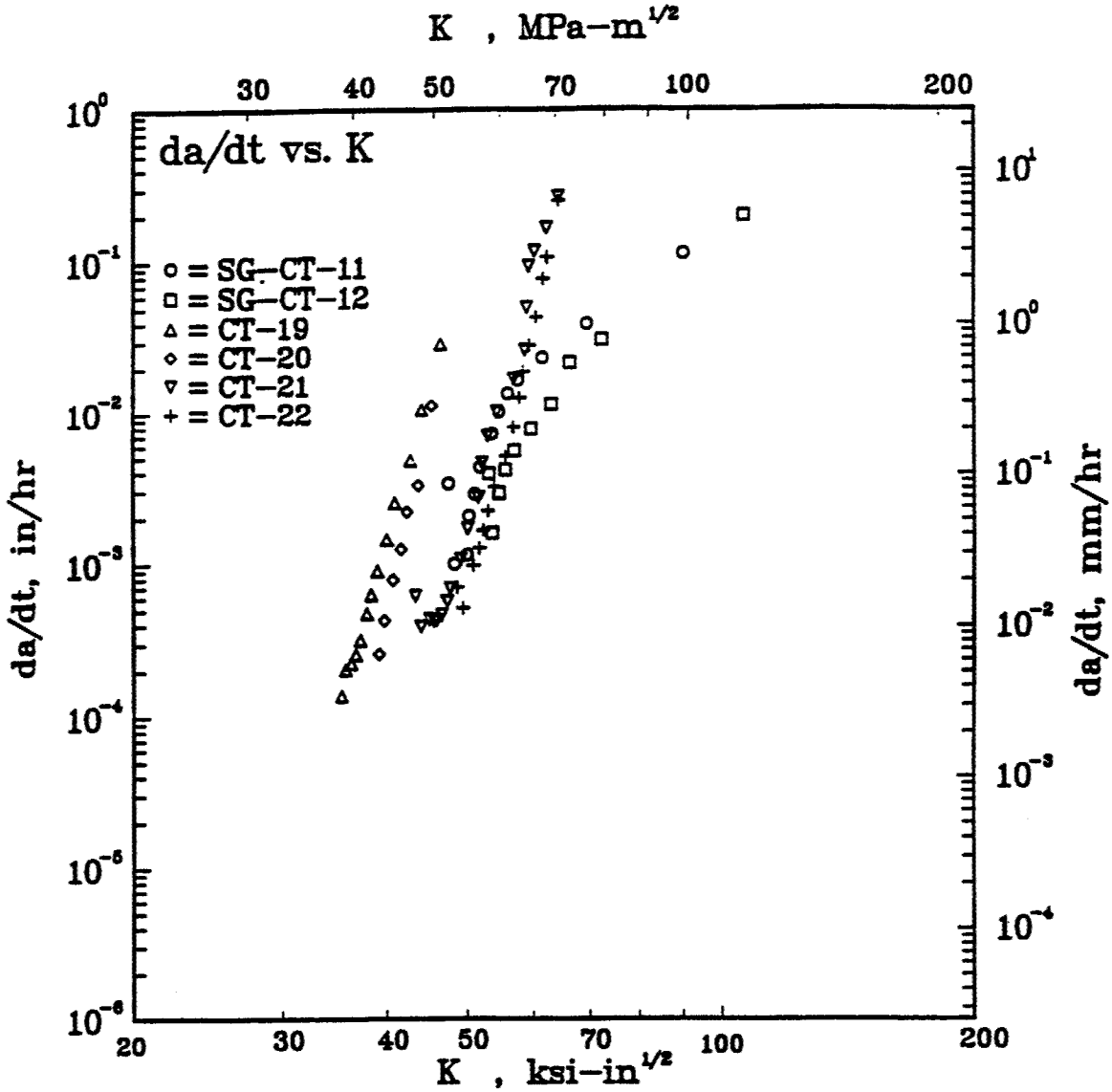

Figure J.1. Creep crack growth, *da/dt*, expressed as a function of stress intensity factor, *K*.

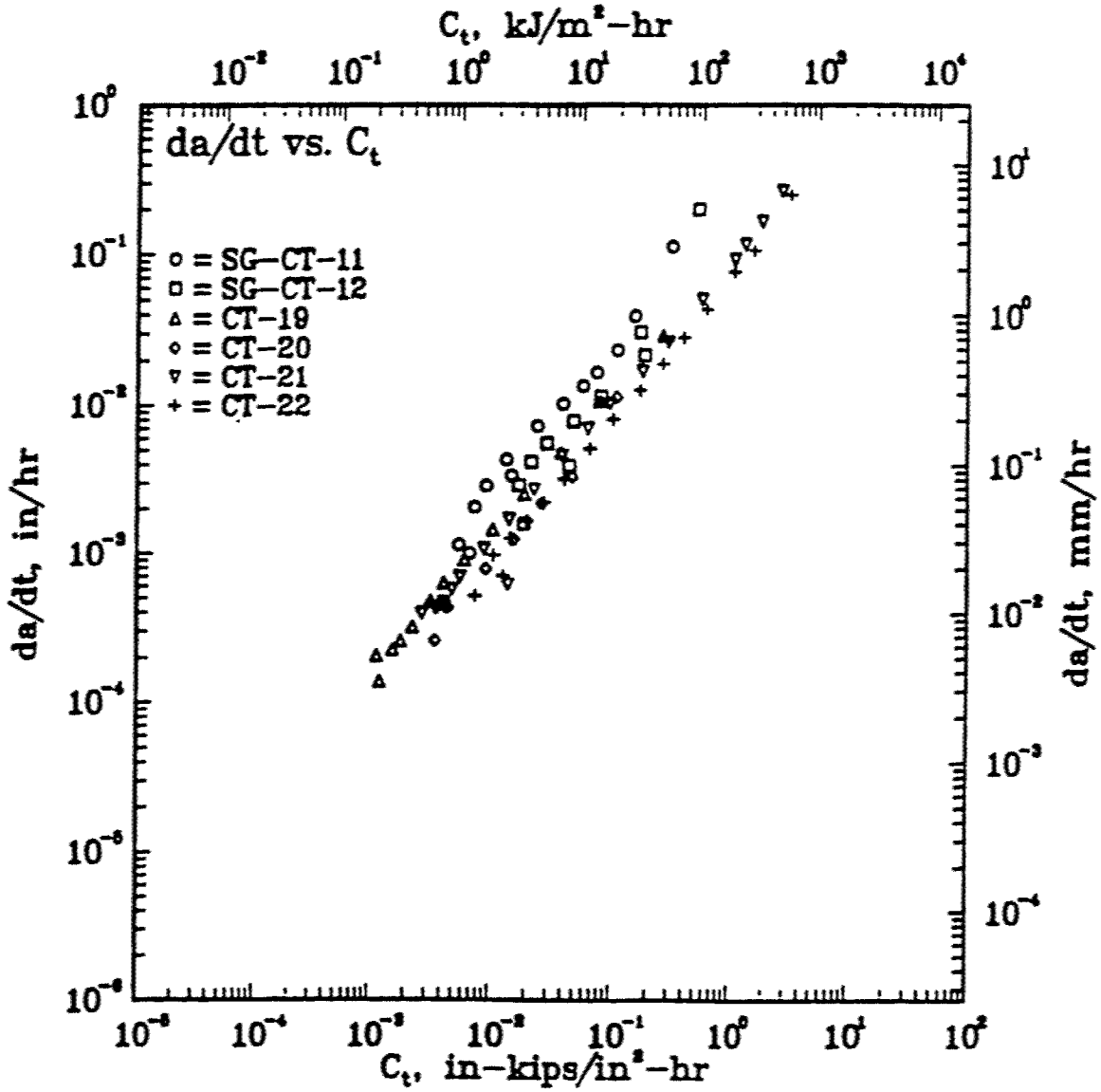

Figure J.2. Creep crack growth data as shown in Figure J.1 expressed as a function of the time dependent fracture mechanics parameter, C_t.

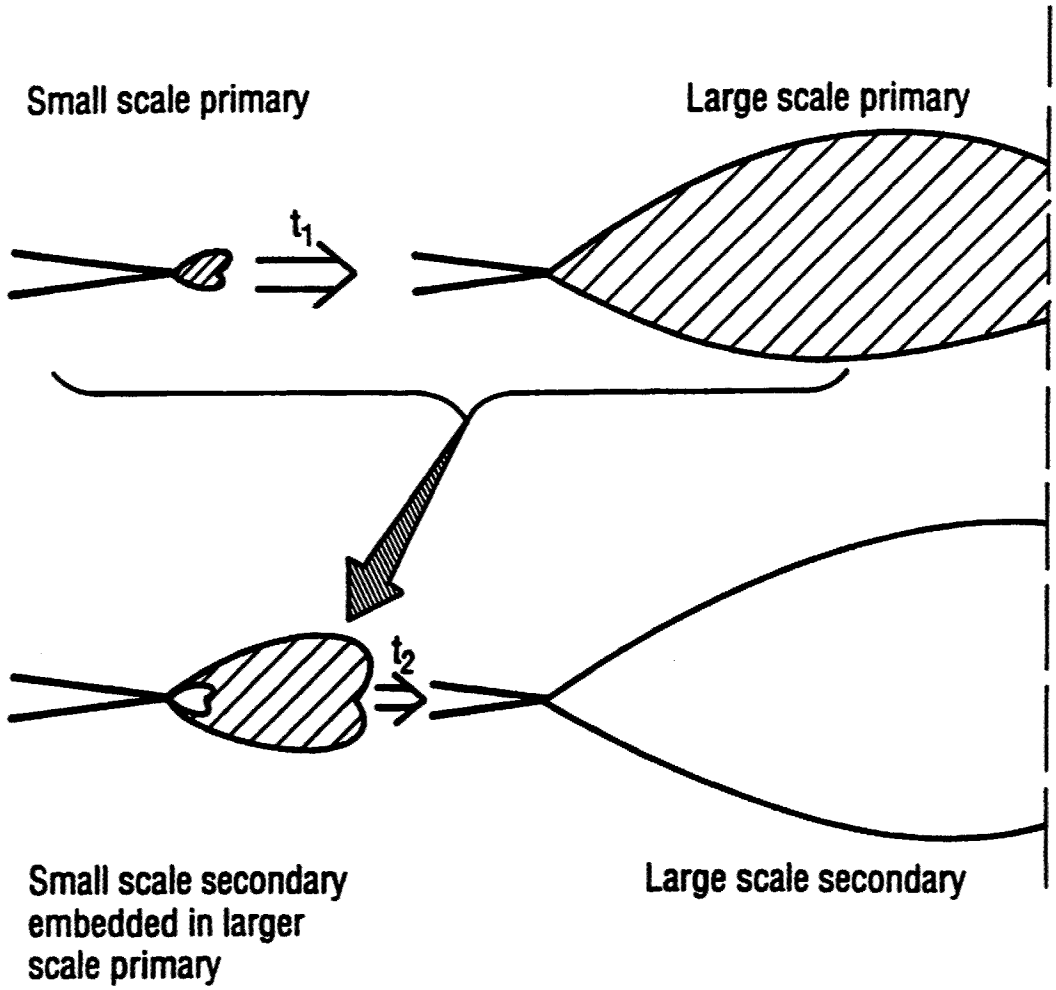

Figure J.3. Schematic showing the development of primary and secondary creep zones at the crack tip, and the transition times t_1 and t_2.

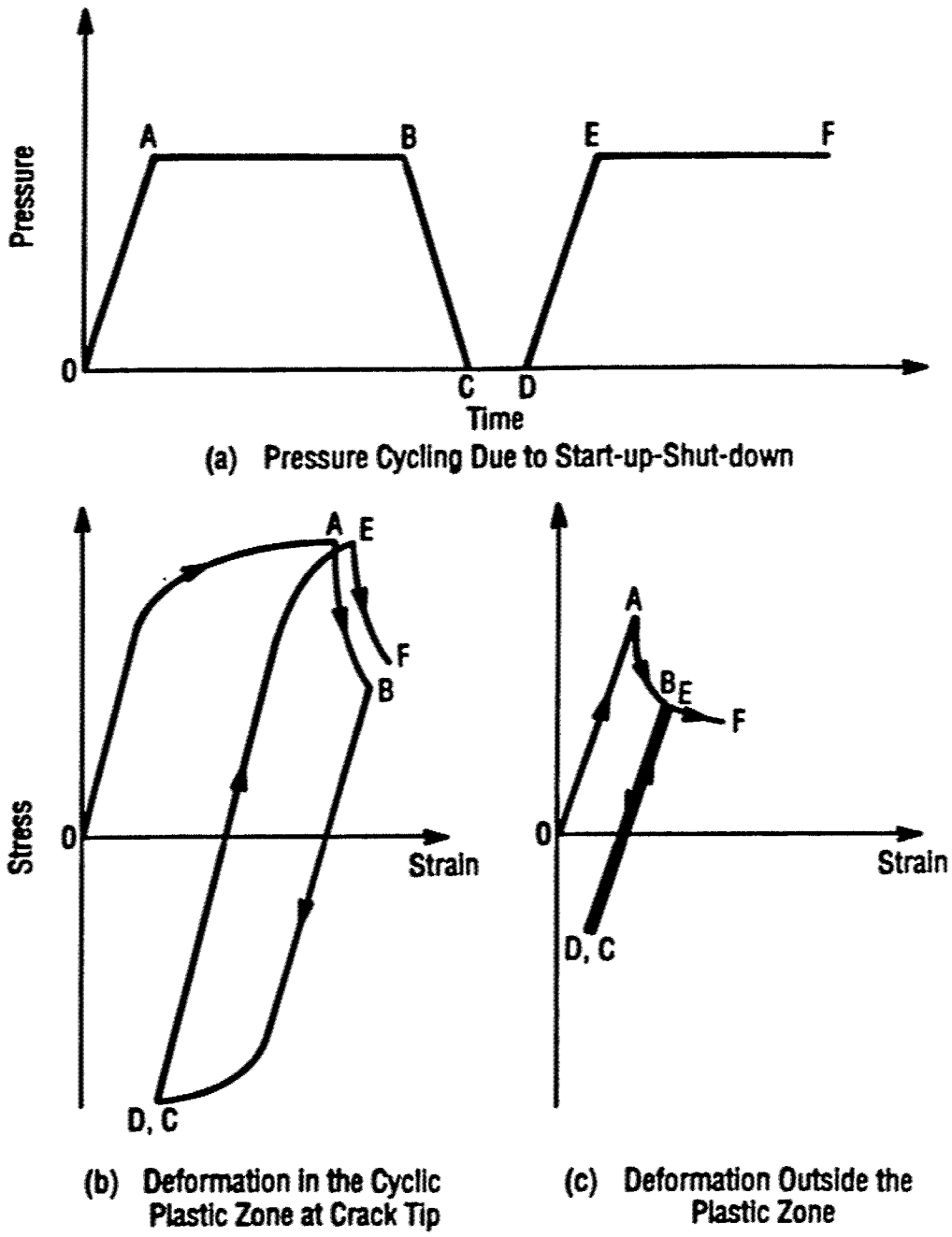

Figure J.4. Effects of cyclic loading: (a) Pressure cycling due to start-up and shut-down, (b) Deformation in cyclic zone at crack tip, (c) Deformation outside the plastic zone.

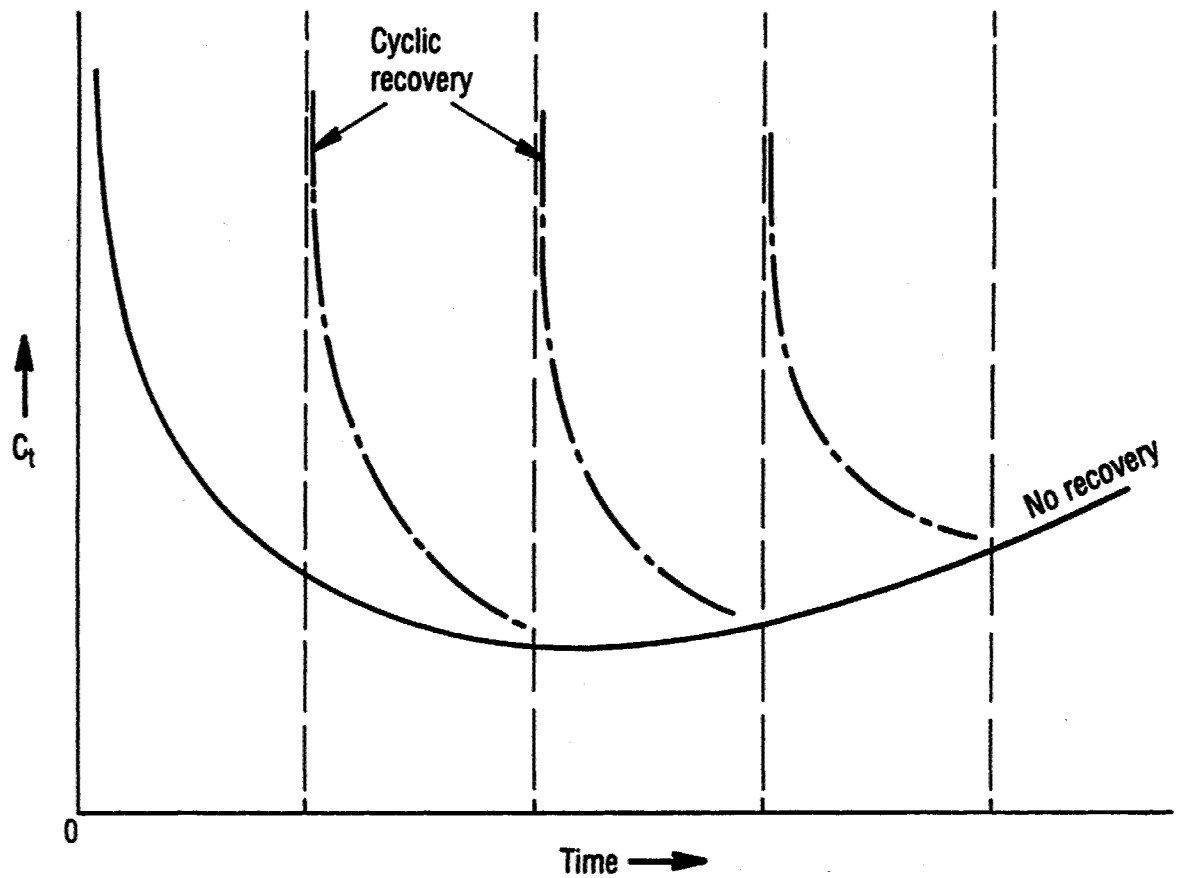

Figure J.5. Schematic showing different C_t behavior for cyclic recovery and no recovery. The vertical lines indicate times at which load cycling occurs.

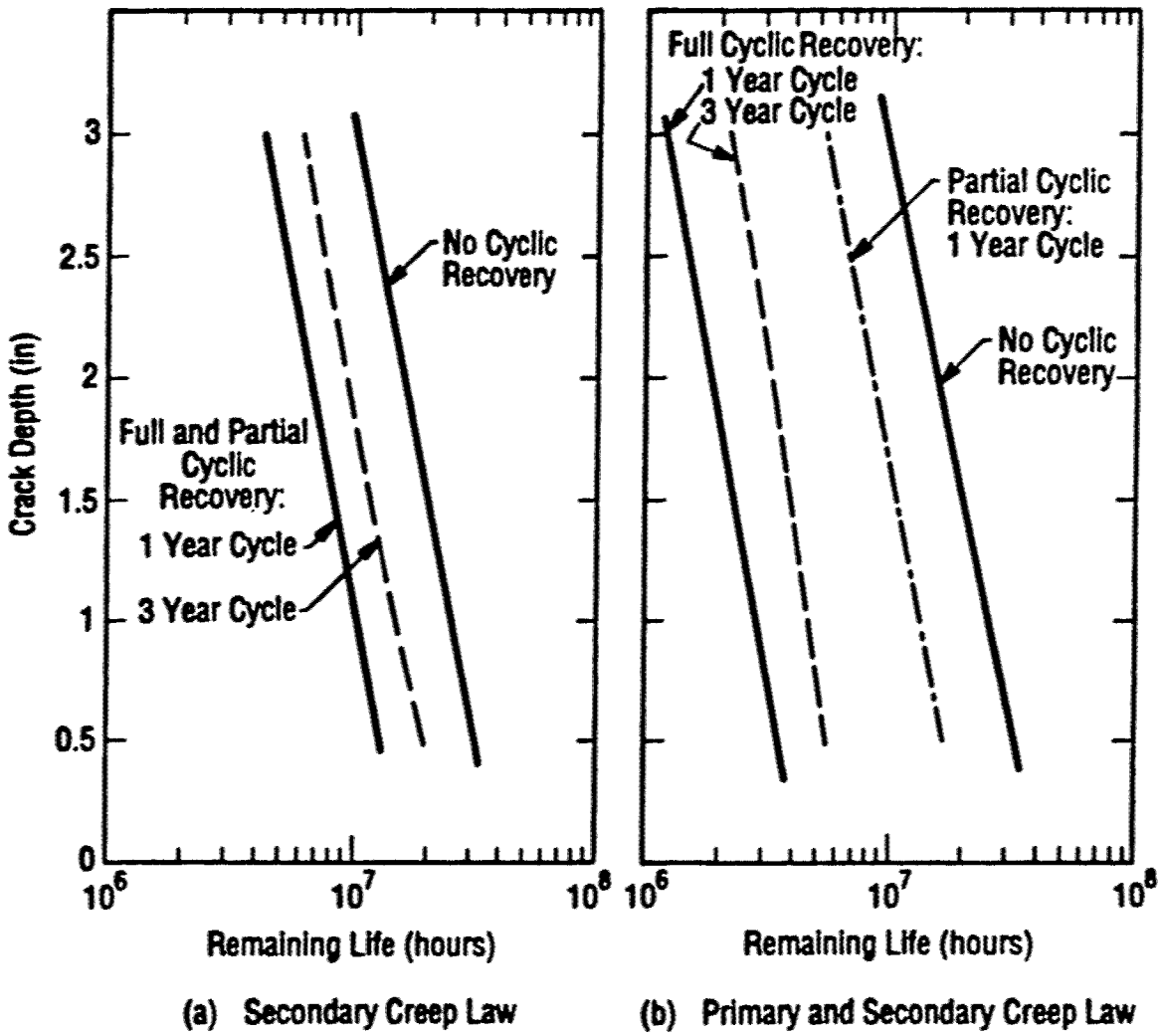

Figure J.6. Examples of the effect on the remaining life of a pressure vessel operating in the creep regime of assuming various recovery models and creep constitutive laws.

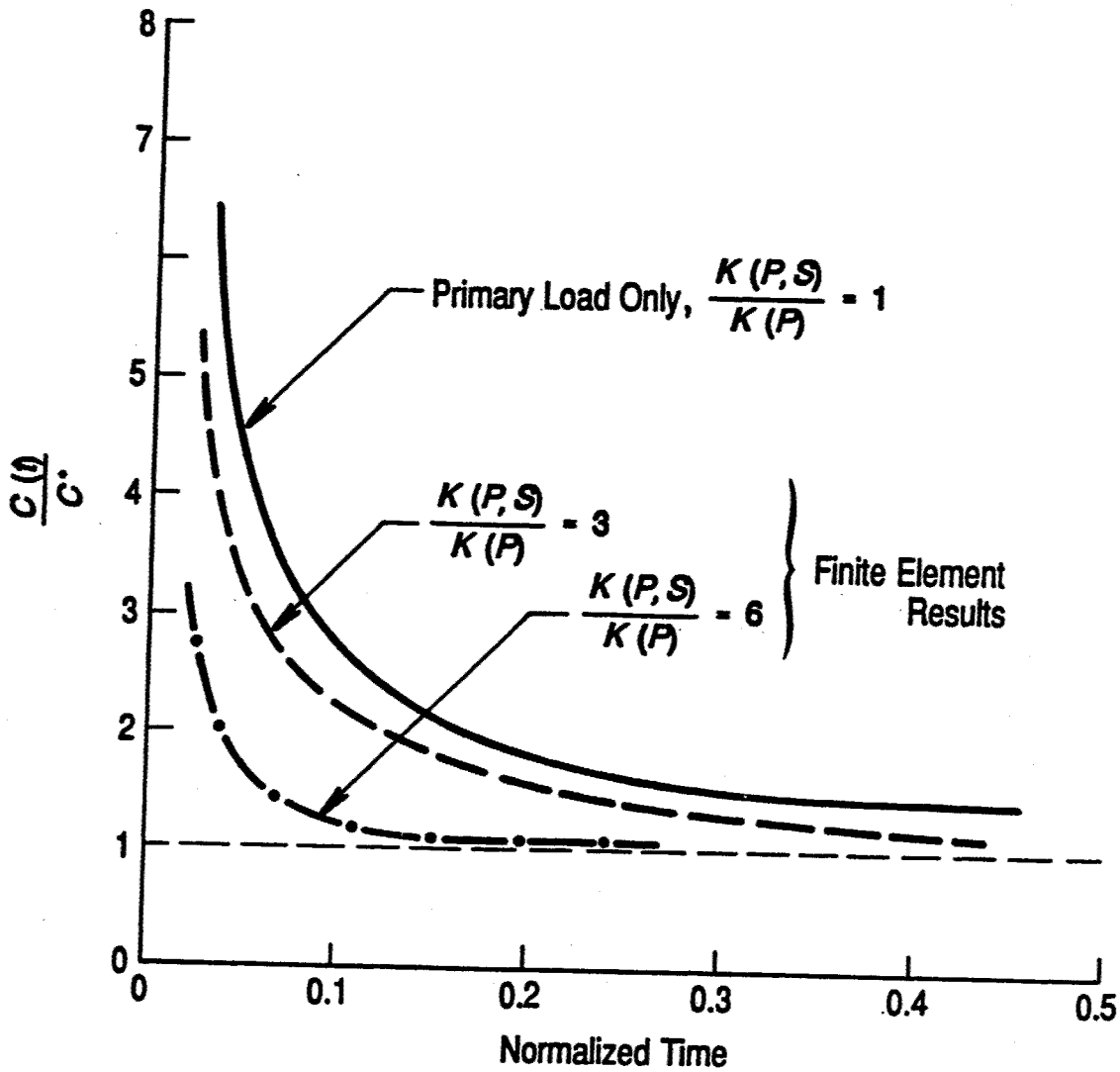

Figure J.7. Illustration showing the effect of increasing thermal loading on the transition of $C(t)$, the crack tip field characterizing TDFM parameter, to its steady state value, C^*, which is determined only by the primary loading. The finite element results are from Joch and Ainsworth (1992b). $K(P)$ is the stress intensity factor due to the primary load, and $K(P,S)$ due to the combined primary and secondary loads.

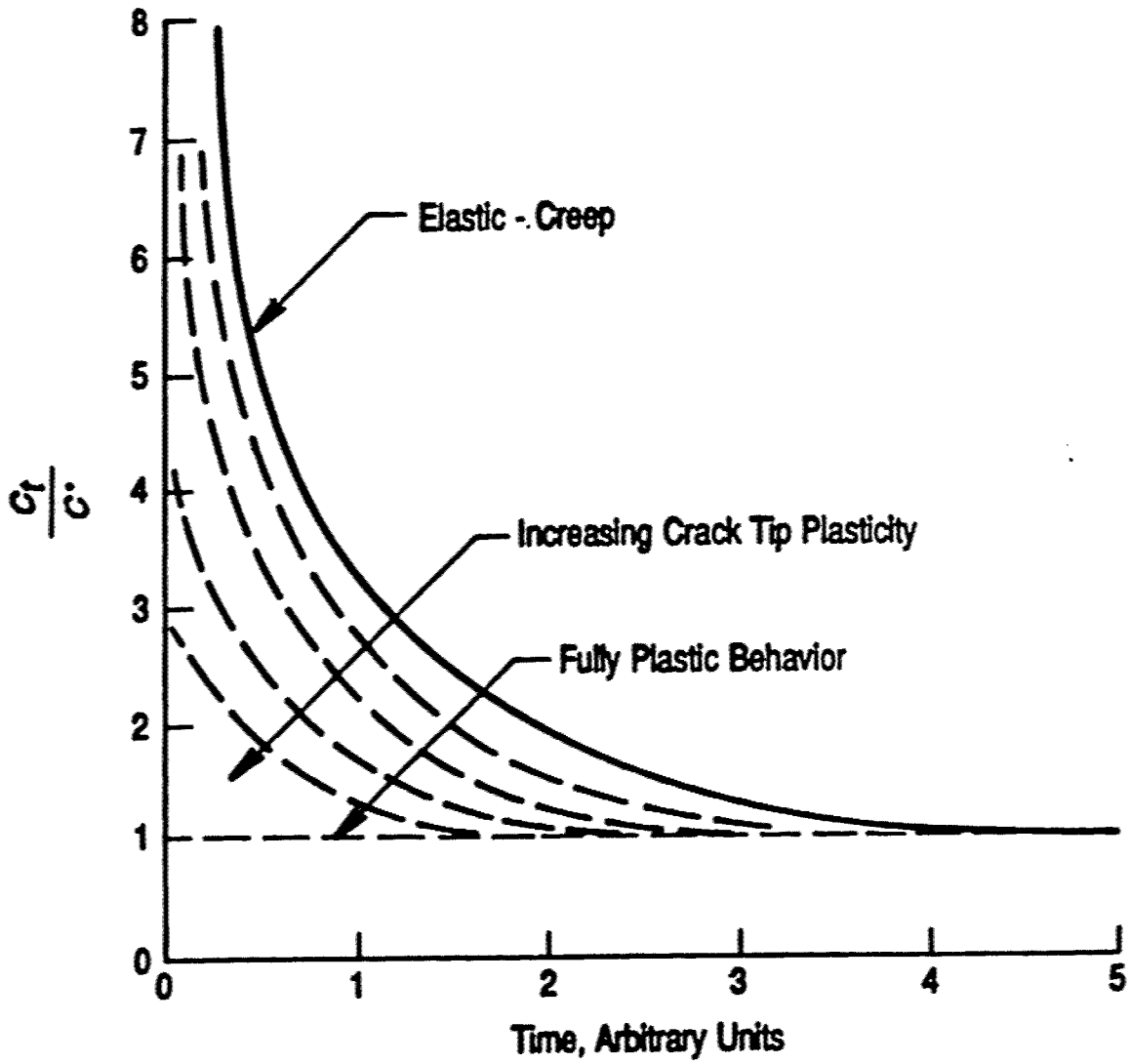

Figure J.8. Illustration showing the effect of increasing crack tip plasticity on the transition of C_t to its steady state value, C^*.

APPENDIX K

USER'S MANUAL FOR NASGRO ELASTIC-PLASTIC FRACTURE MECHANICS MODULES

TABLE OF CONTENTS

		Page
1.0	Introduction to the Elastic-Plastic Fracture Mechanics (EPFM) Module in NASGRO	K.1
2.0	Theoretical Background	K.5
2.1	J and ΔJ Integral	K.5
2.2	EPRI J and ΔJ Estimation Schemes for Combined Primary and Secondary Loads	K.5
	- J Estimation Scheme for Monotonic Loading	K.6
	- ΔJ Estimation Scheme for Cyclic Loading	K.7
2.3	J_p and ΔJ_p Estimation Schemes for Combined Primary and Secondary Loads using Reference Stress Method (RSM)	K.8
	- J_p Estimation Scheme for Monotonic Loading	K.9
	- ΔJ_p Estimation Scheme for Cyclic Loading	K.10
2.4	Brittle and Ductile Fracture Criteria	K.10
	- Brittle	K.10
	- Ductile	K.11
2.5	Elastic-Plastic Fatigue Crack Growth Equation	K.12
2.6	Corrections for Plasticity-Induced Crack Closure	K.12
2.7	Surface Correction Factor due to Crack Closure	K.14
3.0	J_p and ΔJ_p Solutions in the EPFM Module	K.16
3.1	EPRI Solutions	K.16
	- J_p Solutions	K.16
	- ΔJ_p Solutions	K.19
3.2	Optimized Reference Stress Solutions	K.19
	- J_p Solutions	K.19
	- ΔJ_p Solutions	K.20
3.3	Reference Stress Solutions	K.23
	- J_p Solutions	K.23
	- ΔJ_p Solutions	K.24
4.0	Net Section Yield Loads and Moments used in the RSM	K.24
4.1	Net Section Yield Loads for EC01, SC01 and CC01 under Tension	K.24
4.2	Net Section Yield Moments for SC01 and CC01 under Bending	K.24
5.0	Re-characterization of Arbitrary Secondary Stress Fields	K.25
5.1	Linearization of Arbitrary Secondary Stress Field for use with CC01 and TC02	K.25
5.2	Geometry Substitution of SC01 by SC02	K.27
5.3	Uniform Stress Approximation for EC01 and TC01	K.27
6.0	Evaluation of J and ΔJ for Combined Loading	K.28
7.0	Algorithms for Failure Analysis	K.30
7.1	Determining Critical Crack Sizes	K.30
	- Algorithm for Determining the Limit Crack Length (ALIMIT)	K.30
	- Algorithm for Calculating Critical Crack Sizes (Brittle Materials) and Initiation Crack Sizes (Ductile Materials) (ANIT)	K.30

TABLE OF CONTENTS (CONT'D)

		Page
	- Algorithm for Calculating Critical Crack Sizes in Ductile Materials (ACRIT)	K.31
	7.2 Determining Critical Loads	K.32
	- Algorithm for the Limit Primary Load (PLIMIT)	K.32
	- Algorithm for Calculating Critical Loads (Brittle Materials) and Initiation Loads (Ductile Materials) (PINIT)	K.32
	- Algorithm for Calculating Critical Loads for Ductile Materials (PCRIT)	K.32
8.0	Rules for Calculating J, ΔJ and the R ratio	K.38
9.0	Validity Limits for J Solutions	K.39
10.0	How to use the NASGRO EPFM Module	K.39
	10.1 How to run an Elastic-Plastic J-Integral Calculation	K.39
	- Interactive Input Mode	K.40
	- Batch Mode	K.44
	10.2 How to perform a Failure Analysis	K.48
	10.3 How to run an Elastic-Plastic Fatigue Crack Growth Calculation	K.56
11.0	Program Validation	K.65
	11.1 Validation of the RSM J Solutions	K.65
	- TC01 under Tension and TC02 under Tension and Bending	K.65
	- SC01 under Tension and CC01 under Tension	K.69
	a. Validation of optimized RSM	K.69
	b. Validation of the hybrid RSM module of NASGRO	K.72
	c. Additional validation of the hybrid RSM module	K.75
	- Surface Crack under Bending	K.77
	11.2 Validation of the J Solutions due to Secondary Loads	K.81
	11.3 Validation of the EPFM Failure Algorithm	K.81
	- Self-Consistency Between Critical Crack and Critical Load Calculations	K.81
	- Independent Check	K.82
11.4	Validation of the EPFCG Calculation in the NASGRO EPFM Module	K.88
12.0	Acknowledgement	K.88

1.0 Introduction to the Elastic-Plastic Fracture Mechanics Module in NASGRO

The application of linear elastic fracture mechanics (LEFM) to assessing critical crack sizes and critical applied loads is non-conservative in situations where significant crack tip plasticity develops at fracture. This situation is frequently encountered in hardware manufactured from ductile materials that are tough (display a high resistance to crack extension under monotonically increasing loads). Elastic-plastic fracture mechanics (EPFM) was developed in order to extend the concepts of fracture mechanics to defective structures where the influence of plasticity on the crack tip driving force could not be ignored in a safety evaluation without incurring an unacceptable risk of fracture during service.

The *J*-Integral is the most widely employed of the available EPFM parameters. As a result, several successful methods have been developed for evaluating this parameter. For example, the Electric Power Research Institute (EPRI) has sponsored the generation of *J* solutions using the finite element method and their inclusion in a series of elastic-plastic handbooks (Kumar et al., 1981, 1982, 1984a). Relatively simple analytical expressions for *J* have also been derived using so-called reference stress methods (RSM's) (Ainsworth, 1984). The form of these solutions is closely related to the *J* estimation scheme developed by EPRI.

The EPRI and RSM *J* estimation schemes were incorporated into NASGRO in a previous release of this module. These *J* solutions include through central (NASGRO model type TC01) and through edge (TC02) cracks, as well as surface (SC01), corner (CC01) and embedded (EC01) flaws. These *J* solutions utilize the results of elastic-plastic *J* computations obtained from several sources. The EPRI handbook solutions (Kumar et al., 1981) were used for plane strain and plane stress *J* solutions for the TC01 geometry subjected to uniform stressing, and the TC02 geometry subjected to uniform stressing and bending. New *J* solutions derived under the current contract were used to develop the EPFM module solutions for surface (SC01) and corner (CC01) cracks subjected to uniform stressing. The RSM was used to generalize these limited three-dimensional solutions to geometries of arbitrary size, and to provide new *J* solutions for an embedded flaw subjected to uniform stressing (EC01), and surface (SC01) and corner (CC01) cracks subjected to through-wall bending. In addition, guidance on the development of the RSM solutions for the SC01 geometry subjected to bending was provided by the limited *J* solutions reported by Yagawa et al. (1993).

The new, enhanced EPFM module consists of three major routines which perform *J* calculations (JMODULE), failure assessments (FAILALGO) and elastic-plastic fatigue crack growth life predictions (EP_LIFE), respectively. Elastic-plastic *J* solutions to account for the effect of combined (primary and secondary) loading have also been implemented. The position of the three major modules in the NASGRO EPFM program structure is shown in Figure 2 where they are indicated by text boxes highlighted by dashed lines.

The structure for the elastic-plastic J module remains similar to that in the previous release. However, the J estimation routines for various model types have been modified to account for cyclic loading and the effects of secondary loads. The failure algorithm gives users the option to estimate crack lengths and loads at crack initiation and instability. These *critical crack* and *critical load* calculations can be performed for brittle and ductile fracture under combined primary and secondary loads. The effect of blunting and tearing is taken into account in the analysis. The elastic-plastic fatigue crack growth (EPFCG) and life prediction module estimates numbers of fatigue cycles and crack growth rates based on user-defined load spectra or schedules. The definition of load spectrum, or load schedule, is consistent with that of the NASGRO LEFM module. The elastic-plastic fatigue crack growth rate is governed by a modified Paris type of fatigue crack growth equation based on ΔJ_{eff}. The EPFCG computations are terminated when one of the following criteria is satisfied: (1) crack initiation leading to failure or ductile tearing is predicted at the maximum load in a cycle; (2) the load spectrum has been applied for a maximum number of times specified by the user; or (3) LEFM or EPFM geometrical validity limits are violated.

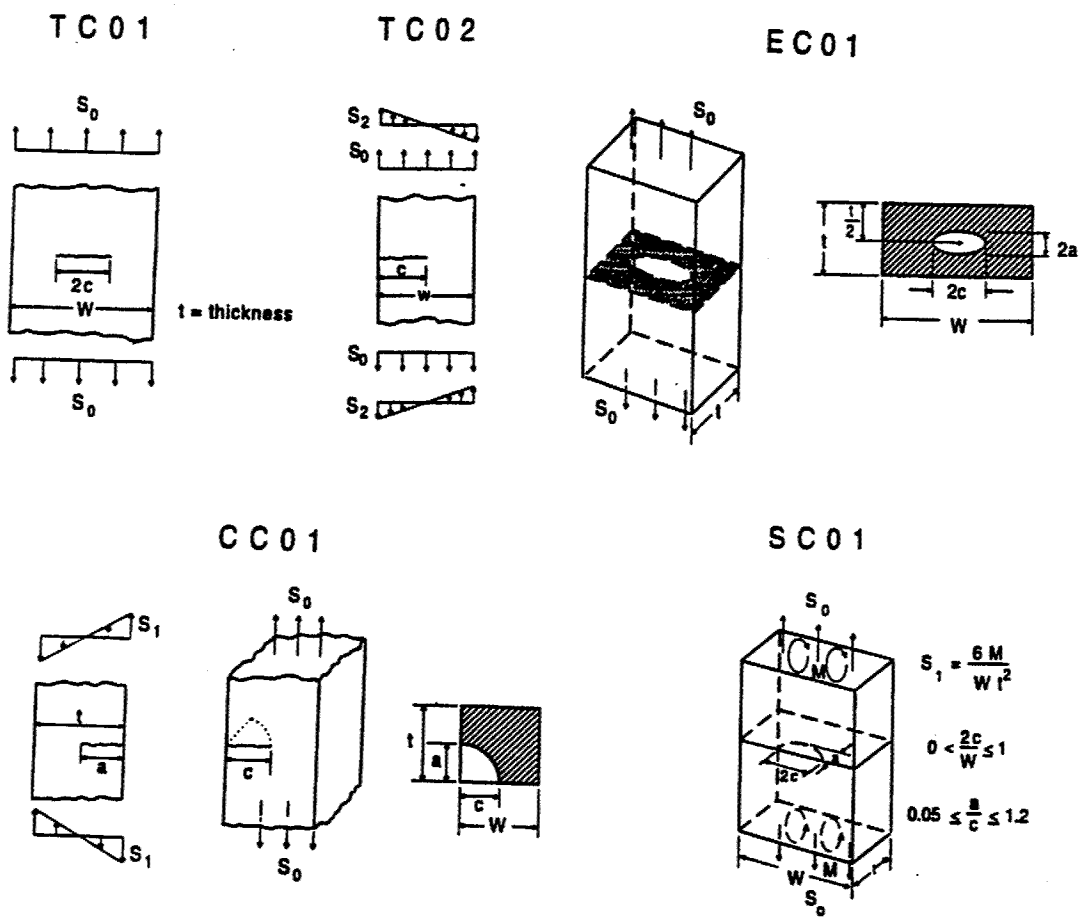

Figure 1. Schematic of the model types included in the EPFM module.

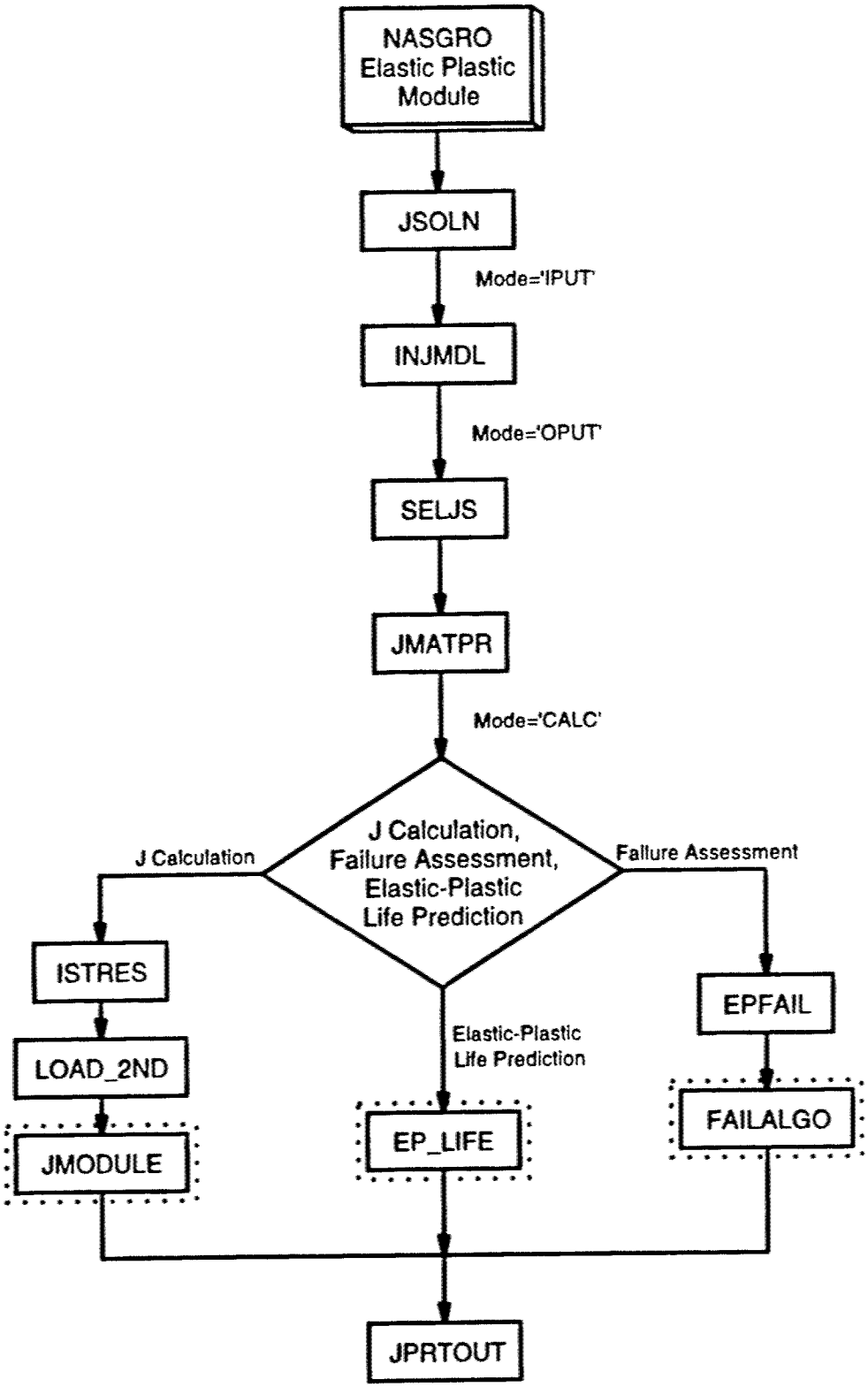

Figure 2. Flow diagram for the NASGRO elastic plastic fracture mechanics module.

2.0 Theoretical Background

2.1 J and ΔJ Integral

The EPFM parameter, J, provides a natural extension of the concepts underpinning LEFM to situations where crack tip plasticity is important. Under conditions of plane strain and plane stress J characterizes the stress and strain fields at a yielded crack tip, and the potential energy release rate due to crack extension. Its value reduces to the value of the elastic strain energy release rate, G, under small scale yielding conditions, and LEFM is recovered in this fracture regime. The relationship between the stress intensity factor, K, and the solution for J in a linear elastic material, J_e, is

$$J_e = G = \frac{K^2}{E'} \tag{1}$$

In this equation, $E' = E/(1-\nu^2)$ for plane strain and $E' = E$ for plane stress, where E is Young's modulus and ν is Poisson's ratio.

Under cyclic loading conditions, the range of J, ΔJ, is the correlating parameter used in the elastic-plastic fatigue crack growth (EPFCG) analysis. By the same token, under small scale yielding conditions, LEFM is recovered in this fracture regime, and the solution for ΔJ_e is related to the range of stress intensity factor ΔK. The relation is given by

$$\Delta J_e = \frac{\Delta K^2}{E'} \tag{2}$$

2.2 EPRI J and ΔJ Estimation Scheme for Combined Primary and Secondary Loads

The EPRI-based J and ΔJ estimation schemes described here are developed for materials whose stress-strain behavior can be described by a Ramberg-Osgood equation. For monotonic loading, the equation is

$$\frac{\varepsilon}{\varepsilon_o} = \frac{\sigma}{\sigma_o} + \alpha\left(\frac{\sigma}{\sigma_o}\right)^n \tag{3}$$

where ε is the total strain (elastic plus plastic) due to the stress, σ, α and n are material constants, and ε_o is a "yield" strain corresponding to the "yield" stress σ_o, where $\varepsilon_o=\sigma_o/E$. The first term on the right hand side of this equation represents the component of elastic strain, ε^e, and the second term represents the plastic strain, ε^p.

Equation (3) also represents the general form of the cyclic stress-strain curve. This curve is derived from the hysteresis stress-strain curve, by replacing ε and σ with $\Delta\varepsilon$ and $\Delta\sigma$, respectively, and ε_o and σ_o, with $2\varepsilon_o$ and $2\sigma_o$, respectively.

$$\frac{\Delta\varepsilon}{2\varepsilon_o} = \frac{\Delta\sigma}{2\sigma_o} + \alpha\left(\frac{\Delta\sigma}{2\sigma_o}\right)^n \tag{4}$$

The Ramberg-Osgood parameters α, n, σ_o, and ε_o in Eqn (4) will be different if the material cyclically hardens or softens.

The Ramberg-Osgood equation can be written in terms of *engineering* stress and strain or *true* stress and strain as derived from tensile test data. True stresses and strains are corrected for changes in the instantaneous cross-sectional area and length of the tensile specimen due to deformation during the test, whereas engineering quantities are based on the original nominal dimensions of the tensile specimen at the beginning of the test (Bannantine et al., 1990). The engineering and true stress-strain curves are very similar except at large values of strain approaching necking, and so values of the Ramberg-Osgood constants will generally be similar for engineering and true quantities unless the data from which they were derived include very large strains. Current usage of the Ramberg-Osgood equation in EPFM applications by various practitioners is mixed between engineering and true quantities. Pragmatically, the engineering stress and strain values will be more commonly available, and their use in this context appears acceptable. Engineering quantities were recommended in the recently completed proof testing handbook (Chell et al., 1997a). However, true values are also acceptable in the current context, and are preferred by some users of J-integral methods.

<u>J Estimation Scheme for Monotonic Loading</u>

In the EPRI elastic-plastic J estimation scheme, J is resolved into elastic and plastic components, J_e and J_p, where

$$J(c,\hat{P}) = J_e\left(c_e,\hat{P}\right) + J_p(c,P) \tag{5}$$

$\hat{P}$ is used to denote a combined primary (P) and secondary (S) load. J_e is a first order plastic corrected value of the linear elastic solution and is used to interpolate between linear elastic and fully plastic behavior. It is a function of primary and secondary loads resulting from thermal, residual, and other self-equilibrated stress fields. In contrast, J_p is a function only of primary loads, since, by definition, secondary loads cannot influence the plastic collapse load of a cracked structure and hence cannot contribute to fully plastic deformation. J_e is related to the stress intensity factor K evaluated at an effective crack length, c_e, by the equation

$$J_e\left(c_e,\hat{P}\right) = \frac{K^2\left(c_e,\hat{P}\right)}{E'} \tag{6}$$

The effective crack length c_e is given by

$$c_e = c + \phi r_y \tag{7}$$

and includes a plastic zone size correction determined by the terms ϕ and r_y that are defined respectively as

$$\phi = \frac{1}{1+\left[\frac{P}{P_o(c)}\right]^2}$$
$$r_y = \frac{1}{\beta\pi}\frac{n-1}{n+1}\left[\frac{K(c,\hat{P})}{\sigma_o}\right]^2 \tag{8}$$

where σ_o and n are Ramberg-Osgood parameters. The non-dimensional parameter, β, equals 2 for plane stress, and 6 for plane strain. $P_o(c)$ is a characteristic normalizing net section yield load corresponding to a crack length c.

Although the analytical forms of the plastic component, J_p, used in the EPRI scheme differ slightly depending on the cracked structure, for illustrative purposes the following expression is used here

$$J_p(c,P) = \alpha\varepsilon_o\sigma_o\frac{c}{W}(W-c)h_1\left(\frac{c}{W},n\right)\left(\frac{P}{P_o(c)}\right)^{n+1} \tag{9}$$

where W is the section width. The values of the function h_1 are tabulated in the EPRI handbooks for various cracked geometries and values of c/W and n. The handbooks also give equations for evaluating the yield load P_o. This parameter depends on the Ramberg-Osgood yield stress, σ_o, and structural dimensions (for example, wall thickness and radius in the case of cylindrical pressure vessels).

The elastic component, $J_e(c_e,\hat{P})$ can be evaluated from the K solutions already available in NASGRO. Hence, the major part of the J modules which have been added to NASGRO address the evaluation of J_p.

<u>ΔJ_{eff} Estimation Scheme for Cyclic Loading</u>

The cyclic change in J due to the cyclic load range, $\Delta\hat{P} = \hat{P}_{max} - \hat{P}_{min}$, comprises elastic and plastic components where

$$\Delta J_{eff}(c,\Delta\hat{P}) = \Delta J_e^{eff}(c_e^{\Delta},\Delta\hat{P}) + \Delta J_p^{eff}(c,\Delta P) \tag{10}$$

and $\hat{P}_{max}$ and $\hat{P}_{min}$ are the combined primary and secondary loads at the maximum and minimum loads in a cycle, respectively. The elastic component, ΔJ_e^{eff}, includes a plastic correction and a crack closure correction, U, and is related to the cyclic range of the stress intensity factor, ΔK, by the equation

$$\Delta J_e^{eff}\left(c_{eff}^{\Delta}, \Delta\hat{P}\right) = \frac{U^2 \Delta K^2\left(c_e^{\Delta}, \Delta\hat{P}\right)}{E'} \tag{11}$$

where the effective crack length for cyclic loading c_{eff}^{Δ} is

$$c_e^{\Delta} = c + \phi^{\Delta} \Delta r_y \tag{12}$$

The effective stress intensity factor range ratio, U, which characterizes crack closure, is defined in Section 2.6. The terms ϕ^{Δ} and Δr_y , respectively, are evaluated as

$$\phi^{\Delta} = \frac{1}{1 + \left[\frac{\Delta P}{2P_o(c)}\right]^2}$$

$$\Delta r_y = \frac{1}{\beta\pi}\frac{n-1}{n+1}\left[\frac{\Delta K\left(c, \Delta\hat{P}\right)}{2\sigma_o}\right]^2 \tag{13}$$

where $\Delta P = P_{max} - P_{min}$ stands for the primary load range, $P_o(c)$ is the normalizing net section yield load corresponding to a crack length c, and σ_o and n are the Ramberg-Osgood parameters defining the cyclic stress-strain curve.

For illustrative purposes, the following expression is used to show one of the analytical forms of the plastic component ΔJ_p used in the EPRI-based scheme in accordance with the definition used in equation (9).

$$\Delta J_p^{eff}(c, \Delta P) = 4U\alpha\varepsilon_o\sigma_o \frac{c}{W}(W - c)h_1\left(\frac{c}{W}, n\right)\left(\frac{\Delta P}{2P_o(c)}\right)^{n+1} \tag{14}$$

The multiplier 4 and the factor 2 multiplying $P_o(c)$ come from the conversion of cyclic stress-strain data into cyclic hysteresis data. Note that the plastic ΔJ_{eff} term includes the factor U, while the elastic ΔJ_{eff} term includes the factor U^2. The energy considerations motivating this formulation are outlined in Section 3.2 of the main body of the final report.

2.3 J_p and ΔJ_p^{eff} Estimation Scheme for Combined Loads using Reference Stress Method (RSM)

The RSM-based J estimation scheme provides an alternative way of estimating J_p and ΔJ_p^{eff} in equations (9) and (14). The details of the method are described in reference [6]. The elastic components, J_e and ΔJ_e^{eff} , are given by equations (6)-(8) and (11)-(13) but with $P_o(c)$ replaced by $P_o^*(c)$, the load at net section yield evaluated using the

Ramberg-Osgood yield stress, σ_o. In general, P_o^* will not equal the EPRI normalizing yield load, P_o, although it may have a form very similar to it.

J_p Estimation Scheme for Monotonic Loading

The RSM approximation to J_p for a Ramberg-Osgood material is

$$J_p^{RSM}(c,P) = \mu V\left(\frac{c}{W}\right)\alpha J_e(c,P)\left(\frac{P}{P_o^*(c)}\right)^{n-1} \tag{15}$$

where V is a dimensionless "structural" parameter that, in general, has a value of around 1, and

$$\mu = \frac{1-\nu_p^2}{1-\nu_e^2}\,(\text{plane strain}),\ \ \mu = 1\,(\text{plane stress}) \tag{16}$$

where ν_e is the elastic value of Poisson's ratio, and ν_p is the plastic value.

The advantages of including the RSM solution in NASGRO are clearly apparent from equation (15). Making the assumption that V=1, then equation (15) provides a relatively simple expression for J_p that can be used for defective hardware for which EPRI handbook solutions are not available. This is possible because J_e can be readily evaluated for a wide range of geometries using existing NASGRO K solutions, and the net section yield load, P_o^*, can be estimated from an available compendium of solutions (Miller, 1988), or estimated using plastic limit analysis. In addition, if the material stress-strain curve cannot be adequately represented by a Ramberg-Osgood equation, then J_p^{RSM} can still be evaluated using a generalized version of equation (15),

$$J_p^{RSM}(c,P) = \mu V J_e(c,P)\left(\frac{E\varepsilon_{ref}^P}{\sigma_{ref}}\right) \tag{17}$$

where the reference stress, σ_{ref}, is defined as

$$\sigma_{ref} = \left(\frac{P}{P_o^*}\right)\sigma_o \tag{18}$$

and the reference plastic strain, ε_{ref}^P, is the uniaxial plastic strain corresponding to σ_{ref}. For a Ramberg-Osgood material ,

$$\varepsilon_{ref}^{P} = \alpha \frac{\sigma_o}{E}\left(\frac{\sigma_{ref}}{\sigma_o}\right)^n \tag{19}$$

Equation (17) can be implemented in a future version of the NASGRO EPFM module to extend the J solutions in the module to materials that display arbitrary stress-strain behavior.

ΔJ_p^{eff} Estimation Scheme for Cyclic Loading

For cyclic loading, the following expression is used to show one of the analytical forms of the plastic component, ΔJ_p^{eff} using the RSM in accordance with the definition used in equation (15).

$$\Delta J_p^{eff}(c,P) = \mu V\left(\frac{c}{W}\right)\alpha U \Delta J_e(c,P)\left(\frac{\Delta P}{2P_o^*(c)}\right)^{n-1} \tag{20}$$

2.4 Brittle and Ductile Fracture Criteria

In the NASGRO EPFM failure algorithm, the J solutions incorporated into NASGRO are used to determine the structural integrity of defective hardware that fractures by brittle or ductile mechanisms. This will enable the user to calculate critical crack sizes and loads based on the following failure criteria.

Brittle

The onset of fracture in brittle materials occurs when the applied crack tip driving force equals or exceeds the fracture toughness of the material. This failure criterion is mathematically expressed as

$$J(c_i + \Delta c_b, P) \geq J_{mat} \tag{21}$$

where the fracture toughness, signified as J_{mat}, is expressed in the same units as the driving force, J. In this equation, c_i is the initial crack length, and Δc_b is the amount of crack tip blunting up to the point of fracture. Δc_b is approximately given by

$$\Delta c_b = J_{mat} / (2\sigma_{ys}) \tag{22}$$

where σ_{ys} is the yield stress. Normally $\Delta c_b / c_i << 1$, and Δc_b can be ignored, but this may not be the case for surface flaws in very thin walled structures, which, for example, are sometimes encountered in the aerospace industry.

J_{mat} can be derived from toughness values expressed in terms of critical stress intensity factors using the expression

$$J_{mat} = \frac{K_{mat}^2}{E'} \tag{23}$$

Here K_{mat} can be equated to the appropriate toughness, such as the plane strain toughness, K_{Ic}; the thickness dependent toughness, K_c; or the surface flaw toughness, K_{Ie}. Alternatively, J_{mat} could be equated directly to J_{Ic}, a measure of fracture toughness as defined in ASTM Standard E813.

Ductile

The ductile fracture toughness does not have a unique value but is dependent on the amount of ductile tearing that has occurred. Hence, as the crack tip driving force (J) increases, the crack will extend and the ductile toughness will increase to balance the increase in the driving force. This situation will not, however, continue indefinitely, and eventually the increase in J with crack extension will exceed the corresponding increase in the toughness. This defines the ductile failure criterion and is expressed mathematically as

$$J(c,P) = J_R(\Delta c_t) \tag{24}$$

while, simultaneously, satisfying the equation

$$\frac{dJ(c)}{dc} = \frac{dJ_R(\Delta c_t)}{d(\Delta c_t)} \tag{25}$$

where $c = c_{inst}$ is the instantaneous crack length corresponding to the load, P, and is given by $c_{crit}+\Delta c_t$, where c_{crit} is the critical crack length and J_R is the toughness corresponding to an amount of tearing, Δc_t which includes crack tip blunting and ductile crack extension. A schematic representation of the failure criterion defined by equations (24) and (25) is shown in Figure 3. The criterion corresponds to the conditions where the applied J curve as a function of crack length forms a tangent to the J_R-curve.

The crack growth resistance curve or J_R-curve is needed for ductile analysis. This can be specified in quadratic form or as a power law. Respectively, they are

(1) Quadratic form:

$$J_R = \begin{cases} J_0 + J_1(\Delta c) + J_2(\Delta c)^2, & \Delta c \le \Delta c_{\max} \\ J_0 + J_1(\Delta c_{\max}) + J_2(\Delta c_{\max})^2, & \Delta c > \Delta c_{\max} \end{cases} \tag{26}$$

(2) Power law:

$$J_R = \begin{cases} J_1(\Delta c)^{J_2}, & \Delta c \le \Delta c_{max} \\ J_1(\Delta c_{max})^{J_2}, & \Delta c > \Delta c_{max} \end{cases} \tag{27}$$

where J_0, J_1 and J_2 are material constants, Δc is the blunting and tear length, and $(\Delta c)_{max}$ is the tear length at which the J_R-curve saturates (i.e., at which J_R attains its maximum value).

2.5 Elastic-Plastic Fatigue Crack Growth

Existing fatigue crack growth (FCG) data bases are nearly all for small scale yielding (SSY) conditions in which ΔK has been used as the parameter characterizing the growth rate per cycle, dc/dN. Fatigue crack growth data correlated with ΔK can be readily converted to a correlation in ΔJ. Typically, the Paris equation is given as

$$\frac{dc}{dN} = C_o(\Delta K)^{m_o} \tag{28}$$

where C_o and m_o are material constants. Equation (28) does not address any crack closure that may occur during the FCG testing. A similar Paris type of elastic plastic fatigue crack growth equation based on ΔJ_{eff}, which does address crack closure, is

$$\frac{dc}{dN} = C(\Delta J_{eff})^m \tag{29}$$

Here the constants C and m can be estimated from C_o and m_o according to $m=m_o/2$ and

$$C = \frac{C_o(E')^{m_o/2}}{U_o^{m_o}} \tag{30}$$

U_o is an estimate of the crack closure in the original FCG tests used to generate the SSY data base from which C_o and m_o were determined. It is a measure of the cyclic driving force determined by the part of the primary load cycle where the crack is open. For typical SSY FCG baseline testing (relatively low stresses and small plastic zone sizes relative to specimen thickness), plane strain conditions are satisfied and U_o is about 0.75.

2.6 Corrections for Plasticity-Induced Crack Closure

The proper form of ΔJ for correlation of EPFCG data must include corrections for plasticity-included crack closure. This correction is particularly important because the crack opening stress σ_{open} under EPFCG conditions can be significantly different from that under typical SSY conditions. The effective stress intensity factor range ratio U is applied to ΔJ_e and ΔJ_p as shown in equations (11), (14) and (20), respectively. The form of U is defined by the following equation.

$$U = \frac{K_{\max} - K_{open}}{K_{\max} - K_{\min}} = \frac{1 - K_{open}/K_{\max}}{1 - R} \tag{31}$$

whre R is the stress ratio due to the combined primary and secondary cyclic loads with no plastic zone correction,

$$R = \frac{K_{\min}}{K_{\max}} \tag{32}$$

and K_{open} is the value of the stress intensity factor at which the crack opens. K_{open} is evaluated using Newman's modified Dugdale crack closure model. This model is used in NASGRO and leads to the following equation for K_{open} as

$$\frac{K_{open}}{K_{\max}} = \begin{cases} A_0 + A_1 R + A_2 R^2 + A_3 R^3 & R \geq 0 \\ A_0 + A_1 R & -2 \leq R < 0 \end{cases} \tag{33}$$

and the coefficients are given by

$$\begin{aligned} A_0 &= \left(0.825 - 0.34\alpha_c + 0.05\alpha_c^{\,2}\right)\left[\cos\left(\frac{\pi}{2}\frac{K_{\max}}{K_{flow}}\right)\right]^{1/\alpha_c} \\ A_1 &= \left(0.415 - 0.071\alpha_c\right)\frac{K_{\max}}{K_{flow}} \\ A_2 &= 1 - A_0 - A_1 - A_3 \\ A_3 &= 2A_0 + A_1 - 1 \end{aligned} \tag{34}$$

K_{flow} is a normalizing parameter given by $\sigma_{flow}\sqrt{\pi a}$ where the flow stress σ_{flow} is the average of the yield stress and the ultimate stress, and a is the crack length at the crack tip location a. For the crack tip location c, $K_{flow} = \sigma_{flow}\sqrt{\pi c}$. The value of the constraint factor α_c is set as an option for the user to feed into the program. Typically it varies from 1 to 3, where α_c=1 corresponds to plane stress and α_c=3 corresponds to plane strain.

No rigorous algorithm is available at the present time to select the optimum value of α_c in a given situation. For elliptical embedded cracks, semi-elliptical surface cracks, quarter-elliptical corner cracks, α_c = 3 (full plane strain) is generally a conservative selection, and this choice is recommended if additional information is not available. Further discussion of stress state effects on the selection of the optimum α_c, including general guidelines for two-dimensional cracks, is provided in Section 3.3.1 in the main body of the final report.

2.7 Surface Correction Factor due to Crack Closure

The evolving shape of cracks with multiple degrees of freedom (e.g., the depth and surface length of a semi-elliptical surface crack) is captured in NASGRO by performing crack growth calculations at two different points around the perimeter of the crack. In current versions of NASGRO, this is done in LEFM with K solutions at the Φ=0° and Φ=90° positions. The new EPFCG module follows a similar approach, but employs J solutions at the Φ = 9° and Φ = 90° locations due to numerical difficulties associated with determining J at the Φ = 0° location. However, since the EPFCG module depends on the current NASGRO capabilities for LEFM calculations, the K solutions employed in the J RSM estimation schemes correspond to the Φ = 0° and Φ=90° positions. Validation exercises have shown that this is an acceptable approach.

An additional surface correction factor β_R is used in the current NASGRO code to multiply ΔK for crack locations where the front intersects a free surface (c-tip for SC01 or a- and c-tips for CC01). It is given by

$$\beta_R = \begin{cases} 0.9 + 0.2R^2 - 0.1R^4, & R \geq 0 \\ 0.9, & R < 0 \end{cases} \tag{35}$$

This factor compensates for surface constraint effects that are not predicted by LEFM, since the ΔK solutions alone do not predict the correct shape of semi-elliptical surface cracks.

The surface constraint effects characterized by the β_R factor are thought to be primarily caused by changes in crack closure at the near-surface crack tip positions. Therefore, it should be possible to account for these effects by choosing different values of the Newman constraint factor α_c at the near-surface positions. However, at the present time, it is not clear how to choose appropriate values of α_c at different positions around the perimeter of a semi-elliptical or quarter-elliptical crack so that the correct crack shape is predicted. It also may be possible that β_R should exhibit some dependency on K_{max}/K_{flow} if crack closure is a key issue in surface constraint. Again, however, insufficient information is available at the present time to formulate a more complex β_R factor for EPFCG conditions. Therefore, until further information is available, it is recommended to choose a common value of α_c at both locations for a two-degree-of-freedom crack, and to use the current NASGRO β_R factor to accommodate near-surface changes in constraint. Although the applicability of the β_R factor to elastic-plastic conditions has not been widely demonstrated, the experimental verification exercises conducted under the current contract (Appendix L) indicate that this approach (near surface β_R factor and a position-independent α_c) gives the correct crack shape for semi-elliptical surface cracks under uniform tension in the SSY, ISY, and LSY regimes.

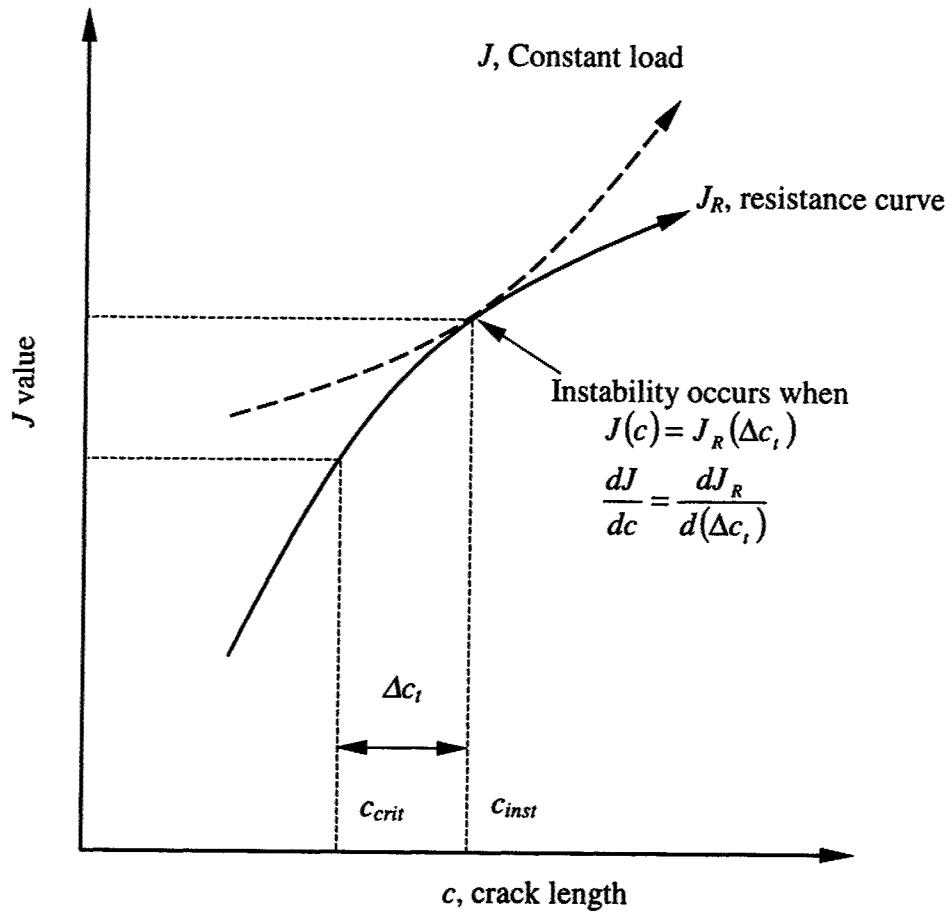

Figure 3. The toughness of ductile materials has no unique value but depends on the tear length. Instability is defined when the applied J curve as a function of crack length, c, becomes tangential to the J_R-curve.

3.0 J_p and ΔJ_p Solutions in the EPFM Module

3.1 EPRI Solutions

J_p Solutions

The EPRI solution scheme defined here is based on equations of the form:

$$J_p = \alpha\sigma_o\varepsilon_o c\left(\frac{b-c}{b}\right)h_1\left(\frac{c}{b},n\right)\left(\frac{P}{P_o}\right)^{n+1}, \text{ for TC01 and TC02 under tension}$$

$$J_p = \alpha\sigma_o\varepsilon_o (b-c)h_1\left(\frac{c}{b},n\right)\left(\frac{M}{M_o}\right)^{n+1}, \text{ for TC02 under bending} \tag{36}$$

where $b=W/2$ for geometry TC01 and $b=W$ for TC02. $2c$ and c are the through crack lengths for TC01 and TC02 respectively. h_1 is a bivariant function of c/b and n. Values of h_1 are available in the EPRI elastic-plastic handbooks for discrete values of c/b and n. These values are shown Tables 1-6 for plane strain and plane stress deformation. The NASGRO Hermite curve fitting routine is used to interpolate h_1 values for values of c/b and n not given in the tables. The characteristic yield load P_o is a function of defect size and σ_0:

TC01:

$$P_0 = \begin{cases} 4(b-c)t\sigma_0/\sqrt{3} & \text{, for plane strain} \\ 2(b-c)t\sigma_0 & \text{, for plane stress} \end{cases} \tag{37}$$

TC02 under tension:

$$P_0 = \begin{cases} 1.455\eta(b-c)t\sigma_0 & \text{, for plane strain} \\ 1.072\eta(b-c)t\sigma_0 & \text{, for plane stress} \end{cases} \tag{38}$$

where $\eta = \sqrt{1+[c/(b-c)]^2} - c/(b-c)$.

TC02 under bending:

$$M_0 = \begin{cases} 0.364\sigma_o t(b-c)^2 & \text{, for plane strain} \\ 0.268\sigma_o t(b-c)^2 & \text{, for plane stress} \end{cases} \tag{39}$$

Table 1. $h_1(2c/W,n)$ values for TC01, plane strain.

	n								
2c/W	1	2	3	5	7	10	13	16	20
0.125	2.80	3.61	4.06	4.35	4.33	4.02	3.56	3.06	2.46
0.250	2.54	3.01	3.21	3.29	3.18	2.92	2.63	2.34	2.03
0.375	2.34	2.62	2.65	2.51	2.28	1.97	1.71	1.46	1.19
0.500	2.21	2.29	2.20	1.97	1.76	1.52	1.32	1.16	0.978
0.625	2.12	1.96	1.76	1.43	1.17	0.863	0.628	0.458	0.300
0.750	2.07	1.73	1.47	1.11	0.895	0.642	0.461	0.337	0.216
0.875	2.08	1.64	1.40	1.14	0.987	0.814	0.688	0.573	0.461

Table 2. $h_1(2c/W,n)$ values for TC01, plane stress.

	n								
2c/W	1	2	3	5	7	10	13	16	20
0.125	2.80	3.57	4.01	4.47	4.65	4.62	4.41	4.13	3.72
0.250	2.54	2.97	3.14	3.20	3.11	2.86	2.65	2.47	2.20
0.375	2.34	2.53	2.52	2.35	2.17	1.95	1.77	1.61	1.43
0.500	2.21	2.20	2.06	1.81	1.63	1.43	1.30	1.17	1.00
0.625	2.12	1.91	1.69	1.41	1.22	1.01	0.853	0.712	0.573
0.750	2.07	1.71	1.46	1.21	1.08	0.867	0.745	0.646	0.532
0.875	2.08	1.57	1.31	1.08	0.972	0.862	0.778	0.715	0.630

Table 3. $h_1(c/W,n)$ values for TC02; plane strain under tension.

	n								
c/W	1	2	3	5	7	10	13	16	20
0.125	4.95	6.93	8.57	11.50	13.50	16.10	18.10	19.90	21.20
0.250	4.34	4.77	4.64	3.82	3.06	2.17	1.55	1.11	0.712
0.375	3.88	3.25	2.63	1.68	1.06	0.539	0.276	0.142	0.0595
0.500	3.40	2.30	1.69	0.928	0.514	0.213	0.0902	0.0385	0.0119
0.625	2.86	1.80	1.30	0.697	0.378	0.153	0.0625	0.0256	0.0078
0.750	2.34	1.61	1.25	0.769	0.477	0.233	0.116	0.0590	0.0215
0.875	1.91	1.57	1.37	1.10	0.925	0.702			

Table 4. $h_I(c/W,n)$ values for TC02; plane stress under tension.

	n								
c/W	1	2	3	5	7	10	13	16	20
0.125	3.58	4.55	5.06	5.30	4.96	4.14	3.29	2.60	1.92
0.250	3.14	3.26	2.92	2.12	1.53	0.960	0.615	0.400	0.230
0.375	2.81	2.37	1.94	1.37	1.01	0.677	0.474	0.342	0.226
0.500	2.46	1.67	1.25	0.776	0.510	0.286	0.164	0.0956	0.0469
0.625	2.07	1.41	1.105	0.755	0.551	0.363	0.248	0.172	0.107
0.750	1.70	1.14	0.910	0.624	0.447	0.280	0.181	0.118	0.067
0.875	1.38	1.11	0.962	0.792	0.677	0.574			

Table 5. $h_I(c/W,n)$ values for TC02; plane strain under bending.

	n								
c/W	1	2	3	5	7	10	13	16	20
0.125	0.936	0.869	0.805	0.687	0.580	0.437	0.329	0.245	0.165
0.250	1.20	1.034	0.930	0.762	0.633	0.523	0.396	0.303	0.215
0.375	1.33	1.15	1.02	0.840	0.695	0.556	0.442	0.360	0.265
0.500	1.41	1.09	0.922	0.675	0.495	0.331	0.211	0.135	0.0741
0.625	1.46	1.07	0.896	0.631	0.436	0.255	0.142	0.0840	0.0411
0.750	1.48	1.15	0.974	0.693	0.500	0.348	0.223	0.140	0.0745
0.875	1.50	1.35	1.20	1.02	0.855	0.690	0.551	0.440	0.321

Table 6. $h_I(c/W,n)$ values for TC02; plane stress under bending.

	n								
c/W	1	2	3	5	7	10	13	16	20
0.125	0.676	0.600	0.548	0.459	0.383	0.297	0.238	0.192	0.148
0.250	0.869	0.731	0.629	0.479	0.370	0.246	0.174	0.117	0.0593
0.375	0.963	0.797	0.680	0.527	0.418	0.307	0.232	0.174	0.105
0.500	1.02	0.767	0.621	0.453	0.324	0.202	0.128	0.0813	0.0298
0.625	1.05	0.786	0.649	0.494	0.357	0.235	0.173	0.105	0.0471
0.750	1.07	0.786	0.643	0.474	0.343	0.230	0.167	0.110	0.0442
0.875	1.086	0.928	0.810	0.646	0.538	0.423	0.332	0.242	0.205

ΔJ_p Solutions

The analytical forms of the plastic component used in the EPRI-based ΔJ estimation scheme are listed below for model types TC01 under tension and TC02 under tension and bending.

TC01 with b=W/2 and TC02 with b=W under tension:

$$\Delta J_p^{eff}(c,\Delta P;b) = 4U\alpha\sigma_o\varepsilon_o c\frac{b-c}{b}h_1\left(\frac{c}{b},n\right)\left(\frac{\Delta P}{2P_o}\right)^{n+1} \tag{40}$$

TC02 under bending:

$$\Delta J_p^{eff}(c,\Delta P;b) = 4U\alpha\sigma_o\varepsilon_o(b-c)h_1\left(\frac{c}{b},n\right)\left(\frac{\Delta M}{2M_o}\right)^{n+1} \tag{41}$$

ΔM is the range of bending moment corresponding to the range of the NASGRO primary bending stress. U is a correction factor related to crack closure and is defined in Section 2.6.

3.2 Optimized Reference Stress Solutions

J_p Solutions

In this approach, the J_p estimate is based on the reference stress method (RSM) which is optimized to reproduce as accurately as possible existing finite element J_p solutions. For the cracked geometries considered here:

TC01 with b=W/2 and TC02 under tension with b=W:

$$J_p^{RSM}\left(\frac{c}{b}\right) = J_e\left(\frac{c}{b}\right)\mu V\left(\frac{c}{b}\right)\alpha\left(\frac{P}{P_0^*}\right)^{n-1} \tag{42}$$

TC02 under bending with b=W:

$$J_p^{RSM}\left(\frac{c}{b}\right) = J_e\left(\frac{c}{b}\right)\mu V\left(\frac{c}{b}\right)\alpha\left(\frac{M}{M_o^*}\right)^{n-1} \tag{43}$$

SC01 (a surface crack) and CC01 (a corner crack) under tension:

$$J_P^{RSM}\left(\frac{a}{t},\frac{a}{c},\frac{c}{b}\right)=J_e\left(\frac{a}{t},\frac{a}{c},\frac{c}{b}\right)\mu V\left(\frac{a}{t},\frac{a}{c}\right)\alpha\left(\frac{P}{P_o^*}\right)^{n-1} \tag{44}$$

The optimized yield loads, P_o^* or M_o^*, and the structural parameter, V, are dependent on geometrical parameters only and are independent of the strain hardening exponent, n. Discrete values of the optimized yield loads and V's are given in Tables 7-10. Values of P_o^* and V that are not shown in the tables are calculated in the program using interpolation procedures based on Hermite or cubic spline curve fitting. Note that the values of P_o^* and V in Tables 9 and 10 are only valid for c/b=0.25. To facilitate generalizing of the RSM solutions to arbitrary c/b values, a hybrid approach is implemented in NASGRO for SC01 and CC01 under tension. The hybrid solution is written as

$$\begin{aligned} J_P^{RSM}\left(\frac{a}{t},\frac{a}{c},\frac{c}{b}\right)&=J_e\left(\frac{a}{t},\frac{a}{c},\frac{c}{b}\right)\mu V\alpha\left(\frac{P}{P_o^*}\right)^{n-1}, \text{for CC01 or SC01 under tension} \\ J_P^{RSM}\left(\frac{a}{t},\frac{a}{c},\frac{c}{b}\right)&=J_e\left(\frac{a}{t},\frac{a}{c},\frac{c}{b}\right)\mu V\alpha\left(\frac{M}{M_o^*}\right)^{n-1}, \text{for SC01 under bending} \end{aligned} \tag{45}$$

where V is a constant associated with each specific model type and the crack front location. It is independent of a/t and a/c ratios. For model type SC01 under tension or bending, two values of V for the deepest crack tip and the near surface crack tip, $(V_a)_{avg}$ and $(V_c)_{avg}$, are evaluated as the arithmetic mean of optimized V values for all a/t and a/c ratios. Respectively, $(V_a)_{avg}$ and $(V_c)_{avg}$ are equal to 1.8164 and 1.2561 for SC01 under tension and 1.0412 and 0.9730 for SC01 under bending (see Table 9). For model type CC01 under tension, V is taken as the maximum of the two arithmetic means at the φ=9° and φ=81° near surface crack tip locations. In this case, $V=V_{max}=\max((V_a)_{avg},(V_c)_{avg})=$ 1.4329 (see Table 10). P_o^* and M_o^* are approximated using plastic limit analysis. For CC01 or SC01 under tension, P_o^* is used, based on load redistribution due to area reduction as described in Section 4.1. These derived values are included in Tables 9 and 10 where they can be compared with the optimized results for P_o^*. For SC01 under bending, M_o^* is used, as described in Section 4.2.

<u>ΔJ_p Solutions</u>

The expressions for ΔJ_p^{eff} derived from the optimized RSM solutions for J_p are given below. Values for the structural parameter V in the ΔJ_p solutions are the same as in the corresponding J_p solutions.

TC01 with b=W/2 and TC02 with b=W under tension:

$$\Delta J_p^{eff}(c,\Delta P;b) = U\Delta J_e(c,\Delta P;b)\mu\alpha V\left(\frac{c}{b}\right)\left(\frac{\Delta P}{2P_o^*}\right)^{n-1} \tag{46}$$

TC02 under bending with b=W:

$$\Delta J_p^{eff}(c,\Delta P;b) = U\Delta J_e(c,\Delta P;b)\mu\alpha V\left(\frac{c}{b}\right)\left(\frac{\Delta M}{2M_o^*}\right)^{n-1} \tag{47}$$

SC01 and CC01 under tension:

$$\Delta J_p^{eff}(a,c,\Delta P;b,t) = U\Delta J_e(a,c,\Delta P;b,t)\mu\alpha V\left(\frac{a}{t},\frac{a}{c}\right)\left(\frac{\Delta P}{2P_o^*}\right)^{n-1} \tag{48}$$

CC01 or SC01 under tension:

$$\Delta J_p^{eff}(a,c,\Delta P;b,t) = U\Delta J_e(a,c,\Delta P;b,t)\mu\alpha V\left(\frac{\Delta P}{2P_o^*}\right)^{n-1} \tag{49}$$

SC01 under bending:

$$\Delta J_p^{eff}(a,c,\Delta P;b,t) = U\Delta J_e(a,c,\Delta P;b,t)\mu\alpha V\left(\frac{\Delta M}{2M_o^*}\right)^{n-1} \tag{50}$$

Note that the EPFM module includes both EPRI and RSM solutions for TC01 and TC02. Since the RSM solutions were derived from the EPRI solutions, the two solutions should give nearly identical results, and the EPRI solution may be preferred within its regime of applicability. The advantage of the RSM formulation is (unlike the EPRI solution) that it permits $n > 20$ and that it will facilitate future extension to materials that do not follow a Ramberg-Osgood stress strain equation.

Table 7. Optimized yield loads and V's for TC01 under tension.

	Plane Strain		Plane Stress	
$2c/W$	$P_o^*/(2bt\sigma_o)$	V	$P_o^*/(2bt\sigma_o)$	V
0.125	1.0055	1.360	0.8537	1.307
0.250	0.8730	1.239	0.7553	1.216
0.375	0.7490	1.189	0.6456	1.129
0.500	0.6074	1.094	0.5260	1.036
0.625	0.4802	1.0248	0.4048	0.9489
0.750	0.3262	0.9233	0.2703	0.8588
0.875	0.1569	0.8241	0.1339	0.7628

Table 8. Optimized yield loads and V's for TC02.

	Tension				Bending			
	Plane Strain		Plane Stress		Plane Strain		Plane Stress	
c/W	$P_o^*/(\sigma_o bt)$	V	$P_o^*/(\sigma_o bt)$	V	$M_o^*/(\sigma_o b^2 t)$	V	$M_o^*/(\sigma_o b^2 t)$	V
0.125	1.0025	1.353	0.8301	1.385	0.3040	1.020	0.2236	0.9654
0.250	0.8693	1.253	0.6748	1.228	0.2238	0.9325	0.1722	0.9536
0.375	0.6445	1.055	0.4411	0.9535	0.1555	0.9317	0.1175	0.9091
0.500	0.4048	0.902	0.2754	0.8090	0.1058	0.8905	0.0790	0.8715
0.625	0.2054	0.847	0.1311	0.7670	0.0614	0.8816	0.0436	0.8491
0.750	0.0750	0.870	0.0516	0.7720	0.0265	0.8948	0.0194	0.8294

Table 9. Optimized yield loads, V's and net section yield loads based on area reduction for SC01 for the case where c/b=0.25.

		Surface Crack (SC01) under Tension				
		Deepest Pt.		Near Surface Pt.		Normalized
a/t	a/c	$P_o^*/(2bt\sigma_o)$	V	$P_o^*/(2bt\sigma_o)$	V	Reduction in Area
0.2	0.2	0.9600	1.6298	0.9598	1.0480	0.9607
0.2	0.6	0.9609	1.6937	0.9712	0.9883	0.9607
0.2	1.0	0.9586	1.7569	0.9720	1.0490	0.9607
0.5	0.2	0.9046	2.2289	0.8756	1.3986	0.9018
0.5	0.6	0.9036	1.9312	0.9093	1.1880	0.9018
0.5	1.0	0.9062	1.9044	0.9197	1.1755	0.9018
0.8	0.2	0.8456	1.6482	0.8369	1.7449	0.8429
0.8	0.6	0.8482	1.7490	0.8679	1.3693	0.8429
0.8	1.0	0.8526	1.8052	0.8763	1.3430	0.8429
		$(V_a)_{avg}$=	1.8164	$(V_c)_{avg}$=	1.2561	
		Surface Crack (SC01) under Bending				
		Deepest Pt.		Near Surface Pt.		
a/t	a/c	$4M_o^*/(bt^2\sigma_o)$	V	$4M_o^*/(bt^2\sigma_o)$	V	
0.2	0.2	1.0616	1.0457	0.9943	1.0848	
0.2	0.6	0.9484	0.8426	1.0129	0.9964	
0.2	1.0	0.9578	1.0397	1.0319	0.9439	
0.5	0.2	0.9868	1.2213	0.9357	0.9305	
0.5	0.6	0.9390	1.0465	1.0736	0.8712	
0.5	1.0	0.9028	1.0511	1.0347	1.0113	
		$(V_a)_{avg}$=	1.0412	$(V_c)_{avg}$=	0.9730	

Table 10. Optimized yield loads, V's and net section yield loads based on area reduction for CC01 for the case where c/b=0.25.

		Corner Crack (CC01)				
		Near Surface Pt. (φ=81°)		Near Surface Pt. (φ=9°)		Normalized
a/t	a/c	$P_o^*/(bt\sigma_o)$	V	$P_o^*/(bt\sigma_o)$	V	Reduction in Area
0.2	0.2	0.9506	1.3895	0.9494	1.0667	0.9607
0.2	0.6	0.9593	1.2132	0.9595	1.1425	0.9607
0.2	1.0	0.9634	1.1667	0.9624	1.1577	0.9607
0.5	0.2	0.8914	1.8186	0.8603	1.5485	0.9018
0.5	0.6	0.9026	1.4200	0.9052	1.3341	0.9018
0.5	1.0	0.9140	1.3087	0.9192	1.3187	0.9018
0.8	0.2	0.8192	1.4976	0.8082	1.9051	0.8429
0.8	0.6	0.8316	1.5387	0.8487	1.4603	0.8429
0.8	1.0	0.8417	1.5432	0.8614	1.4187	0.8429
		$(V_a)_{avg}$=	1.4329	$(V_c)_{avg}$=	1.3725	

3.3 Reference Stress Solutions

J_p Solutions

In the absence of finite element J_p solutions to use as data to optimize the RSM solutions, the RSM approach is still used but with P_o^* and M_o^* estimated from plastic limit theory and with V=1.873. This value of V corresponds to plus two standard deviations from the mean value derived from a statistical analysis of V values for a wide range of cracked structures (Chell et al., 1997b). There is a 97% confidence that computed V values will fall below this statistical upper bound. This approach is used to estimate J_p for an embedded crack under tension (EC01), and a corner (CC01) crack under bending. The equations used in the program are

for EC01:

$$J_p^{RSM}\left(\frac{a}{t},\frac{a}{c},\frac{c}{b}\right)=J_e\left(\frac{a}{t},\frac{a}{c},\frac{c}{b}\right)\cdot 1.873\cdot\mu\alpha\left(\frac{P}{P_o^*}\right)^{n-1} \tag{51}$$

for CC01 under bending:

$$J_p^{RSM}\left(\frac{a}{t},\frac{a}{c},\frac{c}{b}\right)=J_e\left(\frac{a}{t},\frac{a}{c},\frac{c}{b}\right)\cdot 1.873\cdot\mu\alpha\left(\frac{M}{M_o^*}\right)^{n-1} \tag{52}$$

where M is the moment corresponding to the NASGRO bending stress, S_1 (see Figure 1).

ΔJ_p Solutions

For EC01 under tension and CC01 under bending, a RSM ΔJ_p^{eff} estimation scheme is used in which P_0^* and M_o^* are estimated from plastic limit theory and V=1.873 for all crack tip locations. The equations used in the program are

EC01 under tension:

$$\Delta J_p^{eff}(a,c,\Delta P;b,t) = U\Delta J_e(a,c,\Delta P;b,t)\mu\alpha \cdot 1.873 \cdot \left(\frac{\Delta P}{2P_o^*}\right)^{n-1} \tag{53}$$

CC01 under bending:

$$\Delta J_p^{eff}(a,c,\Delta P;b,t) = U\Delta J_e(a,c,\Delta P;b,t)\mu\alpha \cdot 1.873 \cdot \left(\frac{\Delta M}{2M_o^*}\right)^{n-1} \tag{54}$$

4.0 Net Section Yield Load used in the RSM

4.1. Net Section Yield Loads for EC01, SC01 and CC01 under Tension

The net section yield loads for the model types EC01, SC01 and CC01 under tension are derived from the load redistribution due to area reduction. They are given by

$$P_o^* = \begin{cases} \sigma_o\left(Wt - \dfrac{\pi ac}{4}\right), & \text{for CC01 where } W = b \\ \sigma_o(Wt - \pi ac), & \text{for EC01} \\ \sigma_o\left(Wt - \dfrac{\pi ac}{2}\right), & \text{for SC01 where } W = 2b \end{cases} \tag{55}$$

4.2 Net Section Yield Moments for SC01 and CC01 under Bending

The net section yield moments, M_0^*, for model types SC01 and CC01 under bending can be derived from plastic limit analysis assuming a neutral axis midway across the net section thickness, t_{net}. In reference to the cross section defined in Figure 4, the net section thickness varies with the flaw size and is given by

$$t_{net} = \begin{cases} t - a\sqrt{1 - \dfrac{x^2}{c^2}} & ,|x| \le c \\ t & ,|x| > c \end{cases} \tag{56}$$

The net section yield moment or the limit moment for a corner flaw (CC01) and a surface flaw (SC01) can thus be determined analytically as

$$\frac{M_o^*}{\frac{1}{4}bt^2\sigma_o} = \frac{\frac{c}{24}\left(-3at\pi + 6t^2 + 4a^2\right) + \frac{1}{4}t^2(b-c)}{\frac{1}{4}bt^2} \tag{57}$$

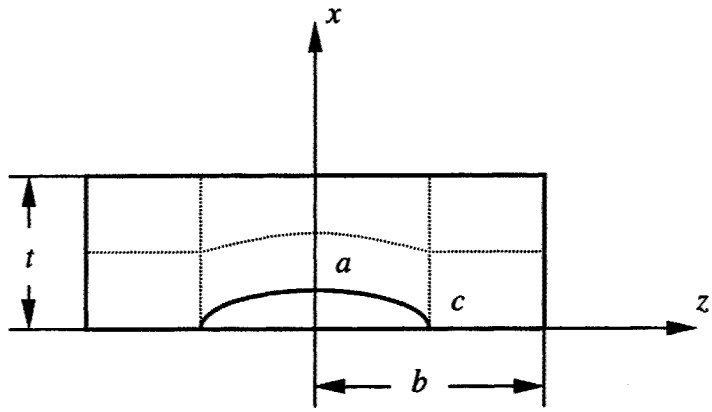

Figure 4. Geometric configuration for plastic limit analysis.

5.0 Re-characterization of Arbitrary Secondary Stress Fields

The effects of secondary loads corresponding to self-equilibrated thermal and residual stresses are taken into account in the Elastic Plastic Fracture Mechanics (EPFM) module of NASGRO. This secondary load capability extends the applicability of NASGRO to the loading conditions shown in Table 11. In contrast to primary loading which is limited to either tension or bending, the secondary loading can be represented by an arbitrary non-linear univariant stress distribution. However, due to the limited *K* solutions in NASGRO for model types TC01, TC02, SC01, CC01 and EC01, approximation techniques are used to conservatively generate uniform and linear stress fields from the user-specified arbitrary stress distributions for secondary loads. These techniques are detailed in the following sub-sections.

5.1 Linearization of Arbitrary Secondary Stress Field for use with CC01 and TC02

For CC01 the univariant secondary stress variation is specified along the thickness direction, and for TC02 it is along the width direction as defined in the NASGRO LEFM module. Since the *K* solutions for CC01 and TC02 are limited to combined tension and bending loads, the arbitrary secondary stress distributions have to be linearized and decomposed into tension and bending components so that the NASGRO

K solutions can be utilized. Referring to Figure 5, the linearized secondary stress variation is represented by a dotted line while the actual loading distribution is indicated by a dash line. The stress level at the position corresponding to the crack tip depends on the stress distribution. The procedure below illustrates how to determine its value.

Step A. Use the actual secondary stress level at the crack tip location as the default value.

Step B. Calculate the load over the crack area corresponding to the linear stress approximation and compare this with that from the actual secondary stress.

Step C. If the approximated load is larger than the actual load, then use the linear stress approximation as a conservative estimate of the actual stress variation as shown in Figure 5(a).

Step D. However, if the actual load is larger than the load corresponding to the linearized stress, then adjust the linear stress approximation until the loads are the same. Use the adjusted linear stress as a conservative representation of the actual secondary stress. The dotted line in Figure 5(b) illustrates a linear stress distribution resulting from this procedure.

The crack tip locations referred to correspond to the c tip in TC02 and the a tip in CC01.

Further decomposition of the linearized secondary stress variation is made to define tension and bending components. For example, in the CC01 model where the univariant secondary stress varies along the thickness or x-direction, the mathematical forms for the tension and bending components are

$$\begin{aligned} \sigma_t &= \frac{\sigma_a - \sigma_0}{2}\frac{t}{a} + \sigma_0 \\ \sigma_b &= \frac{\sigma_a - \sigma_0}{a}\left(x - \frac{t}{2}\right) \end{aligned} \tag{58}$$

respectively, where σ_a is the stress at the location of crack tip a, σ_0 is the secondary stress at the origin of coordinates where the flaw emanates, and t is the thickness. Similar expressions can also be obtained for TC02. These components are used as the input to the NASGRO linear elastic fracture mechanics (LEFM) module for model types TC02 and CC01 to calculate K for the secondary load.

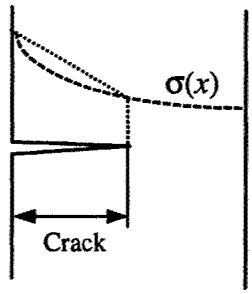

Figure 5(a)

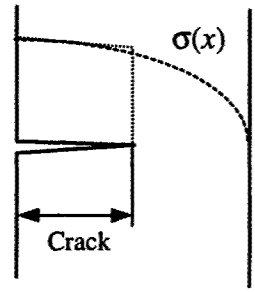

Figure 5(b)

Figure 5. Linear stress approximation for CC01 and TC02.

Model type	Geometry Description	Primary load	Secondary load
TC01	Through crack at center of plate	Tension only	Univariant in width direction
TC02	Through crack at edge of plate	Tension or bending	Univariant in width direction
SC01	Surface crack in a rectangular plate	Tension or bending	Univariant in thickness direction
CC01	Corner crack in a rectangular plate	Tension or bending	Univariant in thickness direction
EC01	Embedded crack in plate	Tension only	Univariant in thickness direction

Table 11. Applicable loading conditions in NASGRO EPFM.

5.2 Geometry Substitution of SC01 by SC02

Since the NASGRO LEFM module for SC01 only accepts uniform tension and bending loads, the SC02 model is used to evaluate K for combined primary and secondary loading. In the SC02 model an arbitrary univariant stress distribution can be specified and no re-characterization of the actual stress distribution is needed.

5.3 Uniform Stress Approximation for EC01 and TC01

Current EC01 and TC01 model types in the NASGRO LEFM module only accept uniform stress distributions. Hence, the actual stress field has to be re-characterized as a uniform stress. In addition, the secondary stress field is restricted to one that is symmetrically distributed about the center of the crack. The mathematical equation for the uniform secondary stress approximation for use with TC01 is

$$\bar{\sigma} = \frac{\int_0^c \sigma(z)dz}{c} \tag{59}$$

Note that for this model, the stress variation is in the z-direction. A similar equation can be derived for the model type EC01 where, however, the uniform stress is evaluated for a secondary stress that varies in the thickness or x-direction, and the integral corresponding to equation (59) is evaluated between x=0 and x=a.

6.0 Evaluation of J and ΔJ for Combined Loading

For TC01 and TC02 in which the crack dimension is described by one parameter, c, equations (6-8) for J_e and equations (10-13) for ΔJ_e are used in the program. However, for SC01, CC01 and EC01 whose crack dimensions are described by two parameters, a and c, the plastic correction needs to be defined differently. For instance, for the surface crack problem (SC01), the material at the deepest point on the crack front is subjected to plane strain deformation, whereas the surface point will undergo plane stress deformation and, accordingly, the equations for the plastic zone correction are different. For model types SC01, CC01 and EC01, the following equations are used to evaluate J_e and ΔJ_e.

<u>J_e Solutions for SC01, CC01 and EC01</u>

$$J(a,c,\hat{P}) = J_e(a_e,c_e,\hat{P}) + J_p(a,c,P) \tag{60}$$

with

$$J_e(a_e,c_e,\hat{P}) = \frac{K^2(a_e,c_e,\hat{P})}{E'} \tag{61}$$

and J_p defined according to equations (44-45) and (51-52). The effective crack lengths a_e and c_e are defined as

$$a_e = a + \phi r_y^a,\ c_e = c + \phi r_y^c \tag{62}$$

with

$$\phi = \frac{1}{1+\left[\frac{P}{P_o(a,c)}\right]^2}$$

and

$$r_y^a = \frac{1}{\beta^a \pi}\frac{n-1}{n+1}\left[\frac{K^a\left(a,c,\hat{P}\right)}{\sigma_o}\right]^2,\ r_y^c = \frac{1}{\beta^c \pi}\frac{n-1}{n+1}\left[\frac{K^c\left(a,c,\hat{P}\right)}{\sigma_o}\right]^2 \tag{63}$$

where superscripts a and c refer to the crack tips at locations a and c, respectively.

<u>ΔJ_e Solutions for SC01, CC01 and EC01</u>

$$\Delta J_{eff}\left(a,c,\Delta\hat{P}\right) = \Delta J_e^{eff}\left(a_e^\Delta, c_e^\Delta, \Delta\hat{P}\right) + \Delta J_p^{eff}\left(a,c,\Delta P\right) \tag{64}$$

with

$$\Delta J_e^{eff}\left(a_e^\Delta, c_e^\Delta, \Delta\hat{P}\right) = \frac{U^2 \Delta K^2\left(a_e^\Delta, c_e^\Delta, \Delta\hat{P}\right)}{E'} \tag{65}$$

and ΔJ_p defined according to equations (48-50) and (53-54). The effective crack lengths a_e^Δ and c_e^Δ are defined as

$$a_e^\Delta = a + \phi^\Delta\left(\Delta r_y^a\right),\ c_e^\Delta = c + \phi^\Delta\left(\Delta r_y^c\right) \tag{66}$$

with terms

$$\phi^\Delta = \frac{1}{1+\left[\frac{\Delta P}{2P_o(a,c)}\right]^2}$$

$$\left(\Delta r_y^a\right) = \frac{1}{\beta^a \pi}\frac{n-1}{n+1}\left[\frac{\Delta K^a\left(a,c,\Delta\hat{P}\right)}{2\sigma_o}\right]^2,\ \left(\Delta r_y^c\right) = \frac{1}{\beta^c \pi}\frac{n-1}{n+1}\left[\frac{\Delta K^c\left(a,c,\Delta\hat{P}\right)}{2\sigma_o}\right]^2 \tag{67}$$

Table 12 shows the values of β^a and β^c for model types SC01, CC01 and EC01.

Table 12. Deformation conditions applied to model types EC01, SC01 and CC01.

Model type	Deformation condition		β	
	a	c	β^a	β^c
EC01	Plane strain	Plane strain	6	6
SC01	Plane strain	Plane stress	6	2
CC01	Plane stress	Plane stress	2	2

7.0 Algorithms for Failure Analysis

The failure algorithm computes critical crack sizes and critical loads for model types TC01, TC02, CC01, SC01, and EC01 subjected to combined primary and secondary loading. The critical load computation is based on the primary load, while the secondary load is held fixed. For brittle materials containing cracks with two degrees of freedom, the assessments are made with respect to J values evaluated at the c-tip or a-tip, whichever is the first to violate the brittle failure criterion. For ductile materials, the assessments are restricted to the a-tip. To facilitate the computations when assessing the critical crack sizes, the crack geometries with more than one degree of freedom (i.e., CC01, SC01, and EC01) are reduced to one degree of freedom flaws by restricting crack shape development to either cracks with constant aspect ratio, or to cracks which can only extend in the a-direction (through the thickness) and whose length in the c-direction remains constant.

7.1 Determining Critical Crack Sizes

Algorithm for Determining the Limit Crack Length (ALIMIT)

The limit crack length a_{limit} is the crack length at which plastic collapse will occur for the given applied load. It serves as an upper bound value in the search for initial and critical crack lengths. Plastic collapse is assumed to occur when the reference stress defined by equation (18) equals the material flow stress $0.5(\sigma_u+\sigma_y)$. While the routine is searching for a_{limit}, a check for geometry bounds and NASGRO validity bounds is constantly carried out. The flow diagram describing the search method is shown in Figure 6.

Algorithm for Calculating Critical Crack Sizes (Brittle Materials) and Initiation Crack Sizes (Ductile Materials) (ANIT)

The initiation crack size a_{init} is determined by numerically solving the equation

$$J\left(a_{init} + \Delta a_b, \hat{P}\right) = J_{mat} \tag{68}$$

where J_{mat} is the material toughness evaluated at the blunting tear length and Δa_b is the blunting length defined as

Brittle materials:

$$\Delta a_b = \frac{J_{mat}}{2\sigma_{ys}} \tag{69}$$

Ductile materials:

$$\Delta a_b = \frac{\sqrt{J_1^2 + 4J_2(J_{mat} - J_0)} - J_1}{2J_2}, \text{for quadratic } J_R \text{ curves}$$

$$\Delta a_b = \left(\frac{J_{mat}}{J_1}\right)^{\frac{1}{J_2}}, \text{for power law } J_R \text{ curves} \tag{70}$$

For brittle materials, the initial crack size will extend by blunting under combined loads $\hat{P}$ to fail at J_{mat}. For ductile materials, this routine provides the crack size at the initiation of ductile tearing which provides a lower bound value in the search for the critical crack size. Figure 7 shows the flow diagram indicating how the search for a_{init} is performed. Note that the initiation crack length does not include the blunting tear length.

Algorithm for Calculating Critical Crack Sizes in Ductile Materials (ACRIT)

This routine calculates the critical crack size for ductile instability preceded by ductile tearing. The following equations simultaneously are solved

$$J(a) = J_R(\Delta a_t)$$

$$\frac{dJ}{da} = \frac{dJ_R}{d(\Delta a_t)} \tag{71}$$

for $a = a_{crit} + \Delta a_t$ by finding the maximum a_{crit} that satisfies both equations. The searching starts from a crack size a_{init} where a_{init} is the initiation crack size. During the search, the tear length Δa_t corresponding to the current J value is needed. This is calculated as follows.

$$\Delta a_t = \frac{\sqrt{J_1^2 + 4J_2(J - J_0)} - J_1}{2J_2}, \text{for quadratic } J_R \text{ - curves}$$

$$\Delta a_t = \left(\frac{J}{J_1}\right)^{\frac{1}{J_2}}, \text{for power law } J_R \text{ - curves} \tag{72}$$

The critical crack size, a_{crit}, is defined as that size that will extend by tear and eventually result in ductile instability under the prescribed combined primary and secondary loads. Hence, the crack size when ductile instability takes place, a_{inst}, is given by

$$a_{inst} = a_{crit} + \Delta a_t \tag{73}$$

The flow diagram describing the search procedure is shown in Figure 8.

7.2 Determining Critical Loads

Algorithm for the Limit Primary Load (PLIMIT)

The limit load P_{limit} is the load at which plastic collapse will occur for the given crack size. It serves as an upper bound in the search for initial and critical loads. The value of the limit load is given by the net section yield load multiplied by the ratio $0.5(\sigma_u+\sigma_y)/\sigma_y$.

Algorithm for Calculating Critical Loads (Brittle Materials) and Initiation Loads (Ductile Materials) (PINIT)

The load to initiate crack growth is determined by numerically solving the equation

$$J(a + \Delta a_b, P_{init} + S) = J_{mat} \tag{74}$$

for P_{init}, where a is the given crack size and P and S indicate primary and secondary loads, respectively. Δa_b is given by equations (69) and (70). For brittle materials, $P_{crit}=P_{init}$, while for ductile materials P_{init} provides a lower bound in the search for the critical load. The flow diagram indicating illustratively how the search routine is performed is shown in Figure 9.

Algorithm for Calculating Critical Loads for Ductile Materials (PCRIT)

The critical load for ductile materials is obtained by finding the maximum value, P_{crit}, of P as a function of tear length, Δa_t, where P is the solution to the equation

$$J(a + \Delta a_t, P + S) = J_R(\Delta a_t) \tag{75}$$

Figure 10 illustrates the search mechanism used to solve for P_{crit}.

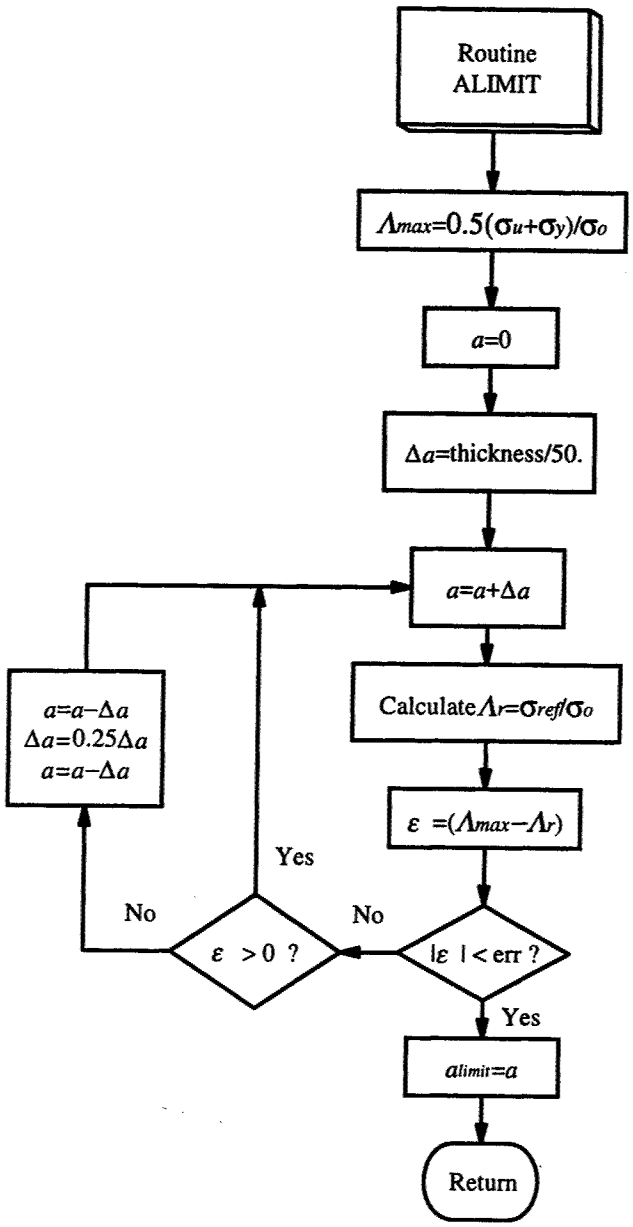

Figure 6. Procedure to determine the limit crack length a_{limit}.

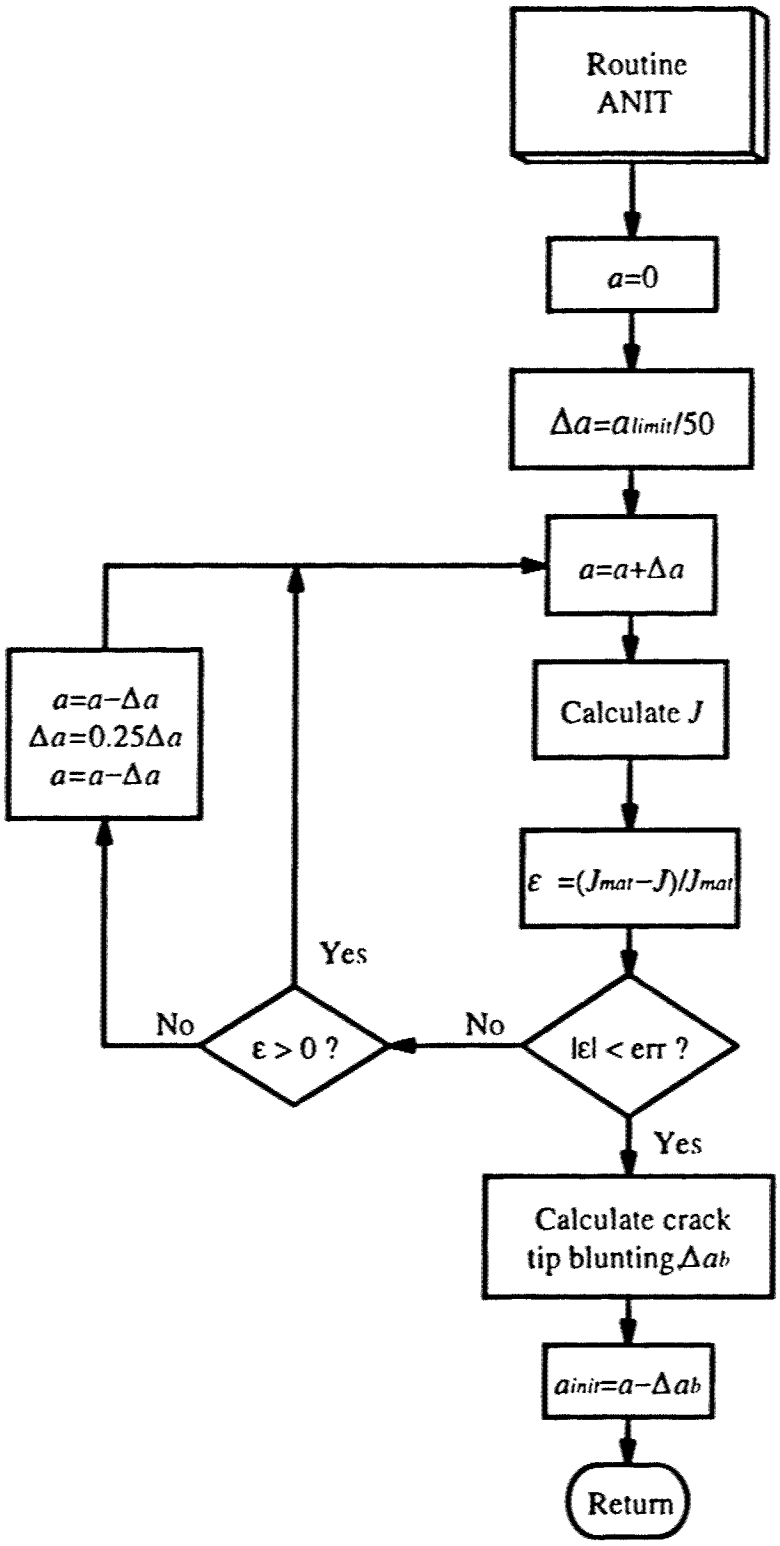

Figure 7. Procedure for the initiation crack length a_{init}.

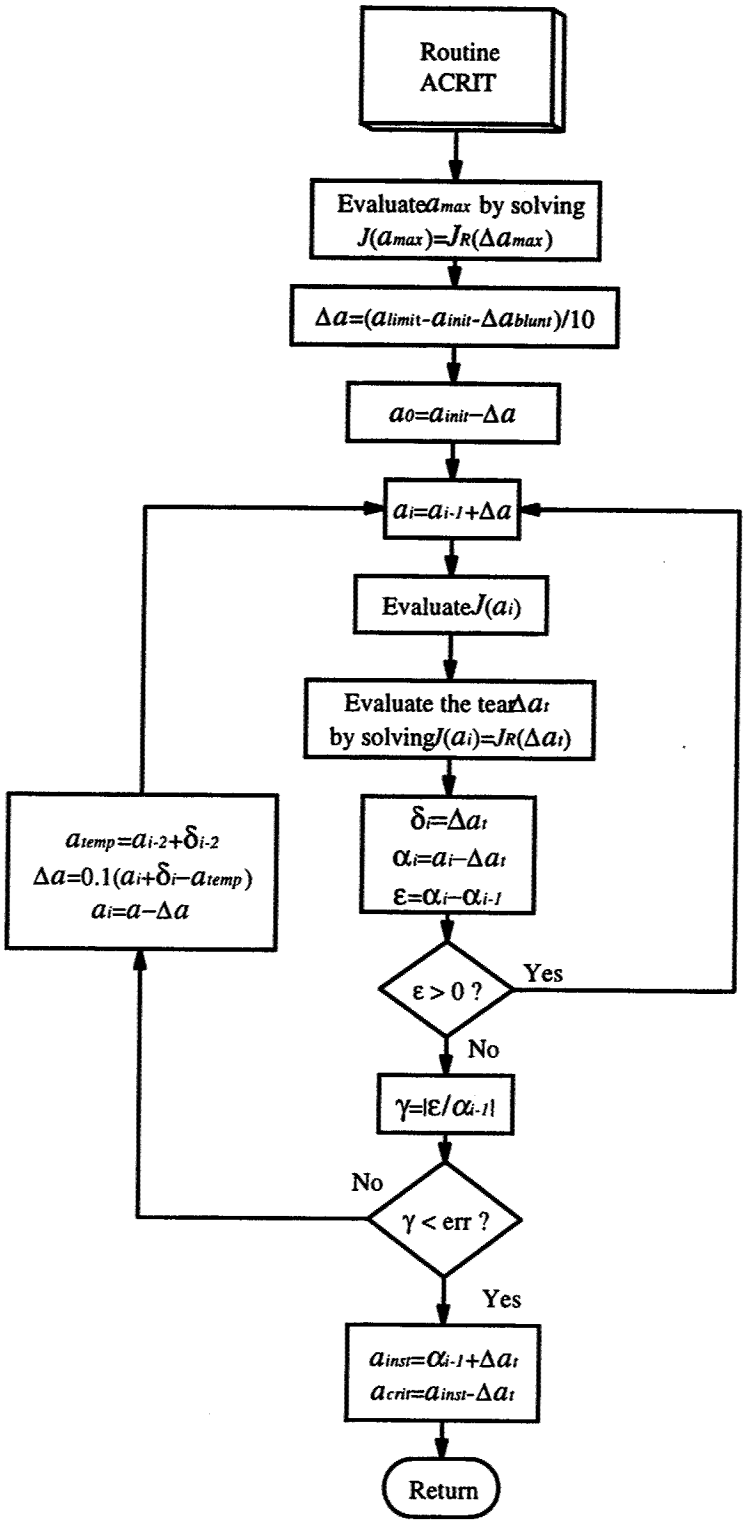

Figure 8. Iteration procedure for the critical crack length a_{crit}.

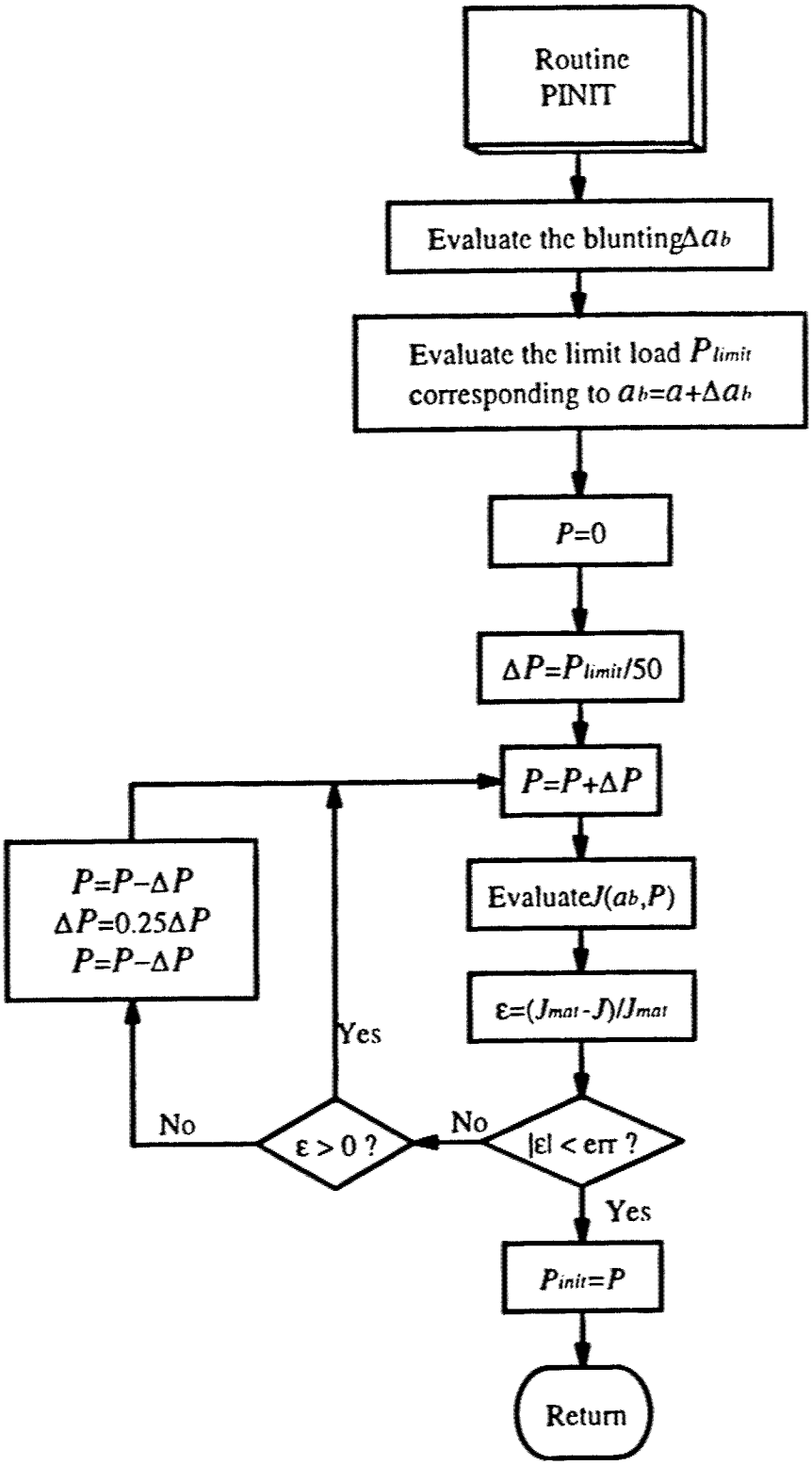

Figure 9. Procedure to determine the initiation load P_{init}.

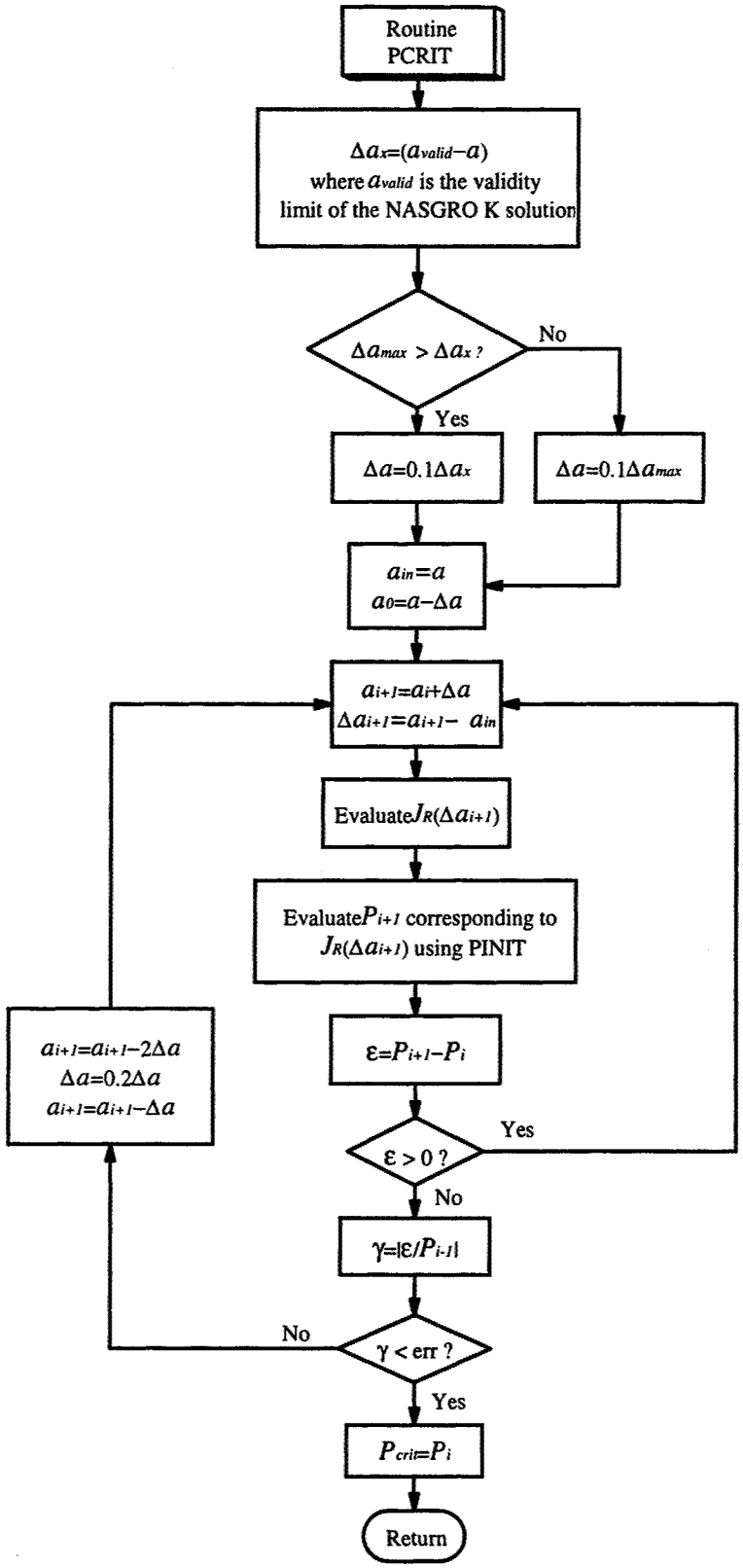

Figure 10. Procedure to determine the critical load P_{crit}.

8.0 Rules for Calculating J, ΔJ and the R ratio

Consistent with similar rules encoded in NASGRO for cyclic crack growth under linear elastic conditions, rules have been drawn up to take into account the relative magnitudes of K_{max} and K_{min}. For instance, under some circumstances the maximum and minimum loads specified by the user may result in a K_{max} value less than the K_{min} value, and, therefore, the values of K_{max} and K_{min} have to be interchanged in determining ΔK. The rules are summarized in Tables 13 and 14, where superscripts P and S refer to primary and secondary loads. Table 13 lists the rules for calculating the elastic components, J_e and ΔJ_e, as well as the R ratio, K_{max}/K_{min}. It identifies the maximum and minimum loads used in the computation for combined loading. Similarly, Table 14 lists the rules for calculating plastic components, J_p and ΔJ_p, in which only the primary load is of consideration.

Table 13. Rules for calculating J_e, ΔJ_e and R.

Initially calculated values			Parameters used in the calculation of J_e, ΔJ_e, and R			
K_{max}^{P+S}	K_{min}^{P+S}	$K_{max}^{P+S} - K_{min}^{P+S}$	Monotonic	Cyclic		
			K_{max}	K_{max}	ΔK	R
Positive	Positive	Positive	K_{max}^{P+S}	K_{max}^{P+S}	$K_{max}^{P+S} - K_{min}^{P+S}$	$1 - \Delta K / K_{max}$
Positive	Positive	Negative	K_{max}^{P+S}	K_{min}^{P+S}	$K_{min}^{P+S} - K_{max}^{P+S}$	$1 - \Delta K / K_{max}$
Positive	Negative	Positive	K_{max}^{P+S}	K_{max}^{P+S}	$K_{max}^{P+S} - K_{min}^{P+S}$	$1 - \Delta K / K_{max}$
Negative	Positive	Negative	Stop	K_{min}^{P+S}	$K_{min}^{P+S} - K_{max}^{P+S}$	$1 - \Delta K / K_{max}$
Negative	Negative	Positive	Stop	Stop	Stop	Stop
Negative	Negative	Negative	Stop	Stop	Stop	Stop

Table 14. Rules for calculating J_p and ΔJ_p.

Initially calculated values			Parameters used in the calculation of J_p and ΔJ_p		
K_{max}^{P}	K_{min}^{P}	$K_{max}^{P} - K_{min}^{P}$	Monotonic	Cyclic	
			K_{max}	K_{max}	ΔK
Positive	Positive	Positive	K_{max}^{P}	K_{max}^{P}	$K_{max}^{P} - K_{min}^{P}$
Positive	Positive	Negative	K_{max}^{P}	K_{min}^{P}	$K_{min}^{P} - K_{max}^{P}$
Positive	Negative	Positive	K_{max}^{P}	K_{max}^{P}	$K_{max}^{P} - K_{min}^{P}$
Negative	Positive	Negative	Stop	K_{min}^{P}	$K_{min}^{P} - K_{max}^{P}$
Negative	Negative	Positive	Stop	Stop	Stop
Negative	Negative	Negative	Stop	Stop	Stop

9.0 Validity Limits for *J* Solutions

Table 15 lists the validity limits of the *J* solutions incorporated in the NASGRO elastic-plastic *J* module and the NASGRO linear elastic fracture mechanics module.

Table 15. Validity limits in elastic-plastic *J* module

Model type	Loading	EPRI	Reference stress method	NASGRO elastic module
TC01	Tension	$10^{-3}<2c/W<0.875$ $1<n<20$	$10^{-3}<2c/W<0.875$ $n>1$	$0<c<W/2$
TC02	Tension	$10^{-3}<c/W<0.875$ $1<n<20$	$10^{-3}<c/W<0.75$ $n>1$	$0<c<W$
	Bending	$10^{-3}<c/W<0.875$ $1<n<20$	$10^{-3}<c/W<0.75$ $n>1$	$0<c<W$
EC01	Tension	N/A	$0<2c<W$, $2c/W\leq0.5$ $0<a<t/2$, $a/c>0$ $n>1$	$0<2c<W$, $2c/W\leq0.5$ $0<a<t/2$, $a/c>0$
CC01	Tension	N/A	$0<c<W$, $0<a<t$ $10^{-3}<a/c<1000$ $n>1$	$0<c<W$, $0<a<t$ $10^{-3}<a/c<1000$
	Bending	N/A	$0<c<W$, $0<a<t$ $10^{-3}<a/c<1000$ $n>1$	$0<c<W$, $0<a<t$ $10^{-3}<a/c<1000$
SC01	Tension	N/A	$0<c<W/2$, $0<a<t$ $0.05<a/c<1.2$ $n>1$	$0<c<W/2$, $0<a<t$ $0.05<a/c<1.2$
	Bending	N/A	$0<c<W/2$, $0<a<t$ $0.05<a/c<1.2$ $n>1$	$0<c<W/2$, $0<a<t$ $0.05<a/c<1.2$

10.0 How to use the NASGRO EPFM Module

Figure 11 shows how the EPFM module interfaces with NASGRO. New users are encouraged to use the flow diagrams illustrated in the following examples as a road map to help them navigate the available options.

10.1 How to Run an Elastic-Plastic J-Integral Calculation

The flow diagram showing the menu structure of the elastic-plastic *J* module is displayed in Figure 12. Figure 13 displays its execution structure. Both figures provide enough information for the available options for the user to navigate the program.

When the program is executed, the main menu of NASGRO shows the available analysis modules. In this release, the menu is

Enter one of the following options:

1 Safe Life Analysis
2 Critical crack size computation
3 Stress-intensity factor solution
4 da/dt life analysis (e.g., for glass)
5 Elastic-Plastic J computation
6 Elastic-Plastic failure analysis
7 Elastic-plastic fatigue life analysis
0 Terminate session

Notes:
1. Once an analysis option is chosen and data input is in progress, entering a minus sign (-) will cause moving back to the previous prompt.
2. Always press Enter key to complete an entry.
SYSTEM_PROMPT> 5

where the system prompt for the user's input is denoted by **SYSTEM_PROMPT>**. Users should choose option 5 for the elastic-plastic *J* calculation. Following this choice, the sub-menu below lets the user choose the type of session.

Enter type of session for elastic-plastic *J* module:

0 — Interactive - input and computation
1 — Interactive input while creating a batch file
2 — Batch - computing only (run using a batch data file)
3 — Edit an existing batch file
(Note: option 1 must be used before option 2 or 3)
SYSTEM_PROMPT> 0

Option 0 provides users a line-by-line interactive input mode. In addition to the simple functions given by option 0, option 1 records every data entry and saves them as a batch file which can be executed later by the user choosing option 2. Option 3 can be used to modify the batch file created by option 1.

Interactive Input Mode

When the interactive input mode (either option 0 or 1) is activated, NASGRO will prompt the user to enter the filename for storing output data and the units for the analysis. The filename can be any alpha-numeric combination up to 12 characters long. The sub-menu shown below follows. This displays the available models in the NASGRO elastic-plastic *J* module. At any data entry stage from this point on, the user can type "-" to go back to the previous prompt.

Enter a model type from the following:
TC Through Crack
CC Corner Crack
EC Embedded Crack
SC Surface Crack
SYSTEM_PROMPT> tc

Select the desired model type. Depending on which model type is chosen, another sub-menu will appear right after your selection. For instance, for a TC (through crack) model, two subsequent sub-menus will be

Which method is to be used for estimating the elastic-plastic *J*?
1... EPRI (Electric Power Research Institute) Solution Scheme
2... RSM (Reference Stress Method) Solution Scheme
SYSTEM_PROMPT> 1

and,

Select the deformation constraint:
1... Plane Strain (PE)
2... Plane Stress (PS)
SYSTEM_PROMPT> 2

However, there are no such options for model types; CC, EC, and SC. After the selection is made, another sub-menu shows available geometries for a specific model type. For the model type TC, the sub-menu should be

Enter a Number from left column to select a THROUGH crack case:
1.... TC01 - in center of plate
2.... TC02 - single edge crack
SYSTEM_PROMPT> 1

After deformation constraint, geometry and model types are selected, another sub-menu indicating the loading type will appear. At present, model types TC02 (edge crack), CC01 (corner crack), and SC01 (surface crack) have available tension and bending loads as separately applied loads, and model types TC01 (center crack) and EC01 (embedded crack) have only tensile loading available. For example, after option 2 (TC02-single edge crack) of the above sub-menu is selected, another sub-menu appears as follows:

Enter a Number from left column to select the loading option for the TC02 geometry:
1.... TENSION - single edge crack in remote tension
2.... BENDING - single edge crack subjected to bending
SYSTEM_PROMPT> 1

The next selection is to define the geometry dimensions. The number of required geometric parameters depends on the model type being selected. Nonlinear material properties are required next in the form of a Ramberg-Osgood uniaxial stress-strain equation

$$\frac{\varepsilon}{\varepsilon_o} = \frac{\sigma}{\sigma_o} + \alpha\left(\frac{\sigma}{\sigma_o}\right)^n \tag{76}$$

where ε is the total strain, σ is the applied stress, and ε_o, σ_o, α and n are material constants. The program will prompt the user to provide the elastic modulus, $E=\sigma_o/\varepsilon_o$,

elastic Poisson's ratio ν, and the Ramberg-Osgood constants α, n and σ_o. The interactive session continues as follows.

```
Geometric Model in use: TC01

Enter Plate Width, W:
SYSTEM_PROMPT> 20

 Plate Width, W =  20.0000

Enter Plate Thickness, t:
SYSTEM_PROMPT> 0.1

 Plate Thickness, t =    .1000

        ELASTIC-PLASTIC J CALCULATION FOR TC01
        ---------------------------------
            DATE: 14-Jul-98  TIME: 14:05:25
         (computed: NASA/FLAGRO Version 3.00, October 1995.)
       Elastic-Plastic Fracture Module (EPFM) V.1.01, Feb. 1998
             SI units [mm, MPa, MPa sqrt(mm)]


      Input  Filename = test.dat
      Output Filename = test.out

      Plate Thickness, t =    .1000
       "  Width, W    =  20.0000

*****************************************************************
Specify the Nonlinear Material Behavior

   Eps/Eps0=Sigma/Sigma0+alpha*(Sigma/Sigma0)**n

with Elastic Modulus defined by Sigma0/Eps0


Enter Elastic Modulus:
SYSTEM_PROMPT> 3000.0

 Elastic Modulus= .3000E+05

Enter Poisson"s Ratio:
SYSTEM_PROMPT> 0.3

 Poissons Ratio= .3000E+00

Enter alpha:
SYSTEM_PROMPT> 1.0

 Alpha =  .1000E+01

Enter Sigma0:
SYSTEM_PROMPT> 100.0
```

```
 Sigma0 =  .1000E+03

Enter n:
SYSTEM_PROMPT> 10.0

 n =  .1000E+02

Enter Material Yield Stress
SYSTEM_PROMPT> 100.0

 Material Yield Stress =       100.00

Enter Material Ultimate Stress
SYSTEM_PROMPT> 150.0

 Material Ultimate Stress =       150.00
```

The next section is to specify the combined primary and secondary loads. The applied loads are defined in terms of nominal (P/A) or linear elastic stresses as indicated in the NASGRO user's manual. The following illustrates the interactive session.

```
*****************************************************************
Specify the loading condition
 1 -- Primary Load only
 2 -- Primary Load and Secondary Load
SYSTEM_PROMPT> 1

PRIMARY LOAD:
 Enter stress, S0: Tensile Stress
SYSTEM_PROMPT> 40.0

      PRIMARY LOADS:     S0: Tensile Stress
                   S0 =   40.00
      NO SECONDARY LOAD SPECIFIED
```

After all the material constants, geometry parameters and applied loads are defined, the next phase is to define the flaw sizes. There are two data input formats as shown in the following prompt.

```
Interactively input the crack size or tabulate the data incrementally?
1...      Interactive input
2...      Tabulate the data incrementally
SYSTEM_PROMPT> 1
```

Option 1 prompts the user to provide the defect size interactively (line-by-line) and use "-1" to terminate the data entry. Option 2 gives the user the option to specify the range of the defect size with a preferred increment size to create a tabular output format. For example, for the model type TC01, a specified number of increments, n_{inc}, with a preferred range of defect sizes defined by c_{max} and c_{min} gives a tabular output of J_e, J_p, and J as a function of defect size with increment size $c_{inc} = (c_{max} - c_{min}) / n_{inc}$. In this example, option 1 is selected.

```
Enter crack size, c (or -1 to stop) :
SYSTEM_PROMPT> 0.3

Enter crack size, c (or -1 to stop) :
SYSTEM_PROMPT> 0.6

Enter crack size, c (or -1 to stop) :
SYSTEM_PROMPT> 1.0

Enter crack size, c (or -1 to stop) :
SYSTEM_PROMPT> 1.5

Enter crack size, c (or -1 to stop) :
SYSTEM_PROMPT> 2.0

Enter crack size, c (or -1 to stop) :
SYSTEM_PROMPT> 3.0

Enter crack size, c (or -1 to stop) :
SYSTEM_PROMPT> -1
```

Once the flaw sizes are specified, NASGRO will start the computation and display the results on screen. The results for the forgoing input are shown as follows.

```
*** EPRI Solution Scheme***

Model Code= TC01 (Plane Stress Condition)
```

c	Je	Jp	J
.3000	.531463E-01	.381383E-04	.531845E-01
.6000	.106655E+00	.930886E-04	.106748E+00
1.0000	.179282E+00	.204742E-03	.179486E+00
1.5000	.273589E+00	.445110E-03	.274034E+00
2.0000	.373905E+00	.893188E-03	.374799E+00
3.0000	.603615E+00	.360880E-02	.607224E+00

```
**********_________________**********
  < PRESS RETURN TO CONTINUE >
```

Batch Mode

Option 1 (interactive input while creating a batch file) in the session menu for elastic-plastic *J* module needs to be completed prior to activating this batch-job mode. The system prompt in the batch mode requests the user to provide the filename of an existing batch data file. This batch data file can also be modified by using option 3 in the session menu for elastic-plastic *J* module without running the time-consuming interactive data input mode again. This editing feature can be used after creating a data file in option 1 without quitting NASGRO. However, users can modify an existing batch file using any ASCII editor. The following lists the content of the batch file just created.

```
test.out    Output file name*12
 2   1=US units; 2=SI units
tc    Crack Model Type
1    1=EPRI, 2=RSM
```

```
2     1=plane strain (PE), 2=plane stress(PS)
1     Crack Model Number
 .2000E+02    Width
 .1000E+00    Thickness
 .3000E+05    Elastic Young"s modulus
  .300    Poisson"s ratio
1.000    Alpha
 .1000E+03    Sigma0
10.000    n
  .1000E+03 material yield stress
  .1500E+03 material ultimate stress
   1 1: Primary, 2: Primary+Secondary
 .4000E+02     loading stress
1    1=Intereactively input, 2=create a table
 .3000E+00    c( 1)
 .6000E+00    c( 2)
 .1000E+01    c( 3)
 .1500E+01    c( 4)
 .2000E+01    c( 5)
 .3000E+01    c( 6)
-.1000E+01    end of input
P    P(1st col.): to print
 0    1:to resume, 0: stop
```

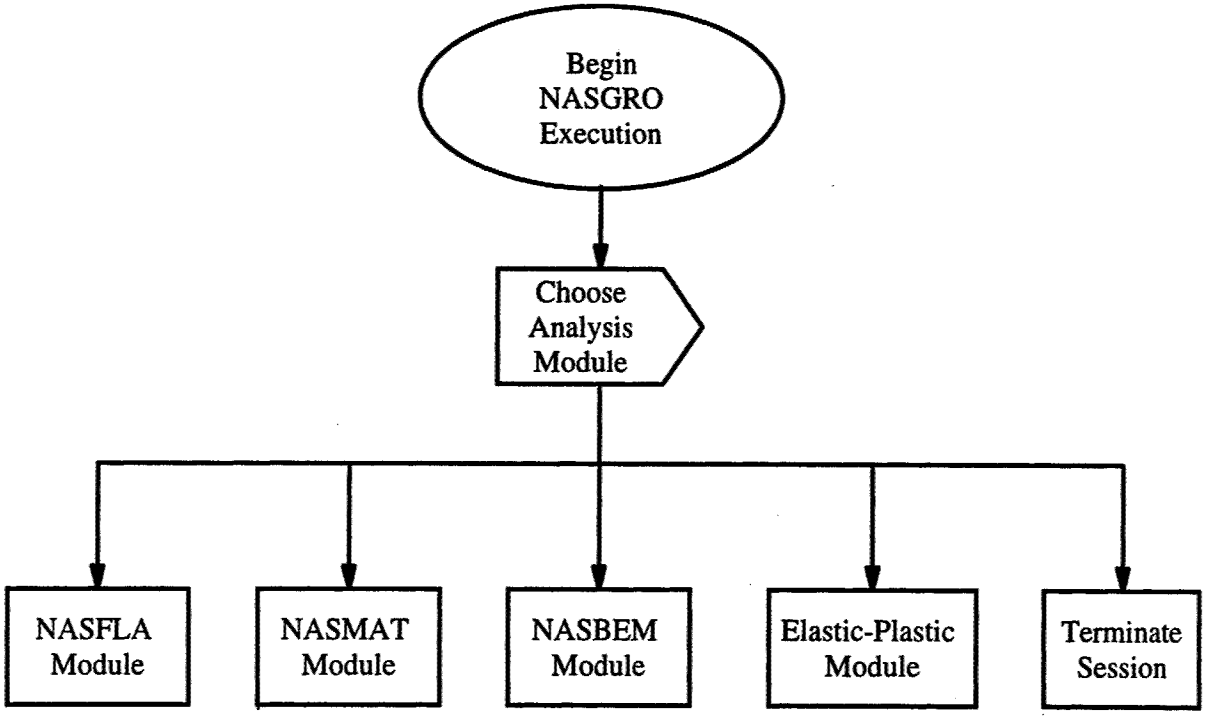

Figure 11. Overall program flow diagram.

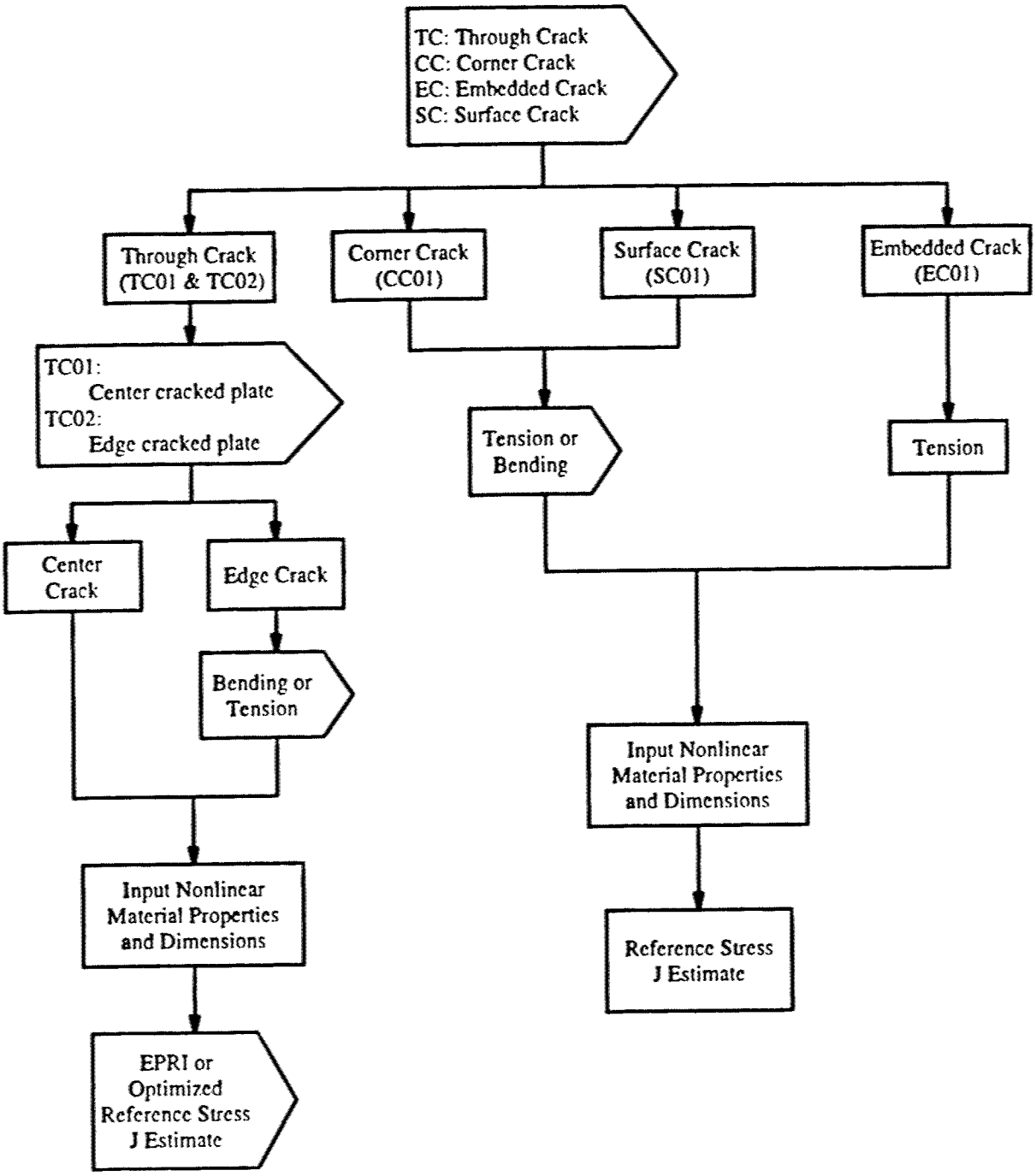

Figure 12. Menu structure of the elastic-plastic *J* module

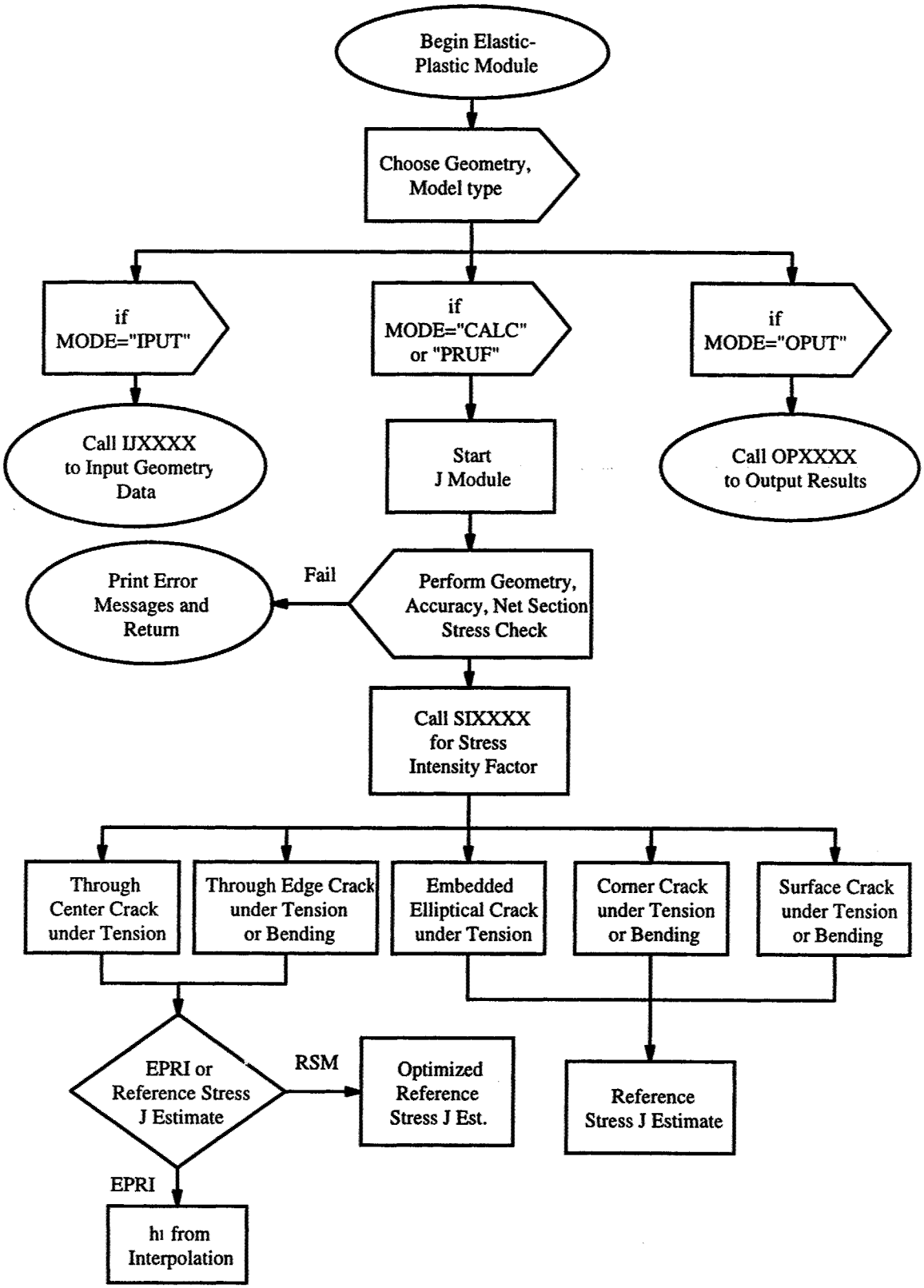

Figure 13. Computing scheme of the elastic-plastic *J* module

10.2 How to Perform a Failure Analysis

An example showing how to perform a step-by-step failure analysis for model type SC01 is demonstrated. After the greeting screens pass, the main menu of NASGRO follows. To activate the option for failure analysis, option 6 should be chosen. The system prompt for user's input is denoted by **SYSTEM_PROMPT>** . The user may refer to Figure 14 for the program structure of this module.

```
Enter one of the following options:

 1  Safe Life Analysis
 2  Critical crack size computation
 3  Stress-intensity factor solution
 4  da/dt life analysis (e.g., for glass)
 5  Elastic-plastic J computation
 6  Elastic-plastic failure analysis
 7  Elastic-plastic fatigue life analysis
 0  Terminate session

 Notes:
 1. Once an analysis option is chosen and data input
    is in progress, entering a minus sign (-)
    will cause moving back to the previous prompt.
 2. Always press Enter key to complete an entry.
SYSTEM_PROMPT>6
```

A sub-menu indicating available ways of file handling mainly concerning input and output appears. It lists the standard NASGRO ways of file processing. Option 0 prompts the user for input without saving. Option 1 lets the user save the input as a separate file and later the user can use (option 2) or modify (option 3) that batch data file. Option 2 is to run the program using the batch file created using option 1. The last option provides the user a line editing capability to modify any text file. In this example, option 1 was selected.

```
Enter type of session for elastic-plastic J module:

 0  Interactive - input and computation
 1  Interactive input while creating a batch file
 2  Batch - computing only (run using a batch data file)
 3  Edit an existing batch file
    (Note: option 1 must be used before option 2 or 3)
SYSTEM_PROMPT>1
```

Following this option, the program proceeds to prompt for filenames of batch processing and data output as well as the units in the analysis.

```
 Enter the name of batch file to use (up to 12 alpha-numeric characters):
  Enter RTN only to return to main menu
SYSTEM_PROMPT>fasc01.dat

 Enter file name for output (up to 12 alpha-numeric characters):
SYSTEM_PROMPT>fasc01.out
```

```
 Enter type of units:

 1  U.S. Customary Units [inches, ksi, ksi sqrt(in)]
 2  SI Units (International System) [mm, MPa, MPa sqrt(mm)]
SYSTEM_PROMPT>2
```

Next, NASGRO will prompt for the model type, the primary loading type, geometric dimensions, and parameters describing nonlinear material behavior. In this release, only Ramberg-Osgood type of material behavior was implemented. Required parameters include σ_0, E, α, and n in the Ramberg-Osgood equation as well as yield and ultimate stresses, σ_{ys} and σ_{ult}, for the assessment of limiting values. The interactive session is given as

```
 Enter a Model type from the following :

 TC  Through Crack
 CC  Corner Crack
 EC  Embedded Crack
 SC  Surface Crack
SYSTEM_PROMPT>SC

 Enter a Number to select a SURFACE crack case:

  1 .. SC01  -  in finite width plate
SYSTEM_PROMPT>1

 SC01

 Geometric Model in use: SC01

 Enter a Number to select the loading option for the SC01 geometry:

  1 .. TENSION  -  surface crack in remote tension
  2 .. BENDING  -  surface crack under bending in the thickness direction
SYSTEM_PROMPT>1

 Enter Thickness, t:
SYSTEM_PROMPT>1.0

 Thickness, t =    1.0000

 Enter Width, W:
SYSTEM_PROMPT>20.0

 Width, W =   20.0000

 [Note: Solution accurate if a/c > or = 0.05 AND a/c < or = 1.2]

      ELASTIC-PLASTIC ANALYSIS FOR CRITICAL CRACK/LOAD FOR SC01
      ---------------------------------------------------------
            DATE: 17-Jun-98  TIME: 15:18:47
        (computed: NASA/FLAGRO Version 3.00, October 1995.)
      Elastic-Plastic Fracture Module (EPFM) V.1.01, Feb. 1998
            SI units [mm, MPa, MPa sqrt(mm)]
```

```
Input  Filename = fasc01.dat
Output Filename = fasc01.out

Plate Thickness, t =    1.0000
 "  Width, W     =  20.0000

*****************************************************************
Specify the Nonlinear Material Behavior

   Eps/Eps0=Sigma/Sigma0+alpha*(Sigma/Sigma0)**n

with Elastic Modulus defined by Sigma0/Eps0


Enter Elastic Modulus:
SYSTEM_PROMPT>30000.

 Elastic Modulus= .3000E+05

Enter Poisson"s Ratio:
SYSTEM_PROMPT>0.3

 Poissons Ratio= .3000E+00

Enter alpha:
SYSTEM_PROMPT>1.0

 Alpha =  .1000E+01

Enter Sigma0:
SYSTEM_PROMPT>100.

 Sigma0 =  .1000E+03

Enter n:
SYSTEM_PROMPT>10.

 n =  .1000E+02

 Enter Material Yield Stress
SYSTEM_PROMPT>100.

 Material Yield Stress =        100.00

 Enter Material Ultimate Stress
SYSTEM_PROMPT>150.

 Material Ultimate Stress =        150.00
```

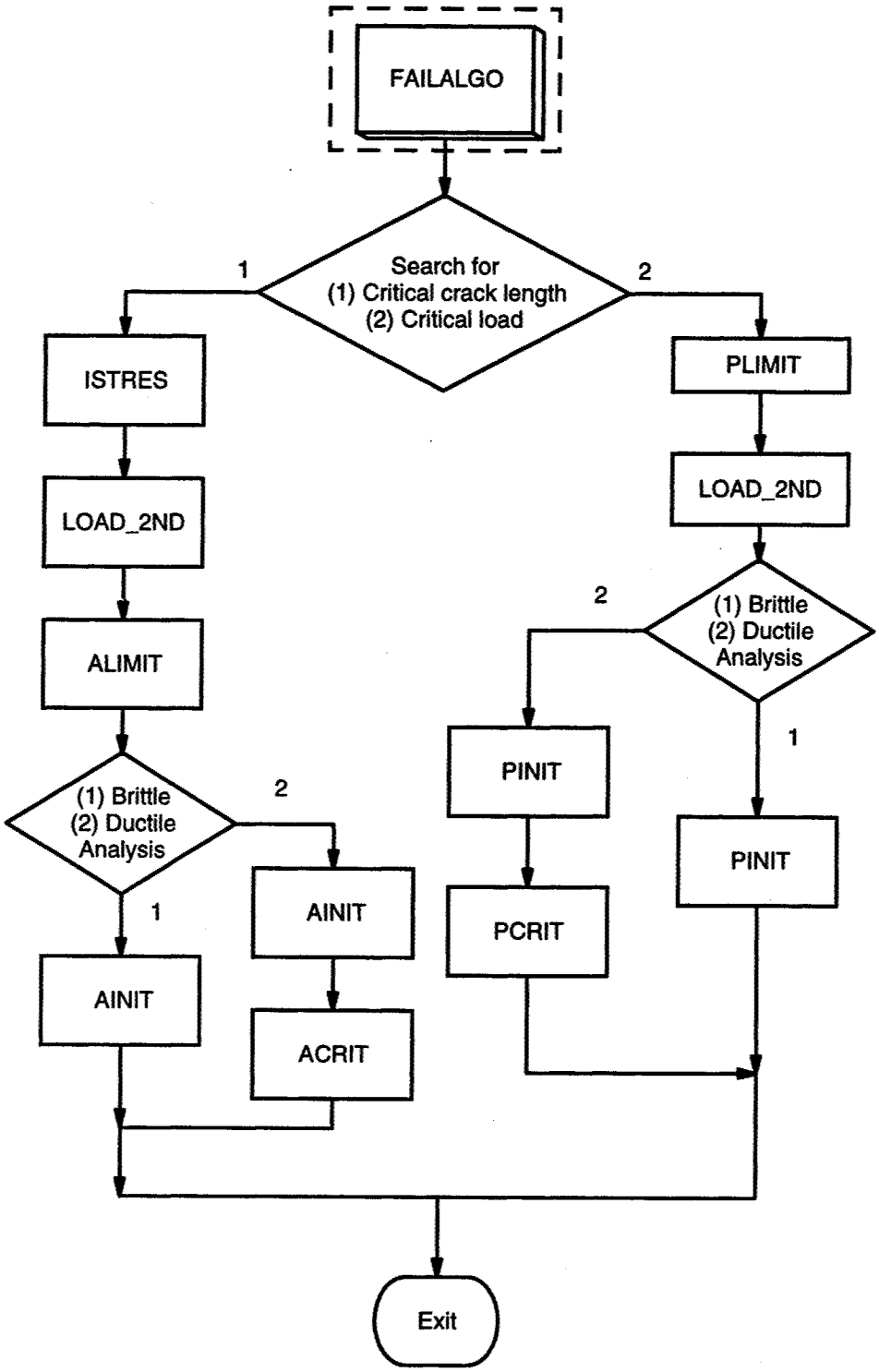

Figure 14. Flow chart for the failure algorithm in the NASGRO EPFM module.

To facilitate the computations when assessing crack geometries with more than one degree of freedom, these are reduced to one degree of freedom flaws by restricting crack shape development either to maintaining a constant aspect ratio, or to cracks extending only in the a-direction (through the thickness) with the c-tip being fixed. The following system prompt asks the user's input for the proper reduction method.

```
Specify the following data for elastic plastic
 failure analysis

  Analysis with constant aspect ratio or constant crack length (c-tip)
    1... constant aspect ratio
    2... constant crack length along c-direction
SYSTEM_PROMPT>1

  iasp =  1

  Enter aspect ratio:
SYSTEM_PROMPT>0.2

  Constant aspect ratio =  .2000E+00
```

Next, the user specifies whether a critical crack or critical load analysis is required.

```
  Search for critical crack length or critical load
    1... critical crack
    2... critical load
SYSTEM_PROMPT>1

  icrit =  1
```

The user then specifies whether a brittle or a ductile failure analysis should be performed.

```
Specify the type of failure analysis
  1... brittle analysis
  2... ductile analysis
SYSTEM_PROMPT>2

  imech =  2 : Ductile analysis is performed
```

A critical toughness, J_{mat}, is required for both types of failure analysis. For ductile failure analysis, that characterizes the onset of crack extension. In addition, the user needs to specify the form of the resistance curve, J_R, as well as the maximum tearing length, Δa_{max} for which the form is valid. J_R can be expressed as either a quadratic or power law in the tear length, Δa_t. In this example, a quadratic form is selected.

```
  Enter material toughness value (Jmat):
SYSTEM_PROMPT>0.2

  Material toughness value (Jmat) =  .2000E+00

  Enter the function type of resistance curve
    1... quadratic form (J=dj0+dj1*x+dj2*x^2)
    2... power law  (J=dj1*x^dj2)
```

```
SYSTEM_PROMPT>1

 npow =  1 (1: quadratic, 2: power law)
 Values for dj0, dj1, dj2, and da(max)
 Enter dj0 first
SYSTEM_PROMPT>0.175

 dj0   = .1750E+00

 Enter dj1
SYSTEM_PROMPT>15.0

 dj1   = .1500E+02

 Enter dj2
SYSTEM_PROMPT>-75.0

 dj2   = -.7500E+02

 Enter da(max)
SYSTEM_PROMPT>0.1

 da(max)= .1000E+00

      Model Code= SC01 under uniform tension
```

The following interactive session illustrates how to provide NASGRO loading information including the specification of primary and secondary loading. In this example, model type SC01 can have univariant stress distribution along x-direction as discussed in Section 5.2. Loads are specified as nominal or linear-elastic stresses.

```
Interactively input the load increment or tabulate the data incrementally?
 1... Interactively input
 2... Tabulate the data incrementally?
SYSTEM_PROMPT>1

 1... Primary Load only
 2... Primary Load plus Secondary Load
SYSTEM_PROMPT>2

 0... Stop input
 1... Input new loading data
SYSTEM_PROMPT>1

 PRIMARY LOAD:
 Enter stress, S0: Tensile Stress
SYSTEM_PROMPT>100

 SECONDARY LOAD:
 Enter values of non-dimensional positions and
     stress for the Secondary Load  (Linear or Nonlinear)

  *Nondimensional positions for SC01 are defined as x/t
   x is along the thickness (t) direction and from the
   surface where the crack initiates
```

```
 Enter Non-dimensional position  1  (terminate input by -1)
SYSTEM_PROMPT>0.
 Enter Stress  1
SYSTEM_PROMPT>100.
 Enter Non-dimensional position  2  (terminate input by -1)
SYSTEM_PROMPT>0.2
 Enter Stress  2
SYSTEM_PROMPT>96.
 Enter Non-dimensional position  3  (terminate input by -1)
SYSTEM_PROMPT>0.4
 Enter Stress  3
SYSTEM_PROMPT>84.
 Enter Non-dimensional position  4  (terminate input by -1)
SYSTEM_PROMPT>0.6
 Enter Stress  4
SYSTEM_PROMPT>64.
 Enter Non-dimensional position  5  (terminate input by -1)
SYSTEM_PROMPT>0.8
 Enter Stress  5
SYSTEM_PROMPT>36.
 Enter Non-dimensional position  6  (terminate input by -1)
SYSTEM_PROMPT>1.0
 Enter Stress  6
SYSTEM_PROMPT>0.
 Enter Non-dimensional position  7  (terminate input by -1)
SYSTEM_PROMPT>-1

      SECONDARY LOAD DISTRIBUTION:
          Norm. x       Stress
            .00       .1000E+03
            .20       .9600E+02
            .40       .8400E+02
            .60       .6400E+02
            .80       .3600E+02
           1.00       .0000E+00

 0... Stop input
 1... Input new loading data
SYSTEM_PROMPT>1

 PRIMARY LOAD:
 Enter stress, S0: Tensile Stress
SYSTEM_PROMPT>130.
 0... Stop input
 1... Input new loading data
SYSTEM_PROMPT>0
```

At this stage, the input phase for the necessary information is completed, and NASGRO will perform the necessary computation and display the results on screen.

```
                TABLE OUTPUT (Fixed a/c= .200E+00):
Pri. Load   a_init      a_crit      a_inst      da(tear)    P/P0_init   P/P0_crit   P/P0_inst
.100E+03    .276E-01    .567E-01    .108E+00    .510E-01    .100E+01    .100E+01    .100E+01

        ERROR[JSC01]: exceeds plastic collapse load!
```

```
a= .198E-01, c= .540E+00 Smax= .130E+03


ERROR[JSC01]: exceeds plastic collapse load!
a= .198E-01, c= .540E+00 Smax= .130E+03


ERROR[JSC01]: exceeds plastic collapse load!
a= .168E-02, c= .540E+00 Smax= .130E+03

.130E+03  .397-308  .397-308  .510E-01                    *( 1)
   * ( 1) : exceed plastic collapse load!

   ********** ------------------------- **********
   < PRESS RETURN TO CONTINUE >

 Press RTN to continue (or P and RTN to obtain the print file)
 (Note: The results will be in the output file.
  Use the appropriate Print command for your machine)
SYSTEM_PROMPT>P
```

The first set of results, for a primary load of 100 ksi, shows calculated values of the significant crack depths (initiation depth, critical depth, instability depth, and the tear length). The second set of results, for a primary load of 130 ksi, demonstrates the error messages that the user receives when the input primary load exceeds the plastic collapse load.

The batch file just created can be used to re-run the program using option 2. For reference, the content of the batch file is listed below.

```
fasc01.out   Output file name*12
 2   1=US units; 2=SI units
sc     Crack Model Type
1    Crack Model Number
1     1=tension, 2=bending
 .1000E+01   Thickness
 .2000E+02   Width
 .3000E+05   Elastic Young"s modulus
  .300   Poisson"s ratio
1.000   Alpha
 .1000E+03   Sigma0
10.000   n
 .1000E+03 material yield stress
 .1500E+03 material ultimate stress
  1   1: const. asp. 2: const. length
 .2000E+00   constant aspect ratio
  1   1: crit. crack 2: crit. load
  2   1: brittle, 2: ductile
 .2000E+00   matl toughness
  1   1: quad. 2: power
 .1750E+00    dj0 -- quadratic
 .1500E+02    dj1 -- quadratic
-.7500E+02    dj2 --  quadratic
 .1000E+00    da(max) -- quadratic
```

```
1    1= interactively input, 2= create a table
 2    1= pri., 2=pri. & sec.
 1    0:stop, 1: cont
.1000E+03    loading stress
 .0000E+00  Non-Dimensional position
 .1000E+03  Stress value
 .2000E+00  Non-Dimensional position
 .9600E+02  Stress value
 .4000E+00  Non-Dimensional position
 .8400E+02  Stress value
 .6000E+00  Non-Dimensional position
 .6400E+02  Stress value
 .8000E+00  Non-Dimensional position
 .3600E+02  Stress value
 .1000E+01  Non-Dimensional position
 .0000E+00  Stress value
-.1000E+01  Non-Dimensional position
 1    0:stop, 1: cont
.1300E+03    loading stress
 0    0:stop, 1: cont
P    P(1st col.): to print
 0    1:to resume, 0: stop
```

10.3 How to Run an Elastic-Plastic Fatigue Crack Growth Calculation

The user should refer to Figure 15 as the roadmap to help them understand the main program flow for the elastic-plastic fatigue crack growth computation. After the program is executed and the screen displays the main menu of NASGRO, option 7 should be chosen to initiate an EPFCG calculation. In this release, the main menu and the user input (after **SYSTEM_PROMPT>**) should be

```
Enter one of the following options:

  1   Safe Life Analysis
  2   Critical crack size computation
  3   Stress-intensity factor solution
  4   da/dt life analysis (e.g., for glass)
  5   Elastic-plastic J computation
  6   Elastic-plastic failure analysis
  7   Elastic-plastic fatigue life analysis
  0   Terminate session

  Notes:
  1.  Once an analysis option is chosen and data input
    is in progress, entering a minus sign (-)
    will cause moving back to the previous prompt.
  2.  Always press Enter key to complete an entry.
SYSTEM_PROMPT> 7
```

A sub-menu for option 7 now appears. It lists the available ways of NASGRO file processing. Option 0 prompts the user for input without saving. Option 1 saves the input as a separate file that can be run later as a batch file. Option 2 is the option to run the program with the batch file created using option 1. Option 3 lets users modify the batch

file and then use option 2 to re-run the program. In this example, option 1 was used to step by step create a batch file for future reference.

```
Enter type of session for elastic-plastic J module:

0   Interactive - input and computation
1   Interactive input while creating a batch file
2   batch - computing only (run using a batch data file)
3   Edit an existing batch file
  (Note: option 1 must be used before option 2 or 3)
SYSTEM_PROMPT> 1
```

Then the program proceeds to prompt for the filenames of the batch and data output files, as well as the units used in the analysis.

```
Enter the name of batch file to use (up to 12 alpha-numeric characters):
 Enter RTN only to return to main menu
SYSTEM_PROMPT> fgsc01.dat

 Enter file name for output (up to 12 alpha-numeric characters):
SYSTEM_PROMPT> fgsc01.out

Enter type of units:

1   U.S. Customary Units [inches, ksi, ksi sqrt(in)]
2   SI Units (International System) [mm, Mpa, Mpa sqrt(mm)]
SYSTEM_PROMPT> 2
```

After filenames for file processing and units have been provided, NASGRO will prompt for the model type, the primary loading type, geometric dimensions, and parameters describing nonlinear material properties used in the elastic-plastic fatigue analysis. The available primary loading type depends on the model type that was chosen. In this example of model type SC01, the primary load can be either tensile or bending. For the material behavior, in addition to yield stress and ultimate stress, NASGRO requires Ramberg-Osgood material parameters to describe the nonlinear material stress-strain relation given by $\varepsilon/\varepsilon_0 = \sigma/\sigma_0 + \alpha(\sigma/\sigma_0)^n$ where α, n, ε_0, and σ_0 are material constants.

Under elastic-plastic cycling, the constitutive properties of some materials change gradually from their monotonic values towards stable cyclic values due to cyclic hardening or softening. The resulting stable cyclic Ramberg-Osgood properties are sometimes denoted by adding a "prime" to the material constant symbols: α', σ_0', ε_0', n'. The selection of monotonic or cyclic constitutive properties can have a significant effect on the calculated values of ΔJ_{eff}. In general, cyclic properties should be chosen when the (uncracked) component in question experiences reversed plastic deformation. In the absence of reversed plastic deformation, monotonic properties are generally an appropriate choice. When in doubt, calculations should be completed with both monotonic and cyclic properties, and the more conservative answer selected. Guidelines for the estimation of these material properties, along with further discussion of these issues, are provided in Section 3.5.2 of the main body of the final report.

The interactive session continues as follows.

```
Enter a Model type from the following :

 TC  Through Crack
 CC  Corner Crack
 EC  Embedded Crack
 SC  Surface Crack
SYSTEM_PROMPT> SC

 Enter a Number to select a SURFACE crack case:

  1 .. SC01  -  In finite width plate
SYSTEM_PROMPT> 1

 SC01

 Geometric Model in use: SC01

 Enter a Number to select the loading option for the SC01 geometry:

  1 .. TENSION  -  surface crack in remote tension
  2 .. BENDING  -  surface crack under bending in the thickness direction
SYSTEM_PROMPT> 1

 Enter Thickness, t:
SYSTEM_PROMPT> 0.2055

 Thickness, t =     .2055

 Enter Width, W:
SYSTEM_PROMPT> 1.24

 Width, W =    1.2400

      ELASTIC-PLASTIC FATIGUE LIFE CALCULATION FOR SC01
      ---------------------------------------------
              DATE: 11-Jun-98  TIME: 10:19:24
          (computed: NASA/FLAGRO Version 3.00, October 1995.)
         Elastic-Plastic Fracture Module (EPFM) V.1.01, Feb. 1998
              SI units [mm, Mpa, Mpa sqrt(mm)]


       Input  Filename = fgsc01.dat
       Output Filename = fgsc01.out

       Plate Thickness, t =     .2055
        *  Width, W    =    1.2400

 ****************************************************************
 Specify the Nonlinear Material Behavior

    Eps/Eps0=Sigma/Sigma0+alpha*(Sigma/Sigma0)**n

 with Elastic Modulus defined by Sigma0/Eps0
 Enter Elastic Modulus:
SYSTEM_PROMPT> 0.2969e+5
```

```
 Elastic Modulus= .2969E+05

 Enter Poisson's Ratio:
SYSTEM_PROMPT> 0.3

 Poisson's Ratio= .3000E+00

 Enter alpha:
SYSTEM_PROMPT> 1.0

 Alpha =  .1000E+01

 Enter Sigma0:
SYSTEM_PROMPT> 158.3

 Sigma0 =  .1583E+03

 Enter n:
SYSTEM_PROMPT> 6.15

 n =  .6150E+01

 Enter Material Yield Stress
SYSTEM_PROMPT> 158.3

 Material Yield Stress =       158.30

 Enter Material Ultimate Stress
SYSTEM_PROMPT> 211.7

 Material Ultimate Stress =       211.70
      Model Code= SC01 under uniform tension
```

It is necessary to create a fatigue load spectrum or schedule for the fatigue analysis. A block case is defined as one cyclic load step with user-specified maximum and minimum loads and the number of cycles this load step is to be applied. A fatigue load spectrum or schedule consists of a random combination of user-defined block cases and the corresponding number of times to be applied. The following illustrates the interactive session of how to build a fatigue load spectrum. Loads are specified as nominal or linear-elastic stresses.

```
BLOCK CASE DEFINITION (max. 60 cases)
 Block Case ID   1: define MAXIMUM cyclic load
    1 -- Primary load only
    2 -- Primary and secondary loads
   -1 -- Terminate input
SYSTEM_PROMPT> 1

 PRIMARY LOAD:
 Enter stress, S0: Tensile Stress
SYSTEM_PROMPT> 135.0

        NO SECONDARY LOAD SPECIFIED!
 Block Case ID   1: define MINIMUM cyclic load
```

```
    1 -- Primary load only
    2 -- Primary and secondary loads
SYSTEM_PROMPT> 1

 PRIMARY LOAD:
 Enter stress, S0: Tensile Stress
SYSTEM_PROMPT> -135.0

        NO SECONDARY LOAD SPECIFIED!
 Specify number of cycles with max/min load applied in Blk Case ID  1
SYSTEM_PROMPT> 1

 Block Case ID   2: define MAXIMUM cyclic load
    1 -- Primary load only
    2 -- Primary and secondary loads
   -1 -- Terminate input
SYSTEM_PROMPT> 1

 PRIMARY LOAD:
 Enter stress, S0: Tensile Stress
SYSTEM_PROMPT> 50.0

        NO SECONDARY LOAD SPECIFIED!
 Block Case ID   2: define MINIMUM cyclic load
    1 -- Primary load only
    2 -- Primary and secondary loads
SYSTEM_PROMPT> 1

 PRIMARY LOAD:
 Enter stress, S0: Tensile Stress
SYSTEM_PROMPT> -80.0

        NO SECONDARY LOAD SPECIFIED!
 Specify number of cycles with max/min load applied in Blk Case ID  2
SYSTEM_PROMPT> 3

 Block Case ID   3: define MAXIMUM cyclic load
    1 -- Primary load only
    2 -- Primary and secondary loads
   -1 -- Terminate input
SYSTEM_PROMPT> -1

        BLOCK CASE DEFINITION:
 Blk Cse.   Maximum Load Values     Minimum Load Values        Cycles
                Primary Load              Primary Load              1
    1          I          Si             I          Si
               0      0.1350E+03         0      -0.1350E+03
               1      0.0000E+00         1       0.0000E+00
               2      0.0000E+00         2       0.0000E+00
               3      0.0000E+00         3       0.0000E+00
                Primary Load              Primary Load              3
    2          I          Si             I          Si
               0      0.5000E+02         0      -0.8000E+02
               1      0.0000E+00         1       0.0000E+00
               2      0.0000E+00         2       0.0000E+00
               3      0.0000E+00         3       0.0000E+00
```

```
Define the Load Spectrum or Schedule using previously-defined block cases
 (max. 80 block cases):
  Input the Block Case ID for the Schedule (end with -1):
SYSTEM_PROMPT> 2

 How many times to apply Block Case ID 2 ?
SYSTEM_PROMPT> 5

  Input the Block Case ID for the Schedule (end with -1):
SYSTEM_PROMPT> 1

 How many times to apply Block Case ID 1 ?
SYSTEM_PROMPT> 2

 Input the Block Case ID the Schedule (end with -1):
SYSTEM_PROMPT> -1


        DEFINITION OF LOAD SPECTRUM (or SCHEDULE):
            Blk. Case ID          No. of Times Applied
                2                        5
                1                        2
```

NASGRO will then prompt for the Paris law fatigue parameters C_0 and m_0 and the fracture toughness J_{mat} which determines the onset of failure. Note that the fatigue life module currently defines failure when $J_{max} > J_{mat}$ at either crack tip location, conservatively taking no credit for rising toughness with tearing in ductile materials (resistance curve analysis). The parameters C_0 and m_0 in the Paris equation (Eqn. (28)) $da/dN = C_0(\Delta K)^{m_0}$ are transformed internally into the material constants that govern fatigue crack growth characterized by ΔJ (see Section 2.5). The baseline crack closure parameter, U_0, consistent with the experimental conditions under which the Paris law constants were derived also needs to be specified. A typical value for U_o when baseline FCG data satisfy plane strain conditions is 0.75. The values of α_c in Newman's closure equation are also needed for each crack tip position. It is currently recommended to select the same value of α_c at both crack tip positions. The interactive session is illustrated as follows.

```
Input matl toughness value J(mat):
SYSTEM_PROMPT> 0.433

        Toughness = .4330E+00

 Input the parameters for the Paris equation
   da/dN=C(dK)^m
 Input C in Paris Law:
SYSTEM_PROMPT> 0.7066e-10

 Input m in Paris Law:
SYSTEM_PROMPT> 3.235

 Input the baseline U0 (possible value 0.75):
```

```
SYSTEM_PROMPT> 0.819

 Input alp for a tip (from 1 to 3) :
SYSTEM_PROMPT> 3.0

 Input alp for c tip (from 1 to 3) :
SYSTEM_PROMPT> 3.0
```

Once the initial crack lengths, the maximum allowable number of times the load spectrum is to be repeated and the print interval are set, NASGRO will start the computation, show the results on screen, and write these to the output file. Step by step interactive input for the forgoing is shown below.

```
Input initial CRACK length(s)
 Input a:
SYSTEM_PROMPT> 0.112e-1

 Input c:
SYSTEM_PROMPT> 0.112e-1

 Specify max. no. of SCHEDULES, N_max, to terminate fatigue analysis?
SYSTEM_PROMPT> 200
 Max. No. of Schedules =     200

 Specify print interval, N_print, to control output?
SYSTEM_PROMPT> 20
 Print interval =     20 schedules

        RESULTS OF FATIGUE ANALYSIS:
Skdl.     a          c        D_Jeff(a)  D_Jeff(c)  Jmax(a)    Jmax(c)   U(a)  U(c)
  20  1.136E-02  1.133E-02  1.702E-02  1.646E-02  1.512E-02  1.796E-02  0.43  0.44
  40  1.151E-02  1.146E-02  1.721E-02  1.672E-02  1.529E-02  1.823E-02  0.43  0.44
  60  1.167E-02  1.159E-02  1.740E-02  1.697E-02  1.547E-02  1.850E-02  0.43  0.44
  80  1.184E-02  1.173E-02  1.760E-02  1.723E-02  1.565E-02  1.877E-02  0.43  0.44
 100  1.201E-02  1.187E-02  1.780E-02  1.749E-02  1.583E-02  1.905E-02  0.43  0.44
 120  1.218E-02  1.201E-02  1.800E-02  1.776E-02  1.602E-02  1.933E-02  0.43  0.44
 140  1.235E-02  1.216E-02  1.822E-02  1.803E-02  1.622E-02  1.962E-02  0.43  0.44
 160  1.253E-02  1.231E-02  1.844E-02  1.831E-02  1.642E-02  1.992E-02  0.43  0.44
 180  1.271E-02  1.246E-02  1.866E-02  1.859E-02  1.662E-02  2.022E-02  0.43  0.44
 200  1.289E-02  1.262E-02  1.889E-02  1.888E-02  1.683E-02  2.052E-02  0.43  0.44

EXCEED MAX. NO. OF LOAD SPECTRUMS (  200) with a= .1289E-01, c= .1262E-01
      , J_bury(max)= .1683E-01, J_surf(max)= .2052E-01, J(mat)= .4330E+00
      , total no. of cycles=   3400

   0  *********_____________________**********
   < PRESS RETURN TO CONTINUE >

 Press RTN to continue (or P and RTN to obtain the print file)
 (Note: The results will be in the output file.
  Use the appropriate Print command for your machine)
SYSTEM_PROMPT> P
```

The batch file created by NASGRO, in this case "fgsc01.dat", can be modified using any text editor or the line editing function embedded in NASGRO. For reference, the following lists the content of the batch file just created.

```
fgsc01.out    Output file name
2  1=US units; 2=SI units
sc     Crack Model Type
1    Crack Model Number
1   1=tension, 2=bending
 .2055E+00   Thickness
 .1240E+01   Width
 .2969E+05   Elastic Young"s modulus
  .300   Poisson"s ratio
1.000  Alpha
 .1583E+03   Sigma0
6.150   n
  .1583E+03 material yield stress
  .2117E+03 material ultimate stress
   1 1: p(max), 2:p+s(max)
 .1350E+03    loading stress
   1 1: p(min), 2:p+s(min)
-.1350E+03    loading stress
    1 no. of cycles
   1 1: p(max), 2:p+s(max)
 .500E+02    loading stress
   1 1: p(min), 2:p+s(min)
-.800E+02    loading stress
3  no. of cycles
  -1   terminate input
   2 block case no.
     5 no. of times
   1 block case no.
     2 no. of times
  -1 block case no.
  .4330E+00    Jmat
  .7066E-10    C in Paris Law
  .3235E+01    m in Paris Law
  .8190E+00   :baseline U0
  .3000E+01   : alp_bury
  .3000E+01   : alp_surf
  .1120E-01   initial a
  .1120E-01   initial c
200  max. no. of cycles
20   print interval
 P    P(1st col.): to print
 0 1:to resume, 0: stop
```

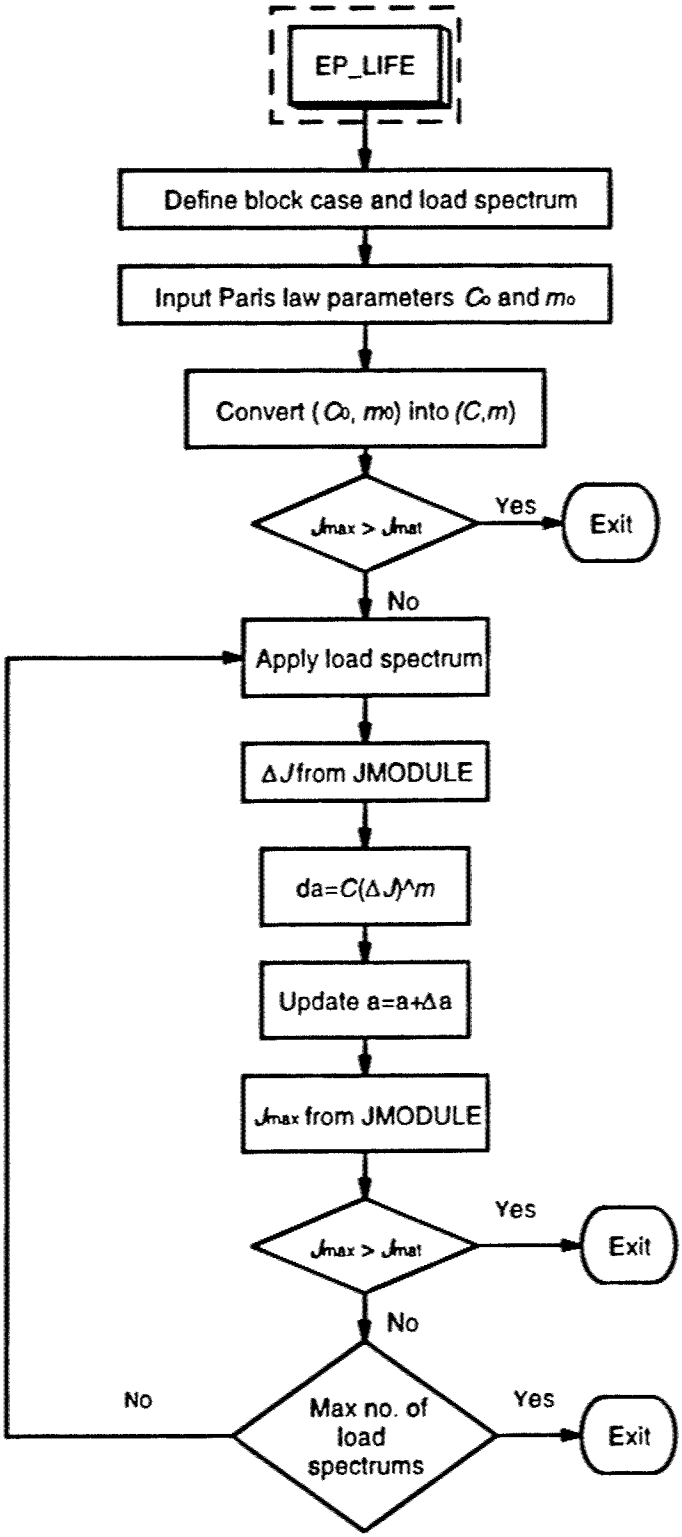

Figure 15. Flow chart for the elastic plastic fatigue crack growth and life prediction analysis in the NASGRO EPFM module.

11.0 Program Validation

11.1 Validation of the RSM J Solutions

Validation of the J solutions in NASGRO is accomplished by comparing the NASGRO results with the results of elastic-plastic finite element computations of J. The J solutions for geometries TC01 and TC02 are compared with the EPRI handbook solutions (Kumar et al., 1981), the geometries SC01 and CC01 under tension with new solutions from the current contract and solutions from Sharobeam and Landes (1995) and geometry SC01 under bending with the Yagawa et al. (1993) solutions. There are no finite element solutions available presently to substantiate the J solutions for geometry CC01 under bending, and EC01 under tension.

<u>TC01 under Tension and TC02 under Tension and Bending</u>

The computed h_1 values evaluated in the EPFM module of NASGRO using the RSM are denoted by $(h_1)^{RSM}$ and are defined in the following equations. They are compared with values of h_1 from EPRI solution scheme as defined in Tables 1-6. The J_p^{RSM} solutions used to derive $(h_1)^{RSM}$ for the TC01 and TC02 models were derived using the optimized RSM.

TC01 under tension:

$$(h_1)^{RSM} = \frac{J_p^{RSM}}{\alpha\sigma_o\varepsilon_o c\left(1-\frac{c}{b}\right)\left(\frac{P}{P_o}\right)^{n+1}} \tag{77}$$

with $b = W/2$. The comparisons are shown in Figures 16 and 17.
TC02 under tension:

$$(h_1)^{RSM} = \frac{J_p^{RSM}}{\alpha\sigma_o\varepsilon_o c\left(1-\frac{c}{b}\right)\left(\frac{P}{P_o}\right)^{n+1}} \tag{78}$$

with b=W. The validation results can be found in Figures 18 and 19.
TC02 under bending:

$$(h_1)^{RSM} = \frac{J_p^{RSM}}{\alpha\sigma_o\varepsilon_o b\left(1-\frac{c}{b}\right)\left(\frac{M}{M_o}\right)^{n+1}} \tag{79}$$

with b=W. Figures 20 and 21 contain the comparison between $(h_1)^{RSM}$ and h_1 from EPRI.

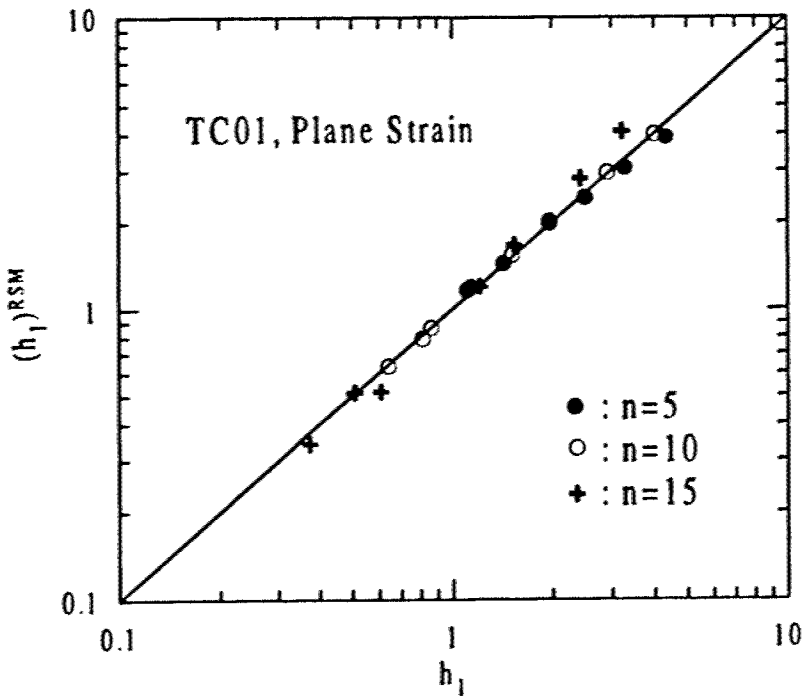

Figure 16. Comparison of computed h_1 values from optimized RSM with EPRI results; TC01, plane strain under tension.

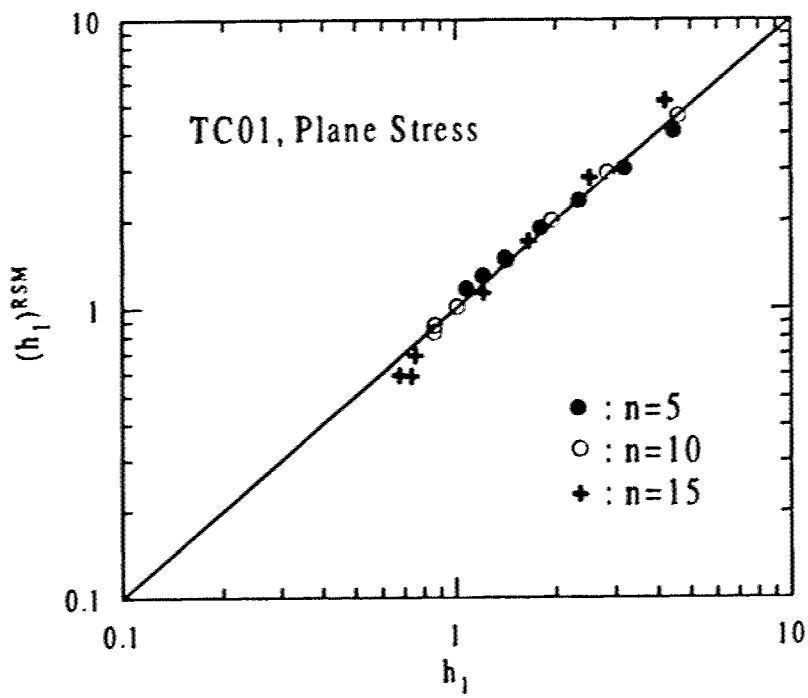

Figure 17. Comparison of computed h_1 values from optimized RSM with EPRI results; TC01, plane stress under tension.

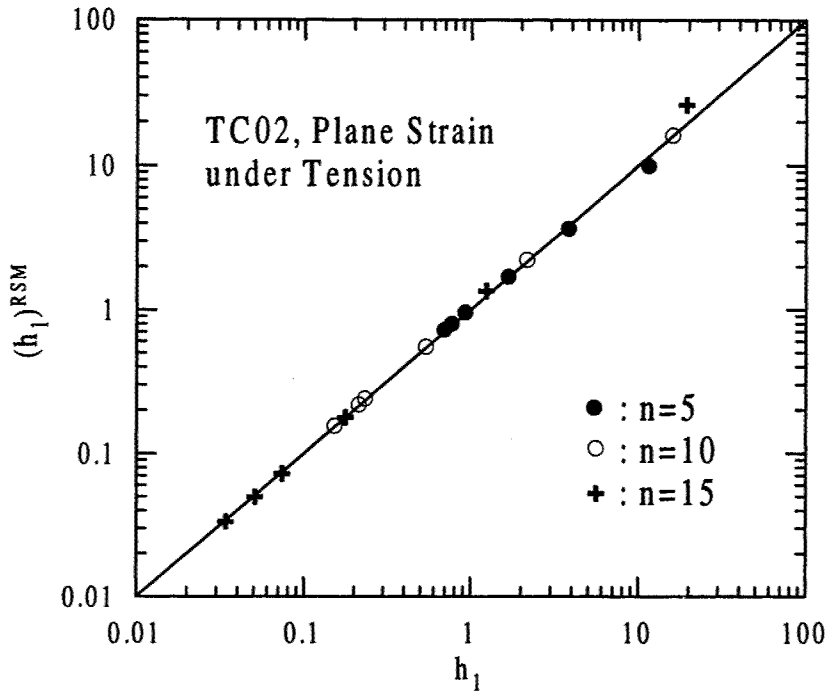

Figure 18. Comparison of computed h_1 values from optimized RSM with EPRI results; TC02, plane strain under tension.

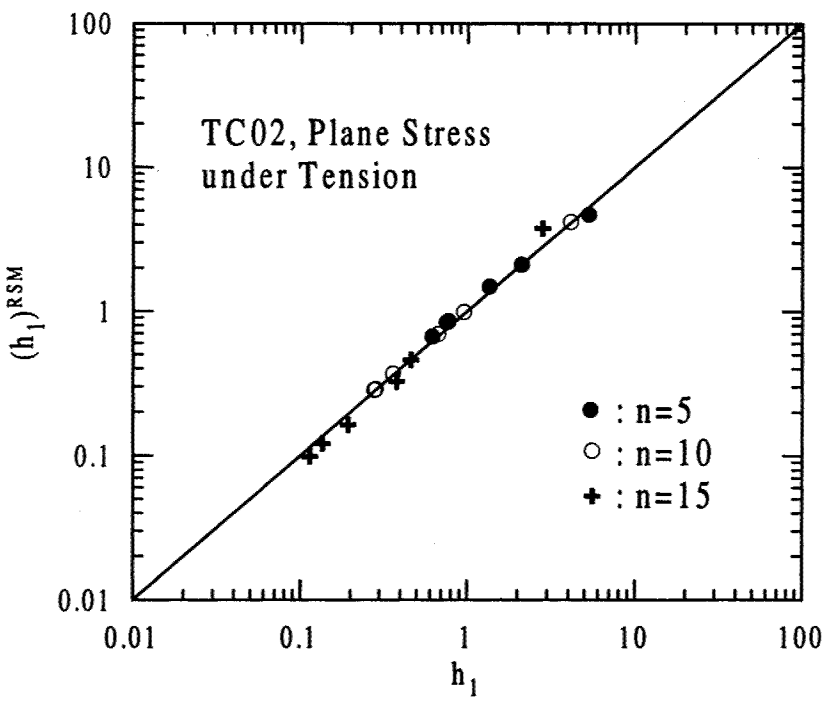

Figure 19. Comparison of computed h_1 values from optimized RSM with EPRI results; TC02, plane stress under tension.

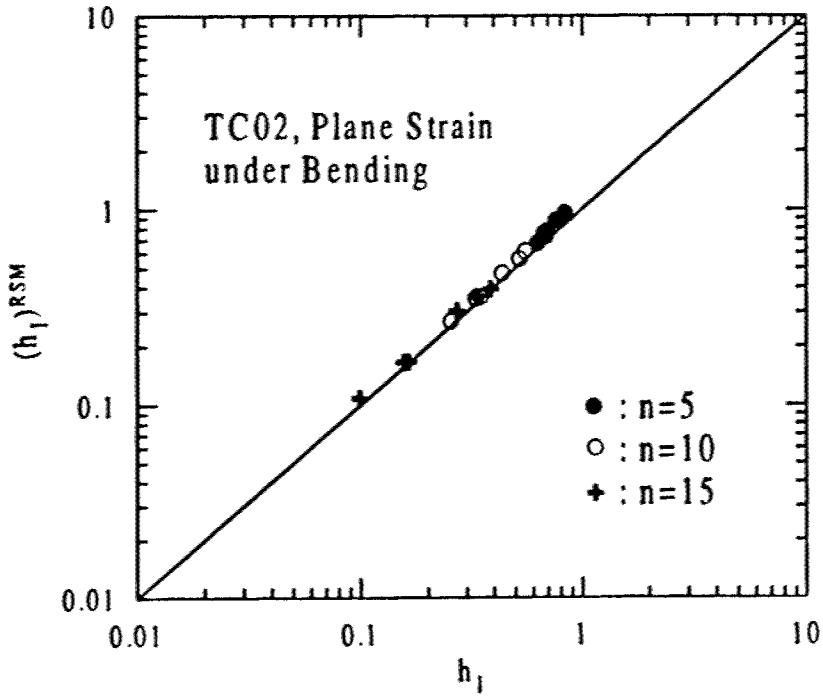

Figure 20. Comparison of computed h_I values from optimized RSM with EPRI results; TC02, plane strain under bending.

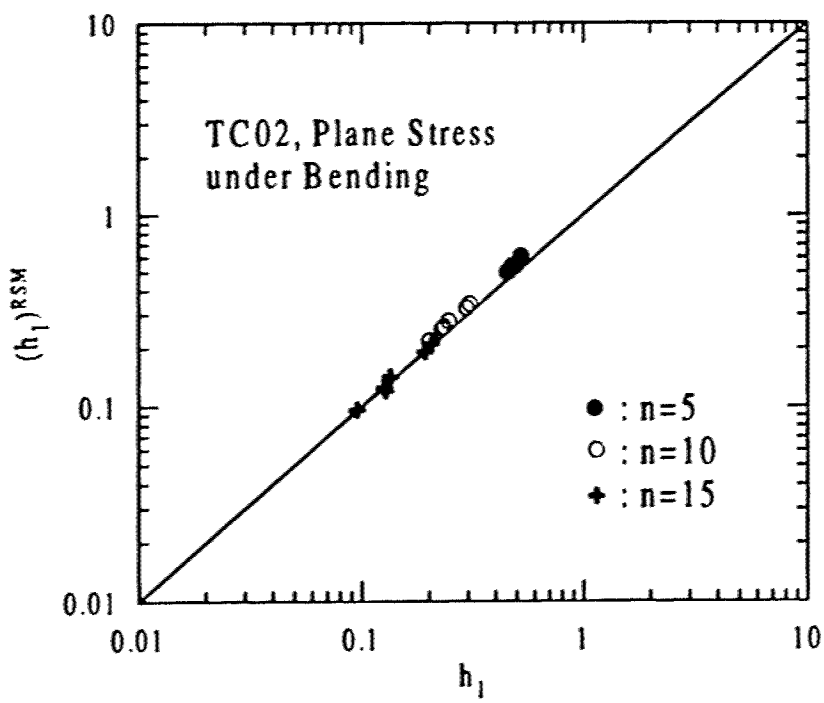

Figure 21. Comparison of computed h_I values from optimized RSM with EPRI results; TC02, plane stress under bending.

SC01 under Tension and CC01 under Tension

Validation of optimized RSM

In this validation, J_p^{RSM} evaluated from equation (44) is based on optimized results of V and P_o^* derived from original FE results (see Appendix C) by Orient[1]. The numerical values of $(h_1)^{RSM}$ are obtained from

$$(h_1)^{RSM} = \frac{J_p^{RSM}}{\alpha\sigma_o\varepsilon_o t\left(\frac{\sigma}{\sigma_o}\right)^{n+1}} \tag{80}$$

and these are validated against Orient's h_1 values, $(h_1)_{Orient}$. The data matrix of these results for h_1 values is shown in Tables 16 and 17 for SC01 and CC01 under tension respectively where, in all cases, c/b=0.25. There are two numerical values of J_p^{RSM}; one for the crack tip location a corresponding to Φ=90° for SC01 (the deepest point) and Φ=81° for CC01 (a near surface point) and the other one corresponding to the near surface crack tip location c corresponding to Φ=9° for both SC01 and CC01. In all cases, the near surface values of J_e that are needed to evaluate J_p^{RSM} were based on the NASGRO surface K solutions. The validation against the finite element results for the SC01 and CC01 geometries are shown in Figures 22-25. These results validate the optimized RSM approach to surface and corner cracks and demonstrate the maximum accuracy that can be expected from using the RSM to derive J solutions for model types SC01 and CC01 in the absence of optimized values for P_o^* and V, as is done in the next section.

Table 16. Matrix of finite element h_1 results for SC01 under tension and c/b=0.25.

		$h_1(\Phi=90°)$			$h_1(\Phi=9°)$		
a/t	*a/c*	*n=5*	*n=10*	*n=15*	*n=5*	*n=10*	*n=15*
0.2	0.2	1.117	1.416	1.644	0.252	0.320	0.370
0.2	0.6	0.672	0.847	0.981	0.352	0.416	0.465
0.2	1.0	0.435	0.556	0.646	0.383	0.450	0.503
0.5	0.2	8.516	14.811	22.309	2.139	4.512	7.615
0.5	0.6	2.976	5.186	7.881	1.916	3.205	4.808
0.5	1.0	1.630	2.804	4.198	1.658	2.599	3.738
0.8	0.2	19.369	47.496	98.941	11.273	29.512	63.511
0.8	0.6	6.178	14.780	30.806	6.449	13.685	25.890
0.8	1.0	3.270	7.625	15.533	4.728	9.472	17.231

[1] In NASGRO, for SC01 and CC01 under tension, a hybrid reference stress method is applied as discussed in Section 3.2. Validation of the hybrid method is presented in the next sub-section.

Table 17. Matrix of finite element h_1 results for CC01 under tension and c/b=0.25.

		$h_1(\Phi=81°)$			$h_1(\Phi=9°)$		
a/t	*a/c*	*n=5*	*n=10*	*n=15*	*n=5*	*n=10*	*n=15*
0.2	0.2	1.337	1.838	2.218	0.269	0.363	0.439
0.2	0.6	0.745	0.913	1.077	0.436	0.552	0.648
0.2	1.0	0.486	0.568	0.659	0.456	0.565	0.657
0.5	0.2	10.408	21.153	32.896	2.620	6.230	10.808
0.5	0.6	3.687	6.399	9.751	2.351	4.069	6.137
0.5	1.0	2.016	3.189	4.673	2.032	3.208	4.611
0.8	0.2	38.762	109.398	260.682	16.218	50.183	130.370
0.8	0.6	14.105	33.628	78.743	9.171	21.145	46.897
0.8	1.0	7.510	17.090	37.577	6.621	14.118	29.158

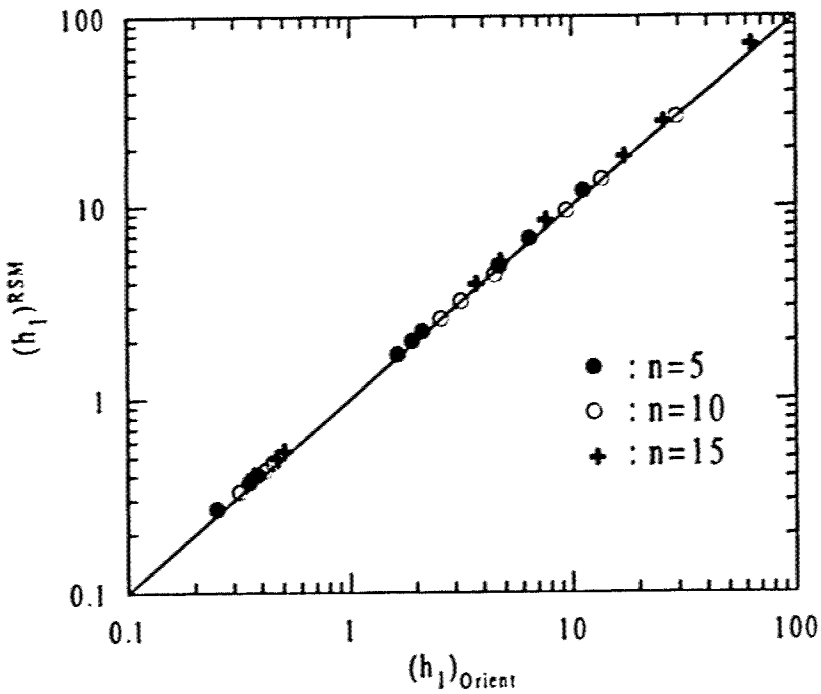

Figure 22. Comparison of predicted h_1 from optimized RSM with FE results for the near surface crack tip location c (Φ=9°); surface crack under tension.

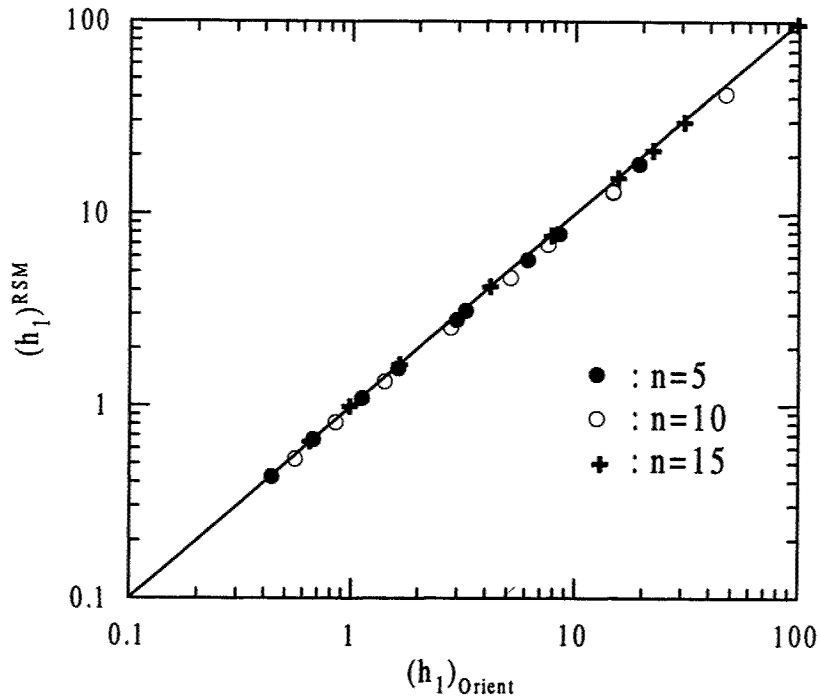

Figure 23. Comparison of predicted h_1 from optimized RSM with FE results for the crack tip location a (Φ=90°); surface crack under tension.

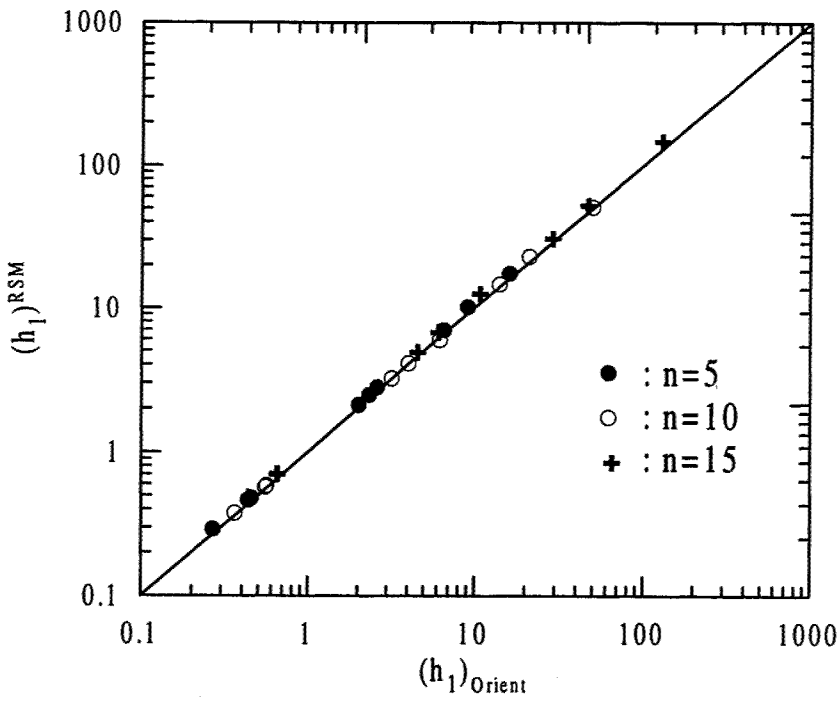

Figure 24. Comparison of predicted h_1 from optimized RSM with FE results for the near surface crack tip location c (Φ=9°); corner crack under tension.

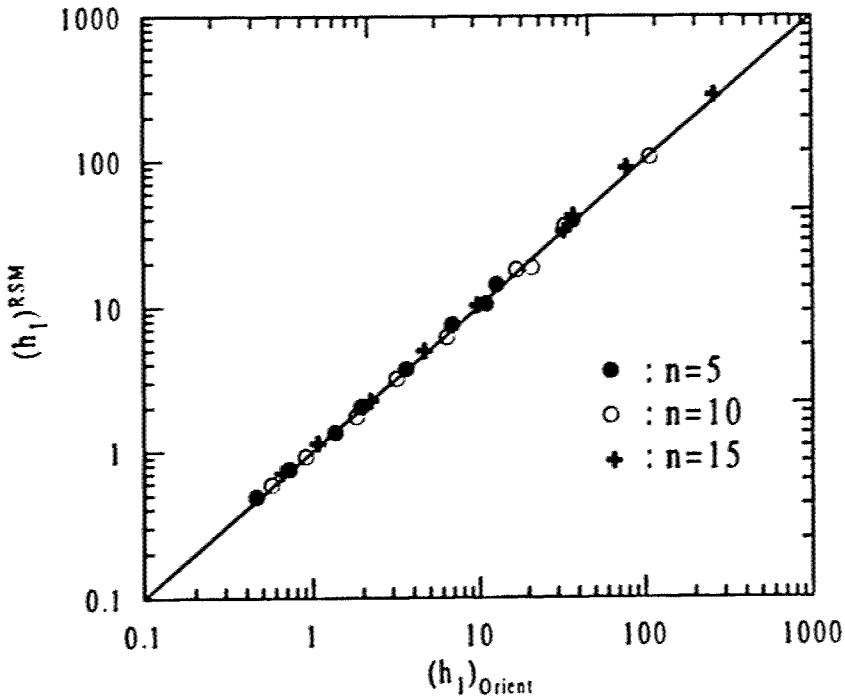

Figure 25. Comparison of predicted h_1 from optimized RSM with FE results for the near surface crack tip location a (Φ=81°); corner crack under tension.

Validation of the hybrid RSM module of NASGRO

In this validation, the $(h_1)^{RSM}$ results derived from the EPFM calculation of NASGRO are compared with original finite element results (Tables 16 and 17). The results are presented in Figures 26-29. In the calculations of $(h_1)^{RSM}$, the net section yield load is based on area reduction (equation (55) and Tables 9 and 10), and the value of V with its associated model type and crack tip position was assumed constant (see equation (45)). The corresponding value used in the analysis can also be found in the figure. Note that arithmetic mean values of optimized V values at crack tip positions a and c were separately used in the RSM solutions for SC01 under tension, while, for CC01 under tension, the maximum of both arithmetic mean values denoted by V_{max} was used. The results from the EPFM module are in good agreement with the FE results even though the hybrid approach was used. The good agreement is demonstrated by the narrow distribution bandwidth of data points which are scattered evenly about the one-to-one line.

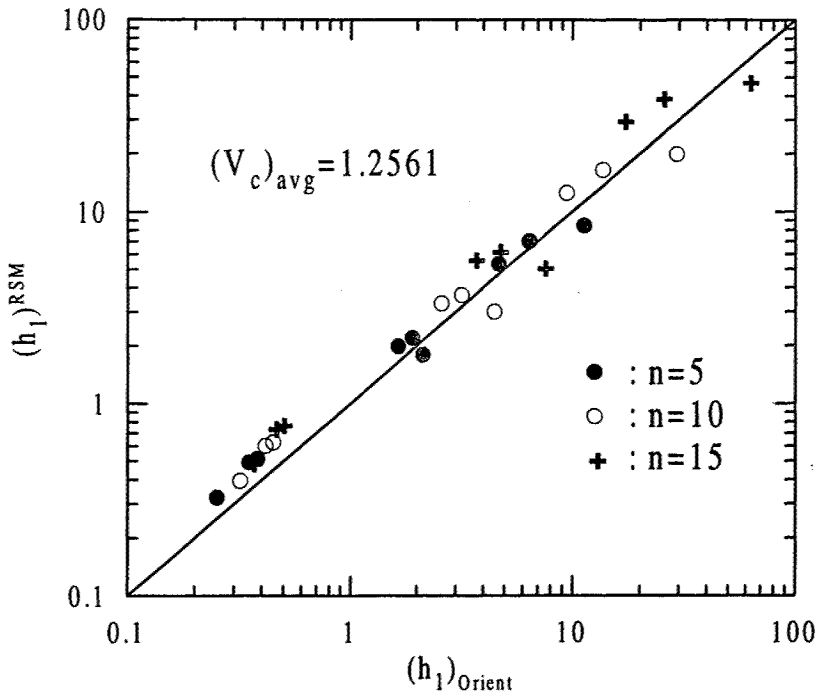

Figure 26. Comparison of predicted h_1 from the EPFM of NASGRO with FE results for the near surface crack tip location c (Φ=9°); surface crack under tension.

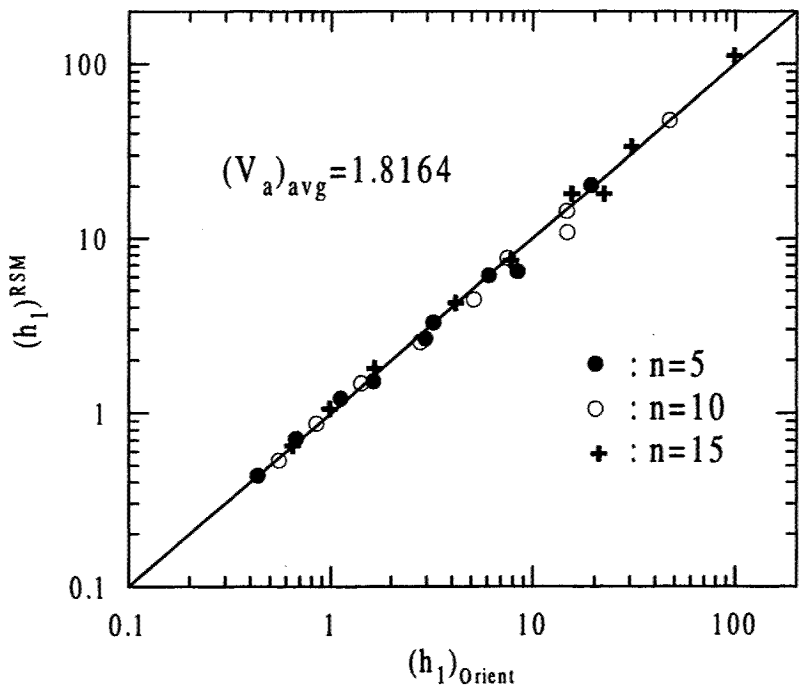

Figure 27. Comparison of predicted h_1 from the EPFM of NASGRO with FE results for the crack tip location a (Φ=90°); surface crack under tension.

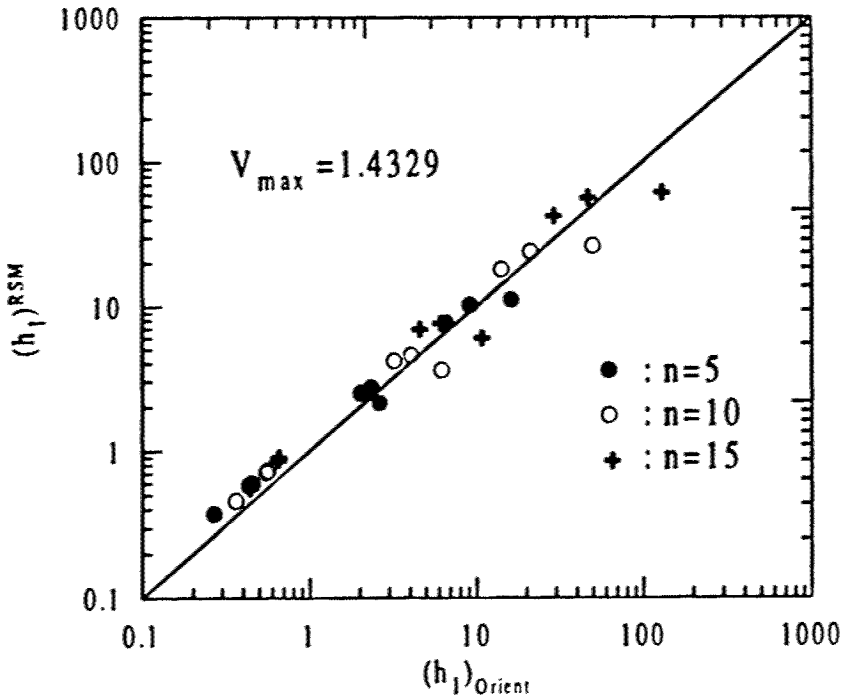

Figure 28. Comparison of predicted h_1 from the EPFM of NASGRO with FE results for the near surface crack tip location c (Φ=9°); corner crack under tension.

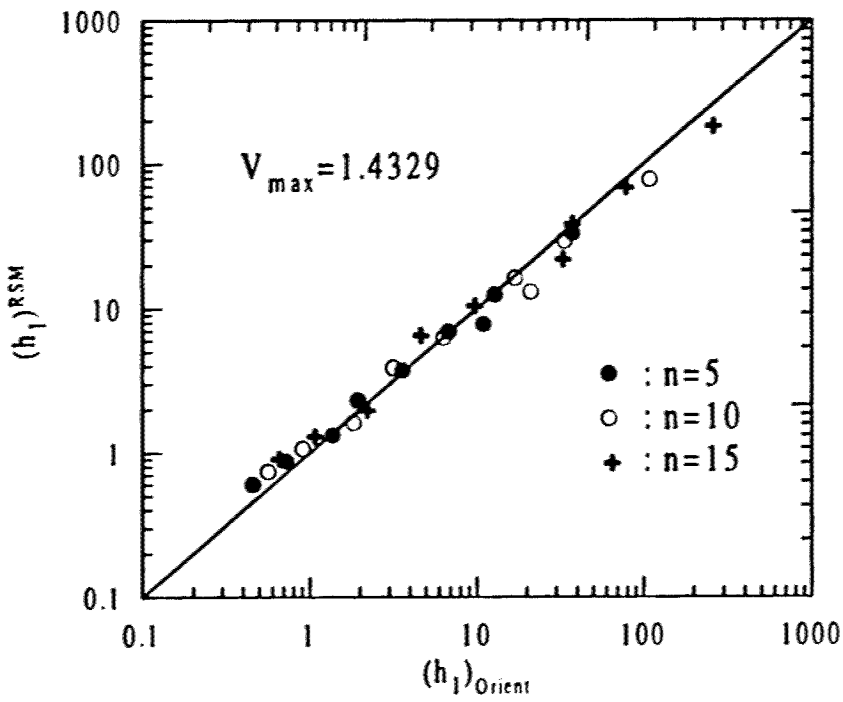

Figure 29. Comparison of predicted h_1 from the EPFM of NASGRO with FE results for the near surface crack tip location a (Φ=81°); corner crack under tension.

Additional validation of the hybrid RSM module

Further validation for the model type SC01 under tension is provided by comparing the results for $(h_1)^{RSM}$ derived from the EPFM module with the finite element results of Sharobeam and Landes (1995), $(h_1)_{Sharobeam}$. Sharobeam investigated an almost random combination of geometric ratios; i.e., *h/t*, *b/c*, *a/t*, and *a/c* (see Table 18). The comparisons[2] are presented in Figures 30 and 31. Note that the validation for the near surface crack tip location *a* is performed at $\Phi=7.5°$. As expected from the comparison with Orient's results, the results for the deepest point obtained from the EPFM module of NASGRO agree well with Sharobeam's finite element results (Figure 31). For the near surface crack tip where plane stress deformation prevails, the RSM solution gives a conservative overestimate of h_1, again consistent with the comparison between the RSM results and Orient's solutions.

Table 18. Matrix of Sharobeam's finite element h_1 results for SC01 under tension.

h/t	*b/c*	*a/t*	*a/c*	*n*	$h_1(\Phi=90°)$	$h_1(\Phi=7.5°)$
8	11.429	0.700	2.000	5	0.772	1.682
4	5.425	0.600	1.627	5	1.007	1.757
4	3.397	0.589	1.000	15	8.313	8.255
4	3.951	0.506	1.000	10	2.887	2.766
8	4.000	0.500	0.500	5	3.760	2.271
12	6.849	0.400	0.457	5	2.352	1.110
8	17.133	0.400	1.713	5	0.472	0.797
4	5.425	0.300	0.814	5	0.874	0.667
4	9.385	0.213	1.000	5	0.436	0.392
4	6.053	0.160	0.484	5	0.542	0.234
4	2.439	0.820	1.000	5	5.172	10.497
4	2.283	0.600	0.685	10	15.268	12.596
4	2.994	0.668	1.000	10	8.103	9.809
4	4.378	0.800	1.751	15	4.742	9.945
16	11.978	0.668	1.000	5	2.097	2.518

[2] For *a/c*>1.2, the validation was not performed because of the validity limitations imposed by the *K* solutions in NASGRO for model type SC01 (see Table 15).

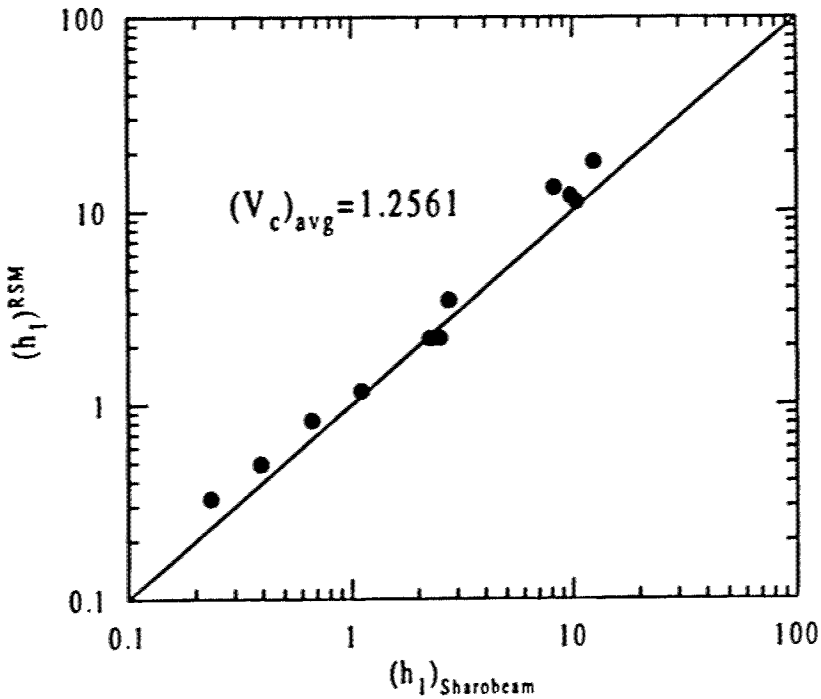

Figure 30. Comparison of predicted h_1 from the EPFM of NASGRO with Sharobeam's FE results for the near surface crack tip location c (Φ=7.5°) for the case of SC01 under tension.

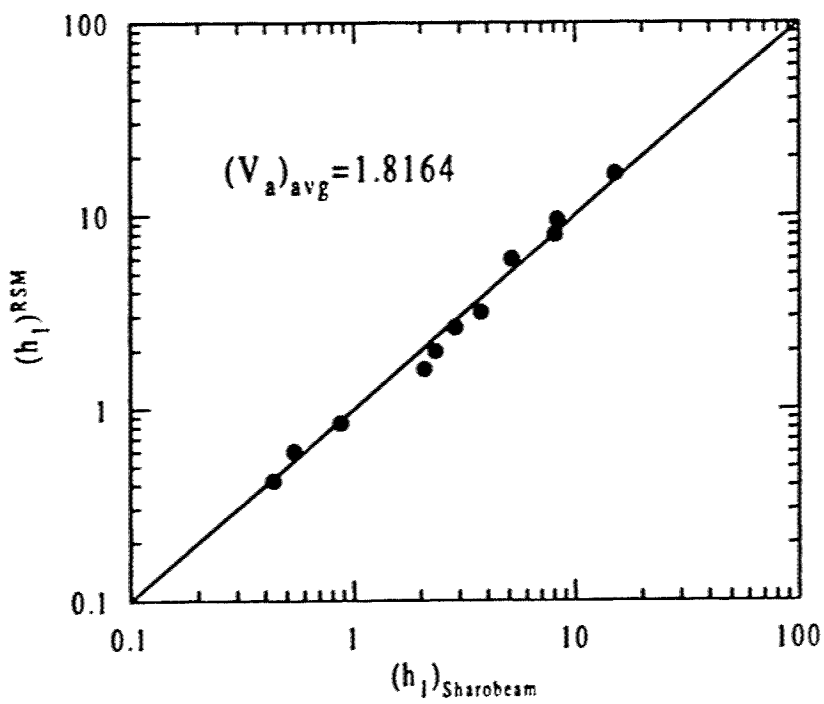

Figure 31. Comparison of predicted h_1 from the EPFM of NASGRO with Sharobeam's FE results for the crack tip location a (Φ=90°) for the case of SC01 under tension.

Surface Crack under Bending

The results of Yagawa et al. (1993) are used in this section for validation purposes. However, two issues need to be addressed. First of all, in Yagawa's paper, the expression for J_p is different from the one used in the EPFM module in NASGRO. Yagawa's expression is of the form

$$J_p = \alpha\sigma_o\varepsilon_o\tilde{h}_1 t\left(\frac{m}{m_o}\right)^{n+1} = \alpha\sigma_o\varepsilon_o\tilde{h}_1 t\left(\frac{\sigma}{3\sigma_o}\right)^{n+1} \tag{81}$$

However, the expression used in NASGRO is

$$J_p^{RSM} = J_e V\alpha\mu\left(\frac{M}{M_o^*}\right)^{n-1} = \alpha\sigma_o\varepsilon_o h_1 t\left(\frac{M}{M_o}\right)^{n+1} = \alpha\sigma_o\varepsilon_o h_1 t\left(\frac{2}{3}\frac{\sigma}{\sigma_o}\right)^{n+1} \tag{82}$$

where $M = \frac{\sigma t^2}{6}\cdot 2b$, $M_o = \frac{\sigma_o t^2}{4}\cdot 2b$, $m = \frac{M}{2b}$, and $m_o = \frac{\sigma_o t^2}{2}$. Therefore, there is a conversion factor between equations (81) and (82) given by

$$\tilde{h}_1 = 2^{n+1} h_1 \tag{83}$$

Secondly, there is a discrepancy between Yagawa's J_e results and NASGRO's. This is demonstrated in Figures 32 and 33 where results using optimized yield loads (determined by applying the RSM) and NASGRO's J_e solutions in equation (82) are compared with Yagawa's results. The discrepancy can be eliminated by replacing NASGRO's J_e solutions by Yagawa's J_e results when evaluating J_p^{RSM} as shown in Figures 34 and 35. The comparisons indicate that Yagawa's elastic solutions for J_e are in error. Therefore, for valid comparisons, the RSM results from NASGRO (based on the hybrid reference stress method and the net section yield moments derived in Section 4.2) are multiplied by a factor equal to the ratio of Yagawa's and NASGRO's values for J_e.

$$(h_1)_{NASGRO}\cdot\frac{(J_e)_{Yagawa}}{(J_e)_{NASGRO}} \text{ versus } (h_1)_{Yagawa} = \frac{\tilde{h}_1}{2^{n+1}}$$

The results shown in Figures 36 and 37 demonstrate that the RSM J solutions in NASGRO are conservative with respect to the finite element results.

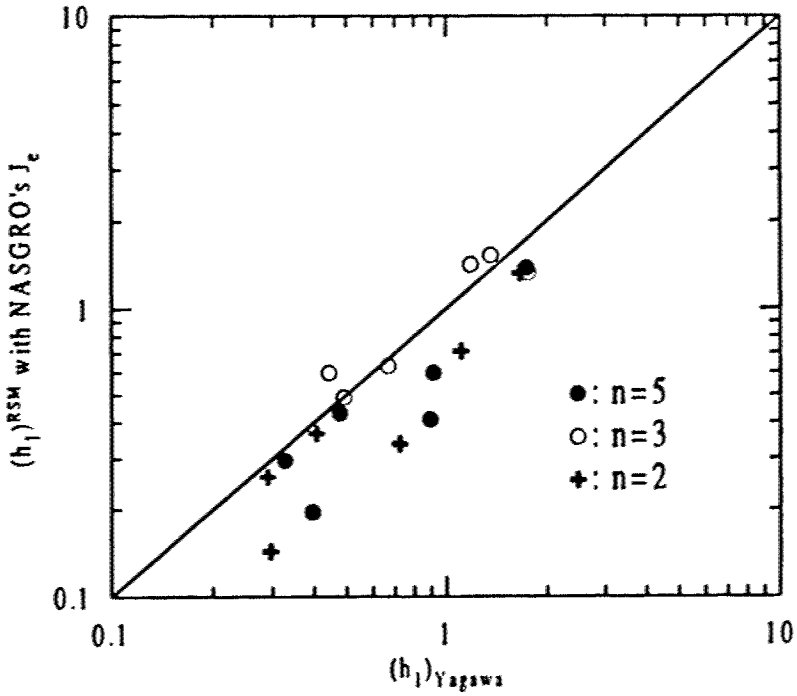

Figure 32. Comparison of $(h_1)_{Yagawa}$ with $(h_1)^{RSM}$ determined using NASGRO's J_e solutions for the crack tip location a (Φ=90°); surface crack under bending.

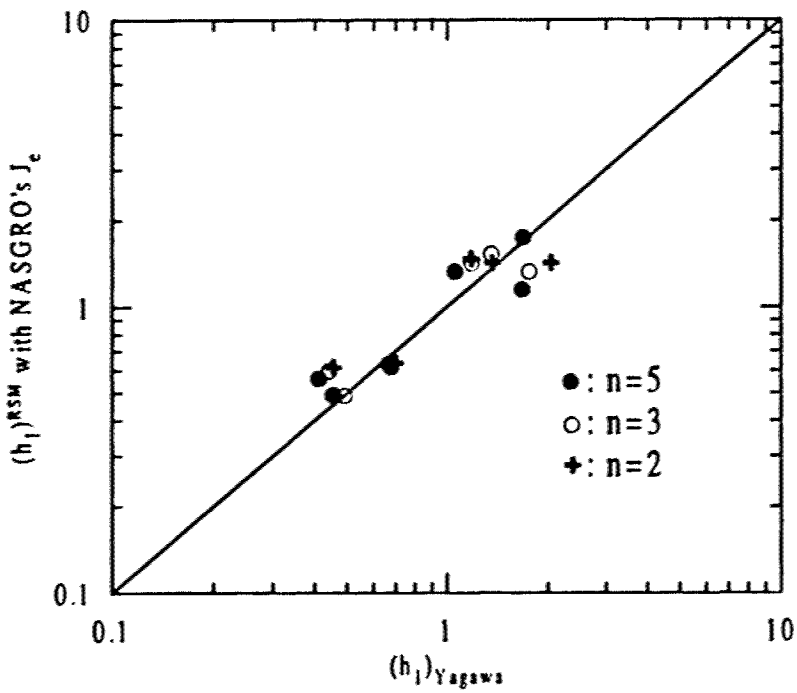

Figure 33. Comparison of $(h_1)_{Yagawa}$ with $(h_1)^{RSM}$ determined using NASGRO's J_e solutions for the near surface crack tip location c (Φ=9°); surface crack under bending.

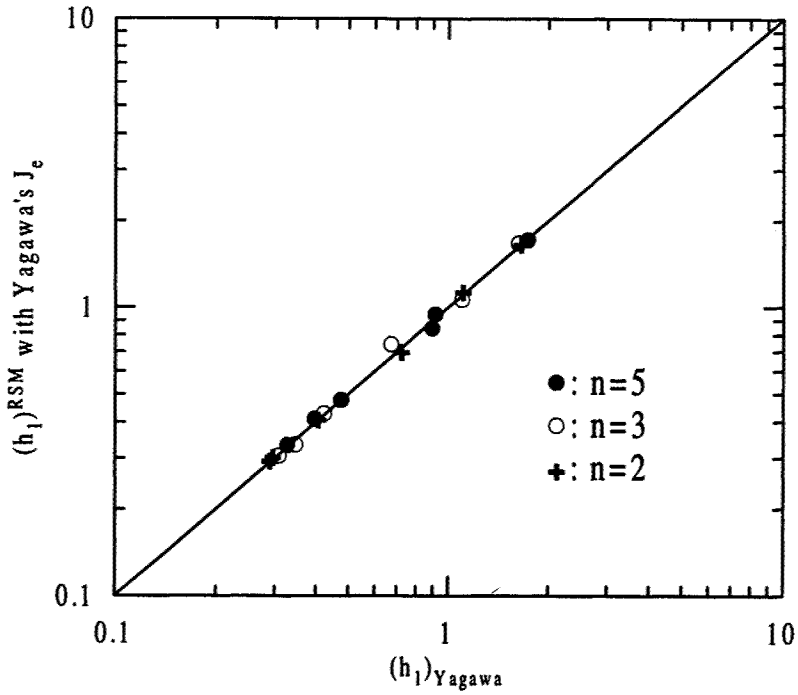

Figure 34. Comparison of $(h_1)_{Yagawa}$ with $(h_1)^{RSM}$ determined using Yagawa's J_e solutions for the crack tip location *a* (Φ=90°); surface crack under bending.

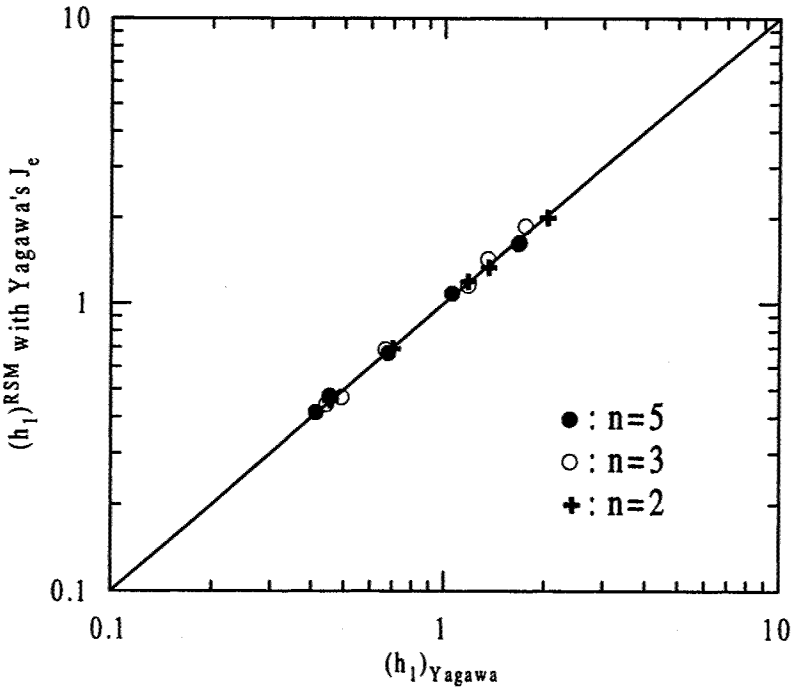

Figure 35. Comparison of $(h_1)_{Yagawa}$ with $(h_1)^{RSM}$ determined using Yagawa's J_e solutions for the near surface crack tip location *c* (Φ=9°); surface crack under bending.

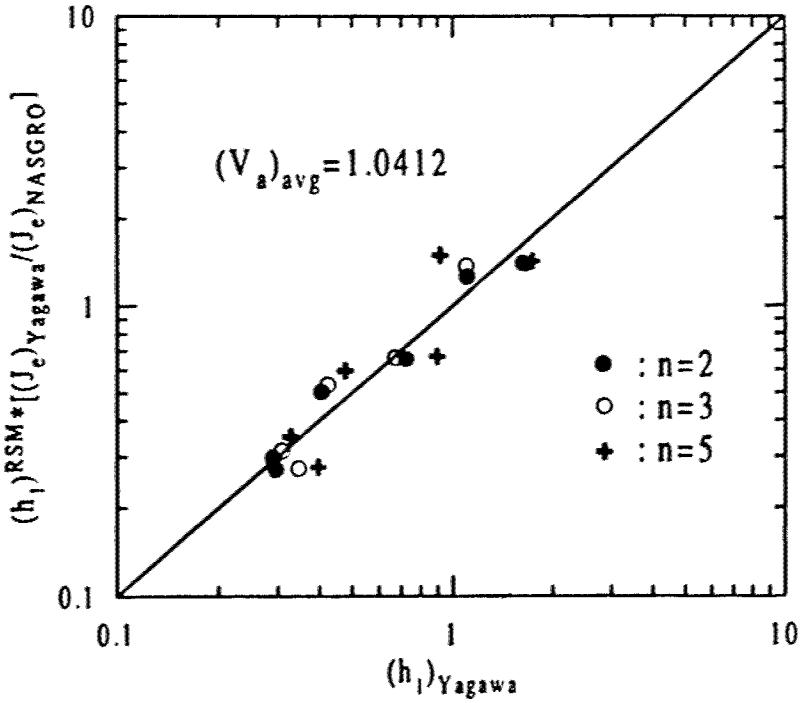

Figure 36. Comparison of RSM results with Yagawa for the crack tip location *a* (Φ=90°); surface crack under bending.

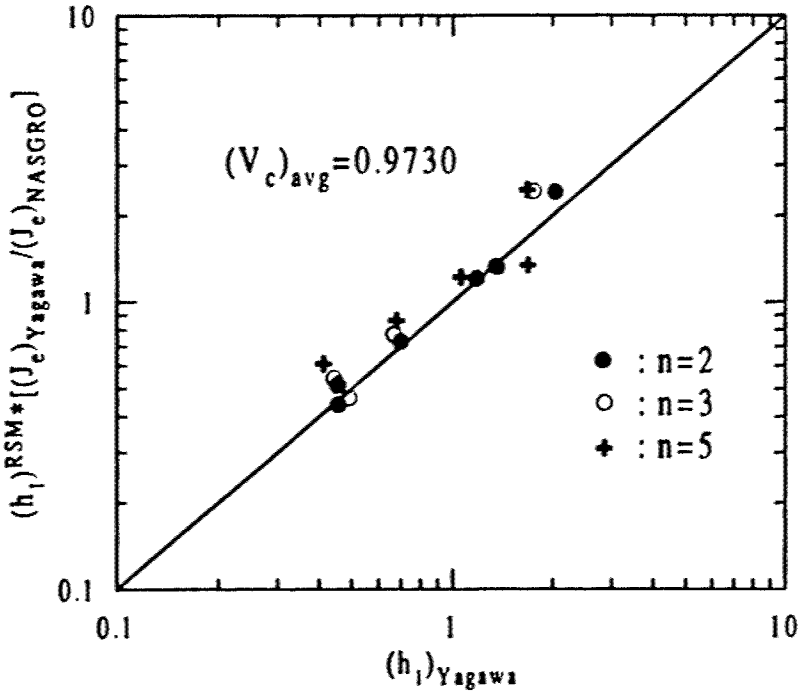

Figure 37. Comparison of RSM results with Yagawa for the near surface crack tip location *c* (Φ=9°); surface crack under bending.

11.2 Validation of the J Solution due to Secondary Loads

Since there are no independent J solutions available characterizing the variety of possible secondary loads, verification of the J routines for secondary loads in NASGRO was based on a self-consistency check. Self-consistency requires that when crack tip plasticity effects are negligible, $J(\sigma_T^P) = J(\sigma_T^S)$ provided $\sigma_T^P = \sigma_T^S$, where superscripts P and S refer to primary and secondary loads, respectively, and the subscript T signifies uniform tension. This self-consistency was confirmed using the test matrix for each model type shown in Table 19.

Model type	Test runs involved	Check
TC01 EC01	1. Primary (uniform tension), $J_e(\sigma_T^P)$ 2. Secondary (uniform tension), $J_e(\sigma_T^S)$ 3. Secondary (tension with triangular variation), $J_e(\bar{\sigma}_T^S)$	$J_e(\sigma_T^P) \cong$ $J_e(\sigma_T^S) \cong$ $J_e(\bar{\sigma}_T^S)$
TC02	1. Primary (uniform tension), $J_e(\sigma_T^P)$ 2. Secondary (uniform tension), $J_e(\sigma_T^S)$	$J_e(\sigma_T^P) \cong$ $J_e(\sigma_T^S)$
SC01	1. Primary (bending), $J_e(\sigma_B^P)$ 2. Secondary (bending), $J_e(\sigma_B^S)$	$J_e(\sigma_B^P) \cong$ $J_e(\sigma_B^S)$
CC01	1. Primary (uniform tension), $J_e(\sigma_T^P)$ 2. Primary (bending), $J_e(\sigma_B^P)$ 3. Secondary (tension & bending), $J_e(\sigma_{T+B}^S)$	$\left[\sqrt{J_e(\sigma_T^P)} + \sqrt{J_e(\sigma_B^P)}\right]^2 \cong$ $J_e(\sigma_{T+B}^S)$

Table 19. Test matrix for the verification of secondary load formulation.

11.3 Validation of the EPFM Failure Algorithm

<u>Self-Consistency Between Critical Crack and Critical Load Calculations</u>

A self-consistency check was done by comparing the results of failure analysis based on critical crack and critical load calculations. The logic of the applied self-consistency check is as follows - If P^c is the calculated critical load corresponding to flaw size, a^c, then a^c should be the calculated critical crack size corresponding to the load P^c. This logic is also valid for combined loading, P^c+S. This consistency requirement was verified using the test matrix shown in Table 20 for a variety of model types. The properties, dimensions and fracture parameters used for the consistency verification are in batch files residing in a sub-directory called OPTION6 included with this release of NASGRO. This sub-directory also contains the corresponding output files.

Independent Check

An independent check of the failure algorithm in the NASGRO EPFM module was made by comparing NASGRO's results with those derived from a SwRI in-house program. This in-house program utilizes the SwRI copyrighted program, KCALC, to calculate stress intensity factors. Table 21 lists the material properties, Ramberg-Osgood parameters and the dimensions used in the verification test matrix. Table 22 shows the comparison between results from NASGRO and the SwRI in-house program for different combinations of loading, constraint, model type, and J_R curve. The two sets of results are close, and the major differences come from different stress intensity factors employed by KCALC and NASGRO.

Model type	Load type	J estimation scheme	Deformation constraint	Load combination	Material behavior	Self-consistency validated
TC01 TC02	Tension	EPRI	Plane strain	P	Brittle	Yes
					Ductile	Yes
				P+S	Brittle	Yes
					Ductile	Yes
			Plane stress	P	Brittle	Yes
					Ductile	Yes
				P+S	Brittle	Yes
					Ductile	Yes
		RSM	Plane strain	P	Brittle	Yes
					Ductile	Yes
				P+S	Brittle	Yes
					Ductile	Yes
			Plane stress	P	Brittle	Yes
					Ductile	Yes
				P+S	Brittle	Yes
					Ductile	Yes

Table 20(a). Test matrix for self-consistency check for TC01 and TC02 under tension.

Model type	Load type	J estimation scheme	Deformation constraint	Load combination	Material behavior	Self-consistency validated
TC02	Bending	EPRI	Plane strain	P	Brittle	Yes
					Ductile	Yes
				P+S	Brittle	Yes
					Ductile	Yes
			Plane stress	P	Brittle	Yes
					Ductile	Yes
				P+S	Brittle	Yes
					Ductile	Yes
		RSM	Plane strain	P	Brittle	Yes
					Ductile	Yes
				P+S	Brittle	Yes
					Ductile	Yes
			Plane stress	P	Brittle	Yes
					Ductile	Yes
				P+S	Brittle	Yes
					Ductile	Yes

Table 20(b). Test matrix for self-consistency check for TC02 under bending.

Model type	Load type	Fixed parameters	Load combination	Material behavior	Self-consistency validated
SC01 CC01 EC01	Tension	Constant aspect ratio	P	Brittle	Yes
				Ductile	Yes
			P+S	Brittle	Yes
				Ductile	Yes
		Constant surface crack size	P	Brittle	Yes
				Ductile	Yes
			P+S	Brittle	Yes
				Ductile	Yes

Table 20(c). Test matrix for self-consistency check for SC01, CC01 and EC01.

Young's module E, kpsi	Poisson's ratio ν	Yield stress σ_y, ksi	Ultimate stress σ_u, ksi	σ_o ksi	α	β
30000	0.3	100	150	100	1	10

Table 21. Material properties used for the comparison between the NASGRO results and those from the program using KCALC for evaluating the fracture toughness.

Model type	Primary Load type	Con-straint	J_R curve	$(\Delta a)_{max}$ in	J_{mat} ksi-in	σ^P ksi	σ^S ksi	NASGRO				Independent check			
								a_{limit} in	a_{init} in	a_{crit} in	$(\Delta a)_{tear}$ in	a_{limit} in	a_{init} in	a_{crit} in	$(\Delta a)_{tear}$ in
TC02 (W=1in, t=10in)	T	PS	0.35+ 30(Δa)- 150(Δa)^2	0.1	0.5	25	100-100x	0.56	0.11	0.14	0.039	0.56	0.11	0.14	0.037
TC02 (W=1in, t=10in)	T	PS	0.35+ 30(Δa)- 150(Δa)^2	0.1	0.5	20	100-100x	0.60	0.12	0.16	0.038	0.60	0.12	0.15	0.038
TC02 (W=1in, t=10in)	B	PS	0.35+ 30(Δa)- 150(Δa)^2	0.1	0.5	15	100	0.75	0.11	0.14	0.034	0.76	0.11	0.14	0.033
TC02 (W=1in, t=10in)	B	PS	0.35+ 30(Δa)- 150(Δa)^2	0.1	0.5	10	100	0.75	0.12	0.15	0.034	0.76	0.12	0.14	0.033
TC02 (W=1in, t=10in)	T	PE	0.35+ 30(Δa)- 150(Δa)^2	0.1	0.5	25	100-100x	0.63	0.16	0.22	0.047	0.63	0.16	0.22	0.046
TC02 (W=1in, t=10in)	T	PE	0.35+ 30(Δa)- 150(Δa)^2	0.1	0.5	20	100-100x	0.66	0.17	0.23	0.047	0.66	0.17	0.23	0.046
TC02 (W=1in, t=10in)	B	PE	0.35+ 30(Δa)- 150(Δa)^2	0.1	0.5	15	100	0.75	0.16	0.21	0.042	0.76	0.16	0.21	0.042
TC02 (W=1in, t=10in)	B	PE	0.35+ 30(Δa)- 150(Δa)^2	0.1	0.5	10	100	0.75	0.17	0.22	0.042	0.76	0.17	0.22	0.042

Table 22(a). Comparison of NASGRO's results with those from a SwRI in-house program; T=tension, B=bend.

Model type	Primary Load type	Con-straint	J_R curve	$(\Delta a)_{max}$ in	J_{mat} ksi-in	σ^P ksi	σ^S ksi	NASGRO				Independent check			
								a_{limit} in	a_{init} in	a_{crit} in	$(\Delta a)_{tear}$ in	a_{limit} in	a_{init} in	a_{crit} in	$(\Delta a)_{tear}$ in
TC01 (W=2in, t=10in)	T	PE	$0.35+30(\Delta a)-150(\Delta a)^2$	0.1	0.5	25	100	0.84	0.24	0.43	0.069	0.84	0.24	0.43	0.068
TC01 (W=2in, t=10in)	T	PE	$0.35+30(\Delta a)-150(\Delta a)^2$	0.1	0.5	20	100	0.88	0.26	0.45	0.068	0.88	0.26	0.45	0.066
TC01 (W=2in, t=10in)	T	PS	$0.35+30(\Delta a)-150(\Delta a)^2$	0.1	0.5	25	20	0.81	0.17	0.30	0.063	0.81	0.17	0.30	0.062
TC01 (W=2in, t=10in)	T	PS	$0.35+30(\Delta a)-150(\Delta a)^2$	0.1	0.5	100	100	0.85	0.18	0.31	0.062	0.85	0.18	0.31	0.061
SC01 (W=10in, t=1in)	T	Fixed c=2	$0.175+15(\Delta a)-75(\Delta a)^2$	0.1	0.2	25	$100(1-x)^2$	1.0	0.11	0.93	0.018				
SC01 (W=10in, t=1in)	T	Fixed c=4	$0.175+15(\Delta a)-75(\Delta a)^2$	0.1	0.2	20	$100(1-x)^2$	1.0	0.128	(*)	(*)				
SC01 (W=10in, t=1in)	T	Fixed a/c= 0.2	$0.175+15(\Delta a)-75(\Delta a)^2$	0.1	0.2	25	$100(1-x)^2$	1.0	0.14	0.569	0.1				
SC01 (W=10in, t=1in)	T	Fixed a/c= 0.1	$0.175+15(\Delta a)-75(\Delta a)^2$	0.1	0.2	20	$100(1-x)^2$	1.0	0.14	0.40	0.079				

Table 22(b). Comparison of NASGRO's results with those from a SwRI in-house program; T=tension, B=bend. (*) outside NASGRO LEFM validity bounds.

11.4 Validation of the NASGRO EPFCG Module

The NASGRO EPFCG module was independently verified by comparing its predictions with actual experimental crack growth data for Inconel 718. Details of this verification exercise are provided in Appendix L.

Experiments included three different specimen geometries (TC01, SC01, and CC01), a wide range of deformation conditions (SSY, ISY, and LSY), and stress ratios ranging from $R = 0$ to $R = -1$. The SSY tests were used to determine baseline crack growth properties, and then these properties were used to make independent predictions for the remaining tests. The NASGRO module was found to be highly successful in predicting crack growth lives and correlating crack growth rate data. All lifetime predictions were conservative and within a factor of two of the actual observed life. The NASGRO module also generally predicted the correct crack shape development for two-degree-of-freedom surface cracks.

12.0 Acknowledgement

The authors wish to acknowledge the invaluable help provided by Sambi R. Mettu at Lockheed/ESC Engineering and Programming Support at Johnson Space Center. His quick responses in answering our many questions concerning NASGRO are much appreciated.

APPENDIX L

EXPERIMENTAL VERIFICATION OF NASGRO ELASTIC-PLASTIC FATIGUE CRACK GROWTH MODULE

L.1 Introduction

Fatigue crack growth tests on specimens of Inconel 718 were used to verify the NASGRO elastic-plastic fatigue crack growth module. Some of these tests were originally performed to support methods development activities under the multiple-cycle proof testing contract (McClung et al., 1996b), while others were performed solely to support NASGRO verification. For completeness, all tests are fully documented in this appendix.

Tests were conducted on three different specimen geometries, identified here according to their NASGRO designation: TC01, central through-crack in a plate; SC01, semi-elliptical surface crack in a plate; and CC01, quarter-elliptical corner crack in a plate. Some tests were conducted under small-scale yielding conditions, while other tests were conducted under intermediate or large-scale yielding. Stress ratios were $R = 0$, $R = 0.1$, or $R = -1$.

The new NASGRO EPFCG module was used to predict the crack growth behavior of all tests. The small scale yielding tests with TC01 specimens were used to determine baseline crack growth properties, and then these properties were used to make independent predictions for the remaining tests.

L.2 Material Characterization

Due to its wide application in SSME components and its use as a model material in related contracts, Inconel 718, a precipitation hardenable, nickel-base superalloy, was chosen for the experimental verification studies. Age hardening in this alloy is achieved through precipitation of a columbium-rich intermetallic phase which results in good corrosion and oxidation resistance, as well as good mechanical properties, which permit its use to temperatures of 1200°F (649°C).

To ensure that the results generated were applicable to SSME components, the test material was purchased according to Rockwell Specification RB0170-153 in the form of 1.25 in. (31.8 mm) diameter round bars. The Inconel 718 was machined into tension specimens and then heat treated according to the following procedures:

(1) Vacuum solution treat at 1900°F (1038°C) for 10-30 minutes

(2) Argon back fill; cool to room temperature

(3) Age in vacuum at 1400°F (760°C) for 10 hrs.

(4) Furnace cool to 1200°F (649°C) and hold for a total time [1400°F (760°C) plus furnace cool plus hold time at 1200°F (649°C)] of 20 hours

(5) Argon back fill; cool to room temperature

This particular heat treatment (denoted STA-1) is used in SSME components to achieve optimum resistance to hydrogen embrittlement.

The chemical composition of the Inconel 718 material used is given in Table L.1. Baseline mechanical properties were determined from standard tensile tests as 0.2% offset yield strength = 166.4 ksi, ultimate tensile strength = 195.1 ksi, elongation = 25.8%, and reduction in area = 32.3%. These tensile test results are in conformance with the RB0170-153 specifications. Analysis of the load-displacement records from these tensile tests produced a relationship between stress (in ksi) and plastic strain of the form

$$\sigma = 248.4\left(\varepsilon_p\right)^{0.0633} \tag{L.1}$$

The elastic modulus is 29.69×10^3 ksi. The stress- total strain relationship may also be written in the general Ramberg-Osgood form,

$$\frac{\varepsilon}{\varepsilon_0} = \frac{\sigma}{\sigma_0} + \alpha\left(\frac{\sigma}{\sigma_0}\right)^n \tag{L.2}$$

where $\epsilon_0 = 0.006$, $\sigma_0 = 179.8$ ksi, $\alpha = 1$, and $n = 15.8$.

Formal cyclic stress-strain curves were not generated. Unpublished Rocketdyne data indicate that Inconel 718 in the STA-1 condition exhibits cyclic softening. Ramberg-Osgood properties generated from stable hysteresis loops obtained in low cycle fatigue tests were $\sigma_0' = 158.3$ ksi, $\epsilon_0' = 0.00533$, $n' = 6.15$, and $\alpha' = 1$.

Table L.1. Chemical Composition of the Inconel 718 Test Material

Heat No.	C	Mn	Si	S	P	Cr	Ni	Mo	Co
6L9364	0.044	0.09	0.12	0.001	0.006	18.5	52.3	3.03	0.31
	Cu	Al	Ti	Cb+Ta	Mg	Pb	Sn	Fe	
	0.05	0.53	0.99	5.17	23 ppm	0.8 ppm	25 ppm	Bal	

L.3 Specimen Geometries

The baseline specimen geometry is shown in Figure L.1. TC01 and SC01 specimens had a rectangular cross-section with a nominal 1.25-in. width and either a 0.2-in. or 0.5-in. thickness. Initial cracks were formed by first electro-discharge machining a narrow notch and then fatigue pre-cracking at low cyclic loads. Different EDM notch configurations were used to generate different

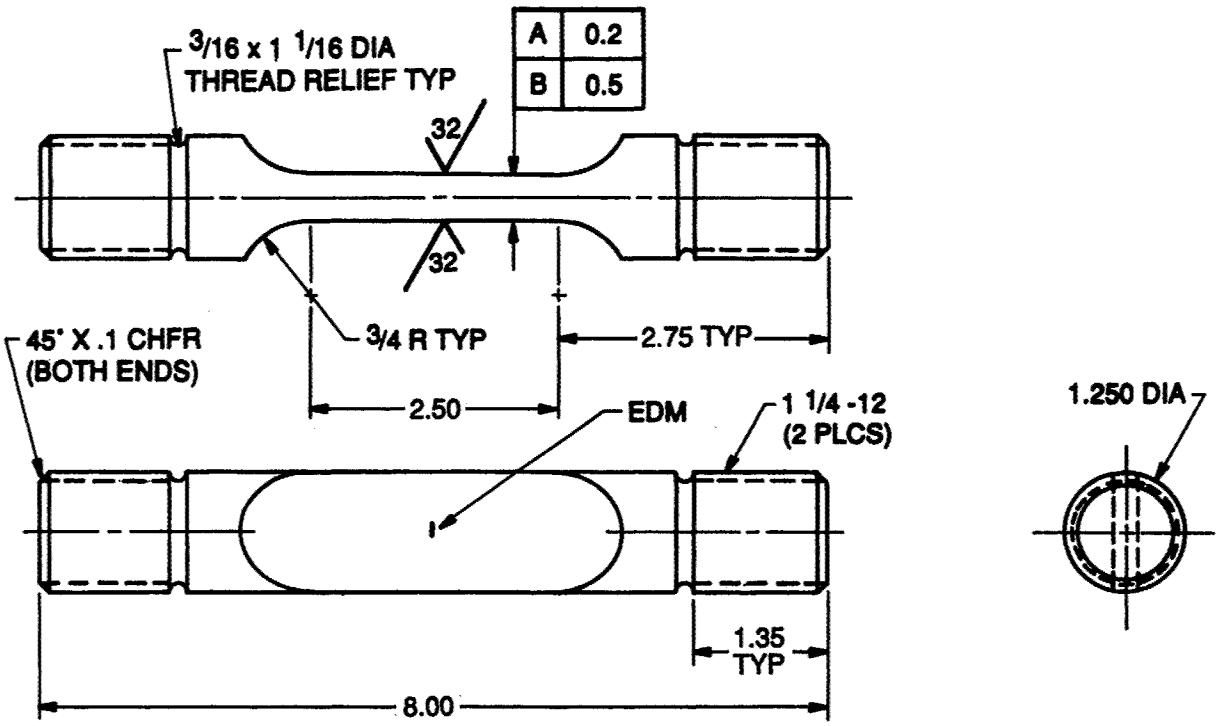

Figure L.1. Baseline specimen geometry for NASGRO EPFCG verification experiments

NASGRO geometries. Shown in Figure L.1 is the placement of the EDM notch for a semi-elliptical surface crack geometry, SC01.

The corner-crack geometry, CC01, tested in this program was generated by electro-discharge machining the width of a 0.5-in. thick specimen down from 1.25-in. to 0.5-in., so that the specimen had approximately a square cross-section. A small EDM notch was then machined into one corner of the specimen.

L.4 Crack Growth Experiments

All experiments were conducted in a laboratory air environment at room temperature. Crack lengths were generally measured by optical inspection at the specimen surface under low magnification, with some supplementary measurements from the fracture surfaces of broken specimens following the test. Some SC01 specimens were heat tinted following the precrack to aid identification of the initial crack size after the specimen was broken open.

TC01 tests were conducted with specimens D1, SD1, and SD2. Specimens SD1 and SD2 were nominally 0.2-in. thick, while D1 was nominally 0.5-in. thick. Initial crack sizes were approximately $2c = 0.3$ in. Constant amplitude load cycling was conducted at a stress ratio of 0.1 and a frequency of 5 Hz. Maximum stresses varied from 20 ksi to 56.3 ksi, and actual specimen lives varied from 9820 cycles to 270,118 cycles.

Six tests were conducted with the SC01 (semi-elliptical surface crack) configuration. Specimens S7 and S33 both contained small semi-circular surface cracks (initial $a = 0.01$ in., initial $2c = 0.02$ in.) in a rectangular cross-section of thickness $t = 0.20$ in. Both specimens were cycled in load control to a maximum stress of 135 ksi. Specimen S7 was cycled at a stress ratio of $R = -1$ (i.e., $\sigma_{min} = -135$ ksi), and specimen S33 was cycled at $R = 0$ (minimum load just slightly greater than zero to avoid backlash in the specimen gripping fixtures). Global strains were monitored with a 0.50-in. extensometer mounted on the side of the specimen.

Cyclic crack growth in specimen S33 continued stably until the surface crack had grown almost completely through the specimen ($a \rightarrow 0.20$ in.). Cyclic crack growth in specimen S7 was interrupted by premature failure of the specimen due to initiation and growth of corner cracks from naturally initiating defects on the specimen edge. The depth of the surface crack just prior to failure was about $a = 0.08$ in.

Nominal cyclic strains in specimen S33 ($R = 0$) were fully elastic, since the total $\Delta\sigma$ was considerably less than $2\sigma_{ys}$. Therefore, the plastic component of ΔJ for this specimen was effectively zero, and the usual ΔK was a valid measure of the cyclic crack driving force. Nominal cyclic strains in specimen S7 ($R = -1$) included both elastic and plastic components. Although the total $\Delta\sigma$ was less than the nominal $2\sigma_{ys}$ based on monotonic properties ($\sigma_{ys} = 165$ ksi), cyclic softening occurred gradually during the test. The cyclic 0.2% offset yield stress is about 135 ksi. As we will see, this cyclic softening is important for the characterization of FCG rates under elastic-plastic conditions.

Specimens S25 and S29 were both SC01 geometries with thickness = 0.2 in. and relatively large initial flaw depths (a_i = 0.149 in. and 0.164 in., respectively, so that a_i/t was approximately 0.8). Constant amplitude load control cycling was conducted at a stress ratio of $R = 0$ and maximum stresses of 145 and 135 ksi, respectively. The initial crack shape was determined following the test to be $a/c = 0.915$ and 0.89, respectively. Cycling continued until specimen failure occurred in 385 and 378 cycles, respectively.

Specimens S11 and S13 were both SC01 geometries subjected to very severe cycling. Both specimens had thickness = 0.2 in. and relatively deep initial crack sizes (a_i = 0.146 in. and 0.129 in., respectively). Initial a/c values were about 0.96 in both specimens.

These two tests were conducted under crack mouth opening displacement (CMOD) control. A small CMOD gage with a gage length of 0.2 in. was placed across the crack mouth, the gage pins located in diamond indentations on the front surface of the specimen. The loads on the specimen were continuously monitored and recorded as CMOD was cycled between zero and a fixed maximum quantity. The maximum stresses on the specimens slowly decreased as cycling continued and the specimen compliance increased. The absolute value of the minimum stresses also slowly decreased with cycling.

Compliance data (load vs. CMOD) were used to estimate changes in crack size on a cycle-by-cycle basis. Initial and final crack depth and length were measured exactly from the specimen surface following the test.

The very first excursion to maximum CMOD produced some crack growth by ductile tearing. The specific amount of crack growth occurring on this first cycle was estimated from similar resistance curve experiments with SC01 specimens in which the specimen was subjected to a single zero-max CMOD ramp and then broken open to determine the amount of crack growth (McClung et al., 1996b).

Fatigue crack growth during these tests was relatively severe. The crack depth in S11 grew from 0.146 in. to 0.162 in.—an increase of 0.016 in.—during only 4 cycles. The crack depth in S13 grew from 0.129 in. to 0.154 in. during only 32 cycles.

Specimen S44 was a CC01 (corner crack) configuration. The initial crack sizes were $a = 0.034$ in. and $c = 0.0345$ in., and the crack grew such that $a \approx c$ throughout the test. Crack growth continued until specimen failure occurred at around $a = 0.275$ in.. However, due to the formation of multiple cracks in the intensely deformed plastic zone ahead of the main crack tip, visual determination of the correct physical crack length was difficult for cracks longer than $a = 0.150$ in. Growth after this point may have also been affected by crack linking. Therefore, only data for cracks shorter than about $a = 0.150$ in. were analyzed as part of the NASGRO verification exercises. These data correspond to the first 2950 fatigue cycles.

For convenience, all test conditions are summarized in Table L.2.

Table L.2. Summary of NASGRO EPFCG verification test conditions

Specimen #	Geometry	R	σ_{max} (ksi)	Cycles	Comments
D1	TC01	0.1	56.4	9820	baseline SSY test, thick specimen
SD1	TC01	0.1	55.8	13470	baseline SSY test
SD2	TC01	0.1	20.0	270118	baseline SSY test
S7	SC01	-1	135	5900	reversed plasticity
S33	SC01	~0	135	44900	
S25	SC01	~0	145	385	deep cracks
S29	SC01	~0	135	378	deep cracks
S11	SC01	~ -1	165 - 157	4	severe reversed plasticity
S13	SC01	~ -1	158 - 138	32	severe reversed plasticity
S44	CC01	-1	135	2950	reversed plasticity

L.5 NASGRO Calculations

The NASGRO EPFCG module was used to predict the crack growth life of all verification experiments. The inputs to NASGRO, as summarized in the User's Manual, Appendix K, include basic tensile properties and baseline fatigue crack growth rate properties, in addition to specification of test conditions such as crack sizes and applied stresses.

Tensile and constitutive property inputs are as summarized in Section L.2. The flow stress (used in the closure model) was estimated as 180 ksi for the monotonic condition and 185 for the stable cyclic condition. This cyclic value was estimated with the procedures outlined in Section 3.6.2.

In the NASGRO calculations, monotonic constitutive properties were employed for all SSY and R = 0 tests, while stable cyclic properties were employed for all $R = -1$ tests (all of which exhibited substantial cyclic plasticity). As discussed in Section 3.5.2, the selection of monotonic or cyclic properties can have a substantial impact on the calculated values of ΔJ_{eff} and total crack growth life. In this particular case, calculations of ΔJ_{eff} for $R = -1$ tests based on monotonic, rather than cyclic, constitutive properties could decrease the calculated ΔJ_{eff} by up to a factor of two. In reality, of course, the actual constitutive response is changing during these short term tests from monotonic towards stable cyclic behavior, but it is not practical to model this transient change, and it is conservative to use stable cyclic properties. This approach follows the recommendations set forth in Appendix K.

Baseline fatigue crack growth properties for input to NASGRO were determined from tests D1, SD1, and SD2. The *da/dN* vs. ΔK data from these SSY tests were regressed to determine appropriate values for the Paris exponent and coefficient, m_0 and C_0 in Eqn 3.28. The resulting values were $m_0 = 3.235$ and $C_0 = 0.706(10)^{-10}$ when the units of stress intensity were taken as ksi√in. Note that crack closure corrections were not included in this regression step, so that the baseline FCG constants would be representative of typical handbook data. The crack closure level for these tests was estimated from the NASGRO closure equations themselves (with $\alpha = 3$) to be $U_0 = 0.819$.

Initial crack sizes for input to NASGRO were based on actual measured values, including independent measurements of *a* and *c* for SC01 and CC01 geometries. NASGRO was used to compute crack sizes with increasing numbers of cycles until observed final crack lengths were reached. No attempt was made in this particular set of verification calculations to predict specimen failure from instability considerations. Therefore, actual and predicted numbers of cycles represent the numbers of cycles for a crack to grow from one fixed crack size to another fixed crack size. For SC01 geometries with two degrees-of-freedom, the crack depth, *a*, was the target parameter.

The key remaining input to the NASGRO EPFCG module is the constraint factor, α, for the crack closure model. As discussed in the User's Manual, Appendix K, α can be chosen based on a number of different considerations. In this verification study, the two limited cases of $\alpha = 1$ and $\alpha = 3$ were both considered. Traditionally, semi-elliptical surface cracks are regarding as having high constraint consistent with a high value of α. However, the severe plasticity associated with the elastic-plastic cycling can be argued to cause some loss of constraint, and therefore a somewhat lower value of α. In the absence of any clear quantitative means to choose α, it seemed prudent to determine the sensitivity to this choice. In these particular experiments, for the particular maximum stress levels (and therefore the particular K_{max}/K_{flow} values) experienced, constraint was found to have only a limited effect on the calculated crack opening levels, because the $\sigma_{open}/\sigma_{max}$ vs. K_{max}/K_{flow} curves for different α values actually cross over at higher values of K_{max}/K_{flow}.

A summary of the comparisons between actual experimental numbers of cycles and predicted numbers of cycles is given in Figure L.2. Note that the open symbols denote predictions based on $\alpha = 3$, while the closed symbols denote predictions based on $\alpha = 1$. In general, all of the predictions are excellent, over a very wide range of cyclic lives. The worst prediction is for the CC01 specimen, S44, which is conservative by about a factor of two. All other predictions are closer than a factor of two, and most of them are much closer. The predictions based on $\alpha = 3$ are always more conservative than the predictions based on $\alpha = 1$, but the differences between these two limiting assumptions are generally not very large. No predictions based on $\alpha = 3$ are non-conservative (predicted numbers of cycles greater than actual numbers of cycles).

Another method of evaluating the quality of the NASGRO calculations is to consider correlations of crack growth rate data based on ΔJ_{eff}. These correlations are shown in Figure L.3. Here the ΔJ_{eff} values calculated with the NASGRO module for specific observed values of crack size are correlated with the actual experimentally observed crack growth data. The crack growth rates were computed from actual *a* vs. *N* data using standard incremental polynomial techniques (2nd order

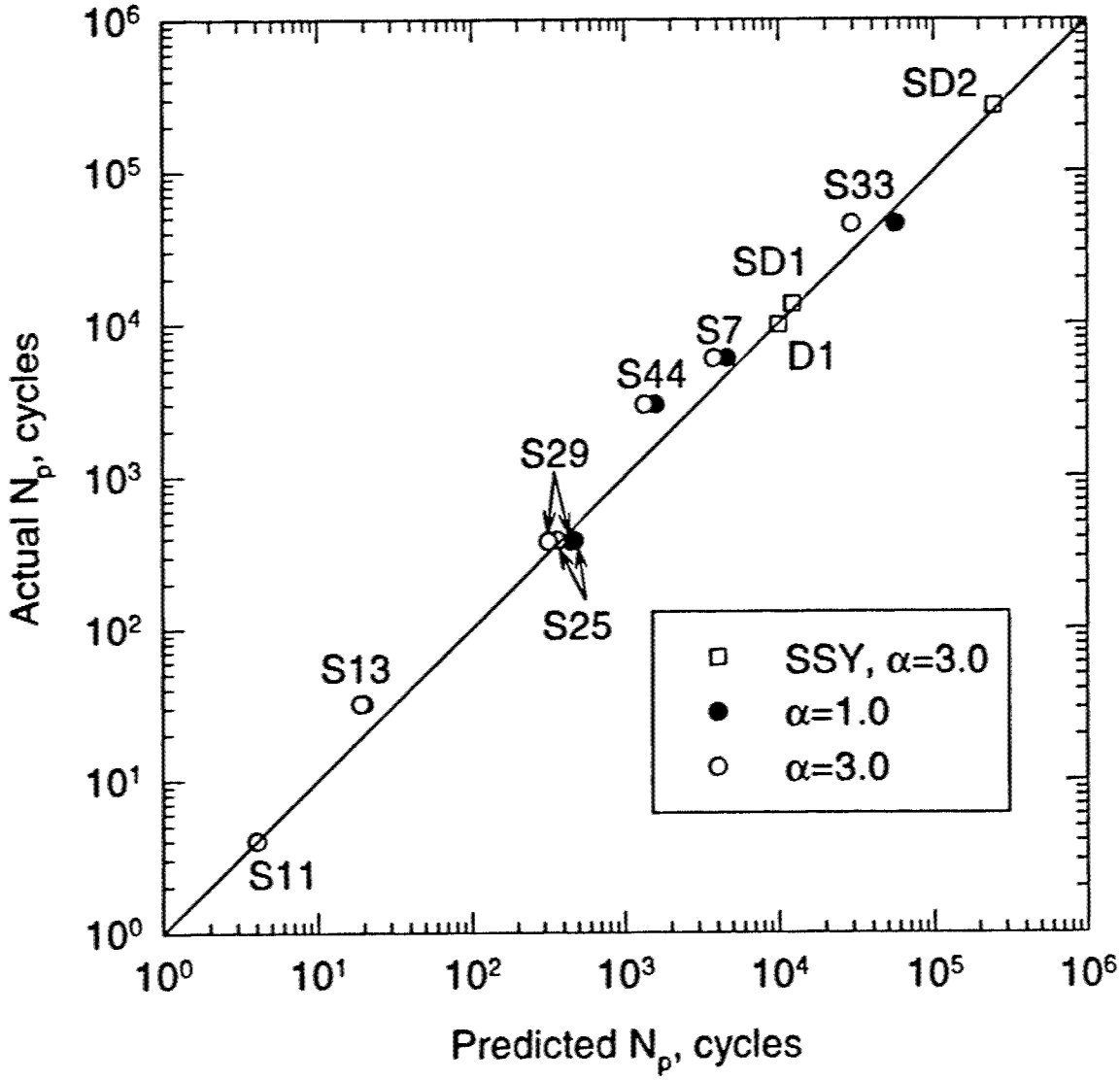

Figure L.2. Comparison of actual and predicted numbers of crack growth cycles

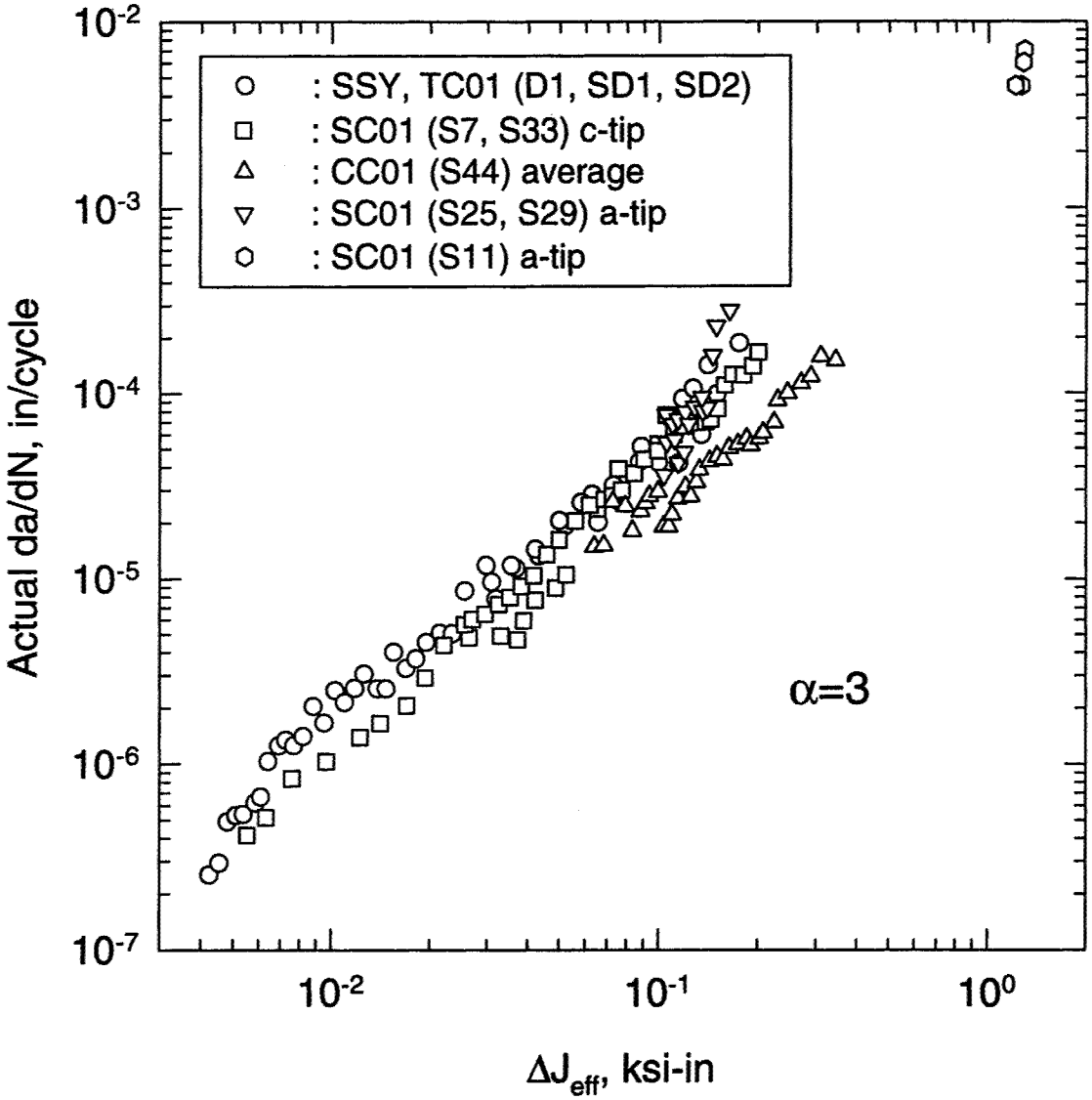

Figure L.3. Correlation of measured crack growth rates with calculated values of ΔJ_{eff}

polynomials with a five-point regression window). The correlation was carried out at either the a-tip or the c-tip for the SC01 cracks depending on which value was most reliably measured experimentally. Specimen S13 was not evaluated in this manner, and therefore does not appear on Figure L.3, because reliable measurements of crack size were not available at cycle numbers other than the first and last cycle of crack growth. The predicted ΔJ_{eff} values were all based on the conservative $\alpha = 3$ value.

The figure demonstrates a very strong correlation of FCG rates by ΔJ_{eff} over a very wide range of FCG rates—more than four orders of magnitude in da/dN. The only test that demonstrates any significant deviation from the central tendencies of the pooled data is the corner crack specimen, S44. Calculated ΔJ_{eff} values for the larger crack sizes in this test appear to be slightly too large, but would have been slightly smaller if a smaller α value was used. All other data generally fall within a factor-of-three scatterband that can be typical of test-to-test scatter under ordinary SSY conditions. It is particularly striking that the ΔJ_{eff} parameter is successful in correlating data from conventional SSY tests with data from tests with significant reversed plasticity. It is this success (the ability to describe all the data in Figure L.3 with a single Paris regression line) that makes it possible to perform accurate EPFCG life predictions based on Paris crack growth constants from baseline SSY tests.

The NASGRO calculations also appear to give the correct trends for the shape of two-degree-of-freedom cracks such as SC01. Comparisons of the predicted a and c values for specimens S7 and S33 (both SC01 geometries) are shown in Figure L.4. The predicted crack aspect ratio a/c is approximately 1 until the crack fronts begin to approach the back surfaces, when a/c begins to slowly decrease. These predictions are in harmony with literature observations of stable semi-circular crack shapes ($a/c \approx 1$) under elastic-plastic conditions (Obrtlik and Polak, 1985; Dowling and Iyyer, 1987; Earthman, 1991). This agreement suggests that the NASGRO β_R factor used to obtain the experimentally observed crack shape under SSY conditions is approximately applicable to EPFCG conditions as well.

L.6 Discussion and Conclusions

This verification study has found the NASGRO EPFCG module to be highly successful in predicting crack growth lives and correlating crack growth rate data. All predictions were conservative and within a factor of two of the actual observed life. It may be prudent to choose $\alpha = 3$ to perform conservative life calculations, but it appears that a somewhat smaller value of α may give slightly more accurate life predictions.

Predictions for the single CC01 specimen were more conservative than any other test. This could indicate that the NASGRO J solution for CC01 is slightly conservative itself. This particular J solution is based on a single set of finite element calculations that exhibited slightly more scatter than similar calculations for other geometries. It may be useful to investigate this J solution further in future work. In the meantime, however, it appears prudent and practical to maintain the current solution in view of its slight conservatism.

This study is not a comprehensive verification of the NASGRO EPFCG module, of course. As with any general purpose FCG code, extensive experience with many different configurations is needed to assess the accuracy and limitations of the code. In particular, further work is needed to investigate the suitability of the code for bending stress fields and alternative materials. However, the current study serves to validate the general ΔJ_{eff} approach to the analysis of fatigue crack growth under elastic-plastic conditions, and to verify that the developed NASGRO modules satisfactorily implement the basic technical approach.

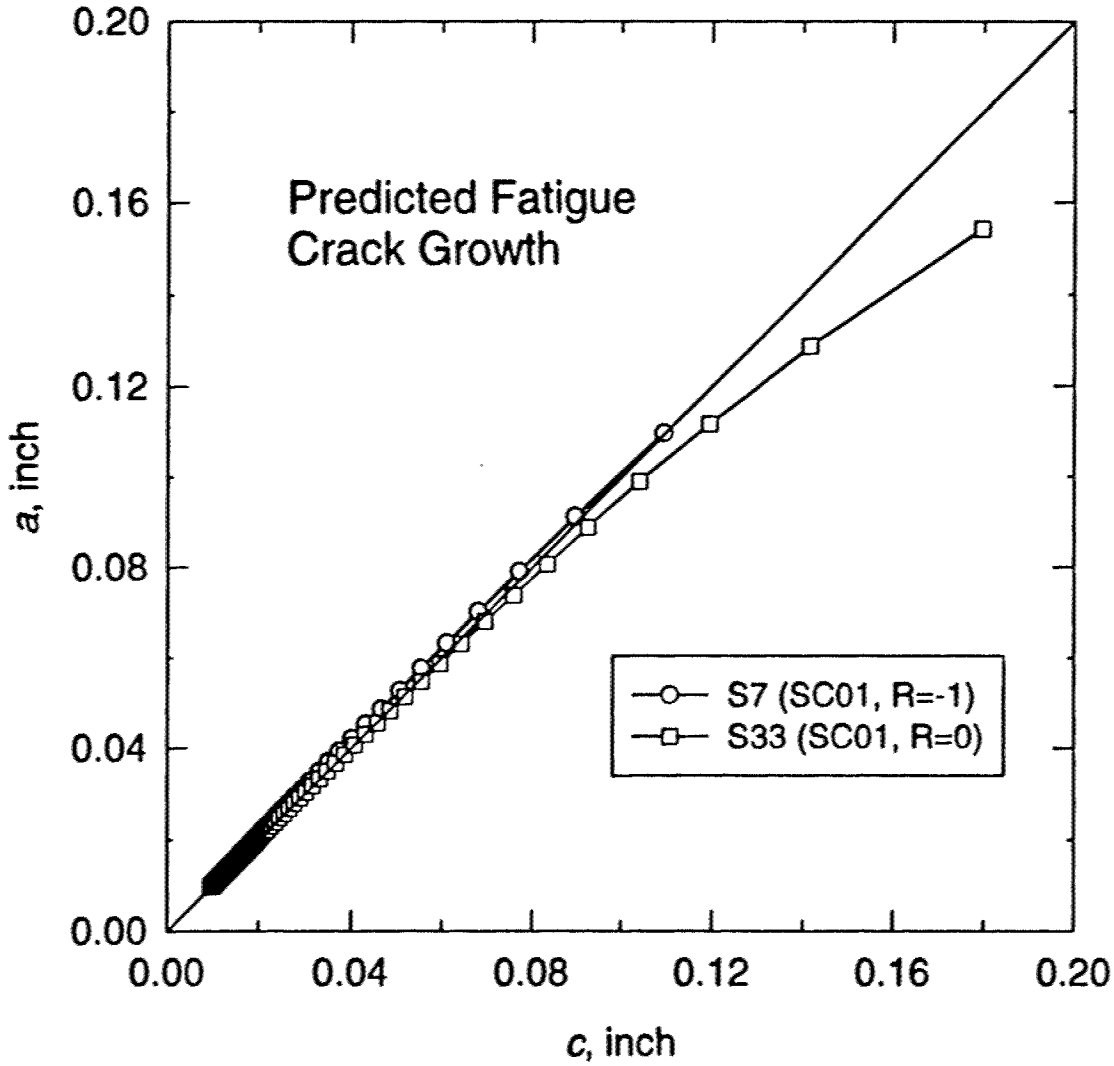

Figure L.4 Comparisons of predicted *a* and *c* values for SC01 geometries under elastic-plastic cycling, demonstrating stable semi-circular shapes

REPORT DOCUMENTATION PAGE

Form Approved
OMB No. 0704-0188

Public reporting burden for this collection of information is estimated to average 1 hour per response, including the time for reviewing instructions, searching existing data sources, gathering and maintaining the data needed, and completing and reviewing the collection of information. Send comments regarding this burden estimate or any other aspect of this collection of information, including suggestions for reducing this burden, to Washington Headquarters Services, Directorate for Information Operation and Reports, 1215 Jefferson Davis Highway, Suite 1204, Arlington, VA 22202-4302, and to the Office of Management and Budget, Paperwork Reduction Project (0704-0188), Washington, DC 20503

1. AGENCY USE ONLY *(Leave Blank)*

2. REPORT DATE
July 1999

3. REPORT TYPE AND DATES COVERED
Contractor Report (Final)

4. TITLE AND SUBTITLE
Development of a Practical Methodology
for Elastic-Plastic and Fully Plastic Fatigue Crack Growth

5. FUNDING NUMBERS
NAS8–37828

6. AUTHORS
R.C. McClung, G.G. Chell, Y.-D. Lee, D.A. Russell,* and G.E. Orient*

7. PERFORMING ORGANIZATION NAMES(S) AND ADDRESS(ES)
Southwest Research Institute
P.O. Drawer 28510
San Antonio, TX 78228–0510

8. PERFORMING ORGANIZATION REPORT NUMBER
M–933

9. SPONSORING/MONITORING AGENCY NAME(S) AND ADDRESS(ES)
George C. Marshall Space Flight Center
Marshall Space Flight Center, Alabama 35812

10. SPONSORING/MONITORING AGENCY REPORT NUMBER
NASA/CR—1999–209428

11. SUPPLEMENTARY NOTES
Prepared for Structures and Dynamics Laboratory, Science and Engineering Directorate.
Technical Monitor: M. Wayne Gregg
*Subcontract Support from Rocketdyne Division, Boeing North American, 6633 Canoga Ave., Canoga Park, CA 91303

12a. DISTRIBUTION/AVAILABILITY STATEMENT
Unclassified-Unlimited
Subject Category 39
Standard Distribution

12b. DISTRIBUTION CODE

13. ABSTRACT *(Maximum 200 words)*

A practical engineering methodology has been developed to analyze and predict fatigue crack growth rates under elastic-plastic and fully plastic conditions. The methodology employs the closure-corrected effective range of the J-integral, ΔJ_{eff}, as the governing parameter. The methodology contains original and literature J and ΔJ solutions for specific geometries, along with general methods for estimating J for other geometries and other loading conditions, including combined mechanical loading and combined primary and secondary loading. The methodology also contains specific practical algorithms that translate a J solution into a prediction of fatigue crack growth rate or life, including methods for determining crack opening levels, crack instability conditions, and material properties. A critical core subset of the J solutions and the practical algorithms has been implemented into independent elastic-plastic NASGRO modules. All components of the entire methodology, including the NASGRO modules, have been verified through analysis and experiment, and limits of applicability have been identified.

14. SUBJECT TERMS
elastic-plastic fracture mechanics, elastic-plastic and fully plastic fatigue crack growth, life prediction, J-integral, Delta J, finite elements, reference stress method, combined loading, primary and secondary loading, notches, multiaxial, crack closure, crack instability, resistance curves, tear-fatigue, creep-fatigue, software, NASGRO

15. NUMBER OF PAGES
485

16. PRICE CODE
A21

17. SECURITY CLASSIFICATION OF REPORT
Unclassified

18. SECURITY CLASSIFICATION OF THIS PAGE
Unclassified

19. SECURITY CLASSIFICATION OF ABSTRACT
Unclassified

20. LIMITATION OF ABSTRACT
Unlimited

National Aeronautics and
Space Administration
AD33
George C. Marshall Space Flight Center
Marshall Space Flight Center, Alabama
35812